

10-5-2016

Investigating the Antiproliferative Activity of Synthetic Troponoids

Eric R. Falcone

University of Connecticut, eric.falcone@uconn.edu

Follow this and additional works at: <https://opencommons.uconn.edu/dissertations>

Recommended Citation

Falcone, Eric R., "Investigating the Antiproliferative Activity of Synthetic Troponoids" (2016). *Doctoral Dissertations*. 1302.
<https://opencommons.uconn.edu/dissertations/1302>

Investigating the Antiproliferative Activity of Synthetic Troponoids

Eric Ryan Falcone, Ph.D.

University of Connecticut, 2016

Troponoid (or more commonly, tropone/tropolone) refers to a family of naturally occurring compounds with a unique seven-membered aromatic ring. As with many secondary metabolites, many of the tropolones display a wide range of biological activity. This activity includes: antibacterial/antifungal, insecticidal, phytotoxic, antimutagenic, anti-diabetic, anti-inflammatory, enzyme inhibition, anticancer, cytoprotective and reactive oxygenated species (ROS) scavenging. Most of this broad-range activity is attributed to the tropolone moiety while side chains are seen as attributing to selectivity. Therefore, tropolone may offer a unique scaffold to develop antiproliferatives since it can chelate metal ions, is relatively small and most likely promiscuous, likely resulting in several mechanisms of action to diminish the development of resistance.

This work focuses on the synthesis of a more diverse library of α -tropolones and tropones with functional groups capable of chelation other than the native hydroxyl. The library was used to assess structure activity relationship on the antiproliferative effects against cancer cell lines. Previous results with α -tropolones in the Anderson and Wright labs suggested selectivity towards hematological malignancies. As a result, α -tropolones were assessed for antiproliferative effects against a panel of malignant hematological cell lines from T-cell, B-cell and myeloid lineage. From this panel, there appears to be selectivity towards cell lines of T-cell lineage. The most susceptible cell line, Molt-4, was explored further to understand the mechanism through which α -tropolones exhibit antiproliferative properties.

Patients with hematological malignancies are at the highest risk of potentially deadly infections typically caused by gram-negative bacteria, with *E. coli*, *K. pneumoniae*, and *P. aeruginosa* being the most common and most lethal. Since several natural tropolones have been found to be bacteriostatic and bactericidal against a broad range of bacteria and exhibit lead-like Gram-negative antibacterial activity, α -tropolones may be developed as antiproliferative agents effective against both hematological malignancies and bacterial infections. The library of α -tropolones was then screened for antiproliferative effects on Gram-negative bacteria. Key potent tropolones were used to explore potential targets using an unbiased target identification approach. These studies show that bacterial enolase is most likely the target through which tropolones exhibit antiproliferative properties against Gram-negative bacteria.

Investigating the Antiproliferative Activity of Synthetic Troponoids

By

ERIC RYAN FALCONE

B.S. (Chemistry), Fairfield University, 2008

M.S. (Bioorganic Chemistry), Syracuse University 2010

A Dissertation

Submitted in Partial Fulfillment of the

Requirements for the Degree of Doctor of Philosophy

At the

University of Connecticut

2016

Copyright by
Eric Ryan Falcone

2016

APPROVAL PAGE

Doctor of Philosophy

Investigating the Antiproliferative Activity of Synthetic Troponoids

Presented by

Eric Ryan Falcone, M.S.

Major Advisor _____
Prof. Dennis L. Wright

Associate Advisor _____
Prof. Charles A. Giardina

Associate Advisor _____
Prof. Akiko Nishiyama

Associate Advisor _____
Prof. M. Kyle Hadden

Associate Advisor _____
Prof. José E. Manautou

University of Connecticut 2016

Dedicated to my grandfathers

Henry and John

who taught me the values of hard work,
dedication and the importance of a good education

ACKNOWLEDGEMENTS

With heart-felt gratitude I wish to extend my thanks to Dr. Amy Anderson, my advisor for the past five years, for believing in my abilities and offering me the opportunity to work in her lab based solely on my work experience and a phone interview. If it were not for her honesty, faith and impressive research, I would not have attended UConn. She was a constant source of inspiration and encouragement. Without her I may never have had the opportunity or confidence to take on such a variety of biological techniques. I believe I have become a better scientist by working with her.

I wish to thank Dr. Dennis Wright, my other major advisor, for his constant support, advice and overall enthusiasm for my projects. His knowledge of chemistry never ceases to amaze me and I strongly believe I have become a better chemist through our numerous discussions, the classes he taught and the many highly skilled chemists he helped develop in his lab.

I would also like to thank the members of my committee, Dr. Charles Giardina, Dr. Akiko Nishiyama, Dr. M. Kyle Hadden and Dr. José Manautou, for making time in their busy schedules to serve as members of my committee and for their advice towards my research and the preparation of this thesis. I especially wish to thank Dr. Andrew Wiemer for providing the Molt-4 and hPBMC cells, allowing me to work in his lab and to learn several different techniques from his graduate student, Jin Li.

Thanks to all the current and former members of the Anderson and Wright research groups, who have contributed in many different ways towards my time in the lab. I especially wish to thank Dr. Michael van Heyst for his guidance and mentoring as well as his tireless efforts

towards broadening the synthetic techniques that could be used to develop new tropolone derivatives. Thanks Jin Li from the Wiemer lab for donating her time to show me the proper techniques for culturing Molt-4 and hPBMCs, Western blot analysis and RNA extraction. I also wish to thank Jolanta Krucinska for her incredible efforts to push the enolase project forward.

Thanks to all the faculty and staff members at the University of Connecticut and other institutions who have contributed in many different ways to my education and research experience. I especially would like to thank Dr. Matthew Kubasik for his continued support and mentoring. I am forever grateful for the undergraduate summer research opportunity and academic advice he provided me as well as his insistence that I declare my undergraduate major as chemistry. Through this I found a world of opportunities and a love for research.

Finally and most importantly, I would like to give my thanks to my family who has supported me throughout my life. Without their constant source of love and encouragement it would have been difficult to accomplish everything I have to date. I would like to especially thank my parents who made sure I was able to have a great education, encouraged and supported my desire to further my graduate education and have always been there for me. I would also like to thank my in-laws for their support and for allowing me to take over their dining room table in order to write part of this thesis. Finally, I would like to thank my wife, Kelly, for her love, support, encouragement, motivation and for making sure I made time to have fun along the way. She helped make this whole experience possible and I am forever indebted to her.

TABLE OF CONTENTS

Chapter 1	Page
Inhibition of Metalloenzymes: Lessons from Clinically Used Inhibitors and Future Directions	
1.1 Introduction	1
1.2 Clinical Inhibitors of Zinc Metalloenzymes	2
1.2.1 Carbonic Anhydrase	3
1.2.2 Angiotensin Converting Enzyme	5
1.2.3 Matrix Metalloproteinase	7
1.2.4 Tumor Necrosis Factor- α Converting Enzyme	10
1.2.5 Histone Deacetylase	13
1.2.6 Farnesyltransferase	16
1.2.7 Leukotriene-A4 Hydrolase	19
1.2.8 Uridine Disphosphate-3-O-(R-3-hydroxymyristoyl)-N-acetylglucosamine Deacetylase	22
1.3 Clinical Inhibitors of Iron Metalloenzymes	25
1.3.1 Hypoxia-Inducible Factor Prolyl Hydroxylase	26
1.3.2 Peptide Deformylase	29
1.3.3 5-Lipoxygenase	32
1.3.4 Cytochrome P450	35
1.4 Clinical Inhibitors of Magnesium Metalloenzymes	38
1.4.1 Human Immunodeficiency Virus-Integrase	39
1.4.2 DNA Gyrase	42
1.5 Clinical Inhibitors of Manganese Metalloenzymes	46
1.5.1 1-deoxy-D-xylulose 5-phosphate Reductoisomerase	47
1.5.2 Arginase	49
1.6 Development of Inhibitors Towards A Copper Metalloenzyme	53
1.5.1 Tyrosinase	54
1.7 Properties of Common Metal Binding Groups	60
1.7.1 Hydroxamates	61
1.7.2 Carboxylates	62
1.7.3 Phosphonates/Phosphates	64
1.7.4 Sulfonamides/Sulfamides/Sulfamates	65
1.7.5 Thiols	65
1.7.6 Other Metal Binding Groups	66

1.8 Tropolone as a Metal Binding Group	74
1.9 Conclusions	77
1.10 References	78

Chapter 2

Development of Lead-like Troponoids Based on the Natural Product α -Thujaplicin

2.1 Background and Significance	115
2.1.1 Discovery of Natural Troponoids	115
2.1.2 Biological Activity of Natural Tropolones	118
2.1.3 Synthesis of the Tropolone Core and the Thujaplicins	125
2.1.4 α -Tropolones as Lead-like Antiproliferative Agents	128
2.1.5 Project Objectives	129
2.2 Results and Discussion	130
2.2.1 Synthesis of α -Tropolones from 2-chlorotropone	130
2.2.2 Synthesis of α -Tropolones from 2-bromo-7-methoxytropone	134
2.2.3 Synthesis of α -Tropolones Using Other Coupling Techniques After Suzuki-Coupling	141
2.2.4 Synthesis of Tropones with Alternative Chelating Moieties	144
2.3 Conclusions	146
2.4 Acknowledgements	147
2.5 References	147

Chapter 3

Development of Synthetic α -Tropolonoids as Antiproliferatives Effective Against T-cell Acute Lymphoblastic Leukemia

3.1 Background and Significance	157
3.1.1 T-cell Acute Lymphoblastic Leukemia	159
3.1.2 Therapies for T-cell ALL and Prognostic Outcomes	162
3.1.3 Strategies Toward Better Therapeutic Options	169
3.1.4 Tropolones as Anti-leukemic Agents	176
3.1.5 Project Objectives	178
3.2 Results and Discussion	178

2.2.1 α -Tropolones Modulate Sirtuin 1 and 2	178
3.2.2 α -Tropolones Exhibit Antiproliferative Selectivity Towards T-cell ALL	183
3.2.3 Elucidating the Activity of α -Tropolones in Molt-4 Cells	194
3.2.4 Effects of α -Tropolones on Non-Tumorigenic Cell Lines	200
3.3 Conclusions	206
3.4 Acknowledgements	207
3.5 References	208

Chapter 4

Development of Synthetic α -Tropolonoids as Antibiotics Effective Against Gram-negative Bacteria

4.1 Background and Significance	224
4.1.1 Characteristics of Gram-negative Bacteria	224
4.1.1.1 Enterobacteriaceae	226
4.1.1.2 <i>Pseudomonas aeruginosa</i>	229
4.1.1.3 Acinetobacter	231
4.1.2 Increased Risk of Infection in Cancer Patients	232
4.1.3 Antibiotic Targets	234
4.1.4 Natural Product Troponoids as Antibacterial Agents	237
4.1.5 Project Objectives	239
4.2 Results and Discussion	240
4.2.1 Novel α -Tropolones are Active Against Gram-negative Bacteria	240
4.2.2 α -Tropolones Display Activity Against Clinical Isolates of <i>Klebsiella pneumoniae</i>	244
4.2.3 Activity of Tropolones Against Other Infectious Microbes	246
4.2.4 Using <i>E. coli</i> Knockout Models to Elucidate Potential Permeability and Efflux Issues	250
4.2.5 Exogenous Metal Effects on α -phenyl Tropolone Activity	252
4.2.6 Elucidation of the Mechanism of Action of Tropolones as Antibacterial Agents	253
4.3 Conclusions	268
4.4 Acknowledgements	269
4.5 References	269
Final Conclusions and Future Directions	281

Chapter 5

Experimental Section

5.1 Materials and Methods - Chemistry	284
5.1.1 General Chemical Methods	284
5.1.2 Synthetic Procedures	285
5.1.3 Tropolone Handling	290
5.2 Materials and Methods - Biology	291
5.2.1 Sirtuin 1 Enzyme Activity Assay	291
5.2.2 Sirtuin 2 Enzyme Activity Assay	291
5.2.3 Mammalian Cell Culturing	292
5.2.4 Mammalian Cell Viability Assay	294
5.2.5 Bacteria Culturing	295
5.2.6 Susceptibility Testing to Determine MIC Values Using Microdilution Method	295
5.2.7 Efflux Pump Evaluation	296
5.2.8 Lipopolysaccharide Permeability Evaluation	296
5.2.9 Drug Affinity Responsive Target Stability (DARTS) Assay	296
Appendix A: Chemical Characterization and Selected Spectra	299
Appendix B: Biological Data	432

LIST OF FIGURES

Chapter 1

1.1 Clinically Used Carbonic Anhydrase Inhibitors. Metal chelating group(s) shown in red.	4
1.2 Crystal structure (PDB: 4m2r) of Azopt (green) bound to CA-II (cyan). The active site consists of three histidine residues (magenta) coordinated to Zn ²⁺ (grey). The sulfonamide (sulfur in yellow, nitrogen in blue and oxygen in red) of Azopt completes the coordination sphere of Zn ²⁺ to inhibit enzyme activity.	5

1.3	Clinically used ACE inhibitors. Metal chelating group shown in red.	6
1.4	Crystal structure (PDB: 2c6n) of Zestril (green) bound to human somatic ACE (cyan). The active site consists of two histidine residues (magenta) and one glutamic acid residue (magenta) coordinated to Zn^{2+} (grey). The carboxylic acid (oxygen in red and nitrogen in blue) of Zestril completes the coordination sphere of Zn^{2+} to inhibit enzyme activity.	7
1.5	MMP inhibitors used in clinical trials. Metal chelating groups shown in red.	8
1.6	Crystal structure (PDB: 1mmb) of Batimastat (green) bound to MMP-8 (cyan). The active site consists of three histidine residues (magenta) coordinated to Zn^{2+} (grey). The hydroxamic acid (oxygen in red and nitrogen in blue) of Batimastat completes the coordination sphere of Zn^{2+} to inhibit enzyme activity.	9
1.7	TACE inhibitors used in clinical trials. Metal chelating groups shown in red.	11
1.8	Crystal structure (PDB: 1zxc) of TMI-001 (green) to TACE (cyan) dimer.	12
1.9	Crystal structure (PDB: 1zxc) of TMI-001 (green) bound to TACE (cyan). The active site consists of three histidine residues (magenta) coordinated to Zn^{2+} (grey). The hydroxamic acid (oxygen in red and nitrogen in blue) of TMI-001 completes the coordination sphere of Zn^{2+} to inhibit enzyme activity.	13
1.10	HDAC inhibitors approved for treatment of hematological malignancies (Belinostat, Panobinostat, Romidepsin and Vorinostat) and in clinical trials (Etinostat and Mocetinostat). Metal chelating groups shown in red.	15
1.11	Crystal structure (PDB: 4lxz) of Vorinostat (green) bound to HDAC2 (cyan). The active site consists of one histidine residue and two aspartic acid residues (magenta) coordinated to Zn^{2+} (grey). The hydroxamic acid (oxygen in red and nitrogen in blue) of Vorinostat completes the coordination sphere of Zn^{2+} to inhibit enzyme activity.	16
1.12	Zinc coordinating Farnesyltransferase inhibitors in clinical	17

trials. Metal binding group shown in red.	
1.13 Crystal structure (PDB: 1sa4) of Zarnestra (green) bound to human farnesyltransferase (cyan). The active site consists of one histidine residue one aspartic acid residue and one cysteine residue (magenta) coordinated to Zn^{2+} (grey). The imidazole (nitrogen in blue) of Zarnestra completes the coordination sphere of Zn^{2+} to inhibit enzyme activity.	18
1.14 LTA4H inhibitors that have proceeded to clinical trials.	20
1.15 Crystal structure (PDB: 1hs6) of Bestatin (green) bound to human leukotriene A4 hydrolase (cyan). The active site consists of two histidine residues and one glutamic acid residue (magenta) coordinated to Zn^{2+} (grey). The amide carbonyl and α -hydroxyl (oxygen in red and nitrogen in blue) of Bestatin completes the coordination sphere of Zn^{2+} to inhibit enzyme activity.	21
1.16 LpxC inhibitors in preclinical development. Metal binding group shown in red.	23
1.17 Crystal structure (PDB: 3nzk) of CHIR-090 (green) bound to LpxC of <i>Yersinia enterocolitica</i> (cyan). The active site consists of two histidine residues and one aspartic acid residue (magenta) coordinated to Zn^{2+} (grey). The hydroxamate (oxygen in red and nitrogen in blue) of CHIR-090 completes the coordination sphere of Zn^{2+} to inhibit enzyme activity.	24
1.18 Inhibitors of PHD2 in clinical trials. Metal binding group shown in red.	27
1.19 Crystal structure (PDB: 2hbt) of FG-2216 (green) bound to human HIF prolyl hydroxylase PHD2 (cyan). The active site consists of two histidine residues and one aspartic acid residue (magenta) coordinated to Fe^{2+} (orange). The isoquinoline nitrogen and β -carbonyl (oxygen in red and nitrogen in blue) of FG-2216 complete the coordination sphere of Fe^{2+} to inhibit enzyme activity.	28
1.20 Inhibitors of PDF based on Actinonin in clinical trials. Metal binding group shown in red.	30
1.21 Crystal structure (PDB: 3u04) of Actinonin (green) bound to PDF of <i>Ehrlichia chaffeensis</i> (cyan). The active site	

	consists of two histidine residues and one cysteine residue (magenta) coordinated to Zn^{2+} (grey). The hydroxamic acid (oxygen in red and nitrogen in blue) of Actinonin completes the coordination sphere of Zn^{2+} to inhibit enzyme activity.	31
1.22	5-LOX inhibitors in clinical trials (Curcumin and Hyperforin) and approved for use.	33
1.23	Crystal structure (PDB: 3v99) of the native ligand arachidonic acid (green) bound to 5-LOX (cyan). The active site consists of three histidine residues (magenta) coordinated to Fe^{2+} (orange).	34
1.24	Antifungal CYP inhibitors approved for clinical use. Metal binding group shown in red.	36
1.25	Crystal structure (PDB: 4wmz) of Fluconazole (green) bound to CYP51A of <i>Saccharomyces cerevisiae</i> (cyan). The active site consists of one cysteine residue (magenta) coordinated to the heme coordinated Fe^{2+} (orange). The triazole (nitrogen in blue) of Fluconazole completes the coordination sphere of Fe^{2+} to inhibit enzyme activity.	37
1.26	HIV integrase inhibitors approved for use (Raltegravir and Elvitegravir) and the first HIV integrase inhibitor to go into clinical trials (S-1360). Metal binding groups shown in red.	40
1.27	Crystal structure (PDB: 3oya) of Raltegravir (green) bound to HIV integrase of Prototype Foamy Virus intrasome (cyan). The active site consists of two aspartic acid residues and one glutamic acid residue (magenta) coordinated to two Mg^{2+} (green). The planar O-O-O motif of the dihydropyrimidine amide (oxygen in red and nitrogen in blue) of Raltegravir completes the coordination sphere of the two Mg^{2+} to inhibit enzyme activity.	41
1.28	Fluoroquinolone inhibitors of DNA gyrase approved for use. Metal binding group shown in red.	43
1.29	Crystal structure (PDB: 5btc) of Ciprofloxacin (magenta) bound to DNA gyrase of <i>Mycobacterium tuberculosis</i> (green). The active site of GyrA appears near the dimer interface and consists of the protein bound to DNA base pairs (blue-green, phosphate backbone in orange). A 3' oxygen on DNA coordinates to Mg^{2+} (green) which is coordinated to DNA gyrase through a water network. The	44

	two carbonyls of the quinolone motif (oxygen in red and nitrogen in blue) of Ciprofloxacin complete the coordination sphere of Mg^{2+} to stabilize the DNA-GyrA complex and prevent further catalysis.	
1.30	Natural products that exhibit potent DXR inhibitory activity (Fosmidomycin is currently in clinical trials). Metal binding group shown in red.	47
1.31	Crystal structure (PDB: 4oee) of Fosmidomycin (green) bound to DXR of <i>M. tuberculosis</i> W203Y mutant (cyan). The active site consists of two glutamic acid residues and one aspartic acid residue (magenta) coordinated to Mn^{2+} (steel blue). The hydroxamate (oxygen in red and nitrogen in blue) of Fosmidomycin completes the coordination sphere of Mn^{2+} to inhibit enzyme activity.	48
1.32	Arginase inhibitors in pre-clinical [S-(2-boronoethyl)-L-cysteine] and clinical (<i>N</i> -hydroxy-nor-L-arginine) development. Metal binding group shown in red.	50
1.33	Crystal structure (PDB: 3kv2) of <i>N</i> -hydroxy-nor-L-arginine (green) bound to human arginase I (cyan). The active site consists of four aspartic acid residues and two histidine residues (magenta) coordinated to two Mn^{2+} (steel blue). The <i>N</i> -hydroxyl group (oxygen in red and nitrogen in blue) of <i>N</i> -hydroxy-nor-L-arginine completes the coordination sphere of Mn^{2+} to inhibit enzyme activity.	52
1.34	Inhibitors of tyrosinase that have been used or tested as topical treatments of hyperpigmentation. Metal binding group shown in red.	56
1.35	Crystal structure (PDB: 3nq1) of kojic acid (cyan) bound to tyrosinase of <i>Bacillus megaterium</i> (green). The active site consists of two Cu^{2+} atoms (copper).	57
1.36	Crystal structure (PDB: 2y9x) of tropolone (green) bound to tyrosinase from <i>Agaricus bisporus</i> (cyan). The active site consists of six histidine residues (magenta) coordinated to two Cu^{2+} (copper). The alpha-hydroxy ketone (oxygen in red) of tropolone completes the coordination sphere of Cu^{2+} to inhibit enzyme activity.	59
1.37	Metal coordination modes of carboxylates.	63

1.38	Hydroxamates and hydroxamate derivatives as metal binding groups.	67
1.39	Carboxylate and carboxylate derivatives as metal binding groups.	68
1.40	New monodentate metal binding groups being explored.	70
1.41	New bidentate metal binding groups being explored.	73
1.42	New tetrahedral metal binding groups being explored.	74

Chapter 2

2.1	Images of the tropone and tropolone scaffold and early isolated natural troponoids.	117
2.2	Structures of some natural tropolones that exhibit antimicrobial activity.	119
2.3	Structures of natural tropolones that exhibit anticancer activity.	124

Chapter 3

3.1	Representation of immunophenotypes of T-cell ALL as categorized by early, cortical or mature subtype.	161
3.2	Chemotherapeutics commonly used to treat both T- and B-cell ALL.	165
3.3	Late stage chemotherapeutic options to treat T-cell ALL.	168
3.4	New anti-leukemic drugs in clinical trials.	176
3.5	% Inhibition of SIRT1 as determined by SIRT1 Direct Fluorescent Screening Assay Kit (n=3) with 10 μ M of each compound. Tenovin-6 was used as a positive control of SIRT1 inhibition. Negative values indicate activation of SIRT1.	179
3.6	% Inhibition of SIRT2 as determined by SIRT2 Direct Fluorescent Screening Assay Kit (n=3) with 10 μ M of each compound. Tenovin-6 was used as a positive control of SIRT2 inhibition. Negative values indicate activation of SIRT2.	180

3.7	Two reported sirutin modulators used as controls.	181
3.8	Non-linear regression analysis of log[inhibitor] versus normalized response.	182
3.9	Depiction of changes in gene expression as determined by microarray analysis of Molt-4 cells treated with MO-OH-Nap and HC-1-OH (A). Genes with greater than 10-fold upregulation found for both treatments as determined by Stanford Tools analysis of microarray data (B). Genes with greater than 4.5-fold downregulation found for both treatments as determined by Stanford Tools analysis of microarray data (C).	195
Chapter 4		
4.1	Diagram of Gram-negative bacteria cell wall.	226
4.2	<i>E. coli</i> 25922 cells treated with a) DMSO, b) HKT-OMe as a negative control, c) HKT , d) BA-pBr-OH.	254
4.3	Gel image of modified DARTS assay using <i>E. coli</i> 25922 treated with DMSO or HC-2-OH and lysed with thermolysin.	257
4.4	Catalytic mechanism of the conversion of 2-PG to PEP by enolase.	258
4.5	% Enolase activity in <i>E. coli</i> lysates as measured by fluorometric analysis of reaction with a peroxide substrate. Peroxide generation of untreated lysate was normalized to 100% activity. Cells were treated with 1 mM, 0.1 mM or 0.001 mM of HC-2-OH, MO-OH-PH or BA-pBr-OH and peroxide generation was compared to untreated lysate and determined as % enolase activity. BA-pBr-OH was not tested at 1 mM.	259
4.6	Structure of Reported Enolase Inhibitor, ENOblock.	265
4.7	Enolase Sequence Identity (%) Compared to <i>E. coli</i> .	266

LIST OF TABLES

Chapter 2

2.1	α -Tropolones from 2-chlorotropone in development.	132
2.2	Synthesis of α -Tropolones from 2-bromo-7-methoxytropolone utilizing lithium chloride for dealkylation of methyl ether.	137

Chapter 3

3.1	Trends in 5-year relative survival rates of select leukemia/lymphoma patients in the United States.	167
3.2	40 year trends in leukemia death rates per 100,000 people for males and females.	169
3.3	GI ₅₀ values (μ M) of first generation and alkyl α -tropolones against a panel of hematological cancer cells from T, B or myeloid lineage.	184
3.4	GI ₅₀ values (μ M) of second generation α -tropolones against a panel of hematological cancer cells from T, B or myeloid lineage.	186
3.5	GI ₅₀ values (μ M) of substituted phenyl α -tropolones against Molt-4 cells.	188
3.6	GI ₅₀ values (μ M) of non-phenyl based α -tropolones and natural troponoids against Molt-4 cells.	190
3.7	GI ₅₀ values (μ M) of α -tropolones and their respective arginate salts against Molt-4 cells.	193
3.8	Gene set enrichment analysis of microarray data from untreated Molt-4 cells versus cells treated for 24 hours with 1 μ M MO-OH-Nap or HC-1-OH. (GO = gene ontology; KEGG = Kyoto Encyclopedia of Genes and Genomes).	197
3.9	Microarray results found for genes of interest.	198
3.10	GI ₅₀ values (μ M) of first generation α -tropolones and hinokitiol against non-tumorigenic cell lines.	200

3.11	GI ₅₀ values (μM) of second generation α-tropolones against hDF cells.	202
3.12	GI ₅₀ values (μM) of two α-tropolones and a control (vorinostat) against hPBMCs and selectivity towards Molt-4 cells.	204
3.13	GI ₅₀ values (μM) of potent α-tropolones and hinokitiol against hPBMCs and selectivity towards Molt-4 cells.	205

Chapter 4

4.1	Resistance profiles (% susceptible) of Gram-negative bacteria against two classes of antibiotics.	235
4.2	Resistance profiles (% susceptible) of Gram-negative bacteria against four classes of antibiotics.	236
4.3	Bacteriostatic Activity of Tropolone Against Gram-negative Bacteria.	238
4.4	Bactericidal Activity of Thujaplicin Related Compounds.	238
4.5	Antibacterial Activity of Thujaplicins against <i>Legionella</i> species (Presented as MIC μg/mL).	238
4.6	MICs (μg/mL) of first generation Tropolones against <i>E. coli</i> 25922 and <i>K. pneumoniae</i> 10031.	241
4.7	MICs (μg/mL) of Key Potent Tropolones Against <i>E. coli</i> 25922 and <i>K. pneumoniae</i> 10031.	243
4.8	MICs (μg/mL) of Key Potent Tropolones Against Clinical Isolates of <i>K. pneumoniae</i> .	245
4.9	MICs (μg/mL) of Key Potent Tropolones Against <i>P. aeruginosa</i> and <i>A. baumannii</i> .	247
4.10	MICs (μg/mL) of Key Potent Tropolones Against Gram-positive and Fungal Species.	249
4.11	MICs of Tropolones Against <i>E. coli</i> and <i>E. coli</i> Knockouts.	251
4.12	Effects of Hydroxyl Substitution on <i>E. coli</i> MIC (μg/mL).	255

4.13	Initial Screening of Tropolones and Small Molecule Chelators (50 μ M) with Purified Enolase.	261
4.14	Evaluation of Key Potent Tropolone Inhibitory Activity on <i>E. coli</i> Enolase (20 μ M).	262
4.15	Evaluation of LPS Limited Tropolone Inhibitory Activity on <i>E. coli</i> Enolase (20 μ M).	263
4.16	Evaluation of Relatively Non-potent Tropolone Inhibitory Activity on <i>E. coli</i> Enolase (20 μ M).	264
4.17	Evaluation of Tropolone and ENOblock Inhibitory Activity on <i>E. coli</i> Enolase (10 μ M).	265
4.18	Evaluation of Alternative Chelating Groups on Tropolone Inhibitory Activity on <i>E. coli</i> Enolase (20 μ M).	267

LIST OF SCHEMES

Chapter 2

2.1	Cook and Coworkers Synthetic Route to Tropolone.	126
2.2	Doering and Knox Synthetic Route to Tropolone and Substituted Tropolones.	126
2.3	Synthesis of α -substituted tropolone from tropolone-copper chelate.	128
2.4	Synthesis of α -tropolones from 2-chlorotropone.	131
2.5	Complications in α -tropolone synthesis from 2-chlorotropone.	133
2.6	Synthesis of α -tropolones from 2-bromo-7-methoxytropone.	135
2.7	Synthesis of <i>para</i> - α -phenyltropolones from 2- <i>para</i> -bromophenyl-7-methoxytropone.	140
2.8	Sonogashira-coupling of alkynes to 2- <i>para</i> -bromophenyl-7-methoxytropone.	142

2.9	Synthesis of <i>N</i> -phenyl-amide α -tropolones.	143
2.10	Synthesis of thio-tropones.	145
2.11	Synthesis of hydroxylamino-tropone.	145
2.12	Synthesis of 2-amido-tropone.	146

Chapter 1

Inhibition of Metalloenzymes: Lessons from Clinically Used Inhibitors and Future Directions

1.1 Introduction

A metalloprotein is any protein that incorporates a metal ion to stabilize protein structure, facilitate electron transport or catalyze chemical transformations. Proteins in the latter group are more commonly referred to as metalloenzymes. Over one third of all human proteins are metalloenzymes.¹ Metalloenzymes incorporate a variety of metal ions in the active site that are essential to their function.² While all metalloenzymes convert substrates into new entities, the majority do not utilize the metal ion for redox chemistry but rather as a means to activate the substrate or to stabilize anionic intermediates and transition states.³ One of the primary research objectives in metallobiochemistry over the past 50 years has been understanding how these metal ions promote function within the active site.⁴ From this work, it has been determined that ligands coordinate directly to the metal ion and this coordination appears to determine the electronic properties of the metal ion and enzyme activity. Once coordinated, the metal ion generally withdraws electron density from ligand to polarize bonds and assist in enzyme turnover.³ Coordination occurs in one of three forms: *syn-monodentate*, *anti-monodentate*, or bidentate. *Syn-monodentate* coordination is the most common and is typical of carboxylic acid coordination in both mono- and dinuclear metalloenzymes. This type of coordination is mostly

observed because the most common amino acids in the active site of metalloenzymes are aspartic acid and glutamic acid. Other common amino acids in the active site that stabilize the metal ion and assist in catalytic function are cysteine and histidine.³

Metalloenzymes are essential to a variety of biological functions including blood pH homeostasis, DNA transcription, gene regulation, matrix degradation and many others.⁵⁻⁷ Therefore, it is not surprising that misregulation of metalloenzymes is associated with diseases including hypertension, inflammation and cancer. Additionally, metalloenzymes have been linked to pathogenic bacterial and fungal infections, antibiotic resistance and viral infections.⁶⁻⁷ As a result, inhibitors have been developed to target these clinically relevant metalloenzymes. These inhibitors all possess a metal binding group linked to a “backbone” structure thought to impart target selectivity.⁸ In this chapter select metalloenzymes and their small molecule inhibitors will be discussed. It should be noted that this is only a partial list of targeted metalloenzymes and inhibitors developed for their inhibition.

1.2 Clinical Inhibitors of Zinc Metalloenzymes

Zinc is essential for the growth and development of all forms of life and is the second most abundant metal in the human body.⁹ The first zinc metalloenzyme, carbonic anhydrase, was discovered in 1940 and served as the basis for metalloenzyme research.¹⁰ Currently more than 300 zinc metalloenzymes have been discovered with approximately 10% of the human proteome consisting of zinc metalloenzymes.¹¹ Zinc is also the only metal ion found in all six enzymatic classes: oxidoreductases, transferases, hydrolases, lyases, isomerases and ligases.⁹

Since zinc exists as Zn^{2+} in metalloenzymes, it has a filled d -orbital and therefore functions as a Lewis acid. As a Lewis acid, zinc is neither “soft” nor “hard” and does not appear to exhibit a coordinating preference. However, the most common binding geometry of zinc metalloenzymes is tetrahedral or trigonal bipyramidal.¹² The active site of these zinc metalloenzymes typically coordinate zinc with histidine or cysteine but several have also been found to use aspartic acid, glutamic acid, tyrosine, asparagines and glutamine.⁹ Additionally, the active site of zinc metalloenzymes is unique in that it must contain at least one water molecule coordinated to zinc that is essential to catalytic activity.¹³ This water molecule may be ionized (as in the case of carbonic anhydrase), polarized to form a nucleophile (found in matrix metalloproteinases), or as an enzyme structure stabilizer that can be displaced by the binding ligand.⁹ Overall, the coordination of zinc in the active site controls acidity of the metal ion which imparts a slight preference towards metal chelating groups. This feature may be exploited for the design of inhibitors against zinc metalloenzymes.

1.2.1 Carbonic Anhydrase

Carbonic anhydrase (CA) is the oldest known class of zinc metalloenzymes.¹⁴ There are 16 isoforms of mammalian CA which all catalyze the conversion of carbon dioxide and water into bicarbonate and protons.¹⁵ CA is essential for blood pH homeostasis, formation of cerebrospinal fluid and urine acidification.¹⁰ Misregulation of CA can lead to neurological disorders, glaucoma, epilepsy, ulcers, edema and cancer.^{10,15} For example, CA-IX is known to regulate pH of tumor cells and can promote tumor growth and survival.¹⁶ Due to its long history

in research and its medical importance, many CA inhibitors have been developed. Clinically available CA inhibitors generally use sulfonamide as the metal binding group (Figure 1.1).

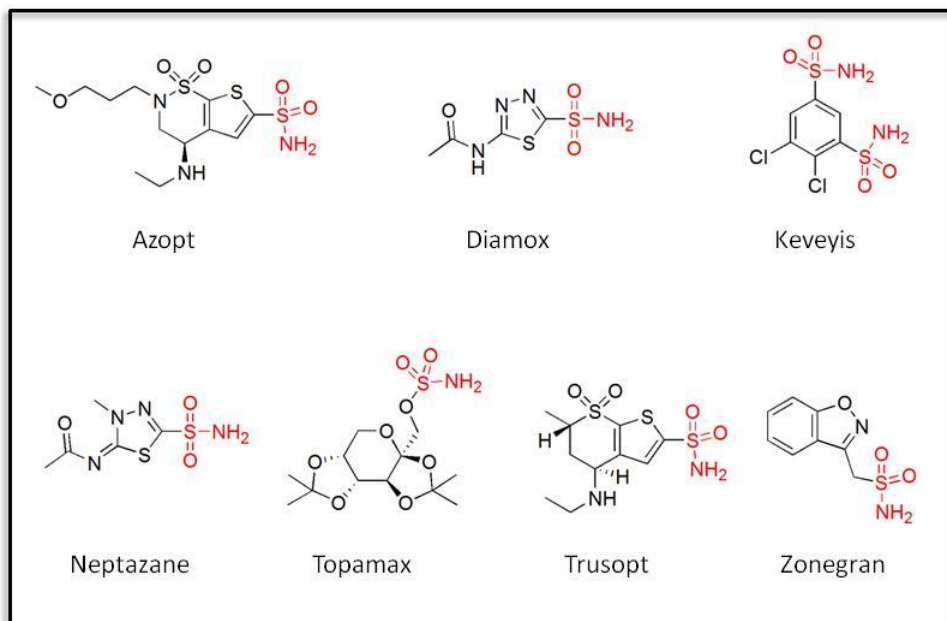


Figure 1.1: Clinically Used Carbonic Anhydrase Inhibitors. Metal chelating group(s) shown in red.

As depicted in Figure 1.1, all the clinically used inhibitors are sulfonamides.

Sulfonamides are a class of metal binding groups that coordinate zinc in a monodentate fashion via a nitrogen atom. A crystal structure of Azopt bound to human CA-II (Figure 1.2) depicts the coordination of zinc by the sulfonamide group of Azopt and three histidine residues (His 94, His 96 and His 119).¹⁷ Although CA IX is linked to tumor growth and survival, inhibitors of CA-IX are not yet approved. Several of the CA inhibitors used in the clinic are CA-II inhibitors (Azopt, Topamax and Trusopt), but most are not isozyme specific. CA-II is the most active isozyme and is found primarily in red blood cells but also in other tissues. Since CA inhibitors mostly act on CA-II, they are approved to treat glaucoma and epilepsy and may be used as diuretics and to treat

altitude sickness.¹⁸ Current research focuses on the development of CA inhibitors to treat hypoxic and metastatic tumors.¹⁹

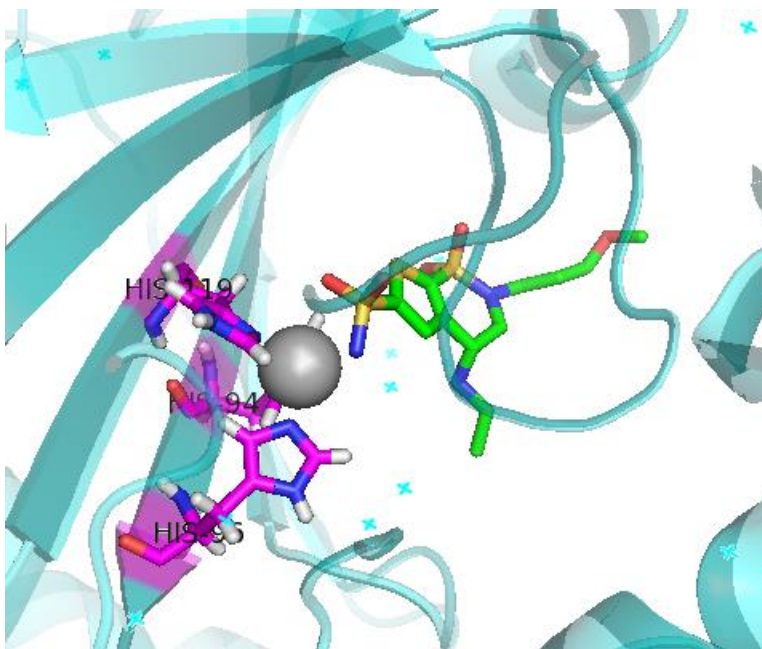


Figure 1.2: Crystal structure (PDB: 4m2r)¹⁷ of Azopt (green) bound to CA-II (cyan). The active site consists of three histidine residues (magenta) coordinated to Zn^{2+} (grey). The sulfonamide (sulfur in yellow, nitrogen in blue and oxygen in red) of Azopt completes the coordination sphere of Zn^{2+} to inhibit enzyme activity.

1.2.2 Angiotensin Converting Enzyme

Angiotensin converting enzyme (ACE) is critical for regulation of the rennin-angiotensin system which maintains blood pressure, electrolyte and fluid balance as well as blood volume.²⁰ It found in endothelial cells, epithelial and neuroepithelial cells, in the blood and other body fluids and as a membrane bound protein in the brain. Another function of ACE is to cleave the C-terminal dipeptide of bradykinin to suppress its function. Active bradykinin results in vasodilation through generating nitric oxide.²¹ As a result, ACE effectively controls

vasoconstriction and electrolyte retention which affect blood pressure.²⁰ Therefore, ACE inhibitors are primarily designed to treat hypertension. All of the ACE inhibitors are analogs of 2-methylpropionyl-L-proline and typically coordinate zinc via a carboxylic acid which exists in pro-drug form for most of the inhibitors. However, Monopril has a phosphinyl group and Capoten contains a thiol which coordinates the zinc. Interestingly, all of the ACE inhibitors have a carboxylic acid as part of the proline scaffold, but this carboxylic acid only interacts with other residues within the hydrophilic active site of ACE.

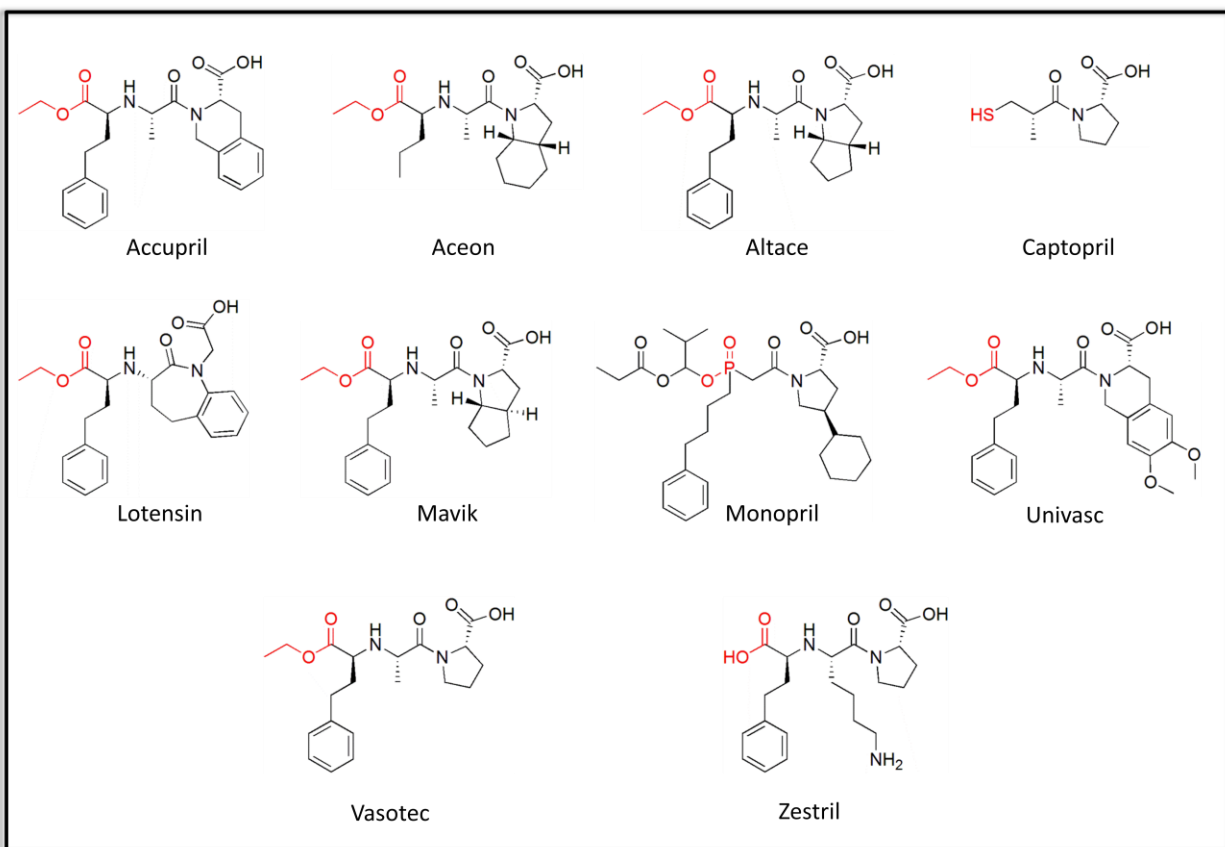


Figure 1.3: Clinically used ACE inhibitors. Metal chelating group shown in red.

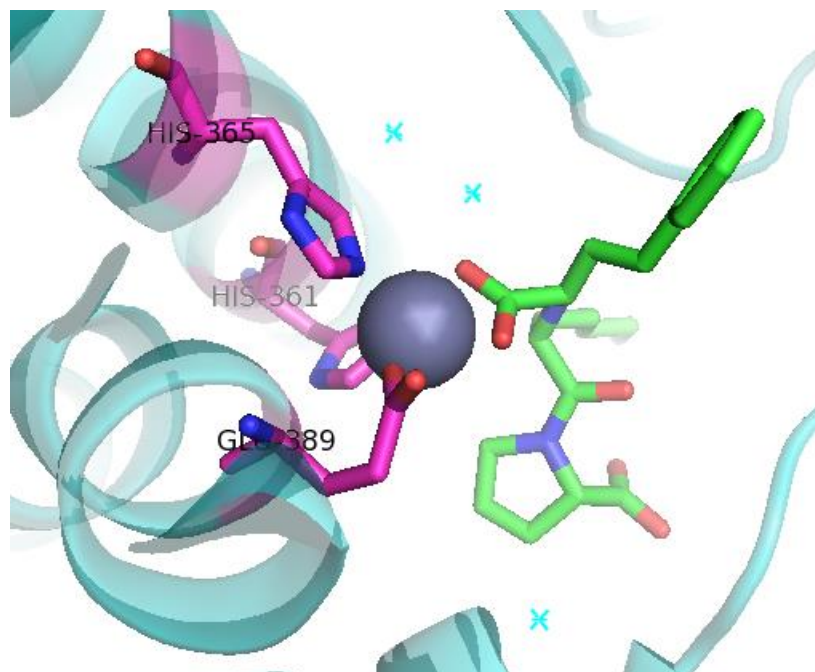


Figure 1.4: Crystal structure (PDB: 2c6n)²² of Zestril (green) bound to human somatic ACE (cyan). The active site consists of two histidine residues (magenta) and one glutamic acid residue (magenta) coordinated to Zn^{2+} (grey). The carboxylic acid (oxygen in red and nitrogen in blue) of Zestril completes the coordination sphere of Zn^{2+} to inhibit enzyme activity.

Figure 1.4 depicts the somatic N domain of human ACE. This domain appears to play an important role in the development of hypertension.²² While the N domain shares nearly 60% sequence homology with the C domain, it has distinct properties and function. The active site of ACE consists of two histidine residues (His 361 and His 365) and one glutamic acid residue (Glu 389) coordinated to Zn^{2+} . There are also several water molecules that assist in coordination, catalytic action and should be accounted for when designing inhibitors.

1.2.3 Matrix Metalloproteinase

Matrix metalloproteinases (MMPs) are a family of 24 extracellular zinc and calcium dependent endopeptidases.²³ The primary function of MMPs is to degrade the extracellular matrix through proteolysis of components such as aggrecan, collagen, elastin, fibronectin, gelatin and laminin.²⁴ Other functions associated with MMPs are cell movement, proliferation, wound healing, angiogenesis and apoptosis. Perhaps most importantly, MMPs are linked to various disease states including arthritis, multiple sclerosis, periodontal disease, atherosclerosis, cardiac injury remodeling and cancer metastasis. As enzymes involved in tumor migration, invasion and angiogenesis, MMPs are ideal targets for the treatment of cancer.

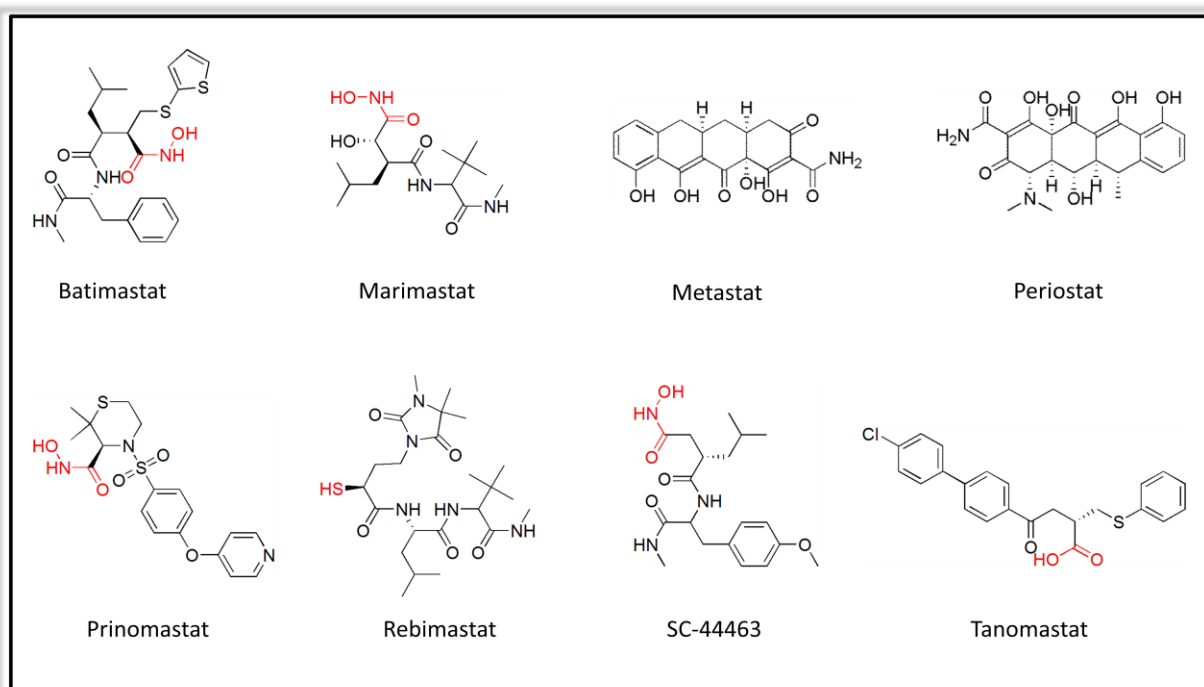


Figure 1.5: MMP inhibitors used in clinical trials. Metal chelating groups shown in red.

Over 50 MMP inhibitors have progressed into clinical trials, but most have failed to gain approval due to lack of isozyme and enzyme selectivity, poor pharmacokinetic profiles, poor oral bioavailability and in many cases a lack of efficacy in human trials.²⁵ To date, the only MMP inhibitor to be approved is Periostat.²⁶ Periostat is a tetracycline based molecule used to treat

periodontal disease. While tetracyclines have several carbonyls and hydroxyls capable of coordinating zinc, it is unknown whether or not tetracyclines directly coordinate the zinc in MMP or exert some other inhibitory effect. However, studies involving selectivity of small molecules with different metal binding groups towards MMP-1 indicate a clear preference of coordination with a hydroxamate (hydroxamate >> formyl hydroxylamine > thiol > phosphinate > α -aminoacrylate > carboxylate/sulfonamide/hydrazide).²⁷

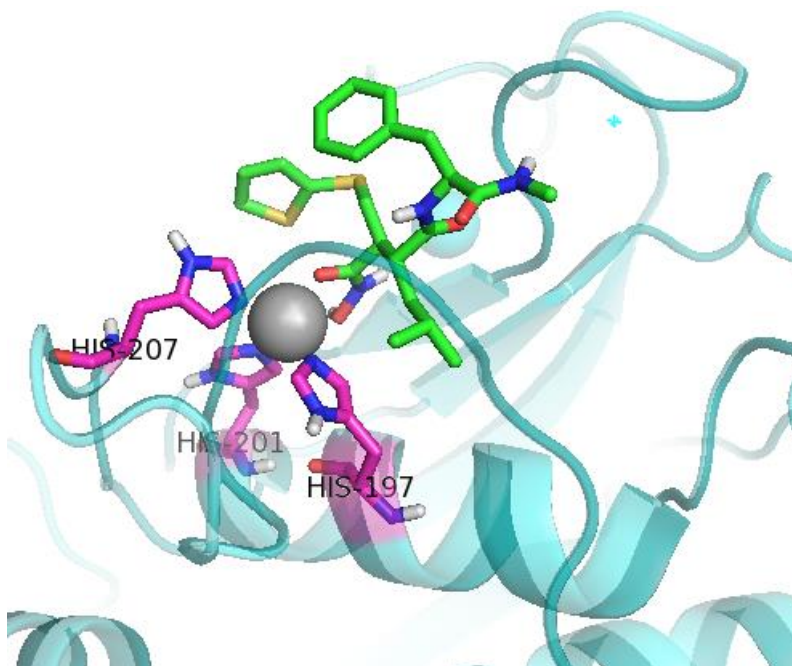


Figure 1.6: Crystal structure (PDB: 1mmb)²⁸ of Batimastat (green) bound to MMP-8 (cyan). The active site consists of three histidine residues (magenta) coordinated to Zn^{2+} (grey). The hydroxamic acid (oxygen in red and nitrogen in blue) of Batimastat completes the coordination sphere of Zn^{2+} to inhibit enzyme activity.

The hydroxamate, Batimastat, exhibits a bidentate coordination of a zinc ion in MMP-8. MMP-8 has two zinc ions and two calcium ions, but Batimastat only appears to coordinate the more accessible zinc ion located in a solvent exposed pocket. The zinc in this site is coordinated by three histidine residues (His 197, His 201 and His 207). Batimastat exhibited significant

inhibitory activity and advanced to Phase III clinical trials but was abandoned due to poor oral bioavailability and inflammation of the inner wall of the abdomen when injected.²⁹ Since hydroxamate based MMP inhibitors have all failed to pass Phase III clinical trials, it is apparent that newer MMP inhibitors should either utilize a different metal binding group or be designed with isozyme selectivity. Isozyme selective inhibitors may be difficult due to high structure homology especially within sub-classes. However, since the zinc of MMPs exhibits a preference towards hydroxamate inhibitors, hydroxamate mimetics of tissue inhibitors of metalloproteinases (TIMPs) might provide better selectivity. There are four TIMPs that inhibit various MMPs with differential efficacy.²³ Complexes of TIMPs and MMPs show inhibition in the subnanomolar range and may provide key insight towards inhibitor design.³⁰

1.2.4 Tumor Necrosis Factor- α Converting Enzyme

Tumor necrosis factor- α converting enzyme (TACE), also known as ADAM-17, is a proteinase which belongs to the same super-family metzincin as MMPs.³¹ TACE is membrane bound and proteolyzes the 26 kDa pro-TNF- α to the active 17 kDa form. In addition to its essential role in TNF- α regulation, TACE is implicated in epidermal growth factor signaling, leukocyte rolling, cell adhesion, JAK-STAT signaling, platelet aggregation and activation and regulation of angiogenesis.³² As a result, TACE inhibitors could potentially treat rheumatoid arthritis, cancer, Alzheimer's, cardiovascular disease, diabetes, Crohn's disease and other autoimmune diseases.

Since TACE is similar to MMP, initial TACE inhibitors were based on MMP inhibitors and utilized hydroxamates as the metal binding group.³³ Interestingly, TACE and MMP share

the same catalytic site structure.³¹ As a result, two MMP inhibitors, Marimastat and Prinomastat, were tested in clinical trials as TACE inhibitors. Similar to the MMP inhibitors, TACE inhibitors have failed to pass Phase III clinical trials due to poor oral bioavailability, musculoskeletal side effects, non-selective inhibition, liver toxicity, and/or poor efficacy in human clinical trials. This is mostly due to the ability of TACE to proteolyze nearly 30 membrane spanning proteins.³²

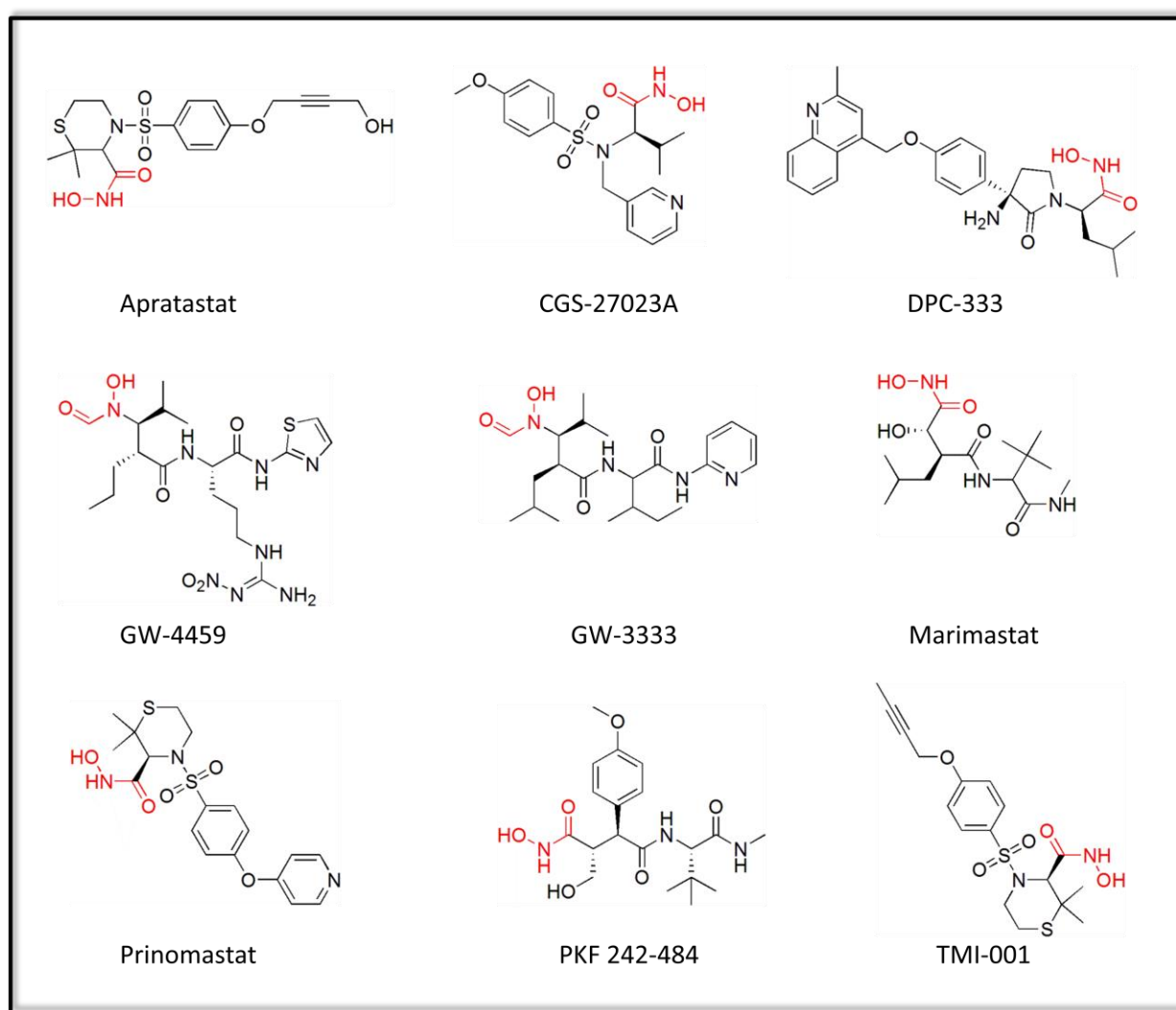


Figure 1.7: TACE inhibitors used in clinical trials. Metal chelating groups shown in red.

Several reviews of TACE inhibitors, their development and clinical trials have been published.^{31,32,35} From these reviews it is clear that many TACE inhibitors have been developed. Most are hydroxamate based and are both MMP and TACE inhibitors while others have been designed to be more selective. The more selective inhibitors include sulfonamides, acetylinic tails, tryptophan, quinolines or macrocycles. While these inhibitors do exhibit some selectivity, none appear to selectively inhibit TACE and not MMP. As a result, the development of TACE inhibitors for diseases other than cancer has mostly been abandoned. Newer TACE inhibitors in development use non-hydroxamate metal binding groups such as thiol, hydantoin or barbiturate, but have not moved into clinical trials.

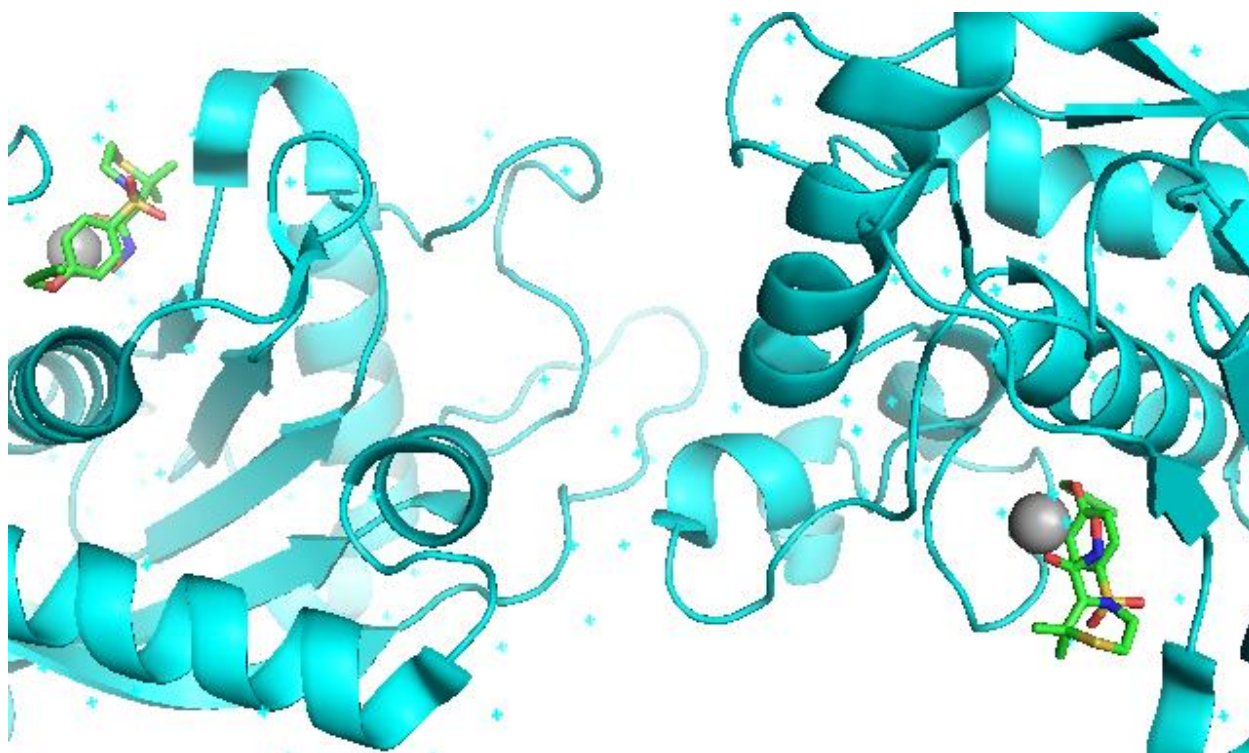


Figure 1.8: Crystal structure (PDB: 1zxc)³⁴ of TMI-001 (green) to TACE (cyan) dimer.

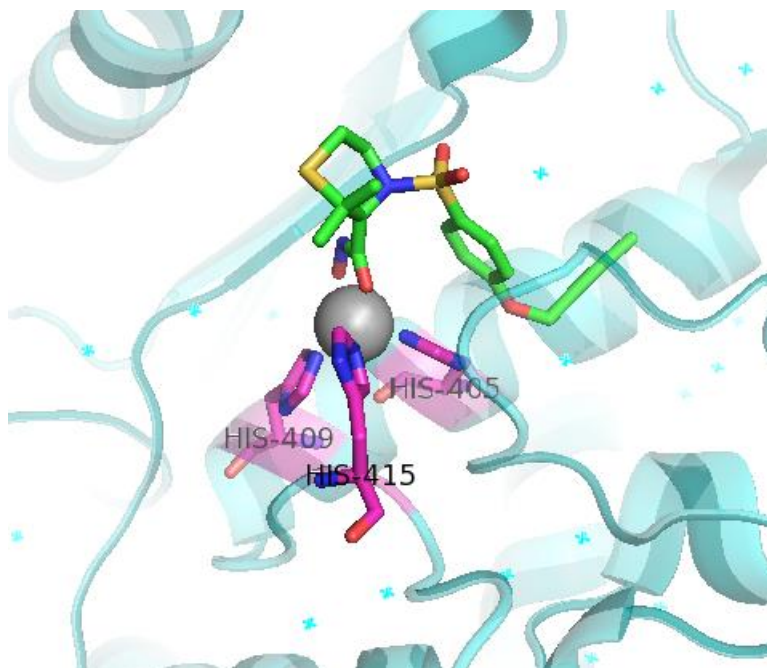


Figure 1.9: Crystal structure (PDB: 1zxc)³⁴ of TMI-001 (green) bound to TACE (cyan). The active site consists of three histidine residues (magenta) coordinated to Zn^{2+} (grey). The hydroxamic acid (oxygen in red and nitrogen in blue) of TMI-001 completes the coordination sphere of Zn^{2+} to inhibit enzyme activity.

As with MMPs, the TACE active site consists of three histidine residues (His 405, His 409 and His 415) coordinated to a zinc ion. The hydroxamate TACE inhibitors coordinate the zinc in a bidentate fashion and may form hydrogen bonds with water molecules in the active site. The more selective TACE inhibitors attempt to overcome the decrease in zinc affinity compared to the hydroxamates by increasing non-covalent interactions with other residues in the active site, especially Leu 348, Gly 349 and Glu 406, and the S1' pocket. The S1' pocket is exploited by the tryptophan and quinoline based inhibitors.

1.2.5 Histone Deacetylase

Histone deacetylase (HDAC) is a class of enzymes which catalyze the deacetylation of lysine residues. Although HDACs are known to deacetylate multiple substrates, the primary substrates appear to be histones. Deacetylation of histone lysines causes the positive charge on the lysine to tightly associate with the negative charge of the phosphate backbone of DNA which results in tighter coiling of the DNA around the histone, repressing gene transcription. There are 18 isoforms of HDAC, but only 11 are zinc dependent.³⁶ In addition to regulation of gene transcription, HDACs are linked to latent human immunodeficiency virus (HIV), cardiac hypertrophy and downregulation of apoptosis and other cellular proteins in cancer cells.¹⁰

As with most zinc metalloenzyme inhibitors, HDAC inhibitors typically use hydroxamate as the metal binding group. Although several HDAC inhibitors have been approved for the treatment of select hematologic malignancies, these inhibitors suffer from lack of isoform selectivity, rapid renal clearance, multiple off target interactions and can be mutagenic.^{25,37} Despite these drawbacks, HDAC inhibitors have the ability to cause hyperacetylation of cancer cells to induce cell cycle arrest and apoptosis.³⁸ Newer HDAC inhibitors currently in clinical trials (see Figure 1.10) utilize benzamide to coordinate zinc in a bidentate fashion similar to the hydroxamate inhibitors. Unlike the hydroxamate based inhibitors, the benzamide inhibitors exhibit isoform selectivity and generally target only class I HDACs.³⁹ Romidepsin is a natural product that resembles a pro-drug since the reduction of the disulfide bond generates a thiol that coordinates zinc in the active site of HDAC.⁴⁰

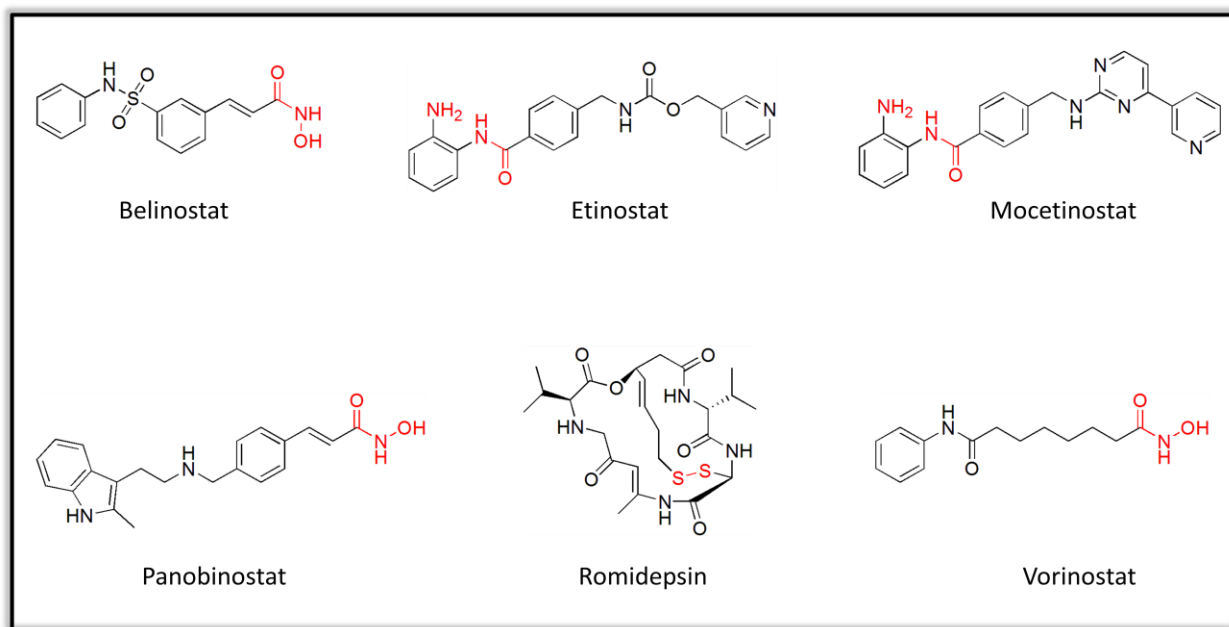


Figure 1.10: HDAC inhibitors approved for treatment of hematological malignancies (Belinostat, Panobinostat, Romidepsin and Vorinostat) and in clinical trials (Etinostat and Mocetinostat).^{37,41} Metal chelating groups shown in red.

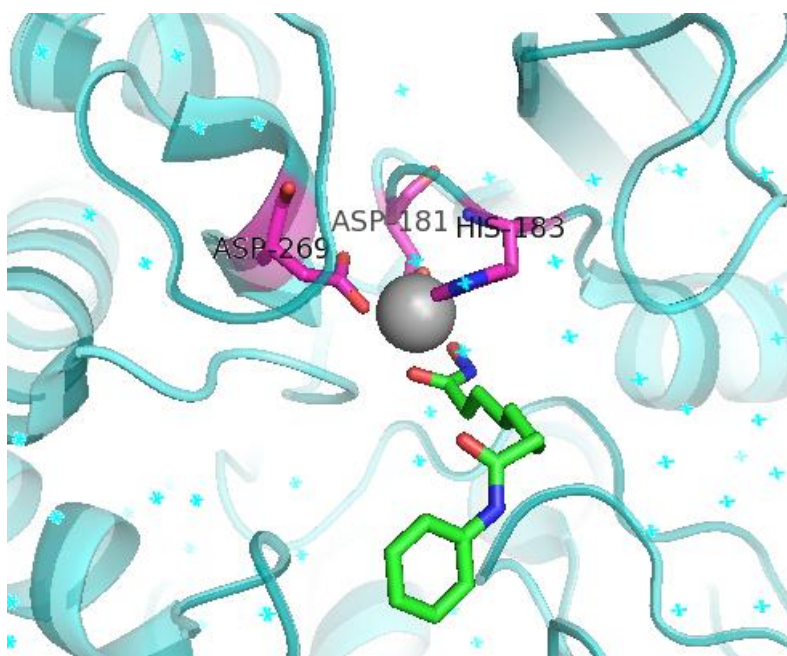


Figure 1.11: Crystal structure (PDB: 4lxz)⁴² of Vorinostat (green) bound to HDAC2 (cyan). The active site consists of one histidine residue and two aspartic acid residues (magenta) coordinated to Zn^{2+} (grey). The hydroxamic acid (oxygen in red and nitrogen in blue) of Vorinostat completes the coordination sphere of Zn^{2+} to inhibit enzyme activity.

The HDAC active site consists of one histidine residue (His 183) and two aspartic acid residues (Asp 181 and Asp 269) coordinated to a zinc ion. HDAC inhibitors coordinate the zinc in a bidentate fashion and may form hydrogen bonds with water molecules in the active site. The more selective HDAC inhibitors exploit a deep hydrophobic foot pocket that extends away from the active site in class I HDACs.⁴³ Although HDACs share significant homology of the active site, especially within sub-classes, better isoform selectivity may be attained through the design of “cap” groups which extend out of the active site to interact with surface residues.³⁶

1.2.6 Farnesyltransferase

Farnesyltransferase (FTase) is a cytoplasmic protein which catalyzes the prenylation of the superfamily of Ras proteins.⁴⁴ Post-translational modification and activation of Ras proteins by FTase requires the C-terminal recognition sequence CaaX, where “a” refers to any aliphatic amino acid and “X” is any amino acid. After binding the Ras protein, FTase will transfer a 15 carbon farnesyl unit from farnesyl pyrophosphate to the cysteine residue.⁴⁵ Inhibition of Ras protein prenylation will prevent cytosolic export to the plasma membrane and subsequent pathway signaling. Since mutated Ras genes are found in approximately 30% of all cancers, inhibition of FTase can inhibit tumor growth and improve survival when combined with standard chemotherapy.⁴⁶ Additionally, FTase inhibitors may treat progeria, glaucoma, neurological diseases and are highly toxic to the malaria causing parasite *Plasmodium falciparum*.⁴⁴

Because FTase catalyzes the transfer of a farnesyl group to a protein, FTase inhibitors are typically either farnesyl pyrophosphate analogs or peptidomimetics.⁴⁵ The peptidomimetics bind

to the CaaX recognition site and coordinate zinc. FTase activity requires binding of a CaaX protein, farnesyl pyrophosphate, Zn^{2+} and water. By binding to the CaaX domain and coordinating zinc, these peptidomimetics effectively compete with the native protein substrates. Other key residues exploited by FTase inhibitors are the hydrophilic residues Lys 164, His 248, Arg 291 and Tyr 300. These residues are essential to hydrogen bonding and proper orientation of farnesyl pyrophosphate for catalysis.

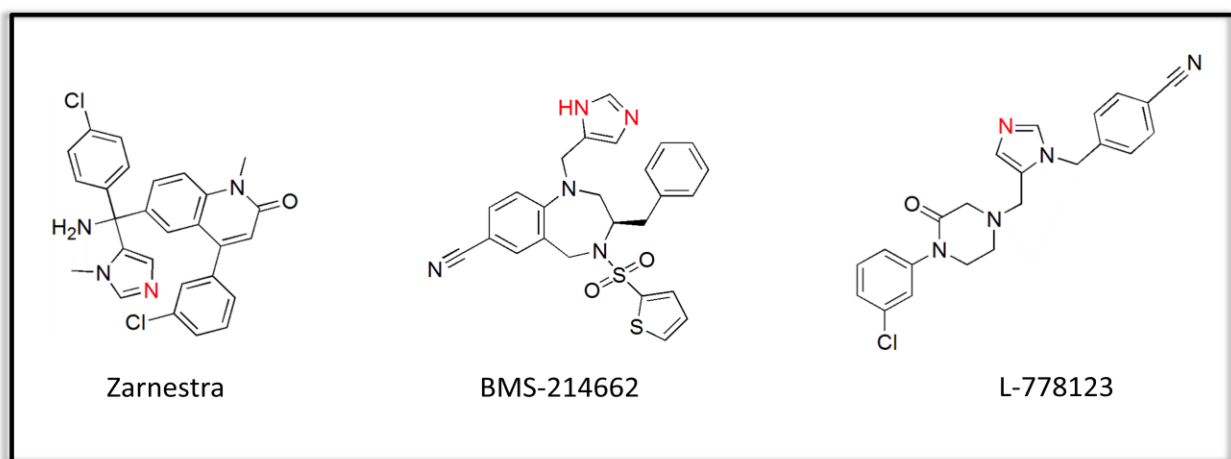


Figure 1.12: Zinc coordinating Farnesyltransferase inhibitors in clinical trials. Metal binding group shown in red.

While FTase inhibitors are not currently approved, several are in late stage clinical trials. Zarnestra was originally investigated as a treatment for myelodysplastic syndromes, but failed to gain approval due to limited *in vivo* activity when used as a single agent.⁴⁷ BMS-214662 is being investigated as a potent inhibitor of H-ras and K-ras for the treatment of acute leukemia and myelodysplastic syndromes.⁴⁸ L-778123 was investigated both as a single agent as in combination with paclitaxel to treat head and neck cancer and non-small cell lung cancer but was abandoned due to adverse effects on heart rate.⁴⁵ The common feature of these three inhibitors is

the monodentate coordination of zinc through an imidazole. Other FTase inhibitors being investigated do not coordinate zinc and act as competitive inhibitors of farnesyl pyrophosphate binding.

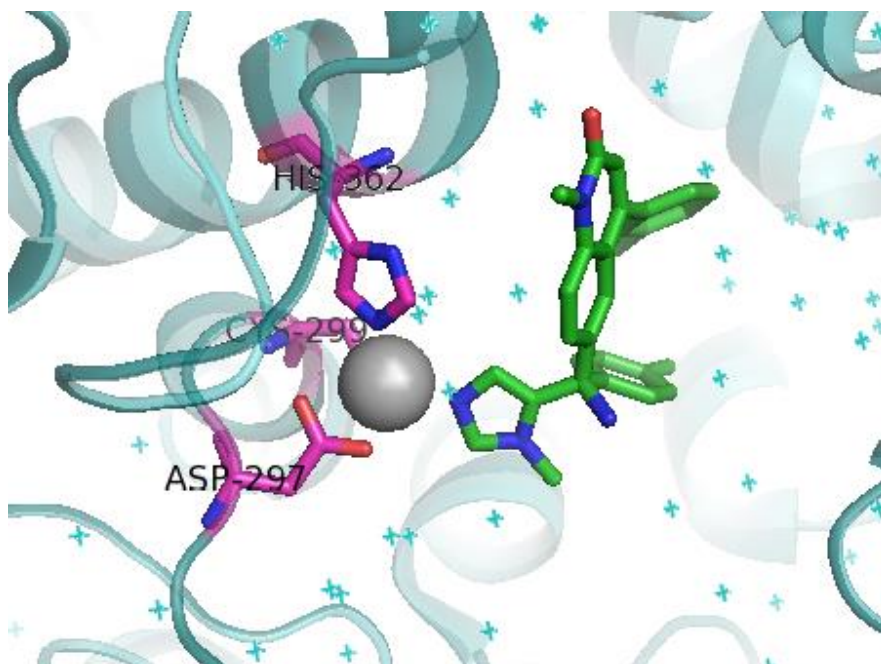


Figure 1.13: Crystal structure (PDB: 1sa4)⁴⁹ of Zarnestra (green) bound to human farnesyltransferase (cyan). The active site consists of one histidine residue one aspartic acid residue and one cysteine residue (magenta) coordinated to Zn^{2+} (grey). The imidazole (nitrogen in blue) of Zarnestra completes the coordination sphere of Zn^{2+} to inhibit enzyme activity.

The FTase active site consists of one aspartic acid residue (Asp 297), one cysteine residue (Cys 299) and one histidine residue (His 362) and coordinated to a zinc ion. Since the active site is highly hydrophilic and contains multiple water molecules, FTase inhibitors typically form hydrogen bonds with water molecules in the active site. Although the metal binding inhibitors in clinical trials utilize imidazole to coordinate zinc, thiol based peptidomimetic inhibitors have also been developed. However, these inhibitors exhibit high levels of toxicity and have been abandoned.⁴⁴ Future FTase inhibitors may benefit from being

designed as an analog of both farnesyl pyrophosphate and the CaaX peptide to increase solubility, bioavailability, membrane transportation and binding potency.⁴⁴

1.2.7 Leukotriene-A4 Hydrolase

Leukotriene-A4 hydrolase (LTA4H) is an enzyme that acts as both an aminopeptidase and epoxide hydrolase.⁵⁰ LTA4H binds the epoxide leukotriene-A4 substrate and hydrolyzes it to the diol leukotriene-B4. Leukotriene-B4 is pro-inflammatory as it activates neutrophils and signals the recruitment of eosinophils, macrophages, mast cells, T-cells, dendritic cells, smooth muscle cells and keratinocytes.⁵¹ Over production of leukotriene-B4 is associated with inflammatory bowel disease, rheumatoid arthritis, atherosclerosis, chronic obstructive pulmonary disease, asthma and cancer.⁵¹ Inhibitors of LTA4H have been designed to treat acute myelocytic leukemia, myocardial infarction and cystic fibrosis.⁵⁰⁻⁵³

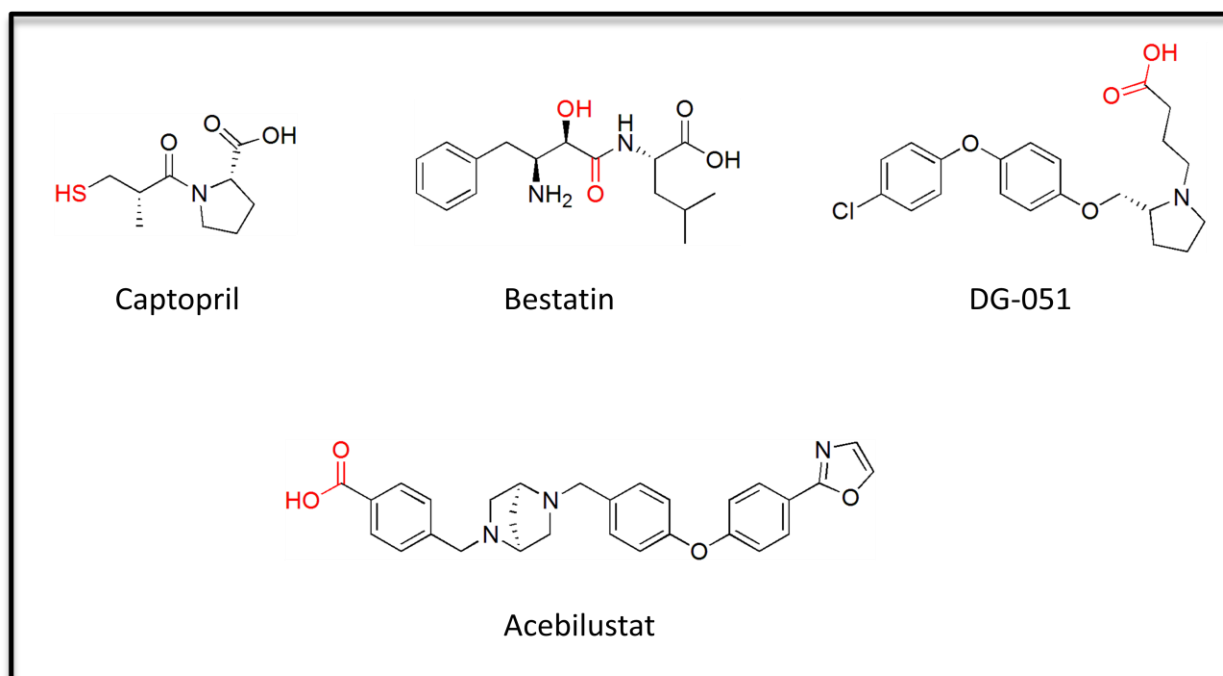


Figure 1.14: LTA4H inhibitors that have proceeded to clinical trials.

Since the active site of LTA4H is structurally similar to ACE, one of the first inhibitors of LTA4H in clinical trials was the ACE inhibitor Captopril. Both ACE and LTA4H belong to the MA family of metallopeptidases which seem to share a HEXXH sequence in the active site.⁵⁴ Because Captopril is a peptide mimetic, other peptide mimetic inhibitors were developed. However, one of the more potent peptide mimetics discovered, Bestatin, was isolated from *Streptomyces olivoreticuli*.⁵⁵ The first crystal structure of LTA4H was solved bound to Bestatin. Here, Bestatin coordinates zinc in a bidentate fashion through the amide carbonyl and α -hydroxyl. Although hydroxamates are known to coordinate zinc in a bidentate fashion and hydroxamate LTA4H inhibitors have been developed, these hydroxamate inhibitors have not progressed to clinical trials most likely due to the clinical failures of other hydroxamate based

inhibitors. However, two carboxylate based inhibitors, DG-051 and Acebilustat, have shown appreciable activity and have proceeded to Phase II clinical trials.^{51,53}

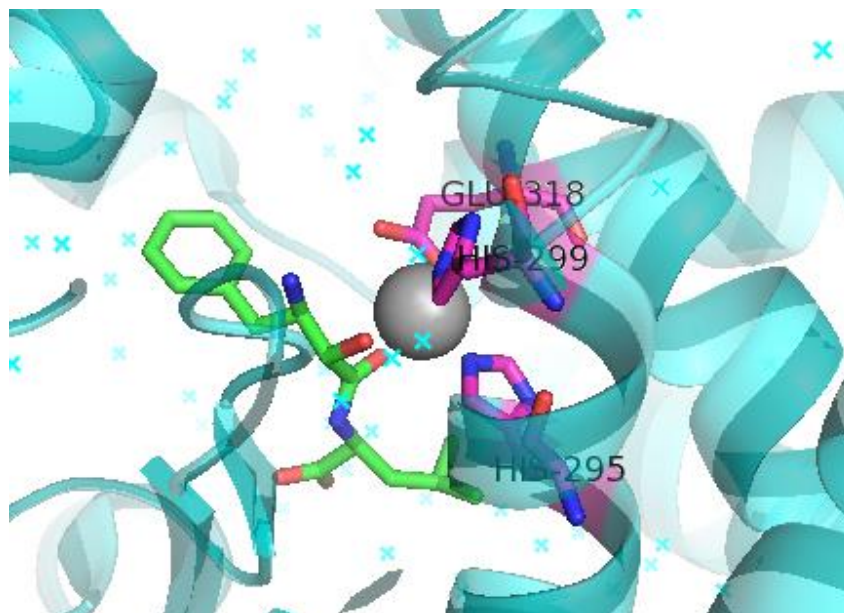


Figure 1.15: Crystal structure (PDB: 1hs6)⁵⁶ of Bestatin (green) bound to human leukotriene A4 hydrolase (cyan). The active site consists of two histidine residues and one glutamic acid residue (magenta) coordinated to Zn^{2+} (grey). The amide carbonyl and α -hydroxyl (oxygen in red and nitrogen in blue) of Bestatin completes the coordination sphere of Zn^{2+} to inhibit enzyme activity.

The LTA4H active site consists of two histidine residues (His 295 and His 299) and one glutamic acid residue (Glu 318) coordinated to a zinc ion. Several water molecules are also present in the active site, suggesting LTA4H inhibitors should be hydrophilic and may exhibit increased potency by forming hydrogen bonds with these water molecules. Although several inhibitors have proceeded to clinical trials, none are currently approved as inhibitors of LTA4H. Captopril is currently only marketed as an ACE inhibitor, but is in Phase II clinical trials as a treatment for patients with non-small cell lung cancer who have previously been treated with radiation therapy.⁴¹ DG-051 does not appear to be in clinical trials and may have been

abandoned or potentially renamed due to financial issues with the company deCODE and subsequent new company Emerald BioStructures. Bestatin is currently in Phase II clinical trials for both the treatment of lymphedema and pulmonary arterial hypertension.⁴¹ Acebilustat went to Phase II clinical trials in late 2015 but does not currently appear to be in any clinical trials.⁴¹ Future inhibitors may benefit from the use of sulfonamides as the metal binding group as seen with the structurally similar enzyme ACE.

1.2.8 Uridine Disphosphate-3-O-(R-3-hydroxymyristoyl)-N-acetylglucosamine Deacetylase

Uridine disphosphate-3-O-(R-3-hydroxymyristoyl)-N-acetylglucosamine deacetylase (LpxC) is a critical enzyme in the cell wall synthesis of gram-negative bacteria.⁵⁷ LpxC is a cytosolic amidase that catalyzes the first step of lipid A biosynthesis by deacetylating the amine of a 3-acyl-N-acetyl-glucoasamine moiety.⁵⁸ Inhibition of LpxC prevents cell wall synthesis and inhibitors prove to be antibacterial.⁵⁸ Since bacterial LpxC lacks a homologous mammalian protein, selective inhibitors without human toxicity may be developed.⁵⁹

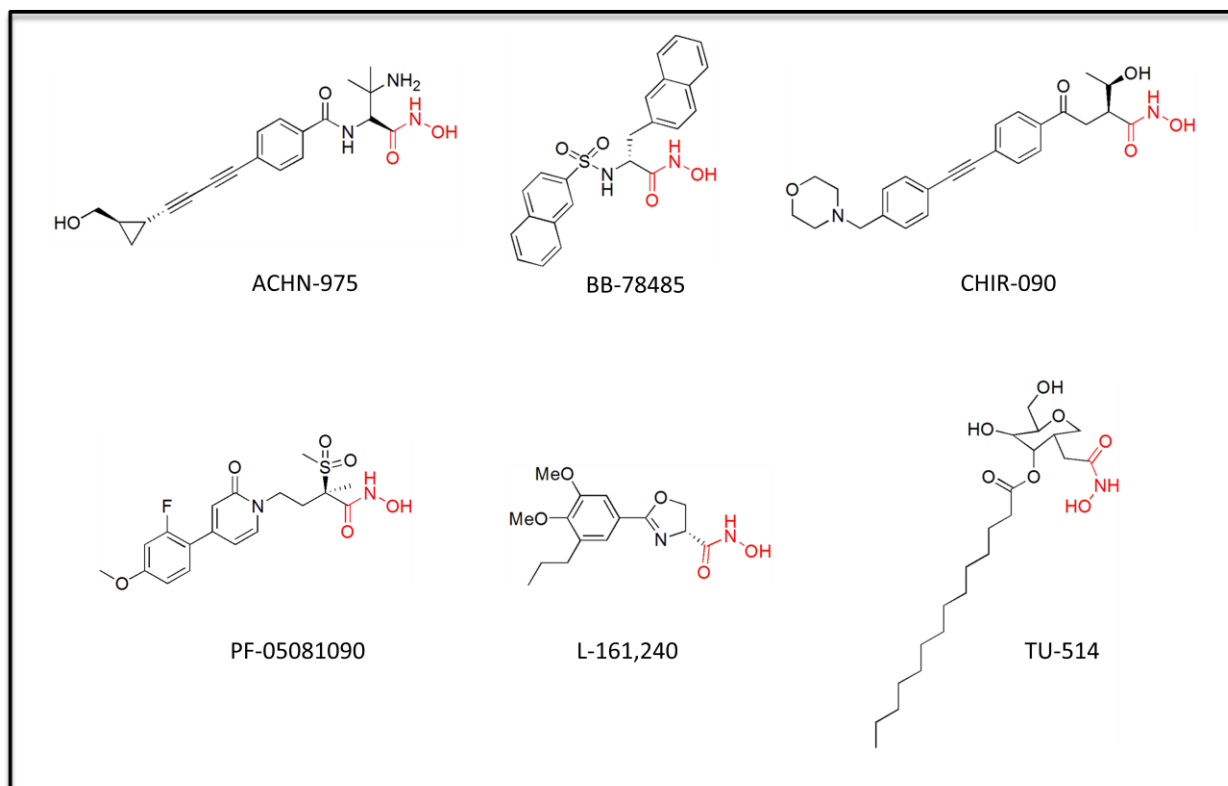


Figure 1.16: LpxC inhibitors in preclinical development. Metal binding group shown in red.

Inhibitors of LpxC exhibit nanomolar activity against the enzyme and are generally lethal to *Escherichia coli*.⁶⁰ Although most gram-negative bacteria share a homologous gene for LpxC, these inhibitors display a range of antibacterial activity in various gram-negative species. CHIR-090 for example exhibits low nanomolar potency against *E. coli*, *Helicobacter pylori*, *Neisseria meningitidis* and *Pseudomonas aeruginosa* but is weakly effective against *Rhizobium leguminosarum*.⁶¹ Despite possessing significant potency, it does not appear that LpxC inhibitors have been tested for toxicity. However, in July 2015 Achaogen was awarded up to \$4.5 million in funding over the next four years by the National Institute of Allergy and Infectious Diseases for the discovery and development of LpxC inhibitors.⁶² Achaogen received this award due to the success of their LpxC inhibitor ACHN-975 which has sub-nanomolar

activity and is bactericidal against *P. aeruginosa*, *E. coli* and *Klebsiella pneumoniae*.⁶³ All of the current LpxC inhibitors are hydroxamates. Although hydroxamates typically are problematic for mammalian targets, it is possible that highly selective hydroxamates for bacterial targets may not exhibit adverse effects in humans while maintaining potency and high zinc affinity in bacteria.

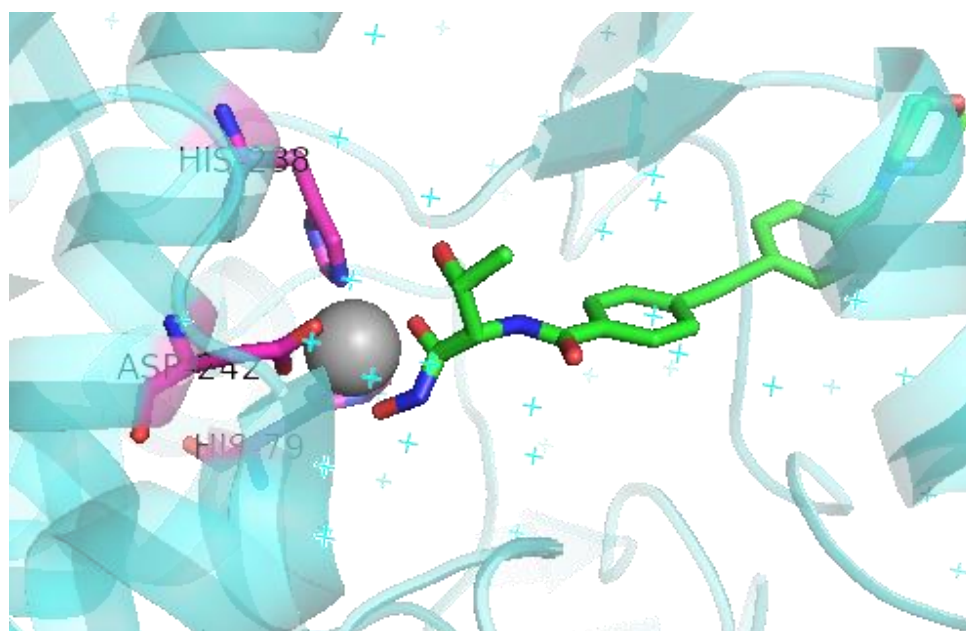


Figure 1.17: Crystal structure (PDB: 3nzk)⁶⁴ of CHIR-090 (green) bound to LpxC of *Yersinia enterocolitica* (cyan). The active site consists of two histidine residues and one aspartic acid residue (magenta) coordinated to Zn^{2+} (grey). The hydroxamate (oxygen in red and nitrogen in blue) of CHIR-090 completes the coordination sphere of Zn^{2+} to inhibit enzyme activity.

The LpxC active site consists of two histidine residues (His 79 and His 238) and one aspartic acid residue (Asp 242) coordinated to a zinc ion. This active site sequence is distinct from other amidases (ie. ACE and LTA4H) since it does not adhere to the standard HEXXH, HXXE or HXXEH sequences.⁵⁷ It may be possible that this unusual active site sequence could reduce off target effects if inhibitors are designed with high affinity. Several water molecules are also present in the active site, suggesting LpxC inhibitors should be highly hydrophilic near the

zinc binding motif. Additionally, there is a hydrophobic passage leading to the active site which binds the acyl chain of the natural substrate. As depicted in Figure 1.17, CHIR-090 exploits this hydrophobic passage with the 4-phenylethynyl-benzyl-morpholine unit. However, CHIR-090 and the other LpxC inhibitors do not occupy the UDP-binding pocket, which may offer enhanced affinity and potency.⁶⁰ Other studies indicate the zinc ion of LpxC exerts a metal binding group preference of: hydroxamate/phosphonate/thioacetoxyacetyl > thiolacetyl > phosphinate > carbonxylate/sulfonamide/hydrazide, suggesting the hydroxamate group may be replaced with either a phosphonate or thioacetoxyacetyl group and maintain potency.⁵⁸

1.3 Clinical Inhibitors of Iron Metalloenzymes

Iron is the most abundant transition metal in the human body with approximately 0.5 mg/mL found in whole blood samples.^{9,65} However, the majority of iron is sequestered by proteins such as ferritin, transferrins, hemosiderin and heme proteins.⁶⁶ These iron sequestering proteins are typically cyto-protective since free iron(II) ions can react with hydrogen peroxide to generate reactive oxygen species. Iron is present in the mitochondria, cytosol and nucleus and is required for most cellular processes. As a key component of redox reactions, iron is critical for electron transfer, ribosome maturation, angiogenesis, respiration, DNA replication and repair and cell cycle control.⁶⁷ Iron regulates the cell cycle by inhibiting cyclins and cyclin dependent kinases. Chelation of iron prevents this activity and leads to cell cycle arrest in either the G1 or S phase. Iron enzymes are involved in biosynthesis of hormones, metabolism of drugs, DNA repair and biosynthesis of antibiotics, making many of these enzymes key drug targets for

treatments of cancer, infection and neurodegenerative disorders.⁶⁸ Iron is generally used to react with oxygen and three types of iron-oxygen active sites have been identified: heme containing iron coordinated to either cysteine, histidine or tyrosine, mononuclear iron coordinated by two histidines and a carboxylate, and dinuclear iron centers coordinated by two histidines and four carboxylates.⁶⁹

1.3.1 Hypoxia-Inducible Factor Prolyl Hydroxylase

Hypoxia-inducible factor (HIF) prolyl hydroxylases are iron and 2-oxoglutarate dependent dioxygenases.⁷⁰ There are two known isoforms of this prolyl hydroxylase, PHD1 and PHD2. Both catalyze the addition of a hydroxyl to proline 402 and proline 564 of HIF- α proteins.⁷¹ This hydroxylation serves as a recognition label for the von Hippel-Lindau protein which ubiquitinates HIF for proteasomal degradation. Activated HIF binds to the hypoxia response element in the enhancer region of genes to transactivate vascular endothelial growth factor (VEGF) and erythropoietin. This activations can lead to angiogenesis, erythropoiesis, apoptosis, cell proliferation and neuroprotection.^{70,72} Inhibition of PHD1 or PHD2 prevents the degradation of HIF- α and inhibitors can be used to treat anemia, ischemic disease, complications from diabetes and provide neuroprotection.⁷¹

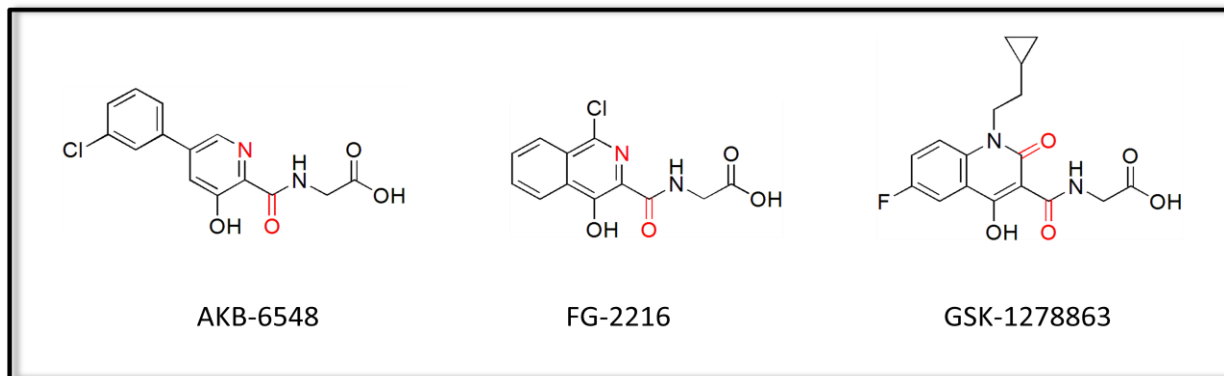


Figure 1.18: Inhibitors of PHD2 in clinical trials. Metal binding group shown in red.

HIF prolyl hydroxylase inhibitors in clinical trials are targeted against PHD2 and are used to treat anemia. Fibrinogen, one of the pioneers in HIF prolyl hydroxylase inhibition, developed FG-2216 which may be used to treat anemia as a result of chronic kidney disease or as a result of cancer chemotherapy. FG-2216 works by stabilizing and activating HIF through PHD2 inhibition to induce erythropoietin. The induction of erythropoietin increases the capacity of blood to transport oxygen and may increase red blood cell count.⁷¹ Following Fibrinogen's lead, GlaxoSmithKline and Akebia Therapeutics Inc. have developed their own PHD2 inhibitors with a similar scaffold. Both GSK-1278863 and AKB-6548 are being investigated for the treatment of anemia, with AKB-6548 specifically targeting anemia associated with chronic kidney disease. All three of these inhibitors coordinate iron in a bidentate fashion. AKB-6548 and FG-2216 coordinate iron using the nitrogen of the pyridine/isoquinoline ring and the β -carbonyl. GSK-1278863 uses a similar β -carbonyl but utilizes the carbonyl of a pyridone for iron coordination. Despite this difference, all three inhibitors form hydrogen bonds with Tyr 303, Tyr 329 and Arg 383 as well as π - π stacking interactions with Tyr 310.

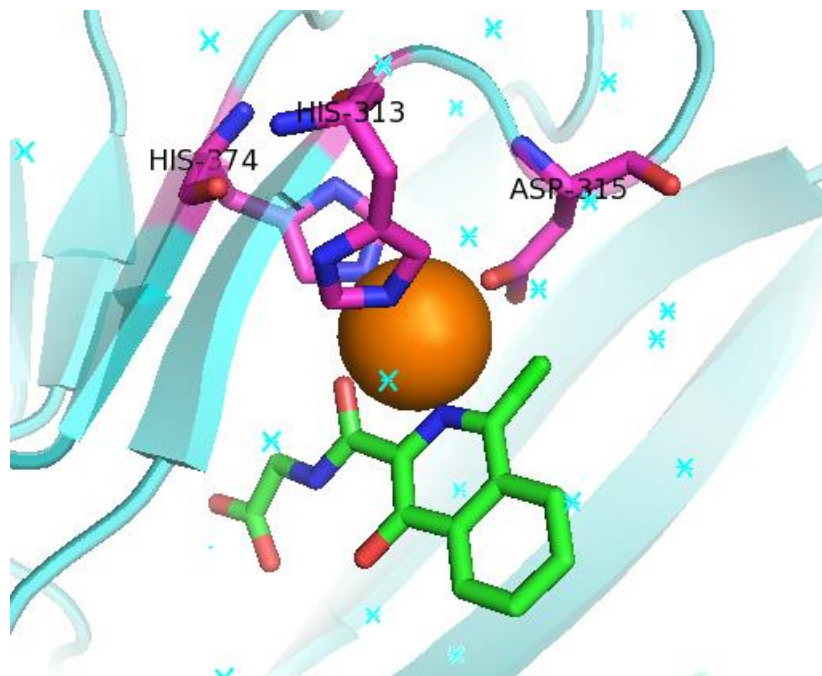


Figure 1.19: Crystal structure (PDB: 2hbt)⁷³ of FG-2216 (green) bound to human HIF prolyl hydroxylase PHD2 (cyan). The active site consists of two histidine residues and one aspartic acid residue (magenta) coordinated to Fe^{2+} (orange). The isoquinoline nitrogen and β -carbonyl (oxygen in red and nitrogen in blue) of FG-2216 complete the coordination sphere of Fe^{2+} to inhibit enzyme activity.

The PHD2 active site consists of two histidine residues (His 313 and His 374) and one aspartic acid residue (Asp 315) coordinated to a ferrous ion. Several water molecules are also present in the active site, suggesting PHD2 inhibitors should be relatively hydrophilic. Additionally, there are hydrophobic pockets near the active site which have not been exploited by current inhibitors.⁷¹ PHD2 is part of a family of prolyl 4-hydroxylases, sometimes referred to as EGLN dioxygenases.⁷² It is unclear if PHD2 inhibitors also inhibit other members of this family, including collagen prolyl 4- hydroxylase, but future efforts should be made to avoid off target inhibition. Additionally, the neuroprotective effects of HIF prolyl hydroxylase inhibition

have not yet been exploited by inhibitors in clinical trials and offer another area of potential for newer inhibitors.

1.3.2 Peptide Deformylase

Peptide deformylase (PDF) catalyzes the removal of *N*-formyl from an N-terminal methionine during protein biosynthesis in bacteria.⁷⁴ This transformation is a critical step in bacterial protein maturation. Two types of PDF have been discovered. Type 1 is found in all gram-negative bacteria and eukaryotes and some gram-positive bacteria. Type 2 is found in gram-positive bacteria and mycoplasma.⁷⁴ Although these two types may be found in gram-positive bacteria, they share very low sequence homology. For example, *E. coli* and *S. aureus* PDF only share 23% homology.⁷⁵ This low homology makes PDF of gram-positive an ideal antibacterial target. Additionally, PDF may serve as a target for some cancers and parasitic diseases such as malaria.⁷⁴

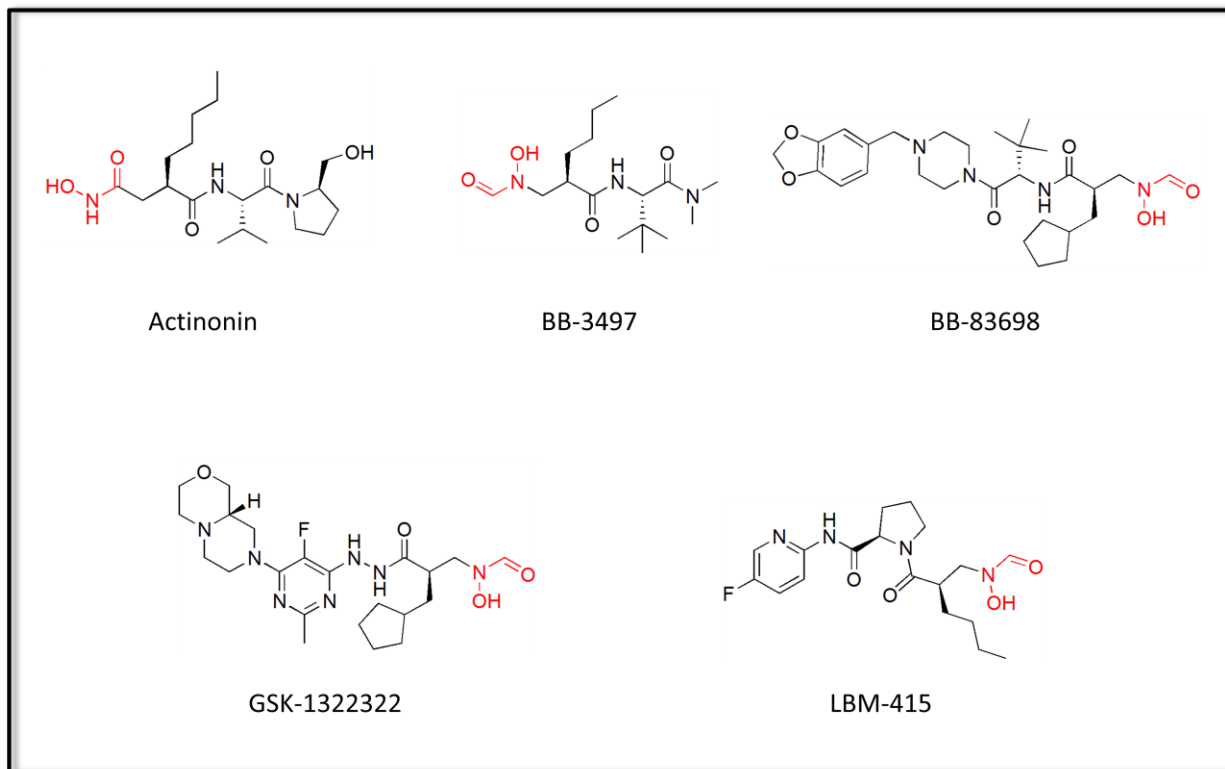


Figure 1.20: Inhibitors of PDF based on Actinonin in clinical trials. Metal binding group shown in red.

Actinonin, isolated from *Streptomyces*, is a PDF inhibitor and known antibiotic, but like most hydroxamates has poor bioavailability.⁷⁴ As a result, actinonin has served as a general scaffold for the development of more potent PDF inhibitors. While many PDF inhibitors with various scaffolds and metal binding groups have been synthesized, only four have proceeded to clinical trials.^{74,76} BB-2497 and BB-83698 were developed by a collaborative effort between British Biotech and Genesoft. They have been investigated for the intravenous treatment of bacterial infections and have shown good efficacy and ideal pharmacokinetic properties for once-daily dosing.⁷⁷ Unfortunately, British Biotech was purchased by Vernalis and the clinical trials for these inhibitors were abandoned.⁷⁴ GSK-1322322 is in Phase IIb trials and is being investigated as both an oral and intravenous treatment for acute bacterial infections and

community acquired pneumonia.⁴¹ LBM-415 was investigated as an oral treatment for respiratory tract infections but was discovered to possess unexpected safety issues due to an increase in methemoglobin and lower blood oxygen saturation.⁷⁸

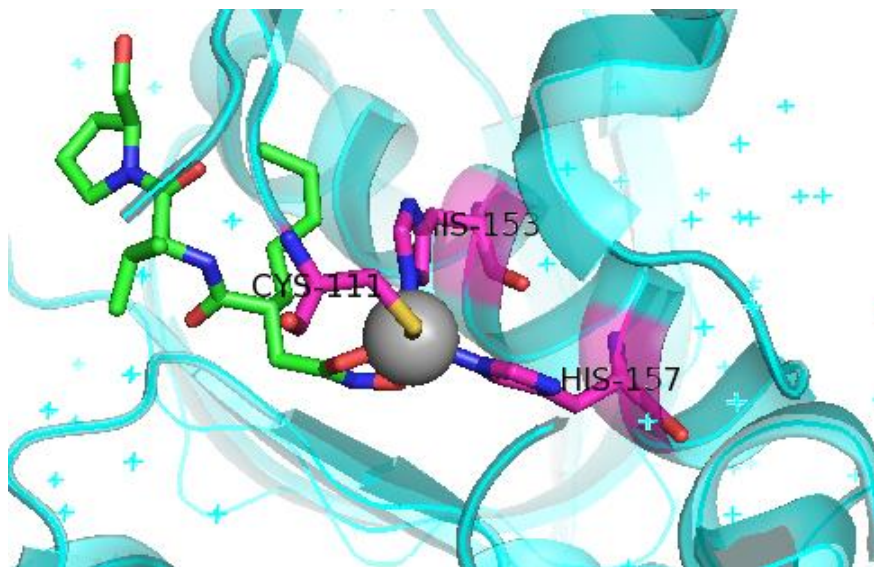


Figure 1.21: Crystal structure (PDB: 3u04)⁷⁹ of Actinonin (green) bound to PDF of *Ehrlichia chaffeensis* (cyan). The active site consists of two histidine residues and one cysteine residue (magenta) coordinated to Zn^{2+} (grey). The hydroxamic acid (oxygen in red and nitrogen in blue) of Actinonin completes the coordination sphere of Zn^{2+} to inhibit enzyme activity.

Although the active site of PDF generally contains a ferrous ion coordinated by two histidine residues, one cysteine residue and two water molecules, the ferrous ion is highly unstable and readily oxidizes to the ferric form. The ferric ion results in an inactive form of the enzyme and cannot be crystallized.⁷⁴ Studies have shown that the ferrous ion can be replaced by either zinc or nickel and maintain activity and stability, which is why this crystal structure depicts zinc as the catalytic metal ion. From this crystal structure and others, it has been determined that inhibitors of PDF must coordinate the ferrous ion as well as form a hydrogen bond with a nearby glutamic acid. Additionally, inhibitors may gain better potency and

selectivity by exploiting three key pockets. The S1 pocket is highly hydrophobic and conserved across species. The S2 pocket is solvent exposed and is considered an open tunnel as residues are typically spaced too far for non-covalent interactions with ligands. The S3 pocket is also solvent exposed but highly variable across species. Therefore, inhibitors may benefit from being designed to interact with the S3 pocket to reduce toxicity and gain better potency. Additionally, it has been determined that the most potent inhibitors of PDF possess either a hydroxamate or reverse hydroxamate metal binding group. It is possible to replace the hydroxamate with either carboxylate or hydrazide, but these groups suffer from a loss in potency. Substitution of hydroxamate with thiol results in greater loss of potency and substitution with phosphonates appears to eliminate inhibitory activity.⁷⁶

1.3.3 5-Lipoxygenase

5-lipoxygenase (5-LOX) is a non-heme iron dioxygenase which catalyzes the lipid peroxidation of arachidonic acid to leukotriene A₄.⁸⁰⁻⁸² 5-LOX is located in both the nucleus and cytosol, but upon activation translocates to the nuclear membrane. This translocation allows it to interact with arachidonic acid to initiate the catalysis of several metabolites. These metabolites may promote cell proliferation and stimulate angiogenesis through the induction of VEGF.⁸² 5-LOX has become a prime target of pharmaceutical and biotech industries due to its role in inflammation.⁸³ Inhibition of 5-LOX has been found to attenuate inflammation after an ischemic event, serving as a neuroprotectant. Additionally, 5-LOX appears to be involved in the progression of prostate, lung, colon and colorectal cancers.

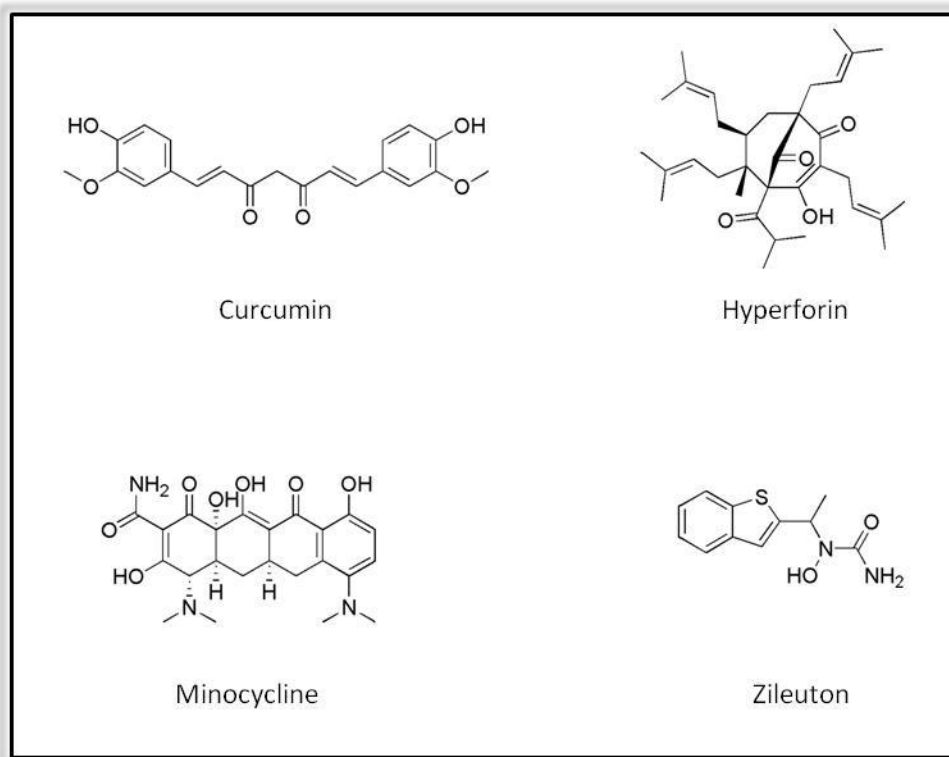


Figure 1.22: 5-LOX inhibitors in clinical trials (Curcumin and Hyperforin) and approved for use.

Currently, two 5-LOX inhibitors are approved but only Zileuton is recognized as a 5-LOX inhibitor. Zileuton is marketed for the treatment of asthma.⁸² Minocycline is also approved by the FDA, but is used as a tetracycline antibiotic for the treatment of several gram-positive and gram-negative infections.⁸⁴ However, Minocycline is known to be both anti-inflammatory and neuroprotective against ischemic events, Parkinson's disease and Huntington's disease.⁸⁵ As a result, Minocycline is currently in clinical trials for the treatment of bipolar depression, Angelman syndrome, schizophrenia, autism, Huntington's, Fragile X syndrome, rheumatoid arthritis, acute stroke recovery, the treatment of several cancers and other inflammation based diseases.⁴¹ Other 5-LOX inhibitors in clinical trials are curcumin and hyperforin.⁴¹ Curcumin inhibits 5-LOX with an $IC_{50} = 8 \mu M$ and displays cytotoxicity against

colorectal cancer with a $GI_{50} = 52 \mu\text{M}$. Although these values are significantly higher than typical chemotherapeutics, curcumin is in Phase II clinical trials as a treatment for pancreatic neoplasms.⁸² Hyperforin is isolated from St. John's wort and has antidepressive, antibacterial and antiproliferative activity.⁸⁶ Another important feature of hyperforin is that it activates pregnane X receptor to regulate expression of cytochrome P450 3A4 monooxygenase, a key enzyme in the oxidative metabolism of over 50% of all drugs.⁸⁷ These important and potent activities has pushed hyperforin into Phase III clinical trials as a dietary supplement for the treatment of depression.⁴¹

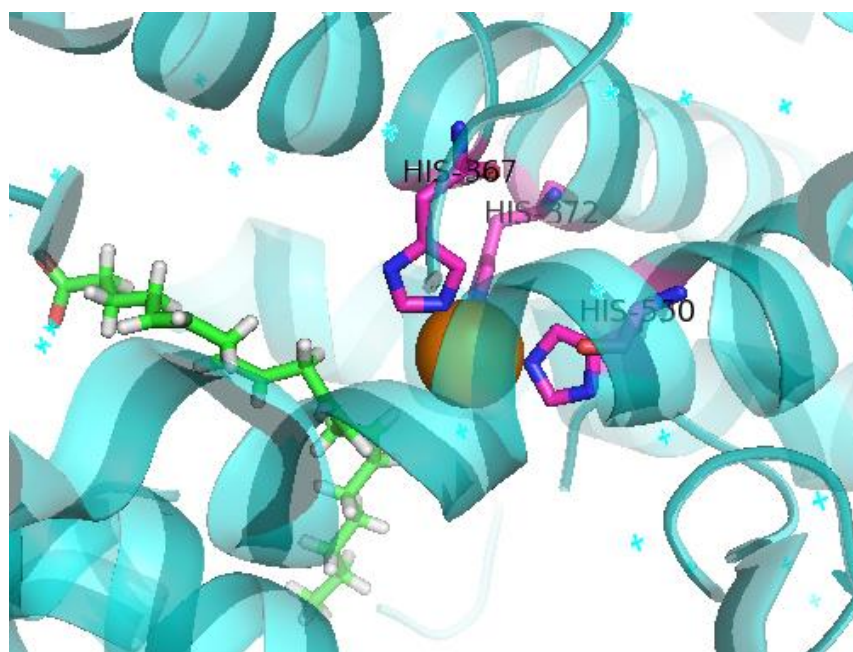


Figure 1.23: Crystal structure (PDB: 3v99)⁸⁸ of the native ligand arachidonic acid (green) bound to 5-LOX (cyan). The active site consists of three histidine residues (magenta) coordinated to Fe^{2+} (orange).

Unfortunately, there is not a crystal structure of an inhibitor bound to 5-LOX. However, from the crystal structure of 5-LOX bound to the native ligand arachidonic acid (Figure 1.23), it is clear three histidine residues (His 372, His 376 and His 530) coordinate the ferrous ion.

Although this is a similar coordination motif to carbonic anhydrase, the active site does not appear to be similar as the 5-LOX active site has a relatively large, mostly hydrophobic tunnel leading to the catalytic metal ion, whereas carbonic anhydrase active site is solvent exposed. This would suggest that 5-LOX inhibitors should be mostly long, hydrophobic molecules with a metal binding head group. However, these inhibitors may benefit from having a hydrophilic “face” to interact with water molecules that line part of the tunnel.

1.3.4 Cytochrome P450

Cytochrome P450 (CYP) is a superfamily of enzymes that catalyze the oxidation of native and xenobiotic chemicals.⁸⁹ Primarily, the CYPs interact with a nitrogenous group on a chemical through a heme-coordinated iron to oxidize the nitrogen via glucuronidation or forming N-oxides.⁹⁰ CYPs are found in all forms of life, with 57 CYP genes present in the human genome and CYP51A a key enzyme in the biosynthesis of the fungal cell wall.⁹¹⁻⁹² It is estimated that nearly 75% of all drugs are metabolized through oxidation by CYP 3A4, 2D6 and 2C9, with CYP 3A4 being the most important and most abundant isoform in humans.⁹²

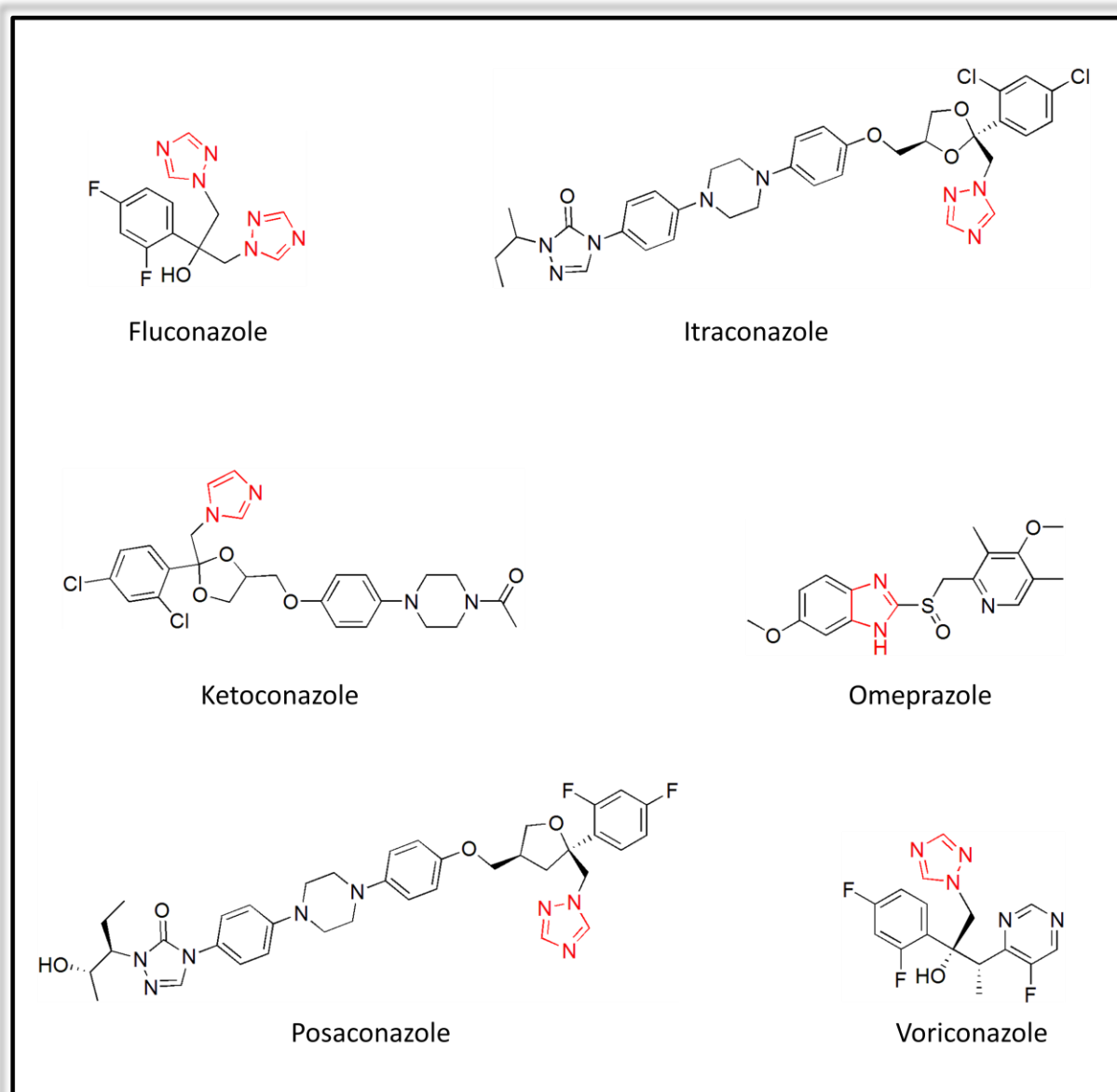


Figure 1.24: Antifungal CYP inhibitors approved for clinical use. Metal binding group shown in red.

While there are many FDA approved drugs that inhibit CYPs, only the imidazole and triazole based antifungal agents have been designed specifically to inhibit CYP.^{89,93} CYP51A, also known as 14 α -sterol demethylase, is essential for ergosterol biosynthesis in fungi. Ergosterol is a critical component of the fungal cell membrane, and inhibition of ergosterol

synthesis compromises the integrity of the membrane.⁹² Since they are nitrogenous and lipophilic, the antifungal CYP inhibitors are themselves substrates for CYP oxidation by CYP 3A4, 2C9 and 2C19.⁹² Inhibition by these antifungals is rapid, competitive and reversible. Interestingly, the triazoles show no inhibitory effect on CYP 1A2, 2D6 and 2E1, and posaconazole also does not inhibit CYP 2C8 or 2C9.⁹⁴⁻⁹⁵

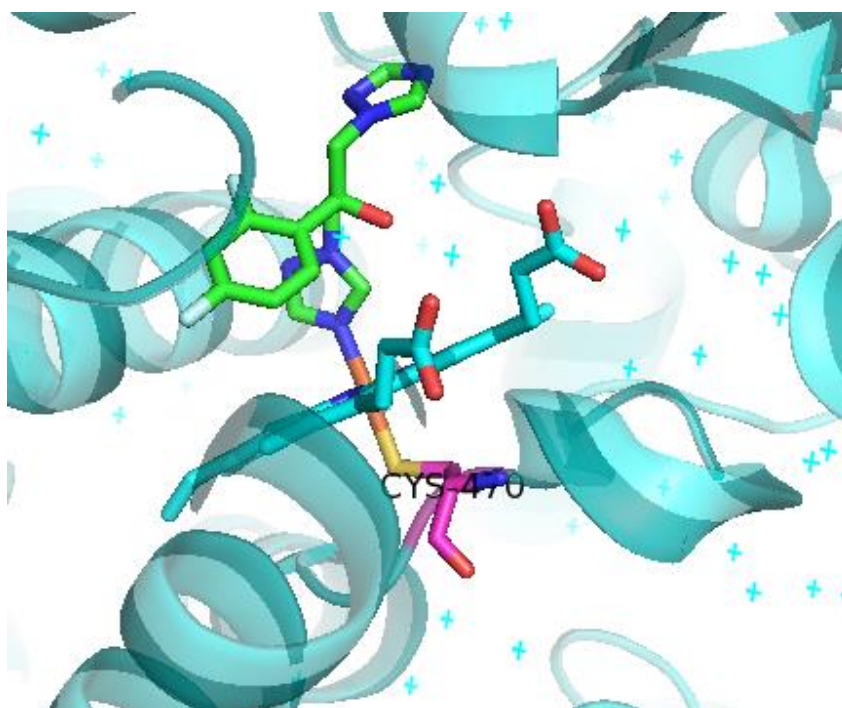


Figure 1.25: Crystal structure (PDB: 4wmz)⁹⁶ of Fluconazole (green) bound to CYP51A of *Saccharomyces cerevisiae* (cyan). The active site consists of one cysteine residue (magenta) coordinated to the heme coordinated Fe^{2+} (orange). The triazole (nitrogen in blue) of Fluconazole completes the coordination sphere of Fe^{2+} to inhibit enzyme activity.

As with all CYPs, the active site of CYP51A contains a heme-coordinated ferrous ion that is also coordinated by a cysteine residue (Cys 470). Due to the lipophilic nature of the heme ring, the active site is largely water-free. However, there is a relatively hydrophilic region extending away from the heme. This explains why the inhibitors are mostly lipophilic near the

triazole/imidazole ring but have mostly hydrophilic tails. Unfortunately, the lipophilic nature of the antifungals results in poor water solubility. Additionally, as CYP inhibitors, especially CYP 3A4, they hinder the metabolism of other drugs such as benzodiazepines, anxiolytics, immunosuppressants, statins and warfarin.⁹² The reduced metabolism of these drugs can cause a highly toxic effect or a reduction in efficacy. This stresses the need to explore derivatives of these antifungals for structure activity relationships to avoid inhibition of the key metabolic CYP enzymes as well as developing an understanding of the inhibition potential of their metabolites.

1.4 Clinical Inhibitors of Magnesium Metalloenzymes

Magnesium is the most abundant divalent cation found in eukaryotic cells.⁹⁷ Free magnesium is essential for the regulation of cell growth as it is an important regulatory cofactor for many enzymes, including: acetyl CoA synthetase, 5'-nucleotidase, phosphorylase kinase, phosphoribosyl pyrophosphate transferase, several ATPases, adenylate cyclase and enzymes in glycolytic pathways.⁹⁸ Potentially due to its abundance, magnesium is one of the most versatile cofactors involved in both intracellular and extracellular processes.⁹⁹ Additionally, magnesium is essential for the activation of enzymes involved in DNA replication.¹⁰⁰ These enzymes typically coordinate the magnesium ion with aspartic acid as part of three structural motifs. RNA polymerase, DNA polymerase I and human immunodeficiency virus reverse transcriptase use the motif NADFDGD while telomerase and reverse transcriptase may use either YXDD or LXDD where X can be any amino acid.⁹⁹ The magnesium ion in the active site of these enzymes is a "hard" ion and prefers binding "hard" ligands with low polarization potential.¹⁰¹⁻¹⁰² Oxygen

and nitrogen are the preferred atoms for magnesium binding, and all magnesium metalloenzymes in the Protein Data Bank are coordinated by at least one carboxylate in a monodentate fashion.¹⁰⁰ The coordination sphere of magnesium is octahedral and always includes at least one water molecule. Unlike other metal ions in metalloenzymes, magnesium will not exchange a first shell water molecule for a protein ligand.⁹² Despite this characteristic, Mg^{2+} is not the preferred metal ion for these enzymes and may be displaced by Zn^{2+} , Cu^{2+} , Co^{2+} , Ni^{2+} , or Fe^{2+} . With the exception of Zn^{2+} , these other metal ions may inhibit the enzyme.⁹⁹

1.4.1 Human Immunodeficiency Virus-Integrase

Human immunodeficiency virus (HIV) integrase is a 32 kDa enzyme that binds both viral and cellular DNA to catalyze the integration of the viral genome into the host DNA.¹⁰³⁻¹⁰⁴ The enzyme consists of three structurally and functionally distinct domains. The N-terminal domain is a zinc finger region that is highly conserved in all retrovirus integrases and is implicated in 3' processing and strand transfer.¹⁰³ The C-terminal domain binds the host DNA and is critical for 3' processing and strand transfer.¹⁰⁵ The catalytic domain contains the catalytic triad of aspartic acids and glutamic acid (DDE motif).¹⁰⁶ This catalytic triad coordinates two metal ions. While magnesium appears to be the preferred ion due to abundance, manganese may also be utilized.¹⁰³

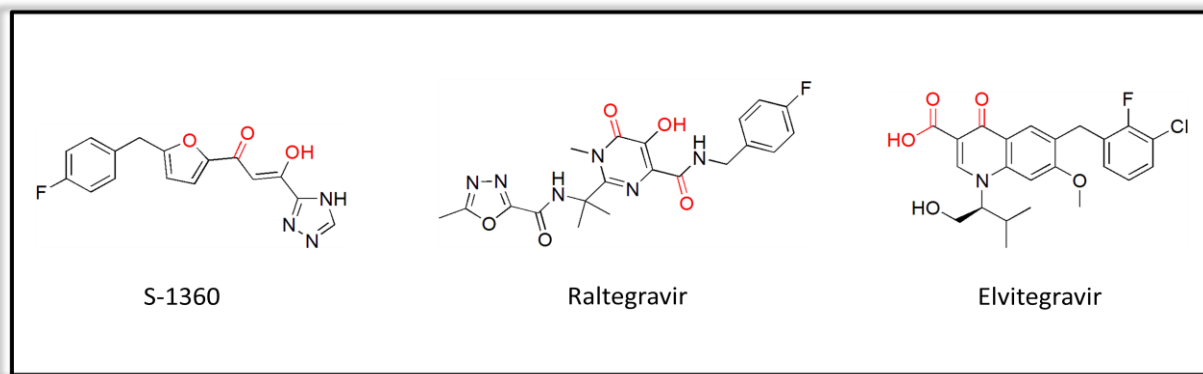


Figure 1.26: HIV integrase inhibitors approved for use (Raltegravir and Elvitegravir) and the first HIV integrase inhibitor to go into clinical trials (S-1360). Metal binding groups shown in red.

Due to limited knowledge about HIV integrase in the early 1990s, initial attempts to develop inhibitors focused on topoisomerase inhibitors, dihydroxynaphthoquinone and caffeic acid phenethyl ester, to coordinate the zinc ion in the N-terminal domain.¹⁰⁷ Although these compounds had some effect, true HIV integrase inhibitors were not determined until 1999. High throughput screening identified diketo acids as potent inhibitors of HIV integrase.¹⁰⁸ The first diketo acid to go into clinical trials was S-1360.¹⁰⁹ Unfortunately, S-1360 failed to show efficacy in humans due to reduction of the carbon linked to the triazole.¹¹⁰ However, this led to the development of another molecule, Raltegravir, which was approved in 2007 and is capable of coordinating the two Mg^{2+} in a bis-bidentate fashion with a planar O-O-O structural motif. Raltegravir forms a 6-membered and 5-membered chelate ring. Upon chelation, Raltegravir can move the fluorophenyl group to displace a 3' adenine and tightly fit in the binding pocket.¹¹¹ Despite the potency of Raltegravir ($IC_{50} = 40$ nM), several resistant strains were discovered. These resistant mutants maintain the same structural motif coordinating the two Mg^{2+} , suggesting that compounds with metal binding groups with higher affinity could be used to inhibit HIV integrase even in Raltegravir resistant strains.¹¹² Eventually Elvitegravir ($IC_{50} = 7$ nM) was developed and approved in 2012. The increased potency of Elvitegravir may be due to

the formation of a 6-membered and a 4-membered chelate ring.¹¹² Although HIV integrase inhibitors could be used as stand-alone treatments of HIV, combination therapy with an HIV protease inhibitor and an antiretroviral is the preferred treatment method.¹¹³

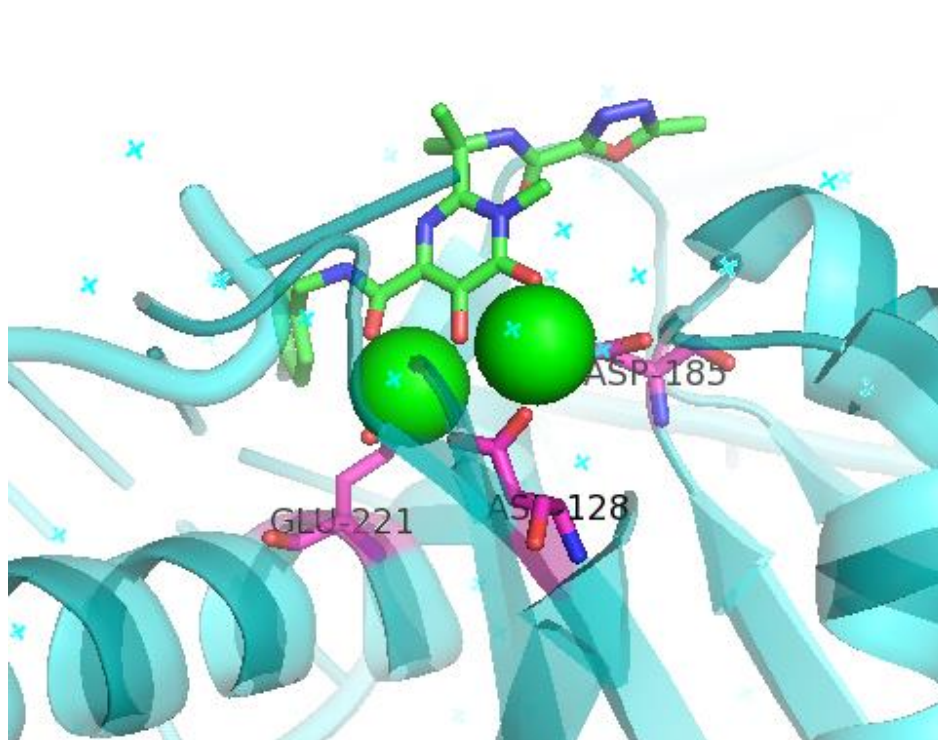


Figure 1.27: Crystal structure (PDB: 3oya)¹¹⁴ of Raltegravir (green) bound to HIV integrase of Prototype Foamy Virus intrasome (cyan). The active site consists of two aspartic acid residues and one glutamic acid residue (magenta) coordinated to two Mg^{2+} (green). The planar O-O-O motif of the dihydropyrimidine amide (oxygen in red and nitrogen in blue) of Raltegravir completes the coordination sphere of the two Mg^{2+} to inhibit enzyme activity.

The HIV integrase active site consists of two aspartic acid residues (Asp 128 and Asp 185) and one glutamic acid residue (Glu 221) coordinated to two magnesium ions. Several water molecules complete the octahedral coordination sphere of each Mg^{2+} . Since the active site is highly hydrophilic and contains multiple water molecules, HIV integrase inhibitors are mostly hydrophilic and may form hydrogen bonds with water molecules in the active site. Because

Mg²⁺ is a “hard” ion and prefers to coordinate with oxygen atoms, inhibitors should contain three planar oxygen atoms. Additionally, inhibitors should be able to displace adenine and tightly bind in the DNA binding pocket to strongly inhibit HIV integrase as well as form π - π stacking interactions with Tyr 143.¹¹² Other research has shown that Van der Waals interactions with Pro 214 may also increase potency.¹¹¹

1.4.2 DNA Gyrase

DNA gyrase is a type IIA topoisomerase. It is an ATP dependent enzyme that catalyzes the supercoiling of DNA in prokaryotes.¹¹⁵ DNA gyrase is also essential for DNA replication, transcription, repair, recombination, bacteriophage λ integrative recombination and decatenation.¹¹⁶⁻¹¹⁸ The enzyme is a tetramer consisting of two subunits, GyrA and GyrB. GyrA forms a covalent bond with a 5' phosphate of DNA to catalyze a double strand break. GyrB hydrolyzes ATP for GyrA to ligate the DNA by forming a new phosphodiester bond.¹¹⁹ DNA gyrase is a popular target for antibiotics and may be a therapeutic target for antitumor agents.¹²⁰ Antibiotics that target DNA gyrase typically belong to one of two classes; quinolones which target GyrA and coumarins which target GyrB. The antibiotics which target GyrB are competitive inhibitors of ATP, do not act by coordinating a metal ion and therefore will not be discussed further.

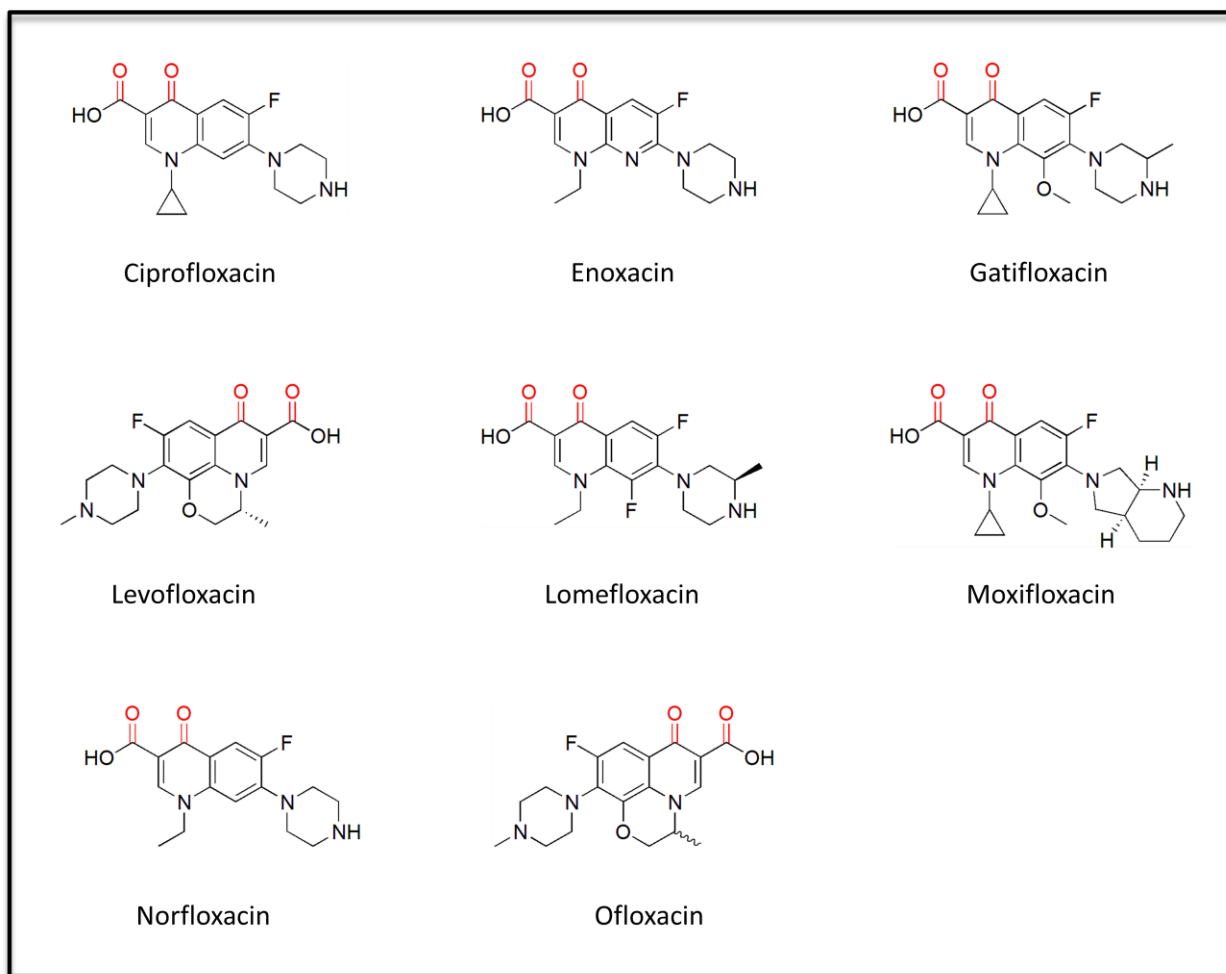


Figure 1.28: Fluoroquinolone inhibitors of DNA gyrase approved for use. Metal binding group shown in red.

The quinolones, which have mostly been replaced by the more effective fluoroquinolones, are one of the most successful classes of antibiotics.¹²¹ Fluoroquinolones can be administered as front-line therapeutics for bacterial infections but are recommended for and often prescribed to treat multi-drug resistant infections. These inhibitors act by stabilizing the cleaved DNA from the first step of the catalytic reaction.¹²² By stabilizing the GyrA-DNA complex, fluoroquinolones prevent DNA replication and transcription as well as the re-ligation of DNA after the double strand break, causing bacteriostasis. At high enough concentrations, fluoroquinolones release the double strand broken DNA from GyrA. Accumulation of the

broken DNA eventually leads to cell death.¹²³ Public interest and demand for fluoroquinolones was drastically heightened in 2001 when Tom Brokaw announced on NBC Nightly News “in Cipro we trust”. This statement was fueled by the terrorist attacks on September 11, 2001 and the subsequent anthrax scares. During this time, Bayer and the United States government provided 60 tablets of Ciprofloxacin to military personnel, first responders and anyone who may have been exposed to anthrax. Medical providers would also prescribe ciprofloxacin to anyone who requested in, placing strains on production and most likely aiding the eventual bacterial resistance.¹²⁴

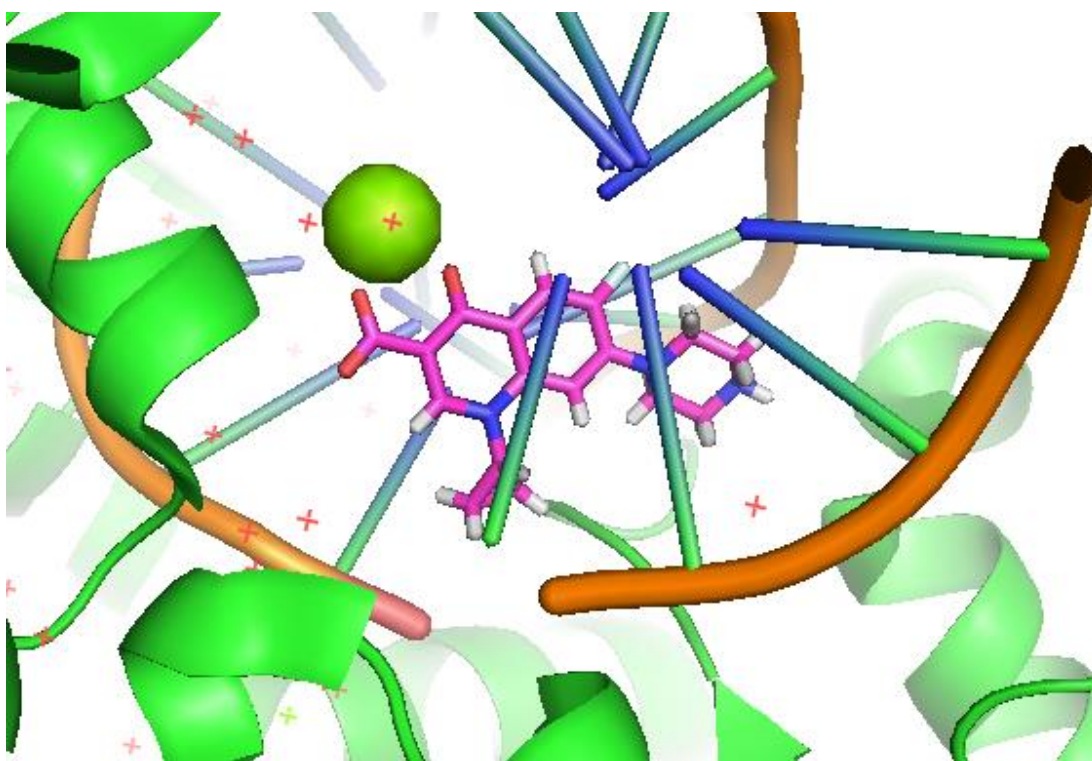


Figure 1.29: Crystal structure (PDB: 5btc)¹²³ of Ciprofloxacin (magenta) bound to DNA gyrase of *Mycobacterium tuberculosis* (green). The active site of GyrA appears near the dimer interface and consists of the protein bound to DNA base pairs (blue-green, phosphate backbone in orange). A 3' oxygen on DNA coordinates to Mg^{2+} (green) which is coordinated to DNA gyrase through a water network. The two carbonyls of the quinolone motif (oxygen in red and nitrogen in blue) of Ciprofloxacin complete the coordination sphere of Mg^{2+} to stabilize the DNA-GyrA complex and prevent further catalysis.

The necessity of a metal ion in the catalytic site has been debated since it has been proposed that intrinsic resistance of certain species to fluoroquinolones results from sequence variation which leads to a loss of metal ion to prevent drug interaction.¹²⁵ However, Figure 1.29 clearly indicates a metal ion forms a “bridge” between the GyrA-DNA complex and the fluoroquinolone through hydrogen bonds with several water molecules. A similar “bridge” between the inhibitor to GyrA by a single water and Mg^{2+} is found in *Staphylococcus aureus* and *Acinetobacter baumannii*.¹²³ Although Mg^{2+} is not directly coordinated by any residues of GyrA, *S. aureus* uses three acidic residues from GyrB to coordinate Mg^{2+} through a water network. These three residues (Glu B435, Asp B508 and Asp B510) are conserved in topoisomerase and primase domains of bacteria.¹²⁶ Additionally, a tyrosine residue (Tyr A123) was found to be essential for the catalytic activity of DNA gyrase in *S. aureus*, helping to cleave the phosphodiester bond of DNA once a 3' oxygen has been coordinated to Mg^{2+} in GyrA.¹²² *Mycobacterium tuberculosis* also has a catalytic tyrosine residue (Tyr 129) but only stabilizes Mg^{2+} with one residue (Asp 94) via a water molecule. This lack of water mediated contacts to Mg^{2+} may explain the resistance of *Mycobacterium* to fluoroquinolones.¹²³ Increased potency and selectivity towards *Mycobacterium tuberculosis* may be achieved through interactions with the nearby residues Arg 482, Thr 500 and Glu 501. Although *S. aureus* also has a nearby arginine residue (Arg A122) it does not have a nearby threonine residue and the homologous glutamic acid residue participates in Mg^{2+} coordination. Therefore, compounds that are designed towards inhibiting DNA gyrase of *Mycobacterium tuberculosis* may not inhibit that of *S. aureus* since there are structural differences in the coordination of Mg^{2+} and some differences in the residues surrounding the active site.

1.5 Clinical Inhibitors of Manganese Metalloenzymes

Manganese is the fourth most common metal ion cofactor and is found in approximately 6% of enzymes.¹²⁷ Similar to iron and copper, manganese is commonly found in redox processes which require electron transfer.⁹⁹ Manganese is essential for enzymes that regulate development, energy metabolism, digestion, immune function, reproduction and antioxidant defense.¹²⁸ Although protein binding characteristics of manganese are scarce, Mn^{2+} exhibits ligand affinity similar to Fe^{2+} .^{99,129} This may be due to Mn^{2+} and Fe^{2+} having similar ionic radii, coordination preferences and free energy of solvation.¹²⁹⁻¹³⁰ It is known that Mn^{2+} and Fe^{2+} are maintained at similar concentrations in the cytosol and this maintenance utilizes a common transporter for cellular uptake.¹³¹ However, Mn^{2+} concentrations are elevated in chloroplasts, as a necessary component of photosystem II, and mitochondria.¹³² Additionally, Mn^{2+} may be replaced by Cu^{2+} or Zn^{2+} at high enough concentrations prior to protein folding. Once a protein is folded properly, Mn^{2+} cannot be displaced by Cu^{2+} or Zn^{2+} .¹³³ It is unknown if Fe^{2+} is able to compete with Mn^{2+} due to key similarities.

1.5.1 1-deoxy-D-xylulose 5-phosphate Reductoisomerase

1-deoxy-D-xylulose 4-phosphate reductoisomerase (DXR) catalyzes the conversion of 1-deoxy-D-xylulose 5-phosphate into 2-C-methyl-D-erythritol 4-phosphate.¹³⁴ DXR is required for the biosynthesis of isoprenoids through the non-mevalonate pathway in bacteria, protozoa, plants

and algae.¹³⁵ The non-mevalonate pathway is not utilized by humans, suggesting the selective inhibition of DXR will not cause toxicity in humans.¹³⁵ Although there is some debate about which metal ion is utilized for catalytic activity, DXR exhibits a high affinity for Co^{2+} , Mn^{2+} and Mg^{2+} in descending order. Similar affinity is displayed for both Co^{2+} and Mn^{2+} , but DXR shows nearly 100-fold less affinity towards Mg^{2+} . While Mg^{2+} is more abundant than Mn^{2+} or Co^{2+} , DXR displays the greatest k_{cat} when Mn^{2+} is in the active site.¹³⁶⁻¹³⁷ Additionally, Mn^{2+} allows the most ligand bond flexibility which better accommodates the transition state geometry.¹³⁸ Together, these results appear to indicate Mn^{2+} as the preferred metal ion for activity.

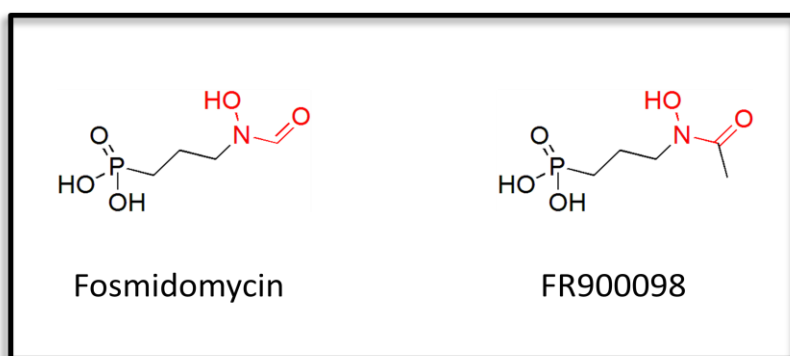


Figure 1.30: Natural products that exhibit potent DXR inhibitory activity (Fosmidomycin is currently in clinical trials). Metal binding group shown in red.

Currently there is only one DXR inhibitor in clinical trials, fosmidomycin, but another natural product exhibits greater DXR inhibition against *Plasmodium falciparum*.¹³⁹ Both of these natural products are isolated from *Streptomyces*, with fosmidomycin isolated from *S. lavendulae* and FR900098 from *S. rubellomurinus*.¹⁴⁰ Fosmidomycin is a slow, tight binding, competitive inhibitor with K_i values of 38-600 nM.¹⁴¹ Despite this potency, fosmidomycin is not very permeable due to the polar, anionic phosphonate group. Additionally, as with most hydroxamates, fosmidomycin displays poor bioavailability.¹³⁵ Although it would appear that

fosmidomycin and FR900098 have two metal chelating groups, only the hydroxamate appears to coordinate Mn^{2+} while the phosphonate hydrogen bonds with several key residues in the active site.

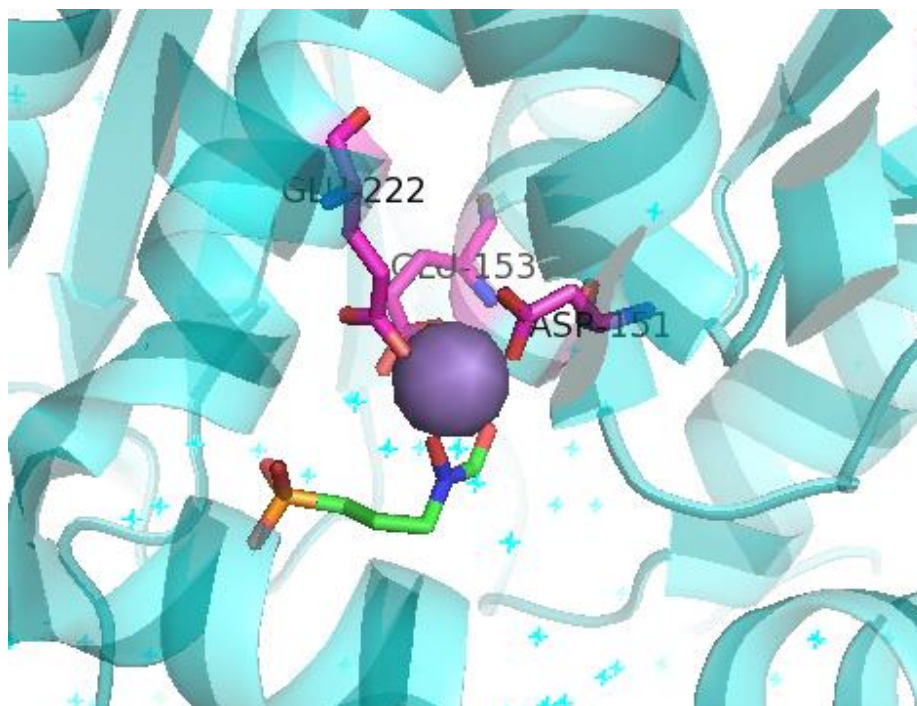


Figure 1.31: Crystal structure (PDB: 4ooe)¹⁴² of Fosmidomycin (green) bound to DXR of *M. tuberculosis* W203Y mutant (cyan). The active site consists of two glutamic acid residues and one aspartic acid residue (magenta) coordinated to Mn^{2+} (steel blue). The hydroxamate (oxygen in red and nitrogen in blue) of Fosmidomycin completes the coordination sphere of Mn^{2+} to inhibit enzyme activity.

In addition to the metal ion, DXR also requires NADPH for activity. DXR is a homodimer with each unit divided into three domains. The N-terminal domain binds NADPH, the central domain contains most of the active site residues as well as a flexible “lid” region, and the C-terminal domain is comprised of mostly α -helices.¹⁴³ The DXR active site consists of two glutamic acid residues (Glu 153 and Glu 222) and one aspartic acid residue (Asp 151) coordinated to Mn^{2+} . Several water molecules are also present in the active site and may be used

to complete an octahedral coordination sphere Mn^{2+} or a ligand may displace the water molecules to create a trigonal bipyramidal coordination sphere.¹⁴⁴⁻¹⁴⁵ Since the active site is highly hydrophilic and contains multiple water molecules, DXR inhibitors are mostly hydrophilic and form hydrogen bonds with hydrophilic residues in the active site. Typically, the phosphonate forms hydrogen bonds with an asparagines, lysine, histidine and two serines. FR900098 may form Van der Waals interactions with a tryptophan residue on the flexible “lid” which may explain its increased potency.¹³⁵ Due to the multiple interactions with the active site, the phosphonate group is essential to proper orientation and binding of the inhibitor.¹⁴⁵ Unfortunately synthetic inhibitors of DXR, with the exception of some sulfur contain isosteres of fosmidomycin, have not been able to produce greater potency.¹⁴⁶ However, these inhibitors typically maintain the hydroxamate moiety and may benefit from the use of an alternative chelating moiety. Additionally, an ester pro-drug form of the phosphonate as well as the addition of more lipid like moieties to interact with the “lid” region may increase the permeability and efficacy of synthetic inhibitors.¹³⁵

1.5.2 Arginase

Arginase is a binuclear metalloenzyme that hydrolyzes L-arginine to L-ornithine and urea.¹⁴⁷ There are two isoforms of human arginase. Arginase I is expressed in the liver and is the major isoform responsible for activity in the human body.¹⁴⁸ Arginase II is mitochondrial and mostly expressed in the kidney and prostate. L-arginine is also the only substrate of nitric oxide synthase (NOS), an enzyme critical for the production of nitric oxide (NO).¹⁴⁹ NO promotes blood flow by regulating vasodilation and inhibiting platelet aggregation, regulates

hemostasis and leukocyte adhesion, exhibits anti-inflammatory effects, scavenges reactive oxygen species and contributes to vascular smooth muscle cell proliferation.¹⁴⁹⁻¹⁵⁰ Both arginase and NOS compete for L-arginine, with NOS having a much higher affinity but approximately 1000-fold less activity than arginase.¹⁵¹ Consumption of L-arginine by arginase impairs the synthesis of NO and may contribute to asthma, cystic fibrosis, glomerular disease, psoriasis, arthritis, sickle cell disease, diabetes mellitus, hypertension, atherosclerosis, erectile dysfunction, ischemia reperfusion injury and aging.^{149, 152-157} Inhibition of arginase restores synthesis of NO and has been shown to protect patients with coronary artery disease from endothelial dysfunction resulting from ischemia reperfusion and reverses impairment of vasodilation.^{147, 149-150, 158}

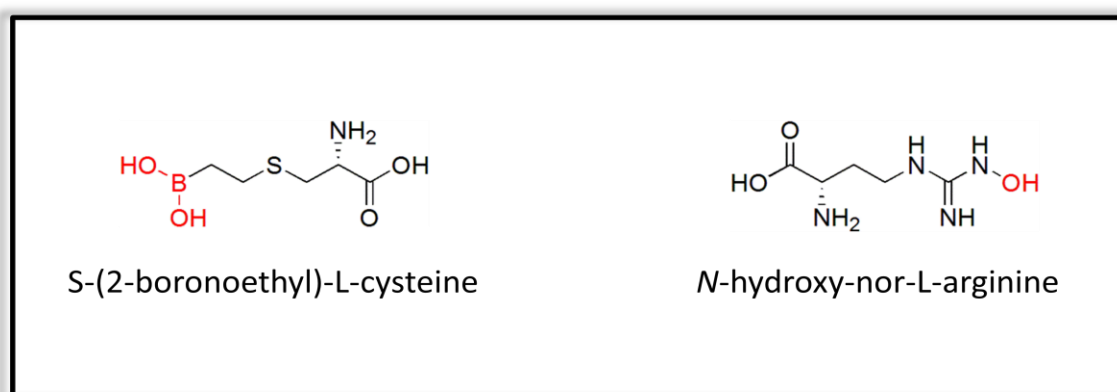


Figure 1.32: Arginase inhibitors in pre-clinical [S-(2-boronoethyl)-L-cysteine] and clinical (N-hydroxy-nor-L-arginine) development. Metal binding group shown in red.

Arginase inhibitors being developed typically belong to one of two classes: boronic acid analogs and N-hydroxy-guanidinium analogs or L-arginine.¹⁴⁹ The boronic acid analogs are able to be trigonal planar, which is the same molecular geometry of the guanidinium group of arginine. This class of inhibitors acts through a nucleophilic attack of the boron atom by a hydroxide bridged to the metal ion. The boronic acid analogs bind to the active site of arginase

approximately 50,000 times stronger than L-arginine, other amino acids, aldehyde based analogs and sulfonamide mimics. S-(2-boronoethyl)-L-cysteine (BEC) is the most studied boronic acid analog and exhibits $K_i = 0.4 \mu\text{M}$ against arginase I and $K_i = 0.31 \mu\text{M}$ against arginase II.¹⁵⁹ BEC also enhances response to acetylcholine which restores vascular tone and normal blood flow in both high and low salt-treated animals.¹⁴⁷ Additionally, BEC can enhance smooth muscle relaxation in human penile corpus cavernosum tissue and may be used to treat erectile dysfunction.¹⁴⁸ Although BEC is has not progressed to clinical trials, it has served as small molecule probe of arginase-NOS responses.

N-hydroxy-nor-L-arginine (nor-NOHA) is a hydroxylamine analog of L-arginine and binds in a similar fashion. The *N*-hydroxy guanidinium side chain maintains the same trigonal planar geometry of the native ligand but the hydroxy group is able to displace the hydroxide ion which attacks the boron of BEC.¹⁶⁰ However, due to the displacement of this hydroxide, nor-NOHA is less specific than BEC against arginase I ($K_i = 0.5 \mu\text{M}$) but more specific against arginase II ($K_i = 50 \text{ nM}$).¹⁶¹ nor-NOHA has recently completed Phase 2 clinical trials as a treatment for cutaneous microvascular endothelial function in patients with type 2 diabetes.⁴¹

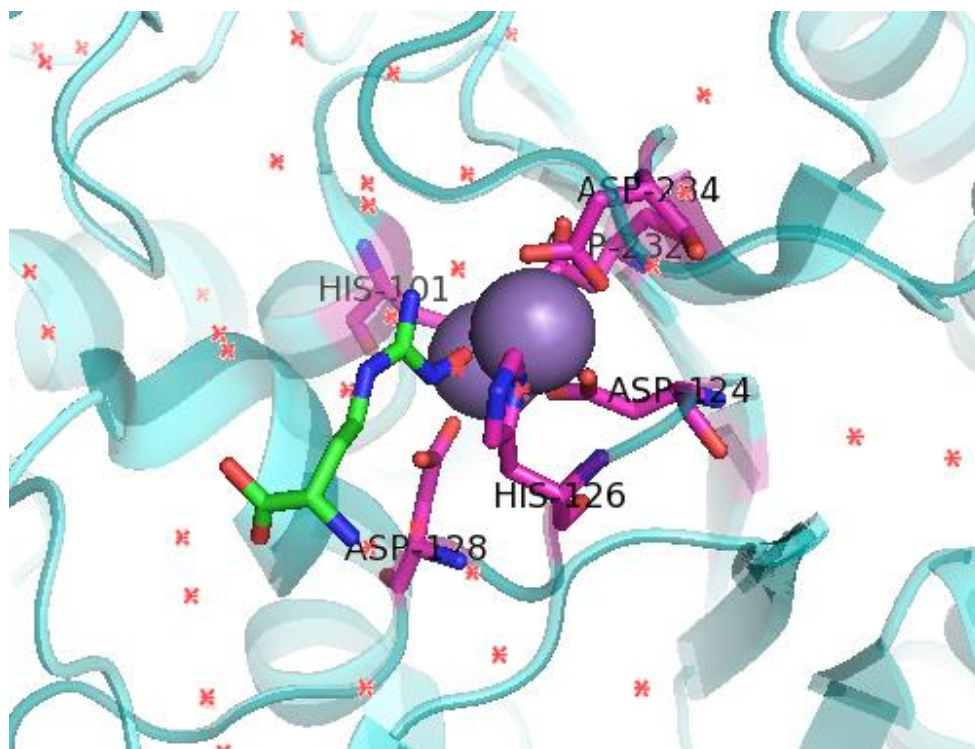


Figure 1.33: Crystal structure (PDB: 3kv2)¹⁶² of *N*-hydroxy-nor-L-arginine (green) bound to human arginase I (cyan). The active site consists of four aspartic acid residues and two histidine residues (magenta) coordinated to two Mn^{2+} (steel blue). The *N*-hydroxyl group (oxygen in red and nitrogen in blue) of *N*-hydroxy-nor-L-arginine completes the coordination sphere of Mn^{2+} to inhibit enzyme activity.

The arginase active site of arginase I and II are nearly identical and consist of four aspartic acid residues (Asp 124, Asp 128, Asp 232 and Asp 234) and two histidine residues (His 101 and His 126) coordinated to two Mn^{2+} . Several water molecules are also present in the active site and are used to complete an octahedral coordination sphere for each Mn^{2+} . The active site is relatively small and highly hydrophilic which is why most arginase inhibitors are an analog of L-arginine. These inhibitors must mimic the trigonal planar geometry of L-arginine to properly fit in the active site and will benefit from interactions with at least three water molecules, Asp 128 and a nearby asparagine. It may be possible to add functionalities to the

backbone of the inhibitor to form contacts with other water molecules and/or a nearby, non-coordinating histidine and aspartic acid. Structure based drug design efforts are currently being made with BEC as a scaffold to identify positions that are amenable to substitution to improve inhibitory activity.¹⁶³⁻¹⁶⁴ X-ray crystallography evidence suggests the α position of the amino acid moiety may be substituted with a two-carbon chain tertiary amine to be in close contact with the aforementioned non-coordinating aspartic acid residue (Asp 181 for arginase I and Asp 200 for arginase II).¹⁶⁵ Unfortunately, the nearly identical active site of arginase I and II makes it seemingly impossible to generate selective inhibitors. However, tissue specific inhibitors could reduce universal arginase inhibition.

1.6 Development of Inhibitors Towards A Copper Metalloenzyme

Copper is the second most abundant transition metal used in biology next to iron.¹⁶⁶ It is also the third most used cell signal modulator after calcium and zinc.¹⁶⁷ In addition to cell signaling regulation, copper also is an essential cofactor for numerous redox enzymes.¹⁶⁸ These enzymes play critical roles in respiration, electron transfer, mitochondrial aerobic metabolism, biosynthesis of neurotransmitters and neuropeptides, antioxidant action, iron uptake, pigmentation, photosynthesis, cross linking of collagen, wound healing, epigenetic modification, tissue integrity, synaptic function, metastasis and cell growth.^{167, 169-170} Despite being essential to these numerous biological processes, whole body copper concentrations are estimated to be 10^{-15} M or less.¹³² However, copper exists in significantly higher concentrations in the blood (5-25 μ M)¹⁷¹ and neurons (100 μ M). The lower estimations of total body copper may be due to 95%

of copper being bound to proteins such as ceruloplasmin.¹⁷² Other areas of high copper content include the liver and the brain.¹⁷³

Copper exists in two oxidized states, with Cu^+ being more kinetically labile and favored in the cellular environment and Cu^{2+} being the primary extracellular state.^{170, 174} To be incorporated into proteins copper requires metallochaperones such as the ATPase Atx1 which incorporates two copper ions into tyrosinase.¹⁷⁵ Since Cu^+ is considered a “soft” acid it has a higher affinity towards “soft” bases such as thiols.¹⁷⁶ Copper containing proteins can be subdivided based on ligands, spectroscopic features and functions as well as number of groups copper ions.¹⁷⁷ Mononuclear copper proteins are divided into two classes: Type 1 and Type 2. Type 1 typically coordinate Cu^+ via histidine, cysteine and sometimes methionine in a trigonal pyramidal or distorted tetrahedral geometry. Type 2 coordinate Cu^+ with histidine, aspartic acid and sometimes tyrosine in a distorted tetragonal geometry. Dinuclear copper proteins are divided into two classes: Type 3 and Cu_A . Type 3 coordinate Cu^+ with histidine and sometimes tyrosine in a tetragonal geometry while Cu_A resemble Type 1 copper proteins. The last class of copper proteins, Cu_Z , is tetranuclear and coordinates copper with histidine and a sulfur ion.¹⁷⁸

1.6.1 Tyrosinase

Tyrosinase is a dinuclear copper metalloenzyme that is a member of the oxidase superfamily.¹⁷⁹ This enzyme can be found in bacteria, fungi, plants and animals.¹⁸⁰⁻¹⁸¹

Tyrosinase has two catalytic functions: the hydroxylation of monophenols and the oxidation of diphenols.¹⁸¹⁻¹⁸² These catalytic functions are directly related to the two copper ions and state of the active site.¹⁸³ The active site can exist in three states: oxy-tyrosinase, deoxy-tyrosinase and

met-tyrosinase. Oxy-tyrosinase is the state when molecular oxygen bridges the two copper ions. Here the copper ions are in the cupric (Cu^{2+}) state. The oxy-tyrosinase catalyzes the hydroxylation of a monophenol to a diphenol. After the hydroxylation the enzyme is converted to the deoxy state. Deoxy-tyrosinase is the reduced form of oxy-tyrosinase and therefore the copper ions are in the cuprous (Cu^+) state. Deoxy-tyrosinase can then bind molecular oxygen to regenerate the oxy state. Oxy-tyrosinase can also oxidize a diphenol to a quinone. After oxidation the enzyme is converted to the met state which resembles the oxy state but has a hydroxide bridge the two Cu^{2+} ions. Met-tyrosinase can also oxidize a diphenol to a quinone. After oxidation, met-tyrosinase is converted to deoxy-tyrosinase.¹⁸⁴

The most studied tyrosinase is mushroom tyrosinase because mushroom tyrosinase is cytosolic, can be purified and is commercially available while human tyrosinase is membrane bound and has yet to be purified.¹⁸⁵ Tyrosinases primarily contribute to pigmentation as part of melanin biosynthesis.¹⁸⁶ Inhibitors of tyrosinase are mostly used as cosmetic agents to treat hyperpigmentary disorders such as melasma, actinic and senile lentigines, ephelide and postinflammatory hyperpigmentation.¹⁸⁷⁻¹⁸⁸ Because tyrosinase in plants contributes to browning, tyrosinase inhibitors may also be used as food additives.¹⁸⁹ Despite the seemingly trivial functions of tyrosinase inhibitors, inhibition of melanin biosynthesis may have more clinical relevance. Fungi melanin has been linked to differentiation of reproductive organs and spore formation, virulence and tissue protection after injury.¹⁹⁰⁻¹⁹² Neuromelanin in the human brain could contribute to dopamine toxicity which may be associated with neurodegenerative diseases such as Parkinson's disease.¹⁹³ Tyrosinase is critical to melanin biosynthesis since it is the rate limiting step.¹⁸²⁻¹⁸³ Therefore, inhibition of tyrosinase and subsequently the inhibition of melanin biosynthesis may lead to treatments of fungal infections and Parkinson's disease.

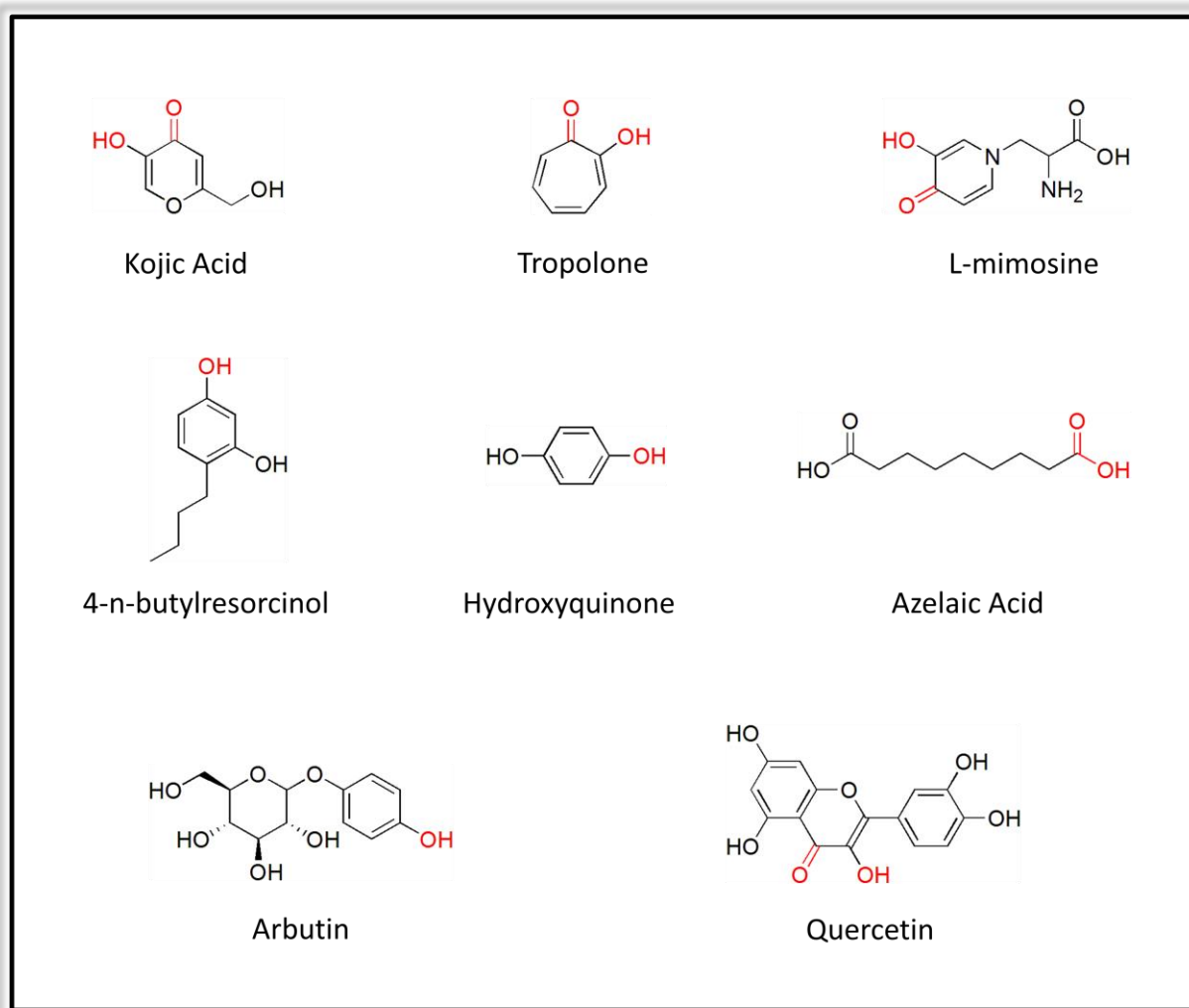


Figure 1.34: Inhibitors of tyrosinase that have been used or tested as topical treatments of hyperpigmentation. Metal binding group shown in red.

Currently, tyrosinase inhibitors are used for cosmetic purposes and as anti-browning food additives.¹⁸⁴ These inhibitors include hydroxyquinone, arbutin, kojic acid and azelaic acid. The “gold standard” of tyrosinase inhibitors is hydroxyquinone, which is used as a topical agent for skin whitening.¹⁸⁸ However, hydroxyquinone can be a skin irritant and may be carcinogenic.¹⁹⁴ Although it is still commonly sold in over-the-counter topical creams in the USA, hydroxyquinone is now banned from cosmetics in Europe and is under investigation by the

FDA.¹⁸⁸ Arbutin is considered to be safe, but is ineffective at the concentrations permitted in cosmetics.¹⁹⁵ While kojic acid is also considered to be safe and is generally used as a positive control when assessing tyrosinase inhibitors, it does not appear to coordinate the copper in the active site of tyrosinase despite its known chelation ability.¹⁹⁶ Azelaic acid is recommended as an alternative to hydroxyquinone and is used to treat melasma and post-inflammatory hyperpigmentation.¹⁹⁷ However, azelaic acid also exhibits antibacterial and anti-inflammatory attributes that are most likely not associated with tyrosinase inhibition.

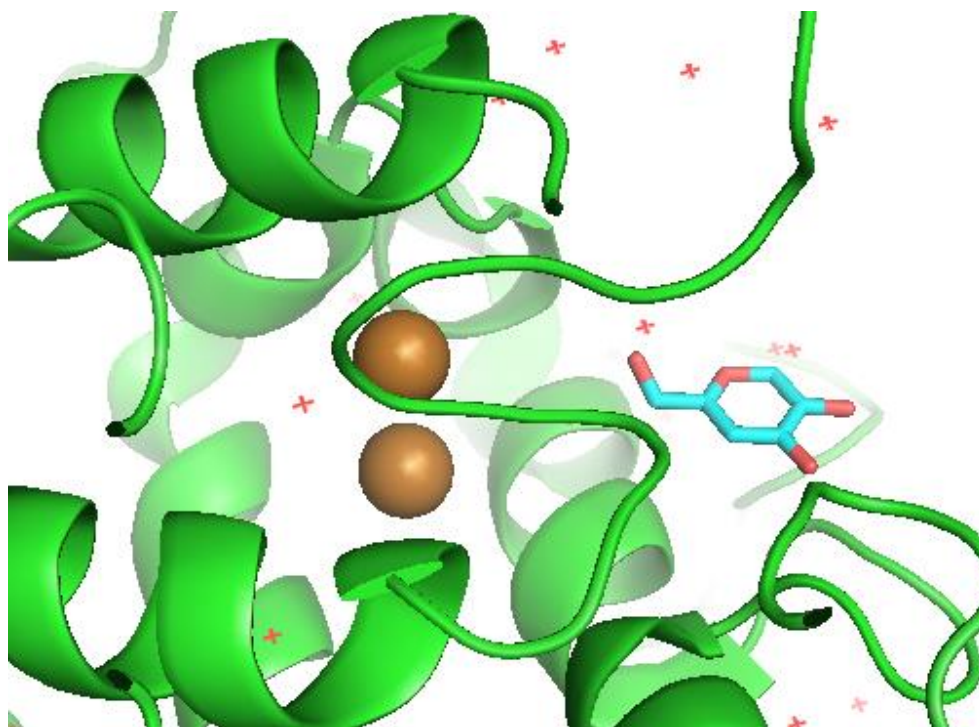


Figure 1.35: Crystal structure (PDB: 3nq1)¹⁹⁶ of kojic acid (cyan) bound to tyrosinase of *Bacillus megaterium* (green). The active site consists of two Cu^{2+} atoms (copper).

Other compounds commonly used as positive controls for tyrosinase inhibition include L-mimosine and tropolone.¹⁸⁴ L-mimosine is a substrate analog of tyrosine, utilizing a hydroxypyridone motif instead of a phenol. The 2-hydroxy-4-pyridone of L-mimosine is similar

to the alpha-hydroxy ketone of kojic acid and tropolone. However, L-mimosine is not a selective inhibitor. Reports indicate L-mimosine is capable of inhibiting DNA replication, causing cell cycle arrest in the G1 phase and inducing apoptosis through chelation of iron.¹⁹⁸⁻¹⁹⁹ As an iron chelator, L-mimosine has recently been linked to inhibition of PHD through coordination of Fe^{2+} in the active site.²⁰⁰ Tropolone is also known to strongly chelate metals, including Cu^{2+} of tyrosinase. The alpha-hydroxy ketone of tropolone coordinates with at least one of the copper atoms in the active site of tyrosinase. This alpha-hydroxy ketone motif is also found in flavanoids, such as quercetin, which also exhibit tyrosinase inhibitory activity. Although quercetin exhibits the highest inhibition activity of the flavonoids, it is a relatively weak inhibitor with only 20% of the inhibitory activity of kojic acid.¹⁸⁴ 4-n-butylresorcinol is another motif found in some flavonoids and has been tested as a topical treatment to reduce the appearance of age spots.²⁰¹⁻²⁰² Not only is 4-n-butylresorcinol a more potent tyrosinase inhibitor, it also exhibits strong effects on reducing the pigmentation of age spots, melasma and other forms of hyperpigmentation.¹⁸⁸

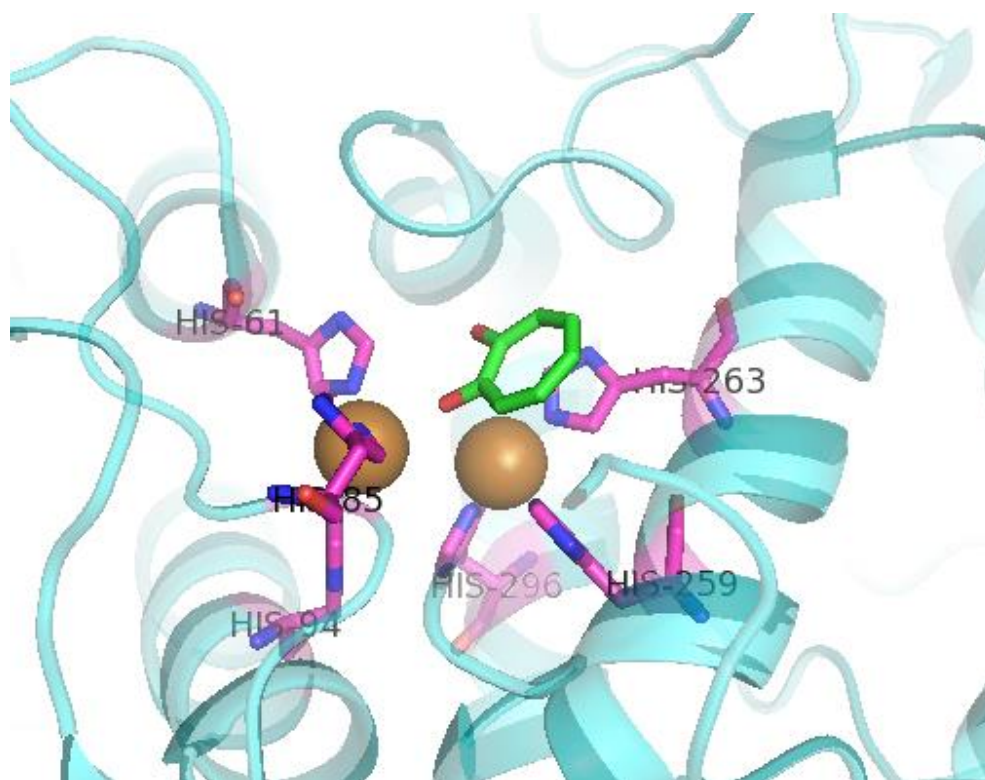


Figure 1.36: Crystal structure (PDB: 2y9x)²⁰³ of tropolone (green) bound to tyrosinase from *Agaricus bisporus* (cyan). The active site consists of six histidine residues (magenta) coordinated to two Cu^{2+} (copper). The alpha-hydroxy ketone (oxygen in red) of tropolone completes the coordination sphere of Cu^{2+} to inhibit enzyme activity.

The active site of mushroom tyrosinase consists of six histidine residues (His 61, His 85, His 94, His 259, His 263 and His 296) coordinated to two Cu^{2+} atoms. Several water molecules are also present in the active site (see Figure 1.35) and may be used in the coordination sphere for Cu^{2+} . The active site is solvent exposed but may be protected by a flexible loop region. Current inhibitors mimic either the monophenol or diphenol substrate and have the ability to coordinate Cu^{2+} in the active site. Due to the small size and relatively simplistic features of these inhibitors, most are not selective towards tyrosinase and may elicit adverse side effects. Additionally, these inhibitors have been developed towards the inhibition of mushroom tyrosinase. While mushroom tyrosinase exists as a cytosolic tetramer, human tyrosinase is a

highly glycosylated monomer which is membrane bound.¹⁸⁴ In order to develop tyrosinase inhibitors capable of treating Parkinson's more information about human tyrosinase is required. This includes kinetic activity and structural characterization of the enzyme. It may also be possible that tyrosinase of melanocytes is different from tyrosinase in the brain and nervous system, which may further be used to develop selective inhibitors.²⁰⁴ Additionally, inhibitors of specific states of tyrosinase (ie. deoxy-tyrosinase) may provide greater selectivity and potency.

1.7 Properties of Common Metal Binding Groups

Chelation is the bonding of ions to metal ions to form a ring-shaped complex and involves the formation of dipolar or coordinate bonds between an organic ligand and a metal atom.²⁰⁵ The organic ligand involved typically utilizes the atoms O, N, S and P to form the coordinate bonds. These organic motifs are referred to as metal binding groups. Metal binding groups can be optimized by size (number of atoms in ring-shaped complex), acidity, number of metal binding groups available, composition (types of atoms and monodentate or bidentate coordination) and relative geometry of coordinating atoms.³ The most common metal binding groups utilized by inhibitors are hydroxamates, carboxylates, phosphonates/phosphates, sulfonamides and thiols.²⁰⁶⁻²⁰⁷ Metalloenzyme inhibitors typically contain a moiety that mimics the natural substrate in addition to these metal binding groups to provide specificity.² However, this may not be enough as many metalloenzymes utilize structurally similar substrates.³ To overcome this issue, one must take into account the local environment of the enzyme as it can play a significant role in the overall binding of the ligand and the metal.²⁰⁸ Additionally, binding

of the inhibitor leads to conformational changes in the active site geometry and these changes should mimic the natural conformational change of the enzyme bound to the native ligand.²⁰⁹

While many clinical inhibitors of metalloenzymes aim to mimic the natural substrate and are designed to maximize interactions within the local environment, many of these inhibitors have poor pharmacokinetic properties, including low oral bioavailability and poor metabolic stability.³ Pro-drug forms have been able to overcome some of these limitations, but there is still a need to better understand how the chemical scaffold may affect the metal binding group and how the metal binding group affects both the metal and the metal-protein interaction.³ For example, most metalloenzymes are zinc based and show high affinity towards sulfur or nitrogen based ligands, but many zinc metalloenzyme inhibitors utilize carboxylic acid as the metal binding group.²⁰⁷ Although this is somewhat misleading since most hydroxamates fail clinical trials and many thiol based inhibitors exhibit poor side effects, this still expresses the need to develop inhibitors with metal binding groups designed for both the metal and the enzyme. Designing inhibitors that balance these interactions may provide better selectivity and biocompatibility.³

1.7.1 Hydroxamates

Hydroxamates are among the most commonly used metal binding groups due to their presence in natural products. Among these natural products are bacterial siderophores. Siderophores are small molecules synthesized by bacteria in response to low levels of iron. Bacteria then utilize the siderophores to sequester iron. The iron-siderophore complex can then be recognized by receptors on the cell wall and actively transported across the membrane to

release iron into the cytoplasm.²¹⁰ While hydroxamates tend to favor chelation of Fe^{2+} , Fe^{3+} or Cu^{2+} , they exhibit good affinity towards first row transition metal ions as well as Mg^{2+} .²⁻³ Chelation of these metals is almost always in a bidentate fashion to form five membered chelate rings. The only instances of monodentate binding of hydroxamates appear in the zinc metalloenzymes carbonic anhydrase and HDAC 4.³

Although hydroxamates are easy to prepare and hydroxamate based inhibitors are typically highly potent in both *in vitro* and *in vivo* experiments, they have only had moderate success in clinical trials.³ One potential reason for their poor clinical success is that most hydroxamate inhibitors have been designed for zinc metalloenzymes. However, hydroxamates exhibit 10^6 - 10^{11} fold greater affinity towards Fe^{3+} than Zn^{2+} .³³ This may explain their weak inhibitory activity towards carbonic anhydrases as well as their lack of selectivity towards many zinc metalloenzymes.^{24,211} Additionally, hydroxamates tend to have poor oral bioavailability, exhibit toxicity due to poor selectivity and have short metabolic half-lives.²⁵ Hydroxamates can readily be hydrolyzed to hydroxylamine and carboxylic acid, are highly prone to glucuronidation and may be oxidized to an acyl nitroso group.^{3,212} Acyl nitroso formation may also lead to formation of reactive oxygen species and oxidative stress.²¹² All of these issues have lead researchers to explore non-hydroxamate and hydroxamate derivatives as potential metal binding groups in order to maintain high metal affinity while reducing metabolic problems.

1.7.2 Carboxylates

The carboxylates aspartic acid and glutamic acid are the most commonly used natural metal binding groups in metalloenzymes to coordinate metal ions.³ While cysteine and histidine

residues are also very common in metalloenzyme metal coordinating motifs, carboxylates are more suitable towards the synthesis of inhibitors. Not only are a wide variety of carboxylic acids commercially available but they can also be readily prepared through a number of well established synthetic methods. In addition to being easily prepared, carboxylic acids are also easy to store and are relatively simple to handle.²¹³ Carboxylic acids may coordinate metal ions in a monodentate or bidentate fashion. The most common coordination is *syn*-monodentate, where both oxygen atoms are oriented towards the metal ion. *Anti*-monodentate, where only one oxygen atom is oriented towards the metal ion, and bidentate coordination are possible but not very common.³ This is most likely due to the unfavorable angle and coordination ring formation of bidentate coordination and the resonance stability of the carboxylate which would suggest a preference for *syn*-monodentate coordination.

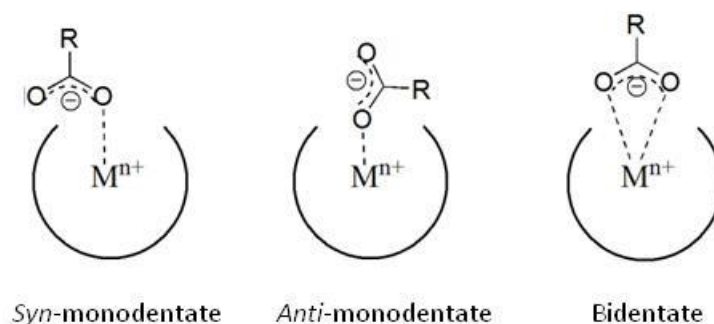


Figure 1.37: Metal coordination modes of carboxylates.

Because carboxylates typically coordinate metals in a monodentate fashion their coordination bonds are generally weaker than those of hydroxamates. As a result, carboxylates tend to coordinate divalent cationic metals.³ A survey of metalloenzymes in the Protein Data Bank (PDB) shows approximately 30% of ligands bound to Zn²⁺ are carboxylates.²⁰⁷ Despite the relatively weaker metal binding of carboxylates compared to hydroxamates, carboxylates exhibit

better bioavailability, are more metabolically stable, and may provide better mimetics for enzyme inhibition.²¹⁴

1.7.3 Phosphonates/Phosphates

Phosphonates and phosphates are generally used as zinc binding groups, with as many examples of phosphonate/phosphate zinc binding ligands found in the PDB as hydroxamate ligands.²⁰⁷ The first natural product inhibitor containing a phosphate was discovered in the 1970s. As a potent inhibitor of zinc dependent proteases, this phosphate based inhibitor led to the development of the ACE inhibitor Monopril.³ Other studies have shown the replacement of a cleavable peptide carbonyl with a phosphate will produce a competitive inhibitor.³ However, phosphate inhibitors are highly charged molecules which critically limits oral bioavailability as well as drastically increases renal clearance.²¹⁵ Phosphonate inhibitors display moderate bioavailability, but similar to phosphate inhibitors suffer from rapid renal clearance.²

Despite the drawbacks of phosphonate/phosphate as a metal binding group, the phosphorus atom is known to conform to a tetrahedral geometry, making it an ideal and stable analog to tetrahedral intermediates formed by hydrolases.³ The tetrahedral geometry of phosphorus favors asymmetric monodentate coordination of metal ions over bidentate coordination. Similar to carboxylates, the preference for monodentate over bidentate coordination reduces phosphorus based inhibitor potency 100-2000 fold compared to identical hydroxamate inhibitors.²⁰⁹ However, phosphonates are known to be tight binding chelators capable of binding divalent and trivalent metal ions. Additionally, phosphonates are stable under harsh conditions, making them acceptable alternatives to hydroxamates.²¹⁶

1.7.4 Sulfonamides/Sulfamides/Sulfamates

Sulfonamides, sulfamides and sulfamates are similar to phosphonates/phosphates/carboxylates in that they bind metals in a predominately monodentate fashion.²⁰⁷ However, sulfonamides, sulfamides and sulfamates are considered to be more desirable because they are more stable in water, are net neutral, and can enhance water solubility and bioavailability.^{215, 218} This class of metal binding groups show high affinity towards zinc and have been found to efficiently coordinate zinc in the active site of enzymes.^{211, 217-218} In fact, sulfonamides are the second most commonly found zinc binding ligands in the PDB.²⁰⁷ Classically, sulfonamides, sulfamides and sulfamates have been used as inhibitors of carbonic anhydrases with low nanomolar potency.²¹⁷⁻²¹⁸ These carbonic anhydrase inhibitors can be primary sulfamides, primary sulfonamides and aromatic or heterocyclic sulfonamides and sulfamates.^{16, 217-218} Additionally, substituted sulfamides can inhibit proteases including: aspartic proteases (HIV-1 protease and γ -secretase), serine proteases (elastase, chymase, tryptase, thrombin, etc.) and metalloproteases (carboxypeptidase A and MMP).²¹⁸ In HIV-1 protease, cyclic sulfamides are able to replace a catalytically active and essential water molecule and interact with a metal coordinating aspartic acid residue to enhance enzyme affinity and potency. Although this class of metal binding groups appears to be promiscuous, they display a much higher affinity towards carbonic anhydrases than MMPs despite identical zinc coordination motifs.²¹⁹⁻²²⁰ This explains why most clinically tested and approved sulfonamides sulfamides and sulfamates are carbonic anhydrase inhibitors.

1.7.5 Thiols

Although thiols are used in both synthetic and biological coordination of metal ions, free thiols are known to have poor pharmacokinetic properties. Most importantly, free thiols are known to form disulfide bonds with cysteine residues which lead to off-target protein binding and toxic side effects.³ However, thiol binds metal ions stronger than carboxylates and is considered to be a relatively potent zinc binding group.²⁵ The strong zinc binding of thiol led to the discovery of Captopril. While Captopril is the only FDA approved free thiol containing inhibitor, considerable efforts are being made to develop pro-drug formulated thiols.²⁵ Romidepsin, despite not being a synthetic inhibitor, is considered a pro-drug form since the disulfide bond can be reduced within the cellular environment to release a free thiol which has been found to coordinate zinc in HDAC.²²¹ Thioacetate pro-drug forms have also been explored with ST7612AA1 advancing to pre-clinical studies against HDAC.²²²

1.7.6 Other Metal Binding Groups

Since many of the classical metal binding groups have limitations in metal affinity, metal binding strength and pharmacokinetic properties, there has been increased focus on developing new metal binding groups. Initial attempts at developing second generation metal binding groups focused on hydroxamate analogs. These analogs include reverse hydroxamates, *N*-substituted hydroxamic acids and *N*-hydroxyureas. Each was developed with the aim of increasing stability and improving target specificity.³ The reverse hydroxamates are more stable than their respective hydroxamates with longer metabolic half lives due to lower susceptibility towards hydrolysis.³ However, similar to hydroxamates, the reverse hydroxamates can only be functionalized in one direction. This limited functionalization potential is overcome by the *N*-

substituted hydroxamates. While the *N*-substituted hydroxamates offer the development of more specialized inhibitors which should increase selectivity, many exhibit a 10-fold decrease in potency towards the zinc metalloenzyme families MMP and ADAM.³ Despite this drawback, the *N*-substituted hydroxamates do not suffer from loss in potency towards PDF and several have been found to be potent inhibitors of LTA4H and fructose biphosphate aldolase.³ *N*-hydroxyureas, such as Zileuton, are similar to hydroxamates, but may be bifunctionalized similar to the *N*-substituted hydroxamates.³

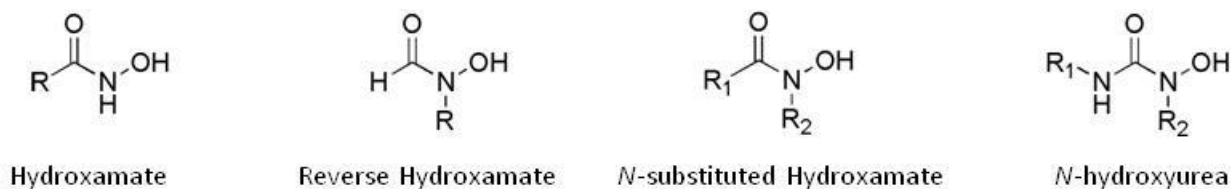


Figure 1.38: Hydroxamates and hydroxamate derivatives as metal binding groups.

Another major class of second generation metal binding groups consists of derivatives of carboxylates. Although carboxylates are typically less potent than their respective hydroxamates, the carboxylates exhibit less pharmacokinetic liabilities. The primary carboxylate derivatives being studied are alpha keto acids, alpha hydroxy acids and picolinic acids. Each of these metal binding groups adds a donor atom alpha to the carboxylic acid which accommodates for the formation of a 5-membered chelate ring instead of the 4-membered chelate ring of carboxylates.³ The alpha keto acids are based on the biological compound α -ketoglutarate which is a key intermediate of the Krebs cycle and is a cofactor of iron dependent oxygenases.³ Alpha keto acids bind metals in a bidentate fashion, as evidenced by the crystal structure of *N*-oxalylglycine bound to prolyl hydroxylase.²²³ Additionally, the alpha keto acids have an amide bond for resonance stabilization.³ Unfortunately, because α -ketoglutarate is used in many

metabolic cycles, it is possible that the alpha keto acids may metabolize too quickly.³ To avoid this, the alpha ketone may be converted to an alcohol to decrease susceptibility to nucleophilic attack. These alpha hydroxy acids utilize the same donor atom as the alpha keto acids but have a different geometry due to the sp^3 hybridized carbon.³ Picolinic acids are also bind metals such as zinc, manganese, copper, iron and molybdenum in a bidentate fashion.²²⁴ Since picolinic acid is a metabolite of tryptophan and a precursor of NAD^+ , it is a well studied functionality.²²⁴ Inhibitors utilizing picolinic acid are primarily inhibitors of iron dependent oxygenases, but have also been found used as inhibitors of zinc β -metallolactamases.³

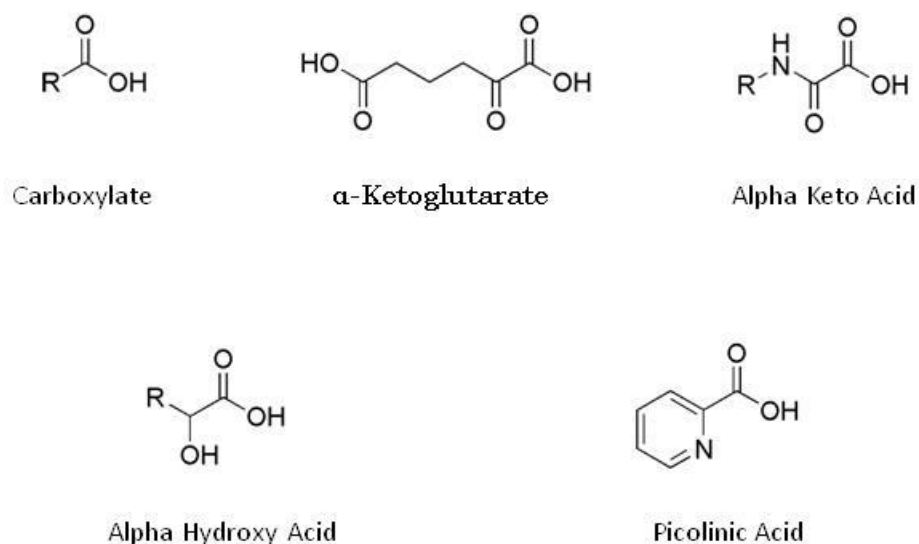


Figure 1.39: Carboxylate and carboxylate derivatives as metal binding groups.

Thiol derivatives are also being developed as metal binding groups. These derivatives attempt to harness the strong monodentate metal binding of the thiol sulfur atom while avoiding the promiscuity and toxic side effects associated with thiol. One type of derivative focuses on replacing the oxygen of a carbonyl with sulfur.³ The most promising of these thiones is the dithiocarbamates. Dithiocarbamates have a lower reduction potential and may be more

biocompatible compared to thiols and have the ability to bind metals in a bidentate fashion. Interestingly, some of these dithiocarbamates appear to function as immunosuppressants.²²⁵ Another class of thiol derivatives being explored is beta mercaptoketone. Beta mercaptoketones bind metals in a bidentate fashion to form a 5-membered chelate ring.³ While this may allow for the development of inhibitors with better potency and selectivity, beta mercaptoketones display a free thiol which may illicit similar toxic side effects of thiols due to off target binding.³

Other metal binding groups explored can be subdivided into monodentate chelators, bidentate chelators and tetrahedral intermediate mimics. The monodentate metal binding groups include amines, alcohols, carbonyls, nitrogen containing heterocycles and oximes. Although these groups all rely on nitrogen or oxygen atoms which are weaker chelators than sulfur, they typically present less pharmacokinetic liabilities. The amine metal binding groups generally do not utilize primary amines, and in many cases utilize the amine in combination with another monodentate metal binding group. However, terminal amines of peptide mimetics have been used as metal chelating groups.³ Similar to the amines, alcohols as metal chelating groups are generally not primary alcohols and many alcohol bearing inhibitors are phenols due to their known metal binding potential.²²⁶ The carbonyls may be part of ketones, amides, urea, or sulfoxides.²⁰⁷ Carbonyls of amides and ureas have better resonance while carbonyls of sulfoxides are polar. Both of these properties can increase the metal binding strength of the oxygen.³ Another way to enhance the nucleophilicity of the carbonyl oxygen is to create an alpha nitromethyl ketone.²²⁷ The nitrogen containing heterocycle nitrogen atom functions as an imine to form a monodentate bond with the metal atom. Potent examples of this class include triazole, imidazole, pyrazole, uridine, pyridine, hydantoin and barbiturate.^{3, 33, 207, 228} Although several of these functional groups are structurally related they appear to show some selectivity

towards isoforms or a certain class of TACE and MMP.^{3, 33} Oximes have been used to develop therapeutic agents capable of transferring acyl groups and are amenable to biotransformation as well as conjugation with both organic and inorganic molecules.²²⁹ Some furan oximes have already been developed which inhibit DNA, RNA and protein synthesis in lipid leukemia cells while quinoline oximes have exhibited antitumor activity.²³⁰⁻²³² Additionally, oximes form stable complexes with metals such as platinum, copper and manganese.²³³⁻²³⁴ While oximes are monodentate chelators, they may be used alpha to a carbonyl to create a bidentate chelator similar to a hydroxamate.²²⁹

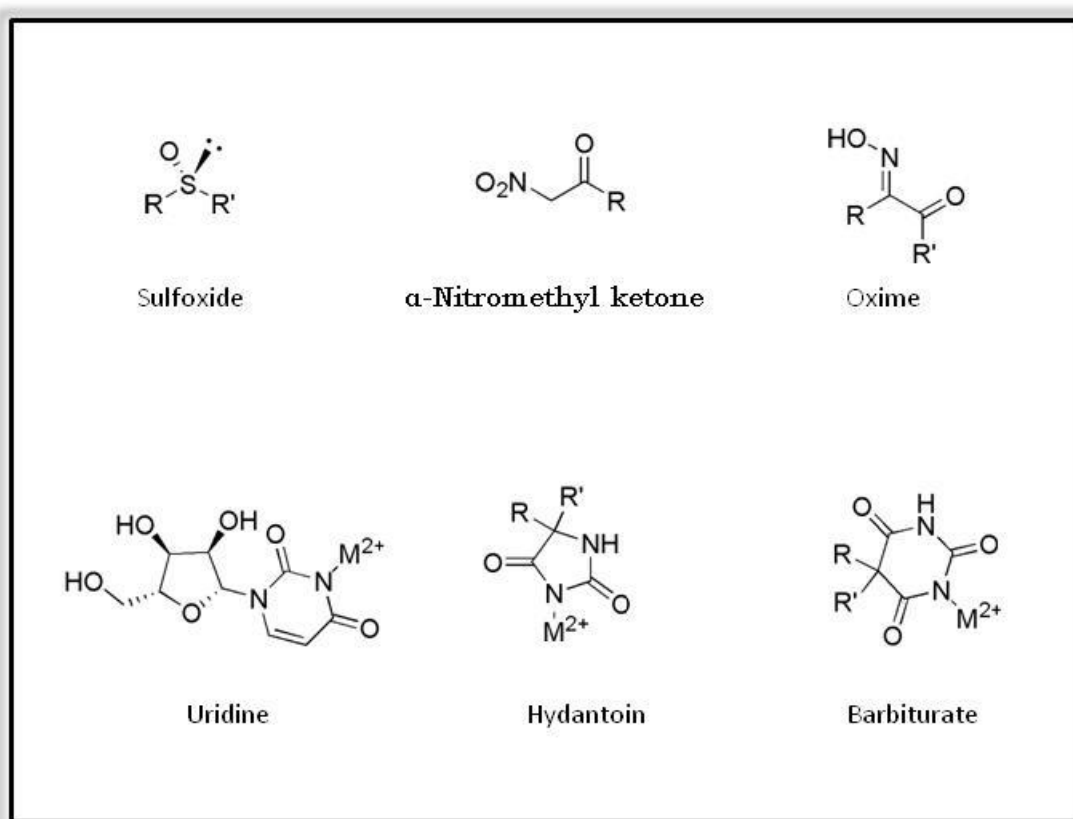


Figure 1.40: New monodentate metal binding groups being explored.

Bidentate metal binding groups being explored include benzamide, 3-hydroxypyridin-2-thione, curcumin, bipyridine, pyrazolylpyridine, 8-hydroxyquinoline and bis-benzimidazol type functional groups. Although benzamide itself is only a monodentate metal binding group, this bidentate metal binding group more accurately refers to *N*-(2-amino-phenyl)-benzamide. Benzamide as a metal binding group is not very common, but have been used to develop the potent HDAC inhibitors Entinostat and Mocetinostat. The bidentate coordination involves the amine on the phenyl ring and the carbonyl of the benzamide to form a trigonal bipyramidal, seven-membered chelate ring.³ Despite aromatic amines not being very nucleophilic, metal coordination with the carbonyl may position the amine to enhance its anionic character.³ 3-hydroxypyridin-2-thione was selected as a novel heterocyclic bidentate metal binding group through a fragment based approach using reported zinc chelation and affinity as well as known ease of synthetic modification.²³⁵ Interestingly, this metal binding group is capable of selectively inhibiting HDAC 6 and 8 and does not exhibit inhibition of HDAC 1. Modifications of 3-hydroxypyridin-2-thione enhance selectivity and cause induction of apoptosis in several cancer cell lines.²³⁵ The bidentate coordination of this group involves the thione and the alpha hydroxyl; similar to the coordination exhibited by hydroxypyrones (ie. kojic acid) and hydroxypyridinones. These heterocyclic bidentate metal binding groups are stronger chelators than their monodentate analogs and are more resistant to hydrolysis.²³⁶ Another anti-cancer, bidentate, metal binding group being explored is curcumin. Curcumin is known to mediate multiple signaling pathways and was discovered to be capable of destabilizing the formation of β -amyloid fibrils associated with Alzheimer's disease.²³⁷⁻²³⁹ Unfortunately curcumin exhibits poor water solubility which leads to poor bioavailability and suffers from rapid metabolism.²⁴⁰ Due to these poor pharmacokinetic properties researchers have focused on developing

“supercurcumins” with a variety of formulations to improve solubility, stability and bioactivity.²⁴⁰ Metal chelation and metal complexes of curcumin have also been studied. Iron-curcumin complexes have displayed the highest potential to treat cancer while gallium complexes exhibit antiviral activity.²⁴¹⁻²⁴² Additionally, copper chelation appears to be involved in many of the anti-cancer properties associated with curcumin.²⁴³ While most metal binding group development has been focused on natural products, some have turned to metal binding groups commonly used in inorganic chemistry.³ These groups include 2,2'-bipyridine, 2-pyrazolylpyridine and 8-hydroxyquinoline. Interestingly, these metal binding groups have primarily been used as mimics of α -ketoglutarate.³ Bis-benzimidazol type groups are similar to the inorganic metal binding groups in that they utilize two known monodentate metal binding groups tethered together in a proper orientation to create a bidentate metal binding group. Benzimidazole is found in nature as part of *N*-ribosyl-dimethylbenzimidazole which coordinates cobalt in vitamin B₁₂.²⁴⁴ The bis-benzimidazol groups have been found to be potent inhibitors of viruses such as rhinovirus, poliovirus and coxsackievirus, target the minor groove of B-DNA, and be effective metal binding groups of Zn²⁺, Mn²⁺, Sc³⁺ and Hg²⁺ for the inhibition of trypsin and zinc-mediated serine proteases.²⁴⁵⁻²⁴⁸

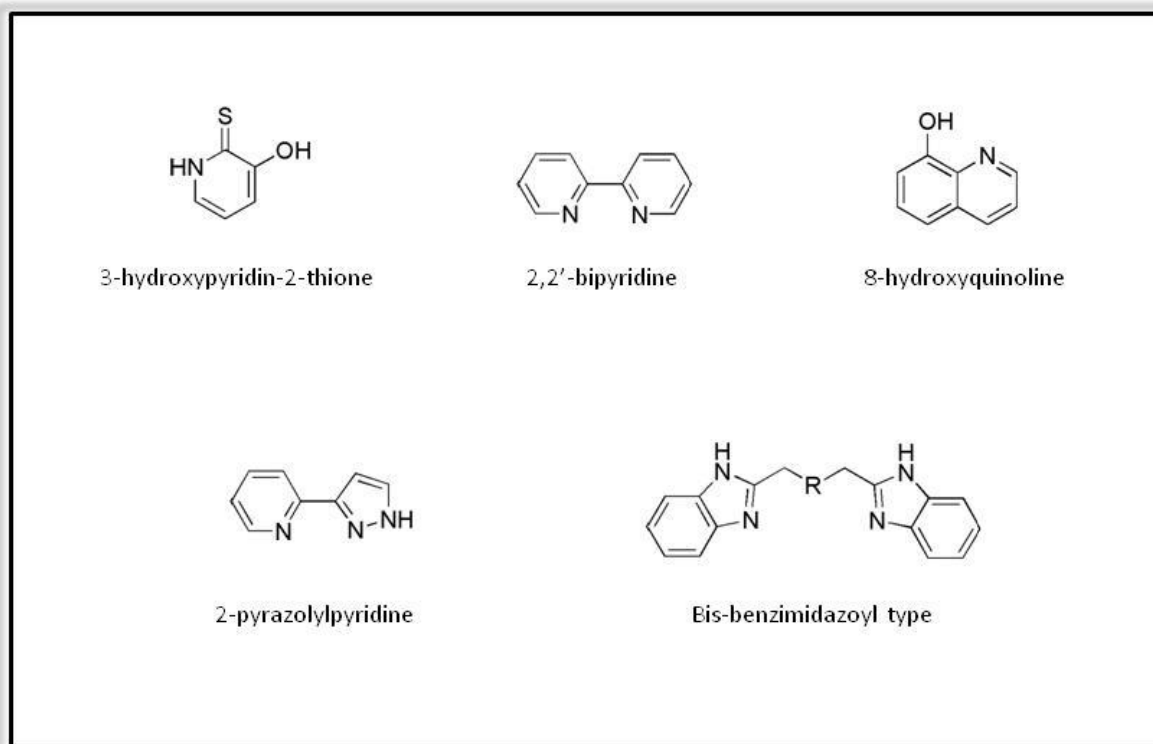


Figure 1.41: New bidentate metal binding groups being explored.

Tetrahedral intermediate mimics may be mono- or bidentate metal binding groups, but form tetrahedral complexes when coordinated to a metal ion. This class of metal binding groups includes silanediols, geminal diols and boronic acids. Silanediols use silicon to generate a stable tetrahedral structure with two hydroxyls. This tetrahedral structure is similar in size and shape to phosphates, but is less acidic.³ Typically they are used to make peptidomimetics by replacing a carbonyl in a peptide backbone. Silanediol peptidomimetics are potent protease inhibitors.²⁴⁹ Currently silanediols have been used as inhibitors of chymotrypsin, thermolysin, ACE and HIV protease.²⁵⁰⁻²⁵³ Geminal diols are similar to the silanediols but with a central carbon atom instead of a silicon atom. As with the silanediols, geminal diols are similar to phosphates in that they bind metals in an asymmetric monodentate fashion and mimic the native tetrahedral intermediate catalyzed by the enzyme. The geminal diols appear to best mimic the intermediates of

hydrolases.³ Boronic acids also mimic the tetrahedral intermediate of hydrolases and have been found to inhibit fatty acid amide hydrolase.²⁵⁴ Additionally, the boronic acids have been found to inhibit many enzymes which are involved in fundamental biological processes such as arginase, serine proteases and the proteasome.²⁵⁵⁻²⁵⁷ One potential drawback to boronic acids as a metal binding group is that the boron atom can covalently bind to serine.³

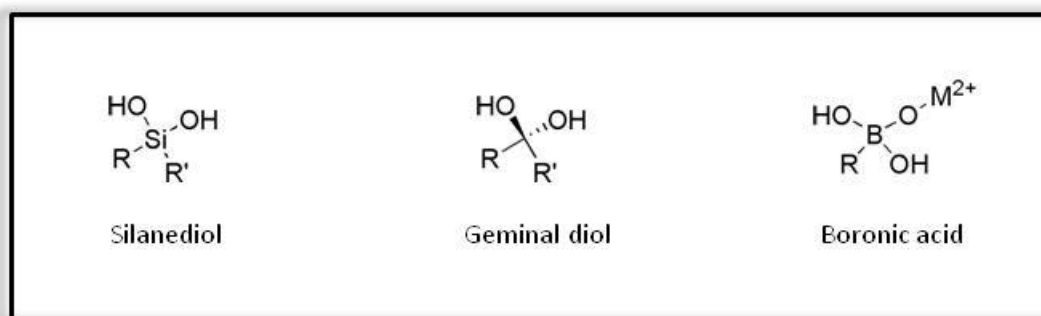


Figure 1.42: New tetrahedral metal binding groups being explored.

Although there are many examples of known metal binding groups, little research has been done to determine how these groups influence selectivity or if weak metal binding groups can be enhanced by maximizing other interactions with the target protein.³ While newer metal binding groups are still being explored (ie. squaric acid, hydroxymethyl oxazoline and 1-hydroxy-2-sulfanyl pyridinium), more information about the interplay between metal-ligand and protein-ligand interactions is essential.^{207, 258} Future research may benefit from combining both a synthetic and structural approach when exploring metal binding groups.³ Additionally, further investigation of the chemical space for new potential metal binding groups could lead to better selectivity and potency.

1.8 Tropolone as a Metal Binding Group

The tropolone motif is a unique cyclic structure which exhibits unusually high resonance energy, an unfavorable oxygen-oxygen distance making it an unusually strong acid and has the ability to form highly stable 5-membered chelate rings.²⁵⁹ Tropolone itself is soluble in both aqueous and organic solvents while tropolone-metal complexes are highly lipid soluble.²⁶⁰ Natural tropolones have low molecular weight, ample sites for diversification and strong metal coordinating potential as seen with both zinc and iron.²⁵⁹⁻²⁶⁰ Additionally, tropolone is known to act as a bidentate metal binding group where the cyclic structure may rigidify the compound to enhance metal affinity relative to a hydroxamate, making tropolone a potential alternative to hydroxamate.²⁶¹

One of the best studied and relatively simplistic natural tropolones, β -thujaplicin, is known to display a wide range of antiproliferative activity²⁶²⁻²⁶⁸ and is safely used in toothpaste, shampoo, cosmetics, hair tonic and as a food preservative in Japan and Russia.²⁶⁹⁻²⁷⁰ Most of this activity is likely due to or has been associated with metal chelation. Research has determined β -thujaplicin is capable of inhibiting many metalloenzymes, especially metalloproteases, with highest levels of activity exhibited against carboxypeptidase A.²⁷⁰ Other metalloprotease inhibited by β -thujaplicin include thermolysin and collagenase. Interestingly, α -thujaplicin does not inhibit thermolysin or collagenase, suggesting various substitutions around the tropolone ring may increase selectivity towards a metal ion or be used to develop enzyme selectivity.²⁷¹

A fragment based library approach to develop novel zinc binding groups determined tropolone displayed strong zinc binding potential.²⁰⁶ Subsequent studies with tropolone and β -thujaplicin determined the tropolone motif showed greater potency against the two zinc metalloenzymes MMP3 and anthrax lethal factor than acetohydroxamic acid (a benchmark for hydroxamate comparison).²⁶¹ The tropolone motif also displayed the strongest zinc binding

compared to the analogous cyclic, aromatic α -hydroxy ketones hydroxypyrrone and hydroxypyridinone. Another fragment based study determined β -thujaplicin binds to the zinc ion of CapF in *S. aureus* to alter the coordination sphere of zinc which destabilizes the enzyme.²⁷² Meanwhile, other studies have shown that β -thujaplicin can bind various heavy metal ions, most notably iron and zinc.²⁷³

As an iron chelator, β -thujaplicin coordinates Fe^{3+} in a 1:1 ratio to generate an oxygen radical.²⁷⁴ Eventually this leads to release of a superoxide radical and Fe^{2+} which can undergo the Fenton reaction with hydrogen peroxide to form a hydroxyl radical. This hydroxyl radical may be the cause of some of the antiproliferative effects associated with β -thujaplicin since a hydroxyl radical may attack membrane lipids, proteins and DNA molecules to exert antimicrobial and cytotoxic effects.²⁷⁴ Binding of β -thujaplicin to Fe^{3+} is also associated with DNA fragmentation and caspase-3 activation.^{264, 273} Interestingly, tropolone-iron complexes display high thermodynamic stability and a stronger binding constant than the transferrin-iron complex.²⁶⁰ This has led to the investigation for clinical use of tropolones as iron chelating agents. Development of tropolones as gram-negative antibacterial agents is based on the hypothesis that tropolones can chelate iron to deprive bacteria of this essential growth factor.²⁶⁹ It is known that small, lipophilic iron chelators inhibit protein and DNA synthesis in myeloid cell lines, which provides a reason to develop tropolones as anticancer agents.²⁷⁵ Additionally, β -thujaplicin and related compounds were found to inhibit the iron metalloenzyme ribonucleotide reductase which is used in DNA synthesis.²⁷⁰

Other biological effects of β -thujaplicin metal binding include the ability to extract Mg^{2+} from the inner mitochondrial compartment,²⁶² stimulation of superoxide formation through copper binding²⁷⁴ and inhibition of the copper metalloenzymes dopamine β -oxygenase²⁷⁶ and

tyrosinase.²⁷⁷ While β -thujaplicin is known to exhibit a wide range of biological activities with multiple potential mechanisms of action, it is generally considered to be a powerful, lipophilic chelator of divalent metal cations. Additionally, most of the biological activity of β -thujaplicin appears to be dependent on metal chelation. This is exemplified by the lack of inhibitory activity of acetylated tropolone and β -thujaplicin methyl ether against metalloproteases²⁷¹ and HDAC respectively.²⁷⁸ Although there has been some concern about the promiscuity of thujaplicins, α - β - and γ -thujaplicin display different activities and exhibit some enzyme selectivity. For example, α -thujaplicin does not appear to inhibit human tyrosinase ($>1000\ \mu\text{M}$) and is only moderately effective against mushroom tyrosinase ($9.53\ \mu\text{M}$) while β -thujaplicin and γ -thujaplicin are effective against human tyrosinase ($8.98\ \mu\text{M}$ and $1.15\ \mu\text{M}$ respectively) but are much more potent towards mushroom tyrosinase ($0.09\ \mu\text{M}$ and $0.07\ \mu\text{M}$ respectively).²⁷⁷ The thujaplicins and tropolone also display some metal binding preference with the highest affinity towards Fe^{3+} , Fe^{2+} and Cu^{2+} , moderate affinity towards Ni^{2+} , Zn^{2+} , Co^{2+} and Mn^{2+} and weaker affinity towards Mg^{2+} and Ca^{2+} .^{259, 279-280} Despite the strong metal binding activity of tropolones, there have been few attempts to utilize this structure as a metal binding group in drug discovery, most likely due to limited synthetic accessibility as a result of its unusual aromatic structure.

1.9 Conclusions

Metals such as calcium, magnesium, potassium, sodium, iron, zinc, cobalt and manganese are essential for most biological activity. In many instances, these metal ions are crucial cofactors for enzymatic reactions. A wide variety of metalloenzymes have been implicated in diseases such as bacterial infections, viral infections, immunological diseases,

neurological diseases and cancer. Targeting the catalytic metal ion of metalloenzymes offers the opportunity to develop new and selective therapeutics and has been a highly fruitful endeavor. Despite recent gains in understanding the function, structure and cellular localization of many metalloenzymes only a limited amount of the chemical space has been explored for metal binding groups. Hydroxamates, carboxylates, phosphates/phosphonates, sulfonamides/sulfamides/sulfamates and thiols are the primary metal binding groups found in clinically used metalloenzyme inhibitors. While each of these metal binding groups has inherent strengths and weakness, none have proven highly selective towards one metal. This has stressed the need to further explore the chemical space for different metal binding groups which may offer better selectivity as well as better potency and pharmacokinetic properties. Additionally, future research should also focus on understanding the interactions of the metal binding group with both the metal and the protein. Meanwhile, natural metal binding groups with known chelating properties offer biologically relevant scaffolds which may be functionalized to provide enzyme selectivity. One such natural metal binding group, tropolone, is a powerful chelating agent with attractive biological activity. Tropolone offers ample sites for diversification where minor changes can drastically alter enzyme inhibitory activity. Development and understanding of structural activity relationships of tropolone modifications may offer exciting new metalloenzyme inhibitors or an alternative metal binding motif for many hydroxamate inhibitors which have failed clinical trials.

1.10 References

1. Franz, K. J. Clawing back: broadening the notion of metal chelators in medicine. *Curr. Opin. Chem. Biol.* **2013**, 17, 143-149.
2. Zingle, C.; Kuntz, L.; Tritsch, D.; Grosdemange-Billiard, C.; Rohmer, M. Modifications around the hydroxamic acid chelating group of fosmidomycin an inhibitor of the metalloenzyme 1-deoxyxylulose 5-phosphate reductoisomerase (DXR). *Bioorg. Med. Chem. Lett.* **2012**, 22, 6563-6567.
3. Storr, T. *Ligand Design in Medicinal Inorganic Chemistry*. John Wiley & Sons Ltd.: United Kingdom, 2014.
4. Cook, S. A.; Hill, E. A.; Borovik, A. S. Lessons from Nature: A Bio-Inspired Approach to Molecular Design. *Biochemistry* **2015**, 24, 4167-4180.
5. Holm, R.; Kennepohl, P.; Solomon, E. I. Structural and Functional Aspects of Metal Sites in Biology. *Chem. Rev.* **1996**, 96, 2239-2314.
6. Rouffet, M.; Cohen, S. M. Emerging Trends in Metalloprotein Inhibition. *Dalton Trans.* **2011**, 40, (14), 3445-3454.
7. Chen, Y.; Cohen, S. M. Investigating the Selectivity of Metalloenzyme Inhibitors in the Presence of Competing Metalloproteins. *Chem. Med. Chem.* **2015**, 10, 1733-1738.
8. Day, J. A. Cohen, S. M. Investigating the Selectivity of Metalloenzyme Inhibitors. *J. Med. Chem.* **2013**, 56, (20), 7997-8007.
9. McCall, K. A.; Huang, C-c.; Fierke, C. A. Function and Mechanism of Zinc Metalloenzymes. *J. Nutr.* **2000**, 130, (5), 14375-14465.
10. Jacobsen, F. E.; Lewis, J. A.; Cohen, S. M. The Design of Inhibitors for Medicinally Relevant Metalloproteins. *Chem. Med. Chem.* **2007**, 2, 152-171.

11. Bertini, I.; Decaria, L.; Rosato, A. The annotation of full zinc proteomes. *J. Biol. Inorg. Chem.* **2010**, 15, 1071-1078.
12. Parkin, G. The Bioinorganic Chemistry of Zinc: Synthetic Analogues of Zinc Enzymes that Feature Tripodal Ligands. *Chem. Commun.* **2000**, 20, 1971-1985.
13. Lee, Y. M.; Lim, C. Physical basis of structural and catalytic Zn-binding sites in proteins. *J. Mol. Biol.* **2008**, 379, (3), 545-553.
14. Meldrum, N. U.; Roughton, F. J. W. Carbonic anhydrase. Its preparation and properties. *J. Physiol.* **1933**, 80, 113-142.
15. Imtaiyaz Hassan, M.; Shajee, B.; Waheed, A.; Ahmad, F.; Sly, W. S. Structure, function and applications of carbonic anhydrase isozymes. *Bioorg. Med. Chem.* **2013**, 21, (6), 1570-1582.
16. Moeker, J.; Mahon, B. P.; Bornaghi, L. F.; Vullo, D.; Supuran, C. T.; McKenna, R.; Poulsen, S-A. Structural Insights into Carbonic Anhydrase IX Isoform Specificity of Carbohydrate-Based Sulfamates. *J. Med. Chem.* **2014**, 57, 8635-8645.
17. Pinard, M. A.; Boone, C. D.; Rife, B. D.; Supuran, C. T.; McKenna, R. Structural study of interaction between brinzolamide and dorzolamide inhibition of human carbonic anhydrases. *Bioorg. Med. Chem.* **2013**, 21, 7210-7215.
18. www.fda.gov : USP Therapeutic Categories Model Guidelines; Carbonic Anhydrase Inhibitors
19. Supuran, C. T. Drug interaction considerations in the therapeutic use of carbonic anhydrase inhibitors. *Expert Opin. Drug Metab. Toxicol.* **2016**, 1-9 [Epub ahead of print].

20. Piepho, R. W. Overview of the angiotensin-converting-enzyme inhibitors. *Am. J. Health-Syst. Pharm.* **2000**, 57, (S1), S3-S7.
21. Brown, N. J.; Vaughan, D. E. Angiotensin converting enzyme inhibitors. *Circulation* **1998**, 97, 1411-1420.
22. Corradi, H. R.; Schwager, S. L. U.; Nchinda, A. T.; Sturrock, E. D.; Acharya, K. R. Crystal Structure of the N Domain of Human Somatic Angiotensin I-Converting Enzyme Provides a Structural Basis for Domain-Specific Inhibitor Design. *J. Mol. Biol.* **2006**, 357, (3), 964-974.
23. Gong, Y.; Chippada-Venkata, U. D.; Oh, W. K. Roles of Matrix Metalloproteinases and Their Natural Inhibitors in Prostate Cancer Progression. *Cancers* **2014**, 6, 1298-1327.
24. Agrawal, A.; Romero-Perez, D.; Jacobsen, J. A.; Villarreal, F. J.; Cohen, S. M. Zinc-Binding Groups Modulate Selective Inhibition of MMPs. *Chem. Med. Chem.* **2008**, 3, 812-820.
25. Shen, S.; Kozikowski, A. P. Why Hydroxamates May Not Be the Best Histone Deacetylase Inhibitors – What Some May Have Forgotten or Would Rather Forget? *Chem. Med. Chem.* **2016**, 11, 15-21.
26. Caton, J.; Ryan, M. E. Clinical studies on the management of periodontal diseases utilizing subantimicrobial dose doxycycline (SDD). *Pharmacol. Res.* **2011**, 63, 114-120.
27. Castelhana, A. L.; Billedeau, R.; Dewdney, N.; Donnelly, S.; Horne, S.; Kurz, L. J.; Liak, T. J.; Martin, R.; Uppington, R.; Yuan, Z.; Krantz, A. Novel indolactam-based inhibitors of matrix metalloproteinases. *Bioorg. Med. Chem. Lett.* **1995**, 5, (13), 1415-1420.

28. Grams, F.; Crimmin, M.; Hinnes, L.; Huxley, P.; Pieper, M.; Tschesche, H.; Bode, W. Structure determination and analysis of human neutrophil collagenase complexed with a hydroxamate inhibitor. *Biochemistry* **1995**, 34, 14012-14020.
29. Rothenberg, M. L.; Nelson, A. R.; Hande, K. R. New Drugs on the Horizon: Matrix Metalloproteinase Inhibitors. *Stem Cells* **1999**, 17, (4), 237-240.
30. Murphy, G. Tissue inhibitors of metalloproteinases. *Genome Biol.* **2011**, 12, (11), 233.
31. DasGupta, S.; Murumkar, P. R.; Giridhar, R.; Yadav, M. R. Current perspective of TACE inhibitors: A review. *Bioorg. Med. Chem.* **2009**, 17, 444-459.
32. Moss, M. L.; Sklair-Tavron, L.; Nudelman, R. Drug Insight: tumor necrosis factor converting enzyme as a pharmaceutical target for rheumatoid arthritis. *Nat. Clin. Pract. Rheumatol.* **2008**, 4, (6), 300-309.
33. Sheppeck II, J. E.; Gilmore, J. L.; Tebben, A.; Xue, C-B.; Liu, R-Q.; Decicco, C. P.; Duan, J. J.-W. Hydantoins, triazolones, and imidazolones as selective non-hydroxamate inhibitors of tumor necrosis factor- α converting enzyme (TACE). *Bioorg. Med. Chem. Lett.* **2007**, 17, 2769-2774.
34. Levin, J. I.; Chen, J. M.; Laakso, L. M.; Du, M.; Du, X.; Venkatesan, A. M.; Sandanayaka, V.; Zask, A.; Xu, J.; Xu, W.; Zhang, Y.; Skotnicki, J. S. Acetylenic TACE inhibitors. Part 2: SAR of six-membered cyclic sulfonamide hydroxamates. *Bioorg. Med. Chem. Lett.* **2005**, 15, 4345-4349.
35. Murumkar, P. R.; DasGupta, S.; Chandani, S. R.; Giridhar, R.; Yadav, M. R. Novel TACE inhibitors in drug discovery: a review of patented compounds. *Expert Opin. Ther. Patents* **2010**, 20, (1), 31-57.

36. Balasubramanian, S.; Verner, E.; Buggy, J. J. Isoform-specific histone deacetylase inhibitors: The next step? *Cancer Letters* **2009**, 280, 211-221.
37. www.fda.gov : histone deacetylase inhibitor
38. Paris, M.; Porcelloni, M.; Binaschi, M.; Fattori, D. Histone Deacetylase Inhibitors: From Bench to Clinic. *J. Med. Chem.* **2008**, 51, (6), 1505-1529.
39. Falkenberg, K. J.; Johnstone, R. W. Histone deacetylases and their inhibitors in cancer, neurological diseases and immune disorders. *Nat. Rev. Drug Discov.* **2014**, 13, 673-691.
40. Ueda, H.; Nakajima, H.; Hori, Y.; Fujita, T.; Nishimura, M.; Goto, T.; Okuhara, M. FR01228, a novel antitumor bicyclic depsipeptide produced by *Chromobacterium violaceum* No. 968. I. Taxonomy, fermentation, isolation, physic-chemical and biological properties, and antitumor activity. *J. Antibiot.* **1994**, 47, (3), 301-310.
41. clinicaltrials.gov
42. Lauffer, B. E.; Mintzer, R.; Fong, R.; Mukund, S.; Tam, C.; Zilberleyb, I.; Flicke, B.; Ritscher, A.; Fedorowicz, G.; Vallero, R.; Ortwine, D. F.; Gunzner, J.; Modrusan, Z.; Neumann, L.; Koth, C. M.; Lupardus, P. J.; Kaminker, J. S.; Heise, C. E.; Steiner, P. Histone Deacetylase (HDAC) Inhibitor Kinetic Rate Constants Correlate with Cellular Histone Acetylation but Not Transcription and Cell Viability. *J. Biol. Chem.* **2013**, 288, 26926-26943.
43. Wang, Y.; Stowe, R. L.; Pinello, C. E.; Tian, G.; Madoux, F.; Li, D.; Zhao, L. Y.; Li, J.-L.; Wang, Y.; Wang, Y.; Ma, H.; Hodder, P.; Roush, W. R.; Liao, D. Identification of Histone Deacetylase Inhibitors with Benzoylhydrazide Scaffold that Selectively Inhibit Class I Histone Deacetylases. *Chemistry & Biology* **2015**, 22, (2), 273-284.

44. Shen, M.; Pan, P.; Li, Y.; Li, D.; Yu, H.; Hou, T. Farnesyltransferase and geranylgeranyltransferase I: structures, mechanism, inhibitors and molecular modeling. *Drug Discov. Today* **2015**, 20, (2), 267-276.
45. Tsimberidou, A. M.; Chandhasin, C.; Kurzrock, R. Farnesyltransferase inhibitors: where are we now? *Expert Opin. Investig. Drugs* **2010**, 19, (12), 1569-1580.
46. Sparano, J. A.; Moulder, S.; Kazi, A.; Vahdat, L.; Li, T.; Pellegrino, C.; Munster, P.; Malafa, M.; Lee, D.; Hoschander, S.; Hopkins, U.; Hershman, D.; Wright, J. J.; Sebti, S. M. Targeted Inhibition of Farnesyltransferase in Locally Advanced Breast Cancer: A Phase I and II Trial of Tipifarnib Plus Dose-Dense Doxorubicin and Cyclophosphamide. *J. Clin. Oncol.* **2006**, 24, (19), 3013-3018.
47. Liu, X.; Sabnis, H.; Bunting, K. D.; Qu, C-K. Molecular Targets for the Treatment of Juvenile Myelomonocytic Leukemia. *Adv. Hematol.* **2012**, 2012: 308252.
48. Rose, W. C.; Lee, F. Y. F.; Fairchild, C. R.; Lynch, M.; Monticello, T.; Kramer, R. A.; Manne, V. Preclinical Antitumor Activity of BMS-214662, a Highly Apoptotic and Novel Farnesyltransferase Inhibitor. *Cancer Res.* **2001**, 61, 7507-7517.
49. Reid, T. S.; Beese, L. S. Crystal Structures of the Anticancer Clinical Candidates R115777 (Tipifarnib) and BMS-214662 Complexed with Protein Farnesyltransferase Suggest a Mechanism of FTI Selectivity. *Biochemistry* **2004**, 43, 6877-6884.
50. Davies, D. R.; Mamat, B.; Magnusson, O. T.; Christensen, J.; Haraldsson, M. H.; Mishra, R.; Pease, B.; Hansen, E.; Singh, J.; Zembower, D.; Kim, H.; Kiselyov, A. S.; Burgin, A. B.; Gurney, M. E.; Stewart, L. J. Discovery of Leukotriene A4 Hydrolase Inhibitors Using Metabolomics Biased Fragment Crystallography. *J. Med. Chem.* **2009**, 52, 4694-4715.

51. Grice, C. A.; Gomez, L. Current status of leukotriene A4 hydrolase inhibitors. *Expert Opin. Ther. Pat.* **2008**, 18, (12), 1333-1350.
52. Hirayama, Y.; Sakamaki, S.; Takayanagi, N.; Tsuji, Y.; Sagawa, T.; Chiba, H.; Matsunaga, T.; Niitsu, Y. Chemotherapy with ubenimex corresponding to patient age and organ disorder for 18 cases of acute myelogeneous leukemia in elderly patients – effects, complications and long-term survival. *Gan To Kagaku Ryoho* **2003**, 30, (8), 1113-1118.
53. Celtaxsys commences acebilustat phase 2 trial in patients with cystic fibrosis in US.
<http://www.news-medical.net/news/20151008/Celtaxsys-commences-acebilustat-phase-2-trial-in-patients-with-cystic-fibrosis-in-US.aspx>
54. Thunnissen, M. M. G. M.; Andersson, B.; Samuelsson, B.; Wong, C-H.; Haeggstrom, J. Z. Crystal structures of leukotriene A4 hydrolase in complex with captopril and two competitive tight binding inhibitors. *FASEB J.* **2002**, 16, (12), 1648-1650.
55. Schorlemmer, H. U.; Bosslet, K.; Dickneite, G.; Luben, G.; Sedlacek, H. H. Studies on the mechanisms of action of the immunomodulator bestatin in various screening test systems. *Behring Inst. Mitt.* **1984**, 157-173.
56. Thunnissen, M. M.; Nordlund, P.; Haeggstrom, J. Z. Crystal structure of human leukotriene A(4) hydrolase, a bifunctional enzyme in inflammation. *Nat. Struct. Biol.* **2001**, 8, 131-135.
57. Barb, A. W.; Zhou, P. Mechanism and Inhibition of LpxC: an essential zinc-dependent deacetylase of bacterial lipid A synthesis. *Curr. Pharm. Biotechnol.* **2008**, 9, (1), 9-15.
58. Pirrung, M. C.; Tumery, L. N.; Raetz, C. R. H.; Jackman, J. E.; Snehathala, K.; McClerren, A. L.; Fierke, C. A.; Gantt, S. L.; Rusche, K. M. Inhibition of the

- Antibacterial Target UDP-(3-O-acyl)-N-acetylglucosamine Deacetylase (LpxC): Isoxazoline Zinc Amidase Inhibitors Bearing Diverse Metal Binding Groups. *J. Med. Chem.* **2002**, 45, 4359-4370.
59. McClerren, A. L.; Endsley, S.; Bowman, J. L.; Andersen, N. H.; Guan, Z.; Rudolph, J.; Raetz, C. R. H. A Slow, Tight-Binding Inhibitor of the Zinc-Dependent Deacetylase LpxC of Lipid A Biosynthesis with Antibiotic Activity Comparable to Ciprofloxacin. *Biochemistry* **2005**, 44, 16574-16583.
60. Barb, A. W.; Jiang, L.; Raetz, C. R. H.; Zhou, P. Structure of the deacetylase LpxC bound to the antibiotic CHIR-090: Time-dependent inhibition and specificity in ligand binding. *Proc. Natl. Acad. Sci. USA* **2007**, 104, (47), 18433-18438.
61. Barb, A. W.; McClerren, A. L.; Snehelatha, K.; Reynolds, C. M.; Zhou, P.; Raetz, C. R. Inhibition of lipid A biosynthesis as the primary mechanism of CHIR-090 antibiotic activity in *Escherichia coli*. *Biochemistry* **2007**, 46, (12), 3793-3802.
62. <http://www.reuters.com/article/idUSnGNXbBGfhK+1d9+GNW20150716>
63. Serio, A. W.; Kubo, A.; Lopez, S.; Gomez, M.; Corey, V. C.; Andrews, L.; Schwartz, M. A.; Kasar, R.; McEnroe, G.; Aggen, J.; Miller, G.; Armstrong, E. S. Structure, Potency and Bactericidal Activity of ACHN-975, a First-in-class LpxC Inhibitor. Presented at 53rd Interscience Conference on Antimicrobial Agents and Chemotherapy **2013**.
64. Cole, K. E.; Gattis, S. G.; Angell, H. D.; Fierke, C. A.; Christianson, D. W. Structure of the Metal-Dependent Deacetylase LpxC from *Yersinia enterocolitica* Complexed with the Potent Inhibitor CHIR-090. *Biochemistry* **2010**, 50, 258-262.
65. Helmer, O. M.; Emerson, C. P. The iron content of the whole blood of normal individuals. *J. Biol. Chem.* **1934**, 104, (1), 157-161.

66. Nappi, A. J.; Vass, E. Iron, metalloenzymes and cytotoxic reactions. *Cell Mol. Biol.* **2000**, 46, (3), 637-647.
67. Zhang, C. Essential functions of iron-requiring proteins in DNA replication, repair and cell cycle control. *Protein Cell* **2014**, 5, (10), 750-760.
68. de Visser, S. P.; Kumar, D. *Iron-Containing Enzymes: Versatile Catalysts of Hydroxylation Reactions in Nature*. Royal Society of Chemistry: England, 2011.
69. Hohenberger, J.; Ray, K.; Meyer, K. The biology and chemistry of high-valent iron-oxo and iron-nitrido complexes.
70. Siddiq, A.; Ayoub, I. A.; Chavez, J. C.; Aminova, L.; Shah, S.; LaManna, J. C.; Patton, S. M.; Connor, J. R.; Cherny, R. A.; Volitakis, I.; Bush, A. I.; Langsetmo, I.; Seeley, T.; Gunzler, V.; Ratan, R. R. Hypoxia-inducible Factor Prolyl 4-Hydroxylase Inhibition: A Target for Neuroprotection in the Central Nervous System. *J. Biol. Chem.* **2005**, 280, (50), 41732-41743.
71. Hong, Y. R.; Kim, H. T.; Lee, S-C.; Ro, S.; Cho, J. M.; Kim, I. S.; Jung, Y. H. [(4-Hydroxyl-benzo[4,5]thieno[3,2-c]pyridine-3-carbonyl)-amino]-acetic acid derivatives; HIF prolyl 4-hydroxylase inhibitors as oral erythropoietin secretagogues. *Bioorg. Med. Chem. Lett.* **2013**, 23, 5953-5957.
72. Mircea, I. HIF-prolyl hydroxylase inhibitors: From basic science to clinical trials. *Medica* **2006**, 1, (2), 67-69.
73. Evdokimov, A. G.; Walter, R. L.; Mekel, M.; Pokross, M. E.; Kawamoto, R.; Boyer, A. Crystal structure of HIF prolyl hydroxylase in complex with a biologically active inhibitor. *To be published*.

74. Sangshetti, J. N.; Khan, F. A. K.; Shinde, D. B. Peptide Deformylase: A New Target in Antibacterial, Antimalarial and Anticancer Drug Discovery. *Curr. Med. Chem.* **2015**, 22, 214-236.
75. Guilloteau, J. P.; Mathieu, M.; Giglione, C.; Blanc, V.; Dupuy, A.; Chevrier, M.; Gil, P.; Famechon, A.; Meinnel, T. The crystal structures of four peptide deformylases bound to the antibiotic actinonin reveal two distinct types: a platform for the structure-based design of antibacterial agents. *J. Mol. Biol.* **2002**, 320, (5), 951-962.
76. Smith, H. K.; Beckett, R. P.; Clements, J. M.; Doel, S.; East, S. P.; Launchbury, S. B.; Pratt, L. M.; Spavold, Z. M.; Thomas, W.; Todd, R. S.; Whittaker, M. Structure-Activity Relationships of the Peptide Deformylase Inhibitor BB-3497: Modification of the Metal Binding Group. *Bioorg. Med. Chem. Lett.* **2002**, 12, 3595-3599.
77. Ramanathan-Girish, S.; McColm, J.; Clements, J. M.; Taupin, P.; Barrowcliffe, S.; Hevizi, J.; Safrin, S.; Moore, C.; Patou, G.; Moser, H.; Gadd, A.; Hoch, U.; Jiang, V.; Lofland, D.; Johnson, K. W. Pharmacokinetics in animals and humans of a first-in-class peptide deformylase inhibitor. *Antimicrob. Agents Chemother.* **2004**, 48(12): 4835-4842.
78. Rolan, P.; Sun, H.; MacLeod, C.; Bracken, K.; Evans, T. G. Pharmacokinetics and unexpected safety issues of LBM415, a novel oral peptide deformylase inhibitor. *Clin. Pharmacol. Ther.* **2011**, 90, (2), 256-262.
79. Abendroth, J.; Clifton, M. C.; Edwards, T. E.; Staker, B. L. Crystal structure of peptide deformylase from *ehrlichia chaffeensis* in complex with actinonin. *To be published*.
80. Liu, Y.; Wang, W.; Li, Y.; Xiao, Y.; Cheng, J.; Jia, J. The 5-Lipoxygenase Inhibitor Zileuton Confers Neuroprotection against Glutamate Oxidative Damage by Inhibiting Ferroptosis. *Biol. Pharm. Bull.* **2015**, 38, 1234-1239.

81. Newcomer, M. E.; Brash, A. R. The structural basis for specificity in lipoxygenase catalysis. *Protein Science* **2015**, 24, 298-309.
82. Bishayee, K.; Khuda-Bukhsh, A. R. 5-Lipoxygenase Antagonist therapy: a new approach towards targeted cancer chemotherapy. *Acta Biochim. Biophys. Sin.* **2013**, 45, (9), 709-719.
83. Anwar, Y.; Sabir, J. S.; Qureshi, M. I.; Saini, K. S. 5-lipoxygenase: a promising drug target against inflammatory diseases-biochemical and pharmacological regulation. *Curr. Drug Targets* **2014**, 15, (4), 410-422.
84. fda.gov: Minocin/Minocycline
85. Song, Y.; Wei, E-Q.; Zhang, W-P.; Zhang, L.; Liu, J-R.; Chen, Z. Minocycline protects PC12 cells from ischemic-like injury and inhibits 5-lipoxygenase activation. *Neuropharmacology and Neurotoxicology* **2004**, 15, (14), 2181-2184.
86. Albert, D.; Zundorf, I.; Dingermann, T.; Muller, W. E.; Steinhilber, D.; Werz, O. Hyperforin is a dual inhibitor of cyclooxygenase-1 and 5-lipoxygenase. *Biochem. Pharmacol.* **2002**, 64, 1767-1775.
87. Moore, L. B.; Goodwin, B.; Jones, S. A.; Wisely, G. B.; Serabjit-Singh, C. J.; Willson, T. M.; Collins, J. L.; Kliewer, S. A. St. John's wort induces hepatic drug metabolism through activation of the pregnane X receptor. *Proc. Natl. Acad. Sci. USA* **2000**, 97, (13), 7500-7502.
88. Gilbert, N. C.; Rui, Z.; Neau, D. B.; Waight, M. T.; Bartlett, S. G.; Boeglin, W. E.; Brash, A. R.; Newcomer, M. E. Conversion of human 5-lipoxygenase to a 15-lipoxygenase by a point mutation to mimic phosphorylation at Serine-663. *Faseb J.* **2012**, 26, 3222-3229.

89. Niwa, T.; Hata, T. The Effect of Genetic Polymorphism on the Inhibition of Azole Antifungal Agents Against CYP2C9-Mediated Metabolism. *J. Pharm. Sci.* **2016**, 105, 1345-1348.
90. Conner, K. P.; Vennam, P.; Woods, C. M.; Krzyaniak, M. D.; Bowman, M. K.; Atkins, W. M. 1,2,3-Triazole-Heme Interactions in Cytochrome P450: Functionally Competent Triazole-Water-Heme Complexes. *Biochemistry* **2012**, 51, 6441-6457.
91. Lamb, D. C.; Lei, L.; Warrilow, A. G.; Lepesheva, G. I.; Mullins, J. G.; Waterman, M. R.; Kelly, S. L. The first virally encoded cytochrome P450. *J. Virol.* **2009**, 83, (16), 8266-8269.
92. Gubbins, P. O. Triazole antifungal agents drug-drug interactions involving hepatic cytochrome P450. *Expert Opin. Drug Metab. Toxicol.* **2011**, 7, (11), 1411-1429.
93. <http://www.fda.gov/drugs/developmentapprovalprocess/developmentresources/druginteractionslabeling/ucm093664.htm#classInhibit>
94. Niwa, T.; Shiraga, T.; Takagi, A. Effect of antifungal drugs on cytochrom P450 (CYP) 1A2, 2D6, and 2E1 activities in human liver microsomes. *Biol. Pharm. Bull.* **2005**, 28, 1813-1816.
95. Wexler, D.; Courtney, R.; Richards, W.; Banfield, C.; Lim, J.; Laughlin, M. Effect of posaconazole on cytochrome P450 enzymes: a randomized, open-label, two-way crossover study. *Eur. J. Pharm. Sci.* **2004**, 21, (5), 645-653.
96. Sagatova, A. A.; Keniya, M. V.; Wilson, R. K.; Monk, B. C.; Tyndall, J. D. Structural Insights into Binding of the Antifungal Drug Fluconazole to *Saccharomyces cerevisiae* Lanosterol 14 α -Demethylase. *Antimicrob. Agents Chemother.* **2015**, 59, 4982-4989.

97. Romani, A.; Scarpa, A. Regulation of cell magnesium. *Arch. Biochem. Biophys.* **1992**, 298, (1), 1-12.
98. Maguire, M. E. Magnesium and Cell Proliferation. *Ann. N. Y. Acad. Sci.* **1998**, 551, 201-215.
99. Dudev, T.; Lim, C. Principles Governing Mg, Ca, and Zn Binding and Selectivity in Proteins. *Chem. Rev.* **2003**, 103, 773-787.
100. Cowan, J. A. *Biological Chemistry of Magnesium*. Wiley-VCH: New York, 1995.
101. Bock, C. W.; Katz, A. K.; Markham, G. D.; Glusker, J. P. Manganese as a Replacement for Magnesium and Zinc: Functional Comparison of the Divalent Ions. *J. Am. Chem. Soc.* **1999**, 121, (32), 7360-7372.
102. Dudev, T.; Cowan, J. A.; Lim, C. Competitive Binding in Magnesium Coordination Chemistry: Water versus Ligands of Biological Interest. *J. Am. Chem. Soc.* **1999**, 121, (33), 7665-7673.
103. Chiu, T. K.; Davies, D. R. Structure and function of HIV-1 integrase. *Curr. Top Med. Chem.* **2004**, 4, (9), 965-977.
104. Pommier, Y.; Johnson, A. A.; Marchand, C. Integrase inhibitors to treat HIV/AIDS. *Nat. Rev. Drug Discov.* **2005**, 4, (3), 236-248.
105. Bushman, F. D.; Engelman, A.; Palmer, I.; Wingfield, P.; Craigie, R. Domains of the integrase protein of human immunodeficiency virus type 1 responsible for polynucleotidyl transfer and zinc binding. *Proc. Natl. Acad. Sci. USA* **1993**, 90, (8), 3428-3432.
106. Venclovas, C.; Siksnys, V. Different enzymes with similar structures involved in Mg(2+)-mediated polynucleotidyl transfer. *Nat. Struct. Biol.* **1995**, 2, (10), 838-841.

107. Fesen, M. R.; Kohn, K. W.; Leteurtre, F.; Pommier, Y. Inhibitors of human immunodeficiency virus integrase. *Proc. Natl. Acad. Sci. USA* **1993**, 90, (6), 2399-2403.
108. Espeseth, A. S.; Felock, P.; Wolfe, A.; Witmer, M.; Grobler, J.; Anthony, N.; Egbertson, M.; Melamed, J. Y.; Young, S.; Hamill, T.; Cole, J. L.; Hazuda, D. J. HIV-1 integrase inhibitors that compete with the target DNA substrate define a unique strand transfer conformation for integrase. *Proc. Natl. Acad. Sci. USA* **2000**, 97, (21), 11244-11249.
109. Rosemond, M. J.; St. John-Williams, L.; Yamaguchi, T.; Fujishita, T.; Walsh, J. S. Enzymology of a carbonyl reduction clearance pathway for the HIV integrase inhibitor, S-1360: role of human liver cytosolic aldo-keto reductases. *Chem. Biol. Interact.* **2004**, 147, (2), 129-139.
110. Serrao, E.; Odde, S.; Ramkumar, K.; Neamati, N. Raltegravir, elvitegravir, and metoogravir: the birth of “me-too” HIV-1 integrase inhibitors. *Retrovirology* **2009**, 6:25.
111. Hare, S.; Gupta, S. S.; Valkov, E.; Engelman, A.; Cherepanov, P. Retroviral intasome assembly and inhibition of DNA strand transfer. *Nature* **2010**, 464, (7286), 232-236.
112. Metifiot, M.; Marchand, C.; Maddali, K.; Pommier, Y. Resistance to integrase inhibitors. *Viruses* **2010**, 2, (7), 1347-1366.
113. fda.gov: elvitegravir
114. Hare, S.; Vos, A. M.; Clayton, R. F.; Thuring, J. W.; Cummings, M. D.; Cherepanov, P. Molecular mechanisms of retroviral integrase inhibition and the evolution of viral resistance. *Proc. Natl. Acad. Sci. USA* **2010**, 107, 20057-20062.

115. Nakada, N.; Gmunder, H.; Hirata, T.; Arisawa, M. Mechanism and Inhibition of DNA Gyrase by Cyclothialidine, a Novel DNA Gyrase Inhibitor. *Antimicrob. Agents Chemother.* **1994**, 38, (9), 1966-1973.
116. Gellert, M. DNA topoisomerase. *Annu. Rev. Biochem.* **1981**, 50, 879-910.
117. Maxwell, A.; Gellert, M. Mechanistic aspects of DNA topoisomerases. *Adv. Protein Chem.* **1986**, 38, 69-107.
118. Dwyer, D. J.; Kohanski, M. A.; Hayete, B.; Collins, J. J. Gyrase inhibitors induce an oxidative damage cellular death pathway in Escherichia coli. *Mol. Sys. Biol.* **2007**, 3:91.
119. Reece, R. J.; Maxwell, A. DNA gyrase: structure and function. *Crit. Rev. Biochem. Mol. Biol.* **1991**, 26, 335-375.
120. Drlica, K.; Franco, R. J. Inhibitors of DNA topoisomerases. *Biochemistry* **1988**, 27, 2253-2259.
121. Suda, K. J.; Hicks, L. A.; Roberts, R. M.; Hunkler, R. J.; Danziger, L. H. A national evaluation of antibiotic expenditures by healthcare setting in the United States. *J. Antimicrob. Chemother.* **2009**, 68, (3), 715-718.
122. Bax, B. D.; Chan, P. F.; Eggleston, D. S.; Fosberry, A.; Gentry, D. R.; Gorrec, F.; Giordano, I.; Hann, M. M.; Hennessy, A.; Hibbs, M.; Huang, J.; Jones, E.; Jones, J.; Brown, K. K.; Lewis, C. J.; May, E. W.; Saunders, M. R.; Singh, O.; Spitzfaden, C. E.; Shen, C.; Shillings, A.; Theobald, A. J.; Wohlkonig, A.; Pearson, N. D.; Gwynn, M. N. Type IIA topoisomerase inhibition by a new class of antibacterial agent. *Nature* **2010**, 466, (19), 935-940.

123. Blower, T. R.; Williamson, B. H.; Kerns, R. J.; Berger, J. M. Crystal structure and stability of gyrase-fluoroquinolone cleaved complexes from *Mycobacterium tuberculosis*. *Proc. Natl. Acad. Sci. USA* **2016**, 113, (7), 1706-1713.
124. Andrew Verderame. "Ciprofloxacin – Bayer Pharmaceuticals' Emergency Response to Anthrax in 2001" presented at BioScience Clubhouse CT at Quinnipiac University February 4, 2016.
125. Matrat, S.; Aubry, A.; Mayer, C.; Jarlier, V.; Cambau, E. Mutagenesis in the $\alpha 3 \alpha 4$ GyrA helix and in the Toprim domain of GyrB refines the contribution of *Mycobacterium tuberculosis* DNA gyrase to intrinsic resistance to quinolones. *Antimicrob. Agents Chemother.* **2008**, 52, (8), 2909-2914.
126. Aravind, L.; Leipe, D. D.; Koonin, E. V. Toprim – a conserved catalytic domain in type IA and II topoisomerases, DnaG – type primases, OLD family nucleases and RecR proteins. *Nucleic Acids Res.* **1998**, 26, 4205-4213.
127. Waldron, K. J.; Rutherford, J. C.; Ford, D.; Robinson, N. J. Metalloproteins and metal sensing. *Nature* **2009**, 460, 823-830.
128. Chen, P.; Chakraborty, S.; Mukhopadhyay, S.; Lee, E.; Paoliello, M. M. B.; Bowman, A. B.; Aschner, M. Manganese homeostasis in the nervous system. *J. Neurochem.* **2015**, 134, 601-610.
129. Dudev, T.; Lim, C. Competition among metal ions for protein binding sites: determinants of metal ion selectivity in proteins. *Chem. Rev.* **2014**, 114, 538-556.
130. Shannon, R. D. Revised Effective Ionic Radii and Systematic Studies of Interatomic Distances in Halides and Chalcogenides. *Acta Cryst.* **1976**, A32, 751-767.

131. Williams, R. J. Free manganese (II) and iron (II) cations can act as intracellular cell controls. *FEBS Lett.* **1982**, 140, 3-10.
132. Foster, A. W.; Osman, D.; Robinson, N. J. Metal Preferences and Metallation. *J. Biol. Chem.* **2014**, 289, (41), 28095-28103.
133. Tottey, S.; Waldron, K. J.; Firbank, S. J.; Reale, B.; Bessant, C.; Sato, K.; Cheek, T. R.; Gray, J.; Banfield, M. J.; Dennison, C.; Robinson, N. J. Protein-folding location can regulate manganese-binding versus copper- or zinc-binding. *Nature* **2008**, 455, 1138-1142.
134. Proteau, P. J. 1-Deoxy-D-xylulose 5-phosphate reductoisomerase: an overview. *Bioorg. Chem.* **2004**, 32, 483-493.
135. Murkin, A. S.; Manning, K. A.; Kholodar, S. A. Mechanism and inhibition of 1-deoxy-D-xylulose-5-phosphate reductoisomerase. *Bioorg. Chem.* **2014**, 57, 171-185.
136. Yin, X.; Proteau, P. J. Characterization of native and histidine-tagged deoxyxylulose 5-phosphate reductoisomerase from the cyanobacterium *Synechocystis* sp. PCC6803. *Biochim. Biophys. Acta.* **2003**, 1652, (1), 75-81.
137. Argyrou, A.; Blanchard, J. S. Kinetic and chemical mechanism of *Mycobacterium tuberculosis* 1-deoxy-D-xylulose-5-phosphate isomeroreductase. *Biochemistry* **2004**, 43, (14), 4375-4384.
138. Crichton, R. *Biological Inorganic Chemistry: A New Introduction to Molecular Structure and Function*. 2nd ed. Elsevier Science & Technology: Amsterdam, Netherlands, **2012**.
139. Jomaa, H.; Wiesner, J.; Sanderbrand, S.; Altincicek, B.; Weidemeyer, C.; Hintz, M.; Turbachova, I.; Eberl, M.; Zeidler, J.; Lichtenthaler, H. K.; Soldati, D.; Beck, E.

- Inhibitors of the nonmevalonate pathway of isoprenoid biosynthesis as antimalarial drugs. *Science* **1999**, 285, (5433), 1573-1576.
140. Eliot, A. C.; Griffin, B. M.; Thomas, P. M.; Johannes, T. W.; Kelleher, N. L.; Zhao, H.; Metcalf, W. W. Cloning, expression, and biochemical characterization of *Streptomyces rubellomurinus* genes required for biosynthesis of antimalarial compound FR900098. *Chem. Biol.* **2008**, 15, (8), 765-770.
141. Grolle, S.; Bringer-Meyer, S.; Sahm, H. Isolation of the *dxr* gene of *Zymomonas mobilis* and characterization of the 1-deoxy-D-xylulose 5-phosphate reductoisomerase. *FEMS Microbiol. Lett.* **2000**, 191, (1), 131-137.
142. Kholodar, S. A.; Tomblin, G.; Liu, J.; Tan, Z.; Allen, C. L.; Gulick, A. M.; Murkin, A. S. Alteration of the Flexible Loop in 1-Deoxy-d-xylulose-5-phosphate Reductoisomerase Boosts Enthalpy-Driven Inhibition by Fosmidomycin. *Biochemistry* **2014**, 53, 3423-3431.
143. Reuter, K.; Sanderbrand, S.; Jomaa, H.; Wiesner, J.; Steinbrecher, I.; Beck, E.; Hintz, M.; Klebe, G.; Stubbs, M. T. Crystal structure of 1-deoxy-D-xylulose-5-phosphate reductoisomerase, a crucial enzyme in the non-mevalonate pathway of isoprenoid biosynthesis. *J. Biol. Chem.* **2002**, 277, (7), 5378-5384.
144. Umeda, T.; Tanaka, N.; Kusakabe, Y.; Nakanishi, M.; Kitade, Y.; Nakamura, K. T. Molecular basis of fosmidomycin's action on the human malaria parasite *Plasmodium falciparum*. *Sci. Rep.* **2011**, 1:9.
145. Bjorkelid, C.; Bergfors, T.; Unge, T.; Mowbray, S. L.; Jones, T. A. Structural studies on *Mycobacterium tuberculosis* DXR in complex with the antibiotic FR-900098. *Acta Crystallogr. D Biol. Crystallogr.* **2012**, 68, 134-143.

146. Kunfermann, A.; Lienau, C.; Illarionov, B.; Held, J.; Grawert, T.; Behrendt, C. T.; Werner, P.; Hahn, S.; Eisenreich, W.; Riederer, U.; Mordmuller, B.; Bacher, A.; Fischer, M.; Groll, M.; Kurz, T. IspC as Target for Antiinfective Drug Discovery: Synthesis, Enantiomeric Separation, and Structural Biology of Fosmidomycin Thia Isosteres. *J. Med. Chem.* **2013**, 56, 8151-8162.
147. Durante, W.; Johnson, F. K.; Johnson, R. A. Arginase: a critical regulator of nitric oxide synthesis and vascular function. *Clin. Exp. Pharmacol. Physiol.* **2007**, 34, (9), 906-911.
148. Jenkinson, C. P.; Grody, W. W.; Cederbaum, S. D. Comparative properties of arginases. *Comp. Biochem. Physiol.* **1996**, 114B, 107-132.
149. Steppan, J.; Nyhan, D.; Berkowitz, D. E. Development of novel arginase inhibitors for therapy of endothelial dysfunction. *Front. Immunol.* **2013**, 4:278.
150. Kovamees, O.; Shemyakin, A.; Pernow, J. Effect of Arginase Inhibition on Ischemia-Reperfusion Injury in Patients with Coronary Artery Disease with and without Diabetes Mellitus. *PLoS One* **2014**, 9, (7), e103260.
151. Wu, G.; Morris, S. M. Arginine metabolism: nitric oxide and beyond. *Biochem. J.* **1998**, 336, 1-17.
152. Meurs, H. Maarsingh, H.; Zaagsma, J. Arginase and asthma: novel insights into nitric oxide homeostasis and airway hyperresponsiveness. *TIPS* **2003**, 24, 450-454.
153. Grasemann, H.; Schwiertz, R.; Mathiesen, S.; Racke, K.; Ratjen, F. Increase arginase activity in cystic fibrosis airways. *Am. J. Respir. Crit. Care Med.* **2005**, 172, 1523-1528.
154. Waddington, S. N.; Cattell, V. Arginase in glomerulonephritis. *Exp. Nephrol.* **2000**, 8, 128-134.

155. Bruch-Gerharz, D.; Schnorr, O.; Suschek, C.; Beck, K. F.; Pfeilschifter, J.; Ruzicka, T.; Kolb-Bachofen, V. Arginase 1 overexpression in psoriasis: limitation of inducible nitric oxide synthase activity as a molecular mechanism for keratinocyte hyperproliferation. *Am. J. Pathol.* **2003**, 162, (1), 203-211.
156. Carraliza, I.; Moncada, S. Increased expression of arginase II in patients with different forms of arthritis: implications of the regulation of nitric oxide. *J. Rheumatol.* **2002**, 29, 2261-2265.
157. Morris, C. R.; Kato, G. J.; Poljakovic, M.; Wang, X.; Blackwelder, W. C.; Sanchdev, V.; Hazen, S. L.; Vichinsky, E. P.; Morris, S. M.; Gladwin, M. T. Dysregulated Arginine Metabolism, Hemolysis-Associated Pulmonary Hypertension and Mortality in Sickle Cell Disease. *JAMA* **2005**, 294, (1), 81-90.
158. Holowatz, L. A.; Thompson, C. A.; Kenney, W. L. Acute ascorbate supplementation alone or combined with arginase inhibition augments reflex cutaneous vasodilation in aged human skin. *Am. J. Physiol. Heart Circ. Physiol.* **2006**, 291, H2965-H2970.
159. Kim, N. N.; Cox, J. D.; Baggio, R. F.; Emig, F. A.; Mistry, S. K.; Harper, S. L.; Speicher, D. W.; Morris, S. M.; Ash, D. E.; Traish, A.; Christianson, D. W. Probing erectile function: S-(2-boronoethyl)-L-cystein binds to arginase as a transition state analogue and enhances smooth muscle relaxation in human penile corpus cavernosum. *Biochemistry* **2001**, 40, (9), 2678-2688.
160. Cox, J. D.; Cama, E.; Colletuori, D. M.; Pethe, S.; Boucher, J. L.; Mansuy, D.; Ash, D. E.; Christianson, D. W. Mechanistic and metabolic inferences from the binding of substrate analogues and products to arginase. *Biochemistry* **2001**, 40, (9), 2689-2701.

161. Shemyakin, A.; Kovamees, O.; Rafnsson, A.; Bohm, F.; Svenarud, P.; Settergren, M.; Jung, C.; Pernow, J. Arginase inhibition improves endothelial function in patients with coronary artery disease and type 2 diabetes mellitus. *Circulation* **2012**, 126, (25), 2943-2950.
162. Di Costanzo, L.; Ilies, M.; Thorn, K. J.; Christianson, D. W. Inhibition of human arginase I by substrate and product analogues. *Arch. Biochem. Biophys.* **2010**, 496, 101-108.
163. Van Zandt, M. C.; Whitehouse, D. L.; Golebiowski, A.; Ji, M. K.; Zhang, M.; Beckett, R. P.; Jagdmann, G. E.; Ryder, T. R.; Sheeler, R.; Andreoli, M.; Conway, B.; Mahboubi, K.; D'Angelo, G.; Mitschler, A.; Cousido-Siah, A.; Ruiz, F. X.; Howard, E. I.; Podjarny, A. D.; Schroeter, H. Discovery of (R)-2-amino-6-borono-2-(2-(piperidin-1-yl)ethyl)hexanoic acid and congeners as highly potent inhibitors of human arginase I and II for treatment of myocardial reperfusion injury. *J. Med. Chem.* **2013**, 56, (6), 2568-2580.
164. Ilies, M.; Di Costanzo, L.; Dowling, D. P.; Thorn, K. J.; Christianson, D. W. Binding of alpha,alpha-disubstituted amino acids to arginase suggest new avenues for inhibitor design. *J. Med. Chem.* **2011**, 54, (15), 5432-5443.
165. Golebiowski, A.; Paul Beckett, R.; Van Zandt, M.; Ji, M. K.; Whitehouse, D.; Ryder, T. R.; Jagdmann, E.; Andreoli, M.; Mazur, A.; Padmanilayam, M.; Cousido-Siah, A.; Mitschler, A.; Ruiz, F. X.; Podjarny, A.; Schroeter, H. 2-Substituted-2-amino-6-borono-hexanoic acids as arginase inhibitors. *Bioorg. Med. Chem. Lett.* **2013**, 23, (7), 2027-2030.

166. Underwood, E. J. *Trace Elements in Human and Animal Nutrition*. 4th ed.; Academic Press: New York, 1977.
167. Grubman, A.; White, A. R. Copper as a key regulator of cell signalling pathways. *Expert Rev. Mol. Med.* **2014**, 16: e11.
168. Boal, A. K.; Rosenzweig, A. C. Structural Biology of Copper Trafficking. *Chem. Rev.* **2009**, 109, (10), 4760-4779.
169. Kaplan, J. H.; Maryon, E. B. How Mammalian Cells Acquire Copper: An Essential but Potentially Toxic Metal. *Biophys. J.* **2016**, 110, 7-13.
170. Cotruvo, J. A.; Aron, A. T.; Ramos-Torres, K. M.; Chang, C. J. Synthetic fluorescent probes for studying copper in biological systems. *Chem. Soc. Rev.* **2015**, 44, 4400-4414.
171. McMillin, G. A.; Travis, J. J.; Hunt, J. W. Direct measurement of free copper in serum or plasma ultrafiltrate. *Am. J. Clin. Path.* **2009**, 131, 160-165.
172. Gaier, E. D.; Eipper, B. A.; Mains, R. E. Copper signaling in the mammalian nervous system: synaptic effects. *J. Neurosci. Res.* **2013**, 91, 2-19.
173. Gaetke, L. M.; Chow-Johnson, H. S.; Chow, C. K. Copper: Toxicological relevance and mechanisms. *Arch. Toxicol.* **2014**, 88, (11), 1929-1938.
174. Kim, H.; Wu, X.; Lee, J. SLC31 (CTR) family of copper transporters in health and disease. *Mol. Aspects Med.* **2013**, 34, (2-3), 561-570.
175. Lin, S. J.; Pufahl, R. A.; Dancis, A.; O'Halloran, T. V.; Culotta, V. C. A role for the *Saccharomyces cerevisiae* ATX1 gene in copper trafficking and iron transport. *J. Biol. Chem.* **1997**, 272, 9215-9220.

176. Lachowicz, J. I.; Nurchi, V. M.; Crisponi, G.; Pelaez, Mde G. J.; Rescigno, A.; Stefanowicz, P.; Cal, M.; Szewczuk, Z. Metal coordination and tyrosinase inhibition studies with Kojic- β Ala-Kojic. *J. Inorg. Biochem.* **2015**, 151, 36-43.
177. Liu, J.; Chakraborty, S.; Hosseinzadeh, P.; Yu, Y.; Tian, S.; Petrik, I.; Bhagi, A.; Lu, Y. Metalloproteins Containing Cytochrome, Iron-Sulfur, or Copper Redox Centers. *Chem. Rev.* **2014**, 114, 4366-4469.
178. Lu, Y. Electron Transfer: Cupredoxins. *Comprehensive Coordination Chemistry II*. McCleverty, J. A.; Meyer, T. J. Eds. Elsevier: Oxford, U. K. 2003, Vol. 8, p 91122.
179. Khan, M. T. H. Molecular design of tyrosinase inhibitors: A critical review of promising novel inhibitors from synthetic origins. *Pure Appl. Chem.* **2007**, 79, (12), 2277-2295.
180. van Gelder, C. W.; Flurkey, W. H.; Wichers, H. J. Sequence and structural features of plant and fungal tyrosinases. *Phytochemistry* **1997**, 45, (7), 1309-1323.
181. Garcia-Borron, J. C.; Solano, F. Molecular anatomy of tyrosinase and its related proteins: Beyond the histidine bound metal catalytic center. *Pigment Cell Res.* **2002**, 15, 162-173.
182. Hearing, V. J.; Jimenez, M. Mammalian tyrosinase – The critical regulatory control point in melanocyte pigmentation. *Int. J. Biochem.* **1987**, 19, 1141-1147.
183. Solomon, E. I.; Sundaram, U. M.; Machonkin, T. E. Multicopper Oxidases and Oxygenases. *Chem. Rev.* **1996**, 96, 2563-2606.
184. Chang, T-S. An Updated Review of Tyrosinase Inhibitors. *Int. J. Mol. Sci.* **2009**, 10, 2440-2475.

185. Parvez, S.; Kang, M.; Chung, H. S.; Bae, H. Naturally occurring tyrosinase inhibitors: mechanism and applications in skin health, cosmetics and agriculture industries. *Phytother. Res.* **2007**, 21, 805-816.
186. Chen, W-C.; Tseng, T-S.; Hsiao, N-W.; Lin, Y-L.; Wen, Z-H.; Tsai, C-C.; Lee, Y-C.; Lin, H-H.; Tsai, K-C. Discovery of Highly Potent Tyrosinase Inhibitor, T1, with Significant Anti-Melanogenesis Ability by zebrafish in vivo Assay and Computational Molecular Modeling. *Sci. Rep.* **2015**, 5: 7995.
187. Solano, F.; Briganti, S.; Picardo, M.; Ghanem, G. Hypopigmenting agents: an update review on biological, chemical and clinical aspects. *Pigment Cell Res.* **2006**, 19, (6), 550-571.
188. Kolbe, L.; Mann, T.; Gerwat, W.; Batzer, J.; Ahlheit, S.; Scherner, C.; Wenck, H.; Stab, F. 4-n-butylresorcinol, a highly effective tyrosinase inhibitor for the topical treatment of hyperpigmentation. *JEADV* **2013**, 27, 19-23.
189. Chen, J. S.; Wei, C.; Marshall, M. R. Inhibition mechanism of kojic acid on polyphenol oxidase. *J. Agric. Food Chem.* **1991**, 39, 1897-1901.
190. Perez-Gilabert, M.; Garcia-Carmona, F. Dimethyl sulfide, a volatile flavor constituent, is a slow-binding inhibitor of tyrosinase. *Biochem. Biophys. Res. Commun.* **2001**, 285, (2), 257-261.
191. Bell, A. A.; Wheeler, M. H. Biosynthesis and Functions of Fungal Melanins. *Ann. Rev. Phytopathol.* **1986**, 24, 411-451.
192. Zimmerman, W. C.; Blanchette, R. A.; Burnes, T. A.; Farrell, R. L. Melanin and perithecial development in *Ophiostoma piliferum*. *Mycologia* **1995**, 87, 857-863.

193. Xu, Y.; Stokes, A. H.; Freeman, W. M.; Kumer, S. C.; Vogt, B. A.; Vrana, K. E.
Tyrosinase mRNA is expressed in human substantia nigra. *Brain Res. Mol. Brain Res.* **1997**, 45, (1), 159-162.
194. Joseph, P.; Klein-Szanto, A. J.; Jaiswal, A. K. Hydroquinones cause specific mutations and lead to cellular transformation and in vivo tumorigenesis. *Br. J. Cancer* **1998**, 78, 312-320.
195. Boissy, R. E.; Visscher, M.; deLong, M. A. DeoxyArbutin: a novel reversible tyrosinase inhibitor with effective in vivo skin lightening potency. *Exp. Dermatol.* **2005**, 14, 601-608.
196. Sendovski, M.; Kanteev, M.; Shuster Ben-Yosef, V.; Adir, N.; Fishman, A. First structures of an active bacterial tyrosinase reveal copper plasticity. *J. Mol. Biol.* **2011**, 405, 227-237.
197. Draelos, Z. D. Skin lightening preparations and the hydroquinone controversy. *Dermatol. Ther.* **2007**, 20, (5), 308-313.
198. Krude, T. Mimosine arrests proliferating human cells before onset of DNA replication in a dose-dependent manner. *Exp. Cell Res.* **1999**, 247, (1), 148-159.
199. Zalatnai, A.; Bocsi, J. Mimosine, a plant-derived amino acid induces apoptosis in human pancreatic cancer xenografts. *Anticancer Res.* **2003**, 23, (5A), 4007-4009.
200. Muller, H. D.; Cvikl, B.; Janjic, K.; Nurnberger, S.; Moritz, A.; Gruber, R.; Agis, H. Effects of Prolyl Hydroxylase Inhibitor L-mimosine on Dental Pulp in the Presence of Advanced Glycation End Products. *J. Endod.* **2015**, 41, (11), 1852-1861.

201. Shimizu, K.; Kondo, R.; Sakai, K. Inhibition of tyrosinase by flavonoids, stilbenes and related 4-substituted resorcinols: structure-activity investigations. *Planta Med.* **2000**, *66*, 11-15.
202. Arung, E. T.; Shimizu, K.; Kondo, R. Artocarpus plants as a potential source of skin whitening agents. *Nat. Prod. Commun.* **2011**, *6*, 1397-1402.
203. Ismaya, W. T.; Rozeboom, H. J.; Weijn, A.; Mes, J. J.; Fusetti, F.; Wichers, H. J.; Dijkstra, B. W. Crystal Structure of Agaricus bisporus Mushroom Tyrosinase: Identity of the Tetramer Subunits and Interaction with Tropolone. *Biochemistry* **2011**, *50*, (24), 5477-5486.
204. Garcia-Molina, F.; Munoz, J. L.; Varon, R.; Rodriguez-Lopez, J. N.; Garcia-Canovas, F.; Tudela, J. A review on spectrophotometric methods for measuring the monophenolase and diphenolase activities of tyrosinase. *J. Agric. Food Chem.* **2007**, *55*, (24), 9739-9749.
205. <http://medical-dictionary.thefreedictionary.com/chelation>
206. Jacobsen, J. A.; Fullagar, J. L.; Miller, M. T.; Cohen, S. M. Identifying Chelators for Metalloprotein Inhibitors Using a Fragment-Based Approach. *J. Med. Chem.* **2011**, *54*, 591-602.
207. Kawai, K.; Nagata, N. Metal-ligand interactions: An analysis of zinc binding groups using the Protein Data Bank. *Eur. J. Med. Chem.* **2012**, *51*, 271-276.
208. Rosato, A.; Valasatava, Y.; Andreini, C. Minimal Functional Sites in Metalloproteins and Their Usage in Structural Bioinformatics. *Int. J. Mol. Sci.* **2016**, *17*, (5), E671.
209. Temperini, C.; Innocenti, A.; Guerri, A.; Scozzafava, A.; Rusconi, S.; Supuran, C. T. Phosph(on)ate as a zinc-binding group in metalloenzyme inhibitors: X-ray crystal

structure of the antiviral drug foscarnet complexed to human carbonic anhydrase I.

Bioorg. Med. Chem. Lett. **2007**, 17, 2210-2215.

210. Hider, R. C.; Kong, X. Chemistry and biology of siderophores. *Nat. Prod. Rep.* **2010**, 27, 637-657.
211. Temperini, C.; Innocenti, A.; Scozzafava, A.; Supuran, C. T. N-hydroxyurea – A versatile zinc binding function in the design of metalloenzyme inhibitors. *Bioorg. Med. Chem. Lett.* **2006**, 16, 4316-4320.
212. Kovacic, P.; Edwards, C. L. Hydroxamic acids (therapeutics and mechanism): chemistry, acyl nitroso, nitroxyl, reactive oxygen species, and cell signaling. *J. Recept. Signal Transduct. Res.* **2011**, 31, (1), 10-19.
213. Gooben, L. J.; Rodriguez, N.; Gooben, K. Carboxylic Acids as Substrates in Homogeneous Catalysis. *Angew. Chem. Int. Ed.* **2008**, 47, 3100-3120.
214. Kontogiorgis, C. A.; Papaioannou, P.; Hadjipavlou-Litina, D. J. Matrix metalloproteinase inhibitors: a review on pharmacophore mapping and (Q)SARs results. *Curr. Med. Chem.* **2005**, 12, (3), 339-355.
215. Choy, C. J. Fulton, M. D.; Davis, A. L.; Hopkins, M.; Choi, J. K.; Anderson, M. O.; Berkman, C. E. Rationally Designed Sulfamides as Glutamate Carboxypeptidase II Inhibitors. *Chem. Biol. Drug Des.* **2013**, 82, 612-619.
216. Svara, J.; Weferling, N.; Hofmann, T. *Ullmann's Encyclopedia of Industrial Chemistry: Phosphorus Compounds, Organic*. Wiley-VCH: New York, 2006.
217. Tuccinardi, T.; Bertini, S.; Granchi, C.; Ortore, G.; Macchia, M.; Minutolo, F.; Martinelli, A.; Supuran, C. T. Salicylaldoxime derivatives as new leads for the

- development of carbonic anhydrase inhibitors. *Bioorg. Med. Chem.* **2013**, 21, 1511-1515.
218. Di Fiore, A.; Monti, S. M.; Innocenti, A.; Winum, J-Y.; De Simone, G.; Supuran, C. T. Carbonic anhydrase inhibitors: Crystallographic and solution binding studies for the interaction of a boron-containing aromatic sulfamide with mammalian isoforms I-XV. *Bioorg. Med. Chem. Lett.* **2010**, 20, 3601-3605.
219. Supuran, C. T.; Scozzafava, A. *Proteinase and Peptidase Inhibition: Recent Potential Targets for Drug Development; Matrix metalloproteinases (MMPs)*. Smith, H. J.; Simons, C. Eds. Taylor & Francis: New York, 2002; 35-61.
220. Scozzafava, A.; Supuran, C. T. Carbonic anhydrase and matrix metalloproteinase inhibitors: sulfonylated amino acid hydroxamates with MMP inhibitory properties act as efficient inhibitors of CA isozymes I, II, and IV, and N-hydroxysulfonamides inhibit both these zinc enzymes. *J. Med. Chem.* **2000**, 43, (20), 3677-87.
221. Furumai, R.; Matsuyama, A.; Kobashi, N.; Lee, K. H.; Nishiyama, M.; Nakajima, H.; Tanaka, A.; Komatsu, Y.; Nishino, N.; Yoshida, M.; Horinouchi, S. FK228 (depsipeptide) as a natural prodrug that inhibits class I histone deacetylases. *Cancer Res.* **2002**, 62, (17), 4916-4921.
222. Vesci, L.; Bernasconi, E.; Milazzo, F. M.; De Santis, R.; Gaudio, E.; Kwee, I.; Rinaldi, A.; Pace, S.; Carollo, V.; Giannini, G.; Bertoni, F. Preclinical antitumor activity of ST7612AA1: a new oral thiol-based histone deacetylase (HDAC) inhibitor. *Oncotarget* **2015**, 6, (8), 5735-5748.
223. Chowdhury, R.; McDonough, M. A.; Mecinovic, J.; Loenarz, C.; Flashman, E.; Hewitson, K. S.; Domene, C.; Schofield, C. J. Structural basis for binding of hypoxia-

- inducible factor to the oxygen-sensing prolyl hydroxylases. *Structure* **2009**, 17, (7), 981-989.
224. Grant, R. S.; Coggan, S. E.; Smythe, G. A. The physiological action of picolinic acid in the human brain. *Int. J. Tryptophan Res.* **2009**, 2, 71-79.
225. Monti, S. M.; Maresca, A.; Viparelli, F.; Carta, F.; De Simone, G.; Muhlschlegel, F. A.; Scozzafava, A.; Supuran, C. T. Dithiocarbamates are strong inhibitors of the beta-class fungal carbonic anhydrases from *Cryptococcus neoformans*, *Candida albicans* and *Candida glabrata*. *Bioorg. Med. Chem. Lett.* **2012**, 22, 859-862.
226. Dunbar, R. C. Metal Cation Binding to Phenol: DFT Comparison of the Competing Sites. *J. Phys. Chem. A* **2002**, 106, 7328-7337.
227. Wang, S-F.; Tian, G. R.; Zhang, W-Z.; Jin, J-Y. Characterization of α -nitromethyl ketone as a new zinc-binding group based on the structural analysis of its complex with carboxypeptidase A. *Bioorg. Med. Chem. Lett.* **2009**, 19, 5009-5011.
228. Taherpour, S.; Lonnberg, T. Metal Ion Chelates as Surrogates of Nucleobases for the Recognition of Nucleic Acid Sequences: The Pd^{2+} Complex of 2,6-Bis(3,5-dimethylpyrazol-1-yl)purine Riboside. *J. Nucleic Acids* **2012**, 2012: 196845.
229. Botta, C. B.; Cabri, W.; Cini, E.; De Cesare, L.; Fattorusso, C.; Giannini, G.; Persico, M.; Petrella, A.; Rondinelli, F.; Rodriguez, M.; Russo, A.; Taddei, M. Oxime Amides as a Novel Zinc Binding Group in Histone Deacetylase Inhibitors: Synthesis, Biological Activity, and Computational Evaluation. *J. Med. Chem.* **2011**, 54, 2165-2182.
230. Abele, E.; Lukevics, E. Furan and thiophene oximes: synthesis, reactions, and biological activity. *Chem. Heterocycl. Compd.* **2001**, 37, 141-169.

231. Abele, E.; Abele, R.; Dzenitis, O.; Lukevics, E. Indole and isatin oximes: synthesis, reactions, and biological activity. *Chem. Heterocycl. Compd.* **2003**, 39, 3-35.
232. Abele, E.; Abele, R.; Rubina, K.; Lukevics, E. Quinoline oximes: synthesis, reactions, and biological activity. *Chem. Heterocycl. Compd.* **2005**, 41, 137-162.
233. Quiroga, A. G.; Cubo, L.; de Blas, E.; Aller, P.; Navarro-Ranninger, C. Trans platinum complexes design: one novel water soluble oxime derivative that contains aliphatic amines in trans configuration. *J. Inorg. Biochem.* **2007**, 101, 104-110.
234. Saglam, N.; Colak, A.; Serbest, K.; Dulger, S.; Guner, S.; Karabocek, S.; Belduz, A. O. Oxidative cleavage of DNA by homo- and heteronuclear Cu(II)-Mn(II) complexes of an oxime-type ligand. *BioMetals* **2002**, 15, 357-365.
235. Patil, V.; Sodji, Q. H.; Kornacki, J. R.; Mrksich, M.; Oyelere, A. K. 3-Hydroxypyridin-2-thione as Novel Zinc Binding Group for Selective Histone Deacetylase Inhibition. *J. Med. Chem.* **2013**, 56, 3492-3506.
236. Puerta, D. T.; Lewis, J. A.; Cohen, S. M. New Beginnings for Matrix Metalloproteinase Inhibitors: Identification of High-Affinity Zinc-Binding Groups. *J. Am. Chem. Soc.* **2004**, 126, (27), 8388-8389.
237. Bar-Sela, G.; Epelbaum, R.; Schaffer, M. Curcumin as an anti-cancer agent: review of the gap between basic and clinical applications. *Curr. Med. Chem.* **2010**, 17, (3), 190-197.
238. Anand, P.; Sundaram, C.; Jhurani, S.; Kunnumakkara, A. B.; Aggarwal, B. B. Curcumin and cancer: an "old-age" disease with an "age-old" solution. *Cancer Lett.* **2008**, 267, 133-164.

239. Yanagisawa, D.; Shirai, N.; Amatsubo, T.; Taguchi, H.; Hirao, K.; Urushitani, M.; Morikawa, S.; Inubushi, T.; Kato, M.; Kato, F.; Morino, K.; Kimura, H.; Nakano, I.; Yoshida, C.; Okada, T.; Sano, M.; Wada, Y.; Wada, K. N.; Yamamoto, A.; Tooyama, I. Relationship between the tautomeric structures of curcumin derivatives and their Abeta-binding activities in the context of therapies for Alzheimer's disease. *Biomaterials* **2010**, 31, (14), 4179-4185.
240. Ferrari, E.; Benassi, R.; Sacchi, S.; Pignedoli, F.; Asti, M.; Saladini, M. Curcumin derivatives as metal-chelating agents with potential multifunctional activity for pharmaceutical applications. *J. Inorg. Biochem.* **2014**, 139, 38-48.
241. Kovacevic, Z.; Kalinowski, D. S.; Lovejoy, D. B.; Yu, Y.; Suryo Rahmanto, Y.; Sharpe, P. C.; Bernhardt, P. V.; Richardson, D. R. The medicinal chemistry of novel iron chelators for the treatment of cancer. *Curr. Top. Med. Chem.* **2011**, 11, (5), 483-499.
242. Zandi, K.; Ramedani, E.; Mohammadi, K.; Tajbakhsh, S.; Deilami, I.; Rastian, Z.; Fouladvand, M.; Yousefi, F.; Farshadpour, F. Evaluation of antiviral activities of curcumin derivatives against HSV-1 in Vero cell line. *Nat. Prod. Commun.* **2010**, 5, (12), 1935-1938.
243. Yoshino, M.; Haneda, M.; Naruse, M.; Htay, H. H.; Tsubouchi, R.; Qiao, S. L.; Li, W. H.; Murakami, K.; Yokochi, T. Prooxidant activity of curcumin: copper-dependent formation of 8-hydroxy-2'-deoxyguanosine in DNA and induction of apoptotic cell death. *Toxicol. In Vitro* **2004**, 18, (6), 783-789.
244. Barker, H. A.; Smyth, R. D.; Weissbach, H.; Toohey, J. I.; Ladd, J. N.; Volcani, B. E. Isolation and properties of crystalline cobamide coenzymes containing benzimidazole or 5,6-dimethylbenzimidazole. *J. Biol. Chem.* **1960**, 235, 480-488.

245. Schleicher, J. B.; Aquino, F.; Rueter, A.; Roderick, W. R.; Appell, R. N. Antiviral activity in tissue culture systems of bis-benzimidazoles, potent inhibitors of rhinoviruses. *Appl. Microbiol.* **1972**, 23, 113-116.
246. Joubert, A.; Sun, X. W.; Johansson, E.; Bailly, C.; Mann, J.; Neidle, S. Sequence-selective targeting of long stretches of the DNA minor groove by a novel dimeric bis-benzimidazole. *Biochemistry* **2003**, 42, (20), 5984-5992.
247. Paul, J. J.; Kircus, S. R.; Sorrell, T. N.; Ropp, P. A.; Thorp, H. H. Effects of coordinating metal ions on the mediated inhibition of trypsin by bis(benzimidazoles) and related compounds. *Inorg. Chem.* **2006**, 45, (13), 5126-5135.
248. Katz, B. A.; Clark, J. M.; Finer-Moore, J. S.; Jenkins, T. E.; Johnson, C. R.; Ross, M. J.; Luong, C.; Moore, W. R.; Stroud, R. M. Design of potent selective zinc-mediated serine protease inhibitors. *Nature* **1998**, 391, (6667), 608-612.
249. Leung, D.; Abbenante, G.; Fairlie, D. P. Protease Inhibitors: Current Status and Future Prospects. *J. Med. Chem.* **2000**, 43, 305-341.
250. Singh, S.; Sieburth, S. M. Serine protease inhibition by a silanediol peptidomimetic. *Org. Lett.* **2012**, 14, (17), 4422-4425.
251. Kim, J.; Sieburth, S. M. A silanediol inhibitor of the metalloprotease thermolysin: synthesis and comparison with a phosphinic acid inhibitor. *J. Org. Chem.* **2004**, 69, (9), 3008-3014.
252. Kim, J.; Hewitt, G.; Carroll, P.; Sieburth, S. M. Silanediol inhibitors of angiotensin-converting enzyme. Synthesis and evaluation of four diastereomers of Phe[Si]Ala dipeptide analogues. *J. Org. Chem.* **2005**, 70, (15), 5781-5789.

253. Chen, C-A.; Sieburth, S. M.; Glekas, A.; Hewitt, G. W.; Trainor, G. L.; Erickson-Viitanen, S.; Garber, S. S.; Cordova, B.; Jeffrey, S.; Klabe, R. M. Drug Design with a New Transition State Analog of the Hydrated Carbonyl: Silicon-Based Inhibitors of the HIV Protease. *Chem. Biol.* **2001**, 8, (12), 1161-1166.
254. Minkkila, A.; Saario, S. M.; Kasnanen, H.; Leppanen, J.; Poso, A.; Nevalainen, T. Discovery of boronic acids as novel and potent inhibitors of fatty acid amide hydrolase. *J. Med. Chem.* **2008**, 51, (22), 7057-7060.
255. Cox, J. D.; Kim, N. N.; Traish, A. M.; Christianson, D. W. Arginase-boronic acid complex highlights a physiological role in erectile function. *Nat. Struct. Biol.* **1999**, 6, (11), 1043-1047.
256. LeBeau, A. M.; Singh, P.; Isaacs, J. T.; Denmeade, S. R. Potent and selective peptidyl boronic acid inhibitors of the serine protease prostate-specific antigen. *Chem. Biol.* **2008**, 15, (7), 665-674.
257. Teicher, B. A.; Ara, G.; Herbst, R.; Palombella, V. J.; Adams, J. The proteasome inhibitor PS-341 in cancer therapy. *Clin. Cancer Res.* **1999**, 5, (9), 2638-2645.
258. Hanessian, S.; Vinci, V.; Auzzas, L.; Marzi, M.; Giannini, G. Exploring alternative Zn-binding groups in the design of HDAC inhibitors: Squaric acid, N-hydroxyurea, and oxazoline analogues of SAHA. *Bioorg. Med. Chem. Lett.* **2006**, 16, 4784-4787.
259. Bryant, B. E.; Fernelius, W. C. Formation Constants of Metal Complexes of Tropolone and its Derivatives. II. Some Alkyltropolones. *J. Am. Chem. Soc.* **1954**, 76, (6), 1696-1697.
260. Hendershott, L.; Gentilcore, R.; Ordway, F.; Fletcher, J.; Donati, R. Tropolone: A Lipid Solubilizing Agent for Cationic Metals. *Eur. J. Nucl. Med.* **1982**, 7, 234-236.

261. Jacobsen, F. E.; Lewis, J. A.; Heroux, K. J.; Cohen, S. M. Characterization and evaluation of pyrone and tropolone chelators for use in metalloprotein inhibitors. *Inorganica Chimica Acta* **2007**, 360, 264-272.
262. Bohme, G.; Schonfeld, P.; Kuster, U.; Kunz, W.; Lyr, H. The multifunctional actions of β -thujaplicin on the oxidative energy transformations as a consequence of its lipophilic and chelating properties. *Acta Biol. Med. Germ.* **1980**, 39, 1153-1163.
263. Lie, S.; Yamauchi, H. Hinokitiol, a metal chelator derived from natural plants, suppresses cell growth and disrupts androgen receptor signaling in prostate carcinoma cell lines. *Biochem. Biophys. Res. Commun.* **2006**, 351, (1), 26-32.
264. Ido, Y.; Muto, N.; Inada, A.; Kohroki, J.; Mano, M.; Odani, T.; Itoh, N.; Yamamoto, K.; Tanaka, K. Induction of apoptosis by hinokitiol, a potent iron chelator, in teratocarcinoma F9 cells is mediated through the activation of caspase-3. *Cell Prolif.* **1999**, 32, (1), 63-73.
265. Miyamoto, D.; Endo, N.; Oku, N.; Arima, Y.; Suzuki, T.; Suzuki, Y. Beta-thujaplicin zinc chelate induces apoptosis in mouse high metastatic melanoma B16BL6 cells. *Biol. Pharm. Bull.* **1998**, 21, (12), 1258-1262.
266. Miyamoto, D.; Kusagaya, Y.; Endo, N.; Sometani, A.; Takeo, S.; Suzuki, T.; Arima, Y.; Nakajima, K.; Suzuki, Y. Thujaplicin-copper chelates inhibit replication of human influenza viruses. *Antiviral Res.* **1998**, 39, (2), 89-100.
267. Liu, S.; Yamauchi, H. p27-Associated G1 arrest induced by hinokitiol in human malignant melanoma cells is mediated via down-regulation of pRb, Skp2 ubiquitin ligase, and impairment of Cdk2 function. *Cancer Lett.* **2009**, 286, 240-249.

268. Zhao, J. Plant Troponoids: Chemistry, Biological Activity, and Biosynthesis. *Curr. Med. Chem.* **2007**, 14, 2597-2621.
269. Morita, Y.; Sakagami, Y.; Okabe, T.; Ohe, T.; Inamori, Y.; Ishida, N. The Mechanism of the Bactericidal Activity of Hinokitiol. *Biocontrol Science* **2007**, 12, (3), 101-110.
270. Bentley, R. A fresh look at natural tropolones. *Nat. Prod. Rep.* **2008**, 25, 118-138.
271. Morita, Y.; Matsumura, E.; Okabe, T.; Shibata, M.; Sugiura, M.; Ohe, T.; Tsujibo, H.; Ishida, N.; Inamori, Y. Biological Activity of Tropolone. *Biol. Pharm. Bull.* **2003**, 26, (10), 1487-1490.
272. Nakano, K.; Chigira, T.; Miyafusa, T.; Nagatoishi, S.; Caaveiro, J. M. M.; Tsumoto, K. Discovery and characterization of natural tropolones as inhibitors of the antibacterial target CapF from *Staphylococcus aureus*. *Sci. Rep.* **2015**, 5: 15337.
273. Nakano, H.; Ikenaga, S.; Aizu, T.; Kaneko, T.; Matsuzaki, Y.; Tsuchida, S.; Hanada, K.; Arima, Y. Human Metallothionein Gene Expression Is Upregulated by β -Thujaplicin: Possible Involvement of Protein Kinase C and Reactive Oxygen Species. *Biol. Pharm. Bull.* **2006**, 29, 55-59.
274. Murakami, K.; Ohara, Y.; Haneda, M.; Tsubouchi, R.; Yoshino, M. Prooxidant Action of Hinokitiol: Hinokitiol-Iron Dependent Generation of Reactive Oxygen Species. *Basic Clin. Pharmacol. Toxicol.* **2005**, 97, (6), 392-394.
275. Kontoghiorghes, G. J.; Piga, A.; Hoffbrand, A. V. Cytotoxic and DNA-inhibitory effects of iron chelators on human leukaemic cell lines. *Hematol. Oncol.* **1986**, 4, (3), 195-204.
276. Meck, C.; D'Erasmus, M. P.; Hirsch, D. R.; Murelli, R. P. The biology and synthesis of α -hydroxytropolones. *MedChemComm* **2014**, 5, (7), 842-852.

277. Yoshimori, A.; Oyama, T.; Takahashi, S.; Abe, H.; Kamiya, T.; Abe, T.; Tanuma, S.
Structure-activity relationships of the thujaplicins for inhibition of human tyrosinase.
Bioorg. Med. Chem. **2014**, 22, 6193-6200.
278. Ononye, S. N.; VanHeyst, M. D.; Oblak, E. Z.; Zhou, W.; Ammar, M.; Anderson, A. C.;
Wright, D. L. Tropolones As Lead-Like Natural Products: The Development of Potent
and Selective Histone Deacetylase Inhibitors. *Med. Chem. Lett.* **2013**, 4, 757-761.
279. Bryant, W.; Fernelius, C.; Douglas, B. E. Formation Constants of Metal Complexes of
Tropolone and Its Derivatives. I. Tropolone. *J. Am. Chem. Soc.* **1953**, 75, (15), 3784-
3786.
280. Oka, Y.; Watanabe, I.; Michio, H. Determination of metals with tropolones. X.
Tropolone chelates of manganese(II), cobalt(II), nickel(II), and zinc(II). *Nippon Kagaku
Zasshi* **1968**, 89, (12), 1220-1223.

Chapter 2

Development of Lead-like Troponoids Based on the Natural Product α -Thujaplicin

2.1 Background and Significance

2.1.1 Discovery of Natural Troponoids

Troponoid refers to a family of naturally occurring compounds with a unique seven-membered aromatic ring, commonly named tropone/tropolone. While this core structure was not determined until the 1940s, the use of the troponoid colchicine dates back to antiquity.¹ A metabolite of the autumn crocus (*Colchicum autumnale*), colchicine was first isolated in 1820 and has typically been used to treat gout but was also reportedly prescribed as a treatment for a disease similarly described as cancer by the Roman emperor Nero's military physician.² Colchicine has since been isolated from at least 37 different plants. It is a tricyclic alkaloid with a trimethoxyphenyl as the A ring, a cycloheptane with an acetamide as the B ring and a methoxytropone C ring. However, the structure of the C ring of colchicine was unknown until 1945 when cyclohepta-2,4,6-trienone (tropone) was proposed as the C ring by Dewar.³ Colchicine is known to bind to tubulin to inhibit microtubule polymerization and exhibits anti-inflammatory properties.⁴ It is approved for the treatment of gout, a prophylactic for cardiovascular disease and familial Mediterranean fever.⁵ Due to its long term use and early discovery, colchicine is one of the best studied tropolones with over 19,000 publications found

on PubMed spanning from 1908 to present. This becomes even more evident when only 875 results are returned by PubMed for the keyword tropolone.

Eventhough colchicine was well studied, a relative expolsion of interest in tropolones began around 1932 with the isolation of puberulonic acid and puberulic acid by Harold Raistrick.⁶ Raistrick and coworkers isolated over 200 fungal metabolites and correctly identified the structures of many, but the structures for puberulonic acid, puberulic acid and stipitatic acid, which he isolated in 1942, eluded him.^{1,7} What Raistrick could determine about the structure of these three metabolites was that each exhibited properties of aromatic hydroxy acids. Again, it was Dewar's 1945 proposal of the tropolone ring that solved the structure of stipitatic acid.⁸

Nozoe independently proposed the same seven membered aromatic ring struture as Dewar in a presentation at the Formosa Branch of the Society of the Chemical Industry in 1941. Although this proposal involved the same tropolone moiety, Nozoe's proposal was for the structure of a compound isolated from the heartwood of taiwanhinoki (*Chamaecyparis taiwanesis*) he termed hinokitiol.¹ However, unlike Dewar's proposal, Nozoe's "tropolonoid" was met with skepticism and there exist no published accounts of this presentation.⁹ Interestingly, Dewar was unaware of Nozoe's work due to the lack of access to global scientific communications and the ongoing conflict of World War II. In fact, Nozoe himself was unaware of Dewar's proposal until 1948 because European and American publications were unavailable to Japan beginning in 1937.¹ After learning of Dewar's proposal, Nozoe finally published his findings in Japanese in 1949 with an English translation in 1950 and a subsequent publication on "compounds having a tropolone nucleus...as initially proposed by Dewar" in 1951.^{1,10}

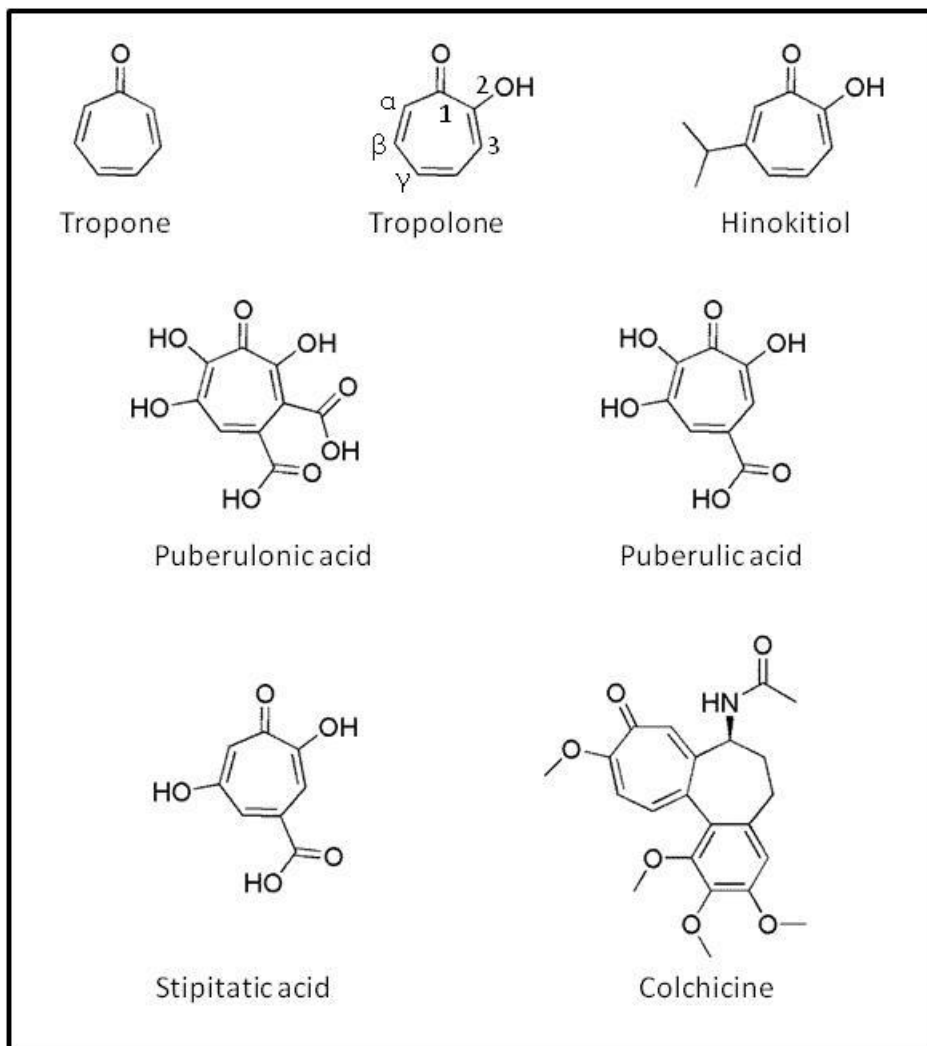


Figure 2.1: Images of the tropone and tropolone scaffold and early isolated natural troponoids.

Since the tropolone ring was proposed by Dewar and Nozoe over 200 natural products have been found to possess this scaffold. These natural products are mainly isolated from fungi and plants but can also be found in some bacteria and can range in complexity from tropolone itself to complex multicyclic systems such as pycnidione and pareirubrine A.¹ As with many secondary metabolites, many of the tropolones display a wide range of biological activity. Most of this activity is attributed to the tropolone moiety while side chains are seen as attributing to selectivity.¹¹ The reason for activity being attributed to the tropolone moiety is because most

tropolones appear to have antimicrobial activity.¹²⁻¹³ It has been proposed that tropolone may offer a unique scaffold to develop novel antibiotics since it can chelate metal ions and most likely has several mechanisms of action to diminish the capability of microorganisms to become resistant.^{11,14-18}

2.1.2 Biological Activity of Natural Tropolones

As mentioned, tropolones exhibited a variety of biological activity including: antibacterial, antifungal, insecticidal, phytotoxic, antimitotic, anti-diabetic, anti-inflammatory, enzyme inhibitory, anticancer, cytoprotective and reactive oxygenated species (ROS) scavenging. Interestingly, the thujaplicins, especially hinokitiol, have been found to exhibit all of the biological activity mentioned with the exception of antimitotic activity; which has only been noted for one natural tropolone, colchicine.¹ Tropolone itself is capable of expressing many of these biological activities. As an antibacterial agent, tropolone produces bacteriostatic effects while the thujaplicins are both bacteriostatic and bactericidal against a broad spectrum of bacterial species.¹⁹ It is believed that tropolone's antibacterial mechanism of action is exerted through effects on the cell wall and the plasma membrane.²⁰ In addition to the thujaplicins, β -dolabrin, 4-acetyltropolone, purpurogallin and black tea theaflavins have also demonstrated antibacterial/antifungal activity. Both β -thujaplicin (hinokitiol) and β -dolabrin exhibit stronger antibacterial activity than gentamycin against *Staphylococcus epidermidis* while α -thujaplicin is more potent than gentamycin against *Enterococcus faecalis*.²¹⁻²² The thujaplicins, β -dolabrin, 4-acetyltropolone and black tea theaflavins are active against both gram-positive and gram-negative bacteria while purpurogallin has only been determined to be active against gram-

positive. However, purpurogallin shows strong antibacterial activity against methicillin resistant *Staphylococcus aureus* (MRSA) with a minimal inhibitory concentration (MIC) of 11.0 $\mu\text{g/mL}$.²³ Antibacterial/antifungal activity of these tropolones may be attributed to their ability to chelate metal as the addition of metal ions was found to reverse antifungal activity.²⁴

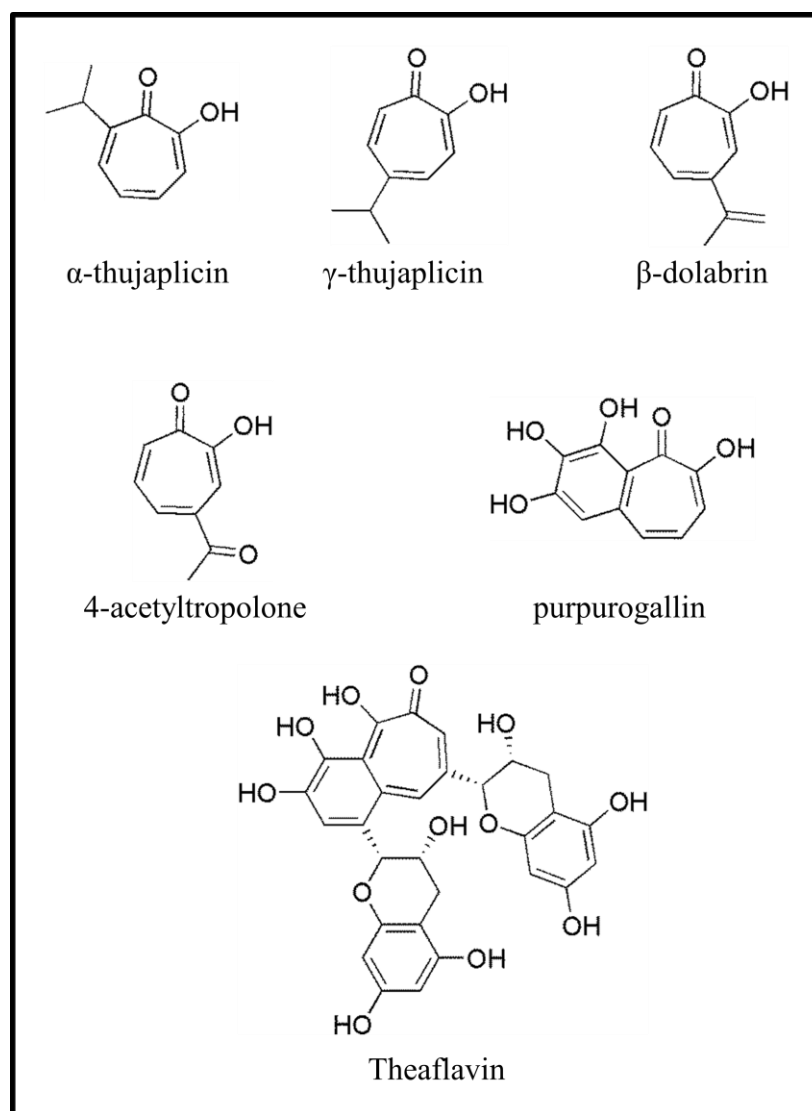


Figure 2.2: Structures of some natural tropolones that exhibit antimicrobial activity.

Tropolone metal chelation appears to be an essential component to most natural tropolone activity. Tropolone and hinokitiol exhibit phytotoxic activity through inhibition of ethylene production and inhibition of ACC oxidase. Addition of Fe^{2+} to the *in vitro* experiments on ACC

oxidase activity eliminates the inhibitory effect of tropolone and hinokitiol.²⁵ Pupurogallin and colchicine have also been found to inhibit ethylene production to inhibit peach seed growth but to a lesser extent than both tropolone and hinokitiol.²⁶ Although the effects of pupurogallin and colchicine on ACC oxidase were not determined, ACC oxidase precedes ethylene production suggesting these tropolones share a similar plant growth inhibitory mechanism of action.

Iron chelation of tropolones imparts activity against the iron metalloenzyme 12-lipoxygenase and is linked to their apoptotic activity in teratocarcinoma F9 cells. 12-lipoxygenase is related to inflammation, platelet homeostasis and thrombosis. Humans have three isoforms of 12-lipoxygenase: epidermis, leukocyte and platelet.²⁷ Hinokitiol has been found to inhibit both the leukocyte (IC₅₀ 50 μ M) and platelet (IC₅₀ 0.1 μ M) isoforms in a reversible manner with a 500-fold selectivity towards the platelet isoform.²⁸ While there is not a crystal structure available to elucidate where hinokitiol binds to 12-lipoxygenase, an iron atom is a key component of the active site of 12-lipoxygenase.²⁷ Since hinokitiol is known to chelate iron and addition of exogenous Fe²⁺ eliminates the activity of hinokitiol against ACC oxidase, it is likely hinokitiol chelates the active site iron of 12-lipoxygenase to inhibit its function. A similar amelioration of hinokitiol activity with the addition of Fe²⁺ or Fe³⁺ was found in teratocarcinoma F9 cells. When treated with hinokitiol, F9 cells would undergo apoptosis due to DNA fragmentation and caspase-3 activation.²⁹ If the F9 cells were pre-incubated with non-toxic concentrations of iron, hinokitiol could no longer induce DNA fragmentation or caspase-3 activation. However, a chelation complex of hinokitiol and Zn²⁺ was determined to be significantly more cytotoxic in mouse melanoma B16BL6 cells than non-complexed hinokitiol.³⁰ Additionally, this (Zn²⁺)hinokitiol complex causes DNA fragmentation in HeLa, Meth A and B16F1 cells but not in normal human fibroblast FS-4 cells.

Despite the strong evidence that tropolones preferentially bind iron and some biological activity can be reduced or eliminated by adding iron, zinc may have a greater effect on tropolone activity. As exhibited by hinokitiol (Zn^{2+})tropolone complexes can have greater biological activity and tropolones have been found to chelate and inhibit several zinc metalloenzymes. In addition to its anticancer activity (Zn^{2+})hinokitiol complex is an insulin-mimetic capable of improving hyperglycemia, tolerance to glucose and responsiveness to insulin.³¹ Although the mechanism is different, hinokitiol chelation of zinc in the active site inhibits carboxypeptidase A.²¹ α -Thujaplicin inhibits carboxypeptidase A (IC_{50} 32.4 μM) but is less potent than hinokitiol (IC_{50} 2.76 μM).²² In a similar chelating mechanism, tropolone has shown potent inhibitory activity against matrix metalloproteinases (MMPs). MMPs degrade connective tissues and deregulation of these enzymes is associated with cancer, arthritis, cardiovascular disease and inflammation.

Iron and zinc are not the only metals associated with the biological activity of tropolones. Chelation of copper by tropolone inhibits polyphenol oxidase to prevent the darkening of fruits and other crops.³²⁻³³ Another copper metalloenzyme commonly associated with inhibition by tropolone is tyrosinase. In 2011, Ismaya and coworkers determined the crystal structure of tropolone bound to mushroom tyrosinase and noticed that it formed a chelation complex with copper in the active site.³⁴ Since then, tropolone has been used as a standard (IC_{50} 400 nM) for inhibitory activity against mushroom tyrosinase.³⁵ Hinokitiol, γ -thujaplicin and nootkatin have also shown potent inhibitory activity against tyrosinase.¹¹ Additionally, copper chelation by hinokitiol inhibits the apoptotic effect of influenza viruses H1N1, H2N2 and H3N2.³⁶ This work led to other research examining the potential of tropolones as antiviral inhibitors of Hepatitis C and human immunodeficiency virus (HIV). While no natural tropolones were discovered to

inhibit Hepatitis C, tropolone derivatives have been developed to inhibit the helicase of this virus.³⁷ Two dihydroxytropolones exhibited inhibitory activity against ribonuclease (RNase) H of HIV-1 reverse transcriptase. These two tropolones, β -thujaplicinol and manicol, inhibit RNase H of HIV-1 and HIV-2 (IC₅₀ 0.2 μ M and 1.5 μ M respectively), but do not inhibit DNA polymerase activity, suggesting metal chelation activity of these two tropolones.³⁸ Later it was discovered that β -thujaplicinol and manicol chelate Mg²⁺ in HIV integrase to prevent viral replication by disrupting the DNA strand transfer reaction.³⁹

Another important biological activity of tropolones is acting as scavengers of reactive oxygenated species (ROS). Unlike most antioxidants that act as weak radical scavengers to prevent generation of ROS, the antioxidant activity of tropolones is most likely due to iron chelation.²⁴ Contradictory to this notion, the (Fe²⁺)hinokitiol complex actually generates ROS which in turn causes DNA damage.⁴⁰ This is similar to the effects seen with Fe³⁺ chelation of hinokitiol to cause single strand DNA breaks. However, this effect was only observed for ratios less than 3:1 hinokitiol to iron. Concentration ratios above 3:1 do not have toxic effects.⁴¹ Adding to this confusion, tropolones elucidate protective effects in a dose dependent manner against hydrogen peroxide induced apoptosis in Jurkat cells. This contradictory effect was attributed to tropolones forming redox-inactive iron complexes to provide protection against hydrogen peroxide. However, formation of lipophilic tropolone-iron complexes can transport redox-active iron inside the cell membrane.⁴¹

Although most tropolone bioactivity is thought to be directly related to metal chelation, the anticancer effects of tropolones are not as well understood. Pareirubrine A, isolated from *Cissampelos pareira*, exhibits strong anti-leukemic activity.⁴² Miltipolone, isolated from *Salvia miltiorrhiza*, is active against a variety of cancer cell lines with GI₅₀s of 0.9 - 6.0 μ M but is

relatively nontoxic towards human umbilical vein endothelial cells with GI_{50} 20 μ M.¹⁸

Theaflavins have been found to inhibit the growth of prostate tumors implanted in athymic nude mice.⁴³ Pycnidione exhibits strong anticancer effects against the lung cancer cell line A549 with a GI_{50} 9.3 nM after 48 hours. Additionally, pycnidione is able to decrease expression of cyclin D1, cyclin E and survivin to induce G1 arrest while activating caspases 8 and 3 and increasing PAI-1 (involved in tumor angiogenesis and invasion) and generation of ROS.⁴⁴ Despite these promising features of these more complex tropolones, most anticancer research has been conducted with the structurally simpler thujaplicins, especially hinokitiol. Hinokitiol has shown multiple anticancer effects across several cell lines. In colon cancer cell lines HCT-116 and SW-620 hinokitiol is growth inhibitory (GI_{50} 4.5 μ M and 4.4 μ M respectively) through induction of S-phase cell cycle arrest. It is also pro-apoptotic as hinokitiol induces caspases 3 and 9, increases expression of p21 and Bax, decreases expression of cyclins A and E, Cdk2 and Bcl-2. Hinokitiol can also reduce tumor sizes of intradermally implanted HCT-116 and SW-620 in BALB/c-nude mice.⁴⁵ In murine melanoma B16-F10 cells, hinokitiol inhibits MMP 1, 3 and 13 and NF κ B and suppresses phosphorylation of ERK 1/2, p38 and JNK to prevent cell migration and tumor growth in C57BL/6 mice.⁴⁶ Hinokitiol also inhibits growth and DNA synthesis in FEM (human melanoma), PC-3 and LNCaP (prostate adenocarcinoma and carcinoma) cells.^{14,47} Additionally, isoforms of hinokitiol have antiproliferative effects against the murine leukemic cell line P388. α -Thujaplicin exhibits a GI_{50} 3.8 μ M after 24 hours incubation but exhibits less acute toxicity.⁴⁸ After 48 hours at this same concentration, γ -thujaplicin inhibits P388 growth by 85%. At 3.8 μ M α -Thujaplicin also inhibits 66% proliferation of the gastric carcinoma cell line KATO-III and 75% of Ehrlich's ascites carcinoma.⁴⁹

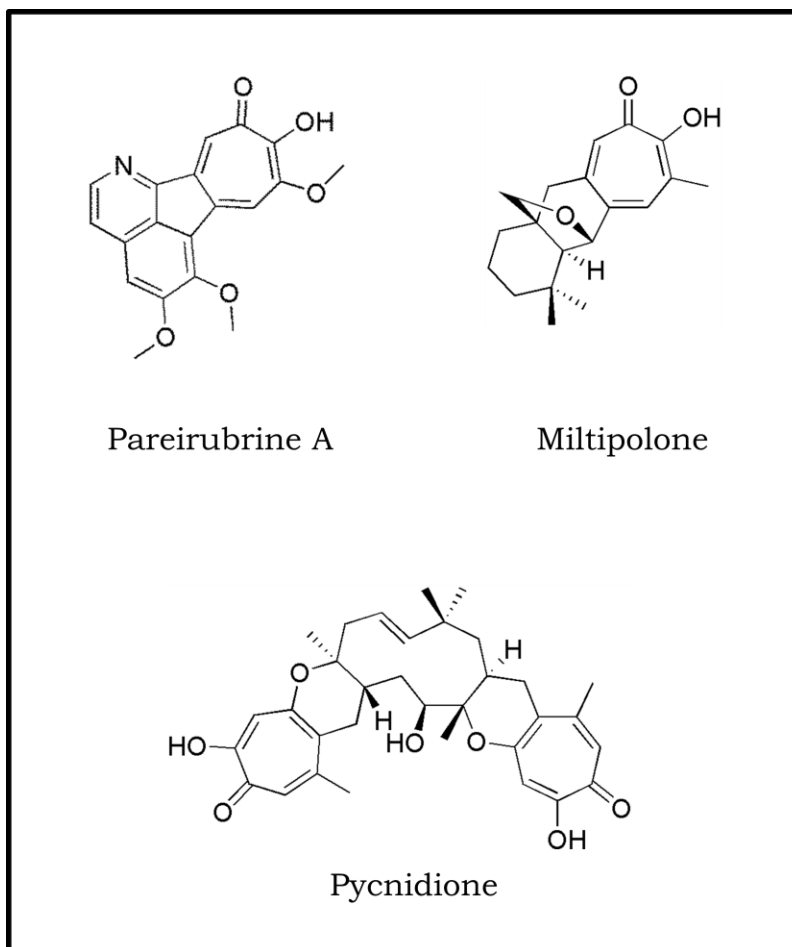
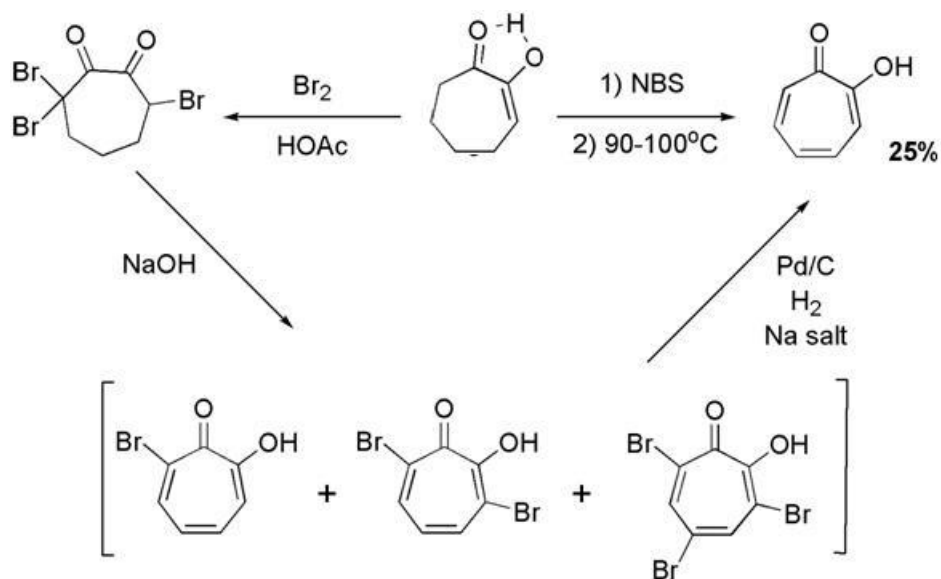
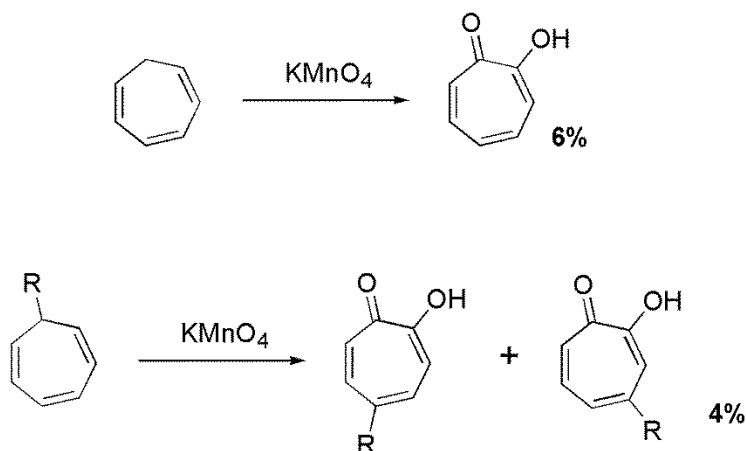


Figure 2.3: Structures of natural tropolones that exhibit anticancer activity.

To summarize, naturally occurring troponoids exhibit a wide range of biological activity. This activity is likely a result of metal chelation. Metal chelation by tropolones typically results in growth inhibition. Tropolones can disrupt the bacterial cell wall and plasma membrane and cause cancer cell cycle arrest. Additionally, tropolones inhibit various metalloenzymes including ACC oxidase, 12-lipoxygenase, carboxypeptidase A, MMP, tyrosinase and HIV integrase. While the activity of natural troponoids is promising, many lack the potency of typical natural products such as taxol and no true targets have been identified. Development of synthetic troponoids offers the potential to increase activity and provide probes for target identification.

2.1.3 Synthesis of the Tropolone Core and the Thujaplicins

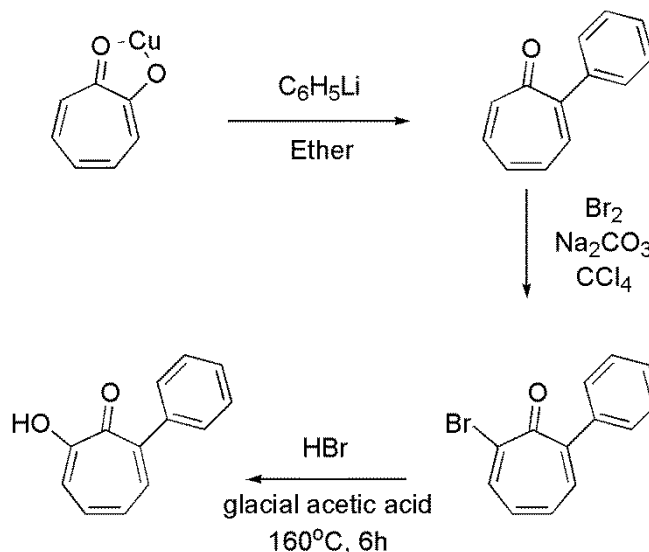
After the tropolone structure was proposed by both Dewar and Nozoe several labs undertook efforts to synthesize this unusual molecule. Most of the early efforts involved the direct oxidation of partially saturated seven-membered rings. In 1950, Cook and coworkers discovered a route that involved the bromination and dehydrobromination of 1,2-cycloheptadione (Scheme 2.1).⁵⁰ Around this same time Doering and Knox reported an alternative route which involved the oxidation of cyclohepta-1,3,5-triene by potassium permanganate (Scheme 2.2).⁵⁰ Interestingly, Doering and Knox also discovered that substitution on the 7 position of cyclohepta-1,3,5-triene followed by a reaction with potassium permanganate could lead to both β and γ substituted tropolones. Unfortunately, both methods to achieve tropolone resulted in poor yields. However, several key reactions were also developed which led to more efficient methods to synthesize tropolone based natural products and tropolone derivatives.⁵⁰

Scheme 2.1: Cook and Coworkers Synthetic Route to Tropolone.**Scheme 2.2:** Doering and Knox Synthetic Route to Tropolone and Substituted Tropolones.

From Cook and coworkers' synthetic route to tropolone, mono-, di- and tri-brominated tropolones were isolated from the reaction of 1,2-cycloheptadione with 2, 3 and 4 moles of bromine at 0°C in glacial acetic acid respectively. They also discovered that the reaction of 2-bromotropolone with diazomethane in ether resulted in the methyl ether 2-bromo-7-

methoxytropone.⁵¹ The work by Doering and Knox also showed that reaction of tropolone with diazomethane resulted in the methyl ether. They also discovered that reaction of the methyl ether with ammonia in methanol at 110°C for 6 days yielded 2-aminotropone.⁵² Hydrolysis of 2-aminotropone with 6 N sodium hydroxide re-generated tropolone. In this same work, Doering and Knox also discovered that 2-methoxytropone could be hydrolyzed by either 3 N hydrochloric acid (52% yield) or 2 N sodium hydroxide (73% yield) to give tropolone in decent yields.⁵²

The initial work by Cook and coworkers and Doering and Knox paved the way towards the synthesis of natural tropolones, namely the thujaplicins. While Cook and coworkers initially abandoned 1,2-cycloheptadione and brominated tropolone they were able to synthesize the thujaplicins from 4-isopropylcycloheptanone (β and γ) and 2-isopropylcycloheptanone (α).⁵³ Meanwhile, they also discovered that the reaction of tropolone in carbon tetrachloride with 0.5 moles bromine at 4°C yielded 2-bromotropolone.⁵⁴ Since palladium catalyzed coupling reactions were still decades away, the first tropolone derivatives typically required built in substitutions. These built in substitutions are still being utilized today and the synthetic history of these tropolone derivatives from non-troponoid scaffolds is the subject of several reviews.^{50,}
⁵⁵⁻⁵⁷ However, in 1952 Doering and Mayer as well as Nozoe and coworkers developed a method to synthesize α -substituted tropolones using an organolithium reagent. This reaction required the copper chelate of tropolone to produce the α -tropone intermediate. The intermediate needed to be brominated then undergo acid catalyzed replacement of the bromide with hydroxyl to yield the α -substituted tropolone.⁵⁸

Scheme 2.3: Synthesis of α -substituted tropolone from tropolone-copper chelate.

Despite these synthetic advances, most tropolone synthesis attempted to generate the natural product and typically did not produce tropolone derivatives. Tropolone derivatives that were developed generally were based on the more complex tropolones or hinokitiol. In 1990 the first Suzuki coupled tropolone derivative from 2-bromo-7-methoxytropolone was reported.⁵⁹ Similar to the synthetic procedures from 1952, conversion to the 2-aryltropolone required hydrolysis of the methyl ether with hydrobromic acid. In 2013, the Wright lab reported a three step synthesis of α -substituted tropolones from the commercially available 2-chlorotropolone.⁶⁰ This work involved a 2-aminotropolone intermediate that was subsequently hydrolyzed similar to that reported by Doering and Knox.

2.1.4 α -Tropolones as Lead-like Antiproliferative Agents

Most work involving α -tropolones has been on α -thujaplicin or other α -substituted natural tropolones. While hinokitiol has been the primary focus of analyzing thujaplicin bioactivity, α -

thujaplicin appears to be equally active. Since the thujaplicins seem to be among the most active natural tropolones, work in the Anderson and Wright labs began with synthesizing simple analogs of both hinokitiol and α -thujaplicin. Histone deacetylases (HDACs) were selected as a class of zinc metalloenzymes which tropolones could potentially inhibit through metal chelation. Screening HDACs 1-2, 4-6, and 8, tropolones were found to possess nanomolar potency in HDACs 2 and 8. While most of the tropolones displayed similar activity, the key potent tropolone from this screen was β -phenyltropolone with IC_{50} 0.06 nM and 1.47 nM in HDAC 2 and 8 respectively.⁶⁰ Following these exciting results, the tropolones were screened against a panel of cancer cell lines. Although all the tropolones showed a preference towards hematological malignancies, the α -substituted tropolones generally exhibited the best activity. Here the key potent derivative was α -(4-methoxyphenyl)tropolone.⁶⁰ When screened against normal human dermal fibroblasts (hDF), the tropolones did not exhibit cytotoxic effects, suggesting α -tropolones are lead-like antiproliferative agents.

2.1.5 Project Objectives

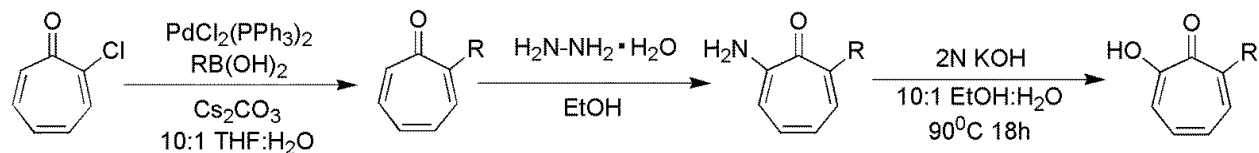
Our goal was to create a more diverse library of α -tropolones to assess structure activity relationship against human leukemia cell lines. Since previous results with a small, phenyl ring based library of α -tropolones suggest para-substitution on the phenyl ring may increase potency against HDAC, a series of α -phenyl tropolone analogs was desired. As the scope of the project expanded to include testing for toxicity in nude mice, a series of α -tropolones with heterocyclic substitutions was desired to increase solubility and activity. To exemplify the versatility of tropolone as a scaffold, reactions other than Suzuki-coupling reactions were also desired.

Additionally, since 2-aminotropones appear to be inactive, our goal was to explore the effect of other chelating group substitutions on tropone.

2.2 Results and Discussion

2.2.1 Synthesis of α -Tropolones from 2-chlorotropone

2-chlorotropone is a commercially available reagent that has proven amenable to the palladium-catalyzed Suzuki-coupling conditions to generate a series of α -aryltropones.⁶⁰ Following Suzuki-coupling, the addition of hydrazine to the 2-aryltropones yielded 2-amino-7-aryltropones. These aminotropones could then be hydrolyzed similar to the aminotropone synthesized by Doering and Knox to generate the desired α -tropolones in good yields (Scheme 2.4).

Scheme 2.4: Synthesis of α -tropolones from 2-chlorotropone.

Tropone	R ^a	Yield (%) ^b	α -Aminotropone	Yield (%) ^b	α -Tropolone	Yield (%) ^b
HC-5-H		97	HC-5-NH ₂	86	HC-5-OH	99
HC-6-H		90	HC-6-NH ₂	67	HC-6-OH	99
HC-7-H		74	HC-7-NH ₂	52	HC-7-OH	63
HC-10-H		100	HC-10-NH ₂	82	HC-10-OH	91
MO-pF-H		100	MO-pF-NH ₂	81	MO-pF-OH	92
MO-pSMe-H		76	MO-pSMe-NH ₂	76	MO-pSMe-OH	79
MO-11-H		94	MO-11-NH ₂	87	MO-11-OH	52
MO-9-H		99	MO-9-NH ₂	88	MO-9-OH	87
MO-10-H		98	MO-10-NH ₂	77	MO-10-OH	65

^a RB(OH)₂; ^b Yield of isolated products.

These results suggested that a large library of α -tropolones could easily be prepared from 2-chlorotropone in three steps. Based on this route, boronic acids with various other functionalities were purchased. These boronic acids contained other heterocycles, various

substitutions on the phenyl ring and alkyl chains. Some analogs still in development are listed in Table 2.1.

Table 2.1: α -Tropolones from 2-chlorotropone in development.

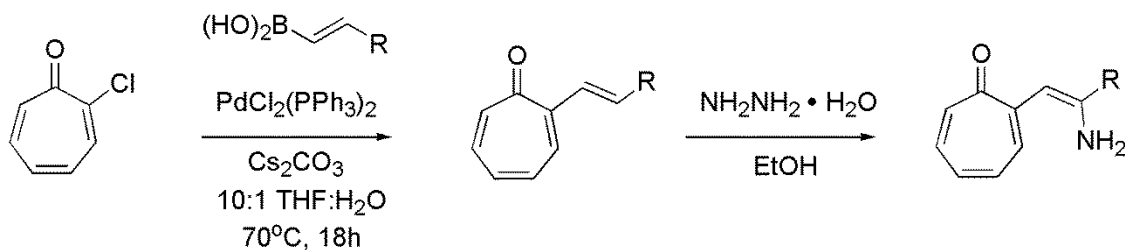
Tropone	R ^a	Yield (%) ^b	α -Aminotropone	Yield (%) ^b	α -Tropolone	Yield (%) ^b
Am-DMe-H		73	Am-DMe-NH2	86	Am-DMe-OH	NA
HC-3-H		54	HC-3-NH2	62	HC-3-OH	NA
HC-11-H		69	---	---	---	---
HC-13-H		crude	HC-13-NH2	58	HC-13-OH	NA

^a RB(OH)₂; ^b Yield of isolated products.

While it appears that this synthetic route is amenable to various substitutions, there are several limitations (Scheme 2.5). First, addition of hydrazine to vinyl substitutions on 2-chlorotropone resulted in a 1,10-conjugate addition of hydrazine resulting in a vinyl amine tropone. This required hydrogenation of the olefin prior to reacting with hydrazine (see Chapter 5 for synthesis of MO-1-OH, MO-2-OH and MO-7-OH). Hydrazine also proved problematic towards a series of furan based derivatives and a substitution containing an aldehyde. Here, hydrazine appeared to over react with these furan derivatives and the methoxy-benzaldehyde substitution and either resulted in no observable product or significantly lower product yields. The other major complication with this synthetic route is the hydrolysis of the aminotropone to the desired α -tropolone. Although 2 N potassium hydroxide is less caustic than the 6 N sodium

hydroxide utilized by Doering and Knox, the reflux of the tropone in this ethanolic solution could affect functional groups on the desired substitution.

Scheme 2.5: Complications in α -tropolone synthesis from 2-chlorotropone.



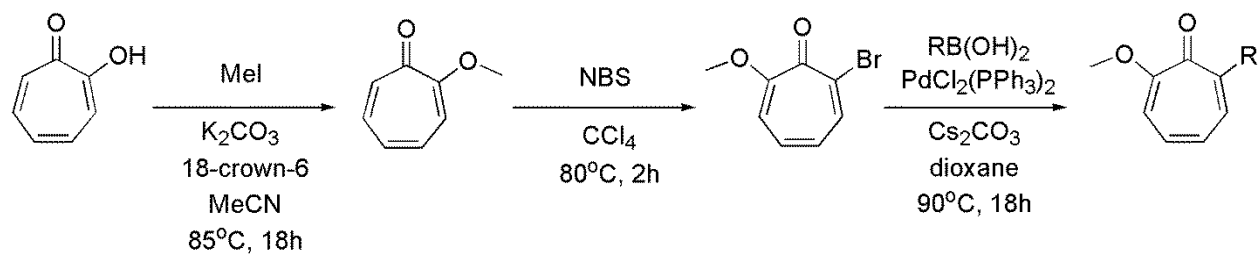
Tropone	R ^a	Yield (%) ^b	α -Aminotropone	Yield (%) ^b	α -Tropolone	Yield (%) ^b
EF-5-H		71	EF-5-NH ₂	NA	---	---
HC-1-H		98	HC-1-NH ₂	80	HC-1-OH	27
HC-2-H		97	HC-2-NH ₂	32 [*]	HC-2-OH	NA
HC-4-H		73	---	---	---	---
HC-8-H		99	HC-8-NH ₂	57	HC-8-OH	NA
HC-9-H		75	HC-9-NH ₂	63	HC-9-OH	NA
HC-12-H		97	HC-12-NH ₂	34	HC-12-OH	NA
Am-Ac-H		97	Am-Ac-NH ₂	NA	---	---

^a RB(OH)₂; ^b Yield of isolated products; ^{*}NMR shows impurities or over reacted material.

Because some of these desired α -tropolones could not be prepared via the 2-chlorotropone synthetic route, a new route was essential. Suri and Nair reported that α -tropolones could be synthesized from 2-bromo-7-methoxytropone.⁵⁹ This synthetic route does not require hydrazine and could potentially avoid several of the issues from the 2-chlorotropone route.

2.2.2 Synthesis of α -Tropolones from 2-bromo-7-methoxytropone

In 1990, Suri and Nair reported a synthetic route from the 2-bromo-7-methoxytropone originally synthesized by Cook and coworkers as well as Doering and Knox. Suri and Nair reported that this compound was amenable to the palladium-catalyzed Suzuki-coupling conditions to generate a series of α -aryltropolones.⁵⁹ However, since diazomethane is explosive and typically requires generation *in situ*, a less hazardous route to the methoxytropone was desired. In 1985, Bass and Gordon reported a simple route to tropolone ethers via reaction with potassium carbonate, an alkyl halide and dicyclohexyl-18-crown-6 in acetonitrile.⁶¹ The methoxytropone could then be brominated according to standard procedures. Comparing the coupling results to those from the 2-chlorotropone route, the 2-bromo-7-methoxytropone route appears to be equally or slightly more amenable to the synthesis of the desired α -tropolones (Scheme 2.6).

Scheme 2.6: Synthesis of α -tropolones from 2-bromo-7-methoxytropone.

Tropone	R ^a	Chloro Route Yield (%) ^b	Bromo Methoxy Route Yield (%) ^b
HC-1		98	95
HC-2		97	84
HC-3		54	88
HC-4		73	65
HC-6		90	36
HC-8		99	83
HC-9		75	87
HC-12		97	59

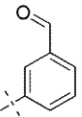
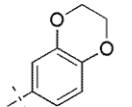
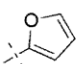
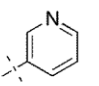
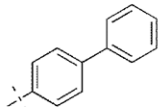
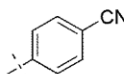
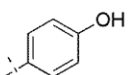
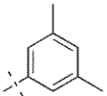
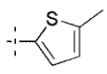
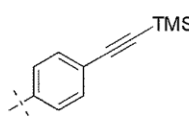
^a RB(OH)₂; ^b Yield of isolated products after Suzuki-coupling

Deprotection of the methyl ether was carried out similar to the procedure used by Doering and Knox. This acid hydrolysis of the methyl ether resulted in precipitation of the tropolone upon cooling. The precipitate could be filtered and dried to yield the pure α -tropolone.

Unlike the 2-chlorotropone route, this method did not have adverse effects on the benzaldehyde substitution. Additionally, benzoic acid methyl ester, nitro-benzene, bromo-benzene, aniline and benzodioxane substitutions were able to be synthesized by this method. However, this acidic deprotection could not be used for the α -furan-tropolone as the furan could be hydrolyzed to the 1,4-dicarbonyl derivative. Acid deprotection of TMS-protected phenylacetylene methoxytropone also proved problematic as it resulted in hydrolysis of the alkyne to a ketone (compound EF-2-OH).

After consulting Greene's Protective Groups in Organic Synthesis, a relatively mild ether deprotection method involving lithium chloride was selected. This method developed by Bernard and coworkers involves the dealkylation of alkyl aryl ethers.⁶² Although Bernard and coworkers heated the dimethylformamide solution to 140°C, the temperature could be reduced for the tropolones to 120°C without sacrificing yields. Additionally, this method reduced the time of deprotection from 6 hours to 2-3 hours.

Table 2.2: Synthesis of α -Tropolones from 2-bromo-7-methoxytropolone utilizing lithium chloride for dealkylation of methyl ether.

Tropone	R ^a	Yield (%) ^b	α -Tropolone	Yield (%) ^b
EF-4-OMe		99	EF-4-OH	40
HC-1-OMe		95	HC-1-OH	64
HC-2-OMe		84	HC-2-OH	11
HC-3-OMe		88	HC-3-OH	5
BA-PH-OMe		80	BA-PH-OH	76
BA-pCN-OMe		72	BA-pCN-OH	24
BA-pOH-OMe		crude	BA-pOH-OH	84
MO-DMe-OMe		87	MO-DMe-OH	70
HC-12-OMe		59	HC-12-OH	27
SG-TMS-OMe		69	SG-TMS-OH	72

^a RB(OH)₂; ^b Yield of isolated products.

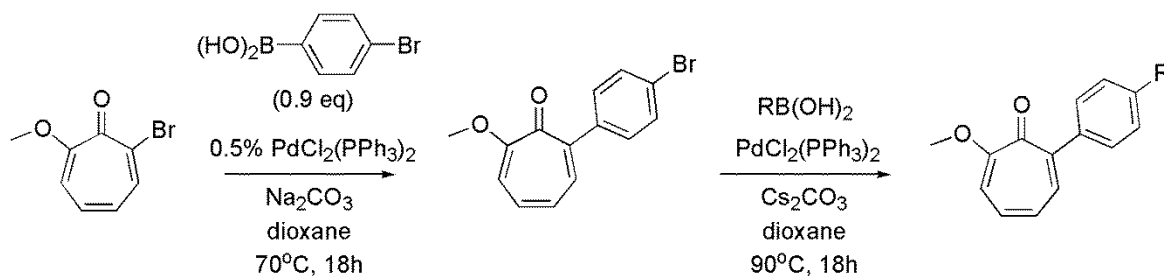
It should be noted that some issues may arise from this process which result in lower yields. First, based on NMR analysis, an impurity interpreted as a high molecular weight

hydrocarbon may be present after standard column chromatography. Recrystallization from acidic water and methanol may be possible in most cases, but several products may be oils or amorphous solids. In order to purify these compounds C-18 column chromatography may be used. Elution from a C-18 column requires mixtures of water and organic solvents. Here, the crude product was added to the column in 4:1 water:methanol and eluted with 50% methanol in water. Although this method required longer evaporation times, all products purified via this technique were free of the high molecular weight hydrocarbon. Another issue discovered was not all boronic acids may be coupled using the conditions depicted in Scheme 2.5. For example, 2-benzofuranboronic acid did not couple. Typical coupling of 2-benzofuranboronic acid requires a solution of benzene/toluene and an aqueous solvent (ie. water or ethanol). Using a solution of toluene and ethanol as reported resulted in minimal coupling.⁶³ Interestingly, the methyl ether on the tropolone appeared to be replaced with ethyl ether. Replacement of ethanol with methanol in the solution yielded the desired product (65%) with the methyl ether intact. This reaction should be explored further to determine if a one-pot Suzuki-coupling and deprotection of 2-bromo-7-methoxytropolone with a boronic acid in toluene and water is possible.

The dealkylation of the tropolone methyl ether appears to be amenable to the generation of a larger α -tropolone library despite some lower yields. Via this method, α -tropolones presenting various heterocycles, alkynes, aldehydes and other functional groups are all able to be synthesized. The next logical step in synthesizing the larger α -tropolone library was to synthesize more analogs with *para*-phenyl substitutions. Although these *para*-phenyl analogs could be synthesized from the aniline, aldehyde, cyano-phenyl, phenol or alkyne tropolones, *para*-bromophenyl was selected to continue utilizing the same Suzuki-coupling conditions already being used. The *para*-bromophenyl analog could also be used later for other coupling

reactions such as Sonogashira, Heck or Buchwald-Hartwig. 4-bromophenylboronic acid could be coupled to 2-bromo-7-methoxytropone using the same Suzuki-coupling conditions utilized for the other tropolone substitutions, but there appeared to be a significant impurity in the aromatic region based on NMR. It was determined that this impurity was most likely a homo-coupled byproduct. To avoid this problem, Suzuki-coupling of 4-bromophenylboronic acid was conducted according to a published method.⁶⁴ While this appeared to reduce the impurity, it did not completely eliminate it. After testing different equivalents of 4-bromophenylboronic acid, it was determined that the addition of 0.9 equivalents would result in a pure product based on NMR. Now a series of *para*- α -phenyltropolones could be synthesized (Scheme 2.7).

Scheme 2.7: Synthesis of *para*- α -phenyltropolones from 2-*para*-bromophenyl-7-methoxytropone.



Tropone	R ^a	Yield (%) ^b	α -Tropolone	Yield (%) ^b
BA-SM-OMe		72	BA-SM-OH	72
BA-DM-OMe		98	BA-DM-OH	72
BA-TM-OMe		99	BA-TM-OH	77
BA-Nap-OMe		96	BA-Nap-OH	63
BA-P5-OMe		99	BA-P5-OH	89
BA-P7-OMe		90	BA-P7-OH	67
BA-P8-OMe		87	BA-P8-OH	68
BA-HC2-OMe		51	BA-HC2-OH	34

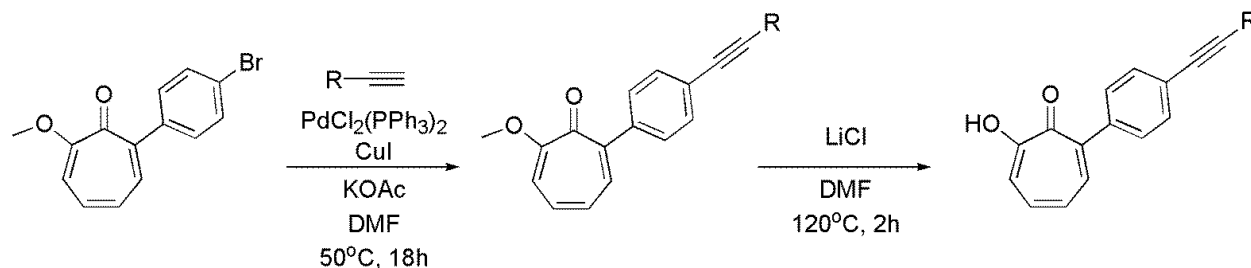
^a RB(OH)₂; ^b Yield of isolated products.

After the successful synthesis of these *para*- α -phenyltropolones, select analogs were attempted directly from the non-protected *para*-bromophenyltropolone (BA-pBr-OH). The normal Suzuki-coupling conditions could produce the desired *para*- α -phenyltropolones but

formed an inseparable mixture of both the coupled product and starting material. Addition of more boronic acid did not overcome this obstacle. Replacement of cesium carbonate with a weaker base, potassium acetate, and a stronger palladium catalyst also failed to yield product. Using a more reactive palladium catalyst and tricyclohexylphosphine to stabilize the transitional metal complex also failed. Replacement of cesium carbonate with potassium fluoride was able to yield the desired product free of starting material. However, this only proved successful for the coupling of 2-furanylboronic acid. Excitingly, this reaction proved more successful than the 2-step coupling/deprotect reaction with 2-*para*-bromophenyl-7-methoxytropone (overall yield 72% vs 17%). Future efforts should be made to successfully synthesize other tropolones from BA-pBr-OH.

2.2.3 Synthesis of α -Tropolones Using Other Coupling Techniques After Suzuki-Coupling

In addition to Suzuki-coupling, BA-pBr-OH can be functionalized via other methods. Sonogashira-coupling to BA-pBr-OH was desired as the product could be used to introduce alkyl linker chains, branched analogs, triazoles via click-coupling, or as a probe for affinity purification by click-chemistry with biotin or a fluorescent tag. To increase the coupling efficiency, potassium acetate was used as a base because acetate ions are thought to bind strongly to soluble palladium (II) and create complexes that are less prone to forming the inactive palladium black.⁶⁵

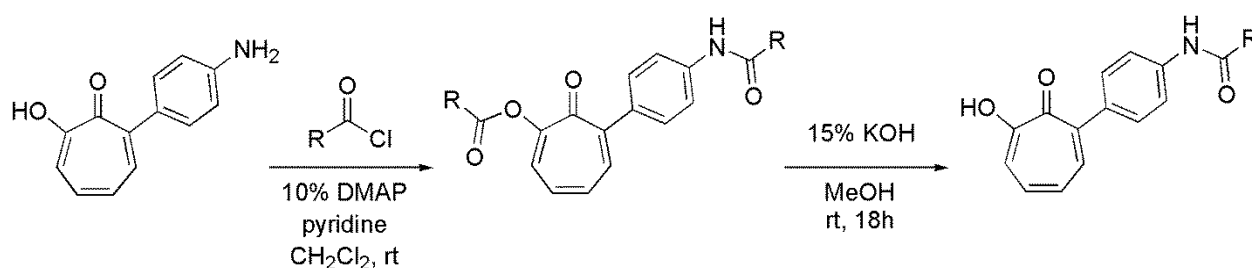
Scheme 2.8: Sonogashira-coupling of alkynes to 2-*para*-bromophenyl-7-methoxytropone.

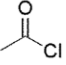
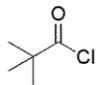
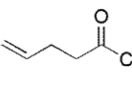
Tropolone	Alkyne	Yield (%) ^b	α-Amido-Tropolone	Yield (%) ^b
BA-pBr-OMe		99	SG-PH-OH	35
		46	SG-iPr-OH	---
		94	SG-EtOH-OH	---

All three alkynes used were successfully coupled, with two in high yields. It is unknown why 3-methyl-1-butyne did not couple as efficiently as the other two alkynes, but it may be possible that not enough copper iodide was in the reaction since a premixed stock of 10% copper iodide in bis(triphenylphosphine)palladium chloride was used as the catalyst. Overall, these Sonogashira-coupling conditions should be useful to couple a variety of alkynes to 2-*para*-bromophenyl-7-methoxytropone. However, the lithium chloride dealkylation of the tropolone methyl ether resulted in a low yield for SG-PH-OH. This may be because the product was precipitated after acidification, filtered and the filtrate which may have contained still soluble product was discarded. It may be possible to avoid this problem by coupling directly to BA-pBr-OH instead of the methyl ether.

As previously mentioned, there are several α -tropolones in this synthesized library that can be further functionalized through subsequent coupling reactions. The amine on α -aniline-tropolone (Am-NH₂-OH) can be utilized in a variety of condensation reactions. Since it has already been shown that γ -aminotropolone can be diacylated and selectively hydrolyzed to maintain the newly formed amide, this diacylation technique was explored.⁶⁶

Scheme 2.9: Synthesis of *N*-phenyl-amide α -tropolones.



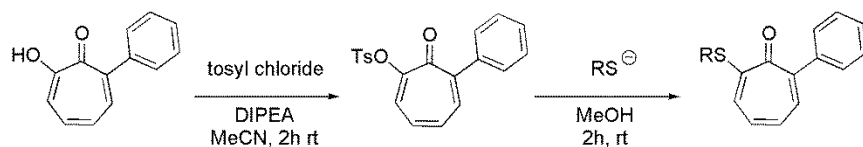
Tropolone	Acyl Chloride	Yield (%) ^b	α -Amido-Tropolone	Yield (%) ^b
Am-NH ₂ -OH		34	Am-Ac-OH	76
		crude	Am-Piv-OH	64
		crude	Am-P5-OH	65

The diacylation of Am-NH₂-OH is successful and can be completed with different acyl chlorides. Unfortunately, the diacylated intermediate tends to broadly diffuse on a column and is not easily purified. Despite the inability to isolate the pure intermediate, the crude product can be washed with water and extracted with dichloromethane to remove DMAP and pyridine. The resultant intermediate is easily dissolved in methanol and the ester hydrolyzed with base. After

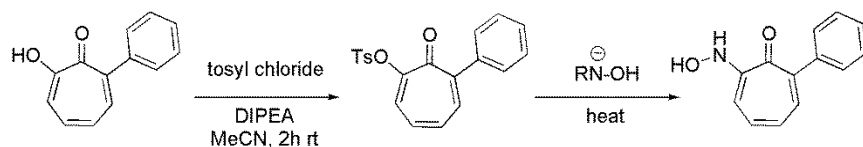
acidic work-up, the product can be purified by column chromatography and collected in good yields.

2.2.4 Synthesis of Tropones with Alternative Chelating Moieties

Previous studies by the Anderson lab determined the aminotropone analogs of the α -tropolones were inactive in cytotoxicity assays. Because this lack of activity was not predicted due to the ability of the amine to act as a chelator with the tropone carbonyl, other potential chelating groups needed to be explored to determine if the hydroxyl is essential to the synthetic α -tropolones activity. It is known that thio-troponoids have biological activity⁶⁷ and hydroxamic acids are commonly used as zinc chelators for histone deacetylase inhibition.⁶⁸ Initial attempts to generate the thio-tropone through nucleophilic displacement of the methyl ether involved α -phenyl-methoxytropone. While it appeared as though some product was formed, the reaction was deemed unsuccessful. Work by Kubo and coworkers discovered that bis-thioditropones could be synthesized through nucleophilic displacement of a tosyl group on the tropone.⁶⁹ Tosylation of α -phenyltropolone with p-toluenesulfonyl chloride was conducted similar to the diacylation of Am-NH₂-OH to form the tosylated α -phenyltropone in good yields (88%). The tosylated α -phenyltropone could then be reacted with either sodium hydrosulfide hydrate or sodium thiomethoxide in methanol at room temperature to form the thio-tropone and thioether-tropone respectively.

Scheme 2.10: Synthesis of thio-tropones.

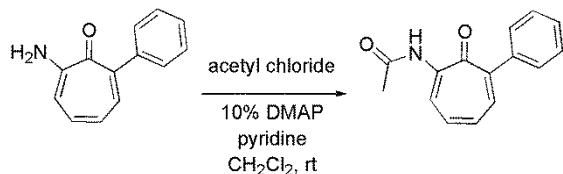
Exploitation of the reactivity of methoxytropones with amines to form aminotropones was attempted to achieve the hydroxylamino-troponone.⁷⁰ Basic Buchwald-Hartwig conditions were used to couple *o*-(*tert*-butyldimethylsilyl)hydroxylamine and α -phenyl-methoxytroponone to generate the hydroxylamino-troponone derivative. Unfortunately, this reaction did not proceed as predicted. However, refluxing *o*-(*tert*-butyldimethylsilyl)hydroxylamine with tosylated α -phenyltroponone yielded the hydroxylamino-troponone (18% yield). Since this reaction undergoes the same nucleophilic substitution mechanism as the thio-derivatives, hydroxylamine hydrochloride salt was neutralized with triethylamine, dissolved in methanol and stirred with tosylated α -phenyltroponone. This reaction appeared to be slow at room temperature so the mixture was heated to 50°C and monitored by TLC. Although this reaction also worked, an oxime may have formed resulting in a significantly lower yield of the hydroxylamino-troponone (7% yield).

Scheme 2.11: Synthesis of hydroxylamino-troponone.

Although it was determined that the aminotropones were biologically inactive in these assays, 2-amido-tropones may have different activity since they could potentially form 6 membered chelate rings instead of the 5 membered chelate ring potentially formed by the

aminotropones. To synthesize this derivative, the amino intermediate of the 2-chlorotropone synthetic route was acylated with acetyl chloride to form the simple acetamide-tropone.

Scheme 2.12: Synthesis of 2-amido-tropone.



Future synthetic work on these tropones with alternative chelating moieties should focus on increasing the yield of the hydroxylamino-tropone. Additionally, synthesis of a carboxy-tropone and phosphonate-tropone should be attempted.

2.3 Conclusions

Synthesis of α -tropolones from commercially available 2-chlorotropone is an efficient but limited synthetic route. A more versatile route towards the synthesis of new α -tropolones is based on elaboration of 2-bromo-7-methoxytropone that can be synthesized in bulk from commercially available tropolone. Lithium chloride dealkylation of the methyl ether provides milder deprotection conditions for the methoxytropone compared to older methods involving reflux in strongly acidic solution. Using this new method, a variety of α -tropolones have been successfully synthesized. The coupling of 4-bromophenylboronic acid to 2-bromo-7-methoxytropone creates a new scaffold for synthesis of α -phenyltropolones with variable substitutions in the *para* position. Additionally, it has been shown that this coupled product can

be utilized in subsequent Suzuki and Sonogashira coupling reactions and the demethylated tropolone (BA-pBr-OH) has the potential to be used in a one step diversification reaction to generate new α -phenyltropolones with substitutions in the *para* position. Other tropolones were synthesized through diacylation of α -anilino-tropolone followed by selective hydrolysis of the ether. A thio-tropone, thioether-tropone and a hydroxylamino-tropone has also been synthesized from tosylated α -phenyltropolone to investigate the necessity of the hydroxyl group for biological activity and/or formation of a 5 membered chelate ring.

2.4 Acknowledgements

Synthesis of compounds MO-1-OH, MO-2-OH, MO-7-OH, MO-9-OH and MO-10-OH were done as a collaborative effort with Dr. Michael van Heyst and Dr. Mohamed Ammar.

2.5 References

1. Bentley, R. A fresh look at natural tropolonoids. *Nat. Prod. Rep.* **2008**, 25, 118-138.
2. Blackwell, W. H. *Poisonous and Medicinal Plants*. Prentice Hall: Englewood Cliffs, NJ, 1990.
3. Dewar, M. J. S. Structure of Colchicine. *Nature* **1945**, 155, 141-142.
4. Wilson, L.; Meza, I. The Mechanism of Action of Colchicine. Colchicine Binding Properties of Sea Urchin Sperm Tail Outer Doublet Tubulin. *J. Cell. Biol.* **1973**, 58, (3), 709-719.

5. Chang, D.-J.; Kim, W.-J. Discovery of structurally simplified analogs of colchicines as an immunosuppressant. *Bioorg. Med. Chem. Lett.* **2014**, 24, 3121-3125.
6. Birkinshaw, J. H.; Raistrick, H. Studies in the biochemistry of micro-organisms: Puberulic acid $C(8)H(6)O(6)$ and an acid $C(8)H(4)O(6)$, new products of the metabolism of glucose by *Penicillium puberulum* Bainier and *Penicillium aurantio-virens* Biourge. With an appendix on certain dihydroxybenzenedicarboxylic acids. *Biochem. J.* **1932**, 26, (2), 441-453.
7. Birkinshaw, J. H.; Chambers, A. R.; Raistrick, H. Studies in the biochemistry of micro-organisms: Stipitatic acid, $C(8)H(6)O(5)$, a metabolic product of *Penicillium stipitatum* Thom. *Biochem. J.* **1942**, 36, (1-2), 242-251.
8. Dewar, M. J. S. Structure of Stipitatic Acid. *Nature* **1945**, 155, (3924), 50-51.
9. Nozoe, T. *Seventy Years in Organic Chemistry*. American Chemical Society: Washington, DC, 1991.
10. Nozoe, T. Substitution products of tropolone and allied compounds. *Nature* **1951**, 167, (4261), 1055-1057.
11. Zhao, J. Plant Troponoids: Chemistry, Biological Activity, and Biosynthesis. *Curr. Med. Chem.* **2007**, 14, 2597-2621.
12. Baillie, A. J.; Freeman, G. G.; Cook, J. W.; Somerville, A. R. Antibacterial and antifungal activity of benzotropolone. *Nature* **1950**, 166, (4210), 65.
13. Dashevskii, V. G. Conformation of the seven-membered ring and biological activity of tricyclic antidepressants. *Pharmaceutical Chemistry Journal* **1981**, 15, (2), 67-71.

14. Lie, S.; Yamauchi, H. Hinokitiol, a metal chelator derived from natural plants, suppresses cell growth and disrupts androgen receptor signaling in prostate carcinoma cell lines. *Biochem. Biophys. Res. Commun.* **2006**, 351, (1), 26-32.
15. Bryant, B. E.; Fernelius, W. C.; Douglas, B. E. Formation Constants of Metal Complexes of Tropolone and Its Derivatives. I. Tropolone. *J. Am. Chem. Soc.* **1953**, 75, (15), 3784-3786.
16. Bryant, B. E.; Fernelius, W. C. Formation Constants of Metal Complexes of Tropolone and its Derivatives. II. Some Alkyltropolones. *J. Am. Chem. Soc.* **1954**, 76, (6), 1696-1697.
17. Bryant, B. E.; Fernelius, W. C. Formation Constants of Metal Complexes of Tropolone and its Derivatives. III. The Benzotropolones and Purpurogallins. *J. Am. Chem. Soc.* **1954**, 76, (14), 3783-3784.
18. Wang, J.; Chen, S.; Cheng, H.; Yang, F.; Wan, J.; Bo, J.; Liu, Y.; Yang, J.; Liu, J.; Zhou, G-C. Identification, structural properties and chelating capacity of miltipolone as a broad-spectrum inhibitor to cancer cells. *Eur. J. Med. Chem.* **2011**, 46, 1117-1121.
19. Trust, T. J. Antibacterial Activity of Tropolone. *Antimicrob. Agents Chemother.* **1975**, 7, (5), 500-506.
20. Halliday, J. E. A Pharmacological Study of Gamma-Thujaplicin. *J. Am. Pharm. Assoc.* **1959**, 48, 722.
21. Inamori, Y.; Shinohara, S.; Tsujibo, H.; Okabe, T.; Morita, Y.; Sakagami, Y.; Kumeda, Y.; Ishida, N. Antimicrobial activity and metalloprotease inhibition of hinokitiol-related compounds, the constituents of *Thujopsis dolabrata*. *Biol. Pharm. Bull.* **1999**, 22, (9), 990-993.

22. Morita, Y.; Matsumura, E.; Tsujibo, H.; Yasuda, M.; Sakagami, Y.; Okabe, T.; Ishida, N.; Inamori, Y. Biological activity of alpha-thujaplicin, the minor component of *Thujaopsis dolabrata*. *Biol. Pharm. Bull.* **2001**, 24, (6), 607-611.
23. Inamori, Y.; Muro, C.; Sajima, E.; Katagiri, M.; Okamoto, Y.; Tanaka, H.; Sakagami, Y.; Tsujibo, H. Biological activity of purpurogallin. *Biosci. Biotechnol. Biochem.* **1997**, 61, (5), 890-892.
24. Diouf, P. N.; Delbarre, N.; Perrin, D.; Gerardin, P.; Rapin, C.; Jacquot, J. P.; Gelhaye, E. Influence of tropolone on *Poria placenta* wood degradation. *Appl. Environ. Microbiol.* **2002**, 68, (9), 4377-4382.
25. Mizutani, F.; Golam Rabbany, A. B. M.; Akiyoshi, H. Inhibition of ethylene production and 1-aminocyclopropane-1-carboxylate oxidase activity by tropolones. *Phytochemistry* **1998**, 48, (1), 31-34.
26. Mizutani, F.; Golam Rabbany, A. B. M.; Akiyoshi, H. Inhibition of ethylene production by tropolone compounds in young excised peach seeds. *J. Jpn. Soc. Hortic. Sci.* **1998**, 67, 166-169.
27. Yeung, J.; Holinstat, M. 12-Lipoxygenase: A Potential Target for Novel Anti-Platelet Therapeutics. *Cardiovasc. Hematol. Agents Med. Chem.* **2011**, 9, (3), 154-164.
28. Suzuki, H.; Ueda, T.; Juranek, I.; Yamamoto, S.; Katoh, T.; Noda, M.; Suzuki, T. Hinokitiol, a selective inhibitor of the platelet type isoxyme of arachidonate 12-lipoxygenase. *Biochem. Biophys. Res. Commun.* **2000**, 275, 885-889.
29. Ido, Y.; Muto, N.; Inada, A.; Kohroki, J.; Mano, M.; Odani, T.; Itoh, N.; Yamamoto, K.; Tanaka, K. Induction of apoptosis by hinokitiol, a potent iron chelator, in

- teratocarcinoma F9 cells is mediated through the activation of caspase-3. *Cell Prolif.* **1999**, 32, (1), 63-73.
30. Miyamoto, D.; Endo, N.; Oku, N.; Arima, Y.; Suzuki, T.; Suzuki, Y. Beta-thujaplicin zinc chelate induces apoptosis in mouse high metastatic melanoma B16BL6 cells. *Biol. Pharm. Bull.* **1998**, 21, (12), 1258-1262.
31. Yamane, M.; Adachi, Y.; Yoshikawa, Y.; Sakurai, H. A New Anti-diabetic Zn(II)-Hinokitiol (β -Thujaplicin) Complex with Zn(O₄) Coordination Mode. *Chem. Lett.* **2005**, 34, (12), 1694-1695.
32. Fuerst, E.; Anderson, J.; Morris, C. Delineating the role of polyphenol oxidase in the darkening of alkaline wheat noodles. *J. Agric. Food Chem.* **2006**, 54, 2378-2384.
33. Dogan, S.; Turan, Y.; Erturk, H.; Arslan, O. Characterization and purification of polyphenol oxidase from artichoke (*cynara scolymus* L.). *J. Agric. Food Chem.* **2005**, 53, (3), 776-785.
34. Ismaya, W. T.; Rozeboom, H. J.; Weijn, A.; Mes, J. J.; Fusetti, F.; Wichers, H. J.; Dijkstra, B. W. Crystal structure of *Agaricus bisporus* mushroom tyrosinase: identity of the tetramer subunits and interaction with tropolone. *Biochem.* **2011**, 50, 5477-5486.
35. Day, J. A.; Cohen, S. M. Investigating the Selectivity of Metalloenzyme Inhibitors. *J. Med. Chem.* **2013**, 56, (20), 7997-8007.
36. Miyamoto, D.; Kusagaya, Y.; Endo, N.; Sometani, A.; Takeo, S.; Suzuki, T.; Arima, Y.; Nakajima, K.; Suzuki, Y. Thujaplicin-copper chelates inhibit replication of human influenza viruses. *Antiviral Res.* **1998**, 39, (2), 89-100.
37. Boguszewska-Chachulska, A. M.; Krawczyk, M.; Najda, A.; Kopanska, K.; Stankiewicz-Drogon, A.; Zagorski-Ostojka, W.; Bretner, M. Searching for a new anti-HCV therapy:

- synthesis and properties of tropolone derivatives. *Biochem. Biophys. Res. Commun.* **2006**, 341, (2), 641-647.
38. Budihas, S. R.; Gorshkova, I.; Gaidamakov, S.; Wamiru, A.; Bona, M. K.; Parniak, M. A.; Crouch, R. J.; McMahon, J. B.; Beutler, J. A.; Le Grice, S. F. Selective inhibition of HIV-1 reverse transcriptase-associated ribonuclease H activity by hydroxylated tropolones. *Nucleic Acids Res.* **2005**, 33, (4), 1249-1256.
39. Semenova, E. A.; Johnson, A. A.; Marchand, C.; Davis, D. A.; Yarchoan, R.; Pommier, Y. Preferential inhibition of the magnesium-dependent strand transfer reaction of HIV-1 integrase by alpha-hydroxytropolones. *Mol. Pharmacol.* **2006**, 69, (4), 1454-1460.
40. Murakami, K.; Ohara, Y.; Haneda, M.; Tsubouchi, R.; Yoshino, M. Prooxidant action of hinokitiol: hinokitiol-iron dependent generation of reactive oxygen species. *Basic Clin. Pharmacol. Toxicol.* **2005**, 97, (6), 392-394.
41. Doulias, P. T.; Nousis, L.; Zhu, B. Z.; Frei, B.; Galaris, D. Protection by tropolones against H₂O₂-induced DNA damage and apoptosis in cultured Jurkat cells. *Free Radic. Res.* **2005**, 39, (2), 125-35.
42. Morita, H.; Matsumoto, K.; Takeya, K.; Itokawa, H.; Iitaka, Y. Structures and solid state tautomeric forms of two novel antileukemic tropoloisoquinoline alkaloids, pareirubines A and B, from *Cissampelos pareira*. *Chem. Pharm. Bull.* **1993**, 41, (8), 1418-1422.
43. Siddiqui, I. A.; Zaman, N.; Aziz, M. H.; Reagan-Shaw, S. R.; Sarfaraz, S.; Adhami, V. M.; Ahmad, N.; Raisuddin, S.; Mukhtar, H. Inhibition of CWR22Rnu1 tumor growth and PSA secretion in athymic nude mice by green and black teas. *Carcinogenesis* **2006**, 27, (4), 833-839.

44. Hsiao, C-J.; Hsiao, S-H.; Chen, W-L.; Guh, J-H.; Hsiao, G.; Chan, Y-J.; Lee, T-H.; Chung, C-L. Pycnidione, a fungus-derived agent, induces cell cycle arrest and apoptosis in A549 human lung cancer cells. *Chemico-Biological Interactions* **2012**, 197, 23-30.
45. Lee, Y-S.; Choi, K-M.; Kim, W.; Jeon, Y-S.; Lee, Y-M.; Hong, J-T.; Yun, Y-P.; Yoo, H-S. Hinokitiol Inhibits Cell Growth through Induction of S-Phase Arrest and Apoptosis in Human Colon Cancer Cells and Suppresses Tumor Growth in a Mouse Xenograft Experiment. *J. Nat. Prod.* **2013**, 26, 2195-2202.
46. Huang, C-H.; Lu, S-H.; Chang, C-C.; Thomas, P. A.; Jayakumar, T.; Sheu, J-R. Hinokitiol, a tropolone derivative, inhibits mouse melanoma (B16-F10) cell migration and in vivo tumor formation. *Eur. J. Pharmacol.* **2015**, 746, 148-157.
47. Liu, S.; Yamauchi, H. p27-Associated G1 arrest induced by hinokitiol in human malignant melanoma cells is mediated via down-regulation of pRb, Skp2 ubiquitin ligase, and impairment of Cdk2 function. *Cancer Lett.* **2009**, 286, 240-249.
48. Morita, Y.; Matsumura, E.; Okabe, T.; Fukui, T.; Shibata, M.; Sugiura, M.; Ohe, T.; Tsujibo, H.; Ishida, N.; Inamori, Y. Biological Activity of α -Thujaplicin, the Isomer of Hinokitiol. *Biol. Pharm. Bull.* **2004**, 27, (6), 899-902.
49. Morita, Y.; Matsumura, E.; Okabe, T.; Fukui, T.; Ohe, T.; Ishida, N.; Inamori, Y. Biological activity of beta-dolabrin, gamma-thujaplicin, and 4-acetyltropolone, hinokitiol-related compounds. *Biol. Pharm. Bull.* **2004**, 27, (10), 1666-1669.
50. Liu, N.; Song, W.; Schienebeck, C. M.; Zhang, M.; Tang, W. Synthesis of naturally occurring tropones and tropolones. *Tetrahedron* **2014**, 70, 9281-9305.
51. Cook, J. W.; Gibb, A. R.; Raphael, R. A.; Somerville, A. R. Tropolones. Part I. The Preparation and General Characteristics of Tropolone. *J. Chem. Soc.* **1951**, 503-511.

52. Doering, W. E.; Knox, L. H. Tropolone. *J. Am. Chem. Soc.* **1951**, 73, 828-838.
53. Cook, J. W.; Gibb, A. R.; Raphael, R. A.; Somerville, A. R. Tropolones. Part II. The Synthesis of α -, β -, and γ -Thujaplicins. *J. Chem. Soc.* **1951**, 695-698.
54. Cook, J. W.; Gibb, A. R.; Raphael, R. A.; Somerville, A. R. Tropolones. Part III. Halogenated Derivatives of Tropolone. *J. Chem. Soc.* **1951**, 2244-2248.
55. Pauson, P. L. Tropones and Tropolones. *Chem. Rev.* **1955**, 55, (1), 9-136.
56. Pietra, F. Seven-membered conjugated carbo- and heterocyclic compounds and their homoconjugated analogs and metal complexes. Synthesis, biosynthesis, structure, and reactivity. *Chem. Rev.* **1973**, 73, (4), 293-364.
57. Banwell, M. G. New Methods for the Synthesis of Troponoid Compounds. *Aust. J. Chem.* **1991**, 44, (1), 1-36.
58. Doering, W. E.; Mayer, J. R. The Synthesis of α -Phenyltropolone from Tropolone. *J. Am. Chem. Soc.* **1953**, 75, (10), 2387-2388.
59. Suri, S. C.; Nair, V. Palladium(0)-Catalyzed Reaction of 2-Bromo-7-methoxytropone with Arylboronic Acids: An Efficient Synthesis of 2-Aryl-7-methoxytropones. *Synthesis* **1990**, 8, 695-696.
60. Ononye, S. N.; VanHeyst, M. D.; Oblak, E. Z.; Zhou, W.; Ammar, M.; Anderson, A. C.; Wright, D. L. Tropolones As Lead-Like Natural Products: The Development of Potent and Selective Histone Deacetylase Inhibitors. *Med. Chem. Lett.* **2013**, 4, 757-761.
61. Bass, R. J.; Gordon, D. W. A Convenient Route to Tropolone Ethers. *Synth. Commun.* **1985**, 15, (3), 225-228.

62. Bernard, A. M.; Ghiani, M. R.; Piras, P. P.; Rivoldini, A. Dealkylation of Activated Alkyl Ethers Using Lithium Chloride in Dimethylformamide. *Synth. Commun.* **1989**, 4, 287-289.
63. Le Guevel, R.; Oger, F.; Lecorgne, A.; Dudasova, Z.; Chevance, S.; Bondon, A.; Barath, P.; Simonneaux, G.; Salbert, G. Identification of small molecule regulators of the nuclear receptor HNF4 α based on naphthofuran scaffolds. *Bioorg. Med. Chem.* **2009**, 17, (19), 7021-7030.
64. Reisner, E.; Lippard, S. J. Synthesis of Dicarboxylate "C-Clamp" 1,2-Diethynylarene Compounds as Potential Transition-Metal Ion Hosts. *Eur. J. Org. Chem.* **2008**, 1, 156-163.
65. Chinchilla, R.; Najera, C. Recent advances in Sonogashira reactions. *Chem. Soc. Rev.* **2011**, 40, 5084-5121.
66. Ebisawa, M.; Ohta, K.; Kawachi, E.; Fukasawa, H.; Hashimoto, Y.; Kagechika, H. Novel Retinoidal Tropone Derivatives. Bioisosteric Relationship of Tropone Ring with Benzoic Acid Moiety in Retinoid Structure. *Chem. Pharm. Bull.* **2001**, 49, (4), 501-503.
67. Chang, D-J.; Kim, W-J. Discovery of Structurally Simplified Analogs of Colchicine as an Immunosuppressant. *Bioorg. Med. Chem. Lett.* **2014**, 24, 3121-3125.
68. Bertrand, P. Inside HDAC with HDAC Inhibitors. *Eur. J. Med. Chem.* **2010**, 45, 2095-2116.
69. Kubo, K.; Mori, A.; Takeshita, H. Synthesis and Mercuriphilic Properties of 2,2'-Oxybis(ethylenethio)ditropone and α -[2-(2-Troponylthio)ethyl]- ω -(2-troponylthio)oligo(oxyethylene). *Bull. Chem. Soc. Jpn.* **1997**, 70, (1), 231-237.

70. Nozoe, T.; Someya, T.; Okai, H. Reactive Troponoids and *o*-Aminophenol. III. The Reaction of 2-Bromo-7-methoxytropone. *Bull. Chem. Soc. Jpn.* **1979**, 52, (4), 1156-1158.

Chapter 3

Development of Synthetic α -Tropolonoids as Antiproliferatives Effective Against T-cell Acute Lymphoblastic Leukemia

3.1 Background and Significance

Acute lymphoblastic leukemia (ALL) is a highly aggressive hematologic malignancy driven by aberrant proliferation of lymphoid precursor cells which primarily accumulate in bone marrow and blood but may spread to other tissues.¹⁻³ While predisposition to ALL is considered uncommon, there is a greater occurrence in children.⁴ ALL is the most common childhood cancer worldwide with 4 to 5 children per 100,000 diagnosed each year and peak incidence between ages 2 and 5.⁵⁻⁶ Although 60% of ALL cases are 20 years old or younger, a second peak occurrence of ALL is found in patients older than 50. Interestingly ALL accounts for 80% of all childhood leukemia but only 20% of adult leukemia.⁶

As the malignant hematopoietic cells expand in bone marrow, patients begin develop symptoms associated with ALL. Typical symptoms include: weakness or fatigue usually associated with anemia, fever which may be caused by neutropenia or infection resulting from suppression of normal hematopoiesis, easy bruising and bleeding caused by thrombocytopenia, shortness of breath caused by a mass formed in the esophagus, trachea, thymus or lymph nodes, weight loss, bone or joint pain or swelling of the abdomen due to high white blood cell (WBC) count, swollen lymph nodes in the neck, armpit or groin, and headache, confusion and nausea as

a result of central nervous systems (CNS) involvement.^{3,7} Because ALL may be of B- or T-progenitor cell origin, diagnosis requires extensive analysis. Diagnosis involves flow cytometry to determine B- or T-cell lineage, morphology assessment and immunophenotyping to determine subtype, cytogenic analysis for common gene rearrangements and bone marrow biopsy to assess bone marrow involvement.^{3,7} Subsequent diagnostic assessments may include complete blood count and well as a chemistry panel to screen for WBC count and potential involvement of other organs, careful screening for any active infection, and lumbar puncture for cytologic analysis of cerebrospinal fluid if CNS involvement is suspected.^{3,7}

Subtyping ALL is critical because each subtype exhibits different responses to therapy and is associated with a different prognosis. Initial subtyping involves morphological assessment to determine L1, L2 or L3 morphology. L1 morphology involves more mature lymphoblasts while L2 is more immature or mixed lineage. L3 morphology is significantly less common and is referred to as Burkitt ALL.³ Burkitt ALL is of B-cell lineage and contains the translocation of MYC typically with IGH@.⁷ Cytogenic analysis of genetic rearrangements further subtypes ALL with L2 morphology. One of the more common genetic rearrangements is the BCR-ABL1 fusion.⁸ Similar to chronic myelogenous leukemia (CML), this fusion results in the Philadelphia chromosome. However, Ph⁺ ALL is characterized by a 190 kDa isoform of the Philadelphia chromosome while CML generally involves a 210 kDa isoform.³ Ph⁺ ALL is of B-cell lineage and is associated with high risk and poor prognosis due to poor detection (unlike CML, Ph⁺ ALL may only be detected by fluorescence *in situ* hybridization or reverse-transcriptase polymerase chain reaction), resistance to asparaginase and daunorubicin and toxicity from treatment with tyrosine kinase inhibitors.^{3-4,9} Finally, flow cytometry and

immunophenotyping further subtype ALL and distinguish the more uncommon cellular subtype, T-cell ALL.³

3.1.1 T-cell Acute Lymphoblastic Leukemia

Lymphoblasts of T-cell ALL are indistinguishable from B-cell ALL since they share many phenotypic features. These lymphoblasts are generally small to medium in size with a thin nuclear membrane and little cytoplasmic space due to a high nuclear to cytoplasmic ratio. Vacuoles may be present within the cytoplasm, resembling more mature lymphocytes. The nucleus may be round, irregular or convoluted in shape. Inside the nucleus the chromatin is finely stippled and moderately condensed and nucleoli are not clearly visible. One key feature which distinguishes T-cell ALL from B-cell ALL is the presence of more mitotic figures. Other key differences involve cell markers. Lymphoblasts of T-cell ALL typically are TdT and CD3 positive. CD3 is the only marker which is T-cell lineage specific. However, CD3 alone is insufficient as a prognostic indicator. Other markers which are variably expressed include CD1a, CD2, CD4, CD5, CD7 and CD8. CD7 and cytoplasmic CD3 are often positive while CD4 and CD8 tend to be co-expressed. Important precursor cell markers are CD99, CD34 and CD1a, with CD99 being the most useful indicator. Interestingly, 19-32% of T-cell ALL cases express the myeloid antigens CD13 and CD33. Although these indicators suggest myeloid cells or mixed lineage, standard T-cell ALL cannot be excluded from diagnosis. Another useful cell marker is CD117 (c-kit) which is associated with aberrant expression of FLT3. Adult cases often express CD25 and large transformed cells may express CD30.¹

Historically T-cell ALL was treated as a single malignancy, but appreciable outcomes in patients receiving uniform treatment prompted extensive research on the molecular biology of the leukemia. Based on immunophenotyping, T-cell ALL cases were originally stratified into 5 subtypes: pro-T, pre-T, cortical, $\alpha\beta$ mature and $\gamma\delta$ mature.¹⁰ Pro-T cells express CD3 and CD7, may express CD34 but do not express CD2 or CD1a. Pre-T cells are similar to pro-T but are CD2 positive. Cortical T-cells express CD3, CD7, CD2 and CD1a, but do not express CD34. Mature T-cells are similar in expression to cortical, but do not express CD1a. Additionally, pro- and pre-T are double negative for CD4 and CD8 while cortical are double positive and mature typically only express one.¹ Due to the high similarity of pro- and pre-T and the similarity of both mature types, T-cell ALL is currently stratified into 3 subtypes: early, cortical and mature.¹¹ Typically patients diagnosed with early or mature T-cell ALL have worse prognostic outcomes than patients diagnosed with cortical T-cell ALL.¹¹ Early T-cell ALL should not be confused with early T-cell precursor ALL (ETP-ALL) which has a distinct immunophenotype.⁴ ETP-ALL expresses the myeloid/stem cell markers CD13, CD33, CD34, CD117 and does not express CD1a or CD8 and may only weakly express CD5. Additionally, ETP-ALL commonly has mutations in FLT3 and RAS; making ETP-ALL more closely resemble acute myeloid leukemia, but is differentiated due to expression of the T-cell marker CD3.^{4,9}

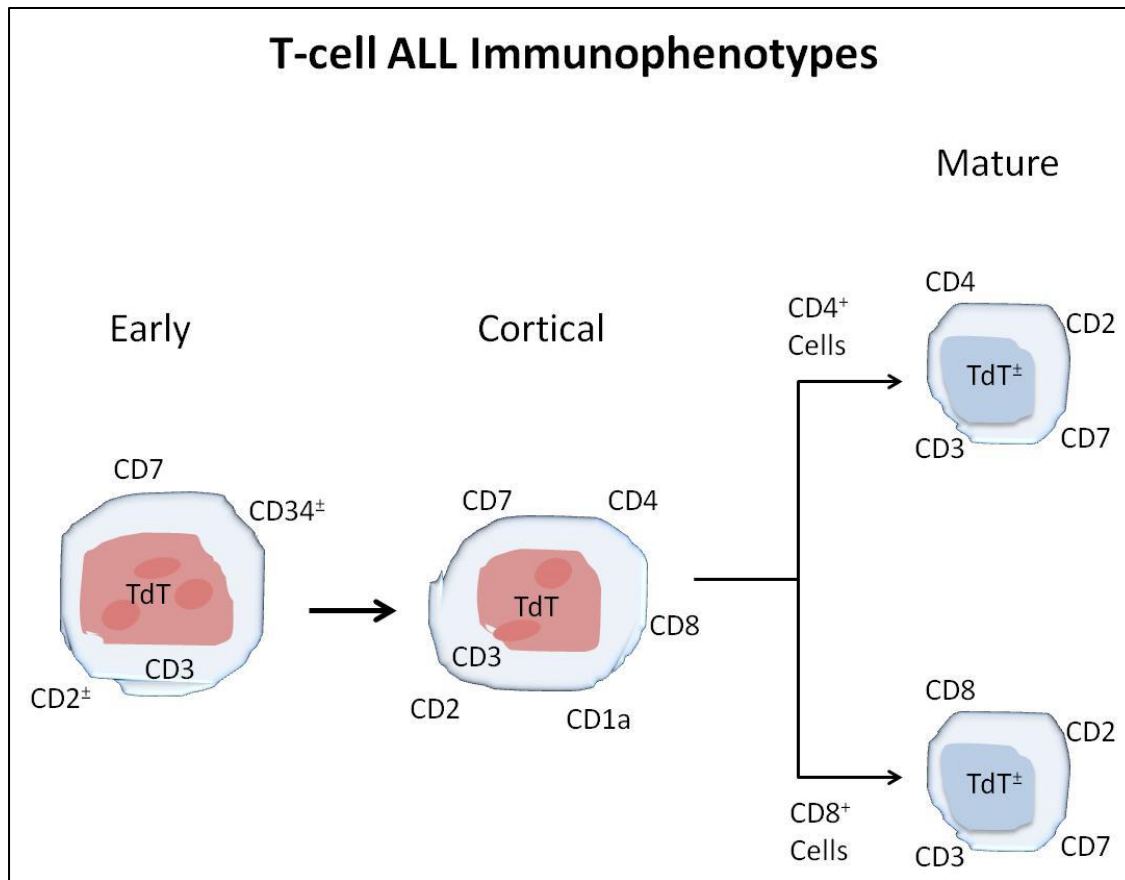


Figure 3.1: Representation of immunophenotypes of T-cell ALL as categorized by early, cortical or mature subtype.

Therapeutic regimens for T-cell ALL may also differ due to cytogenetic analysis. Unlike assessment of morphology and immunophenotyping, cytogenetic analysis cannot be used to subtype T-cell ALL since genetic abnormalities are highly heterogeneous, can be found across all subtypes and each abnormality infrequently occurs.^{10, 12} This is surprising considering approximately 50% of all cases have detectable genetic lesions.¹⁰ Due to the high heterogeneity of T-cell ALL genetic abnormalities, bone marrow samples must be tested to determine precise characteristics.¹³ Genetic abnormalities associated with T-cell ALL involve deregulation of growth, proliferation, chromatin remodeling, differentiation, self-renewal and the cell cycle as well as aberrant expression of transcription factors.^{7, 12} The hallmark of T-cell ALL is genetic

abnormalities in transcription factors of the basic helix loop helix, LIM-only domain, homeobox and MYC families as well as TAN-1.¹⁴ TAN-1 is a C-terminal domain of NOTCH1 and genetic alteration has been found to constitutively activate NOTCH1 in 50-70% of cases.¹⁵⁻¹⁸ Other common genetic abnormalities include deletion of CDKN2A (>70%) and impairment of PRC2.¹⁹⁻²¹ Some cases of T-cell ALL may also contain dysregulation of microRNA and chromosomal rearrangements often adjacent to promoter and enhancer elements of the T-cell receptor genes TRA@, TRB@, TRG@ and TRD@.^{1, 22-27} There are four main subgroups of chromosomal rearrangements: HOX11/TLX1, HOX11L2/TLX3, TAL or LMO genes and fusions involving CALM-AF10, MLL or SET-NUP214.²⁸⁻³⁰ Chromosomal rearrangements involving TAL or LMO genes or HOX11L2/TLX3 tend to be more common with incidences reported in 30% and 24% of cases respectively.²⁹ The other rearrangements and fusions are more rare (4-8% of cases), with HOX11/TLX1 only reported in pediatric cases and unknown prognostic outcomes associated with MLL and SET-NUP214 fusions.²⁸⁻³⁰ As with all cases of T-cell ALL, ETP-ALL lacks consistent genetic abnormalities but tends to contain mutations involving regulators of hematopoietic development (58%), regulators of cytokine receptors and Ras signaling (67%), chromatin modification or epigenetic regulators (48%).^{9, 31} However, more than 60% of adult cases are associated with at least one mutation in DNMT3A, FLT3 or NOTCH1.³²

3.1.2 Therapies for T-ALL and Prognostic Outcomes

Acute lymphoblastic leukemia accounts for 80% of all childhood leukemia and 20% of adult.⁷ In the United States 6,590 new cases of acute lymphoblastic leukemia are estimated to

occur.³ T-cell ALL accounts for 15% of pediatric and 25% of adult cases and occurs more frequently in males.^{12, 21} ETP-ALL is more common in children and accounts for 12-15% of childhood T-cell ALL cases.³³ Although ALL may occur at any age, 60% of cases happen under the age of 20 while 12% of cases occur in people over 65 with two peak incidents: between ages 4 and 5 and over 50.^{7, 34} This makes the management of T-cell ALL highly complex given differences in biological features between children and adults as well as the high risk associated with peak incidence ages.^{13, 35} Other high risk features commonly associated with T-cell ALL include high leukocyte count, high tumor burden and central nervous system involvement.³⁶ On average, the treatment of T-cell ALL lasts 1.5 to 3 years.³ The complexity of T-cell ALL diagnosis and treatment as well as the average length of treatment create a substantial economic burden.¹³

T- and B-cell ALL are initially treated the same and involve remission induction therapy.^{4, 6, 13} Remission induction therapy aims to cause disappearance of detectable leukemia (>5%) in both the bone marrow and other sites through the administration of high doses of multiple chemotherapeutics over a short period of time.³⁷ Chemotherapeutics commonly used are vincristine, an anthracycline (ie. doxorubicin), and a corticosteroid. This treatment regimen may also be supplemented with L-asparaginase. Patients considered to be at high risk of relapse may also receive cyclophosphamide, methotrexate, 6-mercaptopurine, etoposide or cytarabine.³⁷⁻⁴¹ Vincristine is a standard front-line chemotherapeutic for both pediatric and adult T-cell ALL.⁴ It works by binding tubulin of rapidly dividing cells, preventing the separation of chromosomes during metaphase and inducing apoptosis.⁴² Prolonged exposure leads to significant and sometimes irreversible peripheral neuropathy.⁴ Anthracyclines are DNA intercalating agents which prevent replication in rapidly proliferating cells and can cause DNA damage.⁴³ As with

all anthracyclines, doxorubicin can lead to congestive heart failure depending on the cumulative dose. It has been determined that doses exceeding 600 mg/m^2 causes cardiotoxicity in 36% of patients. Additionally, cardiotoxicity caused by doxorubicin results in 50% mortality.⁴⁴ The corticosteroids given as part of remission induction therapy typically include either prednisone or dexamethasone. While neither corticosteroid is considered to be toxic, they may cause depression and anxiety and long term exposure may cause osteoporosis, glaucoma and type 2 diabetes.⁴⁵ L-asparaginase prevents the conversion of L-asparagine to aspartic acid, depriving malignant hematological cells which are unable to synthesize asparagine leading to cell death.⁴⁶ It is not always prescribed to treat T-cell ALL because L-asparaginase is known to cause myelotoxicity and can significantly increase the chances of developing serious bacterial or viral infections.⁴⁷ Remission induction therapy may also be accompanied by central nervous system (CNS) prophylaxis. CNS prophylaxis may involve cranial radiation therapy with intrathecal injection of methotrexate, systemic administration of high doses of methotrexate and intrathecal injection of methotrexate or intrathecal injection of chemotherapeutics.³

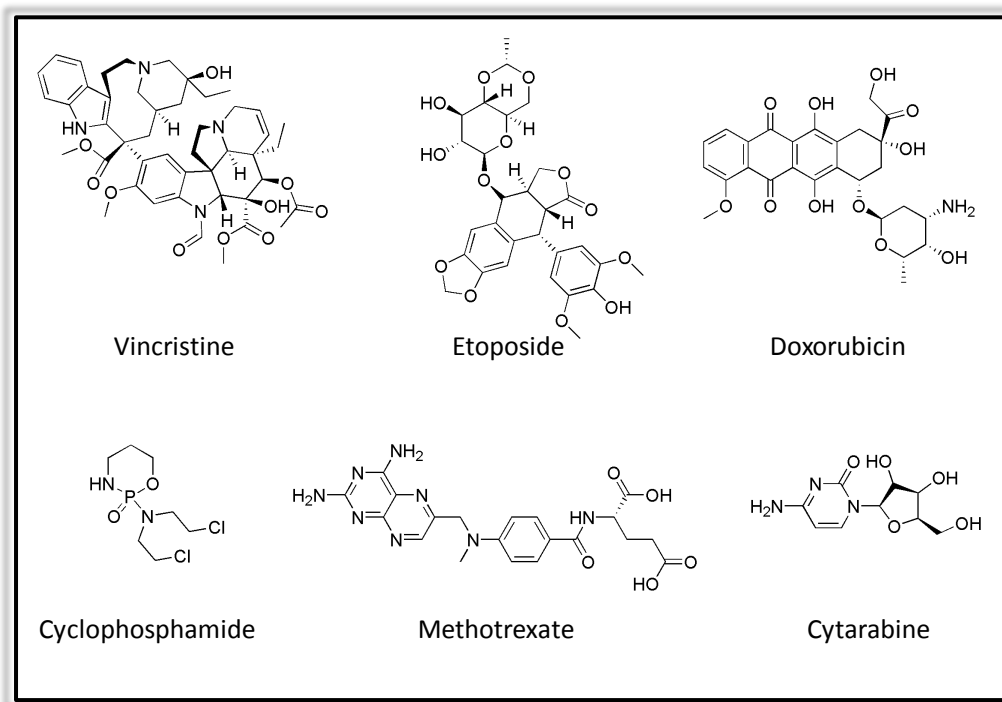


Figure 3.2: Chemotherapeutics commonly used to treat both T- and B-cell ALL.

Despite increased knowledge of subtype biology, genetic abnormalities and general toxicities of prescribed chemotherapeutics, treatment plans for T-cell ALL have not changed much over the past couple of decades and many chemotherapeutic combinations depend on oncology center preference.^{4,21} Although complete remission is achieved in >90% of patients, these gains also come with significant life altering side-effects and higher risk of mortality due to chemotherapeutic toxicity.^{4,48} Additionally, more than 50% of patients will relapse within 3 years.^{41,49} Therefore post remission therapy is critical. Unfortunately, optimal post remission therapy is unknown and mainly consists of autologous or allogeneic bone marrow transplant (alloBMT).³ Typically only patients at high risk are recommended to undergo alloBMT after remission, but recent studies suggest patients with moderate risk benefit significantly more from alloBMT than patients at high risk.⁴ Unfortunately, alloBMT may result in 20-40% mortality due to graft-versus-host disease, veno-occlusive disease or liver and interstitial pneumonitis

despite offering the lowest incidence of relapse.³ The low incidence of relapse associated with alloBMT is why most patients who do relapse typically undergo reinduction chemotherapy followed by alloBMT, especially since chemotherapy alone is highly unlikely to cure relapse cases.³

Patients diagnosed with T-cell ALL generally have worse prognostic outcomes compared to B-cell ALL.⁵⁰⁻⁵³ The worse outcome is associated with a significant risk of relapse and low response to rescue therapy after relapse; with the subtype ETP-ALL linked to the greatest risk of relapse in addition to a high risk of remission therapy failure.^{21, 54} Failure to respond to remission therapy or rescue therapy after relapse is mainly due to chemoresistance.²¹ Surprisingly, 60-80% of adults and greater than 90% of children will achieve complete remission, but more than 50% will relapse.^{3, 55} Despite decades of research, clinical care of T-cell ALL has remained similar and strategies to achieve a second complete remission are severely lacking. The majority of relapses occur within two years of first remission and results in 5-year survival rates of only 7-23%. One factor which leads to relapse is minimal residual disease (MRD) located in the bone marrow.²¹ MRD is a significant prognostic tool since patients who are MRD positive after remission therapy are more suited for alloBM, are considered to be at higher risk of relapse and have a 5-year survival rate of 33% while MRD negative patients have an average 5-year survival rate of 75%.⁴ More than 90% of patients who are MRD positive after remission therapy relapse within 5 months and typically experience chemoresistance.⁵⁶

Table 3.1: Trends in 5-year relative survival rates of select leukemia/lymphoma patients in the United States.

Trends in 5-year relative survival rates (%) in the United States					
Cancer type	1960-1963	1974-1976	1983-1985	1995-2001	2004-2010
Non-Hodgkin's lymphoma	31	47	54	60	72
Leukemia	14	34	41	48	60
Multiple myeloma	12	25	28	32	50
Acute Lymphoblastic Leukemia	N/A	41	52	65	70

Not surprisingly, adults are predisposed to high risk features associated with increased chance of relapse and chemoresistance even during remission therapy.⁴ Predisposition to chemoresistance is thought to involve leukemic stem cells. These stem cells exhibit asymmetric cell division, are capable of self-renewal and production of partially differentiated cells and are typically quiescent, making them relatively unsusceptible to chemotherapy.⁵⁷ Chemoresistance, either initial or acquired after relapse, is the major barrier to achieving a second complete remission and improved survival rates.⁵⁸ Unfortunately, the mechanism(s) through which T-cell ALL becomes chemoresistant is mostly unknown.¹⁴ Current therapeutic options after relapse include cytarabine, etoposide, clofarabine, nelarabine and may include clinical trials with γ -secretase inhibitors. The first line therapeutic option after relapse utilizes cytarabine and etoposide. Cytarabine disrupts DNA synthesis, causing S phase cell cycle arrest.⁵⁹ Side effects of cytarabine include leucopenia and thrombocytopenia, two disorders already associated with high risk T-cell ALL, and may cause cerebellar toxicity. Etoposide is often used in combination with cytarabine or another chemotherapeutic and causes single strand breaks in DNA leading to apoptosis.⁶⁰ Clofarabine is known to be active in relapse and refractory cases, but is a known

hepatotoxin.^{4, 21} While clofarabine may be more active, it has primarily been used to treat children.⁶¹ Nelarabine, like clofarabine, is an analog of 6-mercaptopurine. Despite being the best studied of the two, nelarabine is considered a third line option.⁴ Interestingly, nelarabine selectively accumulates in T-cells but is only prescribed for patients who are refractory to or have relapsed after treatment with at least two other chemotherapeutic regimens.^{6, 54, 62} γ -Secretase inhibitors may be better options to the previously mentioned chemotherapeutics as they block a critical step in Notch activation, but are currently only in clinical trials and may result in gastrointestinal toxicity.⁴

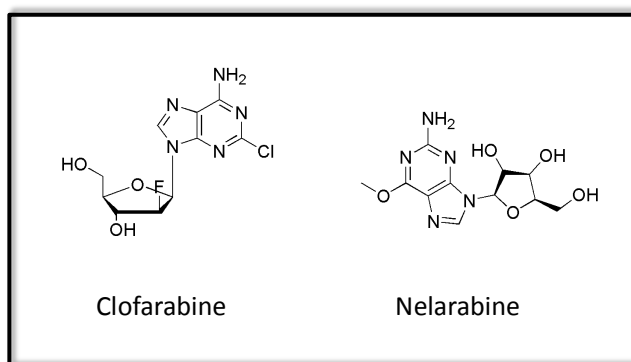


Figure 3.3: Late stage chemotherapeutic options to treat T-cell ALL.

Despite the high risk of relapse, long term remission in children approaches 70-80% and is achieved in approximately 40% of adults.¹⁰ Overall cure rates are reported to be greater than 90% in pediatric cases, 30-40% for adults under the age of 60 and 10% in patients older than 60.^{4, 11} However, when these rates are stratified by risk group survival rates are not as promising as these numbers would suggest. Pediatric cases are categorized into three risk groups: standard (40% of all cases), intermediate (45-50%) and high risk (10-15%). Standard and intermediate risk groups fare the best with 90% and 70-80% survival rates respectively. High risk pediatric cases do not have as successful long term survival rates, with only around 50% achieving long

term survival. Since adults are predisposed to high risk features, adult cases are only categorized into standard (20-25% of cases) and high risk (75-80%) subgroups. Standard risk cases are associated with 60% long term survival while high risk cases only achieve 30% long term survival.⁷ There is an estimated 1,430 deaths that will be attributed to ALL in the United States in 2016.³⁴ Together, the high risk of relapse, increased chemoresistance and poor prognostic outcomes for patients older than 25 or classified as high risk stresses the importance of continued research for better therapeutic options for T-cell ALL.³ This research should aim to better characterize genetic aberrations associated with T-cell ALL, minimizing toxic effects, improving cure rates and long term survival, and developing more options to induce a second remission and eradicate minimal residual disease.¹³

Table 3.2: 40 year trends in leukemia death rates per 100,000 people for males and females.

Trends in cancer death rates per 100,000 of population					
Leukemia	1971-1973	1980	1990	2000	2009-2013
Male	8.9	11.2	10.7	10.3	9.3
Female	5.3	6.5	6.2	5.9	5.2

3.1.3 Strategies Toward Better Therapeutic Options

Current research focused on developing better therapeutic options to treat T-cell ALL is aimed toward inhibition of key genes/gene products or signaling pathways thought to be involved in pathogenesis and progression of the disease. The majority of the aberrant genetic mutations associated with T-cell ALL can be categorized into four classes based on function: cell cycle, impairment of differentiation, self-renewal and proliferation and survival.⁷ CDKN2A and CDKN2B are the two genes commonly altered in T-cell ALL (65-70% of cases) and are linked

to cell cycle progression.⁵⁴ Members of the CDKN2 family inhibit CDK4 and CDK6 to allow progression past the G1/S cell cycle checkpoint. Alteration of CDKN2A/B are mostly deletions but may be point mutations or hypermethylation.⁶³ Unlike most T-cell ALL mutations, deletions in CDKN2A/B tend to be homozygous. These deletions occur in the tumor suppressor locus which contains the code for p14^{ARF} and p16^{INK4a} and promote uncontrolled cell cycle entry.⁷ Loss of p14^{ARF} leads to elevated levels of Mdm2 which inhibits transcriptional activation of p53.⁶⁴ Additionally, aberrant BMI1 which interacts with MYC may also inhibit expression of CDKN2A/B expression.⁵

Impairment of differentiation typically involves MLL, LYL1, TAL1, TAL2, LMO1 and/or LMO2.⁷ As previously mentioned, the MLL gene may form a fusion gene in 5% of T-cell ALL cases. MLL1 is involved in hematopoietic differentiation and leukemogenesis.⁵ LYL1 is known to be important for normal angiogenesis, hematopoiesis and may form a translocation with the T-cell receptor beta locus on chromosome 7.^{10, 65} Aberrant expression of TAL1 is found in 60% of T-cell ALL cases and is associated with the regulation of stem cell development. When TAL1 or LYL1 are deregulated, LMO1 and LMO2 tend to become activated. Malignancies presenting these genetic abnormalities are associated with poor prognosis. These malignancies frequently also have mutations in Ras, cytokine receptor pathways (ie. IL7R and JAK1), transcription factors and histone modifications.³⁶

Gain of self-renewal capability in T-cell ALL is linked to activating mutations in NOTCH1.⁷ It has been determined that more than 60% of T-cell ALL cases have NOTCH1 mutations.¹¹ NOTCH1 encodes a heterodimeric cell membrane receptor that regulates T-cell development, signal transduction, proliferation, adhesion and apoptosis.^{10, 66} Activation results in changes in gene expression within the nucleus.⁶⁷ Overexpression induces ectopic thymocyte

development and prevents other developmental options.¹⁴ Mutations in NOTCH1 are frequently accompanied by heterozygous mutations in FBXW7 (8-30% of cases).⁷ FBXW7 is a ubiquitin ligase which targets Notch1, cMYC, cyclin E and cJun for degradation.^{7, 10} Other genes which may be associated with aberrant NOTCH1 are JMJD3 and JAK1. JMJD3 is a histone demethylase of H3K27 and is essential to the maintenance of NOTCH1 signaling.²¹ Gain of function mutation in JAK1 is found in 10-20% of adults with T-cell ALL. This mutation may cooperate with constitutively activated NOTCH1 in the pathogenesis and progression of T-cell ALL and is associated with chemoresistance, increased risk of relapse and reduced overall survival.⁷

Constitutive activation of NOTCH1 may also cause increased phosphorylation and activation of the PI3K/AKT/mTOR pathway.^{7, 66} The PI3K/AKT/mTOR signaling pathway is highly active in 75-80% of T-cell ALL with mutations within the pathway discovered in 50% of these cases.¹¹ Increased activity of PI3K/AKT/mTOR pathway is linked to chemoresistance and is involved in cell cycle progression, survival, translation, metabolism, and autophagy.^{11, 68} Regulation of the pathway is highly complex with multiple feedback loops. One feedback loop is the activation of mTORC1 by Akt which antagonizes mTORC2 which in turn reduces Akt activity.¹¹ Activation of Akt leads to phosphorylation of multiple protein. Phosphorylation by Akt activates Mdm2 and inactivates pro-apoptotic proteins including FOXO proteins, p21 and p27. Akt also inactivates Bad, pro-caspase 9 and FasL. Akt activates CREB, IKK to regulate expression of gene with anti-apoptotic activity.⁶⁸ mTORC1 limits autophagy and promotes cell growth and proliferation. Another function of mTORC1 is to phosphorylate and promote translation of 4E-BP1 which interacts with eIF4E to regulate mRNA translation. mTORC2 also regulates proliferation through cytoskeleton regulation involving actin fibers, paxillin, RhoA,

Rac1 and PKC α . While mutations in any of these genes could promote the pathogenesis of T-cell ALL, the primary mutation appears in PTEN and rarely ever in PI3K or AKT.¹¹ The mutation in PTEN is commonly a deletion which results in loss of function. Interestingly, this appears to be a secondary event and may serve as a prognostic marker in the progression of T-cell ALL. Loss of PTEN function causes activation of the PI3K/AKT/mTOR pathway, enhances cell size, glucose uptake and proliferation which cumulatively causes a higher risk in failure of remission therapy.⁷

Activation of PI3K/AKT/mTOR is also controlled by the binding of IL-7 to IL7R. This binding event is required for the function of PI3K- γ and - δ to promote thymocyte development and T-cell maturation. Additionally, IL-7 binding activates Akt and mTORC1 which are critical for early and late phase T-cell development. A mutation in IL7R- α results in constitutive activation of the PI3K/AKT/mTOR pathway as well as JAK1 and STAT5.¹⁴ IL-7 signaling also produces reactive oxygenated species critical for the proliferation and survival functions of PI3K/AKT/mTOR.¹¹ Another function of IL-7 signaling is to promote expression of stem cell specific genes and inhibit T-cell transcription factors such as BCL11B.¹⁴ BCL11B is a member of the BCL family and is critical as a T-cell regulator in development, proliferation, differentiation and survival.⁶⁹⁻⁷⁰ It encodes a DNA binding protein essential for the maturation of T-cells from precursors to immature stages and more mature stages of development.¹⁰ Overexpression of BCL11B has been found in T-cell ALL and may be important in leukemogenesis.⁶⁹ BCL11B also regulates the transcriptional activation of EP300 which is important for cell growth, division, differentiation and tumor suppression.^{69, 71}

In addition to IL-7 signaling and the PI3K/AKT/mTOR pathway, another major signaling pathway associated with proliferation and survival commonly mutated in T-cell ALL is p53.

Mutations in TP53 are found in up to 50% of adult cases and 2-10% of pediatric.⁶³ However, these mutations are only discovered in 5% of initially diagnosed patients, making it much more common in relapse cases.⁷ This mutation is generally a point mutation in exons 5-8 and is associated with poor response to prednisone, high risk of treatment failure and poor clinical outcome. The gene product of TP53 is p53 which acts as a checkpoint control for G1/S transition. p53 is also important for senescence and apoptosis and has been found to inhibit Akt/mTOR as well as Notch signaling.⁶³ Genes associated with p53 stabilization and activation, such as USP7 and ATM, may also be mutated in T-cell ALL. USP7 stabilizes p53 and is implicated in transcriptional regulation, cell cycle progression and DNA damage response.²¹ The DNA damage response may be initiated by ATM. ATM senses double strand breaks in DNA and signals multiple effector proteins for cell cycle arrest.⁷² These effector proteins include E2F, which can increase levels of p^{14ARF}, and p53.⁶³ Other DNA damage response signals from ATM include activation of signal transduction, cell cycle regulation, DNA repair, transcription and apoptosis.⁷³ Activation of ATM may also occur due to elevated levels of both endogenous and induced oxidative DNA damage not associated with double strand breaks.⁷⁴ If the DNA damage sensed by ATM is irreparable then ATM will phosphorylate and activate p53 triggering cell cycle arrest and apoptosis.⁷² Mutations in ATM are found in 2-17% of T-cell ALL cases and leads to constitutive activation.⁶³ Constitutive activation of ATM and the DNA damage response is thought to lead to the emergence and selection of malignant cells with non-functional ATM and/or p53.⁷²

Another action which may activate ATM is chromatin remodeling. One reason for this hypothesis is that ATM phosphorylates histone deacetylase (HDAC) 1.⁷³ Maturation of T-cells requires constant chromatin remodeling through DNA methylation and histone

modifications to allow for rapid gene expression.⁷⁵ In addition to ATM, other common mutations in T-cell ALL can cause changes in chromatin structure. As previously mentioned, BCL11B regulates the transcriptional activation of EP300. EP300 and CREBBP have roles in hematopoiesis and acetylate histones as well as MYB, E2F1, TP53 and RB1.⁷⁶⁻⁷⁷ Loss of function mutations in CREBBP may result in chemoresistance.⁷⁸ HDACs may also be implicated in primary T-cell ALL. Somatic mutations in HDAC5 and HDAC7 have been discovered in 5% of pediatric cases and elevated expression or enhanced activity of HDACs are exhibited in T-cell ALL.²¹ While chromatin remodeling and epigenetic modification may be driving forces in the progression of T-cell ALL, enhancer sequences which recognize specific epigenetic modifications also contribute to the pathogenesis. One super-enhancer sequence, BRD4, in particular recognizes acetylated H3K27 and singly methylated H3K4 and is associated with T-cell ALL oncogenes MYB, MYC, ERG, GFI1, CCND3, CDK6, TAL1 and NOTCH1.⁷⁹

While all of the aforementioned genes/gene products or signaling pathways are considered to be therapeutic targets for the development of new anti-leukemic drugs, more research has focused on Notch, PI3K, mTOR, and HDAC inhibitors. γ -Secretase inhibitors have been developed to block the Notch signaling pathway. As mentioned previously, these inhibitors are occasionally prescribed as part of clinical trials for patients who have suffered a relapse after complete remission. These inhibitors prevent the cleavage of and inhibit activation of Notch1.¹² Currently there are two γ -secretase in clinical trials for the treatment of hematologic malignancies: RO4929097 and LY3039478.⁸⁰ The most well researched PI3K inhibitors are wortmannin and LY-294002. Both of these are relatively potent (5 nM and 1.4 μ M respectively) but non-selective inhibitors of PI3Ks. They have also been found to inhibit other enzymes such as mTOR, MAPK, MLCK and BET.⁸¹ Additionally, wortmannin is known to exhibit a

detrimental effect on memory and can impair spatial learning abilities. Because of their off target effects and detrimental side effects, these PI3K inhibitors are not being utilized.⁸²

However, two PI3K inhibitors are currently in clinical trials for various cancers: RP6530 and BKM120.⁸⁰ Rapamycin, an mTOR inhibitor, is FDA approved but is currently in clinical trials as an anticancer therapeutic. Rapamycin binds to FKBP12 which subsequently binds to mTORC1 to inhibit the mTOR pathway.⁸³ Its derivative, everolimus, is also being investigated in clinical trials.⁸⁰ HDAC inhibitors that have been FDA approved or are currently in clinical trials have been discussed in Chapter 1. Briefly, there are 11 zinc-dependent or “classical” HDAC isoforms and 7 non-zinc-dependent isoforms called sirtuins.⁸⁴ Most HDAC inhibitors have been developed to target the classical isoforms, but several have been developed to target sirtuins.⁸⁵ There are other inhibitors being developed which target other factors associated with T-cell ALL but these targets are not as well studied and review of all inhibitors being developed is outside the scope of this chapter.

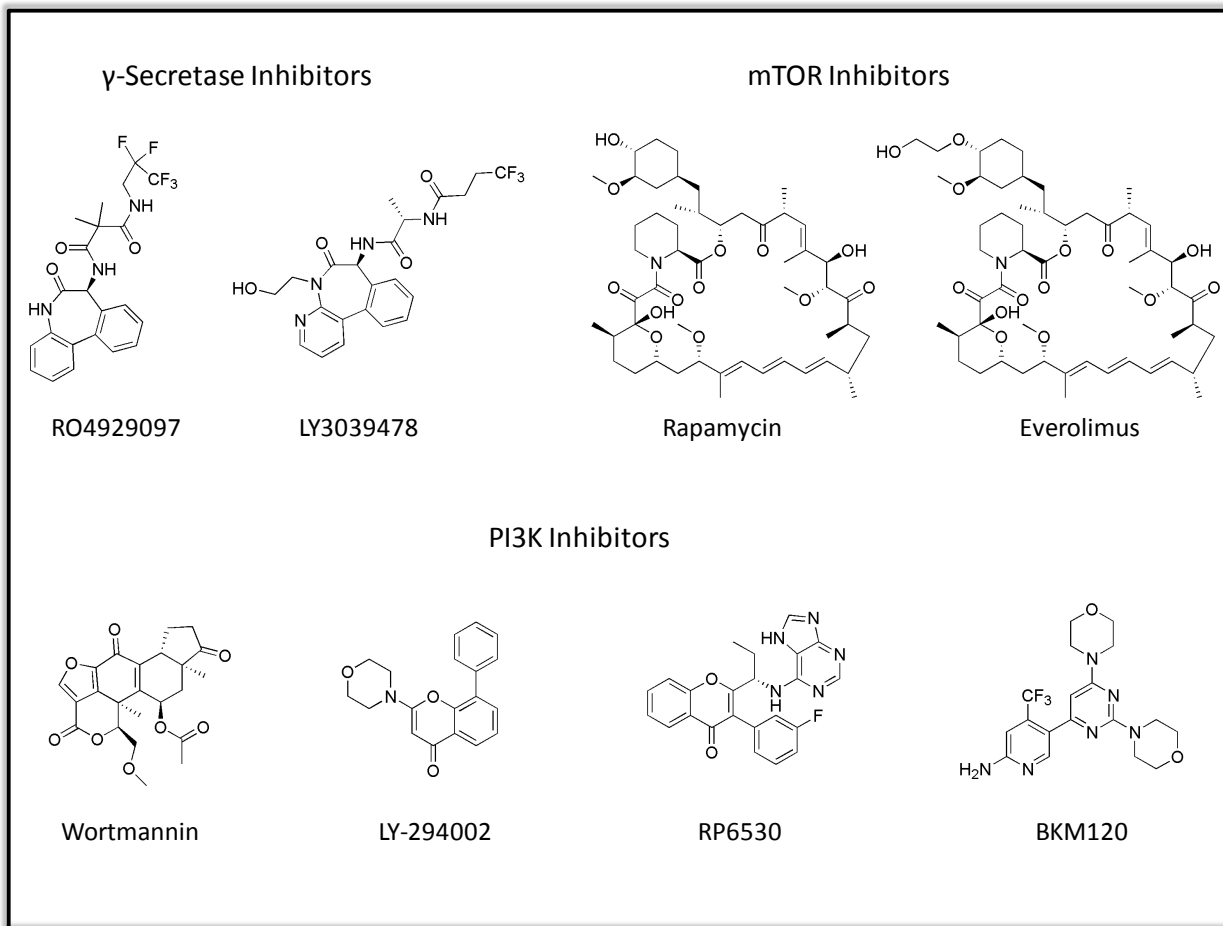


Figure 3.4: New anti-leukemic drugs in clinical trials.

3.1.4 Tropolones as Anti-leukemic Agents

Naturally occurring tropolones are known to exhibit antiproliferative effects.⁸⁶⁻⁸⁸ The best studied tropolone, hinokitiol, has been found to inhibit DNA synthesis, induce cell cycle arrest and exhibit cytotoxic effects in the murine leukemia cell line P388. Other naturally occurring tropolones related to hinokitiol (HKT) also display cytotoxic effects towards P388 which may be associated with inhibition of the metalloenzyme ribonucleotide reductase.⁸⁹ The structural isomer of hinokitiol, α -thujaplicin, displays similar potency against P388 as vincristine after 24 hours but with significantly lower acute toxicity.⁸⁸ Tropolone itself inhibits the uptake

of leucine and thymidine in myeloid leukemia and causes oxidative damage similar to doxorubicin.⁹⁰

The Anderson and Wright labs synthesized and screened tropolone derivatives against two T-cell lymphocytes (Jurkat and HuT-78), a colon cancer cell line (HCT-116) and a pancreatic cancer cell line (BxPC-3). Here the tropolones exhibited significant half maximal growth inhibition (GI_{50}) of the T-cell lymphocytes. This activity differed from that of vorinostat, a HDAC inhibitor, which displayed similar cytotoxic activity towards HuT-78 and HCT-116. The tropolones also did not appear to be toxic ($GI_{50} > 100 \mu M$) towards primary human dermal fibroblasts while vorinostat gave a GI_{50} of $18.95 \mu M$.⁹¹

Research in the Anderson and Wright labs determined the synthetic tropolones are inhibitory towards HDACs with significant selectivity towards HDAC2.⁹¹ It has been shown that HDAC2 inhibition is particularly exciting as a target of aggressive cancers including cutaneous T-cell lymphoma.⁹² Unlike most HDAC inhibitors, the tropolones did not inhibit HDAC6 or cause hyperacetylation of tubulin. The tropolones also displayed different effects on p21 and caspase-8 activation from typical HDAC inhibitors. However, the tropolones were able to enhance the expression of perforin similar to the HDAC inhibitor romidepsin.⁹³ In a collaborative effort with the Giardina lab, the effect of the synthetic tropolones on differentiation regulators was compared to known epigenetic modifiers. Tropolones were found to increase expression of Math1 without changing expression of Muc2. This activity contrasts with that of HDAC inhibitors which increased expression of both Math1 and Muc2, but coincided with the activity displayed by sirtuin modulators. Interestingly, both the tropolones and the sirtuin modulators increased expression of Fabp2 while HDAC inhibitors decreased Fabp2 expression.⁹⁴ These results suggest tropolones may exhibit antiproliferative effects through sirtuin modulation.

This may explain the selectivity towards the hematologic cancer cell lines as sirtuins appear to be involved in many of the processes which facilitate the pathogenesis of leukemia including PI3K/AKT signaling, RAS signaling, p53 activation, regulation of the Foxo family, EP300 and MYC.⁹⁵⁻⁹⁶

3.1.5 Project Objectives

Our goal was to screen a set of tropolone derivatives against sirtuins 1 and 2 to determine if previous anticancer effects exhibited by these tropolones could be attributed to sirtuin inhibition. Because previous research with tropolone derivatives displayed significant anticancer effects against hematologic malignancies, our other primary goal was to assess the activity of both the previously studied tropolones and the newly synthesized tropolones against a panel of leukemic cell lines. These cell lines include T-cell, B-cell and myeloid malignancies to determine if tropolones exhibit lineage specific effects. The most potent tropolones would also be assayed with peripheral blood monocytes to determine whether the cytotoxic effects against the leukemic cell lines were due to general toxicity.

3.2 Results and Discussion

3.2.1 α -Tropolones Modulate Sirtuin 1 and 2

Based on a screen of epigenetically active compounds on intestinal organoid cells derived from cancer-prone *Apc*^{Min/+} mice, synthetic tropolones exhibited activity profiles similar to

sirtuin modulators.⁹⁴ To assess the potential of tropolones to modulate sirtuins, SIRT1 and SIRT2 activity was screened with 10 μ M concentrations of 26 synthetic tropolones, two natural troponoids, three sirtuin inhibitors, a SIRT1 activator and a pan-HDAC inhibitor. Activities were screened using the Direct Fluorescent Screening Assay Kits from Cayman Chemical Company. Following the standard analysis procedures provided, % Inhibition was calculated as:

$$\% \text{ Inhibition} = \left[\frac{\text{Initial Activity} - \text{Sample}}{\text{Initial Activity}} \right] \times 100$$

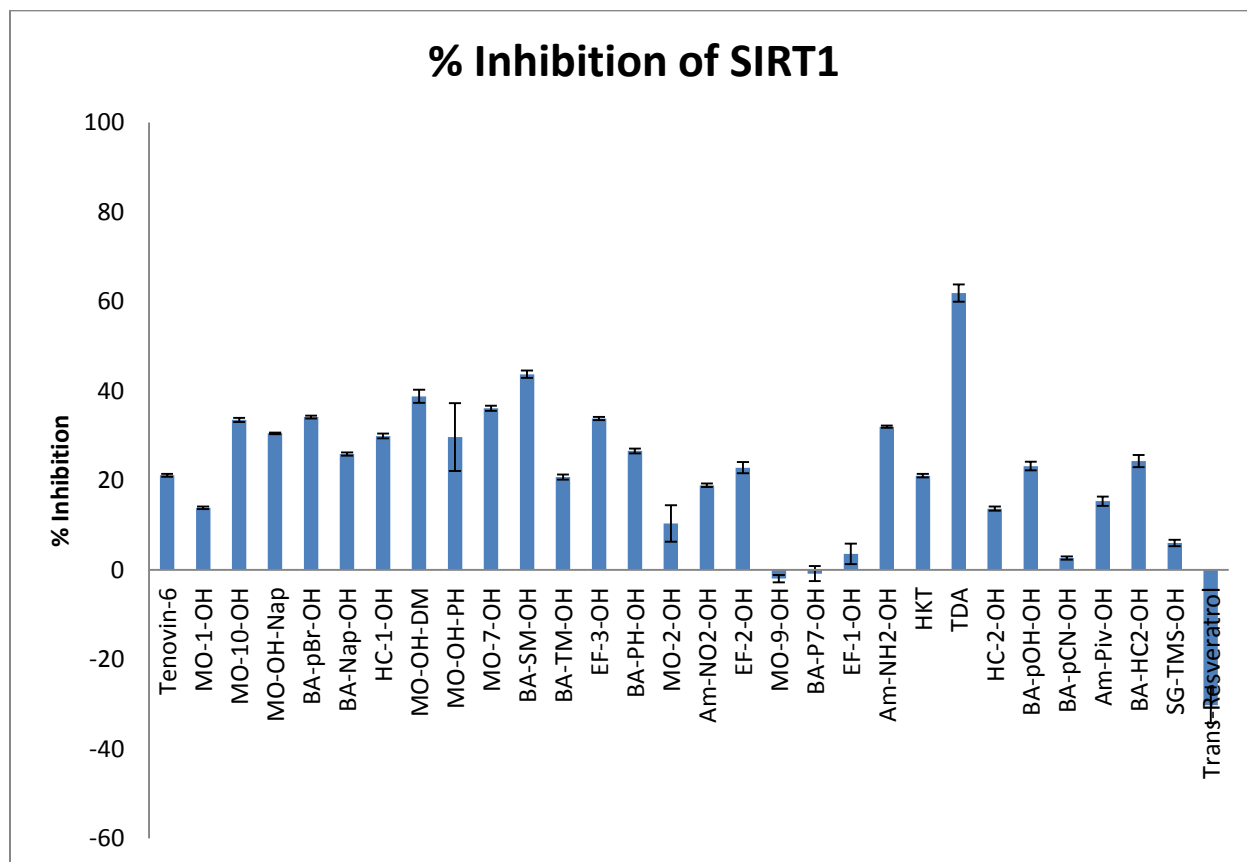


Figure 3.5: % Inhibition of SIRT1 as determined by SIRT1 Direct Fluorescent Screening Assay Kit (n=3) with 10 μ M of each compound. Tenovin-6 was used as a positive control of SIRT1 inhibition. Negative values indicate activation of SIRT1.

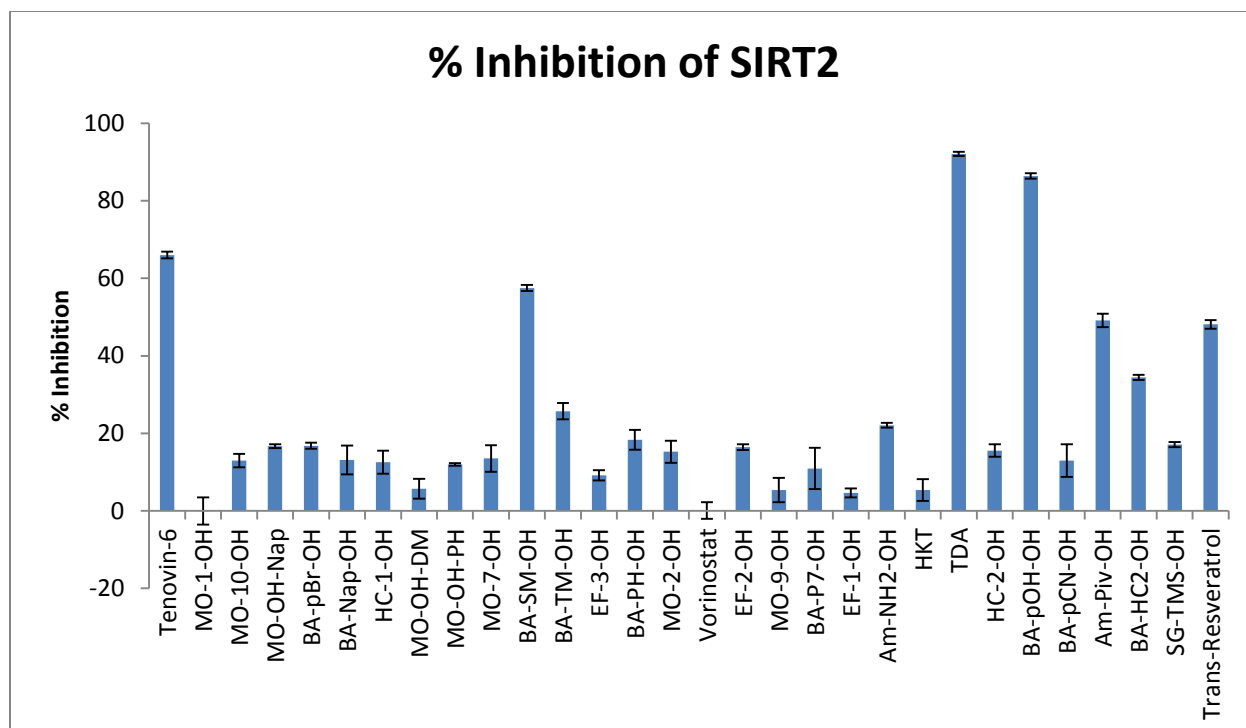


Figure 3.6: % Inhibition of SIRT2 as determined by SIRT2 Direct Fluorescent Screening Assay Kit (n=3) with 10 μ M of each compound. Tenovin-6 was used as a positive control of SIRT2 inhibition. Negative values indicate activation of SIRT2.

The majority of the tropolones screened exhibit inhibitory activity against both SIRT1 and SIRT2. Interestingly, most of the tropolones appear to be more potent against SIRT1 than the sirtuin inhibitor Tenovin-6. Tenovin-6 is one of the more potent sirtuin inhibitors developed and is known to inhibit SIRT1 ($IC_{50} = 21 \mu$ M), SIRT2 ($IC_{50} = 10 \mu$ M) and SIRT3 ($IC_{50} = 67 \mu$ M).⁹⁷ Trans-resveratrol was included in the screen because it is reportedly a SIRT1 activator and does not activate SIRT2.⁹⁸ Because most of the tropolones exhibit similar activity in SIRT1, it is difficult to determine any structure activity relationship. Remarkably, the tropolones that exhibit the least inhibition activity against SIRT1 have substantial pharmaceutical liabilities. EF-1-OH has a benzaldehyde functional group which is a known Michael acceptor. Michael

acceptors can be promiscuous and can form covalent bonds to inactivate enzymes which can lead to substantial toxicity. BA-pCN-OH has a benzonitrile functional group. The cyano group is readily hydrolyzed by acids to generate benzoic acid which can be moderately toxic and decomposition of benzonitrile can generate nitrogen oxides and hydrogen cyanide which is acutely toxic.⁹⁹ Additionally, the two tropolones that slightly activate SIRT1 have a phenyl ring with a *para*-alkyl chain of four (MO-9-OH) or seven (BA-P7-OH) carbons. Surprisingly, a similar compound with a two carbon alkyl chain (MO-10-OH) is among some of the more active inhibitors.

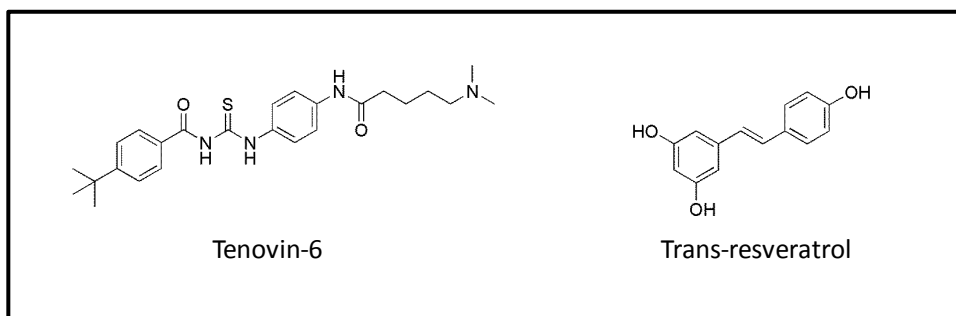


Figure 3.7: Two reported sirutin modulators used as controls.

In contrast to the moderate inhibitory activity of the tropolones towards SIRT1, the majority of the tropolones display weak inhibitory activity towards SIRT2. Again, the similar activity exhibited makes it difficult to determine a structure activity relationship. Interestingly, trans-resveratrol was determined to be an inhibitor of SIRT2 with 48% inhibition at 10 μ M. The inhibitory activity of trans-resveratrol against SIRT2 would explain why it does not activate SIRT2 at 200 μ M and its structure could serve as a template to develop dual action SIRT1 activators/SIRT2 inhibitors; however, these results necessitate more in-depth analysis of trans-resveratrol sirtuin activity which is outside the scope of this project. However, three of the tropolones and the natural tropolonoid, tropodithietic acid (TDA), appear to have IC₅₀ values

around 10 μM or less. Here the most potent tropolone has a phenol substituent. The tropolones and Tenovin-6 were subsequently screened at five different concentrations: 1, 5, 10, 20 and 30 μM ; and IC_{50} s were calculated from the inhibition activity curve.

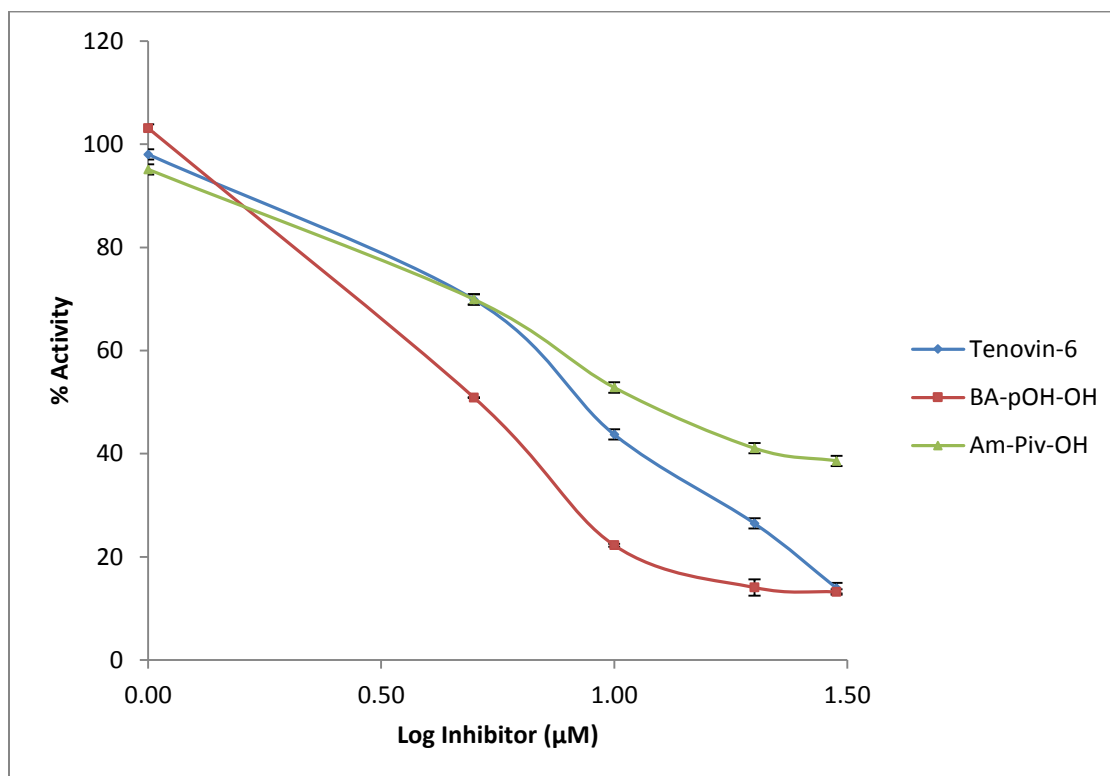


Figure 3.8: Non-linear regression analysis of log[inhibitor] versus normalized response.

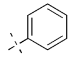
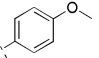
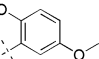
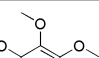
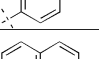
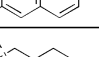
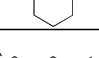
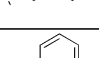
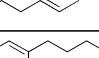
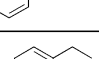
The IC_{50} for Tenovin-6 was determined to be 8.4 μM which is similar to the estimated IC_{50} of 10 μM .⁹⁷ Next, the IC_{50} s of BA-pOH-OH, BA-SM-OH and Am-Piv-OH were determined. BA-pOH-OH proved to be nearly 2-times more potent than Tenovin-6 with $\text{IC}_{50} = 4.9 \mu\text{M}$ while Am-Piv-OH gave $\text{IC}_{50} = 13.3 \mu\text{M}$. Unfortunately, an IC_{50} for BA-SM-OH could not be determined. In the 10 μM screen, two of the three replicates for BA-SM-OH gave similar values while the third replicate was drastically different and omitted. It may be possible that the outlier value was the true value which would explain why an IC_{50} could not be determined.

Although BA-pOH-OH and Am-Piv-OH are among the most potent known SIRT2 inhibitors and the tropolones in general may be among the most potent known SIRT1 inhibitors, the concentrations required to obtain an IC_{50} is significantly greater than the concentrations required for HDAC2 or HDAC8 inhibition by tropolones. This would suggest the tropolones may exhibit similar epigenetic activity profiles to sirtuin modulators due to selective HDAC inhibition, independent of sirtuin activity. It is also possible that the tropolones have a different mechanism than HDAC/sirtuin modulation that effects expression of certain genes including Math1, Muc2 and Fabp2.

3.2.2 α -Tropolones Exhibit Antiproliferative Selectivity Towards T-cell ALL

Since the initial series of tropolones developed in the Wright lab exhibited a growth inhibitory preference towards the hematological cell lines Jurkat and HuT-78 over the colon and pancreatic cancer cell lines HCT-116 and BxPC-3 respectively as well as other cancer cell lines not reported (colon: HT-29; lung: A549; brain: U-87 MG; breast: MCF-7), it was desired to explore any hematological lineage dependent preferences. A panel of leukemic cell lines with T-cell lineage (Jurkat, HuT-78 and Molt-4), B-cell lineage (Daudi and the murine cell line Ba/F3) or myeloid lineage (K562 and HL-60) were screened with the first generation α -substituted tropolones as well as the alkyl chain series of α -tropolones used in the organoid epigenetic controlled differentiation screen by the Giardina lab.

Table 3.3: GI₅₀ values (μM) of first generation and alkyl α-tropolones against a panel of hematological cancer cells from T, B or myeloid lineage.

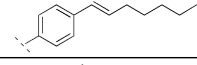
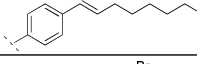
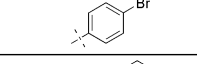
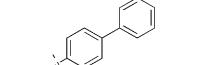
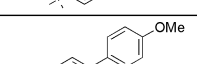
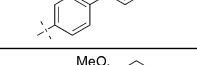
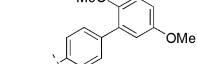
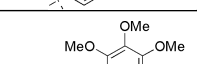
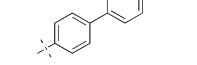
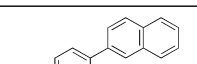
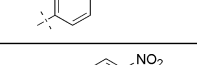
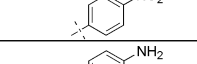
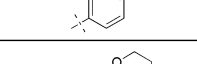
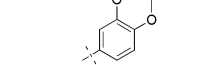
		T-cell			B-cell		Myeloid	
Compound	Functional Group	Jurkat	HuT-78	Molt-4	Daudi	Ba/F3	K562	HL-60
MO-OH-PH		3.33	5.17	0.59	5.77	6.65	8.25	2.79
MO-OH-SM		0.62	2.48	0.58	1.87	5.32	7.47	2.38
MO-OH-DM		0.75	3.62	0.52	3.36	7.22	7.35	3.22
MO-OH-TM		1.86	4.18	0.81	4.20	6.18	7.80	3.00
MO-OH-Nap		1.15	2.09	0.35	1.63	2.34	2.50	1.97
MO-1-OH		NA	1.72	0.24	1.43	3.16	2.74	2.16
MO-2-OH		1.16	5.70	0.81	1.62	1.90	2.92	2.44
MO-7-OH		0.99	4.10	0.62	1.43	1.87	3.32	2.52
MO-9-OH		2.20	2.84	1.33	2.20	2.36	2.82	2.45
MO-10-OH		0.85	3.08	0.34	0.89	2.17	2.38	0.93
Vorinostat		0.51	1.58	0.26	0.49	0.39	1.30	0.16

From this panel of hematological cancer cells there appears to be a preference towards cells of T-cell lineage. While the GI₅₀ values determined for HuT-78 are similar to those for B-cell and myeloid lineage, it should be noted that HuT-78 is a cutaneous T-cell lymphoma whereas Jurkat and Molt-4 are T-cell ALL cell lines. This data suggests tropolones are more potent towards T-cell ALL than the other malignancies tested including Daudi, a B-cell ALL cell line. Interestingly, between the two T-cell ALL cell lines, the tropolones generally exhibit sub-micromolar GI₅₀ values in Molt-4 and micromolar values in Jurkat. Vorinostat, which has been FDA approved to treat cutaneous T-cell lymphoma, was included as a positive control.

Vorinostat exhibited similar potency in most of these cell lines but was weaker against both HuT-78 and K562. While it is unclear why vorinostat is less potent in these two cell lines, it is clear that the tropolones display significantly more selectivity, especially towards Molt-4 cells.

To determine if the selectivity towards T-cell malignancies and Molt-4 cells in particular was directly related to the tropolone pharmacophore or was associated with the α -substitution, a second generation of tropolones was tested on the same panel of cells. This second generation was developed to determine the effects of various *para*-substitutions on the phenyl ring. These substitutions aimed to create a range of hydrophobic/hydrophilic characteristics or to add functional groups which could be readily converted or used to attach other functional groups.

Table 3.4: GI₅₀ values (μM) of second generation α-tropolones against a panel of hematological cancer cells from T, B or myeloid lineage.

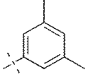
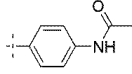
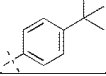
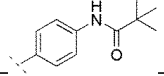
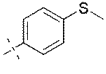
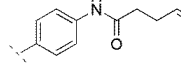
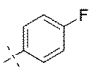
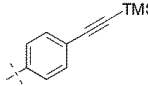
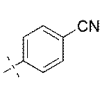
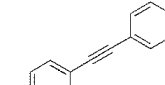
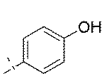
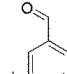
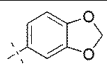
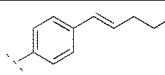
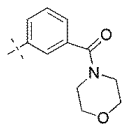
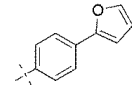
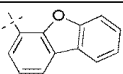
Compound	Functional Group	T-cell			B-cell		Myeloid	
		Jurkat	HuT-78	Molt-4	Daudi	Ba/F3	K562	HL-60
BA-P7-OH		1.93	1.74	1.44	1.45	0.41	6.29	1.67
BA-P8-OH		6.25	2.95	2.20	5.28	1.56	9.60	5.58
BA-pBr-OH		0.71	1.76	0.38	0.92	0.72	2.71	1.14
BA-PH-OH		1.07	2.02	0.80	1.56	1.71	2.47	1.95
BA-SM-OH		0.99	1.78	0.71	1.5	1.05	2.21	0.95
BA-DM-OH		1.66	2.15	0.88	1.45	1.67	2.62	2.24
BA-TM-OH		0.98	2.13	0.77	1.4	1.17	2.53	5.33
BA-Nap-OH		0.77	1.33	0.45	1.23	0.65	2.36	0.79
Am-NO2-OH		1.10	0.75	0.82	0.84	1.01	2.93	1.61
Am-NH2-OH		3.07	1.95	2.68	2.59	1.80	7.54	>10
HC-1-OH		0.92	0.71	0.52	0.83	0.55	7.57	0.98
EF-1-OH		2.18	0.97	0.98	1.00	0.45	5.57	2.86
EF-2-OH		2.76	2.03	2.58	2.31	0.81	>10	3.12
EF-3-OH		1.94	0.87	0.79	1.70	1.62	7.63	2.52

As with the first generation, the second generation of tropolones generally shows a preference towards Molt-4 cells. Interestingly, the overall potency of the second generation tropolones is stronger than the first generation. While this makes the selectivity towards T-cell

malignancies weaker, it offers the ability to develop tropolones capable of treating multiple hematological malignancies. Because the two generations of tropolones mainly rely on substitutions on a phenyl ring and primarily consist of *para*-substitutions, many of the tropolones exhibit similar potency. This could potentially be attributed to the common α -phenyl-tropolone motif. However, as with the sirtuin data, extending the *para*-alkyl chain beyond two carbons reduces potency. The two other functional groups which reduce potency are a ketone and an amine. This is somewhat confusing since a ketone is an electron withdrawing group and an amine is an electron donating group. Additionally, most of the phenyl substitutions with electron withdrawing groups appear to have slightly better potency, but the same is true for the electron donating ether substitutions. Based on these observations, it is clear that more diversity in functional groups and non-phenyl based substitutions needed to be explored to better understand any potential structure activity relationship.

Since the tropolones all appear to exhibit a preference towards Molt-4 cells, all newly synthesized tropolones were screened with Molt-4 to determine relative potency and any structure activity relationship. The next series of tropolones analyzed can be divided into two categories: phenyl-substitutions and non-phenyl based compounds/natural troponoids.


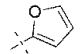
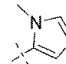
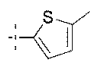
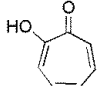
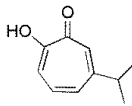
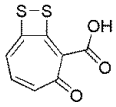
Table 3.5: GI₅₀ values (μ M) of substituted phenyl α -tropolones against Molt-4 cells.

Compound	Functional Group	Molt-4		Compound	Functional Group	Molt-4
MO-DMe-OH		0.39 ± 0.05		Am-Ac-OH		>10
MO-11-OH		0.24 ± 0.05		Am-Piv-OH		1.00 ± 0.10
MO-pSMe-OH		0.16 ± 0.03		Am-P5-OH		1.02 ± 0.08
MO-pF-OH		0.47 ± 0.06		SG-TMS-OH		0.52 ± 0.03
MO-pCN-OH		7.33 ± 0.30		SG-PH-OH		0.28 ± 0.03
MO-pOH-OH		4.39 ± 0.26		EF-4-OH		4.45 ± 0.29
HC-5-OH		4.40 ± 0.29		BA-P5-OH		0.35 ± 0.08
HC-7-OH		>10		BA-HC2-OH		0.34 ± 0.04
HC-10-OH		0.38 ± 0.03		Vorinostat		0.26

Based on these results, the most obvious trend is that *meta*-substitutions on the phenyl ring decrease potency. Upon more critical analysis, it also appears as though functional groups that are strongly electron withdrawing or electron donating can decrease potency. Although the nitrophenyl tropolone (Am-NO₂-OH) is an exception to this statement, it is likely the aromatic nitro moiety causes acute toxicity due to formation of a nitroanion radical known to increase oxidative stress.¹⁰⁰ Further exploration of functional groups is required to validate this notion. Other structural activity observations that can be made are that tropolones with higher

hydrophobicity and aromaticity typically display higher potency and that adding a degree of unsaturation to the *para*-alkyl chain off the phenyl ring appears to increase potency of shorter alkyl chains ($n > 7$). Interestingly, the most potent tropolone has a *para*-thioether on the phenyl ring. MO-pSMe-OH is structurally similar to MO-10-OH but is 2-times more potent. It may be possible that other sulfur atom substitutions may increase potency and should be explored. Additionally, it would appear as though tropolone is amenable to substitutions incorporating peptidomimetics based on the moderate potency displayed by two of the amides: Am-Piv-OH and Am-P5-OH.

Table 3.6: GI₅₀ values (μM) of non-phenyl based α -tropolones and natural troponoids against Molt-4 cells.

Compound	Functional Group/Structure	Molt-4
MO-3-OH		1.06 ± 0.12
HC-2-OH		4.44 ± 0.37
HC-6-OH		1.01 ± 0.12
HC-12-OH		0.51 ± 0.09
Tropolone		9.04 ± 0.67
HKT		1.98 ± 0.31
TDA		2.00 ± 0.33
Vorinostat		0.26

The series of non-phenyl based substituted tropolones is rather limited due to synthetic problems associated with some of these groups (as discussed in Chapter 2). While the furan group should contribute to the therapeutic index of tropolone, it is possible that it increases the solubility too much, making this tropolone unable to bind to its target. Even though the furan is known to be the most reactive of the 5-membered heterocyclic compounds, the *N*-methylpyrrole and thiophene containing tropolones are more potent.¹⁰¹ While furan is generally the most reactive, pyrrole is more prone to electrophilic substitution. Rate of electrophilic substitution for the three 5-membered heterocycles is: pyrrole>>furan>thiophene.¹⁰² These substitutions typically occur on the 2-position, α to the heteroatom. However, the *N*-methylation of pyrrole destroys its aromatic character and alters its electrophilic substitution preference to the 3-position, β to the heteroatom. Together, these traits may help explain the differences in potency between HC-2-OH, HC-6-OH and HC-12-OH, the furan, *N*-methylpyrrole and 2-methyl-thiophene respectively. Being the most reactive and prone to acid hydrolysis, the furan (HC-2-OH) may be quickly metabolized, therefore providing the least potency. The *N*-methylpyrrole may lose potency due to loss of aromatic character, but the electrophilic substitution potential at the 3-position may help maintain potency. This would need to be validated by α -pyrrole tropolone. The 2-methyl-thiophene maintains aromaticity which may enhance potency and already has a substitution at the 2-position which may increase stability. Synthesis of α -thiophene tropolone and 3-substituted-thiophene α -tropolones could validate this notion.

Another structure activity relationship observed from this series is adding a degree of unsaturation to an alkyl chain conjugated to the tropolone decreases potency. This is observed for the difference in Molt-4 potency between MO-2-OH ($GI_{50} = 0.81 \mu\text{M}$) and MO-3-OH ($GI_{50} = 0.99 \mu\text{M}$), a pentyl and 1-pentenyl chain respectively. While neither of these tropolones are

among the ten most potent, this may serve as caution against synthesis of alkyl chain linker substitutions possessing an alkene conjugated to the tropolone.

When comparing the α -synthetic tropolones to the natural troponoids, it is clear the α -synthetic tropolones offer increased potency towards Molt-4. Tropolone itself exhibits a GI_{50} of 9.04 μ M, but its native potency is significantly enhanced by simplistic substitutions on the ring such as the isopropyl of hinokitiol. This effect has been observed in all biological studies with tropolone and hinokitiol and is not surprising that it remains consistent here. However, TDA was expected to be highly potent and potentially toxic due to the disulfide that may be reduced to two thiols, but appears to be less potent than hinokitiol. As discussed in Chapter 1, thiols may form disulfide bonds with cysteine residues which can lead to off-target protein binding and toxic side effects. While it is unclear why TDA is less potent than expected, it is clear that again minor substitutions on the tropolone motif can significantly increase potency towards Molt-4 cells.

One modification which TDA contains compared to tropolone is a carboxylic acid instead of a hydroxyl group. To determine if the hydroxyl group promotes potency or if it may be substituted with another metal coordinating group, a series of alternative metal chelating troponoids based on α -phenyl tropolone were synthesized and screened with Molt-4 cells. These alternative metal chelating groups included: amine, acetamide, thiol, thiomethylether, hydroxylamine and methylether. None of these substitutions exhibited growth inhibitory activity in Molt-4 cells up to 10 μ M. This would suggest that the hydroxyl group is critical for activity. It may be possible to replace the hydroxyl group with a carboxylic acid as with TDA to maintain activity, but this type of troponoid still needs to be synthesized and tested.

Since many of the key potent tropolones are also highly hydrophobic, attempts to increase solubility were made to determine if low water solubility limited potential activity. Previously in the Anderson lab it was determined that the sodium salt of hinokitiol decreased activity in Jurkat cells so this salt formulation was avoided. As discussed in Chapter 2, Zn^{2+} complexes of hinokitiol exhibit greater biological activity and may increase solubility. A zinc complex of α -phenyl tropolone was synthesized and screened with Molt-4 cells. The GI_{50} of the complex was determined to be $0.28 \mu\text{M}$ which is 2.1 times more potent than the zinc-free form (MO-OH-PH). Although this would suggest that zinc complexes of tropolones will increase activity, 2 moles of α -phenyl tropolone make up the zinc complex and would account for doubling the apparent potency. Since the zinc complex did not increase biological activity, a salt formulation involving L-arginine was explored. L-arginine has been used to form an arginate salt of ibuprofen and has proven to increase absorption and increase the rate of effect while not effecting adverse event profiles.¹⁰³ Arginate salts of hinokitiol, MO-pF-OH and HC-1-OH were prepared and screened with Molt-4 cells. Although these salt formulations contained excess L-arginine, comparable concentrations of L-arginine did not exhibit any effects.

Table 3.7: GI_{50} values (μM) of α -tropolones and their respective arginate salts against Molt-4 cells.

Compound	Molt-4		Compound	Molt-4
HKT	1.98 ± 0.31		HKT-Arginate	3.82 ± 0.63
MO-pF-OH	0.47 ± 0.06		MO-pF-Arginate	0.55 ± 0.03
HC-1-OH	0.52		HC-1-Arginate	0.50 ± 0.06

While the arginate salts of hinokitiol and MO-pF-OH suffered a slight decrease in potency, the arginate salt of HC-1-OH exhibited the same potency as the salt-free form. Despite the slight decreases in potency, L-arginine increases the water solubility of the tropolone nearly 3-fold. This increased solubility may be critical for *in vivo* screening of tropolones in animal models. It should also be noted that the excess of arginine in each arginate salt solution was determined based on NMR integration and may not be highly accurate. This lack of accuracy could explain the perceived decrease in activity. More accurate measurements of excess arginine will determine if this salt formulation effects *in vitro* activity.

3.2.3 Elucidating the Activity of α -Tropolones in Molt-4 Cells

Since the tropolones exhibited the greatest potency in the Molt-4 cell line, mRNA samples of untreated Molt-4 cells and Molt-4 cells treated with 1 μ M MO-OH-Nap or HC-1-OH for 24 hours were collected and sent to Boston Children's Hospital Molecular Genetics Core Facility. There the samples were analyzed using an Illumina HumanHT-12 v4 Expression Beadchip. The cubic spline data from the microarray was analyzed using the Stanford Tools plug-in for Excel. This plug-in analyzes the data and determines fold changes in gene expression as well as estimating the false discovery rate by giving a q-value. Based on literature precedence, a fold threshold was imposed at 1.5-fold, meaning only genes up or down regulated above 1.5-fold would be returned by the Stanford Tools plug-in. In general, MO-OH-Nap gave lower q-values than HC-1-OH, but many of the "hits" were similar between the two treatments. With 47,323 genes/gene variants analyzed, 2740 were upregulated 1.5-fold and greater in both treatments and 1751 were downregulated.

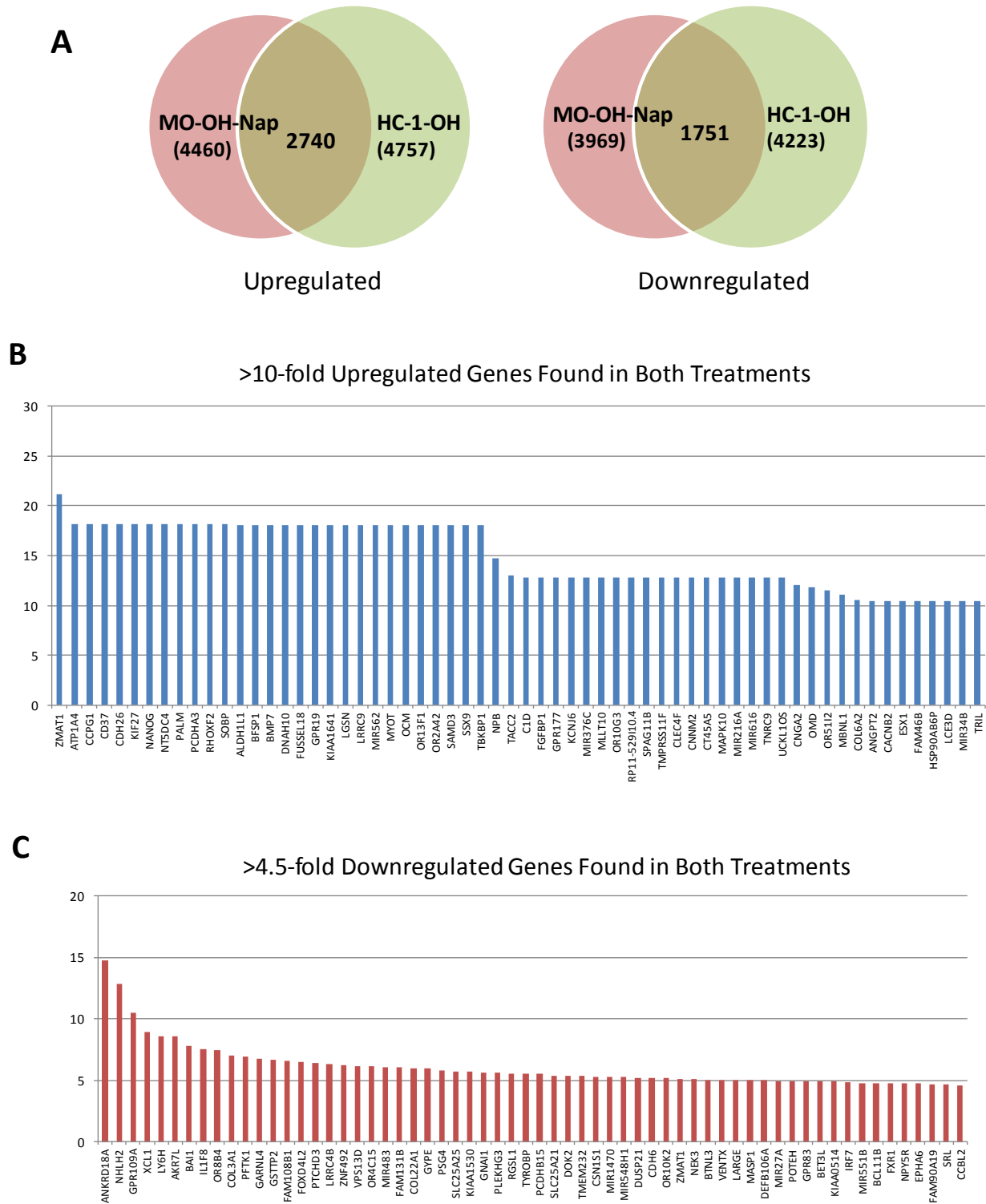


Figure 3.9: Depiction of changes in gene expression as determined by microarray analysis of Molt-4 cells treated with MO-OH-Nap and HC-1-OH (A). Genes with greater than 10-fold upregulation found for both treatments as determined by Stanford Tools analysis of microarray data (B). Genes with greater than 4.5-fold downregulation found for both treatments as determined by Stanford Tools analysis of microarray data (C).

After the Stanford Tools analysis, the “hits” were compared between the two treatments and an average fold change and standard deviation between the two treatment fold change values as well as an average q-value was calculated. Typically “hits” with similar fold changes and low standard deviations also showed lower average q-values. Only “hits” with similar fold changes, low standard deviations and reasonable q-values were investigated further, resulting in 1800 upregulated and 898 downregulated gene/gene variants. From here, each gene was searched in the KEGG Pathway Database and the NCBI Gene Database. Based on these results, 562 upregulated and 48 downregulated gene/gene variants were found to be of interest. These genes were associated with MMP, inflammation, interleukins, HDAC, MAPK, Wnt, major histocompatibility complex, Ras, PI3K, BCL proteins, JAK/STAT, histones, NFkB, Notch, Fanconi anemia, Rho, mTOR, NK-cells, p53, cell-cycle, apoptosis, immune response, hematopoiesis, and T-cell development and signaling.

Meanwhile, a collaboration with the Weimer lab suggested HDAC most likely was not a target due to poor increases in hyperacetylation as determined by Western blot analysis. However, the mTOR pathway appeared to be involved as well as p53 activation of apoptosis. Using this new information combined with results from the microarray, key genes of interest were determined to be involved with apoptosis, caspase induction, p53, the FOXO pathway and the PI3K/AKT/mTOR pathway. Gene set enrichment analysis confirmed this by revealing MO-OH-Nap and HC-1-OH decrease pathways related to protein expression and increase pathways related to DNA damage repair, cell cycle progression, immune cell signaling and cell adhesion and structure.

Table 3.8: Gene set enrichment analysis of microarray data from untreated Molt-4 cells versus cells treated for 24 hours with 1 μ M MO-OH-Nap or HC-1-OH. (GO = gene ontology; KEGG = Kyoto Encyclopedia of Genes and Genomes).

GO-decreased by tropolone	KEGG-decreased by tropolone
<i>Protein expression</i>	<i>Protein expression</i>
TRANSLATION	PROTEASOME
	RIBOSOME
GO-increased by tropolone	<i>Metabolism</i>
<i>DNA/cell cycle</i>	PORPHYRIN AND CHLOROPHYLL METABOLISM
DNA INTEGRITY CHECKPOINT	FRUCTOSE AND MANNOSE METABOLISM
G1 S TRANSITION OF MITOTIC CELL CYCLE	<i>Signaling</i>
DNA DAMAGE RESPONSE SIGNAL TRANSDUCTION	CYTOKINE/CYTOKINE RECEPTOR INTERACTION
MITOTIC CELL CYCLE CHECKPOINT	
<i>Immune function</i>	KEGG-increased by tropolone
MYELOID CELL DIFFERENTIATION	<i>DNA/cell cycle</i>
T CELL ACTIVATION	P53 SIGNALING PATHWAY
REGULATION OF LYMPHOCYTE ACTIVATION	<i>Immune function</i>
<i>Metabolism</i>	LEUKOCYTE TRANSENDOTHELIAL MIGRATION
PEPTIDYL AMINO ACID MODIFICATION	T CELL RECEPTOR SIGNALING PATHWAY
GLYCOPROTEIN BIOSYNTHETIC PROCESS	<i>Structural</i>
CARBOHYDRATE BIOSYNTHETIC PROCESS	ADHERENS JUNCTION
<i>Signaling</i>	GAP JUNCTION
TRANSMEMBRANE RECEPTOR PROTEIN TYROSINE KINASE SIGNALING PATHWAY	REGULATION OF ACTIN CYTOSKELETON
	FOCAL ADHESION

Leading edge analysis of these pathways determined by gene set enrichment analysis confirmed that key genes of interest include: DNA damage response and cell cycle regulators (TP53, RB1, CDK6, BCL2 and CCNE2), phospholipid signaling (PIK3R3, PIK3R1, PIK3CB, PIK3CG, PTEN, PLCG1 and PDPK1), small GTPase signaling (NRAS, RHOA, Rock1, VAV3, RAC1, KRAS, GNAI3 and PAK2) and transcription factors (LEF1, E2F2 and CHUK). Interestingly, many of these genes are targets proposed for the development of better therapeutic options for T-cell ALL and are directly related to the microarray analysis and GO analysis genes of interest. Within the DNA damage response and cell cycle regulators, TP53 may be the most relevant since TP53 codes the p53 protein which may be activated by ATM, regulates G1/S transition and signals cell cycle arrest and promotes apoptosis. CDK6 is inhibited by the CDKN2 family of proteins and serves as a G1/S checkpoint while the BCL family is critical for

T-cell development, proliferation, differentiation and survival. Phospholipid signaling involves the PI3K/AKT/mTOR pathway and regulates the FOXO family and RhoA which is involved in GTPase signaling.

Next, the microarray data was searched for genes of interest determined by leading edge analysis of pathways suggested by gene set enrichment analysis as well as promising therapeutic gene/gene product targets previously discussed.

Table 3.9: Microarray results found for genes of interest.

Gene	Average Fold Change	Standard Deviation
Upregulated		
AKT3	1.89	0.381
ATM	2.27	0.450
CDKN2B	7.18	0.929
EIF4E	4.83	0.001
FOXO3	2.48	0.514
FOXO6	2.51	0.098
HDAC7	2.93	0.980
IL7R	2.11	0.163
LYL1	1.85	0.183
MYCN	2.02	0.159
PIK3R1	1.87	0.138
Downregulated		
BCL11B	4.78	0.807
BCL2	2.43	0.687
CREBBP	2.36	0.559
SIRT2	1.76	0.068

Although not every gene listed by leading edge analysis was determined to be a “hit”, the microarray data clearly indicates that DNA damage response and apoptosis may be the primary target of tropolones while the PI3K/AKT/mTOR pathway may be involved in the apoptotic activity of tropolones. Furthermore, comparing the 151 probable cancer promoting mutated

genes in Molt-4 cells as listed in the NCI60 database to the microarray “hits” discovered 53 of these 151 genes were affected (see Appendix). Again, these genes primarily belong to DNA damage response, apoptosis and the PI3K/AKT/mTOR pathway. Additionally, several of these “hits” suggest tropolones may cause G1 arrest in Molt-4 cells. Future studies should aim to elucidate cell cycle effects of tropolones on Molt-4 cells as well as validate the ability of tropolones to exert apoptotic activity through DNA damage response and the PI3K/AKT/mTOR pathway.

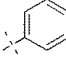
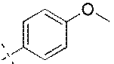
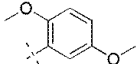
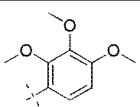
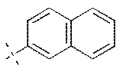
Since these results were found using Molt-4 cells, more information about the cell line may help with determining the validity of these “hits”. Molt-4 cells are human T-lymphoblasts from a 19 year-old male patient with acute lymphoblastic leukemia. This cell line is considered to be a suitable model for studying molecular mechanisms of apoptosis in T-lymphocytes. They express CD1, CD4, CD5 and CD7 and are therefore belong to the mature T-cell ALL subtype.¹⁰⁴ A key characteristic of this cell line is that Molt-4 cells overexpress nonfunctional, truncated p53.¹⁰⁵ However, as with most mutations in T-cell ALL, the p53 mutation is heterozygous meaning Molt-4 cells can still express wild-type p53. Additionally, the truncated p53 has been found to be capable of inducing apoptosis but with significantly lower efficiency.¹⁰⁶ As a result, DNA damage can trigger signals that stabilize the wild-type p53 to induce G1 arrest and apoptosis.¹⁰⁷ While the wild-type p53 can be stabilized and expressed, mutated p53 is upregulated in response to DNA damage and causes Molt-4 cells to only have partially functional DNA damage checkpoints.¹⁰⁵ However, incubation exceeding 24 hours with DNA damaging agents leads to atypical apoptosis. Atypical apoptosis displays features of both apoptosis and necrosis.¹⁰⁷ The Wiemer lab has determined that the tropolone MO-OH-Nap is capable of increasing p53 expression and leads to an accumulation of nuclear p53. Based on this

information, it would appear as though the tropolones may be DNA damaging agents capable of activating and stabilizing p53 in Molt-4 cells. Apoptosis analysis after 24 hours of incubation was conducted by the Wiemer lab using Annexin V and propidium iodide. This determined that tropolones display dose-dependent increases in early apoptotic and late apoptotic/necrotic cells, suggesting the tropolones cause atypical apoptosis. Cell cycle analysis will need to be conducted to determine if incubation with tropolones also causes G1 arrest.

3.2.4 Effects of α -Tropolones on Non-Tumorigenic Cell Lines

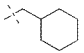
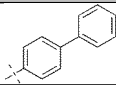

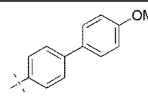
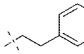
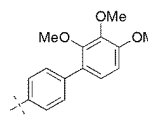
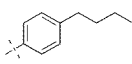
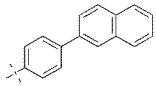
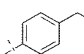
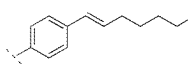
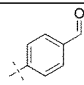
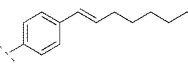
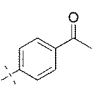
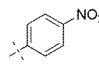
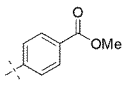
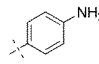
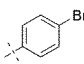
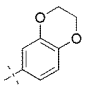
A previous report from the Anderson and Wright labs noted the first generation of α -tropolones and the natural tropolone, hinokitiol, did not exhibit toxicity towards human dermal fibroblasts (hDF) up to 90 μ M. The Priestley lab determined these same α -tropolones and hinokitiol did not exhibit toxicity towards MCF-10A, an epithelial cell line derived from a mammary gland, up to 100 μ M.

Table 3.10: GI₅₀ values (μ M) of first generation α -tropolones and hinokitiol against non-tumorigenic cell lines.

Compound	Functional Group	hDF	MCF-10A
MO-OH-PH		96.46	>100
MO-OH-SM		>100	>100
MO-OH-DM		>100	>100
MO-OH-TM		>100	>100
MO-OH-Nap		93.07	100
HKT		>100	>500

Because the tropolones generally exhibit cytotoxic activity at concentrations less than 10 μ M, the second generation of tropolones were screened against hDF for 72 hours with a maximal concentration of 10 μ M. Again most of the tropolones did not exhibit any cytotoxicity towards hDF cells.

Table 3.11: GI₅₀ values (μM) of second generation α-tropolones against hDF cells.

Compound	Functional Group	hDF		Compound	Functional Group	hDF
MO-1-OH		8.81 ± 2.53		BA-PH-OH		>10
MO-2-OH		>10		BA-SM-OH		>10
MO-7-OH		>10		BA-TM-OH		>10
MO-9-OH		>10		BA-Nap-OH		>10
MO-10-OH		>10		BA-P7-OH		>10
EF-1-OH		>10		BA-P8-OH		>10
EF-2-OH		>10		Am-NO2-OH		>10
EF-3-OH		>10		Am-NH2-OH		>10
BA-pBr-OH		>10		HC-1-OH		>10

Surprisingly, one of the more potent inhibitors of Molt-4, MO-1-OH, appears to be somewhat cytotoxic towards hDF with a GI₅₀ of 8.81 μM. While this is an approximately 37-fold difference in cytotoxicity, it creates some concern about the potential toxicity of this compound. However, it should be noted that MO-1-OH did not exhibit any cytotoxicity activity in MCF-10A nor the hepatocellular carcinoma cell line, HepG2, up to 100 μM and 500 μM respectively. This may be due to the relative age of the DMSO stock solution since the hematological cells, MCF-10A and HepG2 data was obtained early, but the hDF data was obtained after nearly two years of

use and may not be reliable due to potential degradation. The stability of the tropolones in DMSO for long periods of time should be analyzed to determine if the cytotoxicity displayed towards hDF is due to degraded material.

Although the tropolones generally do not exhibit cytotoxic activity towards non-tumorigenic cell lines and only displays limited cytotoxicity towards non-hematological cells, this is not enough to suggest that tropolones are selective towards malignant hematological cells. In order to suggest this selectivity, the tropolones must be screened against non-malignant hematological cells. A suitable model to determine if tropolones are generally cytotoxic towards hematological cells or provide selectivity towards malignant hematological cells is healthy human peripheral blood monocytes (hPBMCs). hPBMCs are any blood cell with a round nucleus (lymphocytes, monocytes, macrophages and dendritic cells) and are essential for immune responses such as cell-mediated cytotoxicity and inflammation.¹⁰⁸⁻¹⁰⁹ First, a potent tropolone from the first generation of synthetic α -tropolones and a more hydrophilic but still potent tropolone from the second generation were assayed with hPBMCs. These two tropolone were selected for both their potency against Molt-4 and for their differences in solubility. The differences in solubility may elucidate if solubility has a role in the activity of tropolones and if highly potent, selective and soluble analogs can be synthesized.

Table 3.12: GI₅₀ values (μM) of two α-tropolones and a control (vorinostat) against hPBMCs and selectivity towards Molt-4 cells.

	GI ₅₀ [μM]		Selectivity
	hPBMC	Molt-4	
MO-OH-Nap	4.89	0.35	14.0
HC-1-OH	6.13	0.52	11.8
Vorinostat	0.86	0.33	2.6

The two α-tropolones tested show some cytotoxicity towards hPBMCs but this cytotoxicity is significantly less than that of vorinostat and their cytotoxicity towards Molt-4. Interestingly, the more potent tropolone, MO-OH-Nap, is also more cytotoxic towards hPBMCs but displays slightly better selectivity than HC-1-OH. This suggests that more soluble and more potent α-tropolones may still be selective towards T-cell hematologic malignancies with minimal cytotoxicity towards healthy lymphocytes. In terms of solubility, there does not appear to be a substantial difference in selectivity between relatively hydrophobic and hydrophilic α-tropolones.

Because the hPBMC data for MO-OH-Nap and HC-1-OH was determined before the Molt-4 data for the compounds listed in Tables 3.5 and 3.6 was obtained, it is necessary to screen some of the most potent and more structurally diverse α-tropolones with hPBMCs. Hinokitiol was also included in this screen to determine if the synthetic α-tropolones possessed better selectivity and potency towards Molt-4 cells.

Table 3.13: GI₅₀ values (μM) of potent α-tropolones and hinokitiol against hPBMCs and selectivity towards Molt-4 cells.

	GI ₅₀ [μM]		Selectivity
	hPBMC	Molt-4	
MO-pSMe-OH	4.84	0.16	30.25
MO-11-OH	5.64	0.24	23.50
SG-PH-OH	8.99	0.28	32.11
BA-HC2-OH	7.23	0.34	21.26
BA-P5-OH	6.93	0.37	18.73
BA-pBr-OH	5.65	0.38	14.87
HC-10-OH	13.10	0.38	34.47
HC-12-OH	6.23	0.51	12.22
SG-TMS-OH	8.50	0.52	16.35
HKT	11.09	1.88	5.90

Surprisingly, some of the most potent tropolones are highly selective towards Molt-4 cells compared to hPBMCs and the natural tropolone, hinokitiol, is less selective than any of the synthetic α-tropolones. This data also suggests that more hydrophobic tropolones may provide more selectivity towards malignant cells. Additionally, the larger the substitution on tropolone appears to increase selectivity. However, this does not explain why BA-pBr-OH, a 4-bromophenyl, is more selective than MO-OH-Nap and HC-1-OH. It is possible that MO-OH-Nap, while hydrophobic, is less selective due to its planar structure which may serve as a DNA intercalating agent. While HC-1-OH should not be planar, it is somewhat similar to MO-OH-Nap and displays DNA damaging characteristics. Therefore, these newer α-tropolones should be screened to determine if they are also potential DNA damaging agents capable of triggering p53 expression and apoptosis in order to rule out a different mechanism of action. It should also be noted that the hPBMC GI₅₀ values listed in Table 3.13 despite being in replicates are only from one biological screen and should be screened another two times in order to validate these numbers.

3.3 Conclusions

Tropolones are antiproliferative agents effective against hematological malignancies with selectivity towards T-cells. As T-cell selective antiproliferative agents, tropolones are most effective against T-cell ALL. Additionally, key potent tropolones are more selective towards malignant T-cells than hPBMCs which partially consist of healthy T-cells. Although a variety of tropolones have been synthesized it is somewhat difficult to determine a structure activity relationship. The more effective analogs typically are aromatic and mainly hydrophobic. Substitutions on the α -phenyl tropolone have determined that *meta* substitutions appear to decrease potency and strongly electron withdrawing and donating groups on the phenyl ring may decrease potency. Additionally, incorporating sulfur atoms in the α -substitution may increase potency. However, more structurally diverse analogs, as well as *ortho*-substituted phenyl rings and furan, pyrrole and thiophene analogs should be synthesized to better understand structure activity trends. One trend that is apparent is that salt formulations may affect activity. Previously, it was determined that a sodium salt drastically decreased activity. Here a zinc salt did not affect activity while arginate salts may have a slight effect on potency, but both increase solubility. Another trend displayed by the tropolones is that larger, relatively hydrophobic substitutions appear to increase selectivity towards malignant T-cells (Molt-4) compared to healthy hPBMCs. As seen from the study utilizing alternative chelating functional groups, the hydroxyl group appears to be essential to tropolone activity. However, as seen with TDA, the

substitution of hydroxyl with a carboxylic acid may yield similar results. Future attempts should be made to make a carboxylic acid substituted tropolone analog.

Based on reports by Anderson lab and the Giardina lab, tropolones appear to act as histone deacetylase modulators. Although the Giardina lab determined tropolones do not exhibit gene expression profiles consistent with known HDAC inhibitors, they could not definitively determine if tropolones were sirtuin modulators. Assays with Sirt1 and Sirt2 determined tropolones are capable of modulating sirtuin activity, mostly through inhibition. However, the inhibitory activity of the tropolones is significantly less than the inhibitory activity previously reported against HDAC2 and HDAC8. While this would suggest the tropolones display different gene expression profiles due to selective inhibition of HDACs, Western blot analysis of histone acetylation levels conducted in the Wiemer lab as well as microarray analysis suggests tropolones have a different mechanism of action. From the microarray analysis it appears as though tropolones activate the apoptotic pathway most likely through DNA damage response and the PI3K/AKT/mTOR pathway. Future studies will need to validate the action of tropolones on these pathways and should aim towards understanding this mechanism of action in order to develop more potent tropolones.

3.4 Acknowledgements

GI₅₀ values for first and second generation tropolones (Tables 3.3 and 3.4 respectively) as well as the GI₅₀ values reported in Table 3.12 were determined by Jin Li. Jin also prepared the mRNA for the microarray and provided information about Western blot analysis of MO-OH-Nap

with histone lysine residues and p53. The arginate salts were prepared by Dr. Santosh Keshipeddy. Gene set enrichment analysis was conducted by Dr. Andrew Wiemer.

3.5 References

1. Swerdlow, S. H.; Campo, E.; Harris, N. L.; Jaffe, E. S.; Pileri, S. A.; Stein, H.; Thiele, J.; Vardiman, J. W. *WHO Classification of Tumours of Haematopoietic and Lymphoid Tissues* 4th ed.; International Agency for Research on Cancer: Lyon, 2008.
2. Inaba, H.; Greaves, M.; Mullighan, C. G. Acute lymphoblastic leukaemia. *Lancet* **2013**, 381, (9881), 1943-1955.
3. PDQ® Adult Treatment Editorial Board. PDQ Adult Acute Lymphoblastic Leukemia Treatment. Bethesda, MD: National Cancer Institute. Updated 05/27/2016. Available at: <http://www.cancer.gov/types/leukemia/hp/adult-all-treatment-pdq>. Accessed 06/21/2016. [PMID: 26389171]
4. Mathisen, M. S.; Kantarjian, H.; Thomas, D.; O'Brien, S.; Jabbour, E. Acute lymphoblastic leukemia in adults: encouraging developments on the way to higher cure rates. *Leukemia & Lymphoma* **2013**, 54, (12), 2592-2600.
5. Van der Meulen, J.; Van Roy, N.; Van Vlierberghe, P.; Speleman, F. The epigenetic landscape of T-cell acute lymphoblastic leukemia. *The International Journal of Biochemistry & Cell Biology* **2014**, 53, 547-557.

6. Jabbour, E.; O'Brien, S.; Konopleva, M.; Kantarjian, H. New Insights into the Pathophysiology and Therapy of Adult Acute Lymphoblastic Leukemia. *Cancer* **2015**, 121, (15), 2517-2528.
7. Guenova, M.; Balatzenko, G. *Leukemia*; InTech: 2013. ISBN: 978-953-51-1127-6
8. Yokota, T.; Kanakura, Y. Genetic abnormalities associated with acute lymphoblastic leukemia. *Cancer Sci.* **2016**, 107, (6), 721-725.
9. Pui, C-H. Genomic and pharmacogenetic studies of childhood acute lymphoblastic leukemia. *Front. Med.* **2015**, 9, (1), 1-9.
10. Kraszewska, M. D.; Dawidowska, M.; Szczepanski, T.; Witt, M. T-cell acute lymphoblastic leukaemia: recent molecular biology findings. *British Journal of Haematology* **2011**, 156, 303-315.
11. Evangelisti, C.; Evangelisti, C.; Charini, F.; Lonetti, A.; Buontempo, F.; Bressanin, D.; Cappellini, A.; Orsini, E.; McCubrey, J. A.; Martelli, A. M. Therapeutic potential of targeting mTOR in T-cell acute lymphoblastic leukemia (Review). *International Journal of Oncology* **2014**, 45, 909-918.
12. Van Vlierberghe, P.; Ferrando, A. The molecular basis of T cell acute lymphoblastic leukemia. *J. Clin. Invest.* **2012**, 122, (10), 3398-3406.
13. Mathisen, M. S.; Kantarjian, H. M.; Jabbour, E. J. Emerging drugs for acute lymphocytic leukemia. *Expert Opin. Emerging Drugs* **2014**, 19, 37-50.
14. Passaro, D.; Quang, C. T.; Ghysdael, J. Microenvironmental cues for T-cell acute lymphoblastic leukemia development. *Immun. Rev.* **2016**, 271, 156-172.
15. Asnafi, V.; Buzyn, A.; Le Noir, S.; Baleyrier, F.; Simon, A.; Beldjord, K.; Reman, O.; Witz, F.; Fagot, T.; Tavernier, E.; Turlure, P.; Leguay, T.; Huguet, F.; Vernant, J. P.;

- Daniel, F.; Bene, M. C.; Ifrah, N.; Thomas, X.; Dombret, H.; Macintyre, E.
NOTCH1/FBXW7 mutation identifies a large subgroup with favourable outcome in adult T-cell acute lymphoblastic leukemia (T-ALL): a GRAALL study. *Blood* **2009**, 113, 3918-3924.
16. Breit, S.; Stanulla, M.; Flohr, T.; Schrappe, M.; Ludwig, W. D.; Tolle, G.; Happich, M.; Muckenthaler, M. U.; Kulozik, A. E. Activating NOTCH1 mutations predict favorable early treatment response and long-term outcome in childhood precursor T-cell lymphoblastic leukemia. *Blood* **2006**, 108, 1151-1157.
17. Larson Gedman, A.; Chen, Q.; Kugel Desmoulin, S.; Ge, Y.; LaFiura, K.; Haska, C. L.; Cherian, C.; Devidas, M.; Linda, S. B.; Taub, J. W.; Matherly, L. H. The impact of NOTCH1, FBW7 and PTEN mutations on prognosis and downstream signaling in pediatric T-cell acute lymphoblastic leukemia: a report from the Children's Oncology Group. *Leukemia* **2009**, 23, 1417-1425.
18. van Grotel, M.; Meijerink, J. P.; Beverloo, H. B.; Langerak, A. W.; Buys-Gladdines, J. G.; Schneider, P.; Poulsen, T. S.; den Boer, M. L.; Horstmann, M.; Kamps, W. A.; Veerman, A. J.; van Wering, E. R.; van Noesel, M. M.; Pieters, R. The outcome of molecular-cytogenetic subgroups in pediatric T-cell acute lymphoblastic leukemia: a retrospective study of patients treated according to DCOG or COALL protocols. *Haematologica* **2006**, 91, 1212-1221.
19. Hebert, J.; Cayuela, J. M.; Berkeley, J.; Sigaux, F. Candidate tumor-suppressor genes MTS1 (p16INK4A) and MTS2 (p15INK4B) display frequent homozygous deletions in primary cells from T- but not from B-cell lineage acute lymphoblastic leukemias. *Blood* **1994**, 84, 4038-4044.

20. Meijerink, J. P. Genetic rearrangements in relation to immunophenotype and outcome in T-cell acute lymphoblastic leukaemia. *Best Pract. Res. Clin. Haematol.* **2010**, 23, 307-318.
21. Peirs, S.; Van der Meulen, J.; Van de Walle, I.; Taghon, T.; Speleman, F.; Poppe, B.; Van Vlierberghe, P. Epigenetics in T-cell acute lymphoblastic leukemia. *Immunol. Rev.* **2015**, 263, 50-67.
22. Correia, N. C.; Durinck, K.; Leite, A. P.; Ongenaert, M.; Rondou, P.; Speleman, F.; Enguita, F. J.; Barata, J. T. Novel TAL1 targets beyond protein-coding genes: identification of TAL1-regulated microRNAs in T-cell acute lymphoblastic leukemia. *Leukemia* **2013**, 27, (7), 1603-1606.
23. Lv, M.; Zhang, X.; Jia, H.; Li, D.; Zhang, B.; Zhang, H.; Hong, M.; Jiang, T.; Jiang, Q.; Lu, J.; Huang, X.; Huang, B. An oncogenic role of miR-142-3p in human T-cell acute lymphoblastic leukemia (T-ALL) by targeting glucocorticoid receptor- α and cAMP/PKA pathways. *Leukemia* **2012**, 26, (4), 769-777.
24. Schotte, D.; Pieters, R.; Den Boer, M. L. MicroRNAs in acute leukemia: from biological players to clinical contributors. *Leukemia* **2012**, 26, (1), 1-12.
25. Miao, M. H.; Ji, X. Q.; Zhang, H.; Xu, J.; Zhu, H.; Shao, X. J. miR-590 promotes cell proliferation and invasion in T-cell acute lymphoblastic leukaemia by inhibiting RB1. *Oncotarget* **2016**, [Epub ahead of print] doi: 10.18632/oncotarget.8414.
26. Luan, C.; Yang, Z.; Chen, B. The functional role of microRNA in acute lymphoblastic leukemia: relevance for diagnosis, differential diagnosis, prognosis, and therapy. *Onco Targets Ther.* **2015**, 8, 2903-2914.

27. De Keersmaecker, K.; Marynen, P.; Cools, J. Genetic insights in the pathogenesis of T-cell acute lymphoblastic leukemia. *Haematologica* **2005**, 90, (8), 1116-1127.
28. Kees, U. R.; Heerema, N. A.; Kumar, R.; Watt, P. M.; Baker, D. L.; La, M. K.; Uckun, F. M.; Sather, H. N. Expression of HOX11 in childhood T-lineage acute lymphoblastic leukaemia can occur in the absence of cytogenetic aberration at 10q24: a study from the Children's Cancer Group (CCG). *Leukemia* **2003**, 17, (5), 887-893.
29. Meijerink, J. P.; den Boer, M. L.; Pieters, R. New genetic abnormalities and treatment response in acute lymphoblastic leukemia. *Sem. Hematol.* **2009**, 46, 16-23.
30. van Grotel, M.; Meijerink, J. P.; van Wering, E. R.; Langerak, A. W.; Beverloo, H. B.; Buijs-Gladdines, J. G.; Burger, N. B.; Passier, M.; van Lieshout, E. M.; Kamps, W. A.; Veerman, A. J.; van Noesel, M. M.; Pieters, R. Prognostic significance of molecular-cytogenetic abnormalities in pediatric T-ALL is not explained by immunophenotypic differences. *Leukemia* **2008**, 22, 124-131.
31. Zhang, J.; Ding, L.; Holmfeldt, L.; Wu, G.; Heatley, S. L.; Payne-Turner, D.; Easton, J.; Chen, X.; Wang, J.; Rusch, M.; Lu, C.; Chen, S. C.; Wei, L.; Collins-Underwood, J. R.; Ma, J.; Roberts, K. G.; Pounds, S. B.; Ulyanov, A.; Becksfort, J.; Gupta, P.; Huether, R.; Kriwacki, R. W.; Parker, M.; McGoldrick, D. J.; Zhao, D.; Alford, D.; Espy, S.; Bobba, K. C.; Song, G.; Pei, D.; Cheng, C.; Roberts, S.; Barbato, M. I.; Campana, D.; Coustan-Smith, E.; Shurtleff, S. A.; Raimondi, S. C.; Kleppe, M.; Cools, J.; Shimano, K. A.; Hermiston, M. L.; Doulatov, S.; Eppert, K.; Laurenti, E.; Notta, F.; Dick, J. E.; Basso, G.; Hunger, S. P.; Loh, M. L.; Devidas, M.; Wood, B.; Winter, S.; Dunsmore, K. P.; Fulton, R. S.; Fulton, L. L.; Hong, X.; Harris, C. C.; Dooling, D. J.; Ochoa, K.; Johnson, K. J.; Obenauer, J. C.; Evans, W. E.; Pui, C. H.; Naeve, C. W.; Ley, T. J.; Mardis, E. R.;

- Wilson, R. K.; Downing, J. R.; Mullighan, C. G. The genetic basis of early T-cell precursor acute lymphoblastic leukaemia. *Nature* **2012**, 481, 157-163.
32. Neumann, M.; Heesch, S.; Schlee, C.; Schwartz, S.; Gokbuget, N.; Hoelzer, D.; Konstandin, N. P.; Ksienzyk, B.; Vosberg, S.; Graf, A.; Krebs, S.; Blum, H.; Raff, T.; Bruggemann, M.; Hofmann, W. K.; Hecht, J.; Bohlander, S. K.; Greif, P. A.; Baldus, C. D. Whole-exome sequencing in adult ETP-ALL reveals a high rate of DNMT3A mutations. *Blood* **2013**, 121, (23), 4749-4752.
33. Coustan-Smith, E.; Mullighan, C. G.; Onciu, M.; Behm, F. G.; Raimondi, S. C.; Pei, D.; Cheng, C.; Su, X.; Rubnitz, J. E.; Basso, G.; Biondi, A.; Pui, C. H.; Downing, J. R.; Campana, D. Early T-cell precursor leukaemia: a subtype of very high-risk acute lymphoblastic leukaemia. *Lancet Oncol.* **2009**, 10, (2), 147-156.
34. National Cancer Institute. SEER Stat Fact Sheet: acute Lymphoblastic Leukemia. Bethesda. 2016. Available from: <http://seer.cancer.gov/statfacts/html/aly1.html>
35. Hunger, S. P.; Lu, X.; Devidas, M.; Camitta, B. M.; Gaynon, P. S.; Winick, N. J.; Reaman, G. H.; Carroll, W. L. Improved survival for children and adolescents with acute lymphoblastic leukemia between 1990 and 2005: a report from the children's oncology group. *J. Clin. Oncol.* **2012**, 30, (14), 1663-1669.
36. You, M. J.; Medeiros, L. J.; Hsi, E. D. T-Lymphoblastic Leukemia/Lymphoma. *Am. J. Clin. Pathol.* **2015**, 144, 411-422.
37. Pui, C. H.; Evans, W. E. Treatment of acute lymphoblastic leukemia. *N. Engl. J. Med.* **2006**, 354, (2), 166-178.
38. Alvarnas, J. C.; Brown, P. A.; Aoun, P.; Ballen, K. K.; Bellam, N.; Blum, W.; Boyer, M. W.; Carraway, H. E.; Coccia, P. F.; Coutre, S. E.; Cultrera, J.; Damon, L. E.; DeAngelo,

- D. J.; Douer, D.; Frangoul, H.; Frankfurt, O.; Goorha, S.; Millenson, M. M.; O'Brien, S.; Petersdorf, S. H.; Rao, A. V.; Terezakis, S.; Uy, G.; Wetzler, M.; Zelenetz, A. D.; Naganuma, M.; Gregory, K. M. Acute Lymphoblastic Leukemia. *J. Natl. Compr. Cancer Netw.* **2012**, 10, (7), 858-914.
39. Linker, C.; Damon, L.; Ries, C.; Navarro, W. Intensified and shortened cyclical chemotherapy for adult acute lymphoblastic leukemia. *J. Clin. Oncol.* **2002**, 20, (10), 2464-2471.
40. Larson, R. A.; Dodge, R. K.; Burns, C. P.; Lee, E. J.; Stone, R. M.; Schulman, P.; Duggan, D.; Davey, F. R.; Sobol, R. E.; Frankel, S.R.; Hooberman, A. L.; Westbrook, C. A.; Arthur, D. C.; George, S. L.; Bloomfield, C. D.; Schiffer, C. A. A Five-Drug Remission Induction Regimen With Intensive Consolidation for Adults With Acute Lymphoblastic Leukemia: Cancer and Leukemia Group B Study 8811. *Blood* **1995**, 85, (8), 2025-2037.
41. Rowe, J. M.; Buck, G.; Burnett, A. K.; Chopra, R.; Wiernik, P. H.; Richards, S. M.; Lazarus, H. M.; Franklin, I. M.; Litzow, M. R.; Ciobanu, N.; Prentice, H. G.; Durrant, J.; Tallman, M. S.; Goldstone, A. H. Induction therapy for adults with acute lymphoblastic leukemia: results of more than 1500 patients from the international ALL trial: MRC UKALL XII/ECOG E2993. *Blood* **2005**, 106, (12), 3760-3767.
42. Jordan, M. A. Mechanism of action of antitumor drugs that interact with microtubules and tubulin. *Curr. Med. Chem. Anticancer Agents* **2002**, 2, 1-17.
43. Tacar, O.; Sriamornsak, P.; Dass, C. R. Doxorubicin: an update on anticancer molecular action, toxicity and novel drug delivery systems. *J. Pharm. Pharmacol.* **2013**, 65, 157-170.

44. Chatterjee, K.; Zhang, J.; Honbo, N.; Karliner, J. S. Doxorubicin cardiomyopathy. *Cardiology* **2010**, 115, 155-162.
45. <http://www.mayoclinic.org/steroids/art-20045692> accessed on 7/14/2016
46. Broome, J. D. L-Asparaginase: discovery and development as a tumor-inhibitory agent. *Cancer Treat. Rep.* **1981**, 65, 111-114.
47. Johnston, P. G.; Hardisty, R. M.; Kay, H. E.; Smith, P. G. Myelosuppressive effect of colaspase (L-asparaginase) in initial treatment of acute lymphoblastic leukaemia. *Br. Med. J.* **1974**, 3, 81-83.
48. Barrett, A. J.; Horowitz, M. M.; Pollock, B. H.; Zhang, M. J.; Bortin, M. M.; Buchanan, G. R.; Camitta, B. M.; Ochs, J.; Graham-Pole, J.; Rowlings, P. A.; Rimm, A. A.; Klein, J. P.; Shuster, J. J.; Sobocinski, K. A.; Gale, R. P. Bone Marrow Transplants from HLA-Identical Siblings as Compared with Chemotherapy for Children with Acute Lymphoblastic Leukemia in a Second Remission. *N. Engl. J. Med.* **1994**, 331, (19), 1253-1258.
49. Fielding, A. K.; Richards, S. M.; Chopra, R.; Lazarus, H. M.; Litzow, M. R.; Buck, G.; Durrant, I. J.; Luger, S. M.; Marks, D. I.; Franklin, I. M.; McMillan, A. K.; Tallman, M. S.; Rowe, J. M.; Goldstone, A. H. Outcome of 609 adults after relapse of acute lymphoblastic leukemia (ALL); an MRC UKALL12/ECOG 2993 study. *Blood* **2007**, 109, 944-950.
50. Vora, A.; Goulden, N.; Wade, R.; Mitchell, C.; Hancock, J.; Hough, R.; Rowntree, C.; Richards, S. Treatment reduction for children and young adults with low-risk acute lymphoblastic leukaemia defined by minimal residual disease (UKALL 2003): a randomised controlled trial. *Lancet Oncol.* **2013**, 14, 199-209.

51. Schrappe, M.; Valsecchi, M. G.; Bartram, C. R.; Schrauder, A.; Panzer-Grumayer, R.; Moricke, A.; Parasole, R.; Zimmermann, M.; Dworzak, M.; Buldini, B.; Reiter, A.; Basso, G.; Klingebiel, T.; Messina, C.; Ratei, R.; Cazzaniga, G.; Koehler, R.; Locatelli, F.; Schafer, B. W.; Arico, M.; Welte, K.; van Dongen, J. J.; Gadner, H.; Biondi, A.; Conter, V. Late MRD response determines relapse risk overall and in subsets of childhood T-cell ALL: results of the AIEOP-BFM-ALL 2000 study. *Blood* **2011**, 118, 2077-2084.
52. Conter, V.; Bartram, C. R.; Valsecchi, M. G.; Schrauder, A.; Panzer-Grumayer, R.; Moricke, A.; Arico, M.; Zimmermann, M.; Mann, G.; De Rossi, G.; Stanulla, M.; Locatelli, F.; Basso, G.; Niggli, F.; Barisone, E.; Henze, G.; Ludwig, W. D.; Haas, O. A.; Cazzaniga, G.; Koehler, R.; Silvestri, D.; Bradtke, J.; Parasole, R.; Beier, R.; van Dongen, J. J.; Biondi, A.; Schrappe, M. Molecular response to treatment redefines all prognostic factors in children and adolescents with B-cell precursor acute lymphoblastic leukemia: results in 3184 patients of the AIEOP-BFM ALL 2000 study. *Blood* **2010**, 115, 3206-3214.
53. Rivera, G. K.; Zhou, Y.; Hancock, M. L.; Gajjar, A.; Rubnitz, J.; Ribeiro, R. C.; Sandlund, J. T.; Hudson, M.; Relling, M.; Evans, W. E.; Pui, C. H. Bone marrow recurrence after initial intensive treatment for childhood acute lymphoblastic leukemia. *Cancer* **2005**, 103, 368-376.
54. Patrick, K.; Vora, A. Update on biology and treatment of T-cell acute lymphoblastic leukaemia. *Curr. Opin. Pediatr.* **2015**, 27, (1), 44-49.
55. Ronson, A.; Tvito, A.; Rowe, J. M. Treatment of Relapsed/Refractory Acute Lymphoblastic Leukemia in Adults. *Curr. Oncol. Rep.* **2016**, 18: 39.

56. Gokbuget, N.; Kneba, M.; Raff, T.; Trautmann, H.; Bartram, C. R.; Arnold, R.; Fietkau, R.; Freund, M.; Ganser, A.; Ludwig, W. D.; Maschmeyer, G.; Rieder, H.; Schwartz, S.; Serve, H.; Thiel, E.; Bruggemann, M.; Hoelzer, D. Adult patients with acute lymphoblastic leukemia and molecular failure display a poor prognosis and are candidates for stem cell transplantation and targeted therapies. *Blood* **2012**, 120, 1868-1876.
57. Clevers, H. The cancer stem cell: premises, promises and challenges. *Nat. Med.* **2011**, 17, 313-319.
58. Kebriaei, P.; Poon, M. L. Future of Therapy in Acute Lymphoblastic Leukemia (ALL) – Potential Role of Immune-Based Therapies. *Curr. Hematol. Malig. Rep.* **2015**, 10, 76-85.
59. Perry, M. J. *The Chemotherapy Source Book*. Wolters Kluwer Health: Philadelphia, 2008.
60. Hande, K. R. Etoposide: four decades of development of a topoisomerase II inhibitor. *Eur. J. Cancer* **1998**, 34, 1514-1521.
61. <http://www.texasoncology.com/types-of-cancer/leukemia/adult-acute-lymphoblastic-leukemia/relapsed-or-refractory-adult-all/> accessed on 7/15/2016
62. Cohen, M. H.; Johnson, J. R.; Justice, R.; Pazdur, R. FDA drug approval summary: nelarabine (Arranon) for the treatment of T-cell lymphoblastic leukemia/lymphoma. *Oncologist* **2008**, 13, 709-714.
63. Bonn, B. R.; Krieger, D.; Burkhardt, B. Cell cycle regulatory molecular profiles of pediatric T-cell lymphoblastic leukemia and lymphoma. *Leukemia & Lymphoma* **2012**, 53, (4), 557-568.
64. Sherr, C. J. Autophagy by ARF: a short story. *Mol. Cell* **2006**, 22, (4), 436-437.

65. <http://www.genecards.org/cgi-bin/carddisp.pl?gene=LYL1> accessed on 7/15/2016
66. Pui, C. H. T Cell Acute Lymphoblastic Leukemia: NOTCHing the Way toward a Better Treatment Outcome. *Cancer Cell* **2009**, 15, 85-87.
67. Kasner, M. T. Novel Targets for Treatment of Adult Acute Lymphocytic Leukemia. *Curr. Hematol. Malig. Rep.* **2010**, 5, 207-212.
68. Vara, J. A. F.; Casado, E.; de Castro, J.; Cejas, P.; Belda-Iniesta, C.; Gonzalez-Baron, M. PI3K/Akt signalling pathway and cancer. *Cancer Treat. Rev.* **2004**, 30, 193-204.
69. Huang, X.; Shen, Q.; Chen, S.; Chen, S.; Yang, L.; Weng, J.; Du, X.; Grabarczyk, P.; Przybylski, G. K.; Schmidt, C. A.; Li, Y. Gene expression profiles in BCL11B-siRNA treated malignant T cells. *J. Hematol. Oncol.* **2011**, 4:23.
70. Huang, X.; Du, X.; Li, Y. The role of BCL11B in hematological malignancy. *Exp. Hematol. Oncol.* **2012**, 1:22.
71. Eckner, R.; Ewen, M. E.; Newsome, D.; Gerdes, M.; DeCaprio, J. A.; Lawrence, J. B.; Livingston, D. M. Molecular cloning and functional analysis of the adenovirus E1A-associated 300-kD protein (p300) reveals a protein with properties of a transcriptional adaptor. *Genes Dev.* **1994**, 8, 869-884.
72. Tang, M. L. F.; Gasser, S. ATM activation mediates anticancer immunosurveillance by natural killer and T cells. *OncoImmunology* **2013**, 2:6.
73. Jang, E. R.; Choi, J. D.; Park, M. A.; Jeong, G.; Cho, H.; Lee, J-S. ATM modulates transcription in response to histone deacetylase inhibition as part of its DNA damage response. *Exp. Mol. Med.* **2010**, 42, 195-204.
74. Yamamoto, K.; Nihrane, A.; Aglipay, J.; Sironi, J.; Arkin, S.; Lipton, J. M.; Ouchi, T.; Liu, J. M. Upregulated ATM Gene Expression and Activated DNA Crosslink-Induced

Damage Response Checkpoint in Fanconi Anemia: Implications for Carcinogenesis.

Mol. Med. **2008**, 14, 167-174.

75. Rothenberg, E. V. The chromatin landscape and transcription factors in T cell programming. *Trends Immunol.* **2014**, 35, 195-204.
76. Blobel, G. A. CREB-binding protein and p300: molecular integrators of hematopoietic transcription. *Blood* **2000**, 95, 745-755.
77. Wang, F.; Marshall, C. B.; Ikura, M. Transcriptional/epigenetic regulator CBP/p300 in tumorigenesis: structural and functional versatility in target recognition. *Cell Mol. Life Sci.* **2013**, 70, 3989-4008.
78. Mullighan, C. G.; Zhang, J.; Kasper, L. H.; Lerach, S.; Payne-Turner, D.; Phillips, L. A.; Heatley, S. L.; Holmfeldt, L.; Collins-Underwood, J. R.; Ma, J.; Buetow, K. H.; Pui, C. H.; Baker, S. D.; Brindle, P. K.; Downing, J. R. CREBBP mutations in relapsed acute lymphoblastic leukaemia. *Nature* **2011**, 471, 235-239.
79. Hnisz, D.; Abraham, B. J.; Lee, T. I.; Lau, A.; Saint-Andre, V.; Sigova, A. A.; Hoke, H. A.; Young, R. A. Super-enhancers in the control of cell identity and disease. *Cell* **2013**, 155, 934-947.
80. <https://clinicaltrials.gov/>
81. Kong, D.; Yamori, T. Phosphatidylinositol 3-kinase inhibitors: promising drug candidates for cancer therapy. *Cancer Sci.* **2008**, 99, 1734-1740.
82. Mizuno, M.; Yamada, K.; Takei, N.; Tran, M. H.; He, J.; Nakajima, A.; Nawa, H.; Nabeshima, T. Phosphatidylinositol 3-kinase: a molecule mediating BDNF-dependent spatial memory formation. *Mol. Psychiatry* **2003**, 8, 217-224.

83. Granata, S.; Dalla Gassa, A.; Carraro, A.; Brunelli, M.; Stallone, G.; Lupo, A.; Zaza, G. Sirolimus and Everolimus Pathway: Reviewing Candidate Genes Influencing Their Intracellular Effects. *Int. J. Mol. Sci.* **2016**, *17*, E735.
84. Paris, M.; Porcelloni, M.; Binaschi, M.; Fattori, D. Histone Deacetylase Inhibitors: From Bench to Clinic. *J. Med. Chem.* **2008**, *51*, (6), 1505-1529.
85. Chen, L.; Medicinal chemistry of sirtuin inhibitors. *Curr. Med. Chem.* **2011**, *18*, 1936-1946.
86. Liu, S.; Yamauchi, H. p27-Associated G1 arrest induced by hinokitiol in human malignant melanoma cells is mediated via down-regulation of pRb, Skp2 ubiquitin ligase, and impairment of Cdk2 function. *Cancer Lett.* **2009**, *286*, (2), 240-249.
87. Liu, S.; Yamauchi, H. Hinokitiol, a metal chelator derived from natural plants, suppresses cell growth and disrupts androgen receptor signaling in prostate carcinoma cell lines. *Biochem. Biophys. Res. Commun.* **2006**, *351*, (1), 26-32.
88. Morita, Y.; Matsumura, E.; Okabe, T.; Fukui, T.; Shibata, M.; Sugira, M.; Ohe, T.; Tsujibo, H.; Ishida, N.; Inamori, Y. Biological activity of α -thujaplicin, the isomer of hinokitiol. *Biol. Pharm. Bull.* **2004**, *27*, 899-902.
89. Morita, Y.; Matsumura, E.; Okabe, T.; Fukui, T.; Ohe, T.; Ishida, N.; Inamori, Y. Biological activity of beta-dolabrin, gamma-thujaplicin, and 4-acetyltropolone, hinokitiol-related compounds. *Biol. Pharm. Bull.* **2004**, *27*, 1666-1669.
90. Kontoghiorghes, G. J.; Piga, A.; Hoffbrand, A. V. Cytotoxic and DNA-inhibitory effects of iron chelators on human leukaemic cell lines. *Hematol. Oncol.* **1986**, *4*, 195-204.

91. Ononye, S. N.; VanHeyst, M. D.; Oblak, E. Z.; Zhou, W.; Ammar, M.; Anderson, A. C.; Wright, D. L. Tropolones As Lead-Like Natural Products: The Development of Potent and Selective Histone Deacetylase Inhibitors. *Med. Chem. Lett.* **2013**, 4, 757-761.
92. Marquard, L.; Gjerdrum, L.; Christensen, L.; Jensen, P.; Sehested, M.; Ralfkiaer, E. Prognostic significance of the therapeutics targets histone deacetylase 1, 2 and 6 and acetylated histone H4 in cutaneous T-cell lymphoma. *Histopathology* **2008**, 53, 267-277.
93. Ononye, S. N.; Van Heyst, M. D.; Giardina, C.; Wright, D. L.; Anderson, A. C. Studies on the antiproliferative effects of tropolone derivatives in Jurkat T-lymphocyte cells. *Bioorg. Med. Chem.* **2014**, 22, (7), 2188-2193.
94. Cao, L.; Kuratnik, A.; Xu, W.; Gibson, J. D.; Kolling, F.; Falcone, E. R.; Ammar, M.; Van Heyst, M. D.; Wright, D. L.; Nelson, C. E.; Giardina, C. Development of Intestinal Organoids as Tissue Surrogates: Cell Composition and the Epigenetic Control of Differentiation. *Mol. Carcinog.* **2015**, 54, (3), 189-202.
95. Peck, B.; Chen, C-Y.; Ho, K-K.; Di Fruscia, P.; Myatt, S. S.; Coombes, R. C.; Fuchter, M. J.; Hsiao, C-D.; Lam, E. W-F. SIRT Inhibitors Induce Cell Death and p53 Acetylation through Targeting Both SIRT1 and SIRT2. *Mol. Cancer Ther.* **2010**, 9, (4), 844-855.
96. Pillai, V. B.; Sundaresan, N. R.; Gupta, M. P. Regulation of Akt Signaling by Sirtuins: Its Implication in Cardiac Hypertrophy and Aging. *Circ. Res.* **2014**, 114, 368-378.
97. Lain, S.; Hollick, J. J.; Campbell, J.; Staples, O. D.; Higgins, M.; Aoubala, M.; McCarthy, A.; Appleyard, V.; Murray, K. E.; Baker, L.; Thompson, A.; Mathers, J.; Holland, S. J.; Stark, M. J.; Pass, G.; Woods, J.; Lane, D. P.; Westwood, N. J. Discovery,

- in vivo activity, and mechanism of action of a small-molecule p53 activator. *Cancer Cell* **2008**, 13, 454-463.
98. Borra, M. T.; Smith, B. C.; Denu, J. M. Mechanism of Human SIRT1 Activation by Resveratrol. *J. Biol. Chem.* **2005**, 280, 17187-17195.
99. Lewis, R. J. *Sax's Dangerous Properties of Industrial Material*. 9th ed. Van Nostrand Reinhold: NY, 1996.
100. Boelsterli, U. A.; Ho, H. K.; Zhou, S.; Leow, K. Y. Bioactivation and hepatotoxicity of nitroaromatic drugs. *Curr. Drug. Metab.* **2006**, 7, 715-727.
101. Banerjee, R.; HKS, K.; Banerjee, M. Medicinal significance of furan derivatives: A Review. *Int. J. Rev. Life Sci.* **2012**, 2, (1), 7-16.
102. Reusch, W. *Virtual Text of Organic Chemistry*. Michigan State University: 1999.
103. Desjardins, P.; Black, P.; Papageorge, M.; Norwood, T.; Shen, D. D.; Norris, L.; Ardia, A. Ibuprofen arginate provides effective relief from postoperative dental pain with a more rapid onset of action than ibuprofen. *Eur. J. Clin. Pharmacol.* **2002**, 58, (6), 387-394.
104. Tichy, A.; Zaskodova, D.; Zoelzer, F.; Vavrova, J.; Sinkorova, Z.; Pejchal, J.; Osterreicher, J.; Rezacova, M. Gamma-Radiation-Induced Phosphorylation of p53 on Serine 15 Is Dose-Dependent in MOLT-4 Leukaemia Cells. *Folia Biologica* **2009**, 55, 41-44.
105. Bozko, P.; Sabisz, M.; Larsen, A. K.; Skladanowski, A. Cross-talk between DNA damage and cell survival checkpoints during G₂ and mitosis: pharmacologic implications. *Mol. Cancer Ther.* **2005**, 4, (12), 2016-2025.

106. Lindgren, T.; Stigbrand, T.; Riklund, K.; Johansson, L.; Eriksson, D. Gene expression profiling in MOLT-4 cells during gamma-radiation-induced apoptosis. *Tumor Biol.* **2012**, *33*, 689-700.
107. Bhatia, U.; Danishefsky, K.; Traganos, F.; Darzynkiewicz, Z. Induction of Apoptosis and Cell Cycle-specific Change in Expression of p53 in Normal Lymphocytes and MOLT-4 Leukemic Cells by Nitrogen Mustard. *Clin. Cancer Res.* **1995**, *1*, 873-880.
108. <https://www.cellapplications.com/human-peripheral-blood-monocytes-hpbm> accessed 7/25/2016
109. <http://www.zen-bio.com/products/cells/pbmcs.php> accessed 7/25/2016

Chapter 4

Development of Synthetic α -Tropolonoids as Antibiotics Effective Against Gram-negative Bacteria

4.1 Background and Significance

4.1.1 Characteristics of Gram-negative Bacteria

One of the most common techniques used to detect and classify bacteria is the Gram stain developed by Hans Christian Gram in 1884.¹ This technique involves the staining of bacterial cultures with crystal violet dye followed by washing with alcohol. Bacteria that retain the dye are considered Gram-positive while the unstained bacteria are considered Gram-negative. Gram-negative bacteria can subsequently be stained using safranin to develop a red or pink color. Although most forms of bacteria fit into these two categories, it should be noted that some bacteria can give false staining, such as Clostridia which stain as Gram-negative despite having characteristics of Gram-positive bacteria, or do not stain using this method, such as *Mycoplasma* spp. and spirochetes.²

Gram-negative bacteria do not retain the crystal violet dye after being washed with alcohol because the peptidoglycan layer for this type of bacteria is relatively thin compared to Gram-positive bacteria.³ While this relatively thin peptidoglycan layer is a clear characteristic of Gram-negative bacteria, the key differentiating feature of Gram-negative bacteria is the presence

of an outer membrane in addition to the typical cytoplasmic membrane. The outer membrane is mostly comprised of lipopolysaccharide and phospholipids and is known to serve complex functions that control the response of the cell to the environment.⁴ One such function is to remove and stop transcription and translation of passive diffusion aqueous channels (porins) when exposed to certain antibiotics.⁵⁻⁶ Removal of porins is one of several methods Gram-negative bacteria employ to develop resistance to antibiotics. Other methods include: production of enzymes capable of degrading the antibiotic, mutations in the antibiotic binding site and up-regulation of efflux pumps capable of removing antibiotics from the cell.⁶ As a result of these innate mechanisms of resistance, Gram-negative infections are becoming increasingly problematic. In particular, the family Enterobacteriaceae is a leading cause of nosocomial infections, *Pseudomonas aeruginosa* is one of the most resistant forms of Gram-negative bacteria, and *Acinetobacter* can be found in virtually 100% of soil and water.⁷

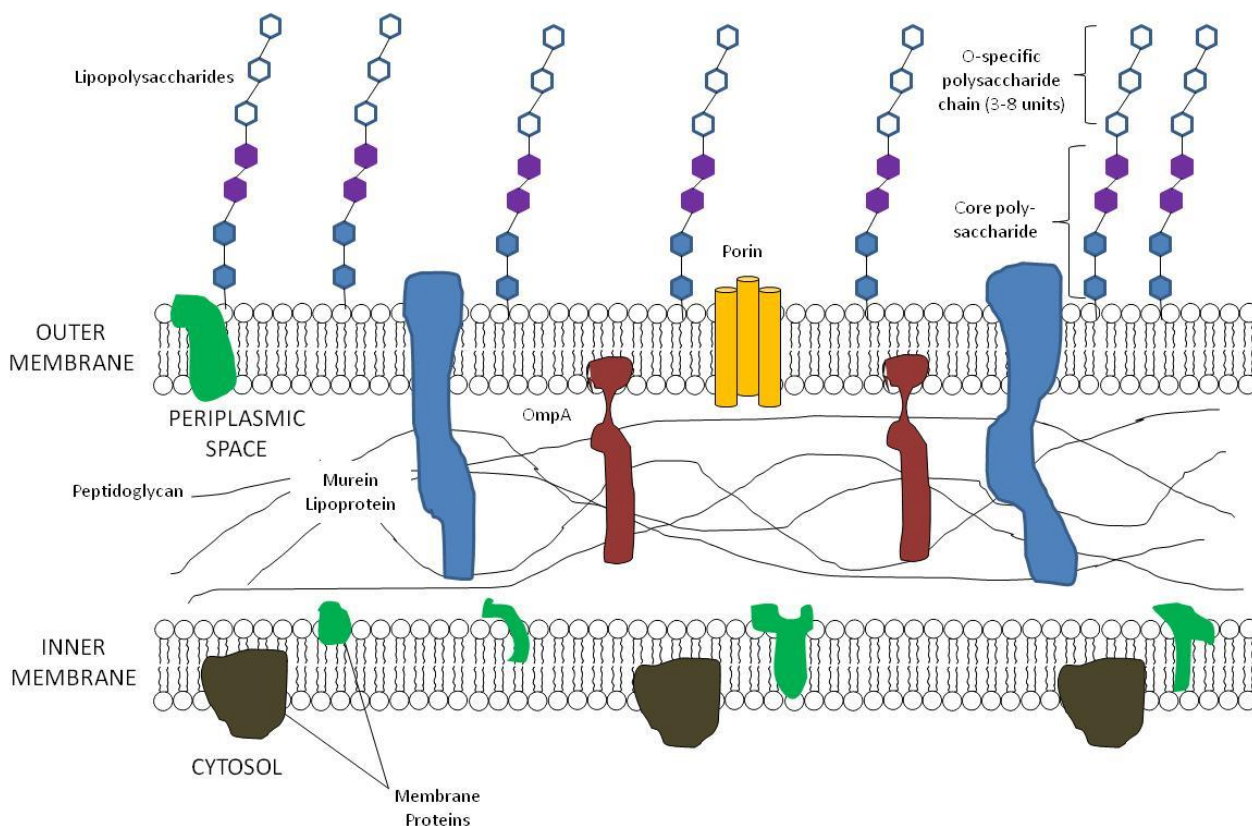


Figure 4.1: Diagram of Gram-negative bacteria cell wall.

4.1.1.1 Enterobacteriaceae

Enterobacteriaceae is a large family of rod shaped, facultatively anaerobic, Gram-negative bacteria.⁸ This family can be subdivided into eight tribes: Escherichieae, Edwardsiellae, Salmonellae, Citrobacterae, Klebsiellae, Proteae, Yersineae, and Erwineae. Among these tribes are some of the most medically important species of bacteria as many are normally found in the gastrointestinal tract and can become pathogenic. Members of this family account for nearly 80% of Gram-negative bacteria clinical isolates. Approximately 75% of all urinary tract infections, two thirds of gastroenteritis cases and one third of all sepsis cases are caused by Enterobacteriaceae.⁷ Infections by Enterobacteriaceae are attributed to their fast

motility, fimbriae which bind tightly to host tissue, endotoxins and enterotoxins.⁸ Two of the most common species that cause nosocomial infections are *Escherichia coli* and *Klebsiella pneumoniae*.

Escherichia coli (*E. coli*) is one of the most studied organisms and can be found worldwide.⁹⁻¹⁰ As a Gram-negative facultative anaerobe, it ferments lactose and possesses an outer membrane. The outer membrane of *E. coli* contains several membrane proteins in addition to the typical lipopolysaccharide and phospholipids. The membrane proteins are mainly the porins OmpC, OmpF and PhoE. Because the porins are small in size, other transport proteins are necessary to provide essential nutrients including oligosaccharides, iron and vitamin B12. While the outer membrane is an important protective barrier, the cytoplasmic membrane of *E. coli* contains over 20 proteins essential for growth and division.¹⁰ Approximately half of these cytoplasmic membrane proteins are able to bind beta lactams, making this membrane a primary target of antibiotics. However, as with most microorganisms, the majority of biochemical processes necessary for growth take place in the cytoplasm.

Although most strains of *E. coli* are considered non-pathogenic, it accounts for most common bacterial infections that result in urinary tract infections, bacteremia, and diarrhea as well as newborn cases of meningitis and clinical cases of pneumonia.⁷ While most infections are easily treated with co-trimoxazole (a dual folate synthesis inhibitor), nitrofurantoin (a bacterial DNA damaging agent), fluoroquinolones (bacterial topoisomerase II inhibitors) or in critical situations, cephalosporins (inhibitors of peptidoglycan synthesis), the number of antibiotic resistant strains has drastically risen since the beginning of the 21st century.¹¹ In 2005, a study by the Bacteraemia Resistance Surveillance Programme determined that 16.6% of bacteraemia cases caused by *E. coli* were resistant to the fluoroquinolone ciprofloxacin.¹² Additionally, there

has been a growing concern of β -lactam resistance since the 1980s due to mutational development of extended spectrum β -lactamases (ESBLs). ESBL producing *E. coli* isolates found in the United Kingdom increased from 0% to 7.3% between 2001 and 2005 with as many as 50.9% harboring the ESBL CTX-M which confers resistance to cephalosporin.¹² Another form of resistance common to Gram-negative bacteria is the use of efflux pumps to remove antibiotics that manage to pass through the cell wall. *E. coli* utilize the AcrAB-TolC pump which is a member of the RND efflux pump family. The RND pumps are multidrug efflux pumps that can export an array of structurally diverse molecules.⁵ Although increasingly resistant strains of *E. coli* are concerning, *Klebsiella pneumoniae*, a more frequently acquired hospital infection, has become poly-resistant and the discovery of resistant isolates has increased at faster rates.

Klebsiella pneumoniae (*K. pneumoniae*) is a rod shaped, facultative anaerobe, capable of fermenting lactose, but unlike most Enterobacteriaceae is non-motile.⁷ It is the second most common cause of Gram-negative bloodstream infections and is associated with lobar pneumonia and urinary tract infections. *K. pneumoniae* can be found worldwide as it is part of the normal flora of the mouth, skin and intestines.¹³ As part of the normal flora, *K. pneumoniae* is an opportunistic pathogen that can lead to high incidences of infection especially in patients undergoing chemotherapy.¹⁴ Other patients at risk of infection include: alcoholics, diabetics, and patients with chronic obstructive pulmonary disease.⁷ For these patients, mortality is high and treatments must be aggressive. Typical treatments involve the use of multiple antibiotics with a preference for cephalosporin and aminoglycosides. However, much like *E. coli*, *K. pneumoniae* has developed ESBLs. The Bacteraemia Resistance Surveillance Programme determined that the incidence of ESBL containing isolates of *K. pneumoniae* increased from 5.6% to 13.1% between

2001 and 2005. Additionally, 81.5% of these isolates were resistant to cephalosporin. Unlike *E. coli*, *K. pneumoniae* is often resistant to trimethoprim (a folate synthesis inhibitor) and fluoroquinolones. Other forms of antibiotic resistance have also increased over the past 20 years, such as carbapenemases (KPC) and β -lactamases. KPC isolates can now be found in most of the United States, France, Sweden, Norway, Scotland, Poland and regions throughout China and Latin America.⁶ The genetic material coding carbapenemases can also be transferred by *K. pneumoniae* to other Enterobacteriaceae.¹⁵ Another resistance mechanism *K. pneumoniae* has developed is the ability to reduce the number of porins in its outer membrane.¹⁶

4.1.1.2 *Pseudomonas aeruginosa*

Belonging to the family Pseudomonadaceae, *Pseudomonas aeruginosa* (*P. aeruginosa*) is a Gram-negative, rod shaped, aerobe.⁷ As an aerobe, it oxidizes aldose sugars, but not maltose. *P. aeruginosa* is found in soil, water, plants and animals and can tolerate a wide variety of physical conditions. It can tolerate these various conditions because it can grow at both 37°C and 42°C, has flagella for motility and can use over 30 organic compounds for growth. Moisture appears to be a critical factor for colonization as *P. aeruginosa* is typically found in the perineum, under arm and ear of humans and has been found on respiratory equipment, cleaning solutions, liquid based medicines, sinks, mops, food sources and processors as well as other sources of moisture in hospitals.

Since *P. aeruginosa* is relatively ubiquitous in the hospital environment, it is not surprising that it is the fourth most frequently isolated pathogen and accounts for 10.1% of all nosocomial infections.⁷ While not always part of the normal human flora, *P. aeruginosa* is an opportunistic pathogen capable of colonizing virtually any tissue, especially the skin of burn

victims, the lower respiratory tract of patients using ventilation, the lungs of cystic fibrosis patients, and the gastrointestinal tract of patients receiving chemotherapy.¹⁷

P. aeruginosa infections are caused by the secretion of a wide variety of molecules and toxins. A key virulence factor is the secretion of lipopolysaccharide that creates a protective barrier called a biofilm. Biofilm formation creates a more favorable environment for bacteria because it traps nutrients and protects the cells from predation or other detriments.¹⁸⁻²¹ Cells embedded in the biofilm matrix closely resemble planktonic cells in the stationary growth phase. As such, biofilms are also characterized by a dramatic decrease in cell growth.²²⁻²⁴ This appearance of stationary growth behavior in biofilms helps further protect the cells from adverse environmental factors such as antibiotics. In fact, biofilms can afford bacterial cells with anywhere from 100-1000 fold resistance to antibiotic treatments.²⁵⁻²⁷ Essentially, there is no major treatment of bacteria once they form biofilms.²⁸⁻³² It is suspected that biofilms cause nearly 80% of all infections.^{26,33} Biofilm formation may also trigger virulence factors which can cause infectious diseases.³⁴

Other virulence factors produced by *P. aeruginosa* include three proteases: elastase, LasA and an alkaline protease. Elastase is a zinc metalloenzyme that causes proteolysis of host proteins and has been linked to biofilm formation.³⁵ LasA is known to cleave elastin, hydrolyze β -casein and lyse *Staphylococci*.⁷ The alkaline protease is not well studied, but some studies indicate it may cleave molecules of the immune system associated with signaling, inflammation and regulation.³⁶ Two other important virulence factors include PrpL and exotoxin A. PrpL is regulated by pyoverdine production and proteolyzes casein, lactoferrin, transferrin, elastase and decorin.³⁷ The degradation of lactoferrin and transferrin increases the ability of siderophores such as pyoverdine to sequester iron and transport it into *P. aeruginosa* to be used for

metabolism. Exotoxin A is the most toxic virulence factor and the most studied.³⁸ Exerting an LD₅₀ of 60-80 ng in a mouse,³⁹ exotoxin A causes the ADP-ribosylation of elongation factor 2 to inhibit host cell protein synthesis.⁴⁰

Treatment of *P. aeruginosa* infections is relatively controversial as antibiotics are often administered before diagnosis.⁷ Because *P. aeruginosa* is intrinsically resistant to many antibiotics due to low hydrophilic molecule permeability and has the ability to acquire genes from other bacteria encoding resistance, many antibiotics are ineffective. *P. aeruginosa* produces β -lactamases, can make structural modifications to its outer membrane to increase resistance to imipenem and colistin, and has the RND type multi-drug efflux pump MexAB-OprM that can export out quinolones, penicillins and cephalosporins and MexXY-OprM that exports out aminoglycosides.¹⁷ These multiple forms of intrinsic resistance necessitates the use of combinatorial treatment typically with an aminoglycoside with either penicillin or a third generation cephalosporin such as ceftazidime or cefoperzone.⁷ However, *P. aeruginosa* resistance to antibiotics continues to increase and it may only be a matter of time before a strain resistant to all conventional antibiotics is discovered.

4.1.1.3 *Acinetobacter*

The genus *Acinetobacter* was first identified in the 1900s and are colorless, non-motile, Gram-negative bacteria that grows on decaying organic matter.⁷ Interestingly, it is rod shaped during the exponential growth phase but spherical in the stationary phase. In the stationary phase, *Acinetobacter* can retain crystal violet dye and are often confused for Gram-positive cocci. Similar to Enterobacteriaceae, *Acinetobacter* is capable of using a variety of organic sources for growth and is found in virtually all sources of soil and water. Although optimal

growth is at 44°C, it has been found in pasteurized milk, frozen foods, hospital air, faucets, bedpans, washcloths, catheters, ventilators, reused needles and plasma protein fractions.⁷ While only present in approximately 25% of health populations, *Acinetobacter* is the most common Gram-negative organism found on the skin of hospital personnel.⁷

The most commonly encountered nosocomial *Acinetobacter* species is *A. baumannii*. Similar to Enterobacteriaceae and *P. aeruginosa*, *A. baumannii* is an opportunistic pathogen and causes a variety of diseases, including: pneumonia, septicemia, meningitis, urinary tract infections, endocarditis, and soft tissue infections in immunocompromised patients.⁴¹ *A. baumannii* also exhibits an assortment of intrinsic resistance mechanisms such as low permeability, reduction in the number of porins, employment of several RND efflux pumps, aminoglycoside modifying enzymes and β -lactamases.⁶⁻⁷ Multi-antibiotic resistance has been increasing at a drastic rate with resistance to three or more antibiotic classes found in 34.2% of all isolates found in the Asia-Pacific region.⁶ While the standard treatment used to include ampicillin, second generation cephalosporins, colistin, minocycline, carbenicillin and gentamicin, *A. baumannii* has now been found to be resistant to most of these antibiotics as well as cefotaxime, chloramphenicol, tobramycin and amikacin.⁷ Imipenem was seen as one of the few treatment options, but outbreaks of imipenem resistance have been documented. Now the current choice of antibiotics is limited to carbapenems, polymyxins and sulbactams.⁴¹

4.1.2 Increased Risk of Infection in Cancer Patients

Many cancers and cancer treatments often leave patients immunocompromised and more susceptible to infections. Patients with hematological malignancies are at the highest risk of potentially deadly infections because they are already considered immunocompromised and most

treatments alter the immune response. In fact, while the survival rates of leukemia and lymphoma have improved to nearly 90%, infections account for the highest mortality rates.⁴² This improvement in patient outcomes is mainly due to intense chemotherapy and newer treatment options such as stem cell transplantation, autologous stem cell reinfusion, granulocyte colony stimulating factors and broad spectrum antibiotics.⁴³ Despite these improvements, the initial 2-3 weeks of acute leukemia is often a period of significant granulocytopenia, a drastic reduction of the innate immune system.⁷ During this time, approximately 50% of acute leukemia patients will develop a fever.² Typically these patients are given broad spectrum antibiotics to combat any potential bacterial or fungal threat, as anywhere from 500-1000 different bacteria may inhabit the human body, mainly in the gastrointestinal tract.⁴⁴ Infections during this time are typically caused by Gram-negative bacteria, with *E. coli*, *K. pneumoniae*, and *P. aeruginosa* being the most common and most lethal.

While Gram-positive bacterial infections have become more frequent in the past several decades, Gram-negative bacteria are of particular concern due to inherent antibiotic resistance. The lipopolysaccharide component of the outer membrane is one of the primary resistance mechanisms of Gram-negative bacteria as it decreases the overall permeability of the cell.⁵ Despite this extra layer of defense, antibiotics have been designed to overcome this permeability issue through utilization of porins within the outer membrane to pass into the peptidoglycan layer. Antibiotics have been developed since the 1940s and have drastically reduced the severity of bacterial infections.⁴⁵ However, this reliance on antibiotics has led to the rise of antibiotic resistant bacteria. Current antibiotics are designed to act on one of four main targets: cell wall synthesis, protein synthesis, DNA replication, or the integrity of the cell membrane.⁵ Antibiotics within the same class usually are based on the same pharmacophore and therefore are closely

related and commonly victim to the same mechanism of resistance. This highlights the need to develop novel antibacterial agents that utilize structurally distinct pharmacophores, target unexploited essential components to bacterial growth, and/or act on several pathways to avoid resistance.

4.1.3 Antibiotic Targets

Current Gram-negative antibiotics target well-studied processes and usually belong to one of 11 basic classes. Aminoglycosides are active against most Gram-negative aerobic and facultative anaerobic bacteria. They act by inhibiting protein synthesis by binding to the 30S ribosome.⁴⁶ The β -lactam class of antibiotics includes penicillin derivatives, cephalosporins, monobactams and carbapenems. All members of this class bind to penicillin binding proteins to inhibit cell wall synthesis.⁴⁷ Glycopeptide antibiotics inhibit peptidoglycan synthesis by binding amino acids within the cell wall to prevent addition of new units of peptidoglycan.⁴⁸ Lincosamides bind 23S of the 50S subunit of the bacterial ribosome to dissociate peptidyl-tRNA from the ribosome.⁴⁹ Similar to lincosamides, macrolide antibiotics cause dissociation of peptidyl-tRNA from the ribosome but bind the P site of the 50S subunit of the ribosome.⁴⁹ Nitrofurans are oxygen acceptors that inhibit cellular respiration and the biosynthesis of nucleic acids.⁵⁰ Polymyxins bind lipopolysaccharide to disturb both the outer and inner membrane similar to a detergent.⁵¹ Ansamycins inhibit transcription through inhibition of bacterial RNA polymerase.⁵² Quinolones are topoisomerase II and IV inhibitors that cause DNA fragmentation.⁵³ Sulfonamides are a class of competitive inhibitors of dihydrofolate reductase which prevents the synthesis of folate necessary to produce nucleic acids.⁵⁴ The last major class of antibiotics effective against Gram-negative bacteria is tetracyclines. Tetracyclines are similar to aminoglycosides as they also bind the 30S ribosomal subunit to prevent the binding of

aminoacyl-tRNA to inhibit protein synthesis.⁵⁵ Despite this array of antibiotics, Gram-negative bacterial resistance has been increasing which stresses the need to develop new antibiotics, especially ones with different biological targets.

Table 4.1: Resistance profiles (% susceptible) of Gram-negative bacteria against two classes of antibiotics.

	Penicillins			Cephalosporins			
	Ampicillin	Amp/Sulbactam	Piperacillin/tazobactam	Cefazolin	Cefepime	Ceftazidime	Ceftriaxone
VCU 2014^a							
<i>E. coli</i>	40	---	96	86	95	---	94
<i>Klebsiella</i>	0	---	91	92	95	---	94
<i>P. aeruginosa</i>		---	90		90	---	
<i>Acinetobacter</i>		---			67	---	
UCLA 2014 non-urine (RRUMC)^b							
<i>E. coli</i>	39	45	91	72	82	81	82
<i>Klebsiella</i>	R	70	89	83	89	88	89
<i>P. aeruginosa</i>	R	R	80	R	83	84	R
<i>Acinetobacter</i>	R	50	44	R	42	41	
UCLA 2014 non-urine (SMH-UCLA) inpatient^b							
<i>E. coli</i>	43	50	94	78	87	87	87
<i>Klebsiella</i>	R	52	71	61	64	64	64
<i>P. aeruginosa</i>	R	R	62	R	67	67	R
MYSTIC 2008^c							
<i>E. coli</i>	---	---	93.6	---	94.5	92.6	89.3
<i>Klebsiella</i>	---	---	85.6	---	93	86.3	87.3
<i>P. aeruginosa</i>	---	---	90.2	---	86.6	85.6	8.9
<i>Acinetobacter</i>	---	---	34.6	---	31.5	31.5	11.8

*R denotes intrinsic resistance

^aData from Virginia Commonwealth University (VCU) Department of Pathology – Microbiology/Immunology 2014.

^bData from University of California Los Angeles (UCLA) Health System Antimicrobial Susceptibility Summary 2014.

^cData from Meropenem Yearly Susceptibility Test Information Collection (MYSTIC) 2008.

Table 4.2: Resistance profiles (% susceptible) of Gram-negative bacteria against four classes of antibiotics.

	Carbapenems			Aminoglycosides			Fluoroquinolone		Other
	Ertapenem	Imipenem	Meropenem	Amikacin	Gentamicin	Tobramycin	Ciprofloxacin	Levofloxacin	TMP/SMX
VCU 2014^a									
<i>E. coli</i>	---	---	100	---	91	---	73	74	74
<i>Klebsiella</i>	---	---	98	---	96	---	94	94	90
<i>P. aeruginosa</i>	---	---	91	---	94	---	81	75	
<i>Acinetobacter</i>	---	---		---	77	---	60	64	72
UCLA 2014 non-urine (RRUMC)^b									
<i>E. coli</i>	99	99	99	99	83	84	63	---	60
<i>Klebsiella</i>	93	96	95	97	92	87	85	---	80
<i>P. aeruginosa</i>	R	76	82	95	89	92	77	---	R
<i>Acinetobacter</i>	R	52	50	52	46	48	44	---	46
UCLA 2014 non-urine (SMH-UCLA) inpatient^b									
<i>E. coli</i>	99	99	99	99	88	88	56	---	60
<i>Klebsiella</i>	73	77	82	82	80	64	66	---	64
<i>P. aeruginosa</i>	R	54	99	99	86	88	51	---	R
MYSTIC 2008^c									
<i>E. coli</i>	98.2	98.6	98.6	---	---	84.8	68.2	68	---
<i>Klebsiella</i>	93.5	94.5	94.2	---	---	85.1	84.1	85.6	---
<i>P. aeruginosa</i>		79.5	85.4	---	---	89.1	77	72.7	---
<i>Acinetobacter</i>		52	45.7	---	---	59.1	32.3	33.9	---

*R denotes intrinsic resistance

^aData from Virginia Commonwealth University (VCU) Department of Pathology – Microbiology/Immunology 2014.

^bData from University of California Los Angeles (UCLA) Health System Antimicrobial Susceptibility Summary 2014.

^cData from Meropenem Yearly Susceptibility Test Information Collection (MYSTIC) 2008.

While druggable targets effective against Gram-negative infections are still being discovered and validated, there is already a growing list of possible targets and agents effective against these targets. One method being studied is the disruption and inhibition of a phenomenon called quorum sensing. Quorum sensing typically causes a simultaneous phenotypic change in a community of the same bacteria.⁵⁶⁻⁵⁷ This synchronization of phenotypes allows bacteria to control certain behaviors that require a large population in order to function properly, such as swarming and biofilm formation.⁵⁸ Quorum sensing inhibitors typically are not

bactericidal, but can be bacteriostatic and can prevent colonization, transfer of resistance genes and production of virulence factors. Anti-virulence factor agents are also being developed for a variety of targets including proteases³⁵ and adhesion proteins.⁵⁹ Other Gram-negative targets with agents being developed include the essential metalloenzymes LpxC⁶⁰⁻⁶¹, DXR⁶², peptide deformylase⁶³ and enolase⁶⁴.

4.1.4 Natural Product Troponoids as Antibacterial Agents

The first troponoid, puberulonic acid, was isolated from *Penicillium puberulum* in 1932, but the first troponoid structure was not proposed until 1941.⁶⁵ Since then more than 200 troponoids have been isolated from various other fungi, bacteria and plants. The most studied troponoids are the thujaplicins, specifically β -thujaplicin (hinokitiol, HKT). As secondary metabolite natural products, thujaplicins have many widespread applications including antibacterial properties. In 1938, it was discovered that HKT exhibits significant antibacterial activity against *tubercle bacillus* and other bacteria.⁶⁶ Because HKT has poor water solubility, many early studies were focused on the unsubstituted thujaplicin, tropolone. Tropolone itself has been found to be bacteriostatic and bactericidal against a broad range of bacteria.⁶⁷

Table 4.3: Bacteriostatic Activity of Tropolone Against Gram-negative Bacteria.⁶⁸

Species	Inoculum (CFU/mL)	MIC (μ M)
<i>Aeromonas hydrophila</i>	6.0×10^3	12
	6.0×10^7	100
<i>Chromobacter violaceum</i>	1.1×10^4	49
	1.1×10^8	100
<i>Escherichia coli</i>	8.0×10^3	410
	8.0×10^7	410
<i>Pseudomonas aeruginosa</i>	9.9×10^3	820
	9.9×10^7	820

Table 4.4: Bactericidal Activity of Thujaplicin Related Compounds.⁶⁹

Compound	% Survival Rate	
	<i>E. coli</i> IFO 3301 (10 min)	<i>S. aureus</i> IFO 12732 (10 min)
Tropone	96	100
Tropolone	65	43
α -Thujaplicin	2	0
Hinokitiol	2	22
Hinokitiol sodium salt	1	5
Hinokitiol-acetate	97	69
β -Dolabrin	5	9

Additionally, α and γ thujaplicin also exhibit antibacterial effects similar to HKT and tropolone.

Table 4.5: Antibacterial Activity of Thujaplicins against *Legionella* species (Presented as MIC μ g/mL).^a

Microorganism	α -thujaplicin ^b	β -thujaplicin	γ -thujaplicin	4-acetyltropolone	β -dolabrin
<i>L. pneumophila</i> SG1	12.5	6.25	50	3.1	6.25
<i>L. pneumophila</i> SG3	50	25	25	12.5	25

^aFrom *Curr. Med. Chem.* 2007, 14, 2597-2621.

^bFrom *Biol. Pharm. Bull.* 2004, 27(6), 899-902.

As exemplified in the bactericidal work done by Morita and coworkers, the efficacy of troponoids appears to be directly related to the alpha hydroxy ketone moiety. Removal of the hydroxyl group (tropone) or acetyl substitution eliminates the bactericidal activity. Activity does

not appear to be affected based on α or β substitution or isopropyl versus isopropenyl; however, there is a significant difference between these versus unsubstituted tropolone. In combination with the known chelation potential of tropolone,⁷⁰ these results suggest that troponoid antibacterial activity is most likely due to metal chelation by the alpha hydroxy ketone. It has been proposed that chelation of Mg^{2+} or Fe^{3+} may allow for more rapid passage through the outer membrane of Gram-negative bacteria where the ion can be dissociated, allowing the drug to pass through the cytoplasmic membrane.⁷¹ Additionally, the lead-like Gram-negative antibacterial activity of α , β and γ thujaplicin as well as β -dolabrin and 4-acetyltropolone suggests the tropolone chemotype offers a unique scaffold amenable to the development of new, potent and metalloprotein selective Gram-negative antibiotics.

4.1.5 Project Objectives

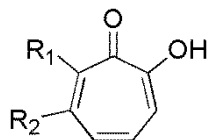
Our goal was to assess the antibacterial activity of tropolone derivatives against Gram-negative bacteria. Because natural product tropolones are known to be biologically active against a variety of targets and are capable of chelating metal ions, the tropolones synthesized should offer antibacterial activity against Gram-negative bacteria. The minimal inhibitory concentration of these tropolones against *E. coli* (ATCC 25922) and *K. pneumoniae* (ATCC 10031) would be assessed first. Tropolones exhibiting lead-like activity would subsequently be screened against *P. aeruginosa* and *A. baumannii* as well as clinical isolates of *K. pneumoniae*. Lipopolysaccharide and efflux pump knockout models of *E. coli* would then be screened to further elucidate the structural activity relationship of the tropolones and any permeability or efflux related problems associated with the tropolone chemotype or substitutions.

4.2 Results and Discussion

4.2.1 Novel α -Tropolones are Active Against Gram-negative Bacteria

The original series of tropolones and aminotropone intermediates synthesized by Dr. Oblak, Dr. van Heyst and Mohamed Ammar,⁷²⁻⁷³ presenting either α or β substitution, were screened for activity against *E. coli* 25922 and *K. pneumoniae* 10031 using the minimal inhibitory concentration (MIC) assay. Initial screening used *E. coli* and the maximum concentration of either 40 or 50 $\mu\text{g/mL}$. Because *K. pneumoniae* is typically more robust than *E. coli*, the maximal concentration of 50 $\mu\text{g/mL}$ was not adequate in most cases and needed to be increased to 125 $\mu\text{g/mL}$.

Table 4.6: MICs ($\mu\text{g/mL}$) of first generation Tropolones against *E. coli* 25922 and *K. pneumoniae* 10031.



Compound	R ₁	R ₂	MW	<i>E. coli</i> 25922 ($\mu\text{g/mL}$)	<i>K. pneumoniae</i> 10031 ($\mu\text{g/mL}$)
Tropolone	H	H	122.12	> 40	> 50
MO-OH-PH		H	198.22	20	25
MO-OH-DM		H	258.27	> 40	100
MO-OH-TM		H	288.28	> 40	100
MO-OH-Nap		H	248.28	40	100
HKT	H		164.2	25	31.25
β -tert	H		178.23	> 50	125
β -cyc	H		190.24	50	62.5
β -PH	H		198.22	25	31.25
β -SM	H		228.24	> 50	62.5
HKT-OMe	H		178.23	> 50	> 500

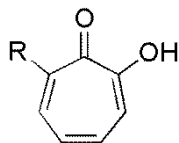
Based on these results, it appears as though there is minimal difference between α and β substituted tropolone activity. Although there might be a slight preference for β versus α for *K. pneumoniae*, this is inconclusive due to the lack of diversity amongst the substitutions.

However, it is clearly apparent that the alpha hydroxy ketone moiety is essential to antibiotic

activity since both the methyl ether form of hinokitiol (HKT-OMe) and the aminotropone intermediates (see Appendix) lack activity in *E. coli* up to 50 $\mu\text{g/mL}$ and in *K. pneumoniae* up to 500 $\mu\text{g/mL}$. Here, the lead-like tropolone from the synthesized analogs is the α -phenyl tropolone (MO-OH-PH).

Although not directly related to these antibacterial results, subsequent tropolones synthesized contained modifications on the α -phenyl substitution, alkyl chains, an alkyl chain connected to a cyclic carbon moiety or heterocyclic substitutions since heterocycles are known to display diverse biological activities.⁷⁴

Table 4.7: MICs ($\mu\text{g/mL}$) of Key Potent Tropolones Against *E. coli* 25922 and *K. pneumoniae* 10031.



Compound	R	MW	<i>E. coli</i> 25922	<i>K. pneumoniae</i> 10031
MO-2-OH		192.25	20/10	10
MO-10-OH		226.27	20	10
MO-pSMe-OH		244.31	20	20
BA-pBr-OH		277.11	20	12.5
BA-PH-OH		274.31	20	12.5
BA-HC2-OH		264.28	20	20
HC-2-OH		188.18	20	10
HC-6-OH		201.22	40/20	40
EF-3-OH		256.25	40/20	20
TDA*		212.25	20	20

*TDA is tropodithietic acid, a tropenoid produced by *Roseobacter gallaeciensis*

While it was anticipated that low molecular weight (< 400 Da), increased polarity and increased relative polar surface area would generate more potent tropolones, it is difficult to determine a trend in modifications to tropolone and Gram-negative MICs (for all tropolone MICs

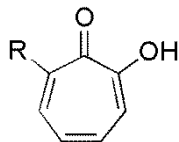
see Appendix). However, many of the key potent tropolones tend to possess a para substitution on the phenyl ring and several substitutions possess hydrogen bonding or chelation potential. Although molecular weight does not appear to be a factor with these tropolones, it appears as though there may be a fine line in developing more potent tropolones with a mix of hydrophilic, aromatic and hydrophobic substitutions. It should be noted that tropodithietic acid (TDA) was included as a natural tropenoid possessing a carboxyl instead of a hydroxyl to determine if this type of substitution affected activity. Interestingly, TDA appears to be one of the more potent tropenoid analogs tested and may provide a scaffold on which to build more potent tropolones utilizing the carboxy-tropone chemotype; however, it should be noted that the dithietane may be reduced to the dithiol which may be responsible for the activity of TDA. Other small molecules with either known metal chelating ability or possessing functional groups with metal chelation potential were also screened against *K. pneumoniae* 10031. Surprisingly, vorinostat, catechol, 6-aminocaproic acid and 3,4-dihydroxyphenylacetic acid did not show any effect up to 40 µg/mL. This suggests the tropolone scaffold is a more suitable metal chelation chemotype, tropolones are more permeable across the outer membrane than the three small molecules tested, tropolones are susceptible to efflux but vorinostat, catechol and 3,4-dihydroxyphenylacetic acid are, or tropolones interact with Gram-negative bacteria in a specific manner in which the other small molecules tested cannot to exhibit an antibacterial effect.

4.2.2 α -Tropolone Display Activity Against Clinical Isolates of *Klebsiella pneumoniae*

Efficacy against *E. coli* 25922 and *K. pneumoniae* 10031 in the 20 µg/mL range is ideal for the development of more potent tropolones, but true lead-like drugs ideally should be

effective against both test strains and clinical isolates. Two clinical isolates of *K. pneumoniae*, *K. p.* UHC1 and *K. p.* UHC3, were obtained from the University of Connecticut Health Center. *K. p.* UHC1 is resistant to trimethoprim (TMP) with an MIC greater than 20 µg/mL while *K. p.* UHC3 is susceptible to TMP.

Table 4.8: MICs (µg/mL) of Key Potent Tropolones Against Clinical Isolates of *K. pneumoniae*.



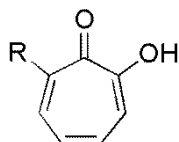
Compound	R	<i>K. p.</i> 10031	<i>K. p.</i> UHC1	<i>K. p.</i> UHC3
MO-OH-PH		25	40/20	20
MO-2-OH		10	40	20
MO-7-OH		25	40	20
MO-10-OH		10	> 40	40
MO-pSMe-OH		20	20	20
BA-pBr-OH		12.5	20	20
HC-1-OH		20	> 40	40
HC-2-OH		10	20	20
EF-2-OH		10	> 40	> 40
EF-3-OH		20	> 40	> 40
HKT		31.25	20	20
TDA		20	20	20

Most of the tropolones show a slight loss of potency against the TMP susceptible *K. pneumoniae* clinical isolate, but several maintain sufficient MICs. This indicates synthetic

tropolones may be developed as clinically useful Gram-negative antibiotics since they are not subjected to the same resistance mechanism utilized against TMP, a commonly prescribed, first-line antibiotic for the treatment of urinary tract infections typically caused by Enterobacteriaceae. Not surprisingly, most of the tropolones lose efficacy against the TMP resistant clinical isolate of *K. pneumoniae*. Although this isolate has not been fully characterized, this decrease in activity may indicate a decrease in the number of porins in the outer membrane to reduce permeability, an increase in multidrug efflux pumps or the mechanism of action of tropolones is similar to TMP. However, several of the key potent tropolones maintain potency against this resistant isolate. BA-pBr-OH and MO-pSMe-OH retain activity in both clinical isolates while MO-OH-PH loses some potency against the TMP resistant isolate. This seems to indicate that a para-substitution on the phenyl ring may increase potency against more resistant isolates, but there appears to be a fine line in selection of functional groups as various alkyl chain lengths, acetyl group, and amide functionality all lose potency. The furan of HC-2-OH may provide a key hydrogen bond acceptor or may covalently bind to a cysteine residue within the target.

4.2.3 Activity of Tropolones Against Other Infectious Microbes

Since the tropolones exhibit lead-like potential against *E. coli* and *K. pneumoniae* it is prudent to screen them for activity against intrinsically more resistant Gram-negative bacteria such as *P. aeruginosa* and *A. baumannii*.

Table 4.9: MICs ($\mu\text{g/mL}$) of Key Potent Tropolones Against *P. aeruginosa* and *A. baumannii*.

Compound	R	<i>P. aeruginosa</i>	<i>A. baumannii</i>
MO-OH-PH		20	20
MO-1-OH		23	23
MO-2-OH		38	19
MO-10-OH		45	23
BA-pBr-OH		28	14
BA-PH-OH		> 55	27
EF-2-OH		48	24
EF-3-OH		51	26
HC-1-OH		51	26
HC-2-OH		> 38	19
HKT		> 164	11
TDA		11	21

The MIC values listed in Table 4.9 were determined in the lab of a collaborator, Dr. Nigel Priestley, at the University of Montana. These experiments were conducted based on the concentration of tropolone in μM and then converted to standard MIC values ($\mu\text{g/mL}$).

Although all the tropolones are relatively potent against *A. baumannii*, there appears to be a preference in potency against *P. aeruginosa* towards small, hydrophobic substitutions and a clear preference towards α -substitution since HKT is non-active. Unlike the activity seen against clinical isolates of *K. pneumoniae*, HC-2-OH does not maintain similar activity to TDA in the more intrinsically resistant *P. aeruginosa*. Interestingly, HC-2-OH is not one of the more potent tropolones in *P. aeruginosa* despite being one of the most potent analogs in all other Gram-negative species examined. This may indicate HC-2-OH and TDA exert activity through different mechanisms. To validate this idea, tropolone analogs with carboxylic acids instead of hydroxyls should be synthesized and tested. Additionally, it appears as though the more potent tropolone analogs against *P. aeruginosa* consist of small, hydrophobic substitutions.

It is known that cytoplasmic targeted Gram-negative antibiotics either enter the cytoplasmic membrane through passive transport through the outer membrane or via solute specific and/or self-promoted uptake. Passive transport is the mechanism which cytoplasmic targeted antibiotics enter the Gram-positive cytoplasm. To further understand the activity of tropolones against Gram-negative bacteria, the tropolones were screened by the Priestly lab against several Gram-positive bacteria and fungal species.

Table 4.10: MICs ($\mu\text{g/mL}$) of Key Potent Tropolones Against Gram-positive and Fungal Species.

Compound	<i>S. aureus</i>	<i>S. pyogenes</i>	<i>B. anthracis</i>	<i>E. faecalis</i>	<i>C. albicans</i>	<i>C. glabrata</i>
MO-OH-PH	39.643	19.822	19.822	19.822	39.643	19.822
MO-1-OH	23.232	11.616	23.232	23.232	23.232	23.232
MO-2-OH	19.212	19.212	19.212	19.212	19.212	19.212
MO-10-OH	22.627	22.627	22.627	45.254	22.627	22.627
BA-pBr-OH	13.856	13.856	138.557	27.711	13.856	13.856
BA-PH-OH	27.431	27.431	27.431	6.858	54.863	27.431
EF-2-OH	48.051	48.051	24.025	> 48.051	24.025	24.025
EF-3-OH	51.251	51.251	25.625	> 51.251	25.625	25.625
HC-1-OH	51.251	25.625	25.625	> 51.251	25.625	25.625
HC-2-OH	37.636	18.818	18.818	37.636	18.818	18.818
HKT	41.05	82.101	82.101	41.05	20.525	10.509
TDA	5.306	21.225	21.225	10.612	21.225	10.612

While the activity of tropolones against Gram-positive and fungal species does not rule out the possibility of interacting with the cytoplasmic membrane to exhibit an antibiotic effect, it does rule out targeting the outer membrane of Gram-negative bacteria. This data shows that α -substituted tropolones are typically more effective against a range of Gram-positive bacteria compared to HKT. However, there does not appear to be a trend in substitutions and activity for the α -tropolones. The carbonyl substituted phenyl rings (EF-2-OH and EF-3-OH) lose significant potency against most of the species tested but maintain similar potency to other tropolones tested against *Bacillus anthracis* (*B. anthracis*). Surprisingly, BA-pBr-OH, which is one of the more potent broad spectrum tropolones, loses 10-fold potency against *B. anthracis*. Due to the lack of trend in structural activity relationship and the perplexing loss of potency of BA-pBr-OH against *B. anthracis*, it is difficult to suggest a reason for tropolone potency or a potential mechanism of action.

All of the tropolones here are relatively potent against *Candida albicans* (*C. albicans*) and *Candida glabrata* (*C. glabrata*) including HKT. Again, the relative consistent potency of the tropolones (~20 µg/mL) makes it difficult to suggest a reason for potency. However, when taking into account the FDA approved antifungal agents, a potential mechanism of action could be explained. The azole antifungals (ie. itraconazole, fluconazole, etc.) are inhibitors of the cytochrome P-450-dependent enzyme lanosterol and act by chelating Fe³⁺ in the active site.⁷⁵ Tropolones are known to bind Fe³⁺ and may act through a similar mechanism since bacteria also express essential cytochrome P-450 enzymes.⁷⁶ Another class of antifungal agents, the echinocandins (ie. caspofungin, micafungin, etc.), inhibit 1,3-β-glucan synthase which synthesizes a critical polysaccharide (1,3-β-glucan) component of the fungal cell wall.⁷⁷ 1,3-β-glucan is analogous to peptidoglycan, suggesting tropolones may disrupt cell wall synthesis in both bacteria and fungi.

4.2.4 Using *E. coli* Knockout Models to Elucidate Potential Permeability and Efflux Issues

After testing the tropolones against a variety of bacterial and fungal species there does not appear to be any specific trend in substitutions and activity. The best trend appears against *P. aeruginosa* where there is a preference towards small, hydrophobic substitutions. The only other potential trend appears against the Enterobacteriaceae, *E. coli* and *K. pneumoniae*, where there is a fine line between tropolones with a mix of hydrophilic, aromatic and hydrophobic substitutions and activity. One reason for the lack of any strong structural activity relationship may be that the tropolones have limited permeability across the outer membrane or that the tropolones can be effluxed out of the cell at different rates to reduce overall efficacy. To assess these possibilities the tropolones were screened against *E. coli* BW25113, which is homologous to 25922, and two knockout strains. JW0451 comes from the Keio collection and is a knockout

model of *E. coli* BW25113 resulting in loss of *acrB*, a member of the RND efflux pump family and the major efflux pump in *E. coli*.⁷⁸ NR698 is an *E. coli* mutant strain with altered LPS to increase permeability to small molecules.⁷⁹

Table 4.11: MICs of Tropolones Against *E. coli* and *E. coli* Knockouts.

Compound	BW25113	JW0451	NR698	Effect on Potency
MO-OH-PH	20	> 40	40	None
MO-9-OH	40	40	20	LPS
BA-pBr-OH	20	20	10	LPS
BA-DM-OH	> 40	20	10	Efflux and LPS
BA-P5-OH	> 20	> 40	20/10	LPS
EF-2-OH	20	20	20	None
HC-1-OH	40	40	40	None
HC-2-OH	20	20	20	None
HC-10-OH	> 40	40/20	10/5	Efflux and LPS
BA-HC2-OH	20	20	20	None
MO-pSMe-OH	20	20	10	LPS
SG-TMS-OH	> 20	> 40	5	LPS
HKT	20	20	20	None

It is encouraging to note many of the tropolones are not affected by reduced permeability across the outer membrane or efflux pumps (for data on additional tropolones see Appendix). While several tropolones do experience permeability issues, they are mostly more hydrophobic than the other analogs. Two tropolones, BA-DM-OH and HC-10-OH, appear to also be effected by efflux. These two present very different substitutions and do not offer real insight into why they are subjected to efflux pumps since structurally similar tropolones such as BA-TM-OH is not. Surprisingly, most of the tropolones with heterocyclic substitutions do not exhibit increased potency in NR698. Again, these results suggest there is a fine line between tropolones with a mix of hydphilic, aromatic and hydrophobic substitutions and activity.

4.2.5 Exogenous Metal Effects on α -phenyl Tropolone Activity

From the broad spectrum activity exhibited against Gram-positive/negative bacteria and fungi it was proposed that one potential mechanism could be the ability to bind Fe^{3+} to inhibit essential cytochrome P-450 enzymes. It was also proposed that tropolones have the potential to bind other metalloenzymes including the zinc metalloenzyme LpxC, magnesium metalloenzymes gyrase and polymerase, the manganese metalloenzyme DXR, or peptide deformylase, another iron metalloenzyme. Based on this, it may be possible that addition of the preferred metal exogenously could eliminate tropolone activity. To test this, solutions of the chloride salts of Fe^{3+} , Zn^{2+} , Mg^{2+} , Mn^{2+} , Ca^{2+} and Cu^{2+} were prepared and co-incubated with MO-OH-PH treated *E. coli* BW25113. First, the metal ions and tropolone were serially diluted in a constant ratio (metal ion: 10 mM - 312 μM ; tropolone: 80 $\mu\text{g/mL}$ – 2.5 $\mu\text{g/mL}$). Most of the metal ions tested had no effect on the MIC but may have precipitated in the 10 mM treated wells. However, the wells treated with Fe^{3+} showed no antibacterial activity. Because the 10 mM concentration of metal ions appeared to precipitate in the wells with 80 $\mu\text{g/mL}$ tropolone it is possible that the excess concentration of metal caused precipitation. To explore this possibility, the concentration of metal ion was held constant at 10 mM and tropolone was still serially diluted. Again, most of metal ions had no effect on the MIC, except for Fe^{3+} and Cu^{2+} . Fe^{3+} treated wells showed no antibacterial activity while wells treated with Cu^{2+} showed drastically increased activity (MIC < 2.5 $\mu\text{g/mL}$). The enhanced antibacterial activity in the Cu^{2+} wells can easily be explained by the bactericidal effect Cu^{2+} at high enough concentrations.⁸⁰ Previous work done in other labs has indicated that the ideal ratio of exogenous Fe^{3+} to tropolone for chelation and activity is 1:3.⁸¹ MIC plates with the ratios of 3:1, 2:1 and 1:1 tropolone to Fe^{3+} were made to determine if these lower concentrations affected potency. Although these lower concentrations (200-75 μM) did

not cause the precipitation seen with the higher concentrations, MO-OH-PH was still found to be inactive at double the MIC (40 $\mu\text{g/mL}$). It should be noted that iron(III) chloride alone had no growth effect on *E. coli*. Furthermore, Fe^{2+} also abolished the activity of MO-OH-PH while 20 μM Fe^{3+} was determined to be the minimal concentration required to abolish activity at 40 $\mu\text{g/mL}$ (10:1 tropolone to iron). This may indicate that tropolones target an iron metalloenzyme.

4.2.6 Elucidation of the Mechanism of Action of Tropolones as Antibacterial Agents

In order to probe the effects of tropolones on the morphology of the cell, Gram-stained preparations of *E. coli* treated with various compounds were imaged using confocal microscopy (see Figure 4.1). Images of the untreated cells and cells treated with the negative control HKT-OMe show little difference in morphology. However, images of cells treated with 20 $\mu\text{g/mL}$ of HKT or BA-pBr-OH show that the cells become filamentous. These results are consistent with incomplete cell division and suggest that the tropolones may directly inhibit biosynthesis of the cell wall or inhibit targets critical to cell division.

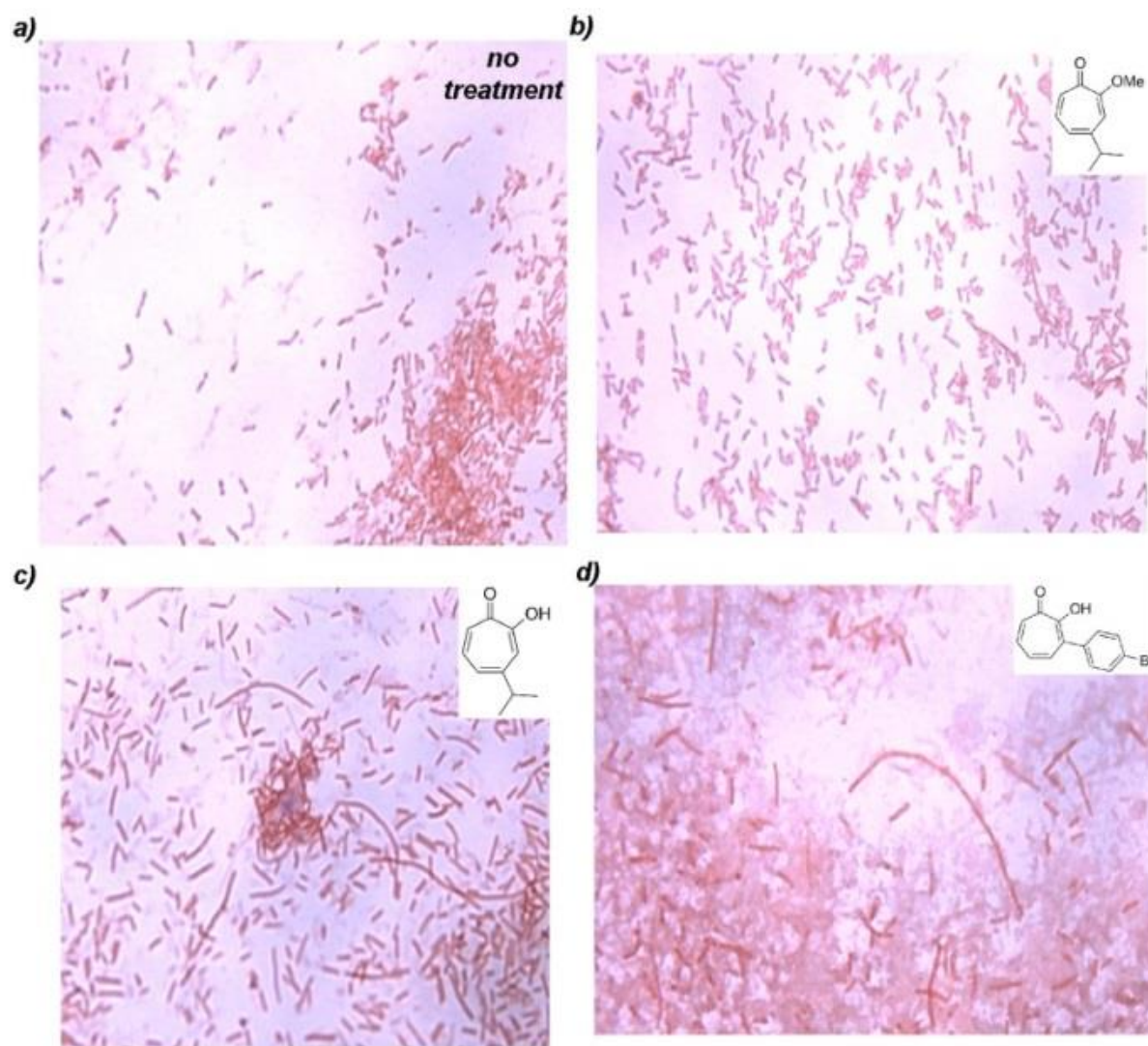


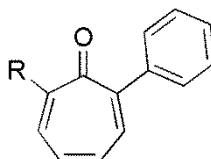
Figure 4.2: *E. coli* 25922 cells treated with a) DMSO, b) HKT-OMe as a negative control, c) HKT, d) BA-pBr-OH.

A report on the antibacterial activity of tropolone did not find filamentous growth for any bacteria treated at sub-inhibitory concentrations.⁶⁸ This would seem to indicate that substitutions on the tropolone ring may change the mechanism of action especially since this study also determined that tropolone expressed only 4% of the bactericidal activity of HKT. Additionally, tropolone was found to lose activity in the presence of 20% sucrose. The author suggests that the lack of filamentous growth means tropolone does not inhibit enzymes involved in cell wall

synthesis while the antagonistic activity of sucrose indicates tropolone acts on the cytoplasmic membrane. To test this hypothesis, several concentrations of MO-OH-PH were co-incubated with 20, 10 or 5% sucrose or glucose in *E. coli* BW25113. Neither sucrose nor glucose appeared to have any effect on the antibacterial activity of MO-OH-PH, suggesting the tropolone analogs may inhibit enzymes involved in cell wall synthesis.

Since many of the enzymes involved in cell wall synthesis are metalloenzymes, phenyl tropones with various substitutions of the hydroxyl group were tested to determine if the hydroxyl group was essential for activity or if activity could be enhanced by incorporation of other metal chelating functionalities.

Table 4.12: Effects of Hydroxyl Substitution on *E. coli* MIC ($\mu\text{g/mL}$).



Compound	R	<i>E. coli</i> BW25113 MIC
MO-OH-PH	-OH	20
MO-NH ₂ -PH	-NH ₂	> 200
MO-OMe-PH	-OCH ₃	> 40
MO-SH-PH	-SH	> 200
MO-Am-PH		> 40
MO-SMe-PH	-SCH ₃	> 40
MO-NHOH-PH	-N(OH)H	> 40
MO-H-PH	-H	> 40

The lack of activity in the tropones with metal chelating functional groups other than hydroxyl indicates metal chelation may not be part of the mechanism of action. The protection of the hydroxyl as a methyl ether and the substitution of the hydroxyl with a hydrogen serve as

negative controls since the methyl ether should have minimal metal chelating potential and hydrogen cannot chelate metal. Combining these results with those from the other metal chelating functional groups shows that the hydroxyl is essential for tropolone activity against Gram-negative bacteria. However, it may be possible that the substitution of the hydroxyl with a carboxylic acid could yield similar results or increase potency as seen with TDA.

Because true structure activity relationship of tropolone derivatives is not well understood, direct target identification approaches such as biotin affinity tags are not ideal. When small molecules exhibit biological activity but have unknown effects due to structural diversity, indirect target identification techniques can be used. Drug affinity responsive target stability (DARTS) is an indirect target identification technique developed by Huang and coworkers “for the initial identification of protein targets of small molecules”.⁸² DARTS uses the idea that the binding of a small molecule to a target protein will stabilize the protein and reduce the sensitivity of the protein to proteases. Based on this principle, two tropolones (BA-pBr-OH and HC-2-OH) were subjected to DARTS analysis. Although the protocol developed by Huang and coworkers requires the incubation of whole cell lysates with the small molecule for 30 minutes prior to thermolysin digestion, this protocol was developed for mammalian cells and not bacteria. Due to this difference, it is not surprising that initial attempts were unsuccessful. To overcome this issue, the protocol was modified to a hybrid of Western Blot and DARTS analysis. In short, tropolones were incubated with 4 mL of *E. coli* 25922 in a 6 well plate overnight before undergoing the standard DARTS protocol (see Chapter 5 for full protocol). Both BA-pBr-OH and HC-2-OH treatment expressed differential bands compared to the untreated (DMSO) lysates, indicating potential targets. Figure 4.2 shows that although there are a couple of differential bands present on the gel, one band is clearly different and able to be

analyzed. The band was excised from the gel and sent to the Keck MS & Proteomics Resource at Yale School of Medicine for LC-MS/MS protein identification. With 83% coverage, the protein in the band was identified as enolase.



Figure 4.3: Gel image of modified DARTS assay using *E. coli* 25922 treated with DMSO or HC-2-OH and lysed with thermolysin.

Enolase is a magnesium metalloenzyme that typically exists as a dimer which catalyzes the conversion of 2-phosphoglycerate (2-PG) to phosphoenolpyruvate (PEP).

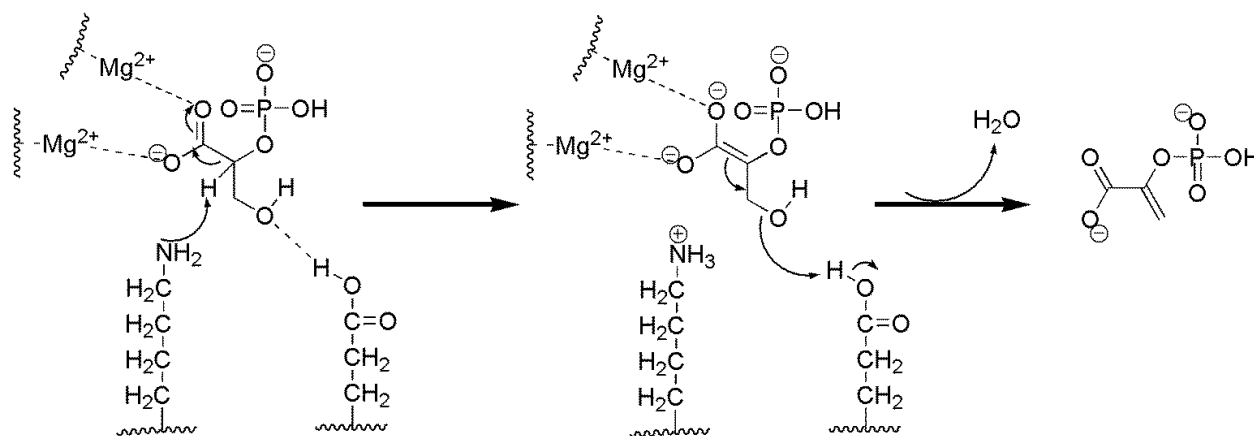


Figure 4.4: Catalytic mechanism of the conversion of 2-PG to PEP by enolase.

The conversion of 2-PG to PEP is an essential step in the degradation of carbohydrates.⁸³

Although this catalytic activity is one of its primary functions, enolase has been implicated in several other important biological processes. In *E. coli*, the enolase gene also contains CTP synthase which is essential for pyrimidine biosynthesis.⁸³ There is an estimated 3131 dimers of enolase per cell in *E. coli* with approximately 1/10 of the total enolase sequestered in the RNA degradosome.⁸⁴⁻⁸⁵ The degradosome is comprised of RNase E, PNPase, RhlB and enolase and is located at the cell surface of bacteria and fungi and is part of the cytoskeletal structure of *E. coli*.^{83,86} As part of the degradosome, enolase stabilizes mRNA that encodes a transmembrane glucose transporter.⁸⁷ Removal of enolase from the degradosome reduces the activity of RNase E nearly 10-fold.⁸³ *E. coli* AT8 cells have abnormalities in RNase E which causes a defect in chromosome segregation and results in filamentous growth possibly due to a defect in attachment of the cytoplasmic membrane to the outer membrane.⁸⁶ Additionally, enolase deficient *E. coli* exhibit interference in cell wall synthesis and repression of metabolic and transport enzymes that would normally remove growth inhibitors.⁸⁸ Because tropolones are known metal chelators and *E. coli* treated with BA-pBr-OH exhibited filamentous growth, enolase is a plausible target.

To validate enolase as a target, the Enolase Activity Assay Kit (Sigma Aldrich) was purchased. This kit uses a whole cell lysate and detects an intermediate of the conversion of 2-PG to PEP. The intermediate can react with a peroxidase substrate to give a fluorometric product that is proportional to the amount of enolase activity present. After establishing a standard curve of peroxide generated indicating 100% enolase activity, peroxide curves of lysates of *E. coli* treated with MO-OH-PH, BA-pBr-OH or HC-2-OH were determined.

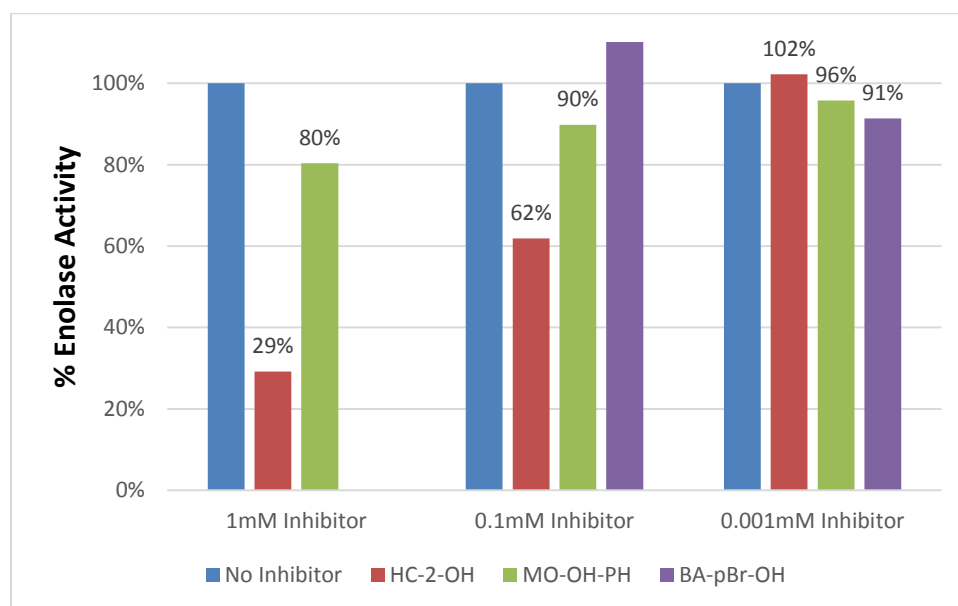


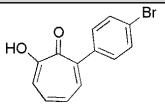
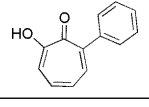
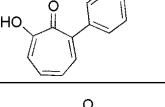
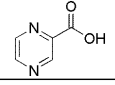
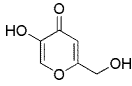
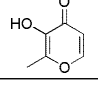
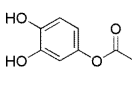
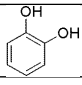
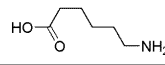
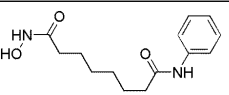
Figure 4.5: % Enolase activity in *E. coli* lysates as measured by fluorometric analysis of reaction with a peroxide substrate. Peroxide generation of untreated lysate was normalized to 100% activity. Cells were treated with 1 mM, 0.1 mM or 0.001 mM of HC-2-OH, MO-OH-PH or BA-pBr-OH and peroxide generation was compared to untreated lysate and determined as % enolase activity. BA-pBr-OH was not tested at 1 mM.

As seen in Figure 4.3, the tropolones tested had some effect on enolase activity, with HC-2-OH having the most substantial effect with an IC_{50} potentially around 200 μ M. MO-OH-PH appears to have a slight effect while BA-pBr-OH did not exhibit any inhibitory effect on enolase. This may indicate that HC-2-OH acts via a different mechanism than the other tropolones and

this mechanism may involve enolase. It should be noted that this assay does not utilize pure enolase enzyme and was developed to detect mammalian enolase activity. Since *E. coli* enolase is known to have low cysteine content compared to mammalian enolases, this kit may not be ideal.⁸⁹

As a result, *E. coli* enolase was expressed, purified, and assessed for activity. The purified *E. coli* enolase exhibited activity similar to reported values and could be used to screen the inhibitory potential of the tropolones. Because enolase is a metalloenzyme and tropolone is a metal chelator, initial inhibition assays included the some of the more potent tropolones and metal chelating small molecules.

Table 4.13: Initial Screening of Tropolones and Small Molecule Chelators (50 μ M) with Purified Enolase.

Compound	Structure	% Enolase Activity	% Inhibition
BA-pBr-OH		22	78
MO-OH-PH		30	70
MO-10-OH		47	53
Pyrazinecarboxylic acid		69	31
Kojic acid		58	42
3-hydroxy-2-methyl-4-pyrone		85	15
3,4-dihydroxyphenyl acetic acid		84	16
Catechol		69	31
6-aminocaproic acid		71	29
Vorinostat		68	32

From this initial screen with the purified enolase it is clear that the tropolones exhibit more inhibitory activity than several small molecule chelators. This suggests tropolones are relatively selective towards enolase and may be used to develop potent enolase inhibitors. To assess the inhibitory potential of tropolones, several key potent, LPS limited and relatively non-potent synthetic α -tropolones were screened at 20 μ M.

Table 4.14: Evaluation of Key Potent Tropolone Inhibitory Activity on *E. coli* Enolase (20 μ M).

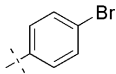
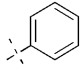
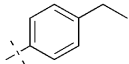
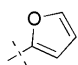
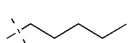
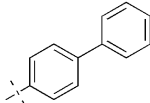
Tropolone	Functional Group	% Inhibition	MIC in <i>E. Coli</i> (WT) μ g/mL
BA-pBr-OH		70	20
MO-OH-PH		33	20
MO-10-OH		35	20
HC-2-OH		52	20
MO-2-OH		82	20/10
BA-PH-OH		58	20

Table 4.15: Evaluation of LPS Limited Tropolone Inhibitory Activity on *E. coli* Enolase (20 μ M).

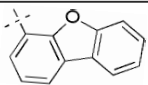
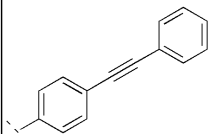
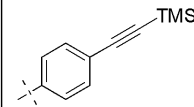
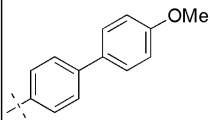
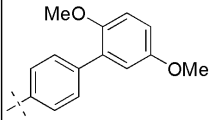
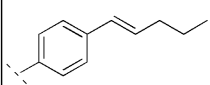
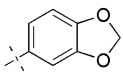
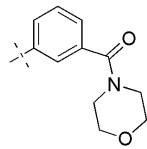
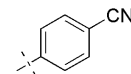
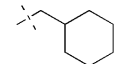
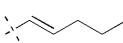
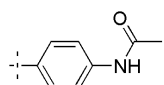
Tropolone	Functional Group	% Inhibition	MIC in <i>E. Coli</i> (WT)	MIC in <i>E. Coli</i> JW0451 (LPS knockout)
HC-10-OH		31	>40	10/5
SG-PH-OH		30	>40	20
SG-TMS-OH		13	>40	5
BA-SM-OH		16	>40	20/10
BA-DM-OH		13	>40	10
BA-P5-OH		8	>40	20/10

Table 4.16: Evaluation of Relatively Non-potent Tropolone Inhibitory Activity on *E. coli* Enolase (20 μ M).

Tropolone	Functional Group	% Inhibition	MIC in <i>E. Coli</i> (WT)	MIC in <i>E. Coli</i> JW0451 (LPS knockout)
HC-5-OH		32	>40	>40
HC-7-OH		61	>40	40
BA-pCN-OH		20	>40	>40
MO-1-OH		35	>40	>40
MO-3-OH		28	40	40
Am-Ac-OH		7	>40	>40

The enolase inhibition data mostly correlates with the *E. coli* MIC data as the most potent growth inhibitors are also the most potent enolase inhibitors. Interestingly, the tropolones which display limited growth inhibition due to LPS are some of the least potent against enolase, exhibiting similar inhibitory activity as the relatively non-potent growth inhibitory tropolones. It is unclear why these tropolones are weakly inhibitory towards enolase yet potent in the *E. coli* LPS knockout model. However, enolase appears to be mainly a cell membrane associated protein in *E.coli* and the knockout model has an abnormal outer membrane, suggesting the LPS limited tropolones may act via a different mechanism. While these tropolones are some of the larger analogs, the biphenyl tropolone, BA-PH-OH, is similar in size yet is potent in both the

growth inhibition assay and enolase inhibition assay, suggesting size may not be a significant factor. Surprisingly, HC-7-OH which is relatively non-potent in the growth inhibition assay is the third most potent analog tested. Again, this is one of the larger analogs, suggesting size does not determine inhibition potential. It is possible HC-7-OH is too polar to have an effect on the growth of *E. coli* even with a defective outer membrane but is a relatively potent enolase inhibitor.

Next, the three most potent tropolones were compared to a reported enolase inhibitor, ENOblock.⁶⁴

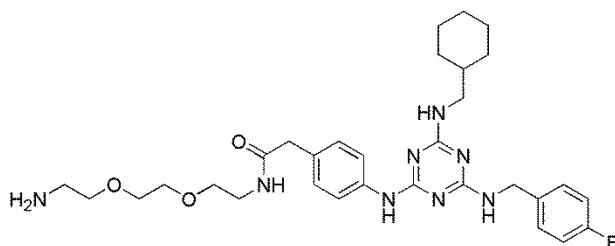


Figure 4.6: Structure of Reported Enolase Inhibitor, ENOblock.

Table 4.17: Evaluation of Tropolone and ENOblock Inhibitory Activity on *E. coli* Enolase (10 μ M).

Compound	% Inhibition
ENOblock	30
BA-pBr-OH	51
MO-2-OH	48
HC-7-OH	37

Here the tropolones were determined to be more potent than ENOblock. ENOblock has been reported to potently inhibit mammalian enolase ENO3 ($IC_{50} = 0.576 \mu M$). The relative lack of potency at 17-times the concentration against *E. coli* enolase suggests ENOblock is more selective towards mammalian enolase than bacterial enolase. Since *E. coli* enolase only shares 55% sequence identity with ENO3, it is not surprising that ENOblock is less effective. Additionally, the MIC of ENOblock in *E. coli* 25922 was determined to be 40 $\mu g/mL$, which is equal to the least effective tropolones. This would suggest that the tropolones may be more selective towards Gram-negative bacteria enolase than mammalian enolase. Gram-negative bacteria such as *K. pneumoniae*, *P. aeruginosa* and *A. baumannii* have 68-97% sequence identity compared to *E. coli*, which is greater than the sequence identity found for Gram-positive, fungal, mammalian and other animal enolase.

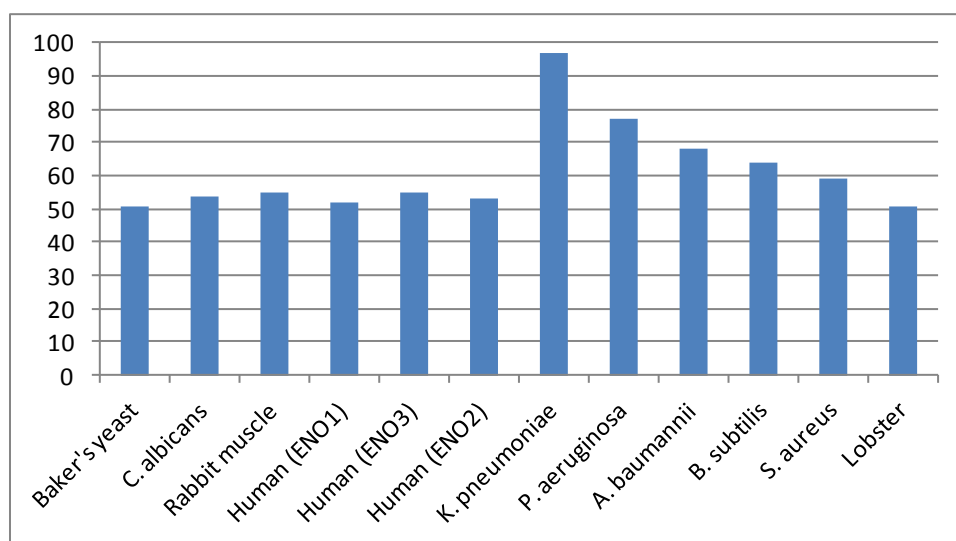


Figure 4.7: Enolase Sequence Identity (%) Compared to *E. coli*.

Because the *E. coli* 25922 MIC and enolase inhibition data suggests tropolones may be selective towards Gram-negative bacteria enolase, yet some potent growth inhibitory tropolones (ie. MO-OH-PH) are relatively non-potent enolase inhibitors and vice versa (ie. HC-7-OH), it

was necessary to determine if enolase inhibition was a function of chelation due to the tropolone moiety or chelation independent and a function of the α -substitution. To assess the activity of the tropolone moiety, the alternative chelator library of α -phenyl substituted tropones was screened with the enolase inhibition assay.

Table 4.18: Evaluation of Alternative Chelating Groups on Tropolone Inhibitory Activity on *E. coli* Enolase (20 μ M).

Compound	Functional Group	% Inhibition
MO-OH-PH	Hydroxyl	33%
MO-OMe-PH	Ether	31%
MO-HNOH-PH	Hydroxylamine	40%
MO-NH ₂ -PH	Amine	55%
MO-SMe-PH	Thioether	22%
MO-SH-PH	Thiol	24%
MO-H-PH	Hydrogen	54%
MO-Am-PH	Amide	51%

Interestingly, some of the alternative chelating functionalities could increase enolase inhibition compared to the α -phenyl tropolone. Based on this data, it would suggest that N>O>S in terms of chelating functionalities. Somewhat surprisingly, the tropone (MO-H-PH) displays inhibitory activity against enolase comparable to the potent nitrogen containing tropones. This suggests that the carbonyl of the tropone can form a monodentate coordination to the magnesium of enolase. This carbonyl is very Lewis basic, making it sufficient for monodentate coordination and potential metalloenzyme inhibition. Additionally, this data could offer alternative scaffolds for the development of enolase inhibitors. While these alternative chelating functionalities are capable of inhibiting enolase, they did not inhibit bacterial growth, suggesting that the ionization in the tropolone scaffold may be critical for Gram-negative penetration.

4.3 Conclusions

Tropolones are antimicrobial agents effective against both Gram-positive and Gram-negative bacteria as well as fungi. As Gram-negative antibacterial agents, tropolones are effective against the most common pathogens: *E. coli*, *K. pneumoniae*, *P. aeruginosa*, and *A. baumannii*. Additionally, key potent tropolones do not experience permeability or efflux issues and maintain potency in TMP resistant clinical isolates of *K. pneumoniae*. Although a variety of tropolones have been synthesized, there is not a clear trend in structure activity relationship. While the more effective analogs typically have some aromaticity and small hydrophilic area, more analogs will need to be synthesized to better understand the structure activity relationship. As seen from the study utilizing alternative chelating functional groups, the hydroxyl group appears to be essential to tropolone growth inhibitory activity. However, as seen with TDA, the substitution of hydroxyl with a carboxylic acid may yield similar results. Future attempts should be made to make a carboxylic acid substituted tropolone analog.

Key potent tropolones cause filamentous growth of *E. coli* at sub-inhibitory concentrations. Filamentous growth and the lack of an antagonistic effect by sucrose are indicative of inhibition of cell wall synthesis enzymes such as enolase. Enolase was determined as a potential target by DARTS analysis, and has been validated through inhibition assays utilizing purified enolase from *E. coli*. From the enolase inhibition assays it was determined that the carbonyl of the tropolone may cause monodentate coordination of the catalytic metal to inhibit enolase activity. Here, the alternative chelating functional groups displayed the preference N>O>S suggesting bacterial growth inhibition may require ionization of the

tropolone, but enolase inhibition does not. Further validation of enolase as the target for the antibacterial activity of tropolones should incorporate a labeled tropolone for pull-down assays.

4.4 Acknowledgements

As previously mentioned, the MICs obtained for *P. aeruginosa*, *A. baumannii*, *S. aureus*, *S. pyogenes*, *B. anthracis*, *E. faecalis*, *C. albicans* and *C. glabrata* were determined by the Priestley lab at the University of Montana. Gram-stain images of *E. coli* and *E. coli* treated with several tropolones was provided by Amy Florian. Experiments utilizing the Enolase Activity Assay Kit were conducted by Jolanta Krucinska. Jolanta also expressed and purified enolase from *E. coli* and determined the activity of the purified enzyme as well as the activity of all the agonists (n=1).

4.5 References

1. Gram, Hans C. Über die isolierte Färbung der Schizomyceten in Schnitt- und Trockenpräparaten. *Fortschr. Med.* **1884**, 2, 185-189.
2. Woods, Gail L; Walker, David H. Detection of Infection or Infectious Agents by Use of Cytologic and Histologic Stains. *Clinical Microbiology Reviews* **1996**, 9 (3), 382-404.
3. Salton, Milton R. J.; Kim, Kwang-Shin. *Medical Microbiology* 4th ed.; The University of Texas Medical Branch at Galveston: Galveston, 1996.

4. Braun, Volkmar. *Bacterial Signaling: Outer Membrane Signaling in Gram-negative Bacteria*. Wiley-VCH Verlag GmbH & Co.: Weinheim, Germany, 2010.
5. Schaechter, Moselio (ed.). *Encyclopedia of Microbiology: Antibiotic Resistance*, 3rd ed.; Elsevier/Academic Press: Boston, 2009.
6. Ho, Jennifer; Tambyah, Paul A.; Paterson, David L. Multiresistant Gram-negative infections: a global perspective. *Curr. Opin. Infect. Dis.* **2010**, 23, 546-553.
7. Mandell, Gerald L; Bennett, John E; Dolin, Raphael. *Mandell, Douglas and Bennett's Principles and Practice of Infectious Disease*, 4th ed.; Churchill Livingstone: New York, 1995.
8. Lerner, K. L.; Lerner, B. W. *World of Microbiology and Immunity*. Gale: Detroit, 2003.
9. Filetoth, Zsolt. *Hospital Acquired Infections*. Whurr Publishers: Philadelphia, 2003.
10. Schaechter, Moselio (ed.). *Encyclopedia of Microbiology: Escherichia coli*, 3rd ed.; Elsevier/Academic Press: Boston, 2009.
11. Anes, J.; McCusker, M. P.; Fanning, S.; Martins, M. The ins and outs of RND efflux pumps in *Escherichia coli*. *Frontiers in Microbiology* **2015**, 6, article 587.
12. Denton, Miles. Enterobacteriaceae. *International Journal of Antimicrobial Agents* **2007**, 29, (3), S9-S22.
13. Ryan, K. J.; Ray, C. G. *Sherris Medical Microbiology*, 4th ed.; McGraw-Hill: New York, 2003.
14. Young, V. M. *Pseudomonas Aeruginosa: Ecological Aspects and Patient Colonization*. Raven Press, New York, 1977.
15. Deshapande, L. M.; Rhomberg, P. R.; Sader, H.S.; Jones, R. N. Emergence of serine carbapenemases (KPC and SME) among clinical strains of Enterobacteriaceae isolated in

the United States Medical Centers: report from the MYSTIC Program (1999-2005).

Diagnostic Microbiology & Infectious Disease **2006**, 56, (4), 367-372.

16. Hernandez-Alles, S.; Alberti, S.; Alvarez, D.; Domenech-Sanchez, A.; Martinez-Martinez, L.; Gil, J.; Tomas, J. M.; Benedi, V. J. Porin expression in clinical isolates of *Klebsiella pneumoniae*. *Microbiology* **1999**, 145, (3), 673-679.
17. Schaechter, Moselio (ed.). *Encyclopedia of Microbiology: Pseudomonas aeruginosa*, 3rd ed.; Elsevier/Academic Press: Boston, 2009.
18. Redfield, R. J., Is quorum sensing a side effect of diffusion sensing? *Trends Microbiol.* **2002**, 10, (8), 365-370.
19. Ammendola, A.; Geisenberger, O.; Andersen, J. B.; Givskov, M.; Schleifer, K.-H.; Eberl, L., *Serratia liquefaciens* swarm cells exhibit enhanced resistance to predation by *Tetrahymena* sp. *FEMS Microbiology Letters* **1998**, 164, (1), 69-75.
20. Nickel, J. C.; Ruseska, I.; Wright, J. B.; Costerton, J. W., Tobramycin resistance of *Pseudomonas aeruginosa* cells growing as a biofilm on urinary catheter material. *Antimicrobial Agents and Chemotherapy* **1985**, 27, (4), 619-24.
21. Welch, R. A.; Burland, V.; Plunkett, G., III; Redford, P.; Roesch, P.; Rasko, D.; Buckles, E. L.; Liou, S. R.; Boutin, A.; Hackett, J.; Stroud, D.; Mayhew, G. F.; Rose, D. J.; Zhou, S.; Schwartz, D. C.; Perna, N. T.; Mobley, H. L. T.; Donnenberg, M. S.; Blattner, F. R., Extensive mosaic structure revealed by the complete genome sequence of uropathogenic *Escherichia coli*. *Proceedings of the National Academy of Sciences of the United States of America* **2002**, 99, (26), 17020-17024.

22. Anderl, J. N.; Zahller, J.; Roe, F.; Stewart, P. S., Role of nutrient limitation and stationary-phase existence in *Klebsiella pneumoniae* biofilm resistance to ampicillin and ciprofloxacin. *Antimicrobial Agents and Chemotherapy* **2003**, 47, (4), 1251-1256.
23. Borriello, G.; Werner, E.; Roe, F.; Kim, A. M.; Ehrlich, G. D.; Stewart, P. S., Oxygen limitation contributes to antibiotic tolerance of *Pseudomonas aeruginosa* in biofilms. *Antimicrobial Agents and Chemotherapy* **2004**, 48, (7), 2659-2664.
24. Rani, S. A.; Pitts, B.; Beyenal, H.; Veluchamy, R. A.; Lewandowski, Z.; Davison, W. M.; Buckingham-Meyer, K.; Stewart, P. S., Spatial patterns of DNA replication, protein synthesis, and oxygen concentration within bacterial biofilms reveal diverse physiological states. *Journal of Bacteriology* **2007**, 189, (11), 4223-4233.
25. Costerton, J. W.; Lewandowski, Z.; Caldwell, D. E.; Korber, D. R.; Lappin-Scott, H. M., Microbial biofilms. *Annual Review of Microbiology* **1995**, 49, 711-45.
26. Mah, T.-F. C.; O'Toole, G. A., Mechanisms of biofilm resistance to antimicrobial agents. *Trends Microbiol.* **2001**, 9, (1), 34-39.
27. Rasmussen, T. B.; Givskov, M., Quorum-sensing inhibitors as anti-pathogenic drugs. *International Journal of Medical Microbiology* **2006**, 296, (2-3), 149-161.
28. Donlan, R. M.; Costerton, J. W., Biofilms: Survival mechanisms of clinically relevant microorganisms. *Clinical Microbiology Reviews* **2002**, 15, (2), 167-193.
29. Chernish Robert, N.; Aaron Shawn, D., Approach to resistant gram-negative bacterial pulmonary infections in patients with cystic fibrosis. *Current opinion in pulmonary medicine* **2003**, 9, (6), 509-15.

30. Gibson Ronald, L.; Burns Jane, L.; Ramsey Bonnie, W., Pathophysiology and management of pulmonary infections in cystic fibrosis. *American journal of respiratory and critical care medicine* **2003**, 168, (8), 918-51.
31. Stewart, P. S.; William Costerton, J., Antibiotic resistance of bacteria in biofilms. *Lancet* **2001**, 358, (9276), 135-138.
32. Hoiby, N.; Frederiksen, B.; Pressler, T., Eradication of early *Pseudomonas aeruginosa* infection. *Journal of cystic fibrosis : official journal of the European Cystic Fibrosis Society* **2005**, 4 Suppl 2, 49-54.
33. Costerton, J. W.; Stewart, P. S.; Greenberg, E. P., Bacterial biofilms: a common cause of persistent infections. *Science (Washington, D. C.)* **1999**, 284, (5418), 1318-1322.
34. Potera, C., Microbiology: Forging a link between biofilms and disease. *Science (Washington, D. C.)* **1999**, 283, (5409), 1837, 1839.
35. Fullagar, J. L.; Garner, A. L.; Struss, A. K.; Day, J. A.; Martin, D. P.; Yu, J.; Cai, X.; Janda, K. D.; Cohen, S. M. Antagonism of a Zinc Metalloprotease Using a Unique Metal-Chelating Scaffold: Tropolones as Inhibitors of *P. aeruginosa* Elastase. *Chemical Communications* **2013**, 49, (31), 3197-3199.
36. Butterworth, M. B.; Zhang, L.; Heidrich, E. M.; Myerburg, M. M.; Thibodeau, P. H. Activation of the Epithelial Sodium Channel (ENaC) by the Alkaline Protease from *Pseudomonas aeruginosa*. *J. Biol. Chem.* **2012**, 287, (39), 32556-32565.
37. Wilderman, P. J.; Vasil, A. I.; Johnson, Z.; Wilson, M. J.; Cunliffe, H. E.; Lamont, I. L.; Vasil, M. L. Characterization of an Endoprotease (PrpL) Encoded by a PvdS-Regulated Gene in *Pseudomonas aeruginosa*. *Infect. Immun.* **2001**, 69, (9), 5385-5394.

38. Middlebrook, J. L.; Dorland, R. B. Bacterial toxins: cellular mechanisms of action. *Microbiol. Rev.* **1984**, 48, 199-221.
39. Armstrong, S.; Yate, S. P.; Merrill, A. R. Insight into the catalytic mechanism of P. aeruginosa exotoxin A strains of toxin interaction with eukaryotic elongation factor. *J. Biol. Chem.* **2002**, 277, (48), 46669-46675.
40. Iglewski, B. H.; Kabat, D. NAD-dependent inhibition of protein synthesis by Pseudomonas aeruginosa toxin. *Proc. Natl. Acad. Sci. USA* **1975**, 72, 2284-2288.
41. Kaur, N.; Khokhar, M.; Jain, V.; Bharatam, P. V.; Sandhir, R.; Tewari, R. Identification of Druggable Targets for Acinetobacter baumannii Via Subtractive Genomics and Plausible Inhibitors for MurA and MurB. *Appl. Biochem. Biotechnol.* **2013**, 171, 417-436.
42. American Cancer Society. *Cancer Facts & Figures 2014*. Atlanta: American Cancer Society; 2014.
43. Mandell, Gerald L; Bennett, John E; Dolin, Raphael. *Mandell, Douglas and Bennett's Principles and Practice of Infectious Disease* 6th ed.; Churchill Livingstone: New York, 2005.
44. Bjarnsholt, T.; Givskov, M. The role of quorum sensing in the pathogenicity of the cunning aggressor Pseudomonas aeruginosa. *Analytical and Bioanalytical Chemistry* **2007**, 387, (2), 409-414.
45. Centers for Disease Control. Health Associated Infections: Gram Negative Bacteria Infections in Healthcare Setting. <http://www.cdc.gov/drugresistance/> (Accessed January 15, 2016).

46. Mingeot-Leclercq, M-P.; Glupczynski, Y.; Tulkens, P. M. Aminoglycosides: Activity and Resistance. *Antimicrobial Agents and Chemotherapy* **1999**, 43, (4), 727-737.
47. Holten, K. B.; Onusko, E. M. Appropriate prescribing of oral beta-lactam antibiotics. *Am. Fam. Physician.* **2000**, 62, (3), 611-620.
48. James, R. C.; Pierce, J. G.; Okano, A.; Xie, J.; Boger, D. L. Redesign of Glycopeptide Antibiotics – Back to the Future. *Chem. Biol.* **2012**, 7, (5), 797-804.
49. Tenson, T.; Lovmar, M.; Ehrenberg, M. The Mechanism of Action of Macrolides, Lincosamides and Streptogramin B Reveals the Nascent Peptide Exit Path in the Ribosome. *J. Mol. Biol.* **2003**, 330, (5), 1005-1014.
50. Dodd, M. C.; Cramer, D. L.; Ward, W. C. The relationship of structure and antibacterial activity in the nitrofurans. *J. Am. Pharm. Assoc.* **1950**, 39, (6), 313-318.
51. Dixon, R. A.; Chopra, I. Polymyxin B and polymyxin B nonapeptide alter cytoplasmic membrane permeability in Escherichia coli. *J. Antimicrob. Chemother.* **1986**, 18, (5), 557-563.
52. Gill, S. K.; Garcia, G. A. Rifamycin inhibition of WT and Rif-resistant Mycobacterium tuberculosis and Escherichia coli RNA polymerase in vitro. *Tuberculosis* **2011**, 91, (5), 361-369.
53. Andersson, M. I.; MacGowan, A. P. Development of the quinolones. *Journal of Antimicrobial Chemotherapy* **2003**, 51, 1-11.
54. Frey, K. M.; Viswanathan, K.; Wright, D. L.; Anderson, A. C. Prospective Screening of Novel Antibacterial Inhibitors of Dihydrofolate Reductase for Mutational Resistance. *Antimicrobial Agents and Chemotherapy* **2012**, 56, (7), 3556-3562.

55. Gale, E. F.; Folkes, J. P. The assimilation of amino acids by bacteria. 15. Actions of antibiotics on nucleic acid and protein synthesis in *Staphylococcus aureus*. *Biochem. J.* **1953**, 53, (3), 493-498.
56. Davies, D. G.; Parsek, M. R.; Pearson, J. P.; Iglewski, B. H.; Costerton, J. W.; Greenberg, E. P. The involvement of cell-to-cell signals in the development of bacterial biofilm. *Science (Washington, D. C.)* **1998**, 280, (5361), 295-298
57. Miller, M. B.; Bassler, B. L. Quorum sensing in bacteria. *Annual Review of Microbiology* **2001**, 55, 165-199.
58. Taga, M. E.; Bassler, B. L. Chemical communication among bacteria. *Proceedings of the National Academy of Sciences of the United States of America* **2003**, 100, (Suppl. 2), 14549-14554.
59. Sharma, G.; Sharma, S.; Sharma, P.; Chandola, D.; Dang, S.; Gupta, S.; Gabrani, R. *Escherichia coli* biofilm: development and therapeutic strategies. *J. Appl. Microbiol.* **2016** [Epub ahead of print] doi: 10.1111/jam.13078
60. Brown, M.; Reilly, U.; Abramite, J.; Arcari, J.; Oliver, R.; Barham, R.; Che, Y.; Chen, J.; Collantes, E.; Chung, S.; Desbonnet, C.; Doty, J.; Doroski, M.; Engtrakul, J.; Harris, T.; Huband, M.; Knafels, J.; Leach, K.; Liu, S.; Marfat, A.; Marra, A.; EMcElroy, E.; Mielnick, M.; Menard, C.; Montgomery, J.; Mullins, L.; Noe, M.; O'Donnell, J.; Penzien, J.; Plummer, M.; Price, L.; Shanmugasundaram, V.; Thoma, C.; Uccello, D.; Warmus, J.; Wishka, D., Potent inhibitors of LpxC for the treatment of Gram-negative Infections. *J. Med. Chem.* **2011**, 55, 914-923.
61. McClerren, A.; Endsley, S.; Bowman, J.; Andersen, N.; Guan, z.; Rudolph, J.; Raetz, C., A slow, tight-binding inhibitor of the zinc-dependent deacetylase LpxC of lipid A

- biosynthesis with antibiotic activity comparable to ciprofloxacin. *Biochemistry* **2005**, 44, 16574-16583.
62. Jackson, E. R.; Dowd, C. S. Inhibition of 1-deoxy-D-xylulose-5-phosphate reductoisomerase (Dxr): a review of the synthesis and biological evaluation of recent inhibitors. *Curr. Top. Med. Chem.* **2012**, 12, (7), 706-728.
63. Peptide deformylase: a new target in antibacterial, antimalarial and anticancer drug discovery. *Curr. Med. Chem.* **2015**, 22, (2), 214-236.
64. Jung, D. W.; Kim, W. H.; Park, S. H.; Lee, J.; Kim, J.; Su, D.; Ha, H. H.; Chang, Y. T.; Williams, D. R. A unique small molecule inhibitor of enolase clarifies its role in fundamental biological processes. *Chem. Biol.* **2013**, 8, (6), 1271-1282.
65. Bentley, R. A fresh look at natural tropolonoids. *Nat. Prod. Rep.* **2008**, 25, 118-138.
66. Nozoe, T. Substitution Products of Tropolone and Allied Compounds. *Nature* **1951**, 167, 1055-1057.
67. Trust, T. J.; Bartlett, K. H. Antibacterial Activity of Tropilidine and Tropone. *Antimicrob. Agents Chemother.* **1975**, 8, (3), 381-383.
68. Trust, T. J. Antibacterial Activity of Tropolone. *Antimicrob. Agents Chemother.* **1975**, 8, (5), 500-506.
69. Morita, Y.; Sakagami, Y.; Okabe, T.; Ohe, T.; Inamori, Y.; Ishida, N. The Mechanism of the Bactericidal Activity of Hinokitiol. *Biocontrol Science* **2007**, 12, (3), 101-110.
70. Bryant, B. E.; Fernelius, W. C.; Douglas, B. E. Formation Constants of Metal Complexes of Tropolone and Its Derivatives. I. Tropolone. *J. Am. Chem. Soc.* **1953**, 75, (15), 3784-3786.

71. Silver, L. L. Are natural products still the best source for antibacterial discovery? The bacterial entry factor. *Expert Opin. Drug Discov.* **2008**, 3, (5), 487-500.
72. Oblak, E. Z.; Bolstad, E. S. D.; Ononye, S. N.; Priestley, N. D.; Hadden, M. K.; Wright, D. L. The furan route to tropolones: probing the antiproliferative effects of β -thujaplicin analogs. *Org. Biomol. Chem.* **2012**, 10, 8597-8604.
73. Ononye, S. N.; VanHeyst, M. D.; Oblak, E. Z.; Zhou, W.; Ammar, M.; Anderson, A. C.; Wright, D. L. Tropolones As Lead-Like Natural Products: The Development of Potent and Selective Histone Deacetylase Inhibitors. *Med. Chem. Lett.* **2013**, 4, 757-761
74. Sekine, S.; Shimodaira, C.; Uesawa, Y.; Kagaya, H.; Kanda, Y.; Ishihara, M.; Amano, O.; Sakagami, H.; Wakabayashi, H. Quantitative Structure-Activity Relationship Analysis of Cytotoxicity and Anti-UV Activity of 2-Aminotropolones. *Anticancer Research* **2014**, 34, 1743-1750.
75. Sheehan, D. J.; Hitchcock, C. A.; Sibley, C. M. Current and Emerging Azole Antifungal Agents. *Clin. Microbiol. Rev.* **1999**, 12, (1), 40-79.
76. Lewis, D. F. V.; Wiseman, A. A selective review of bacterial forms of cytochrom P450 enzymes. *Enzyme and Microbial Technology* **2005**, 36, 377-384.
77. Douglas, C. M. Fungal $\beta(1,3)$ -D-glucan synthesis. *Medical Mycology* **2001**, 39, (1), 55-66.
78. Baba, T.; Ara, T.; Hasegawa, M.; Takai, Y.; Okumura, Y.; Baba, M.; Datsenko, K. A.; Tomita, M.; Wanner, B. L.; Mori, H. Construction of Escherichia coli K-12 in-frame, single-gene knockout mutants: the Keio collection. *Molecular Systems Biology* **2006**, doi: 10.1038/msb4100050.

79. Pierrat, O. A.; Strisovsky, K.; Christova, Y.; Large, J.; Ansell, K.; Bouloc, N.; Smiljanic, E.; Freeman, M. Monocyclic β -Lactams Are Selective, Mechanism-Based Inhibitors of Rhomboid Intramembrane Proteases. *Chem. Biol.* **2011**, 6, 325-335.
80. Zevenhuizen, L. P. T. M.; Dolfing, J.; Eshuis, E. J.; Scholten-Koerselman, I. J. Inhibitory Effects of Copper on Bacteria Related to the Free Ion Concentration. *Microbial Ecology* **1979**, 5, 139-146.
81. Doulias, P-T.; Nousis, L.; Zhu, B-Z.; Frei, B.; Galaris, D. Protection by tropolones against H₂O₂-induced DNA damage and apoptosis in cultured Jurkat cells.
82. Lomenick, B.; Jung, G.; Wohlschlegel, J. A.; Huang, J. Target identification using drug affinity responsive target stability (DARTS). *Curr. Protoc. Chem. Biol.* **2011**, 3, (4), 163-180.
83. Boel, G.; Pichereau, V.; Mijakovic, I.; Maze, A.; Poncet, S.; Gillet, S.; Giard, J-C.; Hartke, A.; Auffray, Y.; Deutscher, J. Is 2-Phosphoglycerate-dependent Automodification of Bacterial Enolases Implicated in their Export? *J. Mol. Biol.* **2004**, 337, 485-496.
84. Dominguez-Malfavon, L.; Islas, L. D.; Luisi, B. F.; Garcia-Villegas, R.; Garcia-Mena, J. The assembly and distribution in vivo of the Escherichia coli RNA degradosome. *Biochimie* **2013**, 95, 2034-2041.
85. Chandran, V.; Luisi, B. F. Recognition of Enolase in the Escherichia coli RNA Degradosome. *J. Mol. Biol.* **2006**, 358, 8-15.
86. Taghbalout, A.; Rothfield, L. RNase E and the other constituents of the RNA degradosome are components of the bacterial cytoskeleton. *Proc. Nat. Acad. Sci.* **2007**, 104, (5), 1667-1672.

87. Worrall, J. A. R.; Gorna, M.; Crump, N. T.; Phillips, L. G.; Tuck, A. C.; Price, A. J.; Bavro, V. N.; Luisi, B. F. Reconstitution and Analysis of the Multienzyme Escherichia coli RNA Degradosome. *J. Mol. Biol.* **2008**, 382, 870-883.
88. Irani, M. H.; Maitra, P. K. Properties of Escherichia coli Mutants Deficient in Enzymes of Glycolysis. *J. Bacteriology* **1977**, 132, (2), 398-410.
89. Wold, F.; Spring, T. G. Enolase from Escherichia coli. *Methods in Enzymology: Carbohydrate Metabolism Part C*. Volume XLII. Academic Press: New York, 1975.

Final Conclusions and Future Directions

Troponoids are an interesting class of natural products which offer a range of biological activity. The tropolones are some of the best studied natural products from this class and the tropolone motif itself offers a scaffold that can be used to develop synthetic troponoids capable of eliciting an antiproliferative response. Here, α -tropolone derivatives were readily synthesized from either 2-chlorotropone or tropolone, both of which are commercially available. While the initial library of synthetic α -tropolones developed in the Wright lab has been expanded and incorporated more diverse functional groups, more synthetic work needs to be done in order to improve overall yield, potentially reduce synthetic steps required and to generate even more diverse functional groups. Additionally, work should be done to make *ortho* substituted α -phenyl tropolones as well as multi-substituted phenyl derivatives in order to assess structure activity relationships.

The α -tropolones synthesized for this work display a range of antiproliferative activity in both hematologic malignancies and Gram-negative bacteria. Generally, derivatives with more aromatic character and more hydrophobicity exhibit more activity. As antiproliferative agents for hematologic malignancies, synthetic α -tropolones appear to have some selectivity towards T-cell leukemia and are most potent towards the T-cell ALL cell line Molt-4. Additionally, the tropolones also exhibit a greater than 10-fold selectivity towards Molt-4 than healthy human peripheral blood monocytes, suggesting synthetic tropolones can be developed as antiproliferative agents of T-cell ALL without substantial risk of being generally toxic. Since the Molt-4 line is derived from a patient in relapse, tropolones may be developed as third line chemotherapeutics similar to nelarabine. While a comprehensive mechanism of action is still unknown, the activity of two of the more potent tropolones was assessed by microarray analysis.

These derivatives displayed activity involving cell cycle regulation, the apoptosis pathway, p53 pathway and PI3K/AKT/mTOR pathway. Some of the more interesting activity involved upregulation of ATM, CDKN2B, IL7R and PIK3R1 and downregulation of BCL11B and BCL2. Although these results need to be validated, Western blot analysis done by the Weimer lab suggests that caspase dependent regulation of p53 and activation of AKT/mTOR is most likely involved. Future work should explore these effects on other cancer cell types as well as determine the selectivity of these new α -tropolones towards hematologic malignancies.

The antiproliferative activity exhibited against Gram-negative bacteria is lead-like with several compounds displaying minimal inhibition concentrations of $\sim 10 \mu\text{g/mL}$ in strains most commonly involved in Gram-negative bacterial infection as well as clinical isolates of *K. pneumoniae*. Several key potent tropolones elicited filamentous growth of *E. coli* consistent with inhibition of cell wall synthesis. An unbiased target identification assay suggested tropolones inhibit enolase, which could explain both the antiproliferative activity as well as the filamentous growth. While many of the tropolones exhibit lead-like inhibition activity towards enolase, the α -phenyl troponoids containing various metal chelating functional groups suggests that the hydroxyl group is unnecessary for inhibition. This concept should be explored further through the synthesis of other troponoids. Additionally, enolase needs to be crystallized with key potent tropolones in order to determine the binding domain. Once the binding domain is determined, structure based drug design can be used to develop potentially more selective and more potent tropolones.

Overall, synthetic α -tropolones are lead-like antiproliferative agents useful against hematologic malignancies and Gram-negative bacteria. Although the mechanism of action for the cancer antiproliferative activity is complex and not well defined at the present, the newer

tropolones have exhibited increased activity. Interestingly, the key potent tropolones against Molt-4 is also one of the most potent analogs against bacterial enolase, *E. coli* and *K. pneumoniae*. While it is unlikely that enolase is involved in the cancer antiproliferative activity due to a low percent identity between Gram-negative bacteria enolase and mammalian enolase, this dual antiproliferative activity may offer the ability to develop synthetic α -tropolones as antiproliferative chemotherapeutics for patients with T-cell ALL as well as Gram-negative infection preventative agents. This dual action potential is important due to the high risk of mortality associated with Gram-negative infections in leukemic patients undergoing remission therapy and should be explored further.

Chapter 5

Experimental Section

5.1 Materials and Methods - Chemistry

5.1.1 General Chemical Methods

All reactions were carried out under an inert atmosphere of argon with dry solvents under anhydrous conditions unless otherwise stated. Commercial grade solvents were used without further purification. Tetrahydrofuran (THF) was used directly from a Baker cycle-tainer system. 1,4-dioxane was used directly from a Sure Seal™ bottle from Sigma Aldrich. N-N-dimethylformamide (DMF) was used directly from an AcroSeal® bottle from Acros Organics. Reagents were purchased at the highest commercial quality and used without further purification unless otherwise stated. Yields refer to chromatographically and spectroscopically (¹H NMR) homogeneous materials. Reactions were monitored by thin layer chromatography (TLC) carried out on Whatman silica 60 Å precoated plates using UV light as the visualizing agent and either a basic aqueous potassium permanganate (KMnO₄) or a solution of ferric chloride (FeCl₃) in methanol and water (1:1) and heated as developing agents. Flash chromatography was performed using Baker silica gel (60 Å particle size). NMR spectra were recorded on Bruker-500 and 400 instruments and calibrated using residual undeuterated solvent as internal reference (ie. CHCl₃ at δ 7.26 ppm ¹H NMR, δ 77.0 ppm ¹³C NMR). The following abbreviations were used to explain the multiplicities: s = singlet, d = doublet, t = triplet, q = quartet, m = multiplet, h

= heptet. IR spectra were recorded on either a Shimadzu FT-IR 8400 or Agilent Cary 630 FTIR Diamond ATR spectrometer. Melting points (m.p.) are uncorrected and were recorded on Mel-Temp digital melting point apparatus. High resolution mass spectra (HRMS) were obtained from the University of Connecticut Spectral Facility by electrospray ionization of flight reflectron experiments.

5.1.2 Synthetic Procedures

General Procedure For Suzuki Couplings to 2-Chloro-2,4,6-cycloheptatrien-1-one: 2-Chloro-2,4,6-cycloheptatrien-1-one (1.0 eq), boronic acid (1.5 eq) and cesium carbonate (3.0 eq) were added to 5:1 dioxane/H₂O (0.3 M) and the mixture was thoroughly degassed by bubbling argon through the solution (10 min). Bis(triphenylphosphine)palladium(II) dichloride (0.1 eq) was added and the mixture was again degassed with argon (5 min). The homogenous solution was heated at 90°C for 16 h before being cooled to room temperature. Water was added and the mixture was extracted with EtOAc (3x). The combined organic layers were washed with brine, dried over Na₂SO₄, filtered and concentrated in vacuo. Flash chromatography of the crude residue (SiO₂, EtOAc in hexanes) provided the desired 2-substituted tropones.

General Procedure for Reduction of C8-C9 Conjugated Olefin: To a flame dried flask was added the 2-substituted-7-methoxy tropone in MeOH (1.0 M). To the solution was added 10% Pd/C (0.5 w/w) and the atmosphere of the flask was evacuated and backfilled with H₂ (3 cycles). The reaction mixture was stirred under an atmosphere of H₂ (balloon) for 2 h before being filtered through a pad of celite, eluting with CH₂Cl₂. The solvent was removed under vacuum and the residue was purified by flash chromatography (SiO₂, EtOAc in hexanes) to provide the desired C8-C9 saturated tropone.

General Procedure For α -Amination of 2-substituted tropone: To a solution of 2-substituted tropone (1.0 eq) in EtOH (0.2 M) was added 65% hydrazine monohydrate (25 eq). The solution was allowed to stir at room temperature until all starting material was consumed as indicated by TLC. The reaction was concentrated in vacuo and then taken up in EtOAc and washed with H₂O (3x). The organic layer was then washed with brine, dried over Na₂SO₄, filtered and concentrated in vacuo. Flash chromatography of the crude residue (SiO₂, EtOAc in hexanes) provided the desired α -amino tropones.

General Procedure For α -amino-2-substituted tropone Hydrolysis: α -amino-2-substituted tropone (1.0 eq) was dissolved in EtOH (0.2 M) to which was added 2N KOH (20 eq). The reaction was heated to 90°C and stirred for 16 h. The reaction was returned to room temperature and diluted with 15% NaOH. The aqueous layer was washed with CH₂Cl₂ (3x) and then acidified to pH 2.0 and extracted with CH₂Cl₂ (3x). The organic layer was then washed with brine, dried over Na₂SO₄, filtered, and concentrated in vacuo.

General Procedure for methyl-protection of 2-hydroxy-2,4,6-cycloheptatrien-1-one: 2-hydroxy-2,4,6-cycloheptatrien-1-one (1.0 eq), potassium carbonate (3.0 eq) and dicyclohexano-18-crown-6 mixture of isomers (0.1 eq) were added to a two-neck flask with a reflux condenser attached and dissolved with acetonitrile (0.2 M). The second neck was covered with a stopper and iodomethane was slowly added to the solution. The solution was heated at 85°C for 16 h before being cooled to room temperature. The solution was filtered through a fritted vacuum funnel and the filtrate was taken up with 0.3 M potassium hydroxide. Water was added and the mixture was extracted with CH₂Cl₂ (3x). The combined organic layers were washed with brine, dried over Na₂SO₄, filtered and concentrated in vacuo.

General Procedure for Bromination of 2-methoxy-2,4,6-cycloheptatrien-1-one: 2-methoxy-2,4,6-cycloheptatrien-1-one was dissolved with carbon tetrachloride (0.2 M) in a pressure vessel. *N*-bromosuccinimide (1.05 eq) was added and the mixture was heated at 80°C for 2 h before being cooled to room temperature. The solution was filtered through a fritted vacuum funnel. Water was added to

the filtrate and the mixture was extracted with CH_2Cl_2 (3x). The combined organic layers were washed with brine, dried over Na_2SO_4 , filtered and concentrated in vacuo. Flash chromatography of the crude residue (SiO_2 , EtOAc in hexanes) provided the desired product.

General Procedure for Iodination of 2-hydroxy-2,4,6-cycloheptatrien-1-one: 2-hydroxy-2,4,6-cycloheptatrien-1-one, potassium carbonate (1.0 eq) and sodium methoxide (1.0 eq) were dissolved in methanol (0.3 M) in a two-neck round bottom flask with a reflux condenser attached. A solid addition funnel was attached to the second neck. Iodine (1.0 eq) was added to the solid addition funnel and was then slowly added to the refluxing solution. Once the iodine was completely added, the solution was refluxed for 1 h before cooling to room temperature. The solution was concentrated in vacuo and flash chromatography of the crude residue (SiO_2 , EtOAc in hexanes) provided the desired product.

General Procedure for Suzuki Couplings to 2-bromo-7-methoxy-2,4,6-cycloheptatrien-1-one: 2-bromo-7-methoxy-2,4,6-cycloheptatrien-1-one (1.0 eq), boronic acid (1.5 eq) and cesium carbonate (3.0 eq) were added to 5:1 dioxane/ H_2O (0.3 M) and the mixture was thoroughly degassed by bubbling argon through the solution (10 min). Bis(triphenylphosphine)palladium(II) dichloride (0.1 eq) was added and the mixture was again degassed with argon (5 min). The homogenous solution was heated at 90°C for 16 h before being cooled to room temperature. Water was added and the mixture was extracted with EtOAc (3x). The combined organic layers were washed with brine, dried over Na_2SO_4 , filtered and concentrated in vacuo. Flash chromatography of the crude residue (SiO_2 , EtOAc in hexanes) provided the desired 2-substituted-7-methoxy tropones.

General Procedure for Sonogashira Couplings to 2-(4-Bromo-phenyl)-7-methoxy-cyclohepta-2,4,6-trienone: 2-(4-Bromo-phenyl)-7-methoxy-cyclohepta-2,4,6-trienone (1.0 eq), alkyne (3.0 eq) and potassium acetate (10.0 eq) were added to DMF (0.3 M) and the mixture was thoroughly degassed by bubbling argon through the solution (10 min). Bis(triphenylphosphine)palladium(II) dichloride (0.1 eq)

and copper (I) iodide (0.1 eq) was added and the mixture was again degassed with argon (5 min). The homogenous solution was heated at 50°C for 16 h before being cooled to room temperature. The reaction is then dried en vacuo using toluene as an azeotrope. Residue is washed with saturated sodium bicarbonate and extracted with EtOAc (3x). The combined organic layers are washed with brine, dried over Na₂SO₄, filtered and concentrated in vacuo. Flash chromatography of the crude residue (SiO₂, EtOAc in hexanes) provided the desired product.

General Procedure for Demethylation of 2-substituted-7-methoxy-2,4,6-cycloheptatrien-1-one with

acid: The 2-substituted-7-methoxy-2,4,6-cycloheptatrien-1-one was added to a 1:1 solution of methanol/HCl (0.3 M) and refluxed for 6 h before cooling to room temperature. Generally the desired product would precipitate from the solution and was filtered and dried without further purification.

General Procedure for Demethylation of 2-substituted-7-methoxy-2,4,6-cycloheptatrien-1-one with

lithium chloride: To a flame dried pressure vessel was added 2-substituted-7-methoxy tropone in DMF (0.6 M) followed by LiCl (3.0 eq). The vessel was heated to 130°C for 3 h before cooling to room temperature. The crude material was acidified to pH 2.0 and diluted with Et₂O and brine. The mixture was then extracted with Et₂O (3x). The combined organic layers were washed with brine, dried over Na₂SO₄, filtered and concentrated in vacuo. Flash chromatography of the crude residue (SiO₂, EtOAc in hexanes) provided the desired α -substituted tropolone. In most cases the tropolone contained an undesired impurity and required filtration through C18 silica gel, eluting with 50% MeOH/H₂O.

General Procedure for Suzuki Coupling to 2-(4-Bromo-phenyl)-7-hydroxy-2,4,6-cycloheptatrien-1-one:

2-(4-bromo-phenyl)-7-hydroxy-2,4,6-cycloheptatrien-1-one (1.0 eq), boronic acid (1.5 eq) and potassium fluoride (3.0 eq) were added to 5:1 dioxane/H₂O (0.3 M) and the mixture was thoroughly degassed by bubbling argon through the solution (10 min). Bis(triphenylphosphine)palladium(II) dichloride (0.1 eq) was added and the mixture was again degassed with argon (5 min). The homogenous solution was

heated at 90°C for 16 h before being cooled to room temperature. Water and a small amount 2 M HCl was added and the mixture was extracted with EtOAc (3x). The combined organic layers were washed with brine, dried over Na₂SO₄, filtered and concentrated in vacuo. Flash chromatography of the crude residue (SiO₂, EtOAc in hexanes) provided the desired 2-substituted-7-hydroxy tropolone.

General Procedure for Diacylation of 2-(4-amino-phenyl)-7-hydroxy-2,4,6-cycloheptatrien-1-one: 2-(4-amino-phenyl)-7-hydroxy-2,4,6-cycloheptatrien-1-one, pyridine (2.0 eq) and 4-(dimethylamino)pyridine (0.1 eq) were dissolved in CH₂Cl₂ (0.2 M). The solution was cooled to 4°C, acyl chloride (2.0 eq) was added and the solution was sealed and stirred for 2 h. Water was added and the mixture was extracted with EtOAc (3x). The combined organic layers were washed with brine, dried over Na₂SO₄, filtered and concentrated in vacuo. Flash chromatography of the crude residue (SiO₂, EtOAc in hexanes) provided the desired product.

General Procedure for Ester Hydrolysis of Diacylated 2-(4-amino-phenyl)-7-hydroxy-2,4,6-cycloheptatrien-1-one: The diacylated 2-(4-amino-phenyl)-7-hydroxy-2,4,6-cycloheptatrien-1-one was dissolved in methanol (0.5 M). A few drops of 3 M potassium hydroxide was added to the solution and stirred for 30 minutes. 2 M HCl was added and the mixture was extracted with EtOAc (3x). The combined organic layers were washed with brine, dried over Na₂SO₄, filtered and concentrated in vacuo. Flash chromatography of the crude residue (SiO₂, EtOAc in hexanes) provided the desired product.

General Procedure for Tosylation of 2-hydroxy-7-phenyl-2,4,6-cycloheptatrien-1-one: 2-hydroxy-7-phenyl-2,4,6-cycloheptatrien-1-one and *N,N*-diisopropylethylamine (1.2 eq) were dissolved in acetonitrile (0.2 M). Next, *p*-toluenesulfonyl chloride (1.1 eq) was added to the solution. The vial was then sealed and stirred at room temperature for 2 h. Water was added and the mixture was extracted with EtOAc (3x). The combined organic layers were washed with brine, dried over Na₂SO₄, filtered and

concentrated in vacuo. Flash chromatography of the crude residue (SiO₂, EtOAc in hexanes) provided the desired product.

General Procedure for Thiol S_N2 Reaction with Toluene-4-sulfonic acid 7-oxo-6-phenyl-cyclohepta-

1,3,5-trienyl ester: Toluene-4-sulfonic acid 7-oxo-6-phenyl-cyclohepta-1,3,5-trienyl ester and the desired thiol (1.9 eq) were dissolved in methanol (0.2 M) and stirred at room temperature for 2 h. The solution was then concentrated in vacuo. Flash chromatography of the crude residue (SiO₂, EtOAc in hexanes) provided the desired product.

General Procedure for O-(tert-Butyldimethylsilyl)hydroxylamine S_N2 Reaction with Toluene-4-sulfonic

acid 7-oxo-6-phenyl-cyclohepta-1,3,5-trienyl ester: Toluene-4-sulfonic acid 7-oxo-6-phenyl-cyclohepta-1,3,5-trienyl ester and O-(tert-Butyldimethylsilyl)hydroxylamine (1.5 eq) were dissolved in dioxane (0.2 M) and stirred at 100°C for 16 h. The solution was then concentrated in vacuo. Flash chromatography of the crude residue (SiO₂, EtOAc in hexanes) provided the desired product.

General Procedure for Formation of Zinc-Tropolone Complex: Tropolone was added to a solution of 1:1 EtOH/H₂O (0.8 M). Next, zinc acetate (0.5 eq) was added to the mixture and stirred for 2 h at reflux. The solution was then cooled to room temperature and the resulting zinc-bistropolone complex precipitated from solution and was collected on filter paper, dried and used without further purification.

5.1.3 Tropolone Handling

Stock solutions of each tropolone (100 mM) were prepared in biology grade DMSO, sealed with parafilm and stored at -20°C. Dilutions of 10 mM were prepared to be used for mammalian cell culture assays and enzyme assays. Assays were designed such that cell cultures were not subjected to more than 2% DMSO by volume. To avoid decomposition, samples were thawed at room temperature and stored as described immediately after use. ¹HNMR and LC

traces show stored samples do not appear to deteriorate after an extended amount of time and use (~1 year).

5.2 Materials and Methods - Biology

5.2.1 Sirtuin 1 Enzyme Activity Assay

Sirtuin 1 enzyme activity was assessed using the SIRT1 Direct Fluorescent Screening Assay Kit from Cayman Chemical. The kit was stored at -80°C until usage. Reagents were thawed on ice and prepared according to supplied protocol. Water used for dilutions was acquired from a Milli-Q Academic water purification system, filtered through a 0.22 µm sterilizing, low protein binding filter and autoclaved. Compounds were tested in triplicate and diluted from 10 mM DMSO stock solutions with SIRT1 Direct Assay Buffer. Tenovin-6, salermide and trans-resveratrol were from the Epigenetics Screening Library (96-Well) from Cayman Chemical. Assay and calculations were performed according to the supplied protocol. The plate was read with a BioTek Synergy™ H1 hybrid reader using excitation at 350 nm and emission at 450 nm.

5.2.2 Sirtuin 2 Enzyme Activity Assay

Sirtuin 2 enzyme activity was assessed using the SIRT2 Direct Fluorescent Screening Assay Kit from Cayman Chemical. The kit was stored at -80°C until usage. Reagents were thawed on ice and prepared according to supplied protocol. Water used for dilutions was acquired from a Milli-Q Academic water purification system, filtered through a 0.22 µm

sterilizing, low protein binding filter and autoclaved. Compounds were tested in triplicate and diluted from 10 mM DMSO stock solutions with SIRT2 Direct Assay Buffer. Tenovin-6, sirtinol and trans-resveratrol were from the Epigenetics Screening Library (96-Well) from Cayman Chemical. Vorinostat (SAHA) was purchased from Sigma Aldrich and dissolved in DMSO to make a 10 mM stock solution. Assay and calculations were performed according to the supplied protocol. The plate was read with a BioTek Synergy™ H1 hybrid reader using excitation at 350 nm and emission at 450 nm.

5.2.3 Mammalian Cell Culturing

Mammalian cell cultures were prepared from cryogenically persevered samples. Normal human adult dermal fibroblast (hDF) cells were generously provided by Dr. Theodore Rasmussen and grown in Dulbecco's Modified Eagle's Medium (DMEM, Life Technologies, cat. no. 11995-065) supplemented with 40% fetal bovine serum (FBS, Atlanta Biologies, cat. no. S11550) and 1% penicillin/streptomycin (Cellgro - Mediatech Inc. cat. no. 30-002-CI). Mammary gland, breast adenocarcinoma, derived from a metastatic site (MCF-7) were generously provided by Dr. Headley Freake and grown in DMEM supplemented with 10% FBS and 1% penicillin/streptomycin. T-lymphoblast, acute lymphoblastic leukemia, derived from a patient in relapse (Molt-4) were generously provided by Dr. Andrew Wiemer and grown in RPMI-1640 supplemented with 10% FCS and 1% penicillin/streptomycin. hPBMCs purified from human blood (purchased from Research Blood Components, Brighton, MA) and frozen in freezing media were generously provided by Dr. Andrew Wiemer. The hPBMCs were thawed and resuspended in RPMI-1640 supplemented with 1x HEPES buffer, pyruvate, non-essential amino acids, 2-mercaptoethanol and 10% FBS and immediately used for the cell viability assay.

Cryo-vials, stored in a liquid nitrogen phase storage container, are placed in a 37°C water bath for 3 to 4 minutes to thaw cryogenically preserved cells. The thawed cells are then moved to a 15 mL conical tube and diluted with 10 mL of media and centrifuged at 125 x g for 5 minutes at 4°C to pellet the cells and to remove DMSO in the cryogenic storage media. After removing and discarding the supernatant, 3 mL of fresh media is used to resuspend the cell pellet. The cell suspension is then added to a 25 mL T-flask with another 3 mL of media. The T-flask is then placed in an incubator at 37°C with 5% carbon dioxide atmosphere.

To preserve (pass) the unused adherent cells (MCF-7 and hDF) from a confluent culture the old media in the T-flask was discarded. The flask is then washed with 6 mL of 0.25% trypsin to remove any residual media and discarded. 3 mL of trypsin was added to the flask and incubated for 5 minutes. After incubation, the flask was viewed under a microscope to ensure the suspension of cells in the solution. Next, 9 mL of DMEM was added to the flask to quench the trypsin. 100 µL of the culture is added to a 1.5 mL Eppendorf tube and combined with 400 µL Trypan Blue and vortexed. 10 µL is then placed on a hemocytometer with a glass cover slide and counted. Meanwhile, the remaining culture is transferred to a 15 mL conical tube and centrifuged at 125 x g for 5 minutes at 4°C. After centrifuging, the supernatant is discarded and the cells are resuspended in fresh media and diluted to $3\text{--}5 \times 10^5$ cells/mL and 6 mL is added to a new T-75 flask. If the cells are not confluent and the media has changed in color, the old media is discarded and fresh media is supplied without trypsinization. MCF-7 media needs to be renewed 2-3 times per week while hDF media needs to be renewed 1-2 times per week. Cryogenic stocks can be made after the third passage for MCF-7 or the first passage for hDF. Stocks are prepared by combining 5 mL of cell culture at 1×10^6 cells/mL with 4 mL FBS and 1 mL DMSO. Approximately 2 mL is added to a cryo-vial. The cryo-vial is placed in a freezer

box and stored at -20°C for 2 hours. The freezer box is then moved to -80°C where it is stored overnight. After this step the cryo-vial can be stored in a liquid nitrogen phase cell storage container for long term storage.

To preserve (pass) the unused Molt-4 cells from a confluent culture the existing cells and media in the T-flask were counted and a dilution factor was determined to maintain the cell culture at $3\text{--}5 \times 10^5$ cells/mL. Depending on the volume required to achieve this cell culture concentration and the age of the media, fresh media could be directly added, some of the existing culture could be discarded and fresh media added or some of the existing culture could be discarded while the remaining culture was centrifuged, old media removed and the cell pellet resuspended in fresh media.

5.2.4 Mammalian Cell Viability Assay

Cell viability assays with hDF and MCF-7 were performed using the Cell Titer 96 Aqueous One Kit (Promega, Madison, WI). 100 μL of cells were seeded in 96 well plates (5×10^4 cells/mL). The cells were then treated with various concentrations of tropolones or vorinostat and incubated at 37°C with 5% CO_2 for 72 h. Formazan content was determined by measuring the absorbance at 490 nm using Synergy H1 Multi-Mode plate reader (Biotek, Winooski, VT). GI_{50} values were determined by non-linear regression analysis. All experiments were repeated independently at least three times ($n = 3$).

Cell viability assays with Molt-4 and hPBMCs were performed using the Quanti-Blue Cell Viability Assay Kit (BioAssay Systems, Hayward, CA). 100 μL of cells were seeded in 96 well plates (10^5 cells/mL for Molt-4 and 10^6 cells/mL for hPBMCs). The cells were then treated with various concentrations of the tropolones or vorinostat and incubated at 37°C with 5% CO_2

for 72 h. 10 μ L of the Quanti-Blue reagent was added into each well for the final 2 h of incubation and the plates were read by a Perkin-Elmer VICTOR X multilabel plate reader (excitation 550 nm, emission 600 nm). GI₅₀ values were determined by non-linear regression analysis. All experiments were repeated independently at least three times (n = 3).

5.2.5 Bacteria Culturing

All reagents were purchased as bacteria culture tested from Fisher Scientific (Pittsburgh, PA) and used according to protocols described. Stock cultures were prepared from overnight cultures by mixing 1 mL of culture (OD₆₀₀ ~1) in a previously autoclaved cryogenic vial containing 200 μ L of glycerol under sterile conditions. Long term stock cultures were stored at -78°C. Luria-Bertani (LB) agar was prepared using 25 g/L LB Broth, Miller (Fisher Scientific) and 15 g/L Agar, molecular genetics powder (Fisher Scientific) dissolved in water obtained from a Milli-Q Academic (Millipore, Billerica, MA), autoclaved and used under sterile conditions to form culture plates. Iso-sensitest broth was prepared from Oxoid Iso-sensitest broth (Thermo Scientific, Waltham, MA) using 23.4 g/L dissolved in water obtained from a Milli-Q Academic and autoclaved. Flat bottomed 96-well microtiter plates (Thermo Scientific) were used for susceptibility testing. Optical densities were measured with a Biospec-Mini DNA/RNA/Protein Analyzer (Shimadzu, Kyoto, Japan).

5.2.6 Susceptibility Testing to Determine MIC Values Using Microdilution Method

All experiments were performed using *Escherichia coli* ATCC 25922 or *Klebsiella pneumoniae* ATCC 10031 as the standard strain. *K. p.* UCHC1 (a TMP resistant strain) and *K. p.* UCHC3 (a TMP susceptible strain) were used as clinical isolates. Bacterial cultures were grown with aeration at 37°C in Iso-sensitest broth or from frozen glycerol stocks on Luria-Bertani (LB)

broth agar plates at 37°C. Tropolones were synthesized as described previously. Trimethoprim (TMP) was purchased from Sigma-Aldrich.

Minimum inhibition concentrations (MICs) were determined using the broth microdilution method according to CLSI standards, using a final inoculum of 5×10^5 CFU/mL. MIC was defined as the lowest concentration of antibiotic or inhibitor preventing visible growth after monitoring cell turbidity at an OD₆₀₀ following an incubation period of 18 hours at 37°C.

5.2.7 Efflux Pump Evaluation

To determine the effects of efflux pumps on the MICs of tropolones, *Escherichia coli* K-12 strain BW25113, a well defined strain that has not been subjected to mutations, was used as the progenitor strain. *Escherichia coli* JW0451, a single gene deletion variant of BW25113, has the gene coding a multidrug efflux pump subunit (acrB) deleted and therefore can be used to determine efflux effects.

MICs were determined using the broth microdilution method according to CLSI standards, using a final inoculum of 5×10^5 CFU/mL. MIC was defined as the lowest concentration of antibiotic or inhibitor preventing visible growth after monitoring cell turbidity at an OD₆₀₀ following an incubation period of 18 hours at 37°C.

5.2.8 Lipopolysaccharide Permeability Evaluation

To determine the effects of lipopolysaccharide solubility being a limiting factor in Gram-negative MICs, *Escherichia coli* K-12 strain BW25113 was used as the progenitor strain. *Escherichia coli* NR698 is a mutant strain that is defective in outer membrane

(lipopolysaccharide) biosynthesis and therefore is reported to impart increased outer membrane permeability to small molecules.

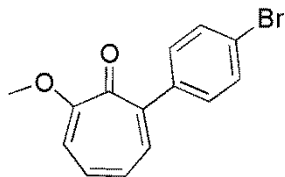
MICs were determined using the broth microdilution method according to CLSI standards, using a final inoculum of 5×10^5 CFU/mL. MIC was defined as the lowest concentration of antibiotic or inhibitor preventing visible growth after monitoring cell turbidity at an OD₆₀₀ following an incubation period of 18 hours at 37°C.

5.2.9 Drug Affinity Responsive Target Stability (DARTS) Assay

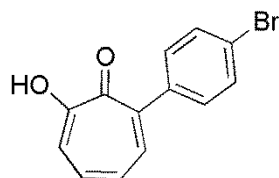
A cryogenically stored sample of *E. coli* 25922 was plated on a LB agar plate and incubated at 37°C overnight. From the culture plate a single colony was picked using a sterile loop and added to 20 mL of LB media in a sterile 50 mL Falcon™ conical tube. The tube was incubated at 37°C and shaken at 225 rpm in a New Brunswick Scientific C25KC incubator shaker overnight. 15 mL of culture was diluted with 10 mL of fresh LB media and OD₆₀₀ was read on a Shimadzu BioSpec-mini. 4 mL of diluted culture was added to each well of a 6-well plate. Appropriate amounts of either DMSO or tropolone were added to each well with less than 4% DMSO in the final volume. The 6-well plate was then incubated at 37°C overnight. The resulting bacterial culture from each well was transferred to separate 1.5 mL Eppendorf tubes and centrifuged at 14,000 rpm for 3 minutes. The supernatant was discarded and the process repeated until all culture had been pelleted. Pellets were then washed with phosphate buffered saline and centrifuged at 14,000 rpm for 3 minutes. Supernatant was discarded and the pellet was broken up by mechanical agitation. Next, 200 µL of bacterial protein extraction reagent (B-PER) with 2 µL of Halt Protease and Phosphatase Inhibitor Cocktail were added to lyse the cells. The lysate was placed on a rocker at 4°C for 45 minutes and then centrifuged at 14,000 rpm for

15 minutes. After centrifuging, the supernatant was transferred to a new 1.5 mL Eppendorf tube and mixed with 200 μ L of DARTS assay buffer and placed on ice. DARTS assay buffer was previously prepared in an autoclaved 100 mL bottle by mixing Tris-HCl (50 mM), sodium chloride (50 mM) and calcium chloride (10 mM) in sterilized, filtered water. The protein content in each tube was measured using the Bradford Assay and 1 μ g of thermolysin (from Promega) was added for every 15 μ g of protein reported. Since the amount of thermolysin required was significantly less than 1 mg, 1 mM stock of thermolysin was prepared in sterilized, filtered water. The samples were then incubated at room temperature for 10 minutes. Proteolysis by thermolysin was quenched by adding 0.5 M EDTA in a 1:10 volumetric ratio (20 μ L). Samples were stained with NuPAGE and run on a 4-12% Bis-Tris gel at 184 volts. After cooling, the gel was stained with coomassie blue. Gel images were recorded using a Nokia Lumia 920. The differential band was excised from the gel using a sterile razor blade and sterile tweezers and placed in 500 μ L of sterilized, filtered water in a sterile 1.5 mL Eppendorf tube. The tube was sealed with parafilm and shipped via FedEx to the Keck MS & Proteomics Resource at Yale School of Medicine for LC-MS/MS protein identification.

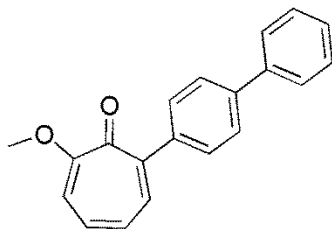
Appendix A: Chemical Characterizations and Selected Spectra



BA-pBr-OMe: yield: 88%. R_f = 0.09 (1:1 EtOAc: Hexanes). M_p = 94.1-95.2. IR (KBr): ν : 3000, 2839, 1593, 1576, 1496, 1356, 1269, 1221, 1161, 1070, 969, 819, 783, 742, 539. ^1H NMR (500 MHz, CDCl_3): δ 7.53 (d, J = 8.5 Hz, 2H), 7.44 (d, J = 9.0 Hz, 1H), 7.36 (d, J = 8.0 Hz, 2H), 7.08 (t, J = 10.5 Hz, 1H), 6.90 (t, J = 10.0 Hz, 1H), 6.77 (d, J = 9.5 Hz, 1H), 3.97 (s, 3H). ^{13}C NMR (125 MHz, CDCl_3): δ 179.1, 166.2, 146.4, 140.3, 137.6, 132.2, 131.3, 131.2, 127.0, 122.3, 112.2, 56.7. HRMS (ESI) calcd for $\text{C}_{14}\text{H}_{11}\text{BrO}_2$ $[\text{M}+\text{H}]^+$: 291.0021; found: 291.0034.

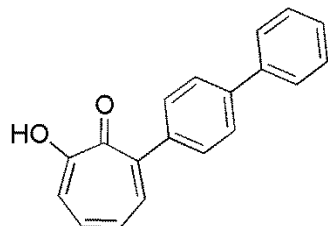


BA-pBr-OH: yield: 82%. R_f = 0.43 (1:1 EtOAc: Hexanes). M_p = 125.7-126.6. IR (KBr): ν : 3182, 1610, 1596, 1556, 1475, 1418, 1395, 1358, 1298, 1238, 1213, 1180, 1105, 1073, 1002, 964, 938, 909, 884, 833, 819, 807, 791, 732, 685, 631, 604, 571, 533, 510, 479, 440. ^1H NMR (500 MHz, CDCl_3): δ 7.61 (d, J = 8.5 Hz, 2H), 7.58 (d, J = 10.0 Hz, 1H), 7.44-7.42 (m, 4H), 7.12 (t, J = 9.5 Hz, 1H). ^{13}C NMR (125 MHz, CDCl_3): δ 172.0, 170.6, 140.4, 138.9, 138.3, 137.2, 131.6, 131.1, 127.6, 122.8, 121.8. HRMS (ESI) calcd for $\text{C}_{13}\text{H}_9\text{BrO}_2$ $[\text{M}+\text{H}]^+$: 276.9864; found: 276.9854.

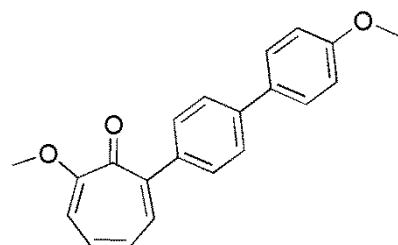


BA-Phe-OMe: yield: 80%. R_f = 0.22 (1:1 EtOAc: Hexanes). M_p = 159.7-161.0. IR (KBr): ν : 3074, 3027, 2967, 2838, 2135, 1590, 1574, 1466, 1354, 1268, 1216, 1170, 1091, 972, 834, 745, 697. ^1H NMR (500 MHz, CDCl_3): δ 7.66 (dd, J = 7.8, 3.1 Hz, 4H), 7.60 (d, J = 8.0 Hz, 2H), 7.53 (d, J = 8.7 Hz, 1H), 7.47 (t, J = 7.6 Hz, 2H), 7.38 (t, J = 7.3 Hz, 1H), 7.05 (t, J = 9.8 Hz, 1H), 6.91 (t, J = 9.6 Hz, 1H), 6.77 (d, J = 9.2 Hz, 1H), 3.97 (s, 3H). ^{13}C NMR

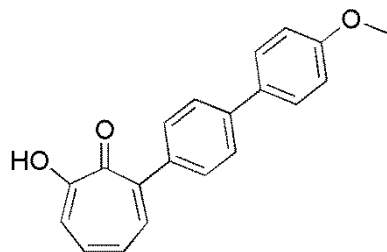
(125 MHz, CDCl₃): δ 179.4, 165.9, 147.1, 140.9, 140.8, 140.3, 137.3, 131.6, 129.8, 128.8, 127.3, 127.2, 126.9, 126.8, 111.9, 56.5. HRMS (ESI) calcd for C₂₀H₁₆O₂ [M+H]⁺: 289.1229; found: 289.1242.



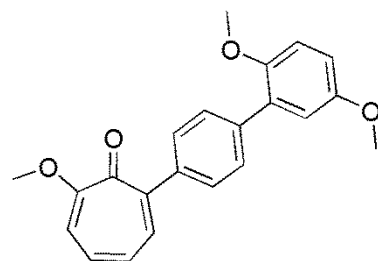
BA-Phe-OH: yield: 76%. R_f = 0.39 (1:1 EtOAc: Hexanes). M_p = 166.1-167.3. IR (KBr): ν : 3136, 3024, 2918, 1591, 1552, 1466, 1357, 1240, 1217, 1170, 764, 699. ¹HNMR (500 MHz, CDCl₃): δ 9.91 (s, 1H), 7.74 (d, J = 7.2 Hz, 2H), 7.72 – 7.68 (m, 3H), 7.66 (d, J = 8.3 Hz, 2H), 7.52 (t, J = 7.4 Hz, 2H), 7.49 – 7.40 (m, 3H), 7.16 (t, J = 9.8 Hz, 1H). ¹³CNMR (125 MHz, CDCl₃): δ 171.33, 170.46, 141.22, 140.68, 140.50, 138.80, 138.63, 136.77, 129.77, 128.85, 127.54, 127.40, 127.20, 127.04, 121.87. HRMS (ESI) calcd for C₁₉H₁₄O₂ [M+H]⁺: 275.1072; found: 275.1062.



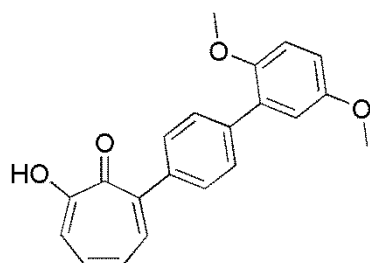
BA-SM-OMe: yield: 72%. R_f = 0.41 (EtOAc). M_p = 160.1-161.3. IR (KBr): ν : 3006, 2958, 2920, 2837, 1590, 1576, 1496, 1250, 1217, 1084, 970, 824, 756. ¹HNMR (500 MHz, CDCl₃): δ 7.63 – 7.53 (m, 7H), 7.08 (t, J = 10.1 Hz, 1H), 7.01 (d, J = 8.7 Hz, 2H), 6.94 (t, J = 10.2, 9.3 Hz, 1H), 6.79 (d, J = 9.6 Hz, 1H), 3.99 (s, 3H), 3.88 (s, 3H). ¹³CNMR (125 MHz, CDCl₃): δ 166.01, 159.41, 147.32, 139.77, 137.46, 132.26, 131.68, 129.95, 128.32, 127.12, 126.48, 114.40, 112.16, 56.67, 55.53. HRMS (ESI) calcd for C₂₁H₁₈O₃ [M+H]⁺: 319.1334; found: 319.1327.



BA-SM-OH: yield: 72%. $R_f = 0.24$ (1:1 EtOAc: Hexanes). $M_p = 167.3-168.5$. IR (KBr): ν : 3156, 3034, 2960, 2917, 2838, 1595, 1541, 1494, 1464, 1414, 1355, 1284, 1240, 1178, 1033, 911, 825. ^1H NMR (500 MHz, CDCl_3): δ 9.90 (s, 1H), 7.70 (d, $J = 8.6$ Hz, 3H), 7.63 (dd, $J = 8.4, 2.0$ Hz, 4H), 7.51 – 7.40 (m, 2H), 7.15 (t, $J = 9.5$ Hz, 1H), 7.05 (d, $J = 8.6$ Hz, 2H), 3.92 (s, 3H). ^{13}C NMR (125 MHz, CDCl_3): δ 171.27, 170.49, 159.40, 140.84, 140.47, 138.64, 138.16, 136.69, 133.19, 129.74, 128.21, 127.37, 126.56, 121.92, 114.32, 55.39. HRMS (ESI) calcd for $\text{C}_{20}\text{H}_{16}\text{O}_3$ $[\text{M}+\text{H}]^+$: 305.1178; found: 305.1177.

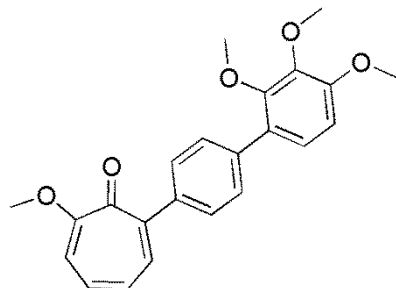


BA-DM-OMe: yield: 98%. $R_f = 0.39$ (EtOAc). $M_p = 155.2-157.8$. IR (KBr): ν : 3086, 2993, 2940, 2904, 2832, 1578, 1549, 1491, 1461, 1270, 1221, 1209, 1178, 1013, 970, 843, 748. ^1H NMR (500 MHz, CD_2Cl_2): δ 7.63 – 7.56 (m, 5H), 7.09 (t, $J = 10.1$ Hz, 1H), 7.01 (d, $J = 3.0$ Hz, 1H), 6.99 – 6.92 (m, 2H), 6.90 (dd, $J = 8.9, 3.0$ Hz, 1H), 6.80 (d, $J = 9.6$ Hz, 1H), 4.01 (s, 3H), 3.86 (s, 2H), 3.82 (s, 3H). ^{13}C NMR (125 MHz, CD_2Cl_2): δ 179.47, 153.82, 150.90, 138.03, 137.32, 131.39, 131.34, 129.55, 129.11, 129.10, 126.90, 116.63, 113.38, 112.75, 111.86, 99.99, 56.51, 56.38, 55.8. HRMS (ESI) calcd for $\text{C}_{22}\text{H}_{20}\text{O}_4$ $[\text{M}+\text{H}]^+$: 349.1440; found: 349.1468.

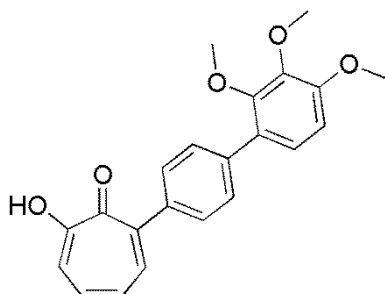


BA-DM-OH: yield: 72%. $R_f = 0.27$ (1:1 EtOAc: Hexanes). $M_p = 144.9-145.8$. IR (KBr): ν : 3144, 3029, 3002, 2953, 2829, 1615, 1548, 1472, 1452, 1364, 1244, 1231, 1206, 1175, 1052, 1024, 798, 718. ^1H NMR (500 MHz, CDCl_3): δ 9.94 (s, 1H), 7.74 – 7.66 (m, 3H), 7.63 (d, $J = 7.6$ Hz, 2H), 7.51 – 7.40 (m, 2H), 7.15 (t, $J =$

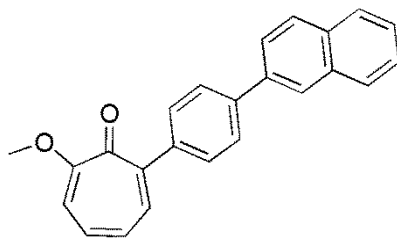
10.6 Hz, 1H), 7.02 (d, $J = 3.1$ Hz, 1H), 6.99 (d, $J = 8.9$ Hz, 1H), 6.93 (dd, $J = 8.9, 3.1$ Hz, 1H), 3.87 (s, 3H), 3.83 (s, 3H). ^{13}C NMR (125 MHz, CDCl_3): δ 171.24, 170.54, 153.84, 150.89, 140.63, 138.73, 138.47, 136.71, 131.08, 129.36, 129.03, 127.39, 121.94, 116.69, 113.47, 112.72, 56.35, 55.85. HRMS (ESI) calcd for $\text{C}_{21}\text{H}_{18}\text{O}_4$ $[\text{M}+\text{H}]^+$: 335.1283; found: 335.1282.



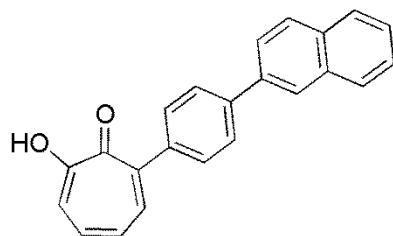
BA-TM-OMe: yield: 99%. $R_f = 0.42$ (EtOAc). $M_p = 132.9$ -134.6. IR (KBr): ν : 3317, 2928, 2837, 1589, 1572, 1461, 1270, 1217, 1165, 1088, 1069, 998, 751. ^1H NMR (500 MHz, CDCl_3): δ 7.60 – 7.55 (m, 5H), 7.13 (d, $J = 8.6$ Hz, 1H), 7.08 (t, $J = 10.4$ Hz, 1H), 6.95 (t, $J = 10.6, 8.9$ Hz, 1H), 6.80 (dd, $J = 9.1, 3.2$ Hz, 2H), 4.00 (s, 3H), 3.98 (s, 3H), 3.95 (s, 3H), 3.76 (s, 3H). ^{13}C NMR (125 MHz, CDCl_3): δ 179.61, 165.97, 153.35, 151.65, 147.28, 142.72, 139.78, 137.98, 137.49, 132.28, 131.61, 129.37, 128.84, 128.44, 127.06, 125.03, 112.10, 107.73, 61.23, 61.17, 56.65, 56.23. HRMS (ESI) calcd for $\text{C}_{23}\text{H}_{22}\text{O}_5$ $[\text{M}+\text{H}]^+$: 379.1546; found: 379.1535.



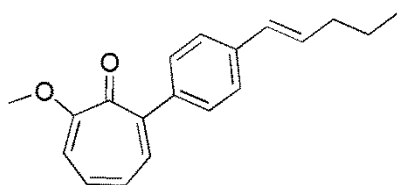
BA-TM-OH: yield: 77%. $R_f = 0.23$ (1:1 EtOAc: Hexanes). $M_p = 150.0$ -151.3. IR (KBr): ν : 3111, 3005, 2978, 2932, 2823, 1596, 1548, 1490, 1475, 1459, 1415, 1290, 1237, 1108, 1079, 1006, 756. ^1H NMR (500 MHz, CDCl_3): δ 9.91 (s, 1H), 7.73 (d, $J = 10.1$ Hz, 1H), 7.64 (q, $J = 8.3, 6.6$ Hz, 4H), 7.52 – 7.41 (m, 2H), 7.16 (dd, $J = 12.1, 9.4$ Hz, 2H), 6.82 (d, $J = 8.7$ Hz, 1H), 3.99 (s, 3H), 3.96 (s, 3H), 3.79 (s, 3H). ^{13}C NMR (125 MHz, CDCl_3): δ 171.5, 170.6, 153.5, 151.7, 142.8, 140.8, 139.0, 138.5, 138.3, 136.8, 129.3, 129.1, 128.3, 127.6, 125.0, 122.0, 107.8, 61.3, 61.2, 56.3. HRMS (ESI) calcd for $\text{C}_{22}\text{H}_{20}\text{O}_5$ $[\text{M}+\text{H}]^+$: 365.1389; found: 365.1373.



BA-Nap-OMe: yield: 85%. R_f = 0.48 (EtOAc). IR (KBr): ν : 3036, 3005, 2940, 2834, 1570, 1492, 1267, 1214, 1159, 1086, 972, 776. ^1H NMR (500 MHz, CDCl_3): δ 8.07 (d, J = 8.3 Hz, 1H), 7.96 (d, J = 10.6 Hz, 1H), 7.92 (d, J = 8.2 Hz, 1H), 7.69 – 7.65 (m, 2H), 7.64 (dd, J = 9.0, 1.0 Hz, 1H), 7.61 – 7.47 (m, 7H), 7.12 (t, J = 10.2, 1H), 6.99 (t, J = 9.3, 10.2 Hz, 1H), 6.83 (d, J = 9.6 Hz, 1H), 4.03 (s, 3H). ^{13}C NMR (125 MHz, CDCl_3): δ 179.4, 165.9, 147.1, 140.3, 140.2, 139.9, 137.4, 133.8, 131.6, 129.7, 129.3, 128.5, 128.2, 127.6, 127.0, 126.9, 126.1, 126.0, 125.7, 125.4, 111.9, 56.5. HRMS (ESI) calcd for $\text{C}_{24}\text{H}_{18}\text{O}_2$ $[\text{M}+\text{H}]^+$: 339.1385; found: 339.1358.

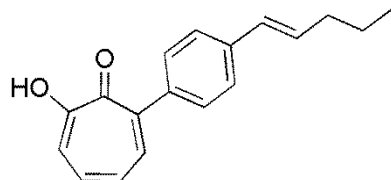


BA-Nap-OH: yield: 63%. R_f = 0.31 (1:1 EtOAc: Hexanes). M_p = 135.6-136.5. IR (KBr): ν : 3152, 3042, 1610, 1594, 1543, 1395, 1357, 1293, 1229, 800, 777, 741, 707. ^1H NMR (500 MHz, CDCl_3): δ 9.96 (s, 1H), 8.06 (d, J = 8.4 Hz, 1H), 7.98 (d, J = 8.2 Hz, 1H), 7.94 (d, J = 8.1 Hz, 1H), 7.78 (d, J = 10.1 Hz, 1H), 7.72 (d, J = 8.0 Hz, 2H), 7.66 (d, J = 8.2 Hz, 2H), 7.61-7.44 (m, 6H), 7.19 (t, J = 9.8 Hz, 1H). ^{13}C NMR (125 MHz, CDCl_3): δ 171.61, 170.32, 140.82, 140.70, 139.74, 138.96, 138.82, 136.79, 133.86, 131.56, 129.99, 129.28, 128.34, 127.86, 127.46, 127.05, 126.14, 126.06, 125.87, 125.44, 121.66. HRMS (ESI) calcd for $\text{C}_{23}\text{H}_{16}\text{O}_2$ $[\text{M}+\text{H}]^+$: 325.1229; found: 325.1251.

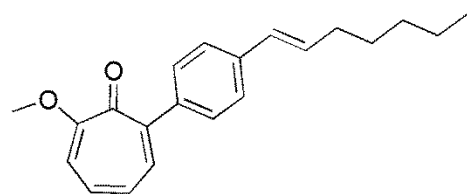


BA-P5-OMe: yield: 95%. R_f = 0.47 (EtOAc). M_p = 104.8-106.0. IR (KBr): ν : 3007, 2950, 2924, 2868, 2834, 1587, 1563, 1490, 1465, 1277, 1220, 1164, 1088, 966, 755. ^1H NMR (500 MHz, CDCl_3): δ 7.49 – 7.43 (m, 3H), 7.40 (d, J = 8.2 Hz, 2H), 7.03 (t, J = 10.6 Hz, 1H), 6.89 (t, J = 8.9 Hz, 1H), 6.75 (d, J = 9.6 Hz, 1H), 6.42 (d, J = 15.9 Hz, 1H), 6.28 (dt, J = 15.8, 6.9 Hz, 1H), 3.95 (s, 3H), 2.22 (q, J = 7.1, 1.4 Hz, 2H), 1.52 (h, J = 7.4 Hz, 2H), 0.98 (t, J = 7.4 Hz, 3H). ^{13}C NMR (125 MHz, CDCl_3): δ 165.91, 147.34, 139.84, 137.84, 137.32,

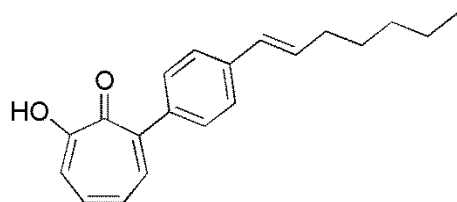
131.62, 131.59, 129.77, 129.72, 127.10, 125.70, 112.13, 56.63, 35.35, 22.71, 13.91. HRMS (ESI) calcd for $C_{19}H_{20}O_2$ $[M+H]^+$: 281.1542; found: 281.1563.



BA-P5-OH: yield: 89%. R_f = 0.44 (1:1 EtOAc: Hexanes). 1H NMR (500 MHz, $CDCl_3$): δ 7.62 (d, J = 10.2 Hz, 1H), 7.52 – 7.37 (m, 6H), 7.10 (t, J = 9.7 Hz, 1H), 6.45 (d, J = 15.8 Hz, 1H), 6.32 (dt, J = 15.7, 6.8 Hz, 1H), 2.25 (q, J = 7.2 Hz, 2H), 1.54 (h, J = 7.4 Hz, 2H), 0.99 (t, J = 7.4 Hz, 3H). ^{13}C NMR (125 MHz, $CDCl_3$): δ 170.96, 170.65, 140.38, 138.50, 138.14, 136.62, 131.96, 129.48, 129.43, 127.31, 125.75, 122.14, 35.18, 22.52, 13.73. HRMS (ESI) calcd for $C_{18}H_{18}O_2$ $[M+H]^+$: 267.1385; found: 267.1399.

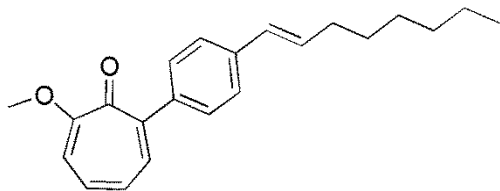


BA-P7-OMe: yield: 90%. R_f = 0.62 (EtOAc). M_p = 113.5-114.4. IR (KBr): ν : 3008, 2952, 2921, 2846, 1587, 1563, 1490, 1467, 1357, 1278, 1221, 1164, 1088, 968, 755. 1H NMR (500 MHz, $CDCl_3$): δ 7.49 – 7.44 (m, 3H), 7.38 (d, J = 8.3 Hz, 2H), 7.04 (t, J = 9.8 Hz, 1H), 6.90 (t, J = 9.8 Hz, 1H), 6.76 (d, J = 9.6 Hz, 1H), 6.42 (d, J = 15.8 Hz, 1H), 6.29 (dt, J = 15.6, 6.8 Hz, 1H), 3.98 (s, 3H), 2.24 (q, J = 14.3, 6.6 Hz, 2H), 1.51 (p, J = 7.7, 2.5 Hz, 2H), 1.40 – 1.34 (m, 4H), 0.92 (t, J = 6.3 Hz, 3H). ^{13}C NMR (125 MHz, $CDCl_3$): δ 179.43, 165.77, 147.24, 139.66, 137.72, 137.05, 131.76, 131.30, 129.56, 129.41, 126.88, 125.54, 111.83, 56.47, 33.10, 31.46, 29.07, 22.59, 14.09. HRMS (ESI) calcd for $C_{21}H_{24}O_2$ $[M+H]^+$: 309.1855; found: 309.1865.

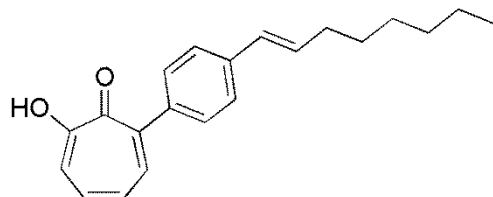


BA-P7-OH: yield: 67%. R_f = 0.49 (1:1 EtOAc: Hexanes). M_p = 98.9-100.0. IR (KBr): ν : 3148, 2950, 2920, 2849, 1619, 1551, 1473, 1362, 1239, 1197, 792, 711. 1H NMR (500 MHz, $CDCl_3$): 9.88 (s, 1H), 7.64 (d, J = 10.2 Hz, 1H), 7.52 (d, J = 8.4 Hz, 2H), 7.49 – 7.44 (m, 3H), 7.41 (t, J = 10.3 Hz, 1H), 7.12 (t, J = 9.9 Hz, 1H), 6.47 (d, J = 16.8 Hz, 1H), 6.35 (dt, J = 15.8, 6.8 Hz, 1H), 2.28 (q, J = 7.9, 6.5 Hz, 2H), 1.54 (p, J = 11.9, 7.2 Hz, 2H), 1.43 – 1.34 (m, 4H), 0.96 (t, J = 6.5 Hz, 3H). ^{13}C NMR (125 MHz, $CDCl_3$): δ 170.99, 170.65, 140.39,

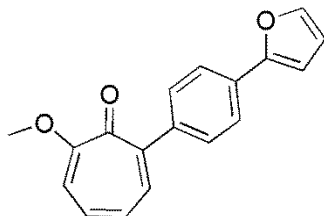
138.52, 138.14, 136.63, 132.25, 129.50, 129.25, 127.32, 125.76, 122.13, 33.11, 31.47, 29.05, 22.59, 14.09. HRMS (ESI) calcd for $C_{20}H_{22}O_2$ $[M+H]^+$: 295.1698; found: 295.1705.



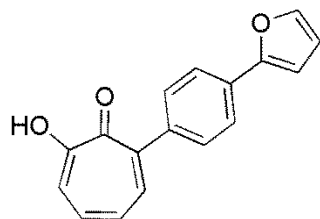
BA-P8-OMe: yield: 87%. R_f = 0.24 (1:1 EtOAc: Hexanes). M_p = 117.2-118.4. IR (KBr): ν : 3007, 2958, 29020, 2850, 1587, 1564, 1491, 1278, 1221, 1164, 1088, 967, 755. 1H NMR (500 MHz, $CDCl_3$): δ 7.47 (dd, J = 13.9, 5.6 Hz, 3H), 7.38 (d, J = 8.3 Hz, 2H), 7.04 (t, J = 10.7 Hz, 1H), 6.90 (t, J = 9.8 Hz, 1H), 6.75 (d, J = 9.6 Hz, 1H), 6.42 (d, J = 13.9 Hz, 1H), 6.29 (dt, J = 15.8, 6.8 Hz, 1H), 3.97 (s, 3H), 2.24 (q, J = 8.3, 6.3 Hz, 2H), 1.50 (p, J = 8.6, 5.6 Hz, 2H), 1.42 – 1.26 (m, 6H), 0.92 (t, J = 7.1 Hz, 3H). ^{13}C NMR (125 MHz, $CDCl_3$): δ 179.57, 165.92, 147.37, 139.81, 137.87, 137.21, 131.91, 131.48, 129.71, 129.57, 127.04, 125.69, 112.01, 56.62, 33.28, 31.93, 29.51, 29.08, 22.81, 14.28. HRMS (ESI) calcd for $C_{22}H_{26}O_2$ $[M+H]^+$: 323.2011; found: 323.2022.



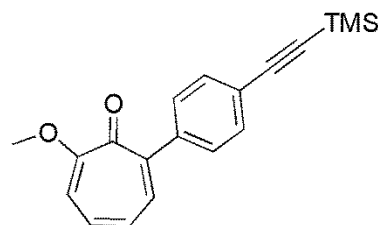
BA-P8-OH: yield: 68%. R_f = 0.70 (1:1 EtOAc: Hexanes). M_p = 85.3-86.4. IR (KBr): ν : 3149, 3018, 2958, 2918, 2850, 1618, 1595, 1553, 1474, 1364, 1275, 1243, 1216, 1197, 965, 787. 1H NMR (500 MHz, $CDCl_3$): δ 9.90 (s, 1H), 7.63 (d, J = 10.0 Hz, 1H), 7.53 – 7.44 (m, 5H), 7.42 (t, J = 9.5 Hz, 1H), 7.12 (t, J = 9.9 Hz, 1H), 6.47 (d, J = 15.8 Hz, 1H), 6.35 (dt, J = 15.7, 6.8 Hz, 1H), 2.32 – 2.25 (m, 2H), 1.57 – 1.49 (m, 2H), 1.43 – 1.32 (m, 6H), 0.95 (t, J = 7.3 Hz, 3H). ^{13}C NMR (125 MHz, $CDCl_3$): δ 140.38, 138.13, 136.61, 132.25, 129.49, 129.25, 127.30, 125.76, 122.12, 33.14, 31.77, 29.33, 28.92, 22.66, 14.12. HRMS (ESI) calcd for $C_{21}H_{24}O_2$ $[M+H]^+$: 309.1855; found: 309.1848.



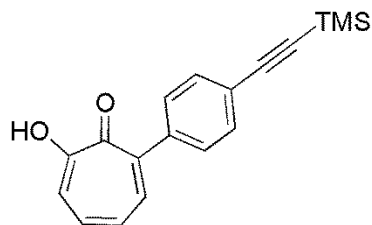
BA-HC2-OMe: yield: % 51. R_f = 0.49 (EtOAc). M_p = 137.4-138.4. IR (KBr): ν : 3127, 3024, 3006, 2924, 2840, 1589, 1573, 1514, 1494, 1465, 1443, 1412, 1355, 1268, 1216, 1168, 1116, 1090, 1071, 1042, 1006, 972. ^1H NMR (500 MHz, CDCl_3): δ 7.74 (d, J = 7.4 Hz, 2H), 7.60 – 7.49 (m, 4H), 7.08 (dd, J = 54.5, 11.3 Hz, 1H), 6.94 (t, J = 9.4 Hz, 1H), 6.79 (d, J = 9.7 Hz, 1H), 6.73 (d, J = 3.3 Hz, 1H), 6.52 (dd, J = 3.3, 1.8 Hz, 1H), 3.99 (s, 3H). ^{13}C NMR (125 MHz, CDCl_3): δ 179.34, 165.85, 153.86, 146.91, 142.20, 140.21, 137.41, 137.19, 132.02, 131.57, 131.14, 131.09, 130.43, 129.81, 128.00, 126.88, 123.39, 111.88, 111.74, 105.36, 56.51. HRMS (ESI) calcd for $\text{C}_{18}\text{H}_{14}\text{O}_3$ $[\text{M}+\text{H}]^+$: 279.1021; found: 279.1005.



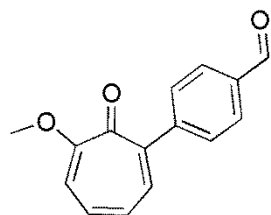
BA-HC2-OH: yield: % 72. R_f = 0.87 (EtOAc). M_p = 87.4-88.2. IR (KBr): ν : 3150, 3069, 2763, 1617, 1549, 1472, 1364, 1272, 1240, 1181, 1155, 1073, 1005, 901, 838, 824, 797, 756. ^1H NMR (500 MHz, CDCl_3): δ 7.80 (d, J = 9.2 Hz, 2H), 7.67 (t, J = 10.2 Hz, 1H), 7.65 – 7.58 (m, 2H), 7.55 (d, J = 1.7 Hz, 1H), 7.49 – 7.41 (m, 3H), 7.14 (t, J = 9.4 Hz, 1H), 6.76 (d, J = 3.2 Hz, 1H), 6.55 (dd, J = 3.4, 1.8 Hz, 1H). ^{13}C NMR (125 MHz, CDCl_3): δ 171.24, 170.47, 153.63, 142.41, 140.38, 140.26, 138.69, 138.48, 137.02, 136.76, 131.46, 130.98, 130.80, 129.76, 127.39, 123.61, 121.90, 121.61, 111.80, 105.66. HRMS (ESI) calcd for $\text{C}_{17}\text{H}_{12}\text{O}_3$ $[\text{M}+\text{H}]^+$: 265.1865; found: 265.0835.



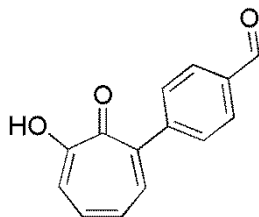
SG-TMS-OMe: yield: 69%. R_f = 0.15 (1:1 EtOAc: Hexanes). M_p = 165.7-166.9. IR (KBr): ν : 3008, 2957, 2898, 2844, 2154, 1588, 1566, 1498, 1279, 1221, 838, 757. ^1H NMR (500 MHz, CDCl_3): δ 7.57 (d, J = 10.1 Hz, 1H), 7.50 (d, J = 9.1 Hz, 2H), 7.44 (d, J = 6.4 Hz, 3H), 7.06 (t, J = 9.1 Hz, 1H), 6.90 (t, J = 10.7 Hz, 1H), 6.76 (d, J = 10.1 Hz, 1H), 3.96 (s, 3H), 0.28 (s, 9H). ^{13}C NMR (125 MHz, CDCl_3): δ 179.24, 166.10, 146.77, 141.60, 137.54, 132.56, 132.03, 131.70, 130.08, 129.46, 126.96, 126.77, 122.81, 112.02, 105.27, 94.95, 56.66, 0.18. HRMS (ESI) calcd for $\text{C}_{19}\text{H}_{20}\text{O}_2\text{Si}$ $[\text{M}+\text{H}]^+$: 309.1311; found: 309.1317.



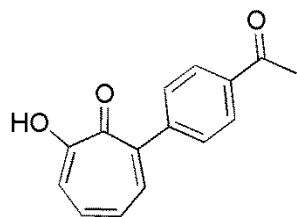
SG-TMS-OH: yield: 72%. R_f = 0.55 (1:1 EtOAc: Hexanes). M_p = 133.4-134.6. IR (KBr): ν : 3159, 2960, 2898, 2865, 2156, 1712, 1617, 1593, 1550, 1472, 1456, 1414, 1365, 1274, 1246, 1202, 1111, 1063, 1018, 913. ^1H NMR (500 MHz, CDCl_3): δ 7.57 (t, J = 9.1 Hz, 3H), 7.49 (d, J = 6.3 Hz, 2H), 7.46 – 7.38 (m, 2H), 7.11 (t, J = 10.4 Hz, 1H), 0.29 (s, 9H). ^{13}C NMR (125 MHz, CDCl_3): δ 171.19, 170.44, 140.38, 139.93, 138.22, 136.95, 131.79, 129.24, 127.35, 123.17, 121.77, 104.80, 95.23, 0.00. HRMS (ESI) calcd for $\text{C}_{18}\text{H}_{18}\text{O}_2\text{Si}$ $[\text{M}+\text{H}]^+$: 295.1154; found: 295.1148.



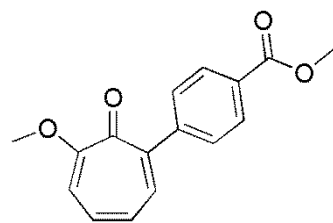
EF-1-OMe: yield: 99%. R_f = 0.5 (EtOAc). M_p = 127.0-128.3. ^1H NMR (500 MHz, CDCl_3): δ 9.98 (s, 1H), 7.94 (s, 1H), 7.82 (d, J = 7.6 Hz, 1H), 7.71 (d, J = 7.7 Hz, 1H), 7.51 (t, J = 7.7 Hz, 1H), 7.45 (d, J = 9.0 Hz, 1H), 7.07 (t, J = 10.7 Hz, 1H), 6.89 (t, J = 10.7 Hz, 1H), 6.77 (d, J = 8.4 Hz, 1H), 3.92 (s, 3H). ^{13}C NMR (125 MHz, CDCl_3): δ 192.34, 179.03, 166.32, 145.99, 142.38, 138.00, 136.43, 135.68, 132.73, 131.22, 128.97, 128.79, 127.05, 112.43, 56.71. HRMS (ESI) calcd for $\text{C}_{15}\text{H}_{12}\text{O}_3$ $[\text{M}+\text{H}]^+$: 241.0865; found: 241.0857.



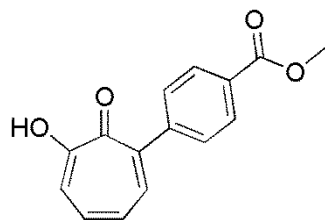
EF-1-OH: yield: 54%. R_f = 0.65 (EtOAc). M_p = 134.0-134.4. IR (KBr): ν : 3182, 2821, 2728, 1695, 1595, 1555, 1474, 1417, 1358, 1302, 1282, 1209, 1149, 655. ^1H NMR (500 MHz, CDCl_3): δ 10.10 (s, 1H), 9.87 (s, 1H), 8.06 (s, 1H), 7.96 (d, J = 7.7 Hz, 1H), 7.85 (d, J = 7.8 Hz, 1H), 7.66 (t, J = 7.8 Hz, 2H), 7.50 – 7.42 (m, 2H), 7.15 (t, J = 10.5 Hz, 1H). ^{13}C NMR (125 MHz, CDCl_3): δ 192.12, 170.15, 140.59, 138.23, 137.42, 136.70, 135.53, 130.79, 129.67, 127.66, 121.39. HRMS (ESI) calcd for $\text{C}_{14}\text{H}_{10}\text{O}_3$ $[\text{M}+\text{H}]^+$: 227.0708; found: 227.0713.



EF-2-OH: yield: 44%. R_f = 0.61 (EtOAc). M_p = 154.1-155.5. IR (KBr): ν : 3150, 3102, 3069, 2958, 2762, 1714, 1617, 1549, 1473, 1365, 1271, 1241, 1218, 1179, 1155, 1073, 1006, 825, 798, 756. ^1H NMR (500 MHz, CDCl_3): δ 9.83 (s, 1H), 8.10 (d, J = 6.9 Hz, 2H), 7.66 (d, J = 6.9 Hz, 2H), 7.63 (d, J = 10.1 Hz, 1H), 7.50 – 7.44 (m, 2H), 7.16 (t, J = 10.5 Hz, 1H), 2.70 (s, 3H). ^{13}C NMR (125 MHz, CDCl_3): δ 197.63, 171.46, 170.32, 144.65, 140.28, 138.10, 137.30, 136.66, 129.60, 128.30, 127.42, 121.55, 26.73. HRMS (ESI) calcd for $\text{C}_{15}\text{H}_{12}\text{O}_3$ $[\text{M}+\text{H}]^+$: 241.0865; found: 241.0829.

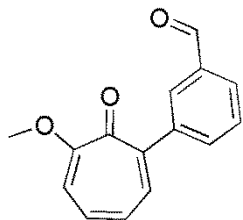


EF-3-OMe: yield: 87%. R_f = 0.44 (EtOAc). M_p = 142.5-143.7. IR (KBr): ν : 3106, 2965, 2762, 1716, 1618, 1589, 1548, 1511, 1474, 1367, 1342, 1291, 1272, 1243, 1180, 1156, 1073, 1007, 839, 825, 799, 767, 755. ^1H NMR (500 MHz, CDCl_3): δ 8.02 (d, J = 8.4 Hz, 2H), 7.64 (ddd, J = 11.8, 5.4, 3.3 Hz, 1H), 7.50 (d, J = 7.4 Hz, 2H), 7.45 – 7.39 (m, 2H), 7.05 (t, J = 10.1 Hz, 1H), 6.87 (t, J = 10.6 Hz, 1H), 6.75 (d, J = 9.6 Hz, 1H), 3.92 (s, 3H), 3.88 (s, 3H). ^{13}C NMR (125 MHz, CDCl_3): δ 179.07, 167.03, 166.24, 146.45, 146.22, 137.92, 132.65, 132.24, 132.16, 129.57, 129.46, 129.40, 128.73, 128.64, 126.99, 112.27, 56.69, 52.25. HRMS (ESI) calcd for $\text{C}_{16}\text{H}_{14}\text{O}_4$ $[\text{M}+\text{H}]^+$: 271.0970; found: 271.0956.

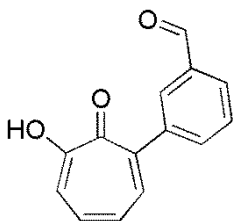


EF-3-OH: yield: 57%. R_f = 0.74 (EtOAc). M_p = 135.4-136.2. IR (KBr): ν : 3235, 3149, 3068, 3013, 2959, 2949, 2862, 2760, 1716, 1617, 1549, 1472, 1364, 1272, 1240, 1182, 1155, 1005, 825, 798, 767, 755. ^1H NMR (500 MHz, CDCl_3): δ 8.17 (d, J = 7.8 Hz, 2H), 7.63 (d, J = 7.9 Hz, 3H), 7.48 (s, 2H), 7.16 (s, 1H), 4.00 (s, 3H). ^{13}C NMR (125 MHz, Methanol- d_4): δ 171.89, 170.29, 166.85, 145.29, 140.22, 138.97, 137.22,

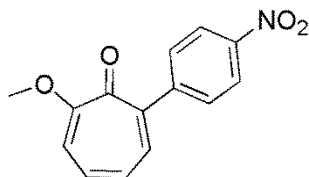
129.36, 129.28, 129.16, 129.14, 128.90, 127.42, 121.25, 51.28. HRMS (ESI) calcd for $C_{15}H_{12}O_4$ $[M+H]^+$: 257.0814; found: 257.0782.



EF-4-OMe: yield: 99%. R_f = 0.43 (EtOAc). M_p = 90.1-91.3. IR (KBr): ν : 3045, 2999, 2814, 2715, 1693, 1612, 1570, 1494, 1462, 1436, 1410, 1380, 1355, 1275, 1216, 1179, 1151, 1095, 1078, 1015, 989. 1H NMR (500 MHz, $CDCl_3$): δ 10.08 (s, 1H), 8.02 (s, 1H), 7.92 (d, J = 7.7 Hz, 1H), 7.81 (d, J = 7.7 Hz, 1H), 7.60 (t, J = 7.6 Hz, 1H), 7.54 (d, J = 9.0 Hz, 1H), 7.16 (t, J = 10.2 Hz, 1H), 6.98 (t, J = 10.6 Hz, 1H), 6.84 (d, J = 9.7 Hz, 1H), 4.02 (s, 3H). ^{13}C NMR (125 MHz, $CDCl_3$): δ 192.21, 178.95, 166.25, 146.00, 142.20, 137.78, 136.38, 135.57, 132.44, 131.06, 128.97, 128.65, 126.87, 112.12, 56.58. HRMS (ESI) calcd for $C_{15}H_{12}O_3$ $[M+H]^+$: 241.0965; found: 241.0845.

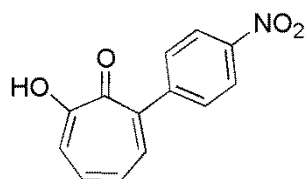


EF-4-OH: yield: 40%. R_f = 0.64 (EtOAc). M_p = 130.0-131.2. IR (KBr): ν : 3179, 3052, 2921, 2818, 2802, 2728, 1683, 1595, 1555, 1473, 1416, 1357, 1302, 1281, 1241, 1207, 1162, 1148, 1089, 734. 1H NMR (500 MHz, $CDCl_3$): δ 10.09 (s, 1H), 8.05 (t, J = 1.8 Hz, 1H), 7.94 (d, J = 7.7 Hz, 1H), 7.83 (d, J = 7.7 Hz, 1H), 7.65 (t, J = 8.6 Hz, 2H), 7.49 – 7.41 (m, 2H), 7.15 (t, J = 10.4 Hz, 1H). ^{13}C NMR (125 MHz, $CDCl_3$): δ 192.14, 172.02, 170.15, 141.03, 140.59, 138.22, 137.42, 136.69, 135.53, 130.79, 129.65, 129.11, 127.67, 121.40. HRMS (ESI) calcd for $C_{14}H_{10}O_3$ $[M+H]^+$: 227.0708; found: 227.0714.

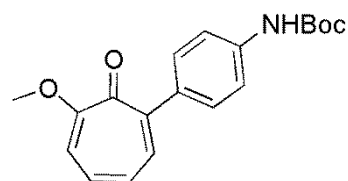


Am-NO₂-OMe: yield: 79%. R_f = 0.50 (EtOAc). IR (KBr): ν : 3169, 3105, 3067, 2976, 2925, 2874, 2848, 2362, 1597, 1577, 1551, 1503, 1459, 1442, 1409, 1341, 1309, 1289, 1273, 1217, 1163, 1118, 1106, 1090, 1063, 1045, 1014, 975. 1H NMR (500 MHz, $CDCl_3$): δ 8.32 – 8.27 (m, 2H), 7.70 – 7.64 (m, 2H), 7.50 (d, J =

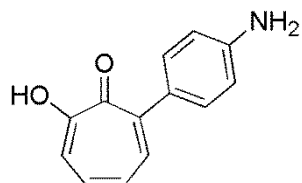
8.9 Hz, 1H), 7.19 (t, J = 9.6 Hz, 1H), 6.98 (t, J = 10.6 Hz, 1H), 6.85 (d, J = 9.8 Hz, 1H), 4.03 (s, 3H). ^{13}C NMR (125 MHz, CDCl_3): δ 166.46, 147.96, 145.22, 137.93, 133.13, 130.40, 126.69, 123.27, 112.12, 56.65. HRMS (ESI) calcd for $\text{C}_{14}\text{H}_{11}\text{NO}_4$ $[\text{M}+\text{H}]^+$: 258.0766; found: 258.0744.



Am-NO₂-OH: yield: 52%. R_f = 0.67 (EtOAc). M_p = 187.6-188.3. IR (KBr): ν : 3248, 3151, 3106, 3070, 3012, 2953, 2848, 2761, 1716, 1617, 1549, 1511, 1474, 1421, 1365, 1342, 1272, 1240, 1179, 1006, 799, 747. ^1H NMR (500 MHz, CDCl_3): δ 9.79 (s, 1H), 8.36 (d, J = 7.6 Hz, 2H), 7.73 (d, J = 9.2 Hz, 2H), 7.63 (d, J = 9.9 Hz, 1H), 7.52 – 7.48 (m, 2H), 7.22 – 7.15 (m, 1H). ^{13}C NMR (125 MHz, CDCl_3): δ 171.92, 169.93, 146.47, 140.19, 137.75, 137.45, 130.40, 127.46, 123.50, 121.00. HRMS (ESI) calcd for $\text{C}_{13}\text{H}_9\text{NO}_4$ $[\text{M}+\text{H}]^+$: 244.0610; found: 244.0588.

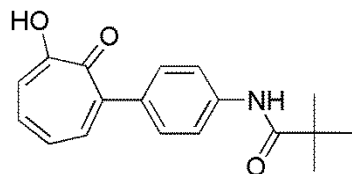


Am-NHBoc-OMe: yield: 84%. R_f = 0.71 (EtOAc). M_p = 194.9-196.2. IR (KBr): ν : 3246, 3149, 3107, 3068, 3046, 2970, 2761, 1709, 1589, 1548, 1512, 1473, 1364, 1321, 1271, 1241, 1218, 1174, 1155, 1050, 1006, 838, 796, 757. ^1H NMR (500 MHz, CDCl_3): δ 7.51 – 7.46 (m, 3H), 7.42 (d, J = 8.4 Hz, 2H), 7.06 (t, J = 10.1 Hz, 1H), 6.96 – 6.89 (m, 1H), 6.78 (d, J = 9.6 Hz, 1H), 6.59 (s, 1H), 3.99 (s, 3H), 1.57 (s, 9H). ^{13}C NMR (125 MHz, CDCl_3): δ 179.43, 165.74, 146.86, 138.17, 137.01, 135.84, 132.16, 132.09, 131.93, 131.17, 130.18, 128.55, 128.46, 126.91, 117.94, 111.85, 56.46, 28.36, 24.89. HRMS (ESI) calcd for $\text{C}_{19}\text{H}_{21}\text{NO}_4$ $[\text{M}+\text{H}]^+$: 328.1549; found: 328.1529.

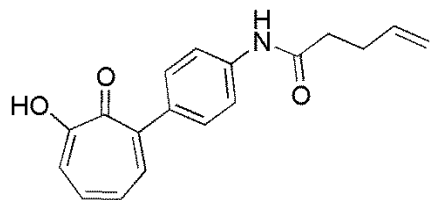


Am-NH₂-OH: yield: 73%. R_f = 0.68 (EtOAc). M_p = 243.2-244.4. IR (KBr): ν : 2979, 2782, 2726, 2650, 2578, 2524, 2487, 1452, 1342, 1313, 1269, 1238, 1217, 1181, 1064, 792, 780, 710. ^1H NMR (500 MHz, $\text{DMSO}-d_6$): δ 7.66 – 7.56 (m, 3H), 7.50 – 7.42 (m, 3H), 7.35 (d, J = 10.1 Hz, 1H), 7.15 (t, J = 9.9 Hz, 1H). ^{13}C NMR

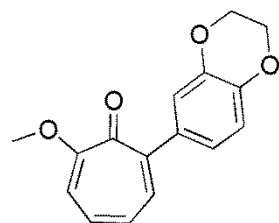
(125 MHz, DMSO- d_6): δ 172.87, 169.52, 140.20, 139.26, 137.09, 131.09, 127.72, 123.04, 120.93. HRMS (ESI) calcd for $C_{13}H_{11}NO_2$ $[M+H]^+$: 214.0868; found: 214.0870.



Am-Piv-OH: yield: 64%. R_f = 0.12 (1:1 EtOAc: Hexanes). M_p = oil. IR (KBr): ν : 3300, 3245, 3106, 3068, 2953, 2926, 2893, 2841, 2761, 1713, 1588, 1572, 1505, 1460, 1310, 1288, 1270, 1238, 1213, 1175, 1062, 749. 1H NMR (500 MHz, $CDCl_3$): δ 7.66 (d, J = 7.9 Hz, 2H), 7.62 (d, J = 10.2 Hz, 1H), 7.54 (d, J = 9.1 Hz, 2H), 7.46 – 7.37 (m, 3H), 7.11 (t, J = 10.7 Hz, 1H), 1.37 (s, 9H). ^{13}C NMR (125 MHz, $CDCl_3$): δ 171.16, 170.46, 166.38, 148.14, 140.40, 138.22, 136.60, 130.09, 127.34, 121.94, 119.50, 117.72, 39.71, 27.65. HRMS (ESI) calcd for $C_{18}H_{19}NO_3$ $[M+H]^+$: 298.1443; found: 298.1474.

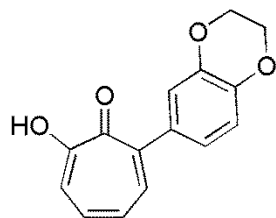


Am-P5-OH: yield: 65%. R_f = 0.13 (1:1 EtOAc: Hexanes). M_p = 127.2–128.5. IR (KBr): ν : 3296, 3178, 3079, 2977, 2922, 2855, 2250, 1770, 1657, 1591, 1515, 1473, 1408, 1361, 1315, 1290, 1275, 1243, 1228, 1180, 1117, 997. 1H NMR (500 MHz, $CDCl_3$): δ 9.85 (s, 1H), 7.63 (d, J = 9.4 Hz, 3H), 7.53 (d, J = 8.1 Hz, 2H), 7.49 – 7.39 (m, 2H), 7.13 (t, J = 9.8 Hz, 1H), 5.93 (ddt, J = 16.6, 10.5, 6.0 Hz, 1H), 5.17 (d, J = 17.1 Hz, 1H), 5.10 (d, J = 11.0 Hz, 1H), 2.54 (q, J = 4.3, 3.2 Hz, 4H). ^{13}C NMR (125 MHz, $CDCl_3$): δ 171.47, 170.65, 170.22, 140.49, 138.59, 137.99, 136.83, 136.64, 135.58, 133.92, 130.08, 127.47, 121.74, 119.50, 116.01, 36.87, 29.44. HRMS (ESI) calcd for $C_{18}H_{17}NO_3$ $[M+H]^+$: 296.1287; found: 296.1259.

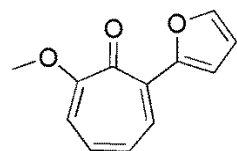


HC-1-OMe: yield: 95%. R_f = 0.47 (EtOAc). M_p = 117.2–118.4. IR (KBr): ν : 2978, 2930, 2876, 2759, 1730, 1588, 1571, 1503, 1456, 1420, 1354, 1304, 1268, 1246, 1211, 1173, 1156, 1126, 1086, 1063, 1047, 990, 933, 916, 888, 862, 815, 740. 1H NMR (500 MHz, $CDCl_3$): δ 7.48 (d, J = 9.0 Hz, 1H), 7.11 – 7.00 (m, 3H),

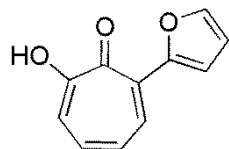
6.94 – 6.87 (m, 2H), 6.77 (d, J = 9.6 Hz, 1H), 4.32 (s, 4H), 3.99 (s, 3H). ^{13}C NMR (125 MHz, CDCl_3): δ 179.46, 165.68, 146.77, 143.57, 142.17, 136.96, 134.53, 131.14, 126.81, 122.75, 118.53, 116.81, 111.83, 64.53, 64.35, 56.48. HRMS (ESI) calcd for $\text{C}_{16}\text{H}_{14}\text{O}_4$ $[\text{M}+\text{H}]^+$: 271.0970; found: 271.0972.



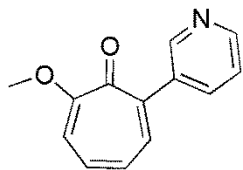
HC-1-OH: yield: 64%. R_f = 0.42 (1:1 EtOAc: Hexanes). M_p = 102.8-103.6. IR (KBr): ν : 3170, 2976, 2932, 2874, 1590, 1578, 1551, 1504, 1470, 1423, 1409, 1356, 1299, 1288, 1250, 1231, 1194, 1158, 1127, 1063, 1045, 1004, 924. ^1H NMR (500 MHz, CD_2Cl_2): δ 9.91 (s, 1H), 7.62 (d, J = 10.2 Hz, 1H), 7.47 – 7.38 (m, 2H), 7.14 – 7.04 (m, 3H), 6.99 (d, J = 8.3 Hz, 1H), 4.34 (s, 4H). ^{13}C NMR (125 MHz, CD_2Cl_2): δ : 170.92, 170.60, 143.79, 143.22, 140.44, 136.58, 133.02, 127.29, 122.66, 122.20, 118.44, 117.13, 64.54, 64.38, 30.99. HRMS (ESI) calcd for $\text{C}_{15}\text{H}_{12}\text{O}_4$ $[\text{M}+\text{H}]^+$: 257.0814; found: 257.0780.



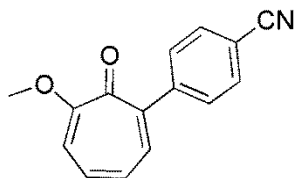
HC-2-OMe: yield: 84%. R_f = 0.65 (EtOAc). M_p = 96.8-97.7. IR (KBr): ν : 3242, 3151, 3105, 3068, 2842, 2761, 1714, 1617, 1549, 1474, 1366, 1271, 1242, 1216, 1180, 1154, 1073, 1017, 1006, 838, 825, 783, 734. ^1H NMR (500 MHz, CDCl_3): δ 8.25 (d, J = 9.2 Hz, 1H), 7.81 (d, J = 3.4 Hz, 1H), 7.56 (d, J = 1.7 Hz, 1H), 7.14 – 7.01 (m, 2H), 6.84 (d, J = 9.3 Hz, 1H), 6.60 (dd, J = 3.5, 1.8 Hz, 1H), 4.02 (s, 3H). ^{13}C NMR (125 MHz, CDCl_3): δ 176.63, 164.69, 150.97, 142.95, 134.57, 132.06, 131.12, 126.92, 115.80, 112.79, 112.05, 56.54. HRMS (ESI) calcd for $\text{C}_{12}\text{H}_{10}\text{O}_3$ $[\text{M}+\text{H}]^+$: 203.0708; found: 203.0722.



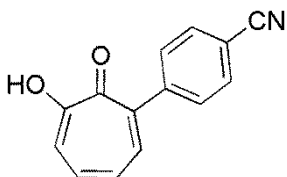
HC-2-OH: yield: 11%. R_f = 0.56 (1:1 EtOAc: Hexanes). ^1H NMR (500 MHz, CDCl_3): δ 10.08 (s, 1H), 8.42 (d, J = 10.4 Hz, 1H), 7.82 (d, J = 3.4 Hz, 1H), 7.61 (s, 1H), 7.43 (d, J = 10.1 Hz, 1H), 7.35 (t, J = 10.0 Hz, 1H), 7.20 (t, J = 10.1 Hz, 1H), 6.64 (dd, J = 3.5, 1.8 Hz, 1H). ^{13}C NMR (125 MHz, CDCl_3): δ 171.10, 167.70, 150.45, 143.51, 135.92, 134.66, 127.54, 119.37, 116.48, 113.02. HRMS (ESI) calcd for $\text{C}_{11}\text{H}_8\text{O}_3$ $[\text{M}+\text{H}]^+$: 189.0552; found: 189.0557.



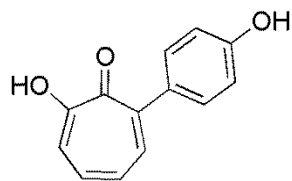
HC-3-OMe: yield: 68%. R_f = 0.08 (EtOAc). M_p = oil. IR (KBr): ν : 3443, 3026, 2965, 2927, 2838, 2769, 2232, 1731, 1615, 1592, 1564, 1495, 1462, 1411, 1359, 1329, 1271, 1216, 1189, 1163, 1091, 1043, 1025, 971. ^1H NMR (500 MHz, CD_2Cl_2): δ 8.64 (d, J = 6.3 Hz, 2H), 7.44 (d, J = 8.9 Hz, 1H), 7.39 (d, J = 6.3 Hz, 2H), 7.13 (d, J = 10.7 Hz, 1H), 6.93 (d, J = 10.7 Hz, 1H), 6.79 (d, J = 11.0 Hz, 1H), 3.98 (s, 3H). ^{13}C NMR (125 MHz, CD_2Cl_2): δ 178.61, 166.48, 149.71, 144.79, 137.90, 133.19, 126.86, 124.23, 112.18, 56.76. HRMS (ESI) calcd for $\text{C}_{13}\text{H}_{11}\text{NO}_2$ $[\text{M}+\text{H}]^+$: 214.0868; found: 214.0898.



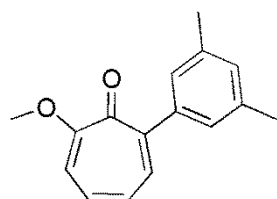
BA-pCN-OMe: yield: 72%. R_f = 0.47 (EtOAc). M_p = 105.7-106.9. IR (KBr): ν : 3056, 3012, 2971, 2941, 2899, 2836, 2224, 1597, 1572, 1538, 1465, 1352, 1272, 1223, 1163, 1092, 972. ^1H NMR (500 MHz, CDCl_3): δ 7.70 – 7.67 (m, 2H), 7.56 (d, J = 8.6 Hz, 2H), 7.44 (d, J = 8.9 Hz, 1H), 7.15 (t, J = 9.6 Hz, 1H), 6.94 (t, J = 10.6 Hz, 1H), 6.81 (d, J = 9.7 Hz, 1H), 3.99 (s, 3H). ^{13}C NMR (125 MHz, CDCl_3): δ 178.60, 166.37, 146.00, 145.49, 137.86, 132.95, 132.12, 132.04, 131.92, 131.77, 130.18, 128.54, 128.45, 126.72, 118.87, 112.13, 111.45, 56.61. HRMS (ESI) calcd for $\text{C}_{15}\text{H}_{11}\text{NO}_2$ $[\text{M}+\text{H}]^+$: 238.0868; found: 238.0857.



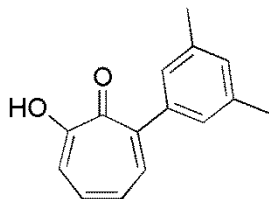
BA-pCN-OH: yield: 24%. R_f = 0.68 (EtOAc). M_p = 144.1-145.2. IR (KBr): ν : 3238, 3106, 3069, 2846, 2763, 1714, 1618, 1510, 1460, 1368, 1321, 1271, 1237, 1178, 827, 799, 781, 769, 758. ^1H NMR (500 MHz, CD_2Cl_2): δ 7.79 (d, J = 8.0 Hz, 2H), 7.67 (d, J = 8.0 Hz, 2H), 7.61 (d, J = 9.6 Hz, 1H), 7.52 – 7.44 (m, 2H), 7.17 (ddd, J = 9.9, 8.4, 2.5 Hz, 1H). ^{13}C NMR (125 MHz, $\text{DMSO}-d_6$): δ 172.91, 169.60, 145.93, 140.18, 138.86, 137.57, 132.32, 130.83, 127.71, 120.79, 119.26, 110.82. HRMS (ESI) calcd for $\text{C}_{14}\text{H}_9\text{NO}_2$ $[\text{M}+\text{H}]^+$: 224.0712; found: 224.0711.



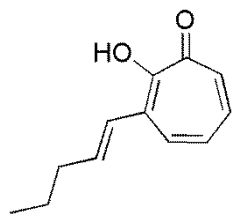
BA-pOH-OH: yield: 84%. R_f = 0.79 (EtOAc). M_p = 178.1-179.0. IR (KBr): ν : 3248, 3108, 3068, 2924, 2762, 1720, 1618, 1587, 1545, 1511, 1433, 1370, 1338, 1291, 1272, 1239, 1175, 1156, 1104, 1072, 838, 825, 800, 780, 767. ^1H NMR (500 MHz, Methanol- d_4): δ 7.66 (d, J = 10.2 Hz, 1H), 7.47 – 7.39 (m, 2H), 7.36 (d, J = 8.3 Hz, 2H), 7.16 (t, J = 9.4 Hz, 1H), 6.85 (d, J = 8.3 Hz, 2H), 5.48 (s, 1H). ^{13}C NMR (125 MHz, Methanol- d_4): δ 173.07, 171.71, 158.92, 142.01, 141.43, 137.84, 132.73, 131.99, 129.11, 123.32, 116.10, 54.95. HRMS (ESI) calcd for $\text{C}_{13}\text{H}_{10}\text{O}_3$ $[\text{M}+\text{H}]^+$: 215.0708; found: 215.0709.



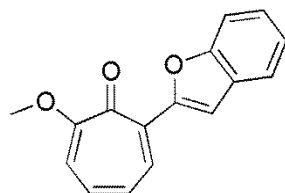
MO-DMe-OMe: yield: 87%. R_f = 0.47 (EtOAc). IR (KBr): ν : 3339, 3033, 3007, 2918, 2855, 2728, 1734, 1595, 1574, 1492, 1458, 1403, 1379, 1352, 1310, 1273, 1242, 1213, 1184, 1150, 1098, 1033, 995. ^1H NMR (500 MHz, CDCl_3): δ 7.45 (d, J = 8.9 Hz, 1H), 7.10 (s, 2H), 7.05 – 6.99 (m, 2H), 6.87 (t, J = 10.6 Hz, 1H), 6.74 (d, J = 9.6 Hz, 1H), 3.95 (s, 3H), 2.36 (s, 6H). ^{13}C NMR (125 MHz, CDCl_3): δ 179.83, 165.86, 148.05, 141.47, 137.62, 137.26, 131.48, 129.75, 127.19, 127.01, 111.98, 56.60, 21.51. HRMS (ESI) calcd for $\text{C}_{16}\text{H}_{16}\text{O}_2$ $[\text{M}+\text{H}]^+$: 241.1229; found: 241.1224.



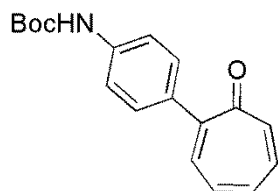
MO-DMe-OH: yield: 70%. R_f = 0.5 (1:1 EtOAc: Hexanes). IR (KBr): ν : 3157, 3034, 2916, 2858, 1614, 1599, 1548, 1474, 1456, 1364, 1314, 1256, 1214, 1093, 987. ^1H NMR (500 MHz, CDCl_3): δ 7.61 (d, J = 10.2 Hz, 1H), 7.48 – 7.40 (m, 2H), 7.17 – 7.08 (m, 4H), 2.42 (s, 6H). ^{13}C NMR (125 MHz, CDCl_3): δ 170.93, 170.74, 140.58, 139.80, 138.87, 137.84, 136.71, 129.96, 127.23, 126.89, 122.45, 21.39. HRMS (ESI) calcd for $\text{C}_{15}\text{H}_{14}\text{O}_2$ $[\text{M}+\text{H}]^+$: 227.1072; found: 227.1073.



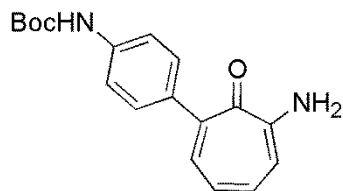
MO-3-OH: yield: 31%. R_f = 0.59 (1:1 EtOAc: Hexanes). M_p = oil. ^1H NMR (500 MHz, CD_2Cl_2): δ 7.76 (d, J = 10.3 Hz, 1H), 7.40 – 7.30 (m, 2H), 7.08 – 7.00 (m, 2H), 6.51 (dt, J = 15.3, 6.9 Hz, 1H), 2.32 (q, J = 7.2, 1.5 Hz, 2H), 1.58 (m, 2H), 1.00 (t, J = 7.4 Hz, 3H). ^{13}C NMR (125 MHz, CD_2Cl_2): δ 170.71, 169.16, 157.19, 137.46, 136.00, 135.75, 127.80, 127.23, 121.73, 35.75, 22.38, 13.77. HRMS (ESI) calcd for $\text{C}_{12}\text{H}_{14}\text{O}_2$ $[\text{M}+\text{H}]^+$: 190.2384; found: 191.1049.



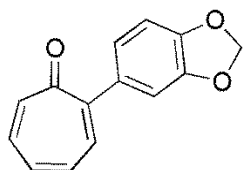
HC-4-OMe: yield: 65%. R_f = 0.29 (1:1 EtOAc: Hexanes). M_p = 151.2-152.1. IR (KBr): ν : 2925, 2853, 2367, 1973, 1734, 1597, 1573, 1537, 1467, 1412, 1364, 1276, 1221, 1191, 1165, 1151, 1142, 1107, 1082, 1017, 981. ^1H NMR (500 MHz, CD_2Cl_2): δ 8.49 (d, J = 9.3 Hz, 1H), 8.21 (s, 1H), 7.70 (d, J = 7.7 Hz, 1H), 7.52 (d, J = 8.2 Hz, 1H), 7.39 – 7.34 (m, 1H), 7.29 (dd, J = 14.9, 7.4 Hz, 1H), 7.15 (dt, J = 32.2, 10.1 Hz, 2H), 6.86 (d, J = 9.4 Hz, 1H), 4.04 (s, 3H). ^{13}C NMR (125 MHz, CD_2Cl_2): δ 164.78, 154.29, 134.13, 133.94, 132.42, 129.72, 126.83, 125.60, 123.01, 122.24, 112.05, 111.95, 110.75, 56.67. HRMS (ESI) calcd for $\text{C}_{16}\text{H}_{12}\text{O}_3$ $[\text{M}+\text{H}]^+$: 253.0865; found: 253.0843.



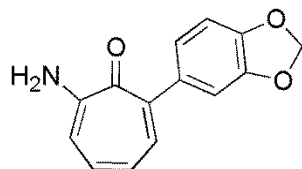
Am-Boc-H: yield: 99%. R_f = 0.34 (1:1 EtOAc: Hexanes). M_p = 175.8-176.4. IR (KBr): ν : 3257, 3176, 3094, 3044, 3002, 2984, 2964, 2927, 1715, 1624, 1597, 1547, 1530, 1501, 1466, 1450, 1414, 1387, 1363, 1317, 1260, 1237, 1153, 1125, 1049, 1028, 1017, 901. ^1H NMR (500 MHz, CDCl_3): δ 7.52 (d, J = 8.5 Hz, 2H), 7.43 (d, J = 8.4 Hz, 2H), 7.40 (d, J = 9.1 Hz, 1H), 7.24 – 7.13 (m, 2H), 7.07 (t, J = 9.6 Hz, 1H), 6.99 (ddt, J = 10.9, 7.5, 1.2 Hz, 1H), 6.66 (s, 1H), 1.57 (s, 9H). ^{13}C NMR (125 MHz, CDCl_3): δ 186.59, 152.61, 151.84, 142.09, 138.75, 135.97, 135.13, 134.41, 133.71, 132.88, 130.05, 117.95, 28.36. HRMS (ESI) calcd for $\text{C}_{18}\text{H}_{19}\text{NO}_3$ $[\text{M}+\text{H}]^+$: 298.1443; found: 298.1430.



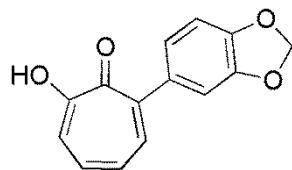
Am-Boc-NH2: yield: 71%. $R_f = 0.39$ (1:1 EtOAc: Hexanes). IR (KBr): ν : 3420, 3243, 3112, 2981, 2937, 2358, 2121, 2017, 1963, 1702, 1587, 1511, 1429, 1345, 1229, 1158, 1056, 833. ^1H NMR (500 MHz, CDCl_3): δ 7.55 (d, $J = 9.6$ Hz, 1H), 7.49 (d, $J = 8.6$ Hz, 2H), 7.44 (d, $J = 8.4$ Hz, 2H), 7.16 (t, $J = 10.8$ Hz, 1H), 6.95 (d, $J = 9.9$ Hz, 1H), 6.82 (t, $J = 9.8$ Hz, 1H), 6.57 (s, 1H), 6.08 (s, 2H), 1.58 (s, 9H). HRMS (ESI) calcd for $\text{C}_{18}\text{H}_{20}\text{N}_2\text{O}_3$ $[\text{M}+\text{H}]^+$: 313.1552; found: 313.1574.



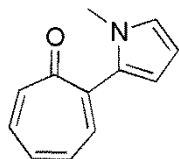
HC-5-H: yield: 97%. $R_f = 0.59$ (1:1 EtOAc: Hexanes). $M_p = 115.7$ -116.8. IR (KBr): ν : 3206, 3084, 3061, 2976, 2902, 2789, 1628, 1570, 1498, 1485, 1461, 1389, 1334, 1295, 1253, 1236, 1102, 1032, 925. ^1H NMR (500 MHz, CDCl_3): δ 7.38 (d, $J = 8.8$ Hz, 1H), 7.22 – 7.12 (m, 2H), 7.10 – 6.96 (m, 4H), 6.88 (d, $J = 8.0$ Hz, 1H), 6.02 (s, 2H). ^{13}C NMR (125 MHz, CDCl_3): δ 186.50, 151.93, 147.97, 147.32, 142.01, 136.04, 135.16, 133.84, 133.60, 133.03, 123.21, 109.98, 109.93, 108.13, 101.24. HRMS (ESI) calcd for $\text{C}_{14}\text{H}_{10}\text{O}_3$ $[\text{M}+\text{H}]^+$: 227.0708; found: 227.0720.



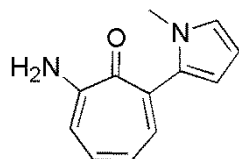
HC-5-NH2: yield: 86%. $R_f = 0.33$ (1:1 EtOAc: Hexanes). $M_p = 133.4$ -134.6. IR (KBr): ν : 3402, 3241, 3182, 3143, 3111, 3011, 2923, 2879, 2852, 2777, 1605, 1500, 1486, 1458, 1429, 1348, 1282, 1228, 1197, 1092, 1034, 930. ^1H NMR (500 MHz, CDCl_3): δ 7.54 (d, $J = 9.7$ Hz, 1H), 7.17 (t, $J = 10.1$ Hz, 1H), 7.07 (d, $J = 1.7$ Hz, 1H), 6.98 – 6.93 (m, 2H), 6.90 (d, $J = 8.0$ Hz, 1H), 6.81 (t, $J = 9.2$ Hz, 1H), 6.11 (s, 2H), 6.02 (s, 2H). ^{13}C NMR (125 MHz, CDCl_3): δ 174.47, 147.14, 146.97, 138.49, 136.31, 135.13, 123.10, 123.03, 112.52, 110.37, 110.00, 108.03, 101.02. HRMS (ESI) calcd for $\text{C}_{14}\text{H}_{11}\text{NO}_3$ $[\text{M}+\text{H}]^+$: 242.0817; found: 242.0804.



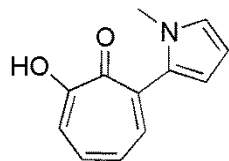
HC-5-OH: yield: 99%. R_f = 0.30 (1:1 EtOAc: Hexanes). IR (KBr): ν : 2892, 2711, 2643, 2547, 2484, 2064, 1944, 1714, 1615, 1587, 1570, 1548, 1435, 1387, 1286, 1230, 1187, 1092, 1034, 933. ^1H NMR (500 MHz, CDCl_3): δ 9.81 (s, 1H), 7.63 (dd, J = 10.2, 1.0 Hz, 1H), 7.48 – 7.38 (m, 2H), 7.14 – 7.08 (m, 2H), 7.02 (dd, J = 8.0, 1.8 Hz, 1H), 6.94 (d, J = 8.0 Hz, 1H), 6.06 (s, 2H). ^{13}C NMR (125 MHz, CDCl_3): δ 170.30, 147.72, 147.46, 140.43, 138.62, 136.60, 133.68, 127.27, 123.16, 121.88, 110.01, 108.28, 101.30. HRMS (ESI) calcd for $\text{C}_{14}\text{H}_{10}\text{O}_4$ $[\text{M}+\text{H}]^+$: 243.0657; found: 243.0666.



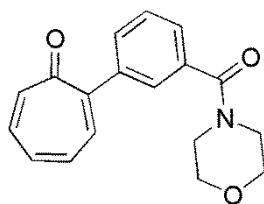
HC-6-H: yield: 67%. R_f = 0.40 (1:1 EtOAc: Hexanes). M_p = 80.0-81.4. IR (KBr): ν : 3116, 3094, 3052, 2979, 2925, 2880, 2361, 1623, 1563, 1510, 1460, 1405, 1379, 1364, 1309, 1275, 1251, 1237, 1217, 1180, 1091, 1054, 1012, 950. ^1H NMR (500 MHz, CDCl_3): δ 7.46 (d, J = 8.8 Hz, 1H), 7.20 – 7.16 (m, 2H), 7.06 (t, J = 11.0 Hz, 1H), 7.02 – 6.96 (m, 1H), 6.79 (t, J = 4.5 Hz, 1H), 6.38 (dd, J = 3.6, 1.8 Hz, 1H), 6.22 (dd, J = 3.7, 2.6 Hz, 1H), 3.57 (s, 3H). ^{13}C NMR (125 MHz, CDCl_3): δ 186.26, 144.92, 141.31, 137.27, 135.33, 133.64, 133.04, 125.11, 112.55, 108.13, 35.51. HRMS (ESI) calcd for $\text{C}_{12}\text{H}_{11}\text{NO}$ $[\text{M}+\text{H}]^+$: 186.0919; found: 186.0938.



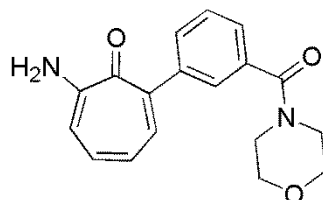
HC-6-NH2: yield: 67%. R_f = 0.71 (EtOAc). M_p = 183.5-184.7. IR (KBr): ν : 3391, 3374, 3243, 3119, 1611, 1517, 1482, 1449, 1421, 1402, 1330, 1304, 1237, 1190, 1087, 1038, 917. ^1H NMR (500 MHz, CD_2Cl_2): δ 7.92 (dd, J = 9.8, 1.3 Hz, 1H), 7.60 (td, J = 10.0, 1.2 Hz, 1H), 7.46 (d, J = 11.4 Hz, 1H), 7.20 – 7.01 (m, 2H), 6.55 – 6.37 (m, 2H), 4.86 (d, J = 5.4 Hz, 2H), 3.74 (s, 3H). ^{13}C NMR (125 MHz, CD_2Cl_2): δ 175.69, 160.74, 142.32, 138.49, 137.38, 135.14, 124.63, 124.18, 115.47, 111.14, 109.11, 36.22. HRMS (ESI) calcd for $\text{C}_{12}\text{H}_{12}\text{N}_2\text{O}$ $[\text{M}+\text{H}]^+$: 201.1028; found: 201.1040.



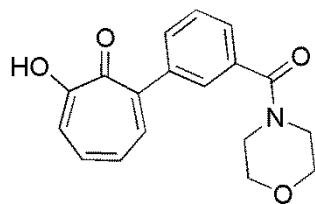
HC-6-OH: yield: 99%. R_f = 0.34 (EtOAc). M_p = 69.8-71.0. IR (KBr): ν : 3197, 2898, 2711, 2642, 1944, 1713, 1606, 1589, 1550, 1483, 1452, 1430, 1415, 1367, 1287, 1088, 1034, 934. ^1H NMR (500 MHz, CDCl_3): δ 7.68 (d, J = 10.2, 1.0 Hz, 1H), 7.49 – 7.39 (m, 2H), 7.10 (t, J = 10.5 Hz, 1H), 6.84 (t, J = 2.2 Hz, 1H), 6.35 – 6.25 (m, 2H), 3.56 (s, 3H). ^{13}C NMR (125 MHz, CDCl_3): δ 171.20, 169.75, 141.43, 136.82, 132.50, 131.19, 127.08, 124.44, 121.94, 111.11, 108.22, 35.29. HRMS (ESI) calcd for $\text{C}_{12}\text{H}_{11}\text{NO}_2$ $[\text{M}+\text{H}]^+$: 202.0868; found: 202.0878.



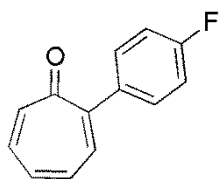
HC-7-H: yield: 74%. R_f = 0.05 (1:1 EtOAc: Hexanes). M_p = oil. ^1H NMR (500 MHz, CDCl_3): δ 7.70 – 7.65 (m, 1H), 7.60 – 7.45 (m, 3H), 7.42 (ddd, J = 8.4, 5.6, 1.3 Hz, 1H), 7.24 – 7.17 (m, 1H), 7.13 – 7.02 (m, 1H), 3.86 – 3.60 (m, 8H). ^{13}C NMR (125 MHz, CDCl_3): δ 186.21, 170.13, 151.46, 142.59, 140.78, 140.05, 136.91, 136.14, 135.57, 134.95, 133.81, 133.75, 130.65, 129.18, 128.55, 128.45, 128.18, 127.23, 126.24, 125.90, 66.91. HRMS (ESI) calcd for $\text{C}_{18}\text{H}_{17}\text{NO}_3$ $[\text{M}+\text{H}]^+$: 296.1287; found: 296.1299.



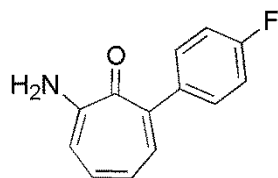
HC-7-NH2: yield: 52%. R_f = 0.29 (EtOAc). IR (KBr): ν : 3408, 3277, 3190, 3051, 2962, 2918, 2852, 1592, 1517, 1455, 1428, 1342, 1300, 1268, 1238, 1208, 1110, 1067, 1022, 949. ^1H NMR (500 MHz, CDCl_3): δ 7.59 (dt, J = 10.0, 1.9 Hz, 2H), 7.55 – 7.47 (m, 2H), 7.43 (dt, J = 7.6, 1.5 Hz, 1H), 7.19 (t, J = 10.0, 1.1 Hz, 1H), 6.96 (d, J = 10.0 Hz, 1H), 6.81 (t, J = 9.8 Hz, 1H), 6.31 (s, 2H), 3.75 (m, 8H). ^{13}C NMR (125 MHz, CDCl_3): δ 174.08, 158.22, 142.66, 140.84, 138.72, 135.85, 134.77, 131.18, 128.57, 128.20, 126.11, 123.08, 112.72, 66.98. HRMS (ESI) calcd for $\text{C}_{18}\text{H}_{18}\text{N}_2\text{O}_3$ $[\text{M}+\text{H}]^+$: 311.1396; found: 311.1379.



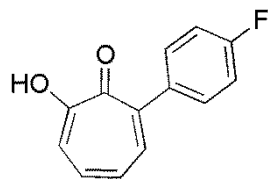
HC-7-OH: yield: 63%. R_f = 0.16 (EtOAc). M_p = 224.7-225.8. IR (KBr): ν : 2961, 2812, 2651, 2540, 1673, 1594, 1546, 1472, 1416, 1381, 1356, 1311, 1282, 1247, 1190, 1175, 1120, 1090, 998, 936. ^1H NMR (500 MHz, $\text{DMSO}-d_6$): δ 12.98 (s, 1H), 8.06 (d, J = 1.8 Hz, 1H), 7.98 (d, J = 7.7 Hz, 1H), 7.74 (d, J = 7.3 Hz, 1H), 7.67 (d, J = 9.8 Hz, 1H), 7.59 (t, J = 7.7 Hz, 1H), 7.47 (t, J = 10.1 Hz, 1H), 7.36 (d, J = 10.3 Hz, 1H), 7.16 (t, J = 9.9 Hz, 1H), 3.35 (s, 8H). ^{13}C NMR (125 MHz, $\text{DMSO}-d_6$): δ 172.85, 169.61, 167.59, 141.20, 140.26, 139.29, 137.15, 134.16, 130.99, 130.65, 129.09, 128.81, 127.78, 120.99. HRMS (ESI) calcd for $\text{C}_{18}\text{H}_{17}\text{NO}_4$ $[\text{M}+\text{H}]^+$: 311.3319; found: 311.3307.



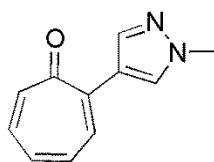
MO-pF-H: yield: 99%. R_f = 0.47 (1:1 EtOAc: Hexanes). M_p = 69.6-70.4. IR (KBr): ν : 3033, 2967, 2924, 2862, 1628, 1558, 1519, 1503, 1451, 1416, 1383, 1266, 1233, 1216, 1197, 1161, 1097, 981. ^1H NMR (500 MHz, CDCl_3): δ 7.54 – 7.49 (m, 2H), 7.36 (d, J = 8.6 Hz, 1H), 7.23 – 7.15 (m, 2H), 7.15 – 7.08 (m, 2H), 7.07 – 6.97 (m, 2H). ^{13}C NMR (125 MHz, CDCl_3): δ 186.29, 163.82, 161.85, 151.32, 142.33, 136.45, 135.87, 135.84, 135.33, 133.61, 133.41, 131.13, 131.06, 115.12, 114.95. HRMS (ESI) calcd for $\text{C}_{13}\text{H}_9\text{FO}$ $[\text{M}+\text{H}]^+$: 201.0716; found: 201.0745.



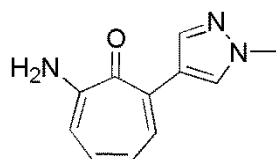
MO-pF-NH₂: yield: 81%. R_f = 0.81 (EtOAc). M_p = 200.7-202.0. IR (KBr): ν : 3427, 3271, 3149, 1595, 1498, 1449, 1429, 1400, 1347, 1268, 1215, 1154, 1091, 1011, 912. ^1H NMR (500 MHz, CDCl_3): δ 7.57 – 7.46 (m, 3H), 7.17 (dt, J = 25.4, 9.4 Hz, 3H), 6.97 (d, J = 9.9 Hz, 1H), 6.83 (t, J = 9.8 Hz, 1H), 6.13 (s, 2H). ^{13}C NMR (125 MHz, CDCl_3): δ 174.35, 163.15, 157.78, 141.24, 138.60, 135.42, 131.26, 131.20, 123.15, 114.92, 114.75, 112.56. HRMS (ESI) calcd for $\text{C}_{13}\text{H}_{10}\text{FNO}$ $[\text{M}+\text{H}]^+$: 216.0825; found: 216.0845.



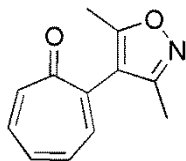
MO-pF-OH: yield: 92%. R_f = 0.59 (EtOAc). M_p = 134.1-135.0. IR (KBr): ν : 2536, 2214, 1896, 1603, 1541, 1507, 1489, 1459, 1422, 1384, 1363, 1294, 1279, 1243, 1227, 1191, 1166, 1103, 914. ^1H NMR (500 MHz, CDCl_3): δ 7.62 (d, J = 10.1 Hz, 1H), 7.57 – 7.52 (m, 2H), 7.50 – 7.40 (m, 2H), 7.19 (t, J = 8.7 Hz, 2H), 7.14 (t, J = 9.7 Hz, 1H). ^{13}C NMR (125 MHz, CDCl_3): δ 171.50, 170.24, 140.46, 138.17, 136.83, 135.75, 131.18, 131.12, 127.36, 121.65, 115.36, 115.19. HRMS (ESI) calcd for $\text{C}_{13}\text{H}_9\text{FO}_2$ $[\text{M}+\text{H}]^+$: 217.0665; found: 217.0669.



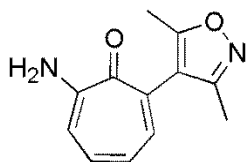
HC-8-H: yield: 99%. R_f = 0.13 (1:1 EtOAc: Hexanes). M_p = 59.8-61.0. IR (KBr): ν : 3163, 3014, 2925, 2852, 1624, 1570, 1537, 1500, 1460, 1436, 1408, 1393, 1378, 1274, 1226, 1188, 1159, 1118, 1063, 1024, 981. ^1H NMR (500 MHz, CDCl_3): δ 8.48 (s, 1H), 7.88 (s, 1H), 7.68 (d, J = 9.2 Hz, 1H), 7.17 – 7.10 (m, 2H), 7.07 (t, J = 10.0 Hz, 1H), 6.94 (ddd, J = 10.0, 7.0, 2.0 Hz, 1H), 3.92 (s, 3H). ^{13}C NMR (125 MHz, CDCl_3): δ 185.11, 143.50, 140.39, 138.84, 134.94, 133.74, 132.83, 132.19, 132.09, 132.01, 131.92, 131.71, 119.66, 39.08. HRMS (ESI) calcd for $\text{C}_{11}\text{H}_{10}\text{N}_2\text{O}$ $[\text{M}+\text{H}]^+$: 187.0871; found: 187.0899.



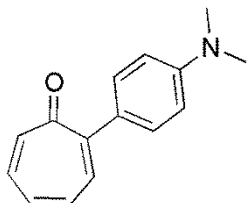
HC-8-NH2: yield: 57%. R_f = 0.38 (EtOAc). M_p = 143.6-144.8. IR (KBr): ν : 3383, 3274, 3154, 3053, 2957, 2923, 2852, 1627, 1594, 1569, 1515, 1475, 1434, 1410, 1369, 1298, 1236, 1171, 1117, 1058, 991. ^1H NMR (500 MHz, CDCl_3): δ 8.55 (s, 1H), 7.95 (s, 1H), 7.91 (d, J = 10.0 Hz, 1H), 7.14 (t, J = 9.9 Hz, 1H), 6.97 (d, J = 10.0 Hz, 1H), 6.85 (t, J = 9.9 Hz, 1H), 6.17 (s, 2H), 3.99 (s, 3H). ^{13}C NMR (125 MHz, CDCl_3): δ 173.00, 156.44, 138.81, 134.74, 134.39, 133.12, 132.20, 132.06, 123.38, 121.74, 113.33, 39.03. HRMS (ESI) calcd for $\text{C}_{11}\text{H}_{11}\text{N}_3\text{O}$ $[\text{M}+\text{H}]^+$: 202.0980; found: 202.0999.



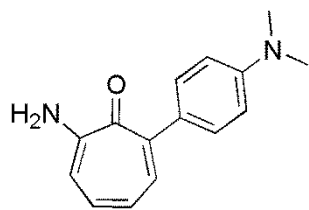
HC-9-H: yield: 75%. $R_f = 0.34$ (1:1 EtOAc: Hexanes). ^1H NMR (500 MHz, CDCl_3): δ 7.28 – 7.24 (m, 1H), 7.23 – 7.20 (m, 1H), 7.10 – 7.05 (m, 2H), 2.39 (s, 3H), 2.22 (s, 3H). ^{13}C NMR (125 MHz, CDCl_3): δ 166.96, 143.19, 141.78, 137.88, 135.64, 134.44, 133.24, 115.76, 12.02, 10.95. HRMS (ESI) calcd for $\text{C}_{12}\text{H}_{11}\text{NO}_2$ $[\text{M}+\text{H}]^+$: 202.0868; found: 202.0892.



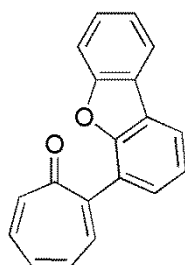
HC-9-NH₂: yield: 63%. $R_f = 0.65$ (EtOAc). $M_p = 210.0\text{--}211.1$. IR (KBr): ν : 3403, 3236, 3179, 3113, 3018, 2927, 2851, 1609, 1513, 1450, 1409, 1366, 1332, 1279, 1238, 1211, 1119, 1049, 1034, 971. ^1H NMR (500 MHz, CDCl_3): δ 7.36 (d, $J = 9.6$ Hz, 1H), 7.24 (t, $J = 10.1$ Hz, 1H), 6.99 (d, $J = 10.1$ Hz, 1H), 6.80 (t, $J = 10.2$ Hz, 1H), 6.29 (s, 2H), 2.35 (s, 3H), 2.20 (s, 3H). ^{13}C NMR (125 MHz, CDCl_3): δ 173.82, 165.83, 159.83, 157.11, 139.26, 136.44, 132.13, 132.05, 131.06, 128.60, 128.51, 122.54, 117.47, 112.59, 11.80, 10.95. HRMS (ESI) calcd for $\text{C}_{12}\text{H}_{12}\text{N}_2\text{O}_2$ $[\text{M}+\text{H}]^+$: 217.0977; found: 217.0982.



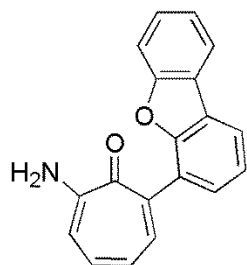
Am-DMe-H: yield: 73%. $R_f = 0.43$ (1:1 EtOAc: Hexanes). $M_p = 136.8\text{--}138.1$. IR (KBr): ν : 3116, 3064, 2994, 2949, 2920, 2878, 2852, 2800, 1624, 1599, 1563, 1523, 1502, 1479, 1460, 1444, 1350, 1326, 1291, 1260, 1226, 1209, 1193, 1164, 1120, 1062, 976. ^1H NMR (500 MHz, CDCl_3): δ 7.59 – 7.53 (m, 2H), 7.41 (d, $J = 9.1$ Hz, 1H), 7.18 (d, $J = 12.0$ Hz, 1H), 7.12 (ddd, $J = 12.0, 7.7, 1.2$ Hz, 1H), 7.05 (t, $J = 9.9$ Hz, 1H), 6.92 (dd, $J = 10.8, 7.8$ Hz, 1H), 6.80 – 6.75 (m, 2H), 3.04 (s, 6H). ^{13}C NMR (125 MHz, CDCl_3): δ 186.90, 152.22, 150.80, 141.28, 135.57, 134.83, 134.62, 133.74, 131.70, 131.48, 130.45, 127.41, 111.72, 40.36. HRMS (ESI) calcd for $\text{C}_{15}\text{H}_{15}\text{NO}$ $[\text{M}+\text{H}]^+$: 226.1232; found: 226.1251.



Am-DMe-NH₂: yield: 86%. R_f = 0.69 (EtOAc). M_p = 190.0-191.2. IR (KBr): ν : 3403, 3230, 3140, 3036, 2877, 2838, 2796, 1602, 1511, 1446, 1427, 1355, 1317, 1272, 1238, 1227, 1192, 1162, 1119, 1061, 1031, 1004, 947. ¹HNMR (500 MHz, CDCl₃): δ 7.58 (d, J = 9.7 Hz, 1H), 7.50 (d, J = 8.6 Hz, 2H), 7.10 (t, J = 10.0 Hz, 1H), 6.91 (d, J = 10.6 Hz, 1H), 6.85 – 6.76 (m, 3H), 6.10 (s, 2H), 3.03 (s, 6H). ¹³CNMR (125 MHz, CDCl₃): δ 174.71, 157.28, 150.04, 142.44, 137.99, 134.11, 130.54, 123.22, 112.60, 112.02, 40.62. HRMS (ESI) calcd for C₁₅H₁₆N₂O [M+H]⁺: 241.1341; found: 241.1363.

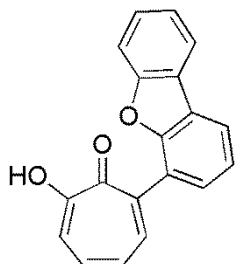


HC-10-H: yield: 99%. R_f = 0.59 (1:1 EtOAc: Hexanes). M_p = 115.1-116.2. IR (KBr): ν : 3051, 3028, 2922, 2257, 1627, 1568, 1449, 1385, 1266, 1185, 840. ¹HNMR (500 MHz, CDCl₃): δ 8.01 (ddd, J = 7.8, 4.0, 1.2 Hz, 2H), 7.64 (d, J = 8.5 Hz, 1H), 7.60 – 7.55 (m, 2H), 7.50 – 7.42 (m, 2H), 7.38 (t, J = 7.5 Hz, 1H), 7.31 (d, J = 12.1 Hz, 1H), 7.23 (ddd, J = 12.1, 7.6, 1.5 Hz, 1H), 7.14 – 7.03 (m, 2H). ¹³CNMR (125 MHz, CDCl₃): δ 186.04, 156.07, 153.24, 148.26, 142.09, 137.61, 135.30, 134.08, 133.58, 128.17, 127.20, 124.79, 124.61, 124.24, 122.80, 122.75, 120.84, 120.65, 111.87. HRMS (ESI) calcd for C₁₉H₁₂O₂ [M+H]⁺: 273.0916; found: 273.0925.

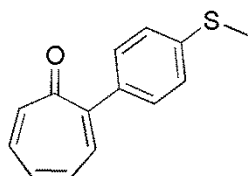


HC-10-NH₂: yield: 82%. R_f = 0.77 (EtOAc). M_p = 218.3-219.2. IR (KBr): ν : 3413, 3240, 3181, 3142, 3053, 1599, 1518, 1469, 1448, 1435, 1408, 1349, 1315, 1279, 1259, 1234, 1188, 1115, 1055, 847. ¹HNMR (500 MHz, CDCl₃): δ 8.00 (t, J = 7.7 Hz, 2H), 7.74 (d, J = 9.5 Hz, 1H), 7.54 (d, J = 7.9 Hz, 2H), 7.45 (td, J = 7.4, 2.6 Hz, 2H), 7.37 (t, J = 7.5 Hz, 1H), 7.27 (t, J = 10.1 Hz, 1H), 7.01 (d, J = 10.0 Hz, 1H), 6.88 (t, J = 9.8 Hz, 1H),

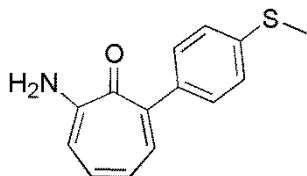
6.20 (s, 2H). ^{13}C NMR (125 MHz, CDCl_3): δ 174.13, 157.51, 156.10, 153.74, 139.30, 137.54, 136.11, 128.35, 126.91, 124.49, 124.39, 122.88, 122.61, 122.57, 120.55, 119.93, 112.43, 111.86. HRMS (ESI) calcd for $\text{C}_{19}\text{H}_{13}\text{NO}_2$ $[\text{M}+\text{H}]^+$: 288.1025; found: 288.1042.



HC-10-OH: yield: 91%. R_f = 0.64 (EtOAc). M_p = 53.8-55.0. IR (KBr): ν : 3051, 3028, 2922, 2852, 2538, 2359, 1923, 1627, 1568, 1449, 1386, 1266, 1185, 1117, 804. ^1H NMR (500 MHz, CDCl_3): δ 8.05 (ddd, J = 12.0, 7.7, 1.3 Hz, 2H), 7.82 (d, J = 10.0 Hz, 1H), 7.59 – 7.47 (m, 6H), 7.40 (t, J = 7.5 Hz, 1H), 7.19 (ddd, J = 10.4, 6.6, 4.0 Hz, 1H). ^{13}C NMR (125 MHz, CDCl_3): δ 170.81, 170.80, 156.11, 153.32, 141.05, 137.56, 133.64, 132.17, 128.43, 128.00, 127.33, 127.16, 124.74, 124.19, 122.88, 122.75, 122.42, 120.85, 120.72, 111.83. HRMS (ESI) calcd for $\text{C}_{19}\text{H}_{12}\text{O}_3$ $[\text{M}+\text{H}]^+$: 289.0865; found: 289.0863.

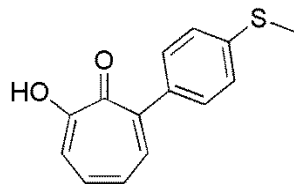


MO-pSMe-H: yield: 76%. R_f = 0.43 (1:1 EtOAc: Hexanes). M_p = 93.0-94.1. IR (KBr): ν : 3092, 3060, 3037, 3019, 2975, 2920, 1729, 1627, 1563, 1514, 1486, 1464, 1431, 1406, 1379, 1319, 1265, 1234, 1189, 1091, 1014, 970. ^1H NMR (500 MHz, CDCl_3): δ 7.48 (d, J = 8.3 Hz, 2H), 7.37 (d, J = 8.9 Hz, 1H), 7.30 (d, J = 8.3 Hz, 2H), 7.21 – 7.12 (m, 2H), 7.05 (t, J = 10.7 Hz, 1H), 7.01 – 6.95 (m, 1H), 2.53 (s, 3H). ^{13}C NMR (125 MHz, CDCl_3): δ 186.42, 151.77, 142.13, 139.32, 136.54, 136.08, 135.22, 133.67, 133.15, 129.63, 125.95, 15.64. HRMS (ESI) calcd for $\text{C}_{14}\text{H}_{12}\text{OS}$ $[\text{M}+\text{H}]^+$: 229.0687; found: 229.0668.

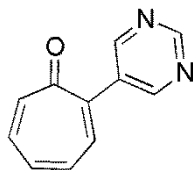


MO-pSMe-NH2: yield: 76%. R_f = 0.37 (1:1 EtOAc: Hexanes). M_p = 112.4-114.0. IR (KBr): ν : 3397, 3236, 3183, 3147, 2914, 1650, 1588, 1516, 1491, 1428, 1397, 1341, 1316, 1299, 1269, 1238, 1189, 1113, 1089, 1013, 967. ^1H NMR (500 MHz, CDCl_3): δ 7.54 (d, J = 9.6 Hz, 1H), 7.47 (d, J = 9.5 Hz, 2H), 7.37 – 7.32 (m, 2H), 7.17 (t, J = 10.0 Hz, 1H), 6.93 (d, J = 10.0 Hz, 1H), 6.82 (t, J = 9.8 Hz, 1H), 6.17 (s, 2H), 2.55 (s, 3H).

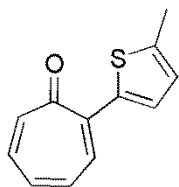
^{13}C NMR (125 MHz, CDCl_3): δ 174.34, 157.78, 141.57, 139.28, 138.42, 137.58, 135.27, 130.01, 126.29, 123.13, 112.60, 16.00. HRMS (ESI) calcd for $\text{C}_{14}\text{H}_{13}\text{NOS}$ $[\text{M}+\text{H}]^+$: 244.0796; found: 244.0788.



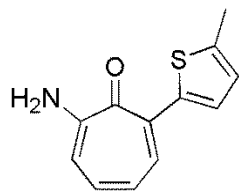
MO-pSMe-OH: yield: 79%. R_f = 0.61 (EtOAc). M_p = 122.0-123.4. IR (KBr): ν : 3139, 2919, 1619, 1592, 1555, 1547, 1470, 1433, 1397, 1362, 1319, 1300, 1274, 1262, 1241, 1216, 1200, 1190, 1112, 1094, 1059, 1014, 972. ^1H NMR (500 MHz, CDCl_3): δ 7.63 (d, J = 10.2 Hz, 1H), 7.51 (d, J = 8.1 Hz, 2H), 7.49 – 7.41 (m, 2H), 7.38 (d, J = 8.8 Hz, 2H), 7.13 (ddd, J = 10.1, 9.4, 1.4 Hz, 1H), 2.58 (s, 3H). ^{13}C NMR (125 MHz, CDCl_3): δ 171.28, 170.35, 140.34, 139.14, 138.43, 136.66, 136.44, 129.75, 127.38, 126.11, 121.83, 15.66. HRMS (ESI) calcd for $\text{C}_{14}\text{H}_{12}\text{O}_2\text{S}$ $[\text{M}+\text{H}]^+$: 245.0636; found: 245.0623.



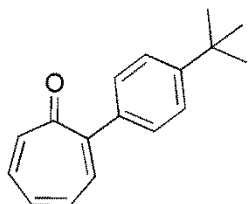
HC-11-H: yield: 69%. R_f = 0.27 (EtOAc). M_p = 174.9-176.0. IR (KBr): ν : 3024, 2975, 2361, 2336, 1672, 1628, 1557, 1518, 1465, 1433, 1413, 1398, 1352, 1271, 1238, 1190, 1167, 1114, 1046, 979. ^1H NMR (500 MHz, CDCl_3): δ 9.24 (s, 1H), 8.93 (s, 2H), 7.43 – 7.39 (m, 1H), 7.26 (dd, J = 3.8, 1.6 Hz, 2H), 7.13 (tt, J = 4.0, 1.7 Hz, 2H). ^{13}C NMR (125 MHz, CDCl_3): δ 185.28, 158.11, 156.73, 145.91, 142.89, 137.13, 136.01, 134.92, 133.56, 133.48, 109.99. HRMS (ESI) calcd for $\text{C}_{11}\text{H}_8\text{N}_2\text{O}$ $[\text{M}+\text{H}]^+$: 185.0715; found: 185.0719.



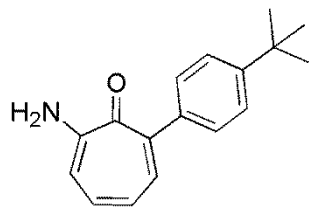
HC-12-H: yield: 97%. R_f = 0.57 (1:1 EtOAc: Hexanes). M_p = 66.4-67.5. IR (KBr): ν : 3076, 3060, 3009, 2962, 2912, 2852, 2362, 1754, 1618, 1563, 1490, 1461, 1439, 1391, 1379, 1326, 1286, 1235, 1208, 1161, 1060, 1033, 877. ^1H NMR (500 MHz, CDCl_3): δ 7.86 (d, J = 9.5 Hz, 1H), 7.56 (d, J = 3.9 Hz, 1H), 7.26 – 7.14 (m, 2H), 7.12 (t, J = 10.0 Hz, 1H), 6.99 (t, J = 10.6 Hz, 1H), 6.83 (d, J = 3.8 Hz, 1H), 2.56 (s, 3H). ^{13}C NMR (125 MHz, CDCl_3): δ 184.12, 146.52, 143.98, 139.99, 136.82, 135.16, 133.52, 132.34, 131.32, 128.43, 125.27, 15.44. HRMS (ESI) calcd for $\text{C}_{12}\text{H}_{10}\text{OS}$ $[\text{M}+\text{H}]^+$: 203.0531; found: 203.0563.



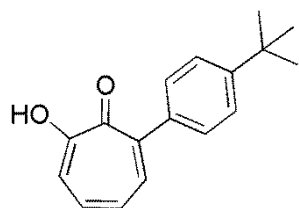
HC-12-NH2: yield: 34%. R_f = 0.56 (1:1 EtOAc: Hexanes). M_p = 101.8-103.0. IR (KBr): ν : 3445, 3399, 3281, 3178, 3143, 3065, 2922, 2853, 1735, 1595, 1561, 1505, 1425, 1376, 1353, 1311, 1266, 1239, 1216, 1164, 1107, 1063, 1006, 976. ^1H NMR (500 MHz, CDCl_3): δ 8.14 (d, J = 10.2 Hz, 1H), 7.52 (d, J = 3.8 Hz, 1H), 7.18 (t, J = 9.9 Hz, 1H), 6.99 (d, J = 10.1 Hz, 1H), 6.91 – 6.82 (m, 2H), 6.19 (s, 2H), 2.59 (s, 3H). ^{13}C NMR (125 MHz, CDCl_3): δ 171.81, 156.64, 143.58, 139.38, 134.76, 134.27, 134.11, 126.37, 124.31, 123.24, 113.87, 15.25. HRMS (ESI) calcd for $\text{C}_{12}\text{H}_{11}\text{NOS}$ $[\text{M}+\text{H}]^+$: 218.0640; found: 218.0654.



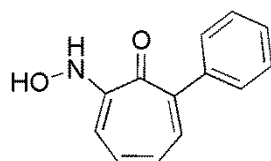
MO-11-H: yield: 94%. R_f = 0.67 (1:1 EtOAc: Hexanes). IR (KBr): ν : 3031, 2952, 2902, 2864, 2714, 1693, 1626, 1564, 1518, 1505, 1461, 1435, 1405, 1383, 1360, 1257, 1229, 1200, 1123, 1110, 1095, 1053, 1016, 979. ^1H NMR (500 MHz, CDCl_3): δ 7.49 (q, J = 8.5 Hz, 4H), 7.42 (d, J = 8.8 Hz, 1H), 7.22 (d, J = 12.0 Hz, 1H), 7.19 – 7.13 (m, 1H), 7.08 (t, J = 9.8 Hz, 1H), 6.99 (dd, J = 10.9, 7.6 Hz, 1H), 1.39 (s, 9H). ^{13}C NMR (125 MHz, CDCl_3): δ 186.66, 152.41, 151.53, 142.18, 136.96, 136.15, 135.07, 133.69, 132.91, 128.88, 125.13, 34.68, 31.32. HRMS (ESI) calcd for $\text{C}_{17}\text{H}_{18}\text{O}$ $[\text{M}+\text{H}]^+$: 239.1436; found: 239.1419.



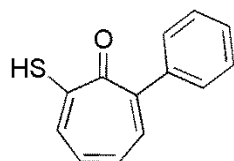
MO-11-NH2: yield: 87%. R_f = 0.80 (EtOAc). IR (KBr): ν : 3396, 3229, 3138, 2949, 2901, 2863, 2715, 1693, 1602, 1591, 1503, 1460, 1434, 1342, 1309, 1271, 1232, 1179, 1119, 1097, 1016, 986. ^1H NMR (500 MHz, CDCl_3): δ 7.58 (d, J = 9.7 Hz, 1H), 7.48 (d, J = 1.3 Hz, 4H), 7.16 (t, J = 10.0 Hz, 1H), 6.94 (d, J = 10.0 Hz, 1H), 6.82 (t, J = 9.8 Hz, 1H), 6.12 (s, 2H), 1.40 (s, 9H). ^{13}C NMR (125 MHz, CDCl_3): δ 174.55, 157.66, 150.20, 142.30, 139.34, 138.58, 134.97, 129.16, 124.92, 123.18, 112.45, 34.60, 31.40. HRMS (ESI) calcd for $\text{C}_{17}\text{H}_{19}\text{NO}$ $[\text{M}+\text{H}]^+$: 254.1500; found: 254.1508.



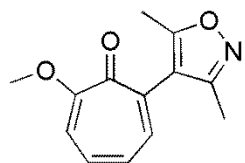
MO-11-OH: yield: 52%. R_f = 0.5 (1:1 EtOAc: Hexanes). IR (KBr): ν : 3169, 2962, 2902, 2867, 1714, 1615, 1592, 1550, 1475, 1455, 1435, 1416, 1360, 1236, 1202, 1110, 1065, 1022, 996. ^1H NMR (500 MHz, CDCl_3): δ 7.66 (d, J = 10.1 Hz, 1H), 7.53 (s, 4H), 7.49 – 7.38 (m, 2H), 7.12 (t, J = 9.7 Hz, 1H), 1.42 (s, 9H). ^{13}C NMR (125 MHz, CDCl_3): δ 171.11, 170.59, 151.35, 140.64, 138.77, 136.87, 136.59, 129.02, 127.38, 125.26, 122.07, 34.72, 31.36. HRMS (ESI) calcd for $\text{C}_{17}\text{H}_{18}\text{O}_2$ $[\text{M}+\text{H}]^+$: 255.1385; found: 255.1386.



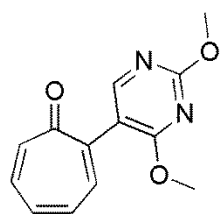
MO-NHOH-PH: yield: 18%. R_f = 0.79 (1:1 EtOAc: Hexanes). IR (KBr): ν : 3418, 2923, 2851, 2356, 1731, 1611, 1490, 1456, 1413, 1377, 1288, 1253, 1224, 1178, 1097, 1073, 1026, 996. ^1H NMR (500 MHz, CDCl_3): δ 10.16 (s, 1H), 8.34 (s, 1H), 7.64 (d, J = 7.5 Hz, 2H), 7.49 (dd, J = 89.2, 7.7 Hz, 3H), 7.43 – 7.39 (m, 2H), 7.24 (dd, J = 7.7, 1.7 Hz, 1H), 7.05 (t, J = 7.6 Hz, 1H). ^{13}C NMR (125 MHz, CDCl_3): δ 154.46, 153.32, 137.74, 132.58, 130.27, 129.78, 129.39, 128.15, 127.25, 119.77, 116.69. HRMS (ESI) calcd for $\text{C}_{13}\text{H}_{11}\text{NO}_2$ $[\text{M}+\text{H}]^+$: 214.0868; found: 214.0879.



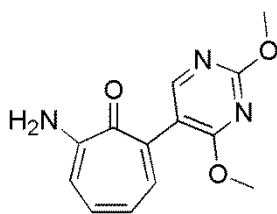
MO-SH-PH: yield: 59%. R_f = 0.68 (1:1 EtOAc: Hexanes). IR (KBr): ν : 3089, 3052, 3034, 3017, 2963, 2922, 2852, 2008, 1960, 1581, 1546, 1479, 1439, 1390, 1352, 1315, 1285, 1255, 1220, 1193, 1115, 1092, 1076, 1031, 1012, 987. ^1H NMR (500 MHz, CDCl_3): δ 10.06 (s, 1H), 8.61 (d, J = 10.4 Hz, 1H), 7.56 – 7.45 (m, 6H), 7.32 – 7.27 (m, 1H), 7.22 (t, J = 9.9 Hz, 1H). ^{13}C NMR (125 MHz, CDCl_3): δ 180.40, 172.11, 142.00, 140.90, 140.56, 136.44, 132.81, 131.88, 129.09, 128.39, 128.35. HRMS (ESI) calcd for $\text{C}_{13}\text{H}_{10}\text{OS}$ $[\text{M}+\text{H}]^+$: 215.0531; found: 215.0504.



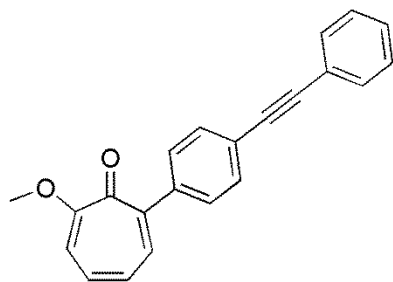
HC-9-OMe: yield: 87%. $R_f = 0.3$ (EtOAc). IR (KBr): ν : 3417, 3055, 2966, 2925, 2839, 1591, 1573, 1503, 1464, 1437, 1417, 1357, 1274, 1215, 1167, 1118, 1095, 968. ^1H NMR (500 MHz, CDCl_3): δ 7.37 (d, $J = 9.0$ Hz, 1H), 7.18 (t, $J = 10.2$ Hz, 1H), 6.94 (t, $J = 9.1$ Hz, 1H), 6.85 (d, $J = 9.7$ Hz, 1H), 4.02 (s, 3H), 2.36 (s, 3H), 2.20 (s, 3H). ^{13}C NMR (125 MHz, CDCl_3): δ 178.06, 166.43, 165.43, 159.56, 138.71, 137.46, 132.90, 132.15, 132.07, 131.93, 128.55, 128.46, 126.45, 116.65, 112.14, 56.58, 11.97, 11.00. HRMS (ESI) calcd for $\text{C}_{13}\text{H}_{13}\text{NO}_3$ $[\text{M}+\text{H}]^+$: 232.0974; found: 232.0984.



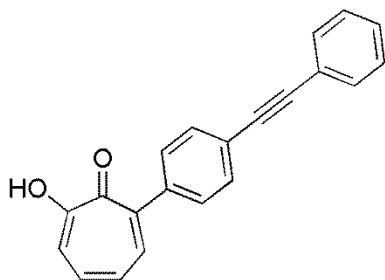
HC-13-H: yield: 99%. $R_f = 0.18$ (1:1 EtOAc: Hexanes). IR (KBr): ν : 3020, 3005, 2957, 2362, 1580, 1557, 1460, 1394, 1377, 1324, 1303, 1280, 1257, 1239, 1224, 1199, 1080, 1005, 936. ^1H NMR (500 MHz, CDCl_3): δ 8.22 (s, 1H), 7.37 – 7.32 (m, 1H), 7.22 – 7.13 (m, 2H), 7.07 – 7.00 (m, 2H), 4.06 (s, 3H), 4.00 (s, 3H). ^{13}C NMR (125 MHz, CDCl_3): δ 185.67, 168.08, 165.20, 158.04, 146.35, 141.34, 136.85, 135.35, 134.08, 133.32, 132.14, 132.06, 131.94, 128.55, 128.46, 115.67, 54.92, 54.22. HRMS (ESI) calcd for $\text{C}_{13}\text{H}_{12}\text{N}_2\text{O}_3$ $[\text{M}+\text{H}]^+$: 245.0926; found: 245.0900.



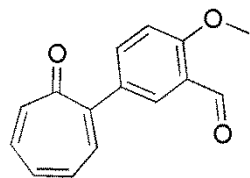
HC-13-NH2: yield: 58%. $R_f = 0.29$ (EtOAc). IR (KBr): ν : 3374, 3264, 3164, 2987, 2953, 2927, 2359, 1612, 1594, 1556, 1469, 1454, 1397, 1380, 1359, 1312, 1291, 1253, 1238, 1207, 1132, 1082, 1035, 1008, 974. ^1H NMR (500 MHz, CDCl_3): δ 8.18 (s, 1H), 7.41 (d, $J = 9.6$ Hz, 1H), 7.18 (t, $J = 10.1$ Hz, 1H), 6.95 (d, $J = 10.0$ Hz, 1H), 6.76 (t, $J = 9.8$ Hz, 1H), 6.39 (s, 2H), 4.04 (s, 3H), 3.96 (s, 3H). ^{13}C NMR (125 MHz, CDCl_3): δ 173.87, 168.52, 164.75, 157.81, 157.15, 138.77, 136.39, 134.50, 132.11, 132.03, 128.62, 128.52, 122.47, 117.57, 112.60, 60.40, 54.80, 54.10. HRMS (ESI) calcd for $\text{C}_{13}\text{H}_{13}\text{N}_3\text{O}_3$ $[\text{M}+\text{H}]^+$: 260.1035; found: 260.1049.



SG-PH-OMe: yield: 99%. R_f = 0.46 (EtOAc). ^1H NMR (500 MHz, CDCl_3): δ 7.63 – 7.56 (m, 4H), 7.52 (dd, J = 8.7, 5.6 Hz, 3H), 7.42 – 7.37 (m, 3H), 7.11 (t, J = 8.7 Hz, 1H), 6.95 (t, J = 8.6 Hz, 1H), 6.80 (d, J = 9.7 Hz, 1H), 4.01 (s, 3H). ^{13}C NMR (125 MHz, CDCl_3): δ 179.17, 165.98, 146.71, 141.21, 137.37, 131.83, 131.66, 131.23, 131.16, 131.08, 129.45, 128.35, 128.26, 126.82, 123.35, 122.86, 111.87, 89.46, 56.53. HRMS (ESI) calcd for $\text{C}_{22}\text{H}_{16}\text{O}_2$ $[\text{M}+\text{H}]^+$: 313.1229; found: 313.1225.

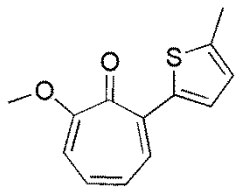


SG-PH-OH: yield: 35%. R_f = 0.5 (1:1 EtOAc: Hexanes). IR (KBr): ν : 3175, 3109, 3052, 3032, 3008, 2915, 2887, 2830, 2358, 1981, 1701, 1594, 1550, 1509, 1474, 1441, 1416, 1357, 1298, 1271, 1238, 1216, 1178, 1158, 1107, 1069, 1004, 974. ^1H NMR (500 MHz, CDCl_3): δ 9.86 (s, 1H), 7.70 – 7.62 (m, 3H), 7.62 – 7.55 (m, 4H), 7.52 – 7.43 (m, 2H), 7.43 – 7.37 (m, 3H), 7.15 (t, J = 8.1 Hz, 1H). ^{13}C NMR (125 MHz, CDCl_3): δ 173.68, 170.40, 147.03, 140.39, 139.72, 138.34, 136.93, 131.69, 131.45, 129.39, 128.39, 127.38, 123.36, 123.21, 121.73, 90.3, 89.19. HRMS (ESI) calcd for $\text{C}_{21}\text{H}_{14}\text{O}_2$ $[\text{M}+\text{H}]^+$: 299.1072; found: 299.1081.

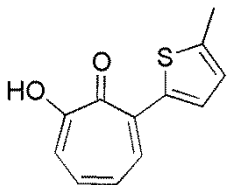


EF-5-H: yield 71%. R_f = 0.34 (1:1 EtOAc: Hexanes). IR (KBr): ν : 3060, 3018, 3000, 2959, 2842, 2751, 2362, 1679, 1624, 1602, 1572, 1513, 1497, 1461, 1442, 1423, 1390, 1379, 1275, 1259, 1244, 1230, 1205, 1187, 1168, 1115, 1023, 1007, 951. ^1H NMR (500 MHz, CDCl_3): δ 10.49 (s, 1H), 7.93 (d, J = 2.4 Hz, 1H), 7.88 (dd, J = 8.7, 2.5 Hz, 1H), 7.41 (d, J = 8.8 Hz, 1H), 7.21 – 7.13 (m, 2H), 7.07 (d, J = 9.4 Hz, 2H), 7.00 (t, J = 8.5 Hz, 1H), 3.99 (s, 3H). ^{13}C NMR (125 MHz, CDCl_3): δ 189.35, 186.24, 161.95, 150.72, 142.22, 137.13,

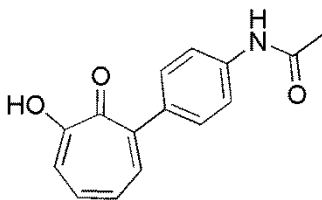
136.24, 135.43, 133.69, 133.45, 132.42, 129.39, 124.59, 111.31, 55.92. HRMS (ESI) calcd for $C_{15}H_{12}O_3$ $[M+H]^+$: 241.0865; found: 241.0874.



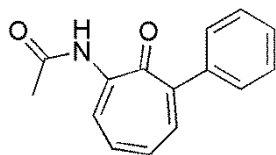
HC-12-OMe: yield 59%. R_f = 0.54 (EtOAc). IR (KBr): ν : 3049, 2997, 2967, 2917, 2854, 2836, 1722, 1584, 1551, 1466, 1444, 1408, 1379, 1361, 1323, 1267, 1232, 1217, 1199, 1165, 1086, 1051, 1017, 973. 1H NMR (500 MHz, $CDCl_3$): δ 7.99 (d, J = 9.4 Hz, 1H), 7.52 (d, J = 3.8 Hz, 1H), 7.07 (t, J = 10.0 Hz, 1H), 6.97 (t, J = 10.0 Hz, 1H), 6.88 – 6.79 (m, 2H), 3.99 (s, 3H), 2.56 (s, 3H). ^{13}C NMR (125 MHz, $CDCl_3$): δ 177.10, 164.52, 145.16, 138.98, 138.10, 132.79, 130.74, 127.46, 126.77, 124.80, 112.75, 56.58, 15.39. HRMS (ESI) calcd for $C_{13}H_{12}O_2S$ $[M+H]^+$: 233.0636; found: 233.0663.



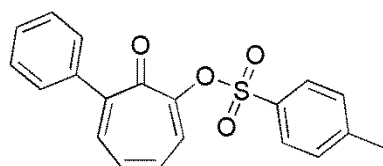
HC-12-OH: yield 27%. R_f = 0.29 (1:1 EtOAc: Hexanes). IR (KBr): ν : 3182, 3166, 3143, 2910, 2359, 2342, 1596, 1584, 1539, 1508, 1478, 1443, 1418, 1364, 1293, 1270, 1241, 1220, 1166, 1117, 1068, 1028, 1004, 950. 1H NMR (500 MHz, $CDCl_3$): δ 9.88 (s, 1H), 8.23 (dd, J = 10.3, 0.8 Hz, 1H), 7.68 (d, J = 3.8 Hz, 1H), 7.46 (d, J = 10.0 Hz, 1H), 7.36 (t, J = 10.0 Hz, 1H), 7.17 (t, J = 10.1 Hz, 1H), 6.89 (d, J = 3.5 Hz, 1H), 2.61 (s, 3H). HRMS (ESI) calcd for $C_{12}H_{10}O_2S$ $[M+H]^+$: 219.0480; found: 219.0474.



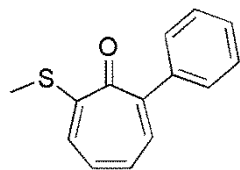
Am-Ac-OH: yield 76%. R_f = 0.61 (1:1 EtOAc: Hexanes). IR (KBr): ν : 3280, 3064, 2926, 2852, 2359, 1689, 1594, 1549, 1496, 1478, 1454, 1437, 1395, 1346, 1276, 1224, 1202, 1176, 1072, 1023, 987. 1H NMR (500 MHz, $CDCl_3$): δ 9.70 (s, 1H), 9.11 (d, J = 9.9 Hz, 1H), 7.64 (d, J = 9.1, 1.1 Hz, 1H), 7.48 (d, J = 4.4 Hz, 4H), 7.43 (h, J = 4.4 Hz, 1H), 7.32 (t, J = 10.5 Hz, 1H), 7.14 (t, J = 9.8 Hz, 1H), 2.31 (s, 3H). ^{13}C NMR (125 MHz, $CDCl_3$): δ 177.47, 170.15, 147.88, 147.54, 141.06, 139.20, 134.99, 130.02, 129.16, 128.16, 128.11, 121.30, 25.75. HRMS (ESI) calcd for $C_{15}H_{13}NO_3$ $[M+H]^+$: 256.0974; found: 256.0966.



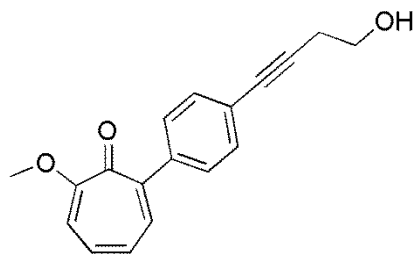
MO-Am-PH: yield 76%. $R_f = 0.61$ (1:1 EtOAc: Hexanes). IR (KBr): ν : 3499, 3278, 3243, 3007, 2962, 2953, 2924, 2852, 2358, 1687, 1540, 1497, 1473, 1456, 1438, 1396, 1377, 1347, 1274, 1240, 1226, 1198, 1182, 1110, 1083, 1019, 965. ^1H NMR (500 MHz, CDCl_3): δ 9.70 (s, 1H), 9.16 – 9.05 (m, 1H), 7.64 (dd, $J = 9.2, 1.1$ Hz, 1H), 7.48 (d, $J = 4.4$ Hz, 4H), 7.35 – 7.27 (m, 1H), 7.14 (dd, $J = 10.3, 9.2$ Hz, 1H), 2.31 (s, 3H). ^{13}C NMR (125 MHz, CDCl_3): δ 147.86, 147.54, 141.06, 139.18, 134.97, 130.00, 129.17, 128.15, 128.10, 121.27, 25.75. HRMS (ESI) calcd for $\text{C}_{15}\text{H}_{13}\text{NO}_2$ $[\text{M}+\text{H}]^+$: 240.1025; found: 240.1042.



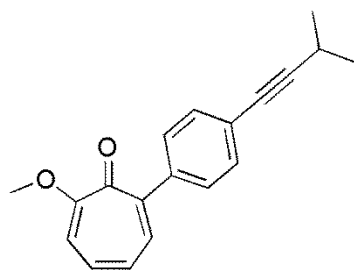
MO-OTs-PH: yield 88%. $R_f = 0.71$ (1:1 EtOAc: Hexanes). ^1H NMR (500 MHz, CDCl_3): δ 7.97 (d, $J = 8.8$ Hz, 2H), 7.51 (d, $J = 9.2$ Hz, 1H), 7.46 (d, $J = 8.9$ Hz, 1H), 7.40 (dt, $J = 6.0, 2.5$ Hz, 3H), 7.38 – 7.33 (m, 4H), 7.17 (t, $J = 9.7$ Hz, 1H), 6.99 (t, $J = 10.6$ Hz, 1H), 2.47 (s, 3H). ^{13}C NMR (125 MHz, CDCl_3): δ 178.42, 154.77, 151.89, 145.43, 139.76, 136.70, 133.85, 133.21, 129.66, 129.44, 129.41, 129.02, 128.76, 128.68, 128.13, 21.74. HRMS (ESI) calcd for $\text{C}_{20}\text{H}_{16}\text{O}_4\text{S}$ $[\text{M}+\text{H}]^+$: 353.0848; found: 353.0857.



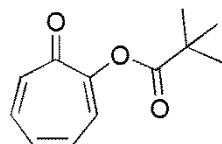
MO-SMe-PH: yield 98%. $R_f = 0.61$ (1:1 EtOAc: Hexanes). IR (KBr): ν : 3078, 3046, 2953, 2917, 2851, 2358, 1603, 1578, 1546, 1489, 1475, 1458, 1438, 1420, 1396, 1353, 1316, 1271, 1253, 1200, 1153, 1098, 1071, 1028, 1014, 950. ^1H NMR (500 MHz, CDCl_3): δ 7.50 (t, $J = 9.9$ Hz, 3H), 7.44 (t, $J = 7.6, 6.7$ Hz, 2H), 7.40 (d, $J = 7.6$ Hz, 1H), 7.13 – 7.05 (m, 2H), 7.00 (t, $J = 9.3$ Hz, 1H), 2.42 (s, 3H). ^{13}C NMR (125 MHz, CDCl_3): δ 181.71, 161.15, 144.94, 140.82, 137.23, 131.31, 129.53, 128.89, 128.04, 127.97, 126.54, 15.95. HRMS (ESI) calcd for $\text{C}_{14}\text{H}_{12}\text{OS}$ $[\text{M}+\text{H}]^+$: 229.0687; found: 229.0714.



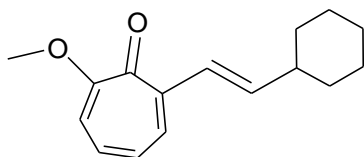
SG-EtOH-OMe: yield 94%. $R_f = 0.23$ (EtOAc). IR (KBr): ν : 3395, 2924, 1710, 1677, 1589, 1557, 1491, 1463, 1438, 1407, 1355, 1326, 1271, 1216, 1160, 1111, 1089, 1043, 1014, 972. ^1H NMR (500 MHz, CDCl_3): δ 7.50 – 7.43 (m, 5H), 7.09 (t, $J = 10.1$ Hz, 1H), 6.93 (t, $J = 11.2$ Hz, 1H), 6.79 (d, $J = 9.6$ Hz, 1H), 3.99 (s, 3H), 3.85 (t, $J = 6.3$ Hz, 2H), 2.74 (t, $J = 6.9$ Hz, 2H). ^{13}C NMR (125 MHz, CDCl_3): δ 179.16, 165.95, 146.74, 140.88, 137.41, 131.84, 131.28, 129.34, 126.86, 122.97, 111.94, 87.06, 82.43, 61.19, 56.50, 23.94. HRMS (ESI) calcd for $\text{C}_{18}\text{H}_{16}\text{O}_3$ $[\text{M}+\text{H}]^+$: 281.1178; found: 281.1194.



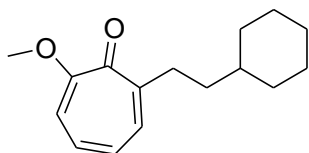
SG-iPr-OMe: yield 46%. $R_f = 0.49$ (EtOAc). ^1H NMR (500 MHz, CDCl_3): δ 7.48 – 7.43 (m, 4H), 7.07 (t, $J = 10.5$, 9.6 Hz, 1H), 6.92 (t, $J = 10.1$ Hz, 1H), 6.77 (d, $J = 9.6$ Hz, 1H), 3.98 (s, 3H), 1.31 (d, $J = 6.9$ Hz, 6H). ^{13}C NMR (125 MHz, CDCl_3): δ 179.20, 165.88, 162.60, 146.84, 140.38, 137.28, 135.23, 135.18, 131.66, 131.13, 130.24, 129.24, 127.65, 126.83, 123.67, 111.86, 96.46, 79.74, 56.48, 36.51, 23.06, 21.21. HRMS (ESI) calcd for $\text{C}_{19}\text{H}_{18}\text{O}_2$ $[\text{M}+\text{H}]^+$: 279.1385; found: 2789.14041.



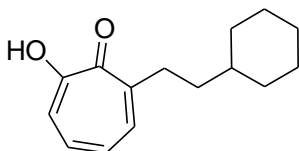
PIV-tropolone: yield 86%. ^1H NMR (500 MHz, CDCl_3): δ 7.21 (d, $J = 10.8$ Hz, 2H), 7.14 (t, $J = 10.4$ Hz, 2H), 7.06 (t, $J = 9.7$ Hz, 1H), 1.41 (s, 9H). ^{13}C NMR (125 MHz, CDCl_3): δ 175.86, 137.80, 133.94, 133.16, 123.97, 39.20, 27.25, 27.09. HRMS (ESI) calcd for $\text{C}_{12}\text{H}_{14}\text{O}_3$: 207.1021; found: 207.1044.



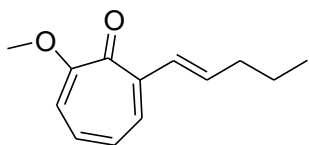
MO-1-unsat-OMe: yield 94%. R_f = 0.26 (1:1 EtOAc: Hexanes). M_p = N/A. IR (KBr): ν : 2925, 2918, 2849, 1632, 1610, 1595, 1570, 1488, 1466, 1448, 1364, 1270, 1249, 1217, 1178, 1043, 969, 750. ^1H NMR (500 MHz, CDCl_3): δ 7.54 (d, J = 9.2 Hz, 1H), 6.96-6.93 (m, 2H), 6.80 (t, J = 19.7, 9.7, 10 Hz, 1H), 6.68 (d, J = 9.7 Hz, 1H), 6.24 (dd, J = 16, 7.2, 7.2 Hz, 1H), 3.88 (s, 3H), 2.17-2.13 (m, 1H), 1.79-1.62 (m, 5H), 1.32-1.11 (m, 5H). ^{13}C NMR (126 MHz, CDCl_3): δ 178.8, 164.0, 143.9, 141.3, 132.3, 130.6, 126.8, 126.6, 112.1, 56.2, 41.6, 32.6, 25.8. HRMS (ESI) calcd for $\text{C}_{16}\text{H}_{20}\text{O}_2$ $[\text{M}+\text{H}]^+$: 245.1542; found: 245.1533.



MO-1-OMe: yield: 86%. R_f = 0.27 (1:1 EtOAc: Hexanes). M_p = N/A. IR (KBr): ν : 3053, 2945, 2842, 2662, 1738, 1575, 1568, 1556, 1504, 1455, 1372, 1128, 1062, 1055, 1042, 1037, 837, 798, 748. ^1H NMR (500 MHz, CDCl_3): δ 7.37 (d, J = 8.9 Hz, 1H), 6.99 (t, J = 20.2, 10.5, 9.8 Hz, 1H), 6.82 (t, J = 19.5, 9.5, 10.0 Hz, 1H), 6.74 (d, J = 9.7 Hz, 1H), 3.92 (s, 3H), 2.79-2.76 (m, 2H), 1.81-1.62 (m, 5H), 1.48-1.44 (m, 2H), 1.36-1.11 (m, 4H), 0.99-0.91 (m, 2H). ^{13}C NMR (126 MHz, CDCl_3): δ 179.2, 163.4, 150.5, 135.2, 130.3, 126.8, 111.7, 55.9, 37.5, 36.5, 33.6, 26.4, 26.0. HRMS (ESI) calcd for $\text{C}_{16}\text{H}_{22}\text{O}_2$ $[\text{M}+\text{H}]^+$: 247.1698; found: 247.1696.

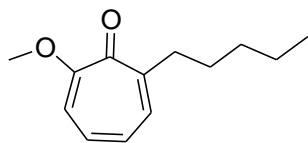


MO-1-OH: yield: 76%. R_f = 0.54 (1:1 EtOAc: Hexanes). M_p = N/A. IR (KBr): ν : 3204, 2919, 2901, 2848, 1599, 1547, 1537, 1475, 1418, 1380, 1229, 1205, 1125, 996, 731. ^1H NMR (500 MHz, CD_2Cl_2): δ 9.65 (bs, 1H), 7.47 (d, J = 9.9 Hz, 1H), 7.32-7.25 (m, 2H), 7.00-6.96 (m, 1H), 2.84-2.80 (m, 2H), 1.80 (d, J = 13.6 Hz, 2H), 1.72-1.64 (m, 3H), 1.50-1.46 (m, 2H), 1.36-1.13 (m, 5H), 1.00-0.92 (m, 2H). ^{13}C NMR (126 MHz, CD_2Cl_2): δ 172.7, 168.9, 142.6, 139.9, 136.2, 127.9, 121.7, 38.4, 37.5, 33.8, 33.3, 27.3, 26.9. HRMS (ESI) calcd for $\text{C}_{15}\text{H}_{20}\text{O}_2$ $[\text{M}+\text{H}]^+$: 233.1541; found: 233.1550.

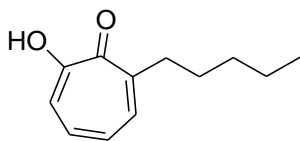


MO-2-unsat-OMe: yield: 88%. R_f = 0.25 (1:1 EtOAc: Hexanes). M_p = N/A. IR (KBr): ν : 2958, 2929, 2870, 1633, 1610, 1590, 1570, 1560, 1489, 1465, 1438, 1364, 1270, 1250, 1218, 1177, 1057, 1039, 969, 782,

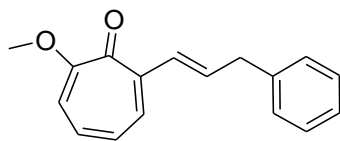
750, 671. ^1H NMR (500 MHz, CDCl_3): δ 7.40 (d, J = 9.1 Hz, 1H), 6.84-6.79 (m, 2H), 6.68 (t, J = 19.7, 9.7, 10 Hz, 1H), 6.58 (d, J = 9.7 Hz, 1H), 6.22-6.16 (m, 1H), 3.74 (s, 3H), 2.05 (q, J = 23.1, 7.3, 7.4, 8.4 Hz, 2H), 1.33 (h, J = 36.9, 7.4, 7.4, 7.4, 7.4, 7.4 Hz, 2H), 0.77 (t, J = 14.8, 7.4, 7.4 Hz, 3H). ^{13}C NMR (126 MHz, CDCl_3): δ 178.3, 163.7, 143.2, 135.2, 132.2, 130.5, 128.8, 126.5, 111.9, 55.9, 35.1, 21.9, 13.3. HRMS (ESI) calcd for $\text{C}_{13}\text{H}_{16}\text{O}_2$ $[\text{M}+\text{H}]^+$: 205.1229; found: 205.1247.



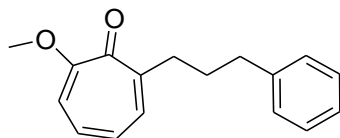
MO-2-OMe: yield 84%. R_f = 0.26 (1:1 EtOAc: Hexanes). M_p = N/A. IR (KBr): ν : 2954, 2923, 2869, 2855, 1595, 1567, 1556, 1496, 1466, 1463, 1446, 1435, 1413, 1375, 1270, 1254, 1218, 1175, 1114, 1045, 1022, 795, 748. ^1H NMR (500 MHz, CDCl_3): δ 7.34 (d, J = 8.9 Hz, 1H), 6.96 (t, J = 20.3, 10.6, 9.8 Hz, 1H), 6.79 (t, J = 19.6, 10.5, 9.1 Hz, 1H), 6.70 (d, J = 9.7 Hz, 1H), 3.90 (s, 3H), 2.75-2.72 (m, 2H), 1.56 (m, 2H), 1.32 (m, 4H), 0.86 (m, 3H). ^{13}C NMR (126 MHz, CDCl_3): δ 179.5, 163.7, 150.3, 135.6, 130.5, 127.0, 111.9, 56.2, 36.3, 31.8, 28.7, 22.4, 13.9. HRMS (ESI) calcd for $\text{C}_{13}\text{H}_{18}\text{O}_2$ $[\text{M}+\text{H}]^+$: 207.1385; found: 207.1410.



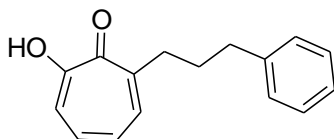
MO-2-OH: yield: 75%. R_f = 0.6 (1:1 EtOAc: Hexanes). M_p = N/A. IR (KBr): ν : 3172, 3161, 3153, 3140, 2957, 2927, 2924, 2869, 2857, 1616, 1601, 1549, 1488, 1477, 1468, 1422, 1381, 1293, 1240, 1232, 850, 799, 743, 718, 696. ^1H NMR (500 MHz, CD_2Cl_2): δ 9.60 (bs, 1H), 7.46 (d, J = 9.9 Hz, 1H), 7.31-7.24 (m, 2H), 6.96 (t, J = 18.7, 9.0, 9.7 Hz, 1H), 2.80 (t, J = 15.5, 7.6, 7.9 Hz, 2H), 1.61 (m, 2H), 1.35 (m, 4H), 0.89 (m, 3H). ^{13}C NMR (126 MHz, CDCl_3): δ 172.9, 169.1, 142.1, 139.9, 136.2, 127.7, 121.8, 35.9, 32.4, 29.4, 23.1, 14.4. HRMS (ESI) calcd for $\text{C}_{12}\text{H}_{16}\text{O}_2$ $[\text{M}+\text{H}]^+$: 193.1229; found: 193.1249.



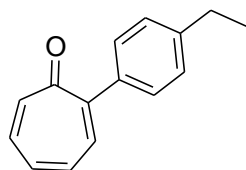
MO-7-unsat-OMe: yield: 85%. R_f = 0.28 (1:1 EtOAc: Hexanes). M_p = 77.4-79.0. IR (KBr): ν : 3057, 3024, 3005, 2964, 2936, 2897, 2835, 1632, 1587, 1564, 1489, 1466, 1452, 1438, 1409, 1364, 1272, 1247, 1217, 1175, 1154, 1059, 1042, 1030, 971, 937, 819, 799, 751, 700, 674. ^1H NMR (500 MHz, CDCl_3): δ 7.46 (d, J = 9.0 Hz, 1H), 7.24-7.12 (m, 5H), 7.03 (d, J = 15.7 Hz, 1H), 6.89 (t, J = 20.0, 9.95, 10.1 Hz, 1H), 6.42-6.36 (m, 1H), 6.63 (d, J = 9.7 Hz, 1H), 6.42-6.36 (m, 1H), 3.82 (s, 3H), 3.51 (d, J = 6.9 Hz, 2H). ^{13}C NMR (126 MHz, CDCl_3): δ 178.3, 163.9, 142.8, 139.4, 133.3, 132.6, 130.9, 129.9, 128.2, 128.1, 126.5, 125.8, 111.9, 55.9, 39.4. HRMS (ESI) calcd for $\text{C}_{17}\text{H}_{16}\text{O}_2$ $[\text{M}+\text{H}]^+$: 253.1229; found: 253.1258.



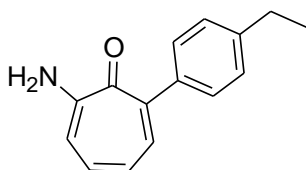
MO-7-OMe: yield: 82%. R_f = 0.29 (1:1 EtOAc: Hexanes). M_p = N/A. IR (KBr): ν : 3024, 2929, 2913, 2853, 1594, 1574, 1497, 1466, 1453, 1374, 1271, 1219, 1177, 751, 700. ^1H NMR (500 MHz, CDCl_3): δ 7.33 (d, J = 8.9 Hz, 1H), 7.28-7.14 (m, 5H), 6.97 (t, J = 20.3, 10.6, 9.7 Hz, 1H), 6.79 (t, J = 19.6, 9.6, 10.0 Hz, 1H), 6.71 (d, J = 9.6 Hz, 1H), 3.92 (s, 3H), 2.82 (t, J = 15.4, 7.6, 7.8 Hz, 2H), 2.70 (t, J = 15.5, 7.6, 7.9 Hz, 2H), 1.96-1.90 (m, 2H). ^{13}C NMR (126 MHz, CDCl_3): δ 179.4, 163.8, 149.7, 142.1, 135.7, 130.7, 128.3, 128.2, 126.9, 125.6, 56.2, 36.1, 35.7, 30.5. HRMS (ESI) calcd for $\text{C}_{17}\text{H}_{18}\text{O}_2$ $[\text{M}+\text{H}]^+$: 255.1385; found: 255.1406.



MO-7-OH: yield: 73%. R_f = 0.35 (1:1 EtOAc: Hexanes). M_p = N/A. IR (KBr): ν : 3026, 2927, 2923, 2857, 1616, 1600, 1550, 1473, 1459, 1453, 1424, 1382, 1293, 1263, 1247, 1233, 1214, 738, 699. ^1H NMR (500 MHz, CD_2Cl_2): δ 7.47 (d, J = 9.8 Hz, 1H), 7.34-7.17 (m, 7H), 6.98 (t, J = 20.6, 9.9, 10.7 Hz, 1H), 2.88 (t, J = 15.5, 7.6, 7.9 Hz, 2H), 2.72 (t, J = 15.4, 7.6, 7.8 Hz, 2H), 1.99-1.93 (m, 2H). ^{13}C NMR (126 MHz, CD_2Cl_2): δ 173.0, 168.7, 142.8, 141.8, 140.0, 136.4, 129.0, 128.8, 127.9, 126.3, 121.5, 36.3, 35.7, 31.2. HRMS (ESI) calcd for $\text{C}_{16}\text{H}_{16}\text{O}_2$ $[\text{M}+\text{H}]^+$: 241.1229; found: 241.1253.

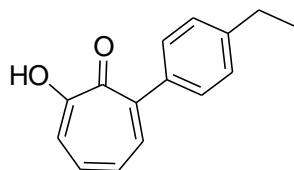


MO-10-H: yield: 97%. R_f = 0.29 (25% EtOAc in Hexanes). M_p = N/A. IR (KBr): ν : 3024, 2964, 2931, 2873, 1638, 1575, 1464, 1384, 1261, 833, 791, 690. ^1H NMR (500 MHz, CDCl_3): δ 7.45 (d, J = 15.0 Hz, 2H), 7.38 (dd, J = 10.0, 1.0, 1.0 Hz, 1H), 7.26 (d, J = 8.5 Hz, 2H), 7.20 (d, J = 12.0 Hz, 1H), 7.13 (ddd, J = 21.0, 9.0, 9.0, 1.5, 1.5, 1.5, 1.5 Hz, 1H), 7.05 (t, J = 19.5, 10.5, 9.0 Hz, 1H), 6.96 (dd, J = 18.5, 7.5, 8.0 Hz, 1H), 2.71 (q, 23.0, 8.0, 7.5, 7.5 Hz, 2H), 1.29 (t, J = 15.5, 8.0, 7.5 Hz, 3H). ^{13}C NMR (126 MHz, CDCl_3): δ 186.8, 175.5, 152.7, 144.9, 142.3, 137.4, 136.3, 136.0, 135.3, 133.9, 133.1, 129.3, 127.8, 41.4, 29.4, 28.9, 15.6. HRMS (ESI) calcd for $\text{C}_{16}\text{H}_{16}\text{O}_2$ $[\text{M}+\text{H}]^+$: 211.1124; found 211.1152.

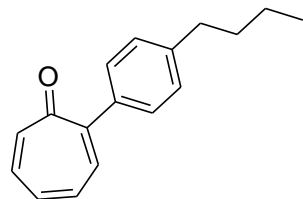


MO-10-NH2: yield: 77%. R_f = 0.44 (1:1 EtOAc: Hexanes). M_p = 131.0-132.2. IR (KBr): ν : 3388, 3254, 3242, 3233, 3206, 3176, 3152, 3147, 3118, 2960, 1606, 1512, 1453, 1433, 1410, 1343, 1273, 1240, 1180, 1113, 915, 833, 757, 707, 584. ^1H NMR (500 MHz, CD_2Cl_2): δ 7.52 (dd, J = 11.0, 1.5, 1.0 Hz, 1H), 7.41 (d, J

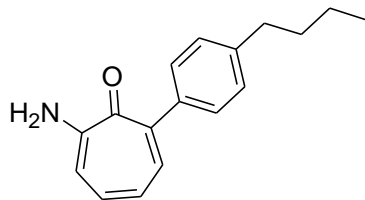
= 8.0 Hz, 2H), 7.29 (d, J = 8.5 Hz, 2H), 7.16 (td, J = 21.5, 11.5, 11.5, 1.5, 1.5, 1.0 Hz, 1H), 6.95 (dd, J = 10.5, 0.5, 0.5 Hz, 1H), 6.80 (t, J = 20.5, 10.0, 10.5 Hz, 1H), 6.16 (s, 2H), 2.74 (q, J = 23.0, 8.0, 7.5, 7.5 Hz, 2H), 1.32 (t, J = 15.0, 7.5, 7.5 Hz, 3H). ^{13}C NMR (126 MHz, CD_2Cl_2): δ 174.6, 157.9, 143.6, 142.2, 140.2, 138.4, 135.1, 129.6, 127.4, 123.0, 112.3, 28.8, 15.6. HRMS (ESI) calcd for $\text{C}_{15}\text{H}_{15}\text{NO}$ $[\text{M}+\text{H}]^+$: 226.1236; found 226.1262.



MO-10-OH: yield: 65%. R_f = 0.47 (1:1 EtOAc: Hexanes). M_p = 60.7-61.9. IR (KBr): ν : 3168, 3022, 2964, 2929, 2872, 1615, 1595, 1549, 1474, 1418, 1380, 1365, 1276, 1247, 914, 835, 751. ^1H NMR (500 MHz, CD_2Cl_2): δ 7.63 (d, J = 10.5 Hz, 1H), 7.49-7.34 (m, 6H), 7.13 (t, J = 20.5, 10.5, 10.0 Hz, 1H), 2.77 (q, J = 23.0, 7.5, 8.0, 7.5 Hz, 2H), 1.34 (t, J = 15.5, 7.5, 8.0 Hz, 3H). ^{13}C NMR (126 MHz, CD_2Cl_2): δ 171.6, 170.3, 144.7, 140.6, 139.1, 137.6, 136.6, 129.4, 127.8, 121.5, 28.8, 15.5. HRMS (ESI) calcd for $\text{C}_{15}\text{H}_{14}\text{O}_2$ $[\text{M}+\text{H}]^+$: 227.1072; found 227.1103.

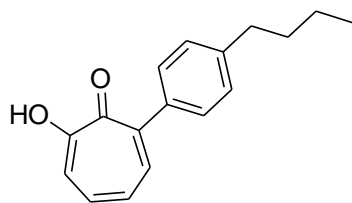


MO-9-H: yield: 97%. R_f = 0.47 (25% EtOAc in Hexanes). M_p = N/A. IR (KBr): ν : 3024, 2956, 2929, 2869, 2856, 1630, 1582, 1508, 1463, 1382, 1259, 1230, 1183, 902, 830, 781, 687, 558. ^1H NMR (500 MHz, CDCl_3): δ 7.43 (d, J = 8.0 Hz, 2H), 7.29 (d, J = 8.8 Hz, 1H), 7.20 (d, J = 8.0 Hz, 2H), 7.12 (d, J = 12.0 Hz, 1H), 7.03 (t, J = 19.9, 7.8, 12.1 Hz, 1H), 6.94 (t, J = 19.6, 10.6, 9.0 Hz, 1H), 6.85 (t, J = 19.4, 8.6, 10.8 Hz, 1H), 2.63 (t, J = 15.5, 7.6, 7.9 Hz, 2H), 1.62 (p, J = 30.4, 7.4, 7.7, 7.5, 7.8 Hz, 2H), 1.38 (h, J = 37.0, 7.4, 7.4, 7.4, 7.4, 7.4 Hz, 2H), 0.94 (t, J = 14.7, 7.4, 7.3 Hz, 3H). ^{13}C NMR (126 MHz, CDCl_3): δ 186.6, 152.4, 143.4, 142.1, 137.5, 136.3, 135.3, 133.9, 133.1, 129.3, 128.3, 35.6, 33.7, 22.6, 14.2. HRMS (ESI) calcd for $\text{C}_{18}\text{H}_{20}\text{O}_2$ $[\text{M}+\text{H}]^+$: 239.1437; found: 239.1498.

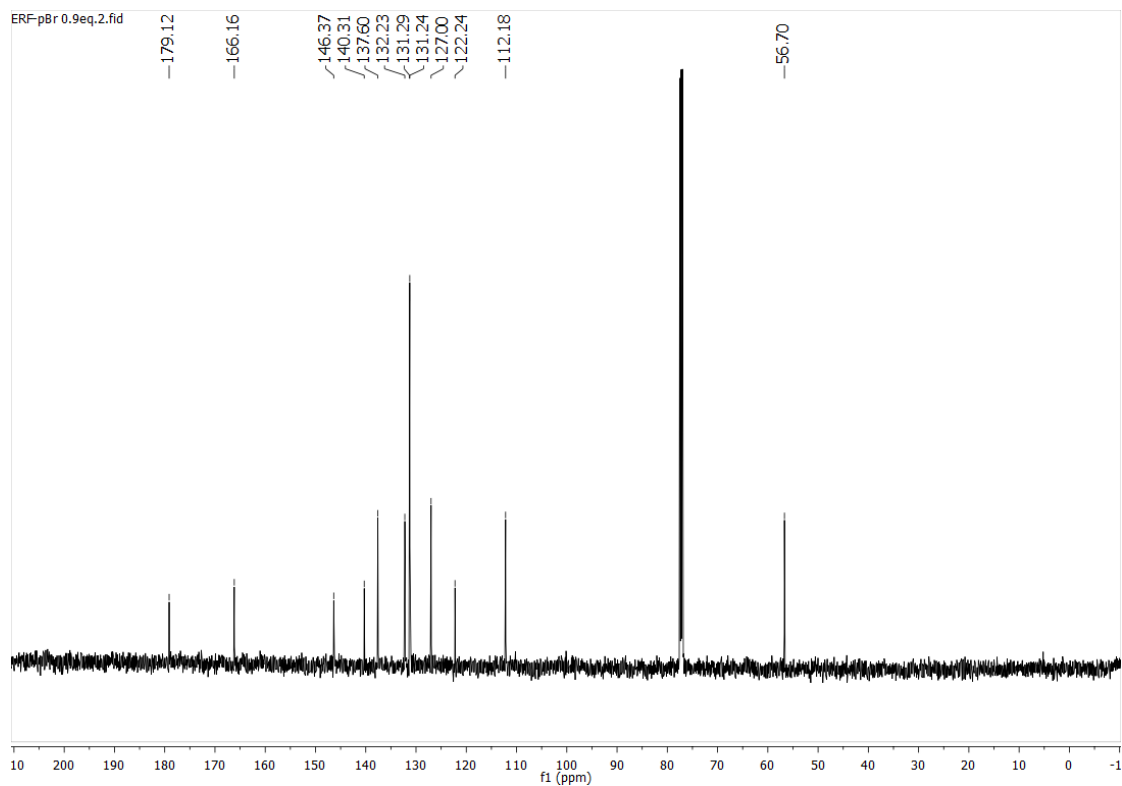
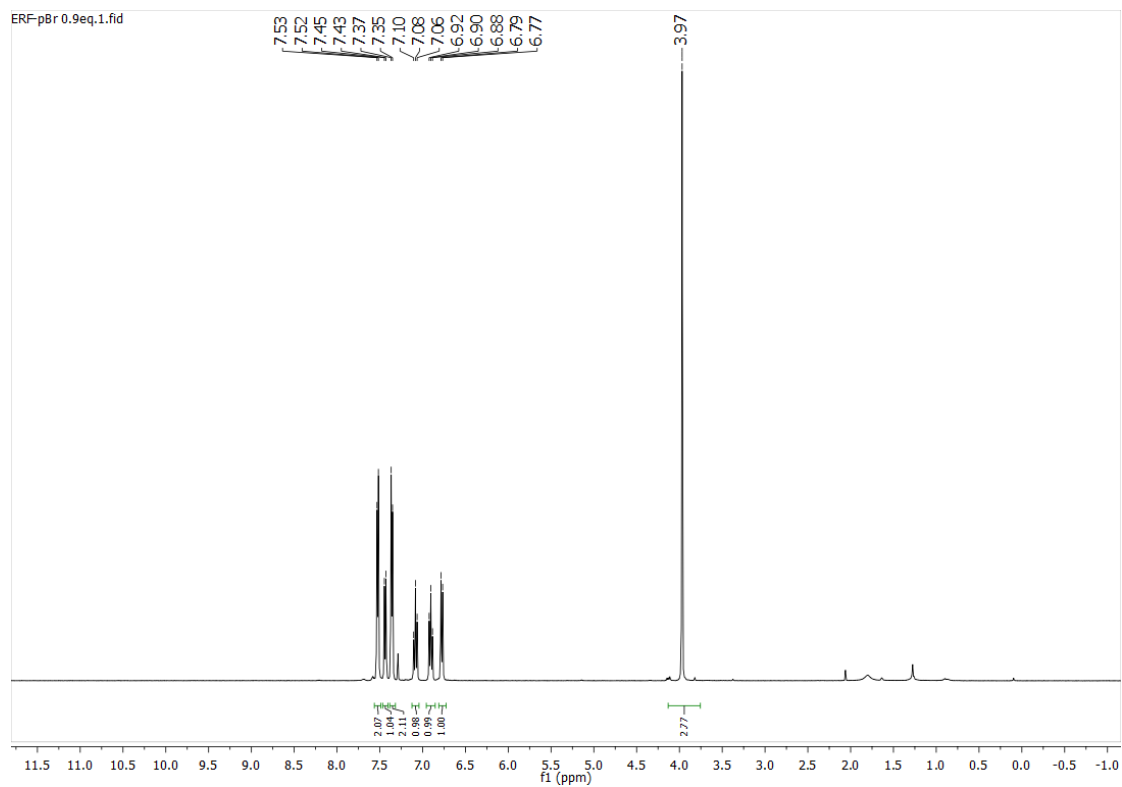


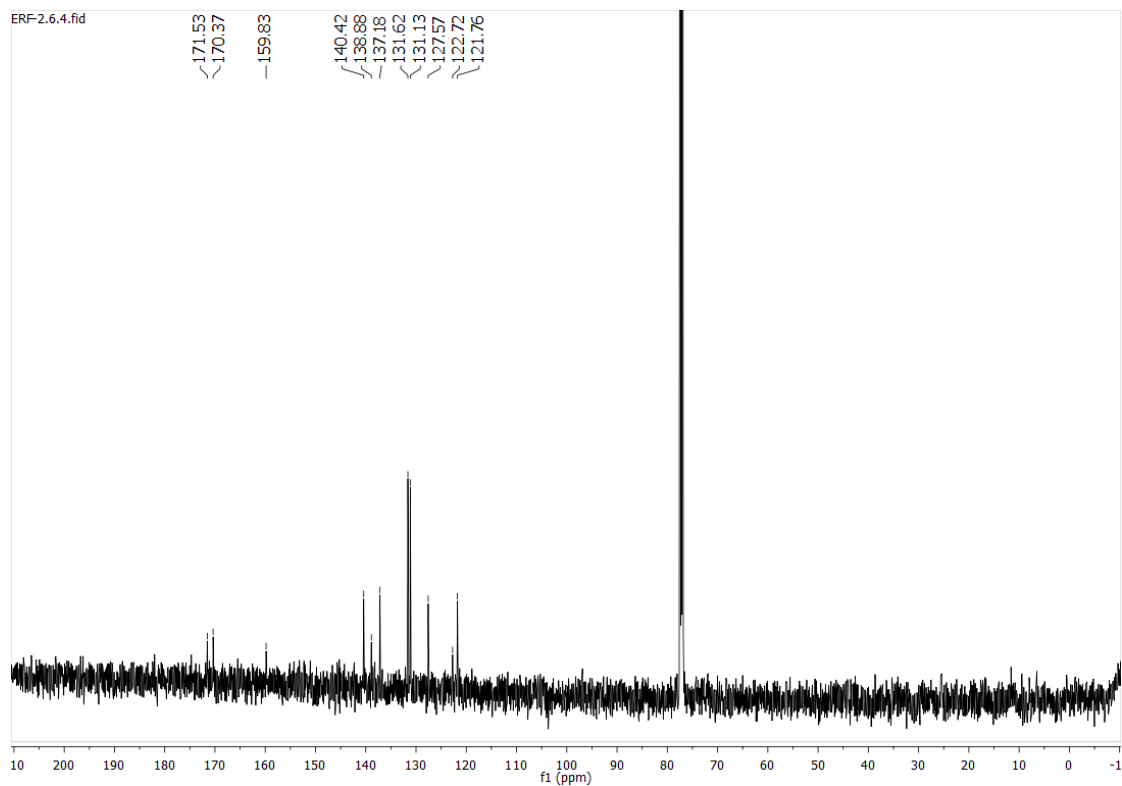
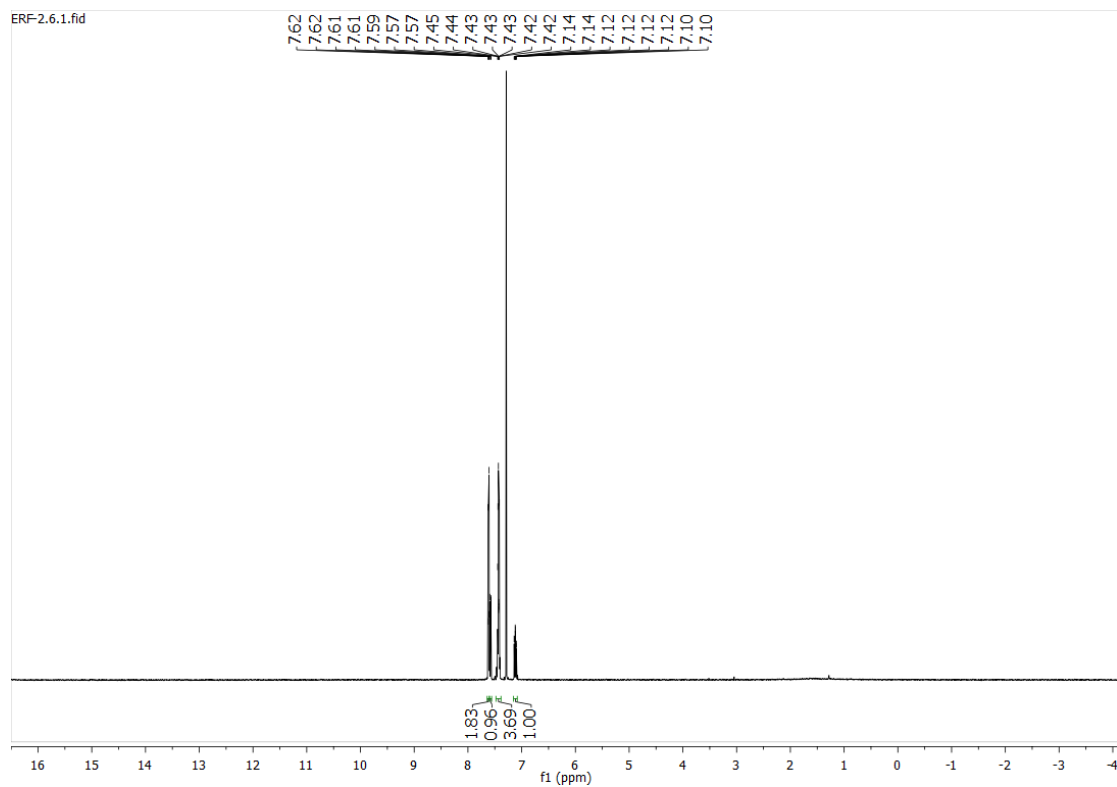
MO-9-NH2: yield: 88%. R_f = 0.50 (1:1 EtOAc: Hexanes). M_p = 133.7-135.0. IR (KBr): ν : 3398, 3240, 3232, 3200, 3140, 3124, 3118, 2954, 2925, 1607, 1520, 1507, 1433, 1335, 1266, 1239, 916, 759, 706, 573. ^1H NMR (500 MHz, CD_2Cl_2): δ 7.51 (d, J = 9.6 Hz, 1H), 7.43 (d, J = 8.0 Hz, 2H), 7.25 (d, J = 7.9 Hz, 2H), 7.06 (t, J = 20.0, 10.0, 10.0 Hz, 1H), 6.84 (d, J = 10.0 Hz, 1H), 6.74 (t, J = 19.6, 9.8, 9.8 Hz, 1H), 6.25 (s, 2H), 2.66 (t, J = 15.4, 7.4, 8.0 Hz, 2H), 1.65 (p, J = 30.4, 7.4, 7.7, 6.8, 8.5 Hz, 2H), 1.41 (h, J = 36.9, 7.3, 7.4, 7.4, 7.5,

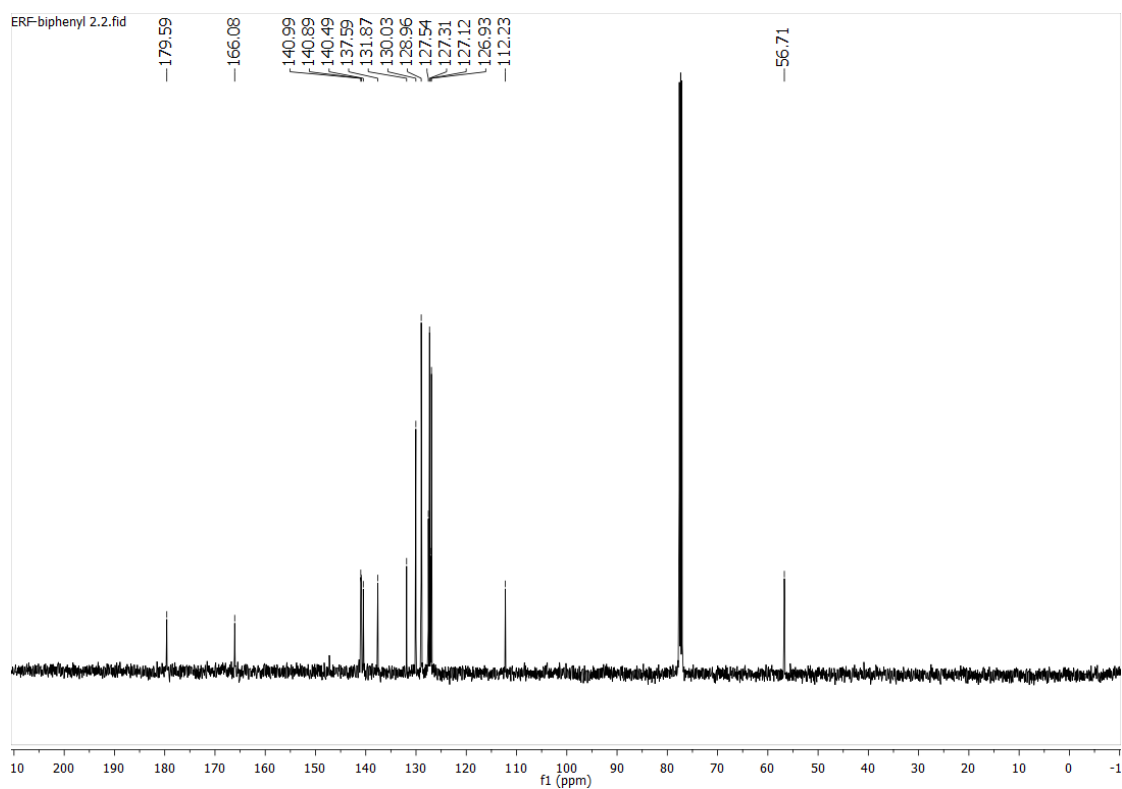
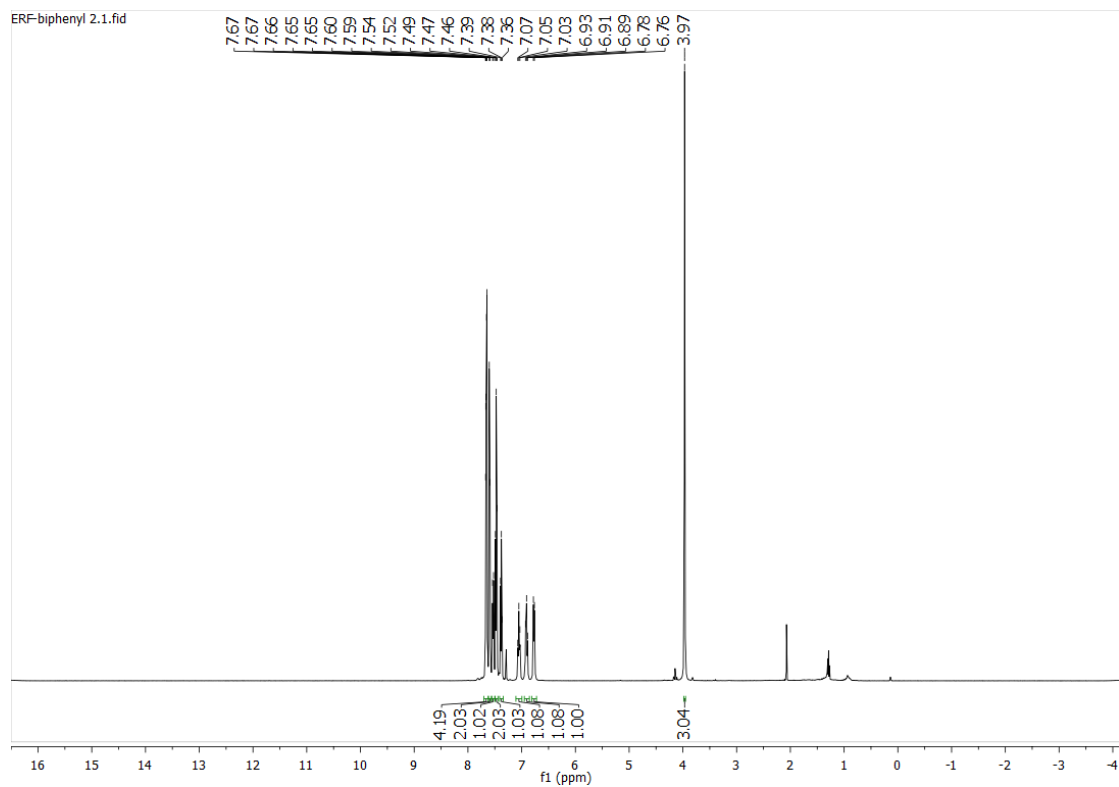
7.4 Hz, 2H), 0.96 (t, J = 14.7, 7.4, 7.3 Hz, 3H). ^{13}C NMR (126 MHz, CD_2Cl_2): δ 174.0, 158.1, 141.8, 141.6, 139.7, 138.4, 135.1, 129.2, 127.8, 122.6, 112.8, 35.3, 33.4, 22.3, 13.8. HRMS (ESI) calcd for $\text{C}_{17}\text{H}_{19}\text{NO}$ $[\text{M}+\text{H}]^+$: 254.1545; found: 254.1526.



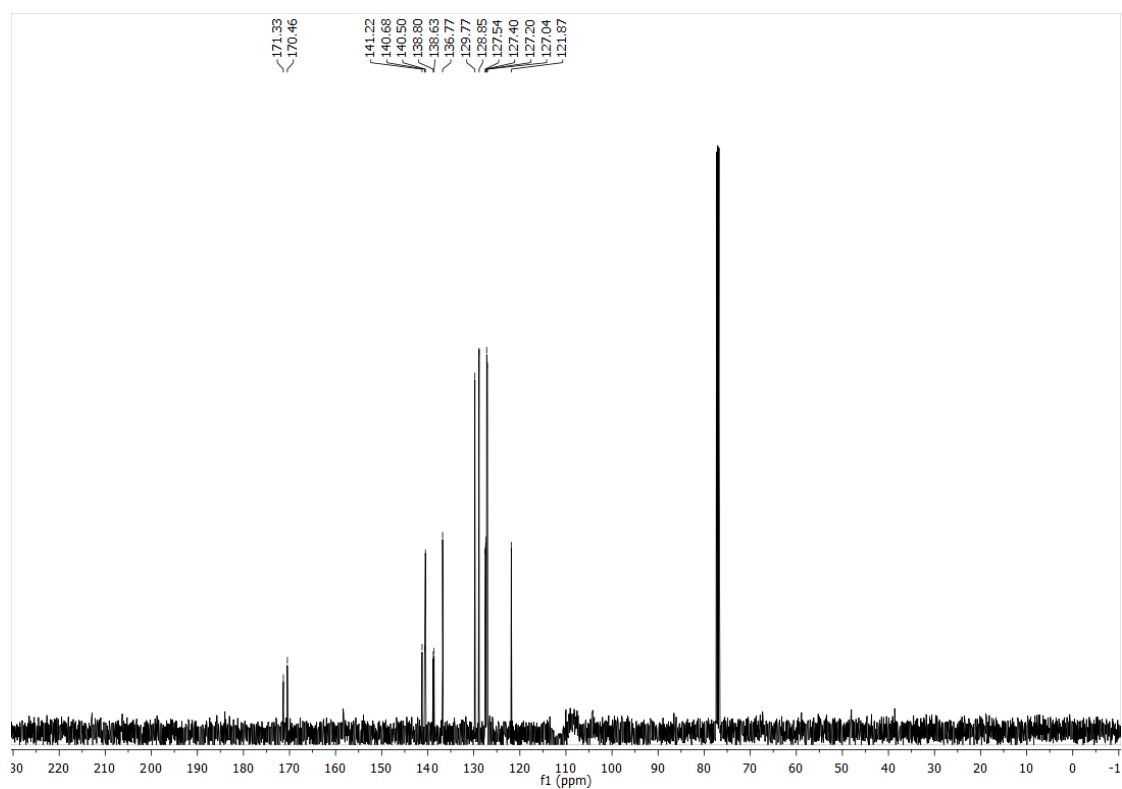
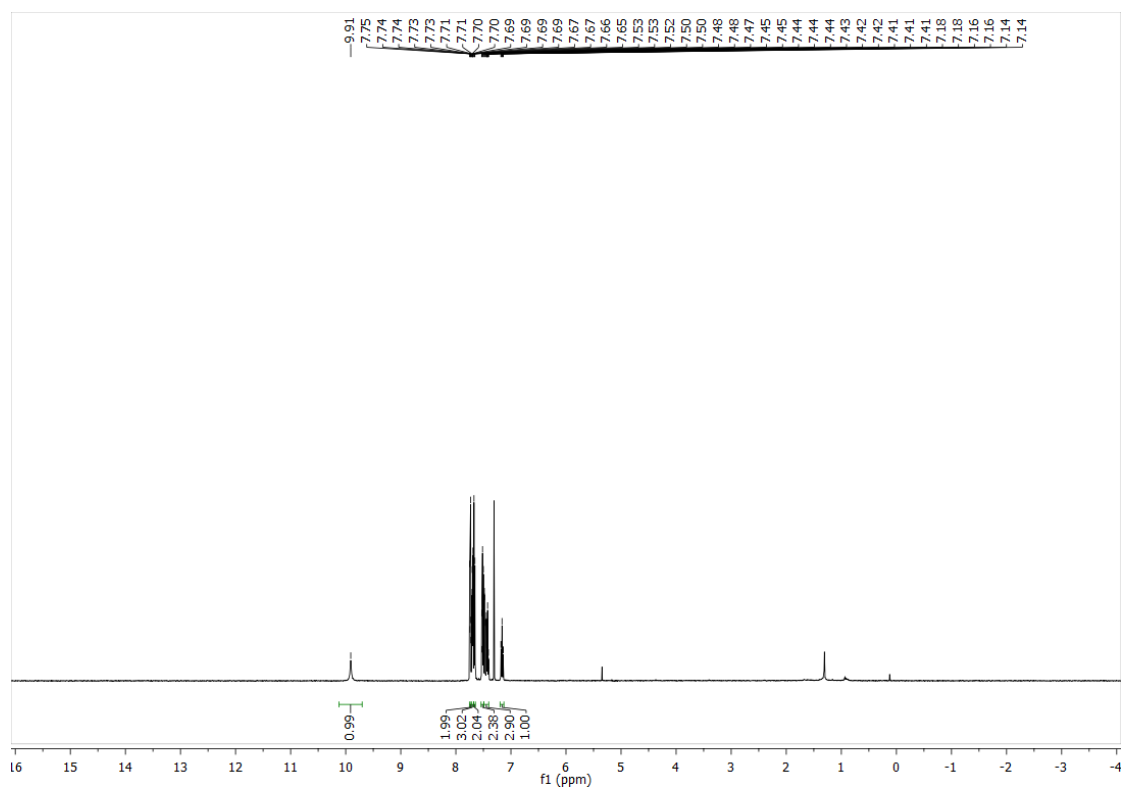
MO-9-OH: yield: 87%. R_f = 0.37 (1:1 EtOAc: Hexanes). M_p = N/A. IR (KBr): ν : 2957, 2928, 2856, 1613, 1595, 1549, 1474, 1466, 1455, 1419, 1376, 1363, 1291, 1276, 1246, 1182, 730. ^1H NMR (400 MHz, CD_2Cl_2): δ 7.60 (d, J = 10.1 Hz, 1H), 7.43-7.37 (m, 4H), 7.27 (d, J = 8.1 Hz, 2H), 7.11-7.06 (m, 1H), 2.70 (t, J = 15.5, 7.5, 8.0 Hz, 2H), 1.70 (p, J = 30.4, 7.2, 7.8, 7.6, 7.8 Hz, 2H), 1.40 (h, J = 36.9, 7.3, 7.4, 7.5, 7.4, 7.3 Hz, 2H), 1.00 (t, J = 14.6, 7.3, 7.3 Hz, 3H). ^{13}C NMR (101 MHz, CD_2Cl_2): δ 172.0, 170.7, 143.8, 141.0, 139.6, 137.9, 137.0, 129.8, 128.7, 127.9, 121.9, 35.9, 34.3, 23.0, 14.3. HRMS (ESI) calcd for $\text{C}_{17}\text{H}_{18}\text{O}_2$ $[\text{M}+\text{H}]^+$: 255.1385; found: 255.1390.

BA-pBr-OMe

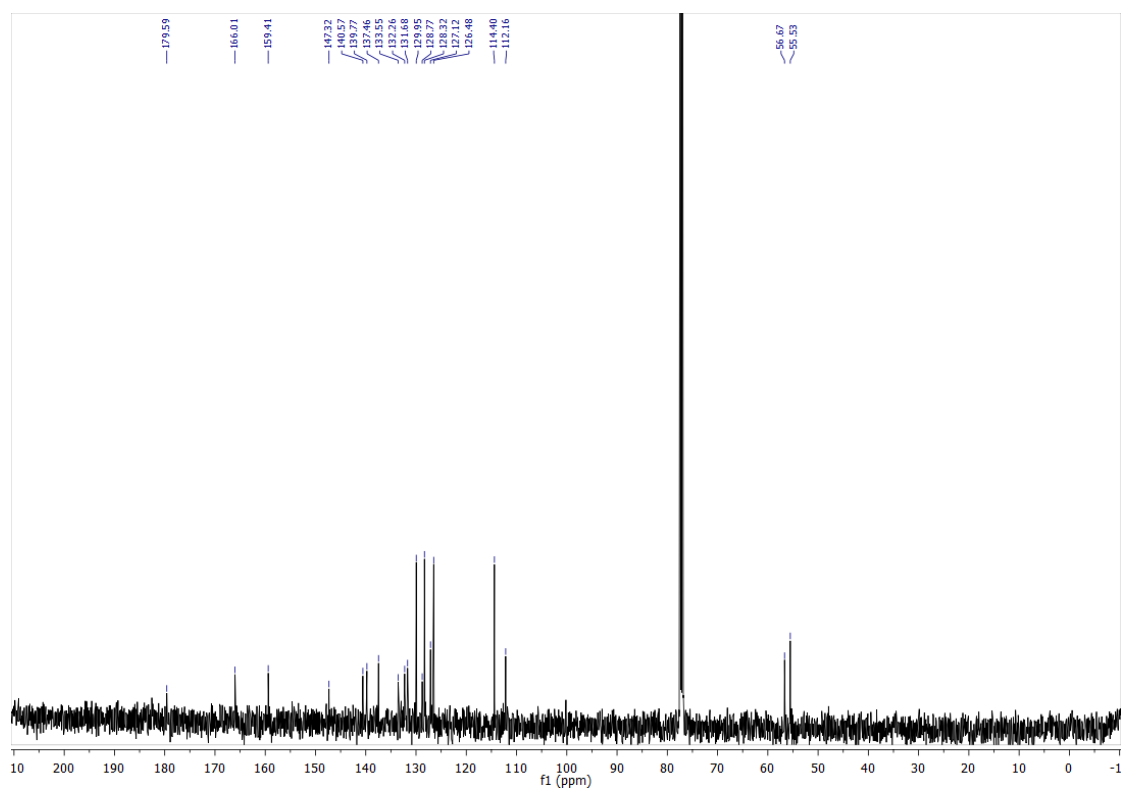
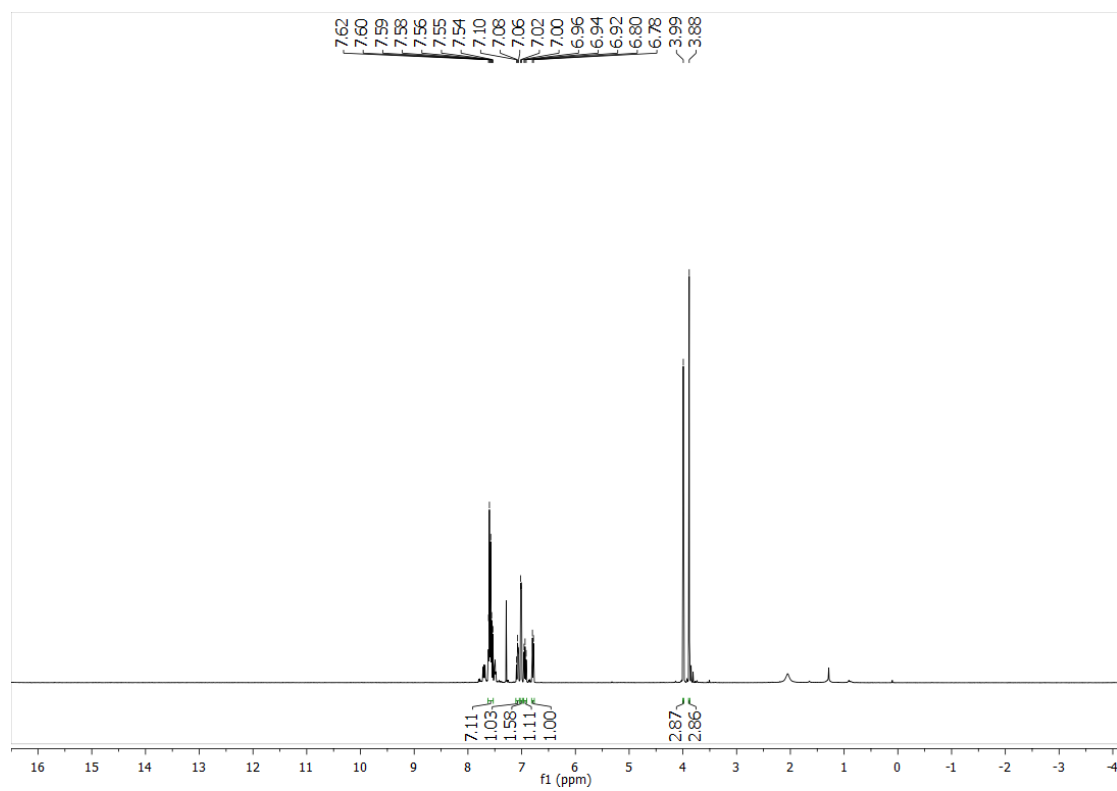
BA-pBr-OH

BA-PH-OMe

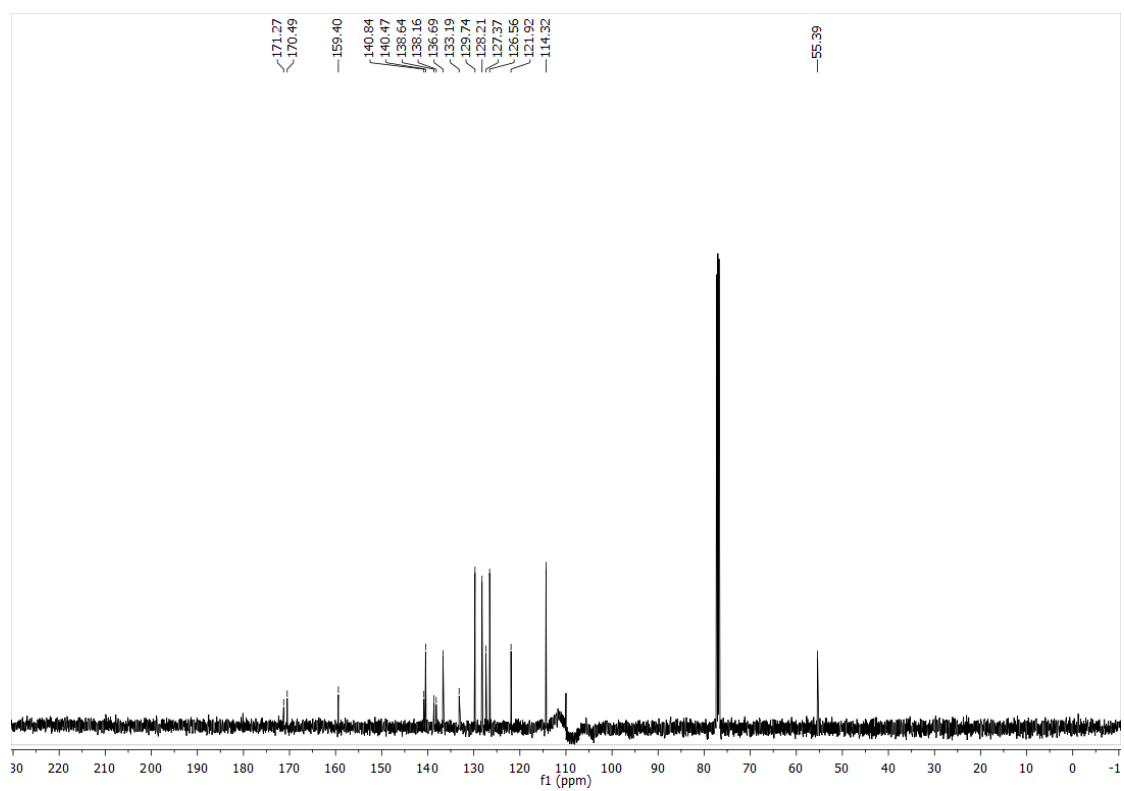
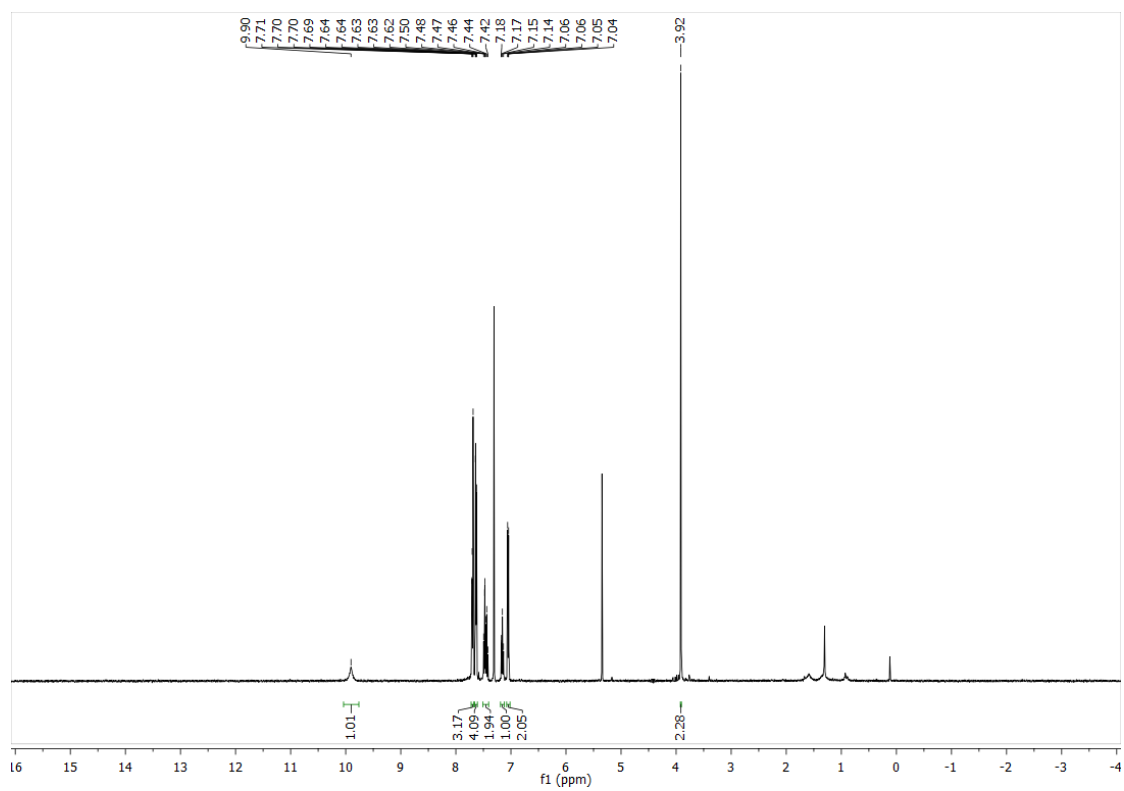
BA-PH-OH



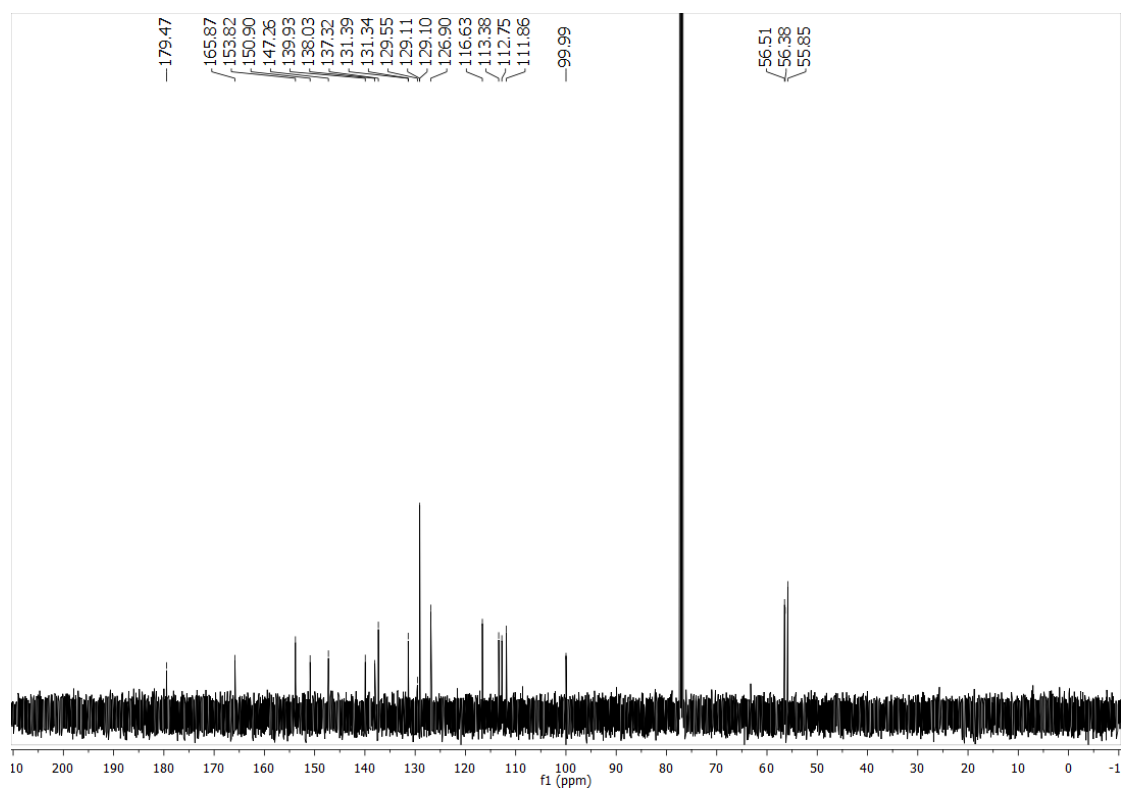
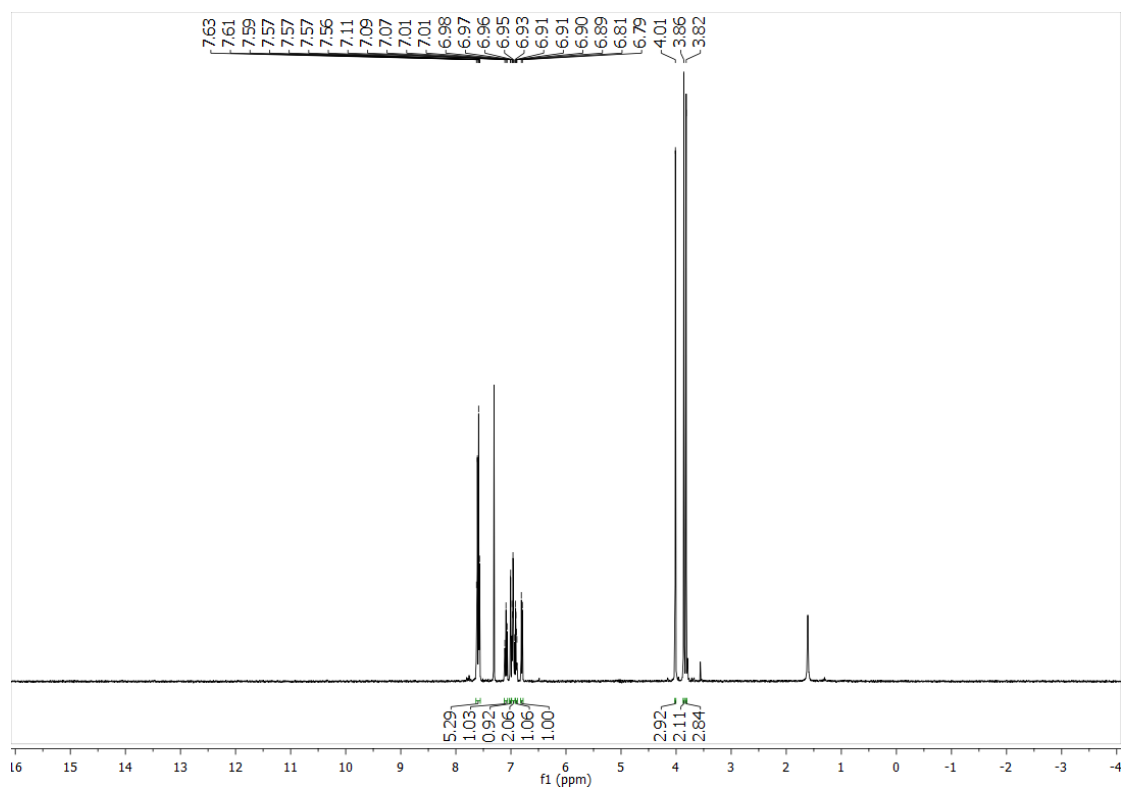
BA-SM-OMe



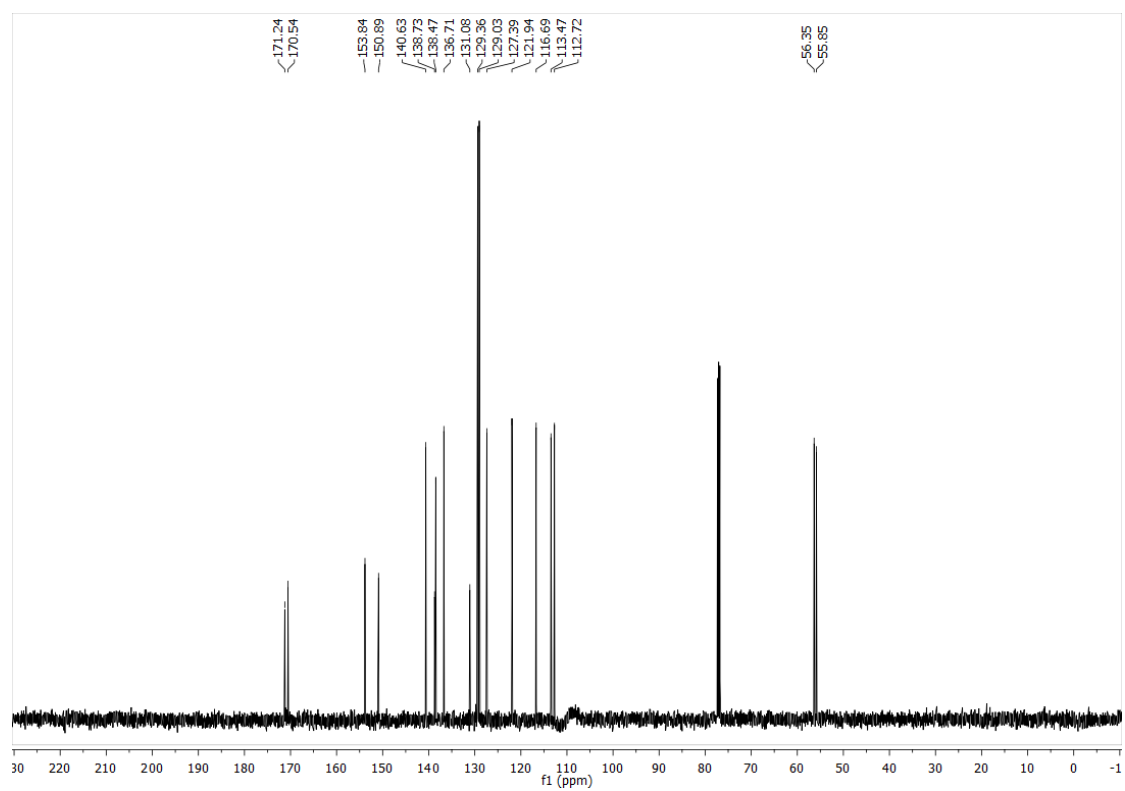
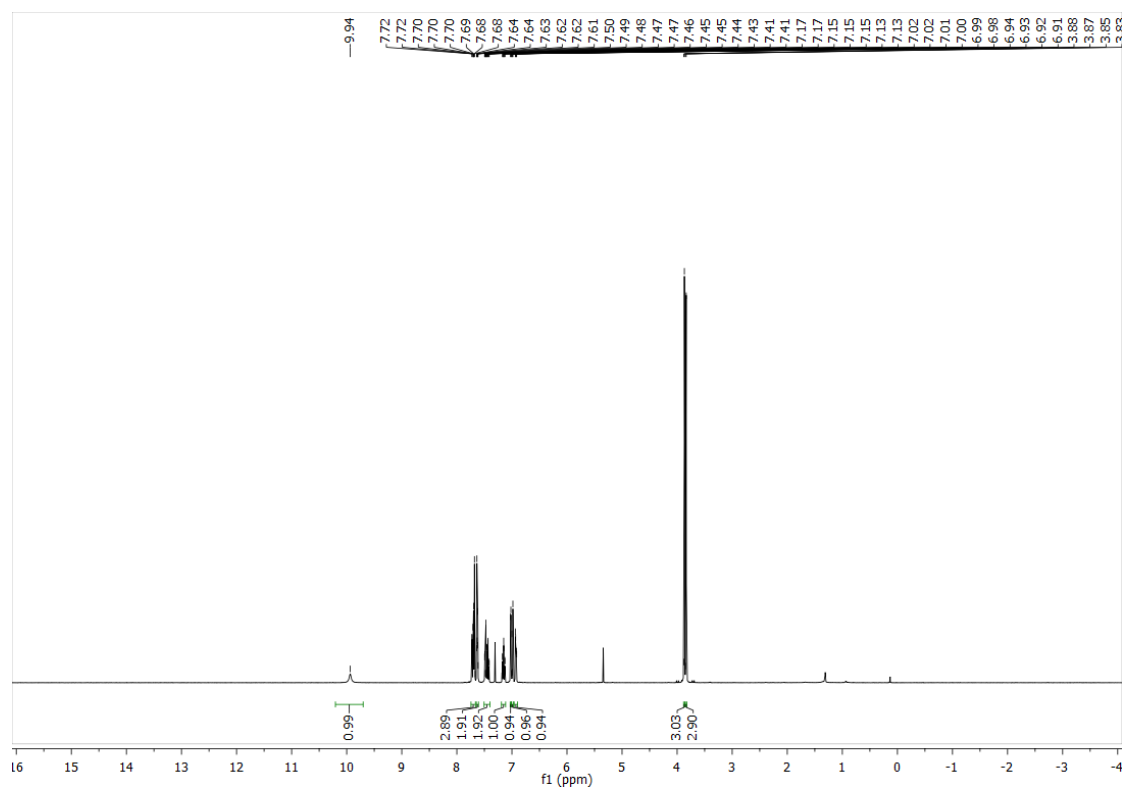
BA-SM-OH



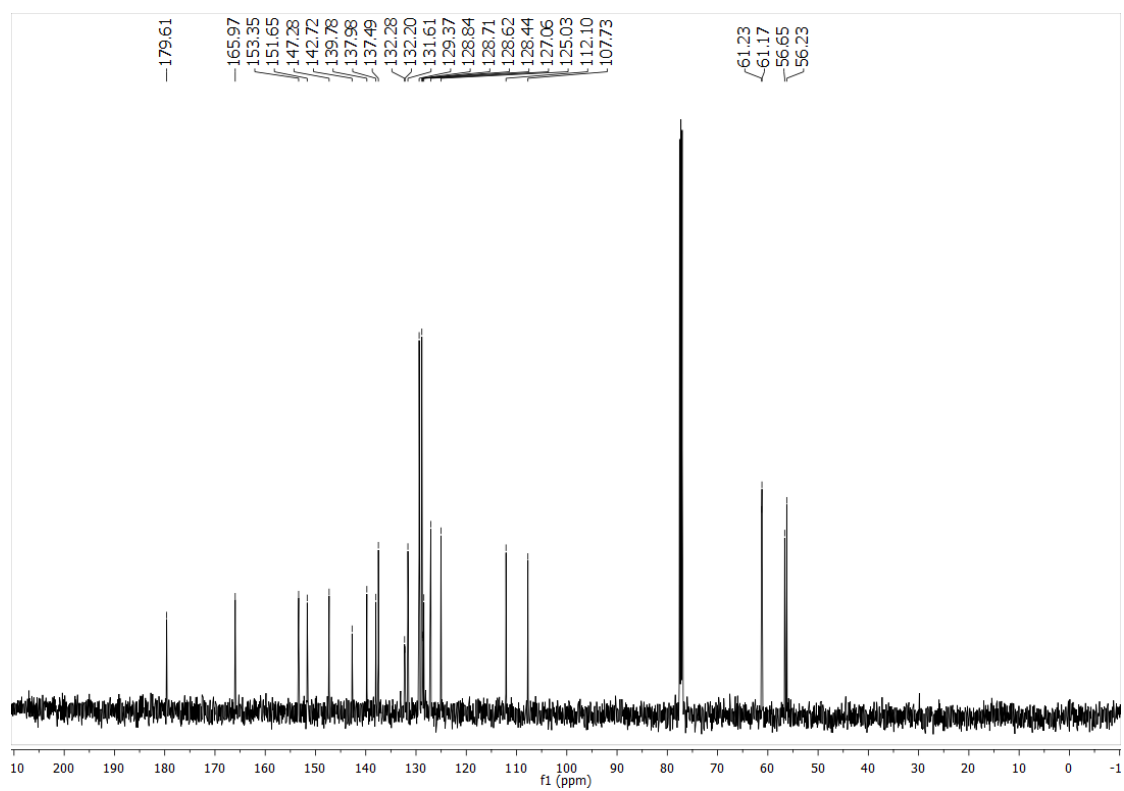
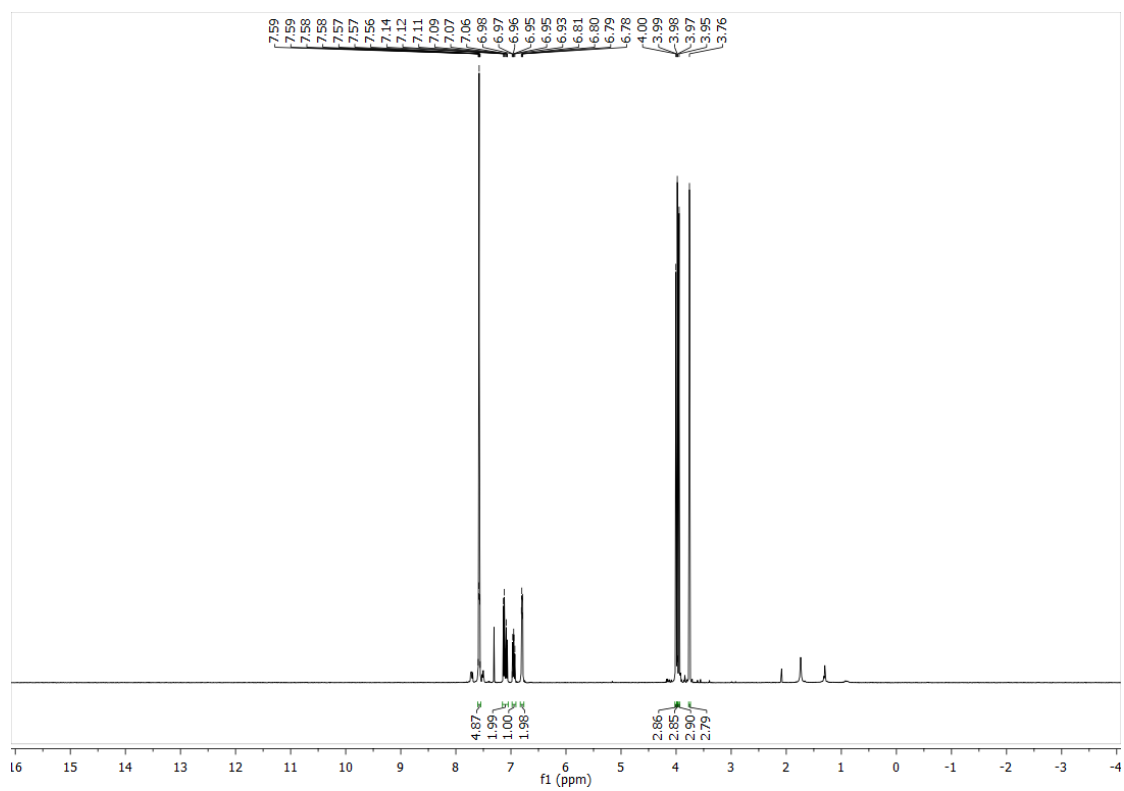
BA-DM-OMe



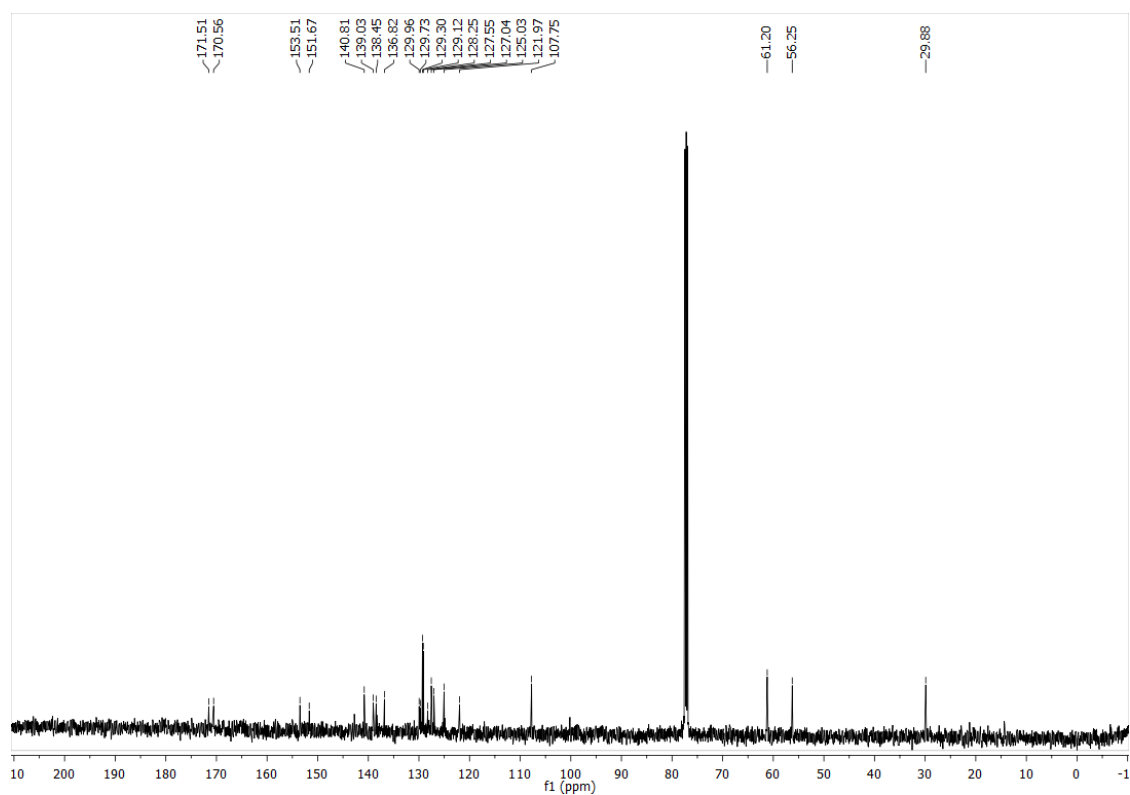
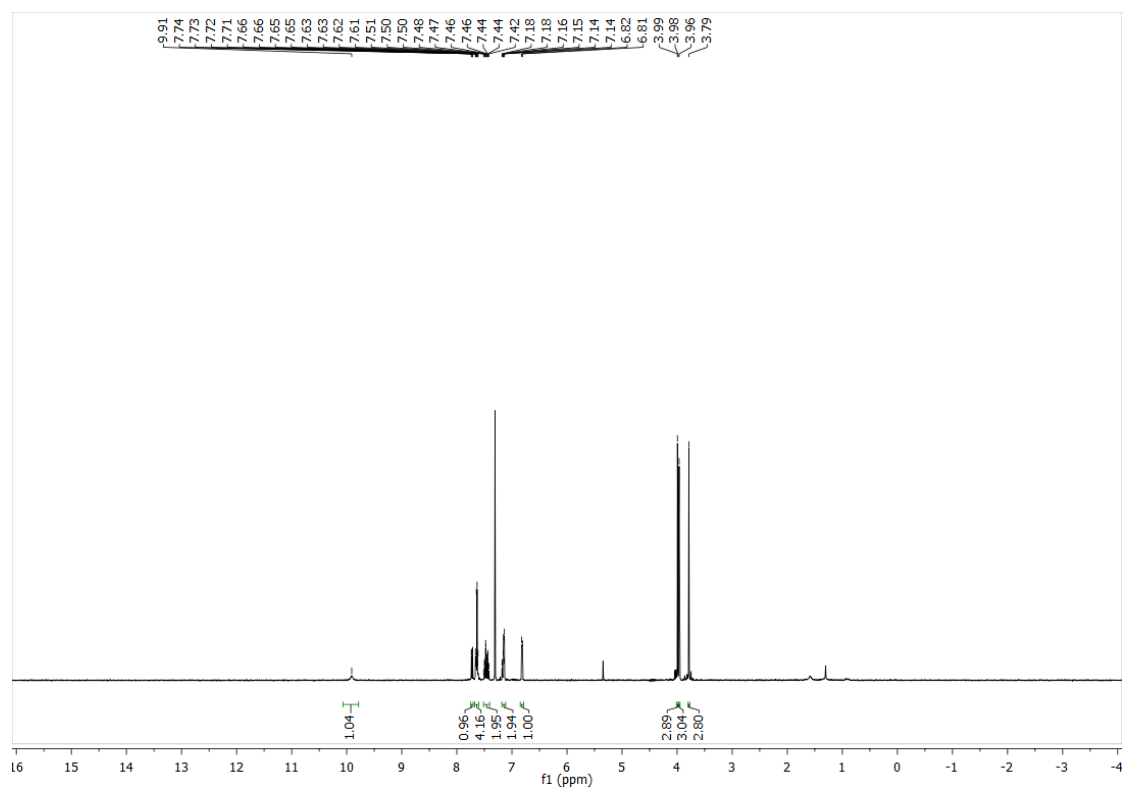
BA-DM-OH



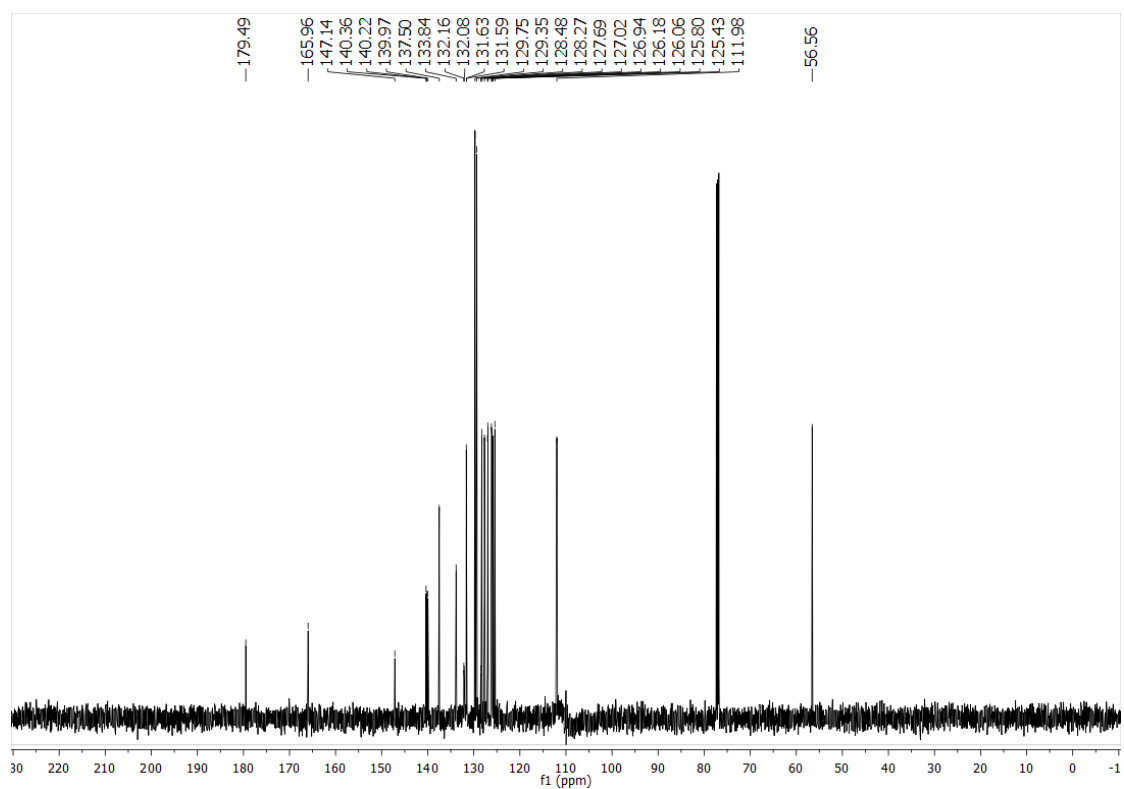
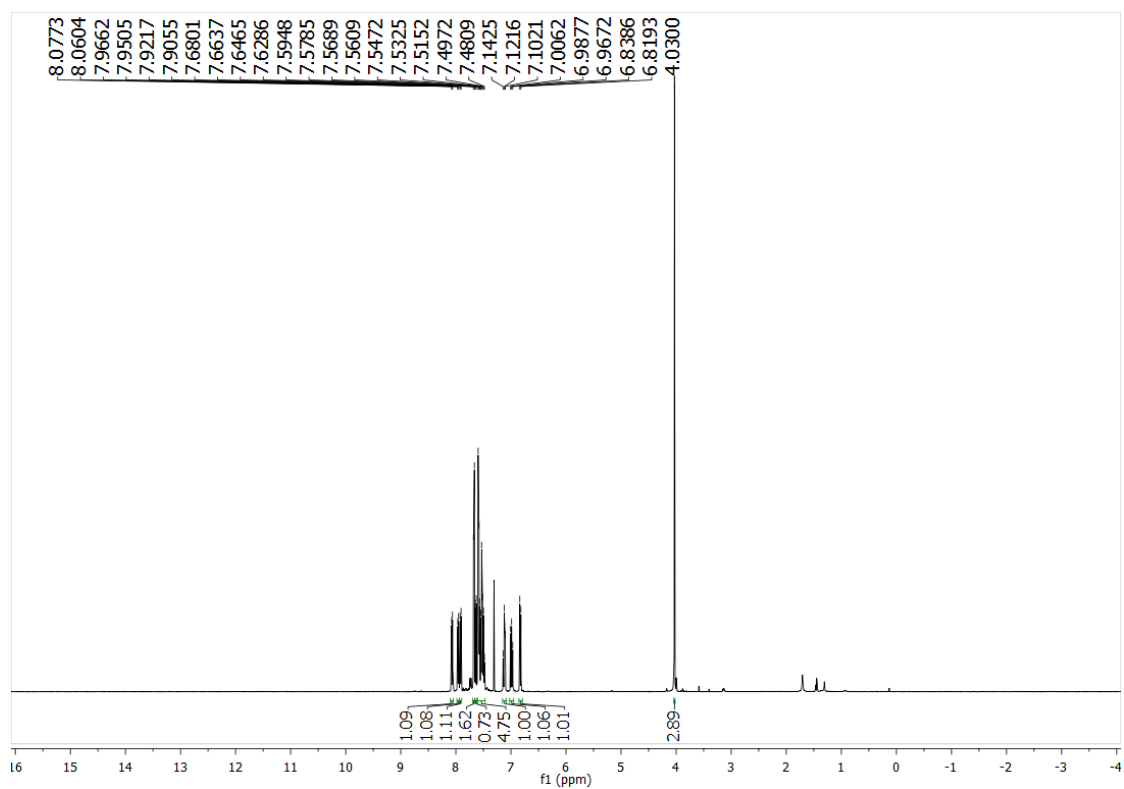
BA-TM-OMe



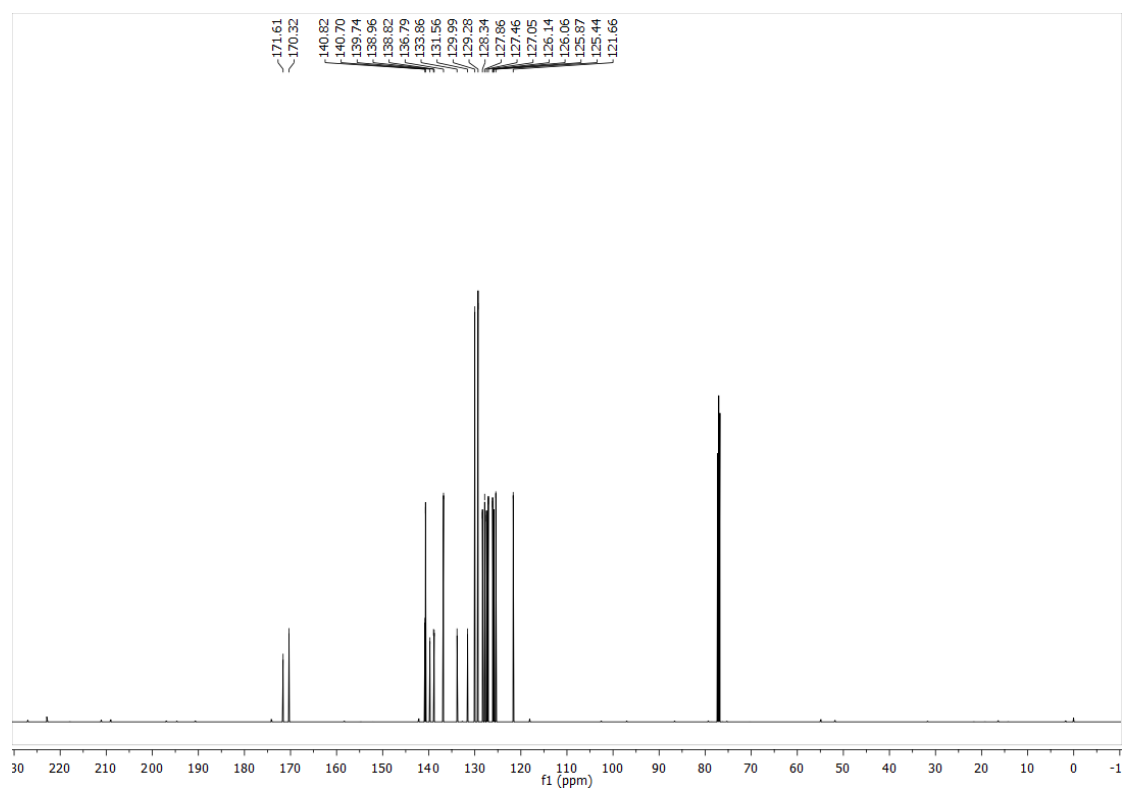
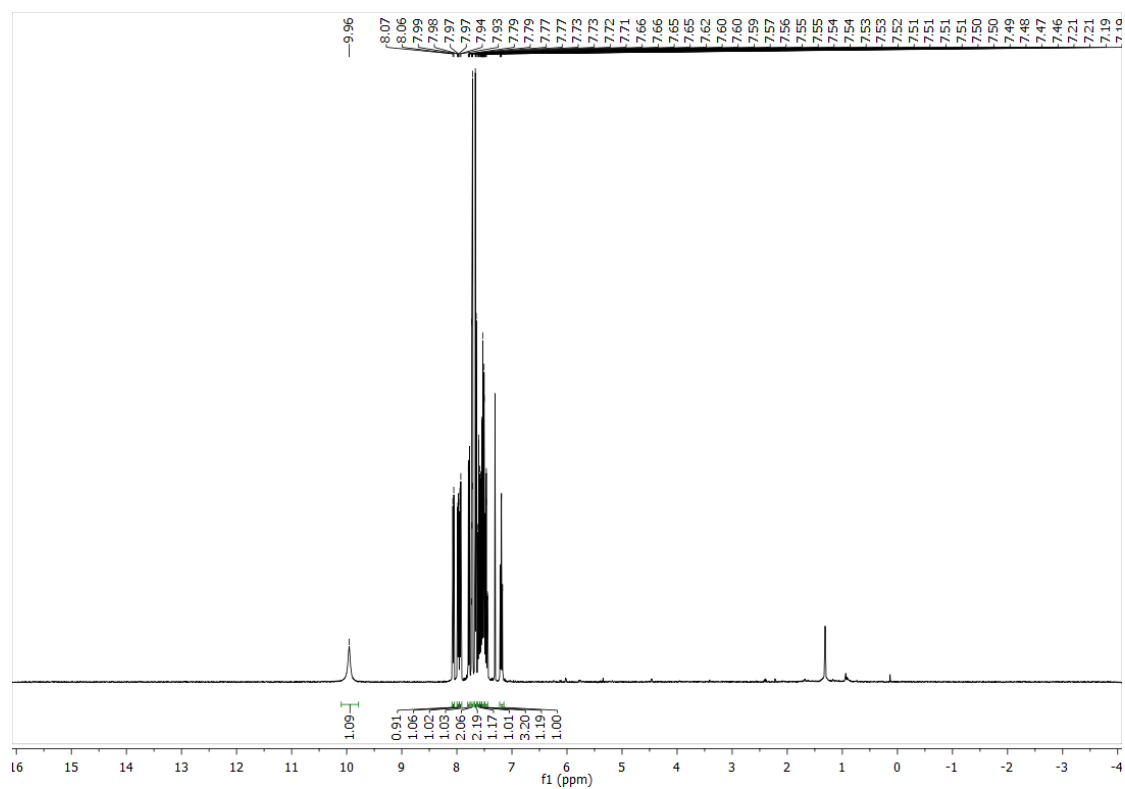
BA-TM-OH

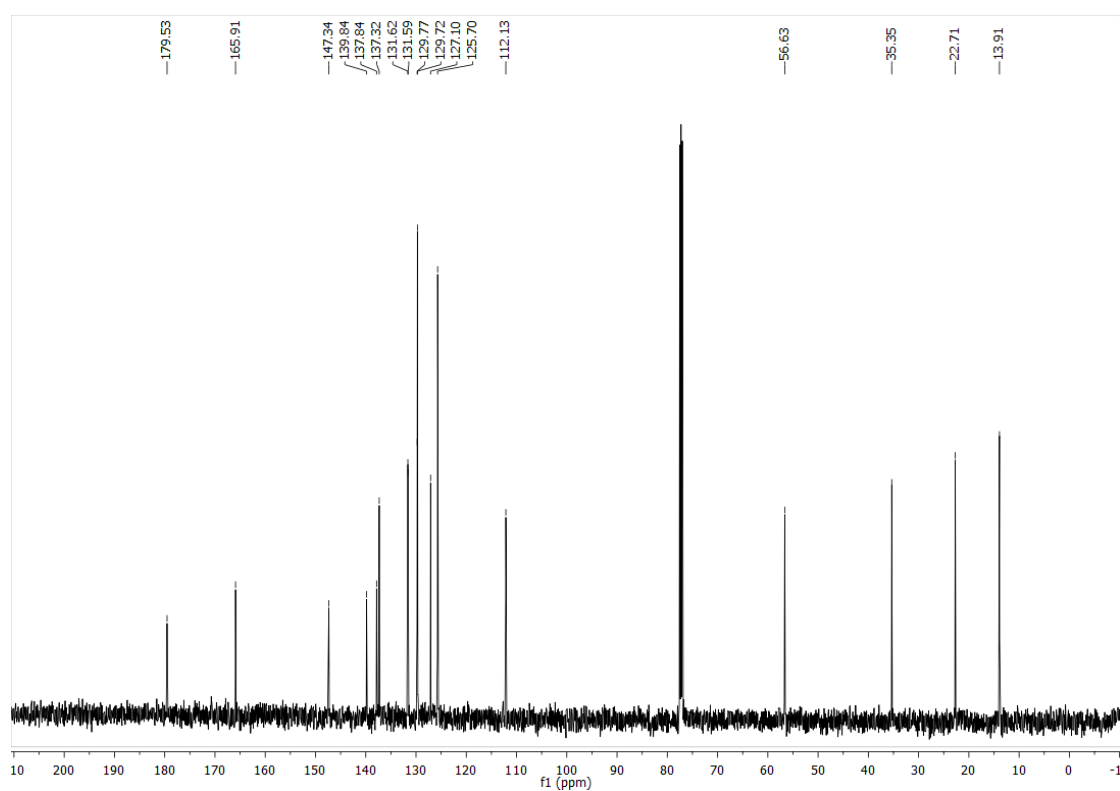
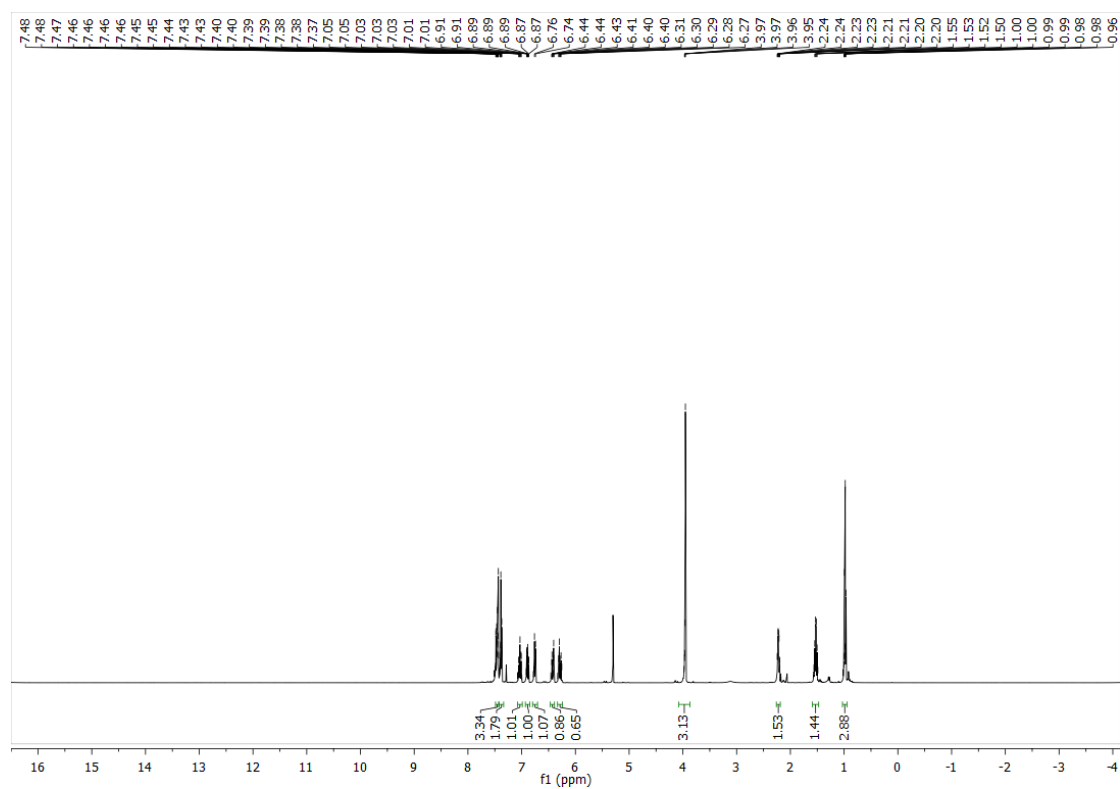


BA-Nap-OMe

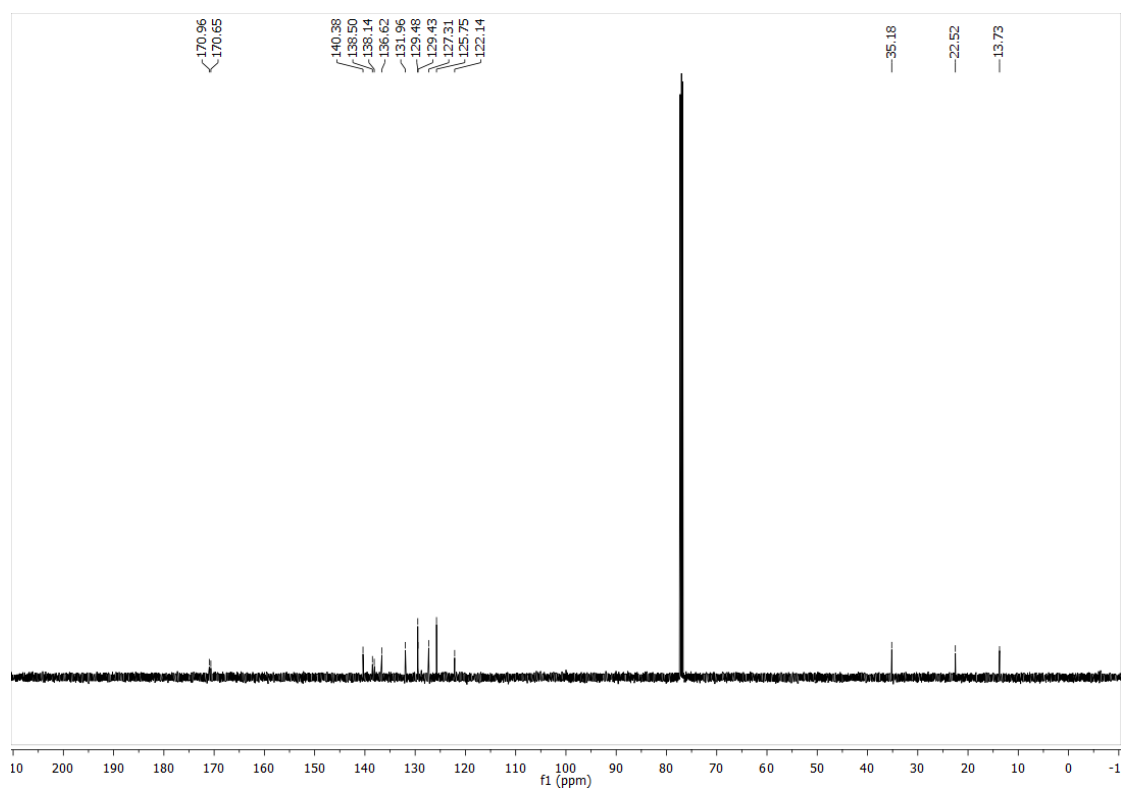
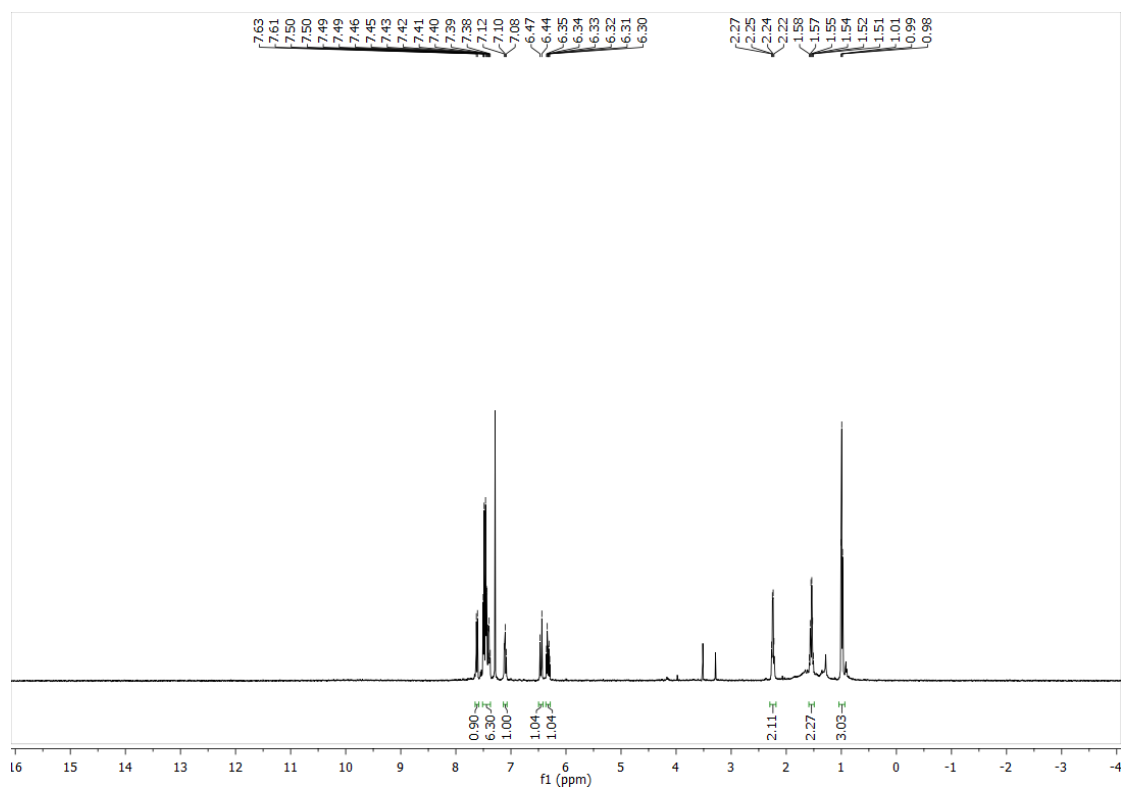


BA-Nap-OH

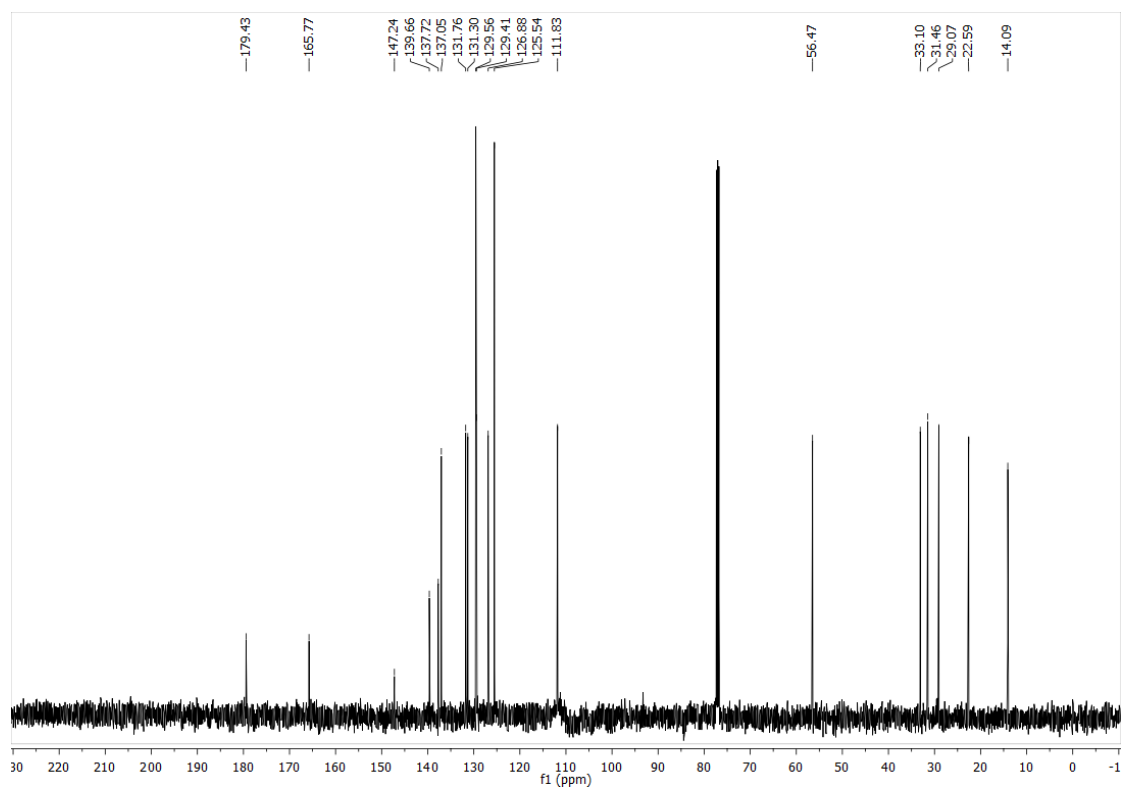
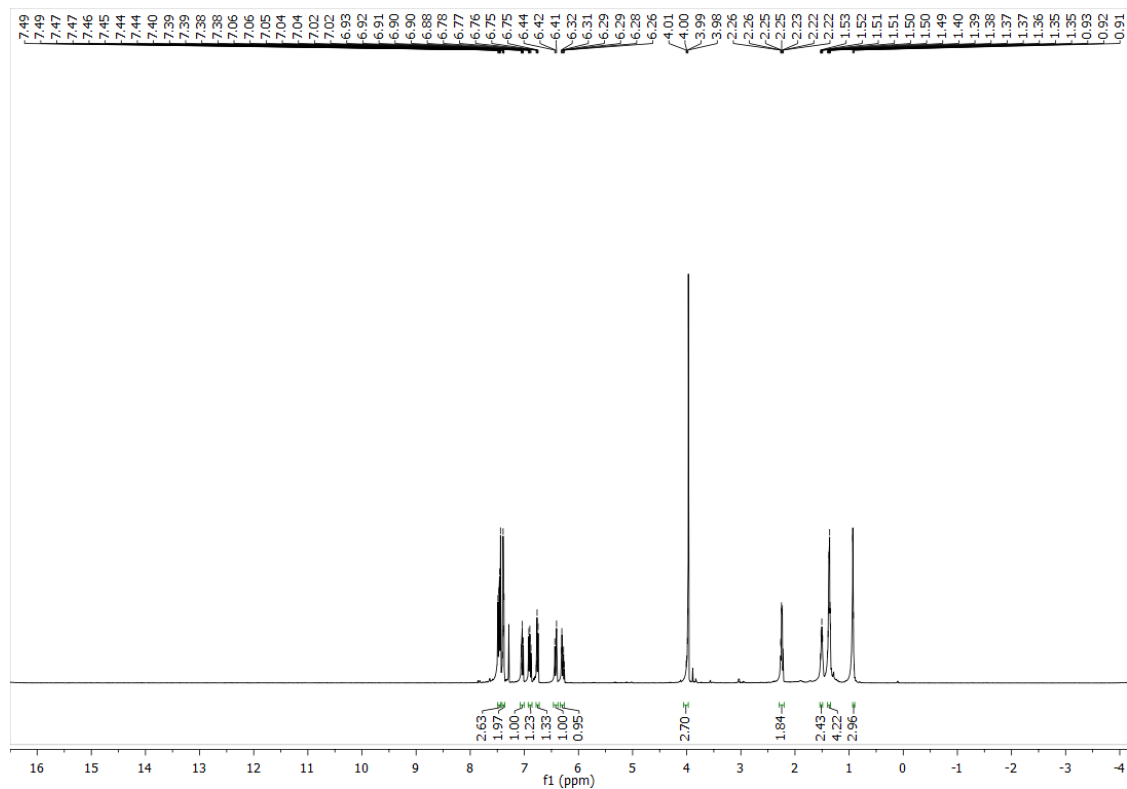




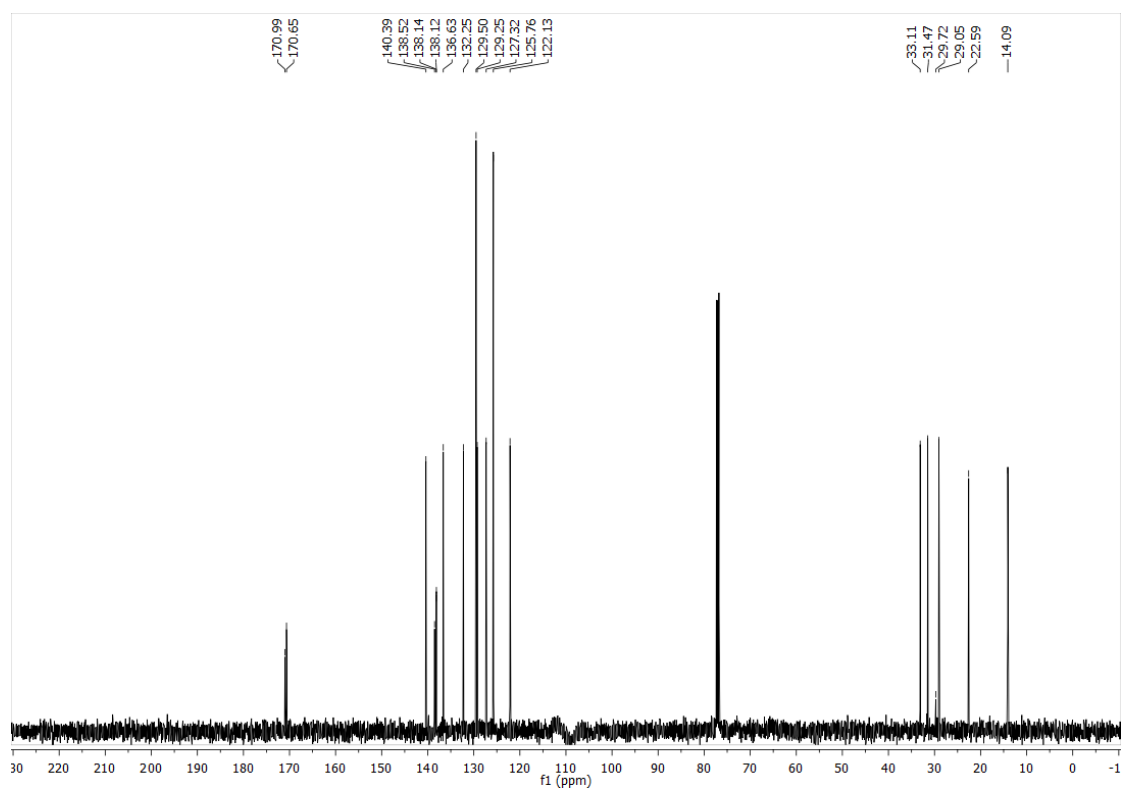
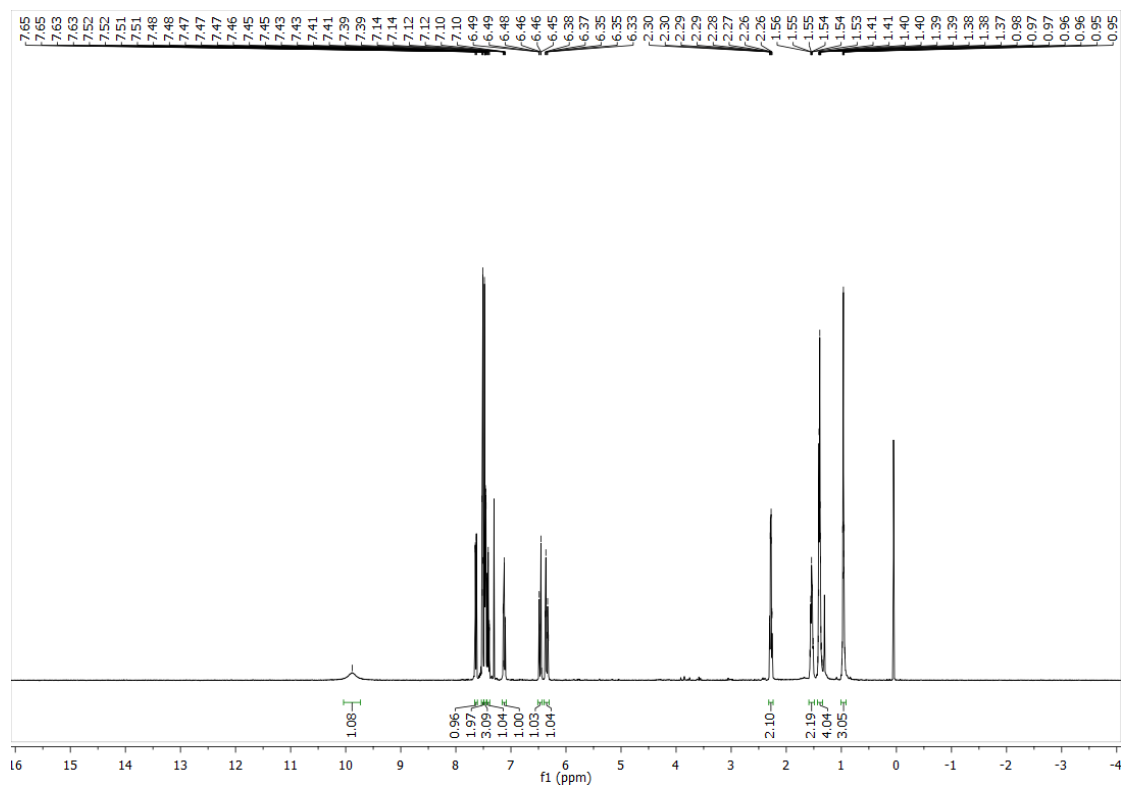
BA-P5-OH



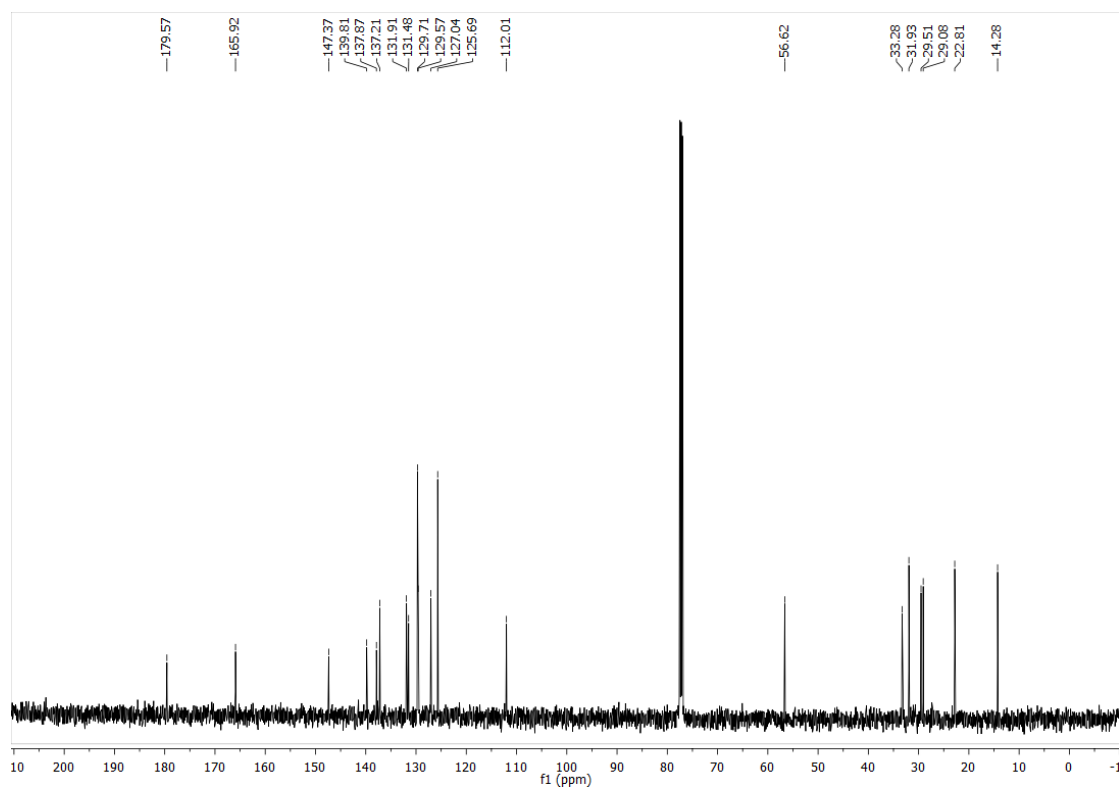
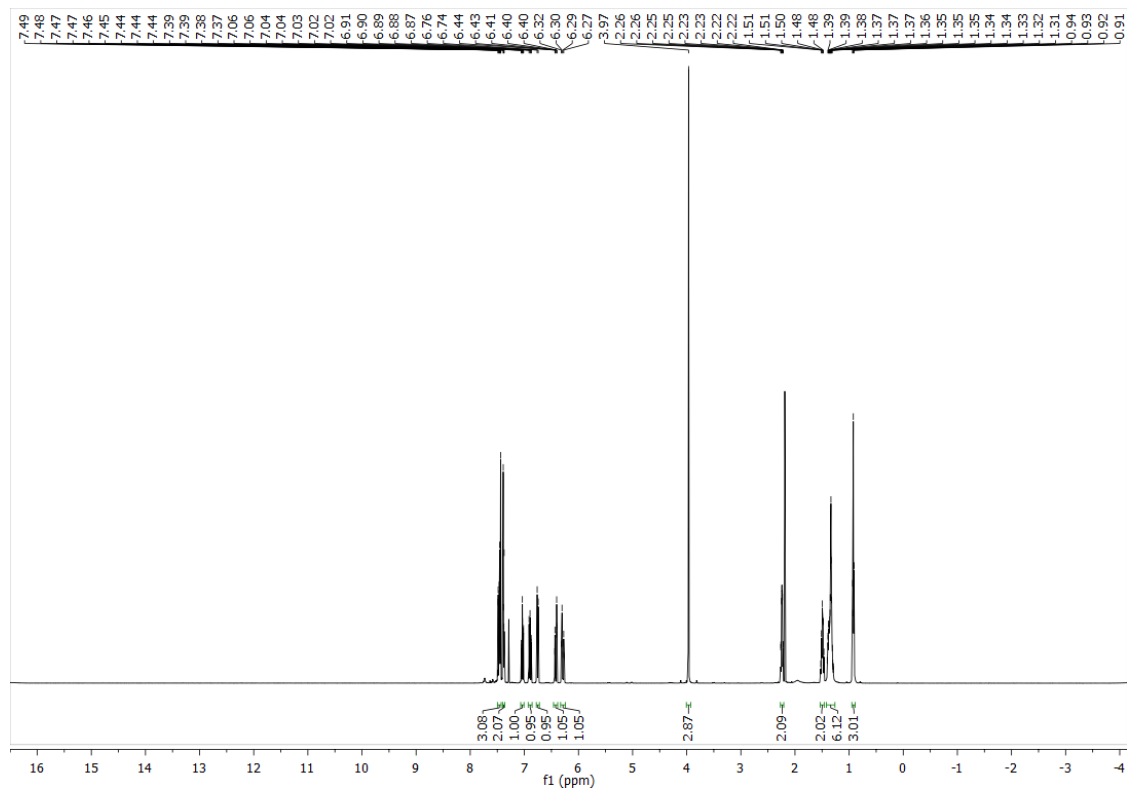
BA-P7-OMe



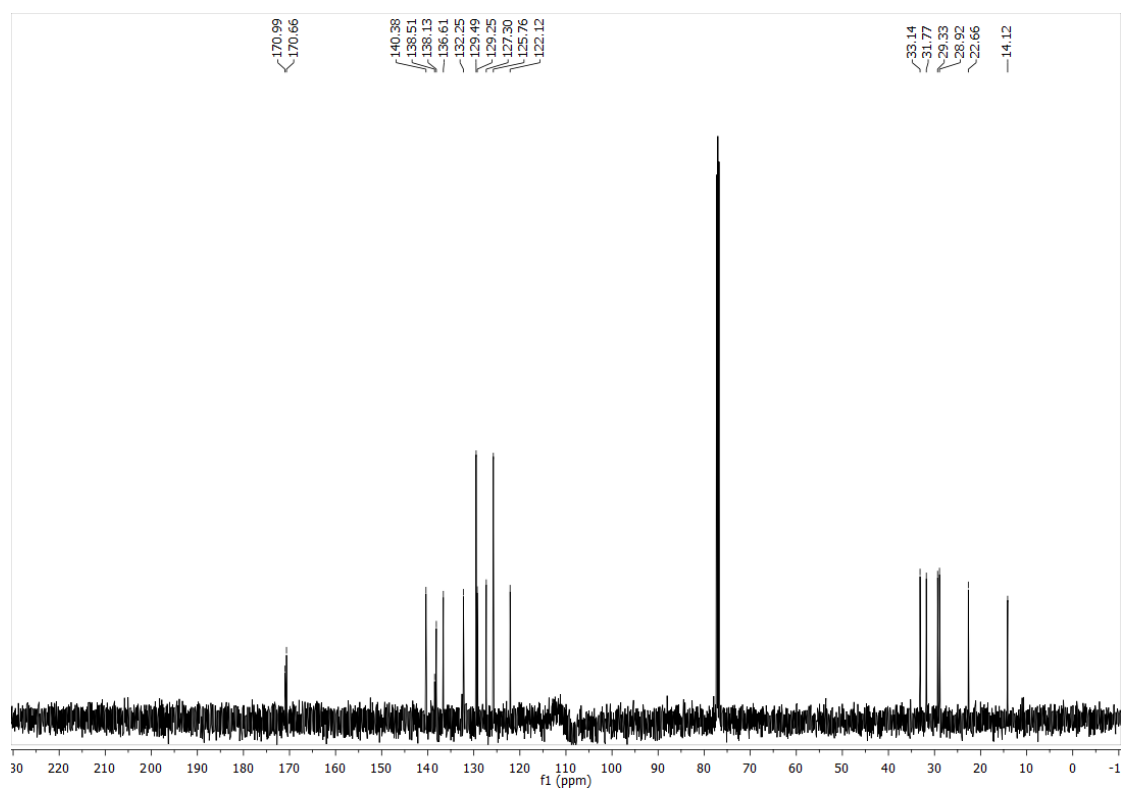
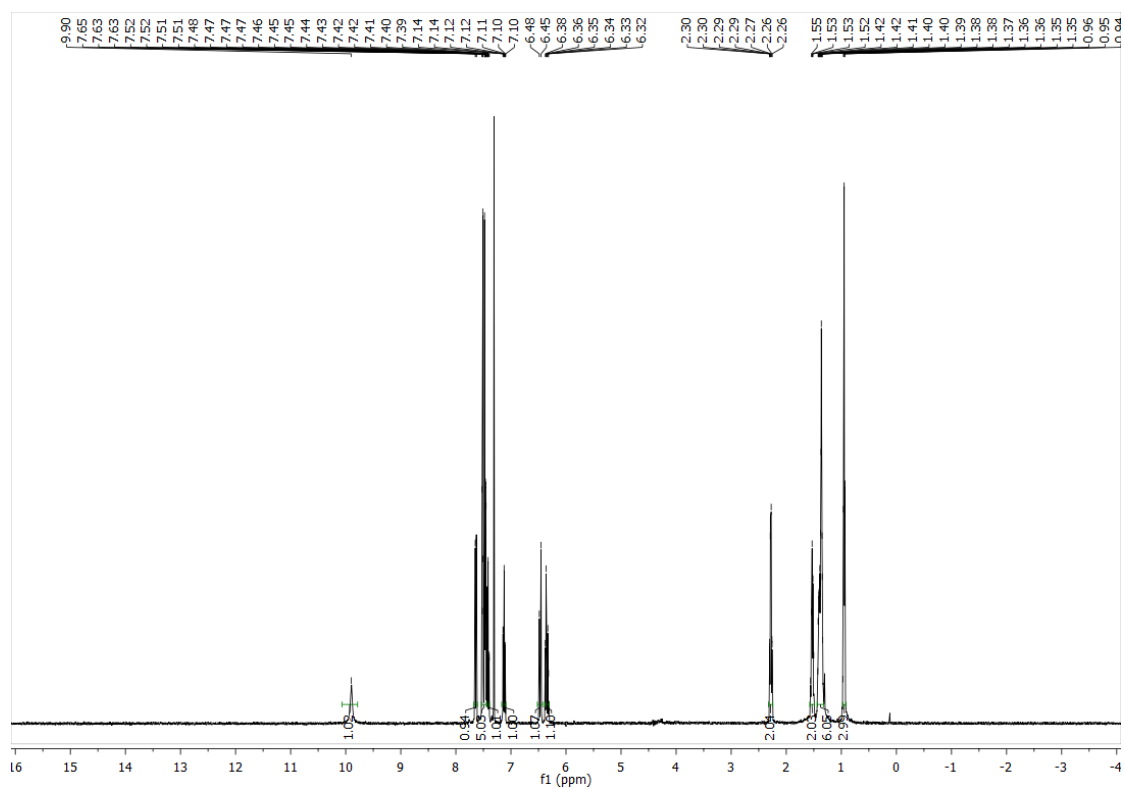
BA-P7-OH



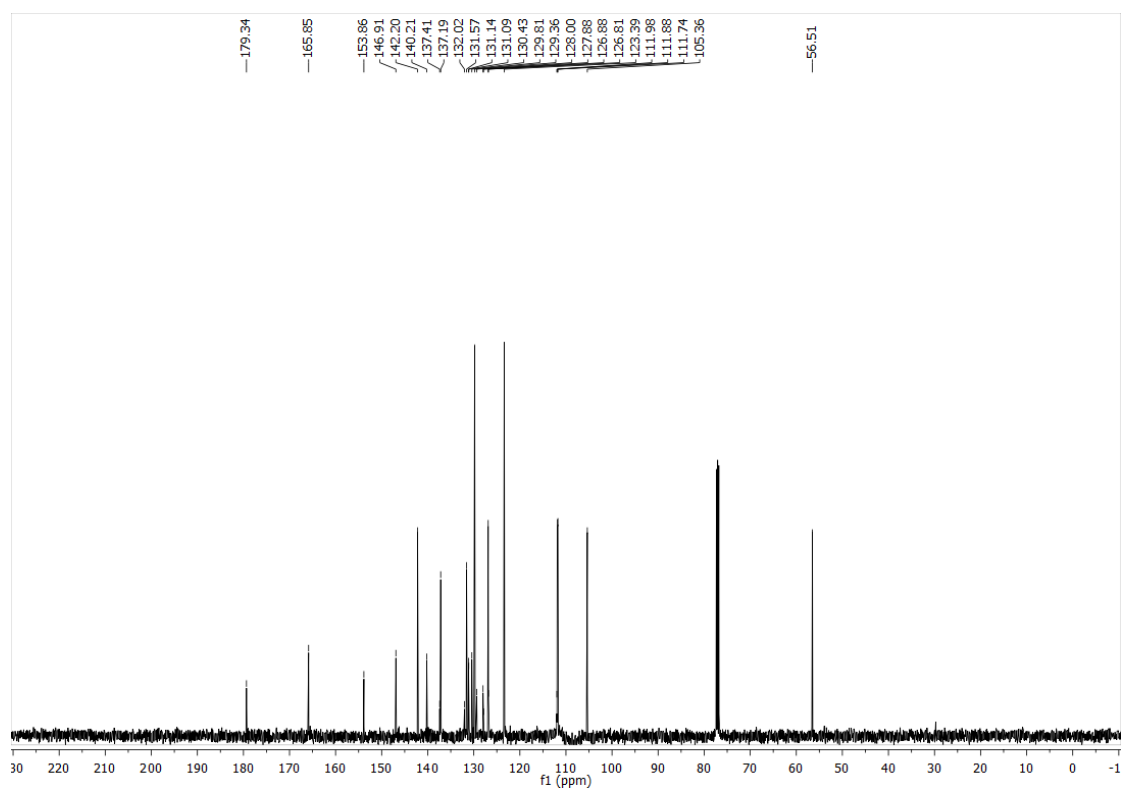
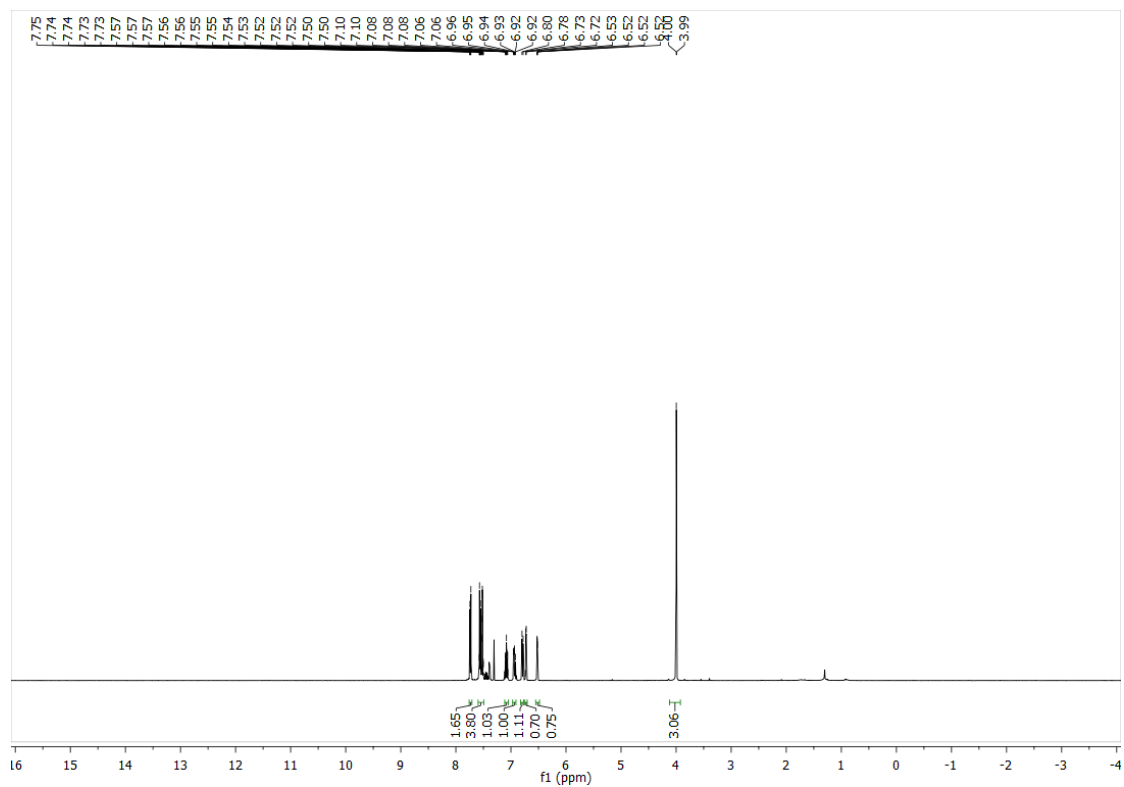
BA-P8-OMe



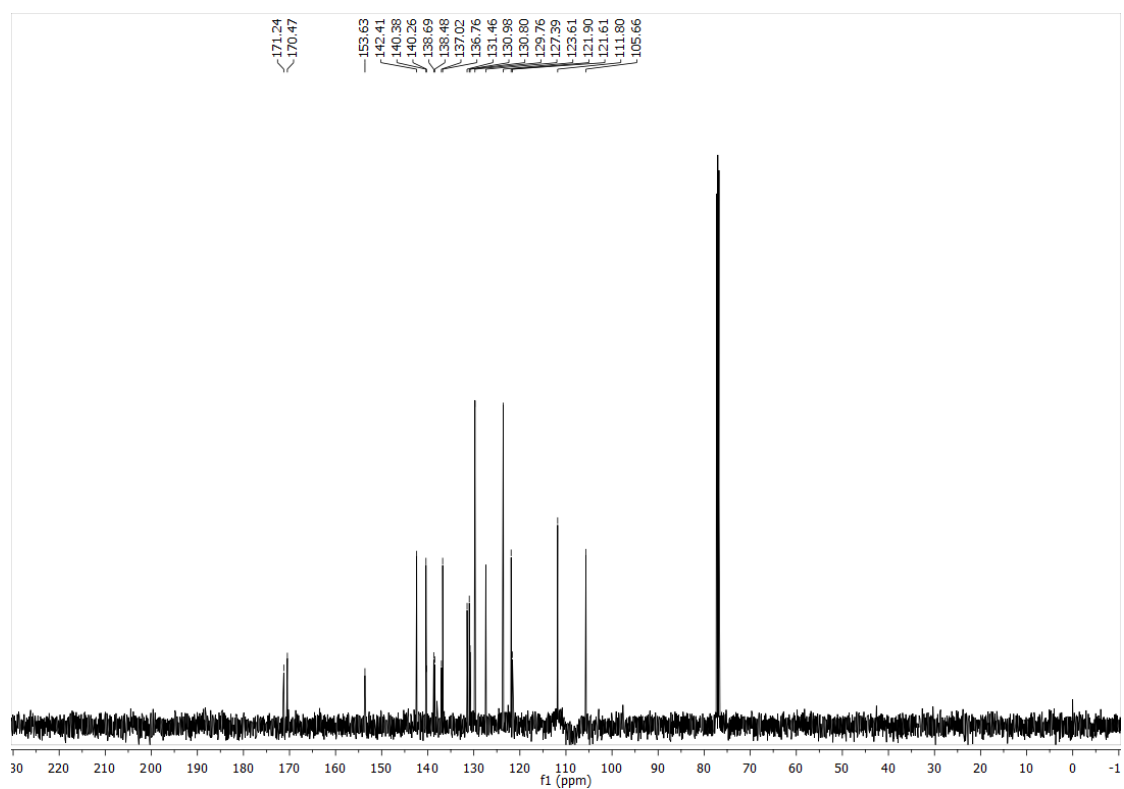
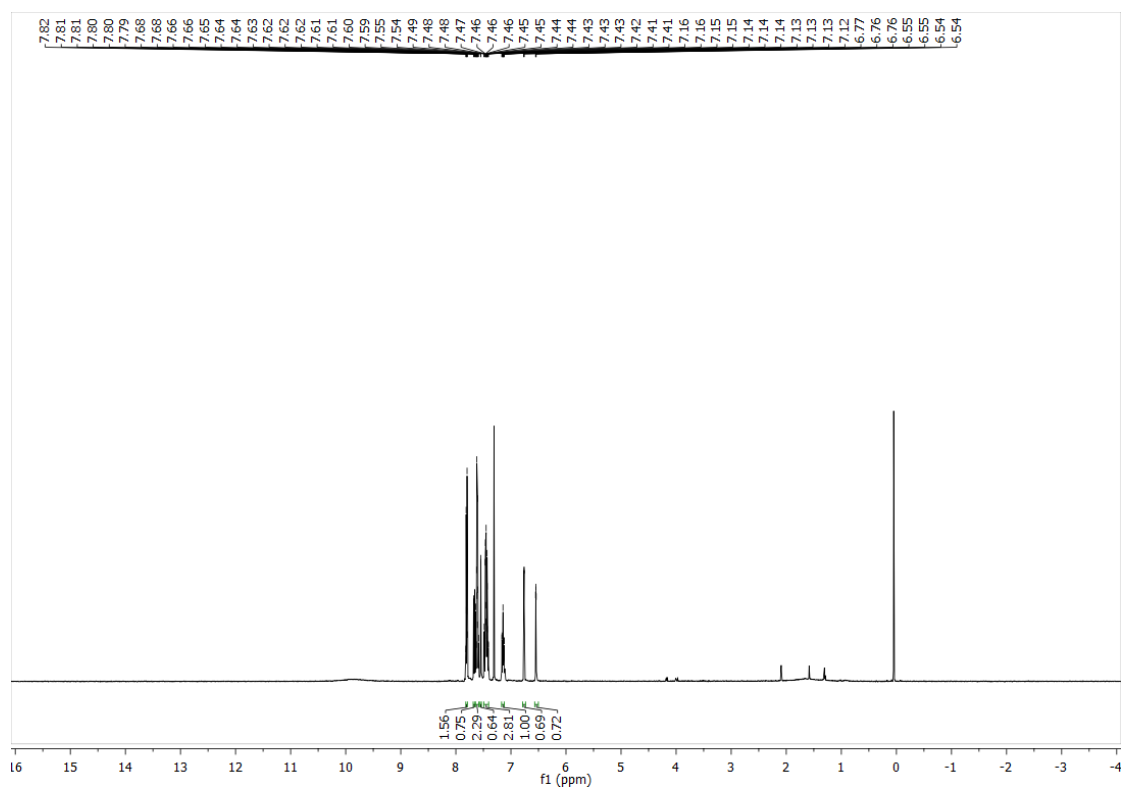
BA-P8-OH



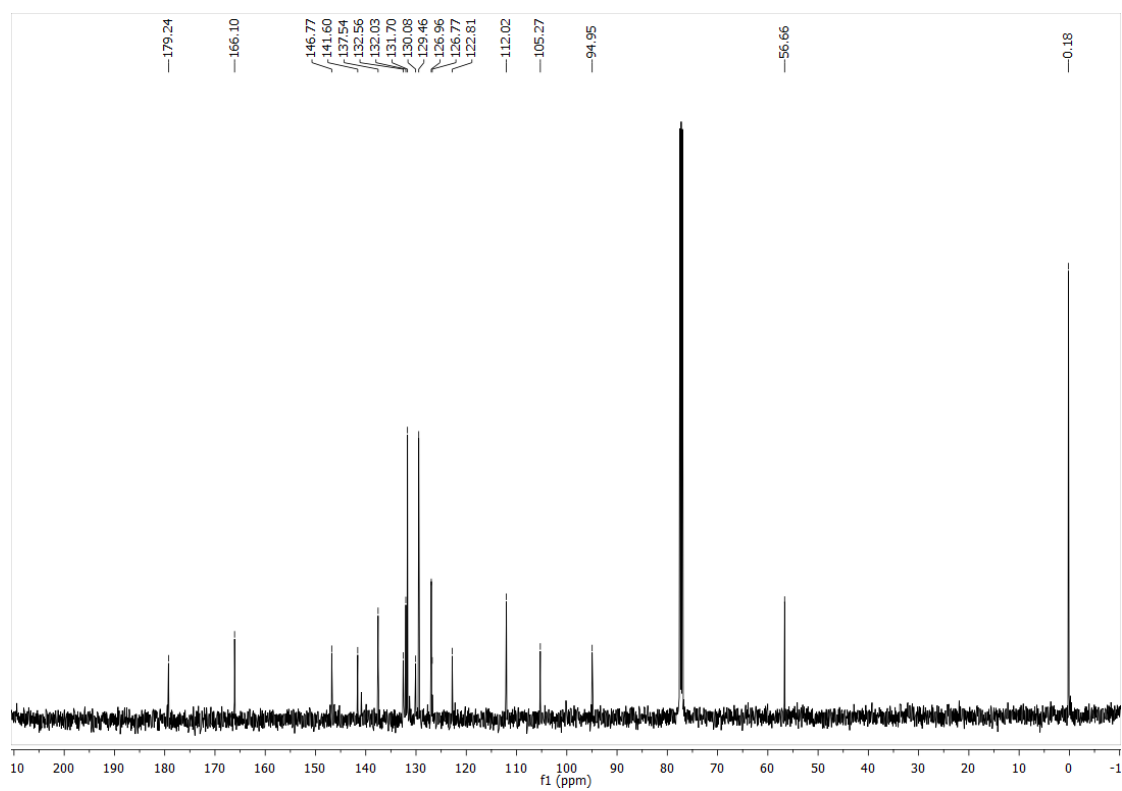
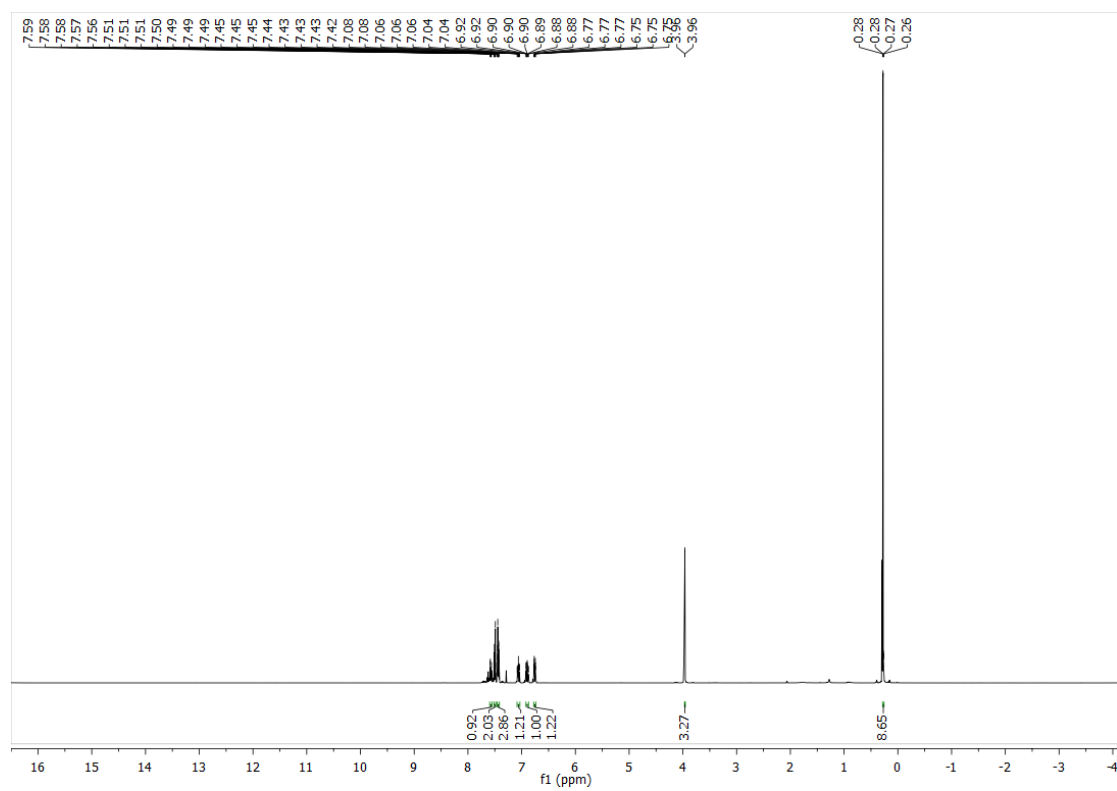
BA-HC2-OMe



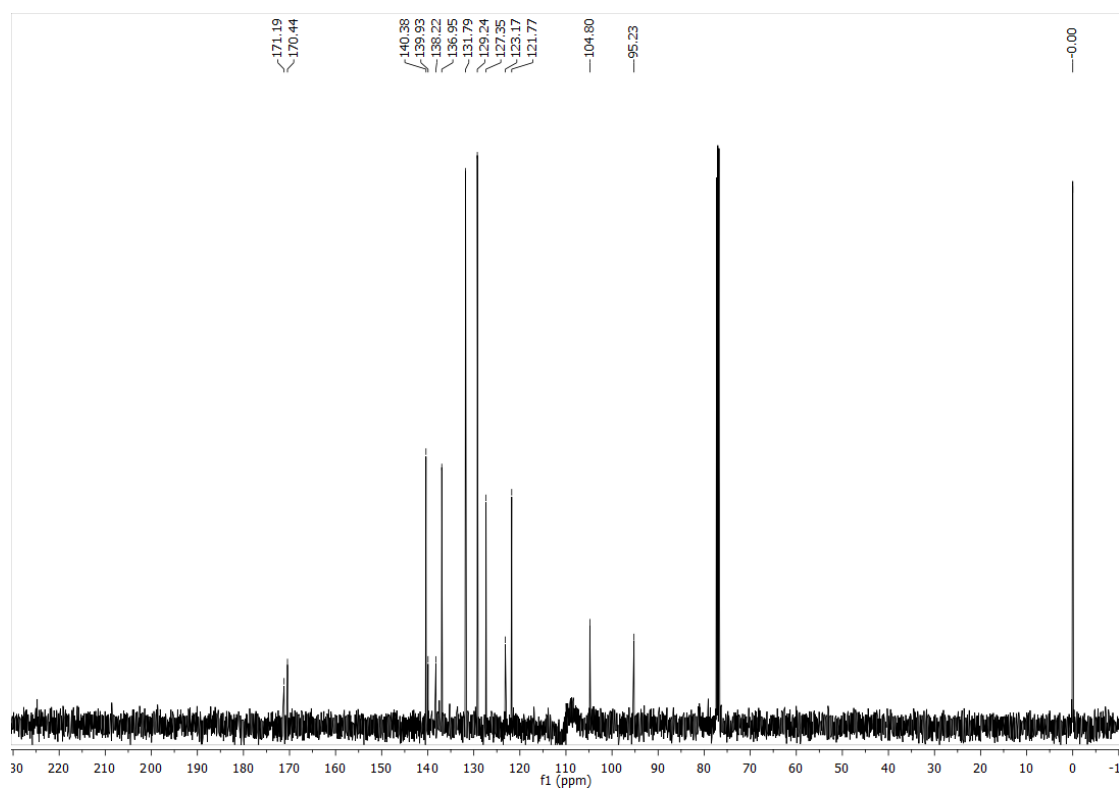
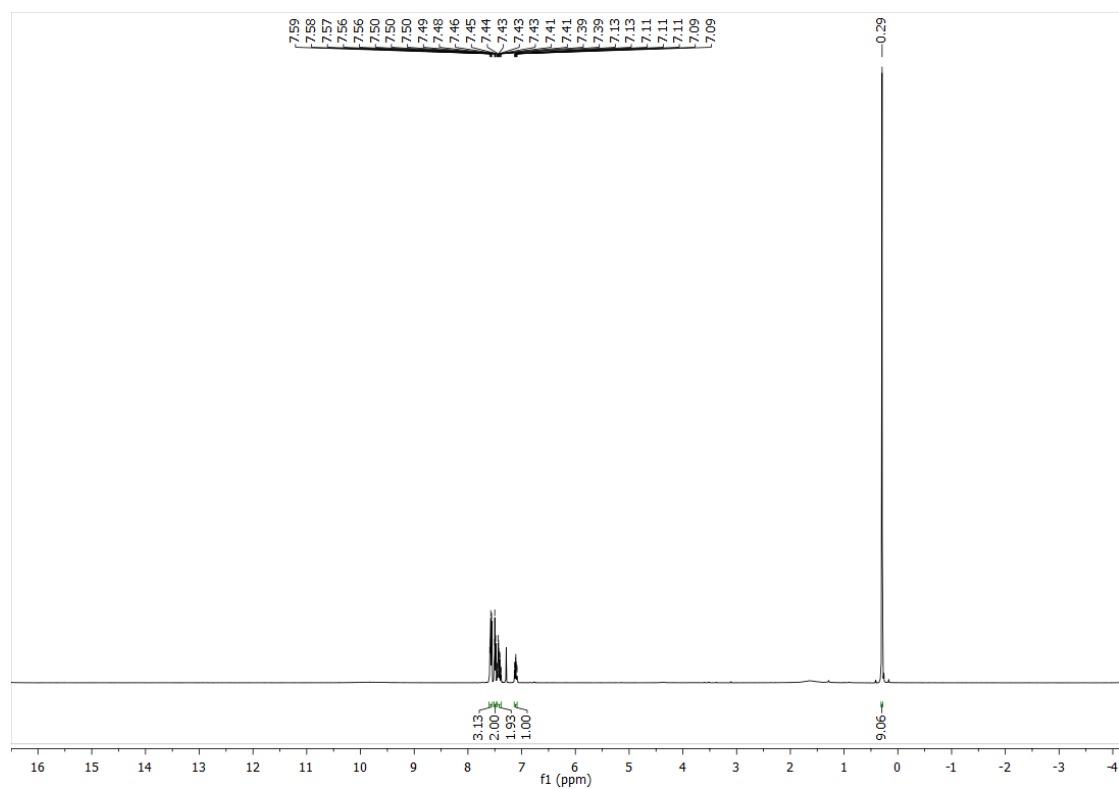
BA-HC2-OH



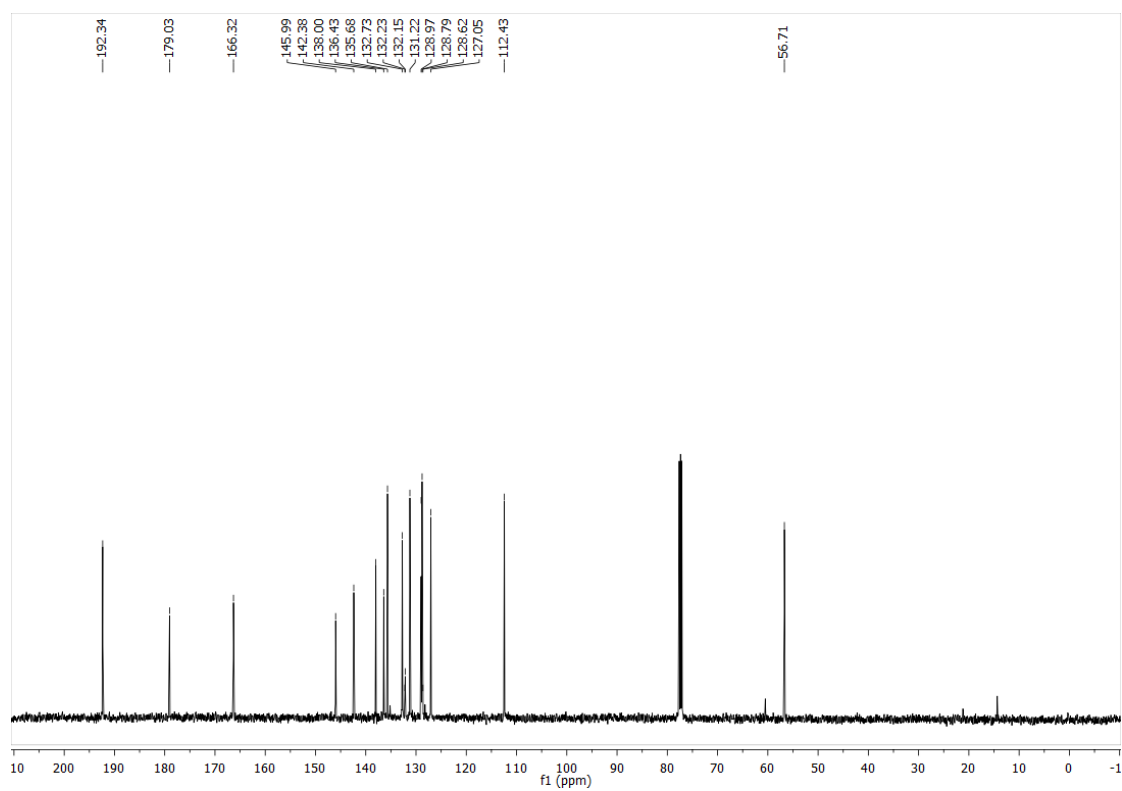
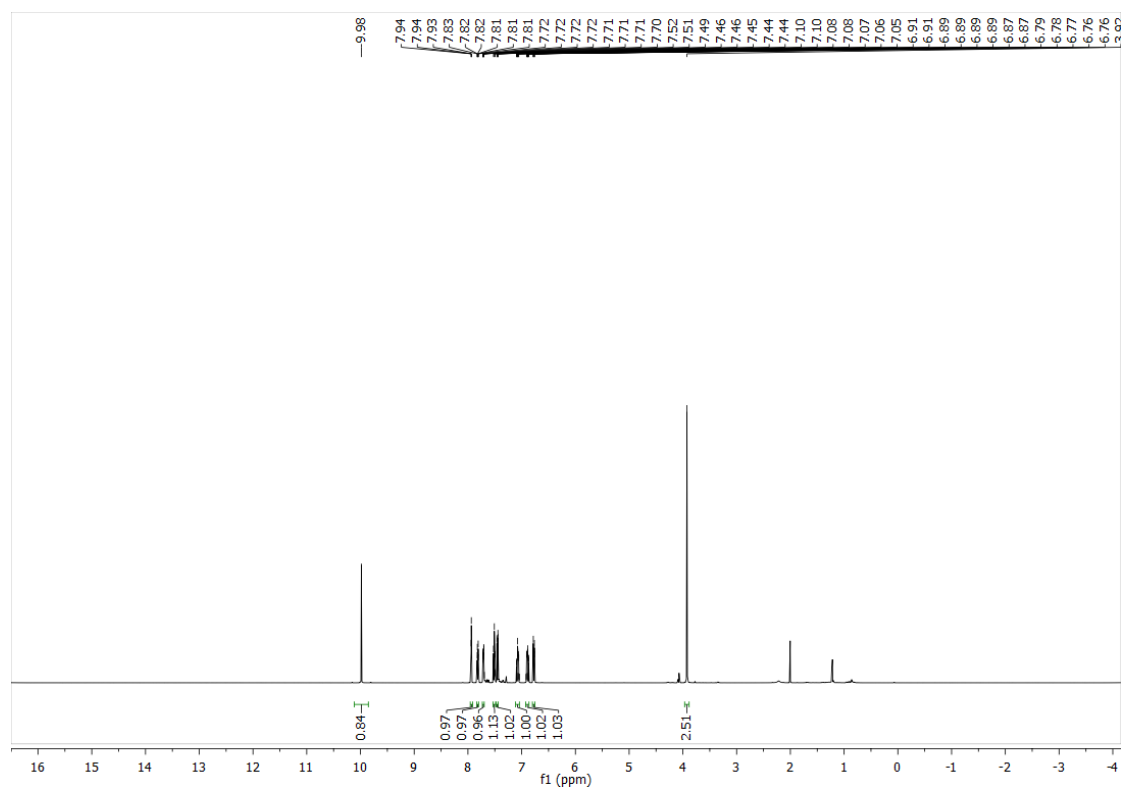
SG-TMS-OMe

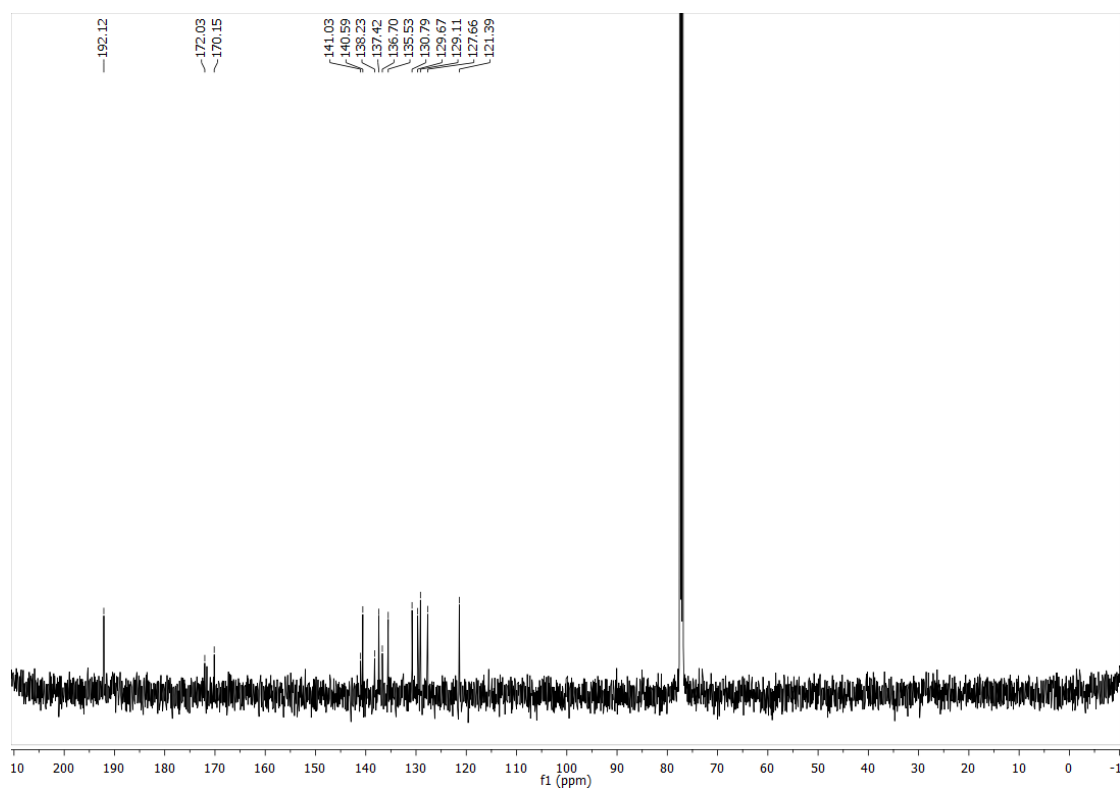
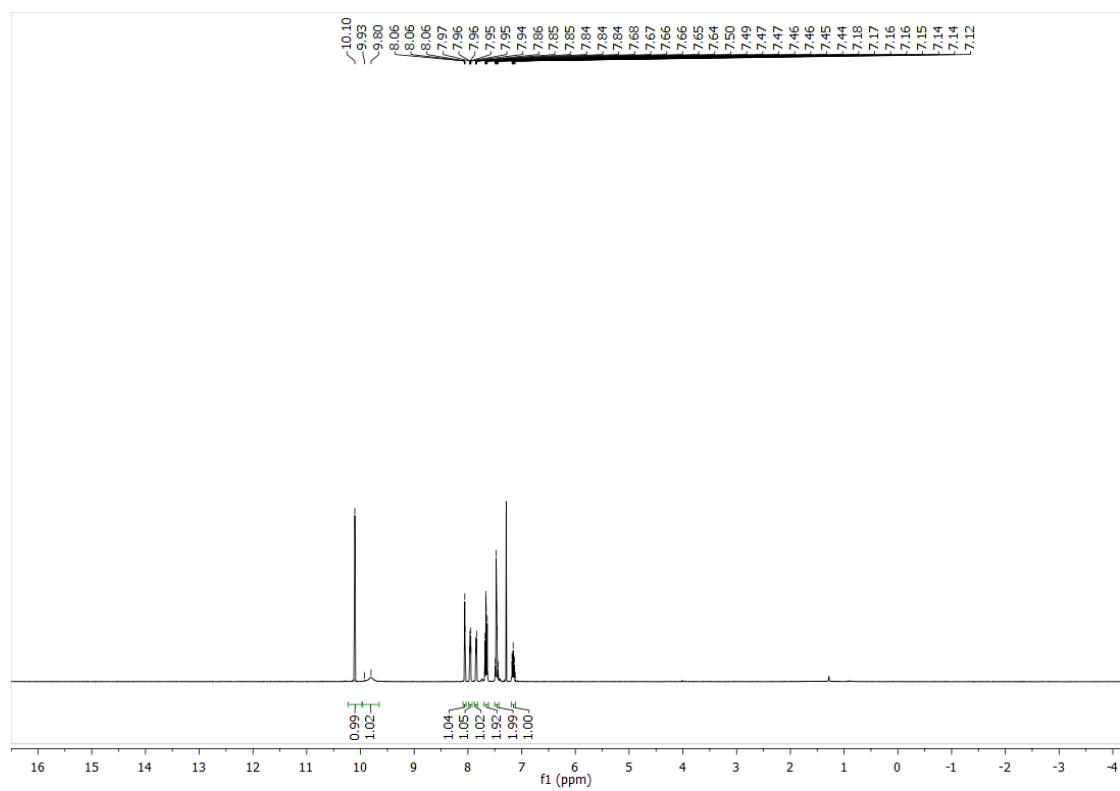


SG-TMS-OH

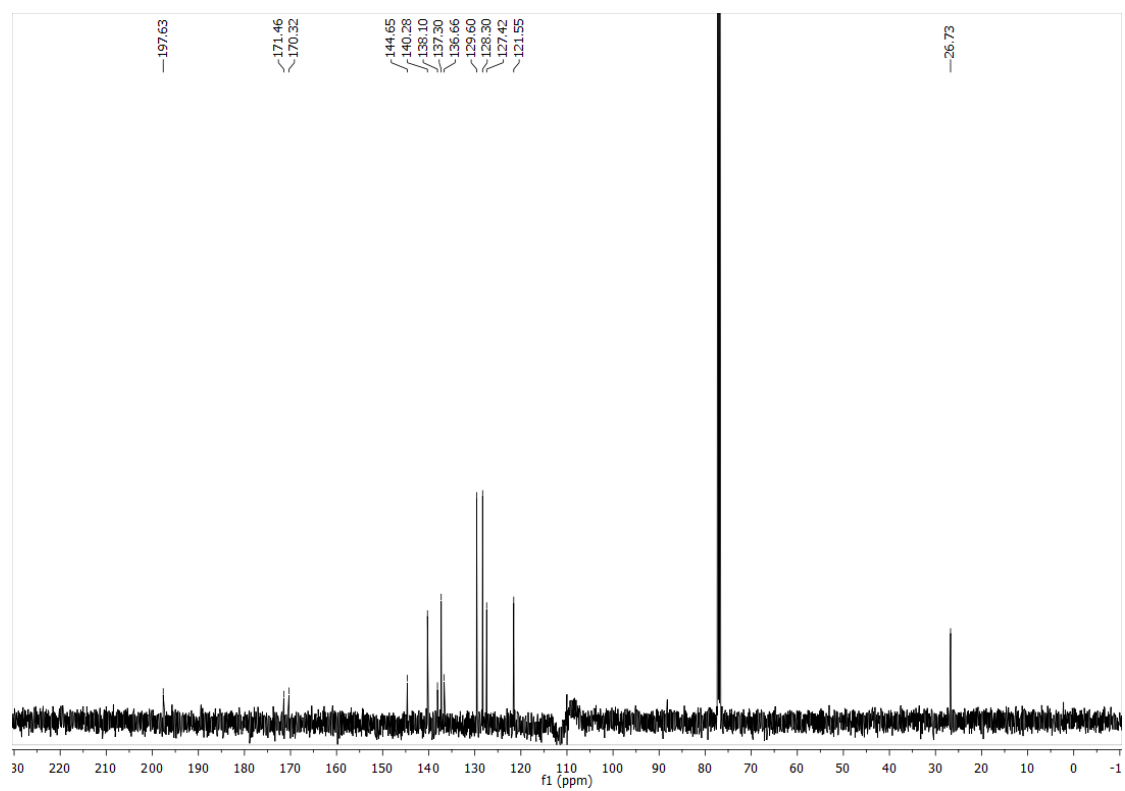
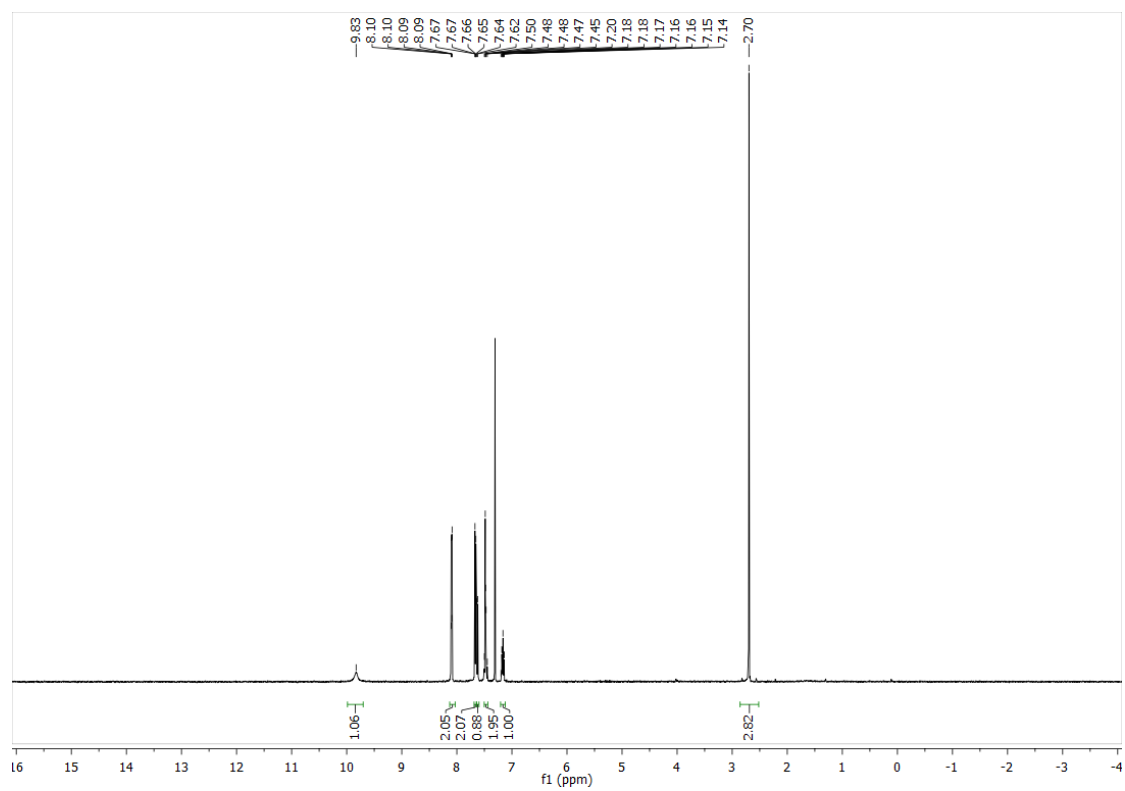


EF-1-OMe

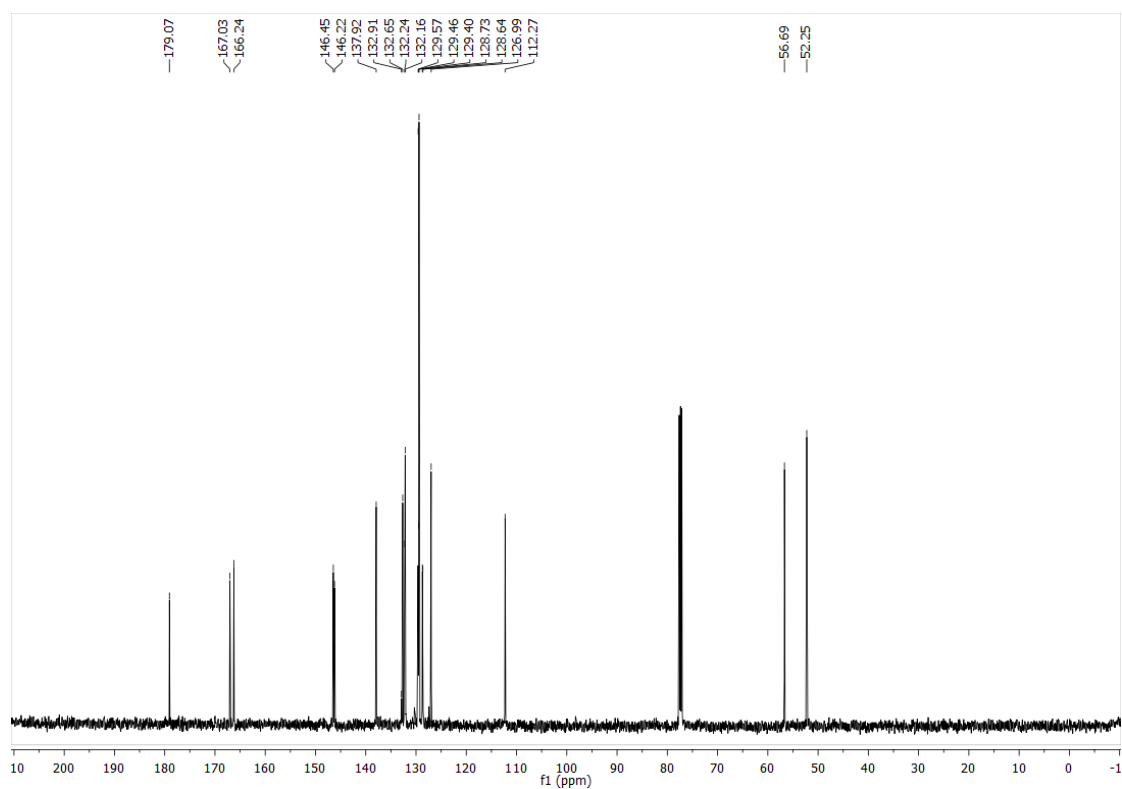
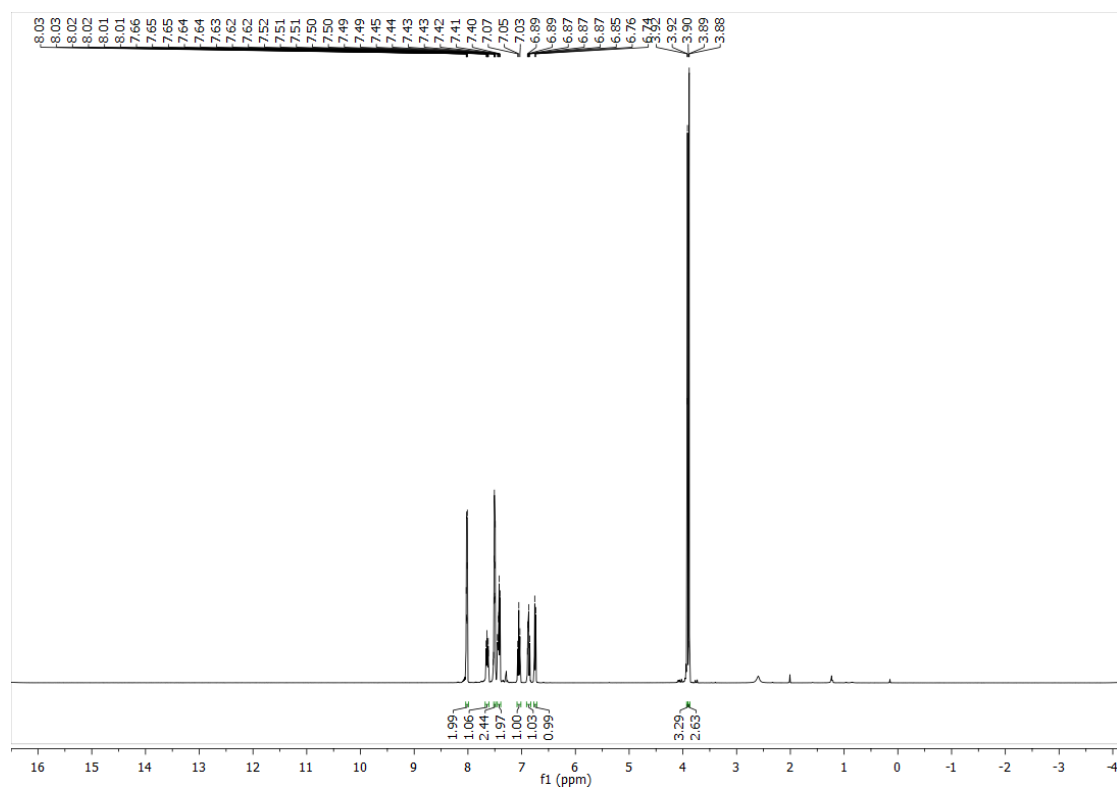


EF-1-OH

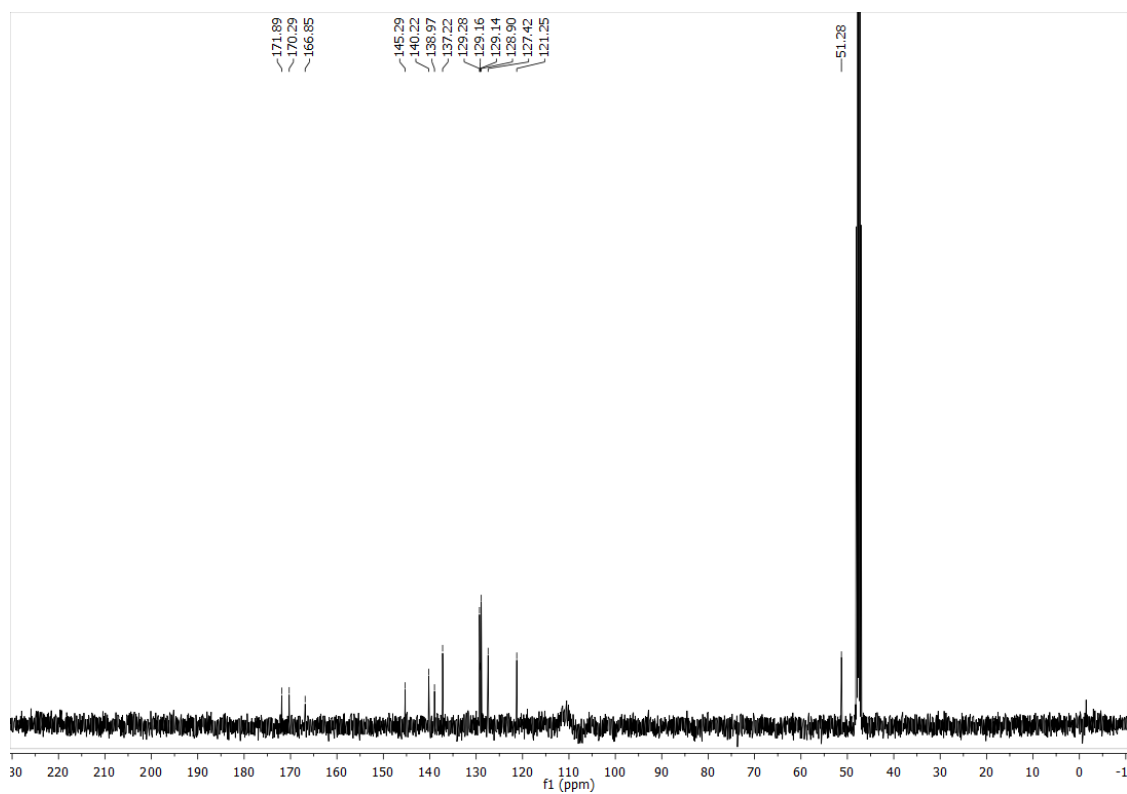
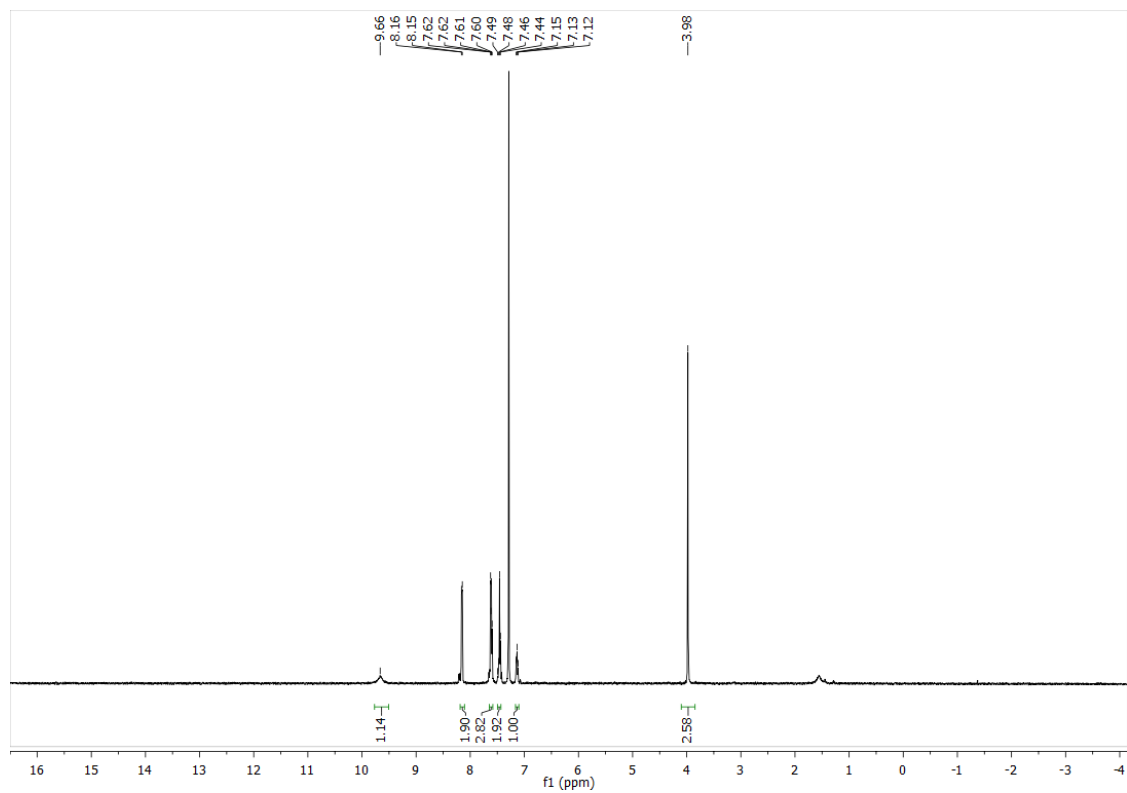
EF-2-OH



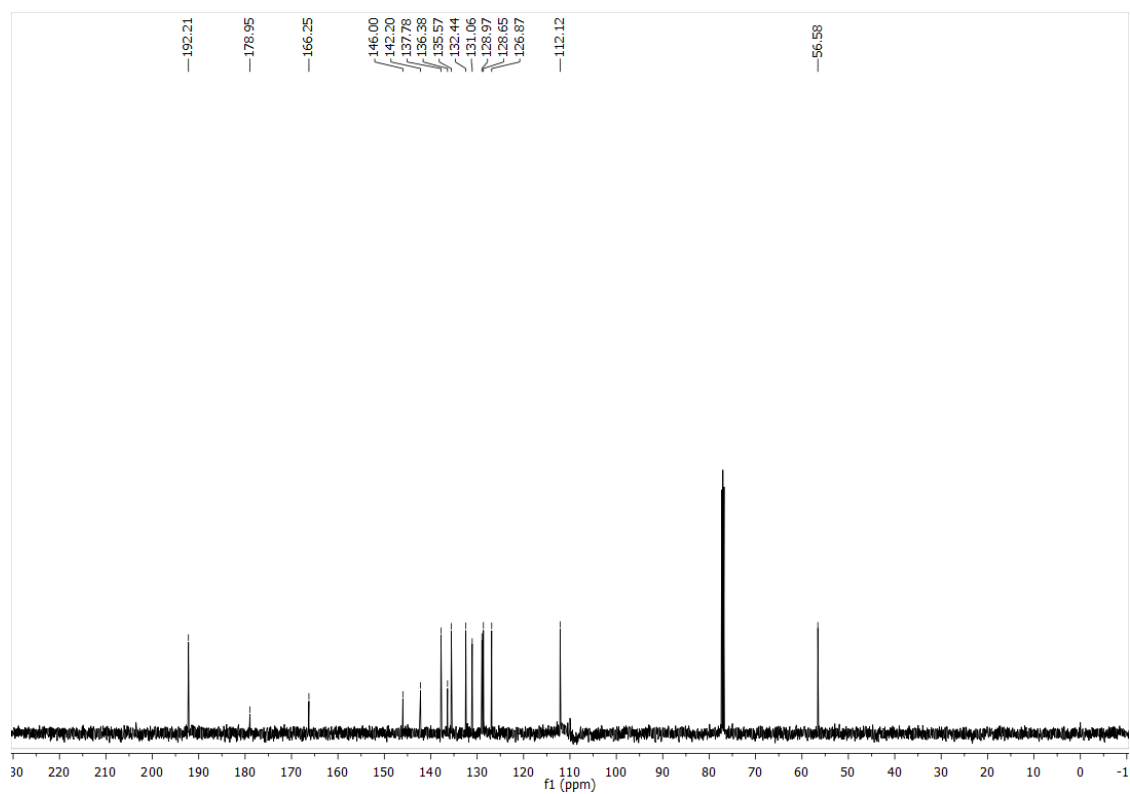
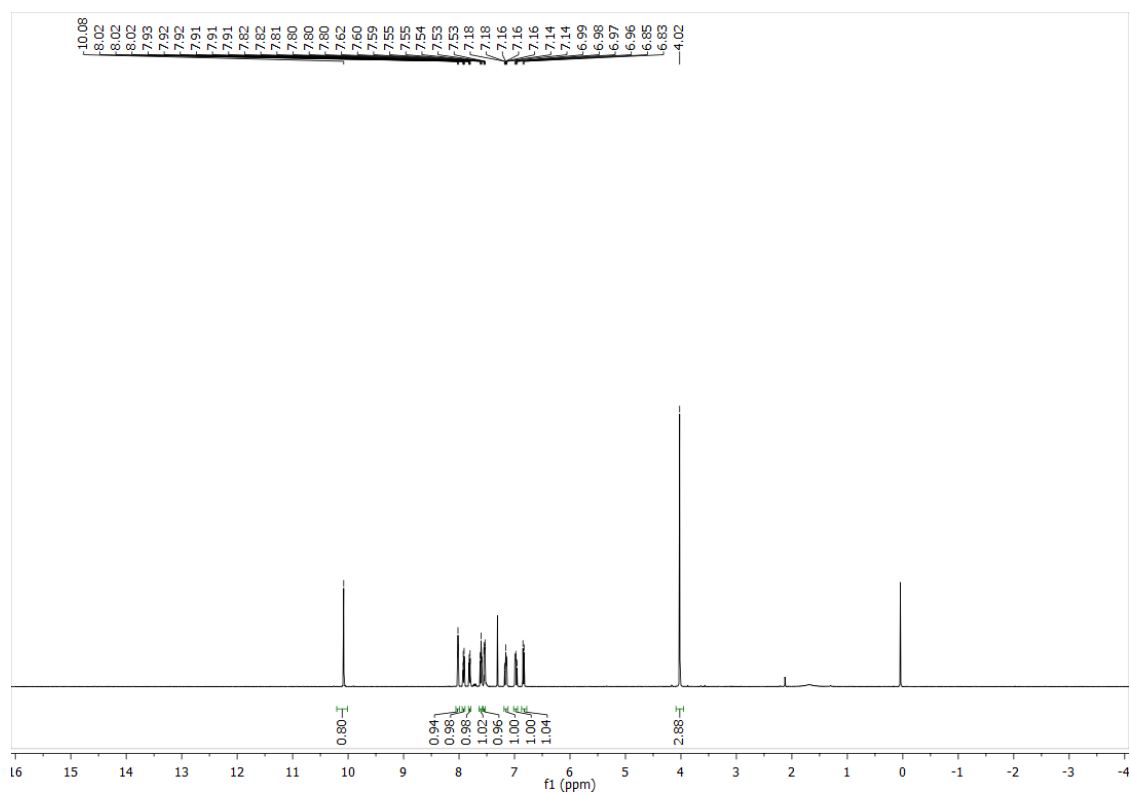
EF-3-OMe

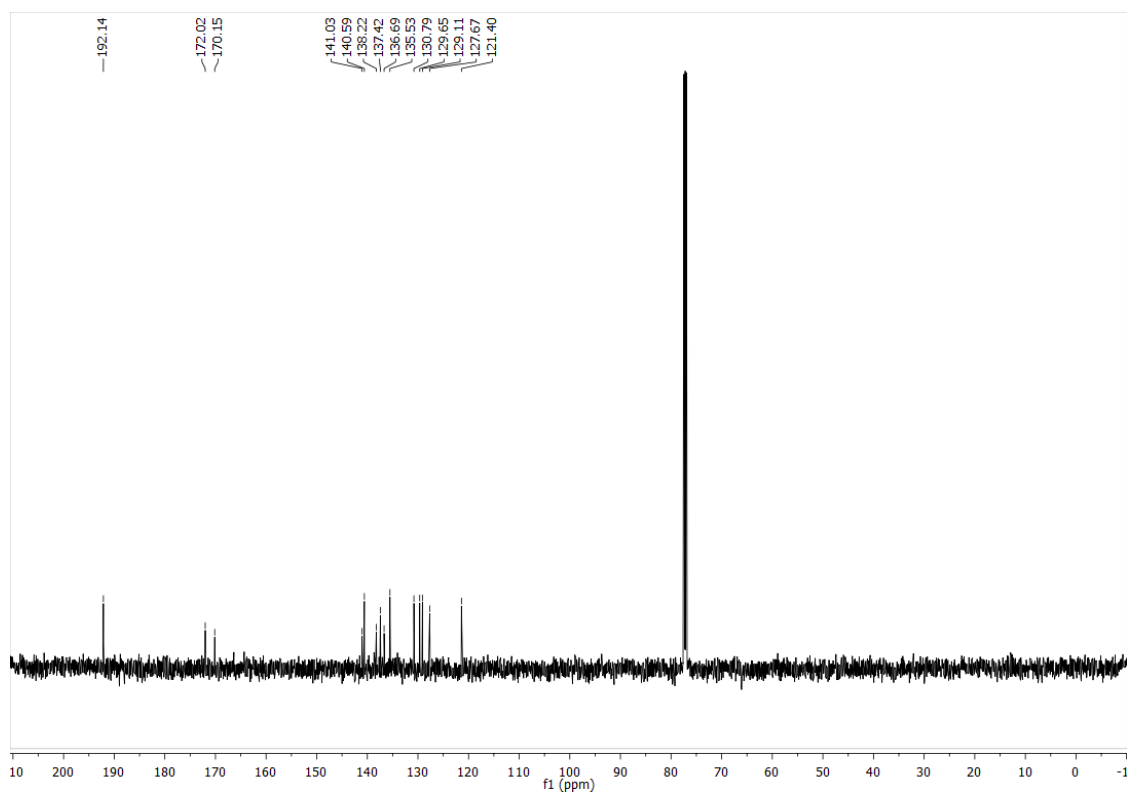
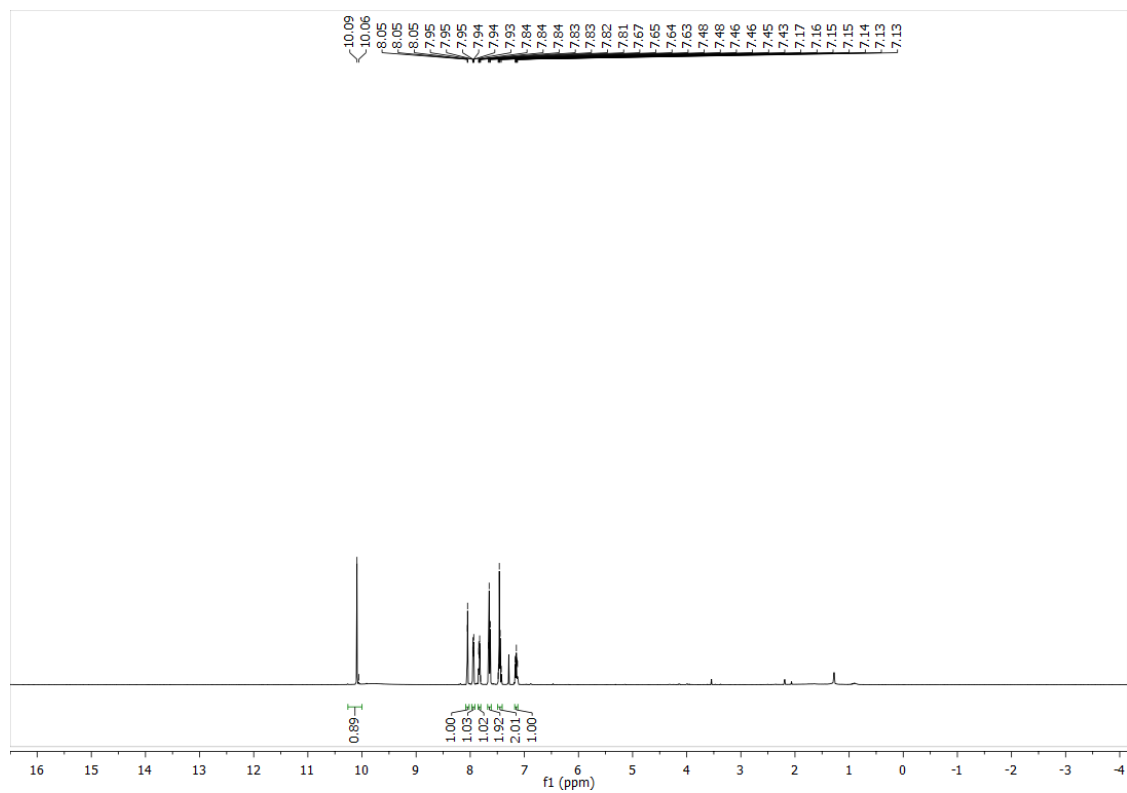


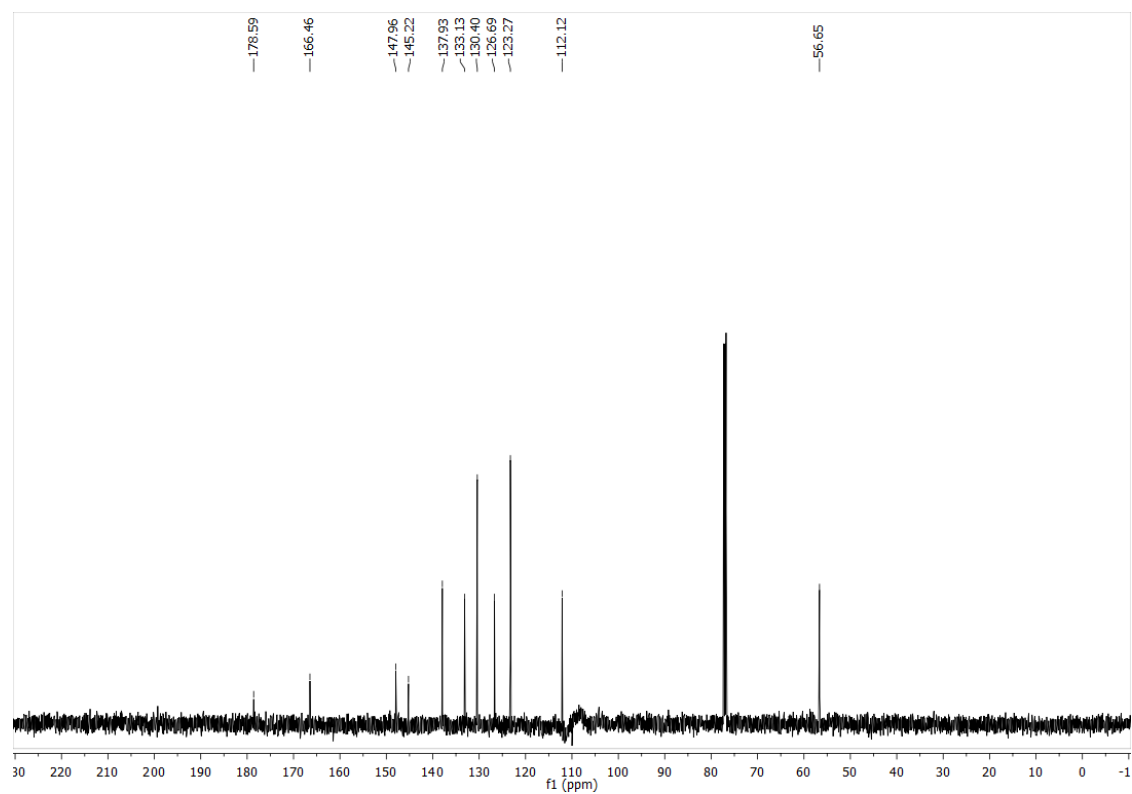
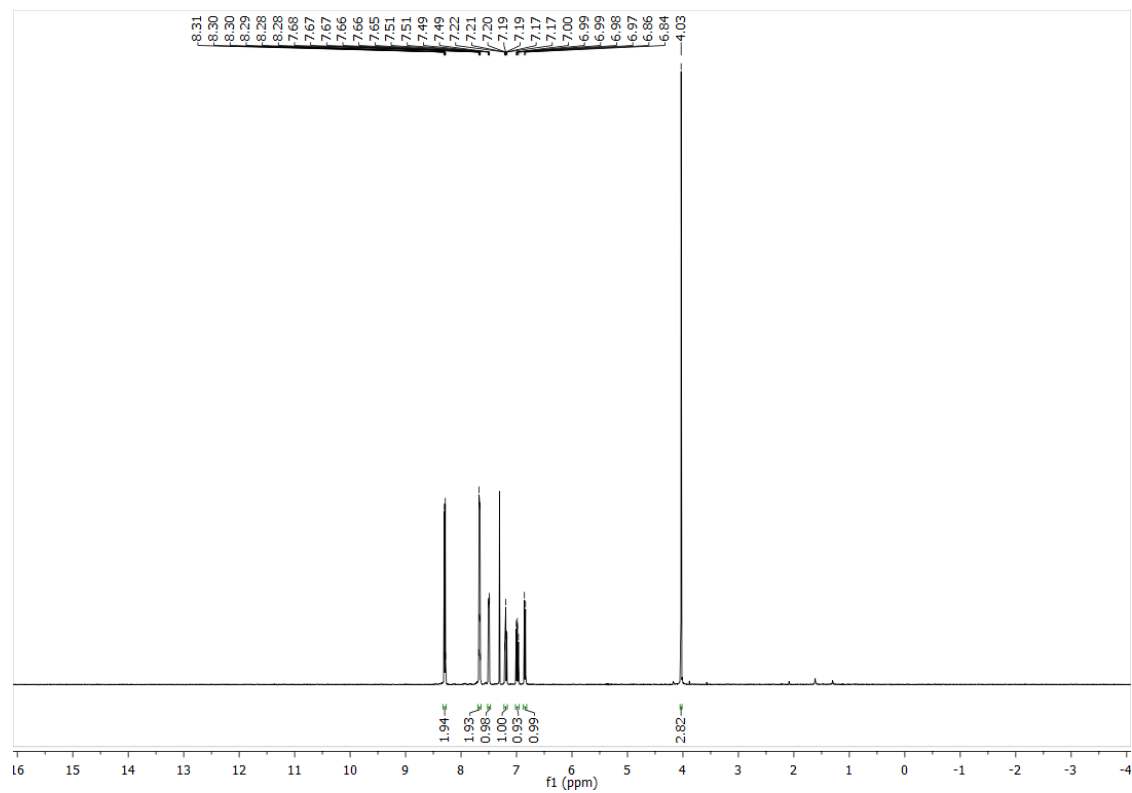
EF-3-OH

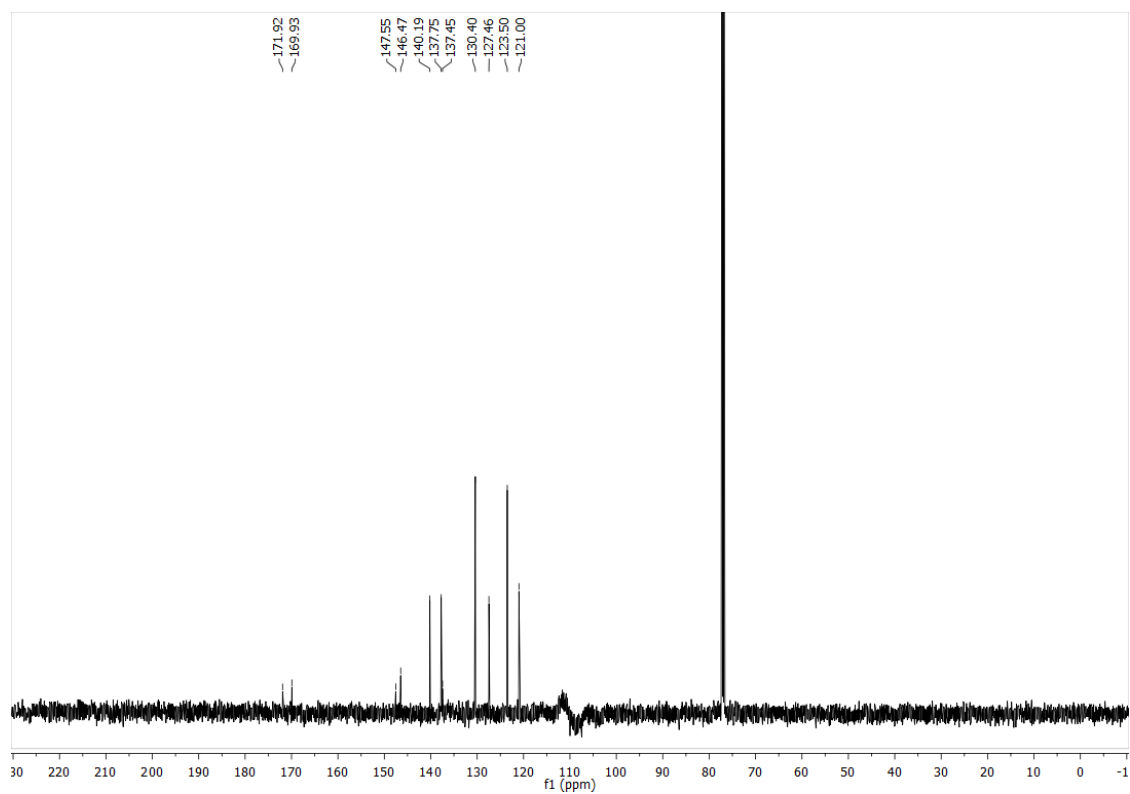
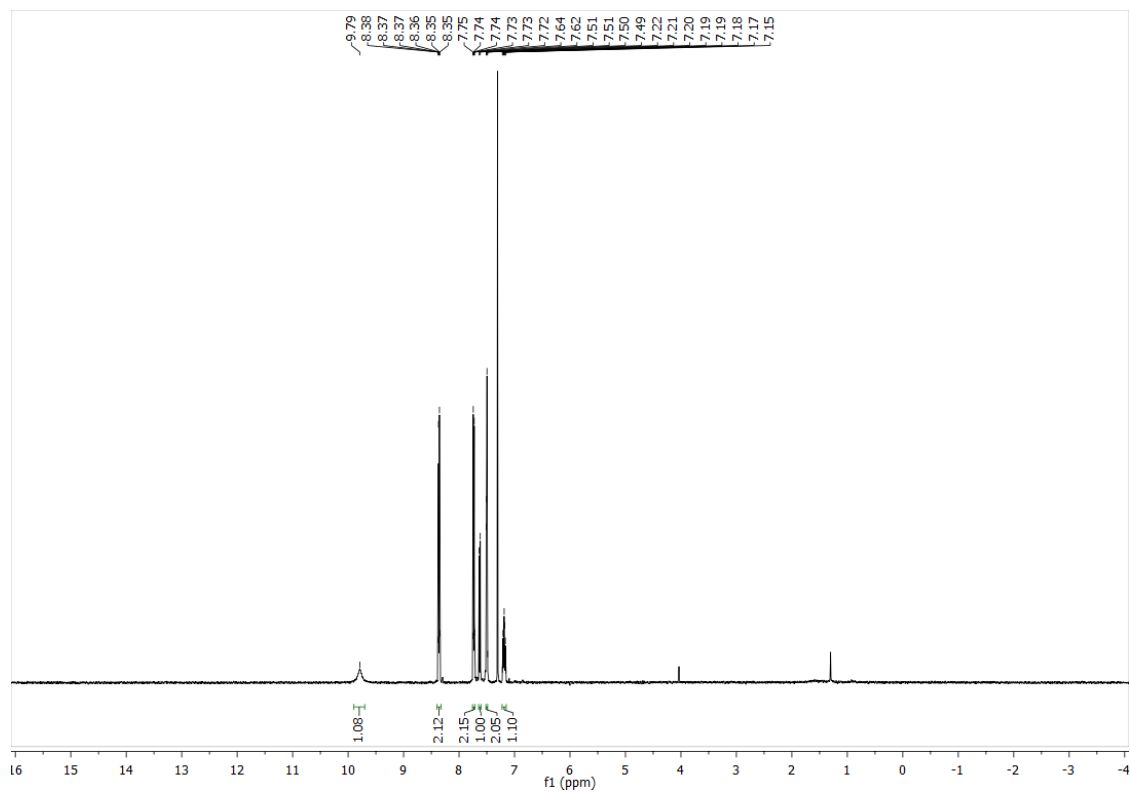


EF-4-OMe

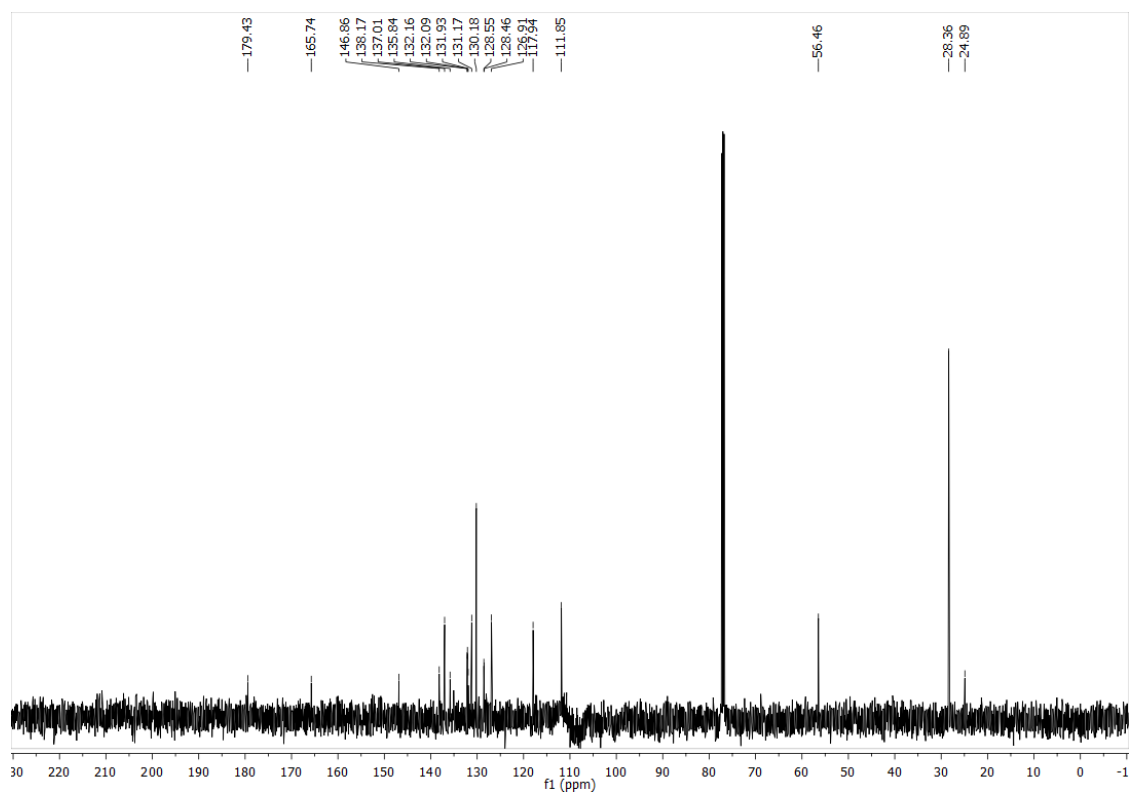
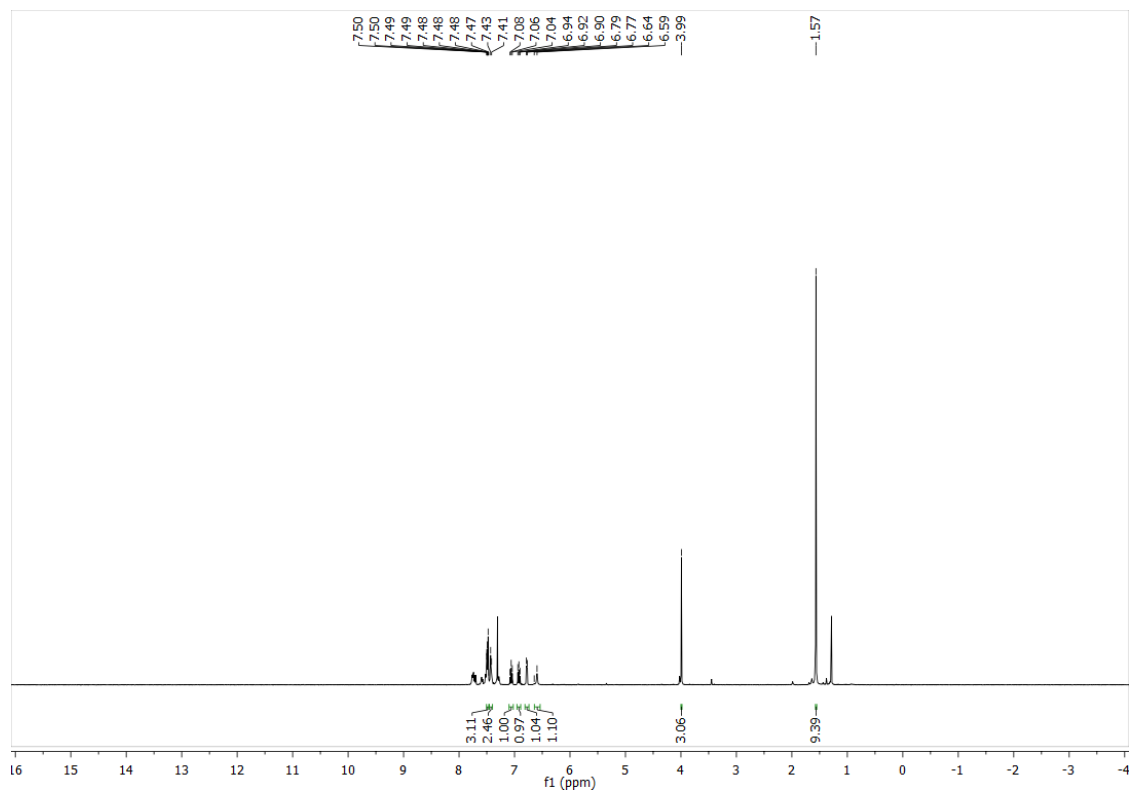


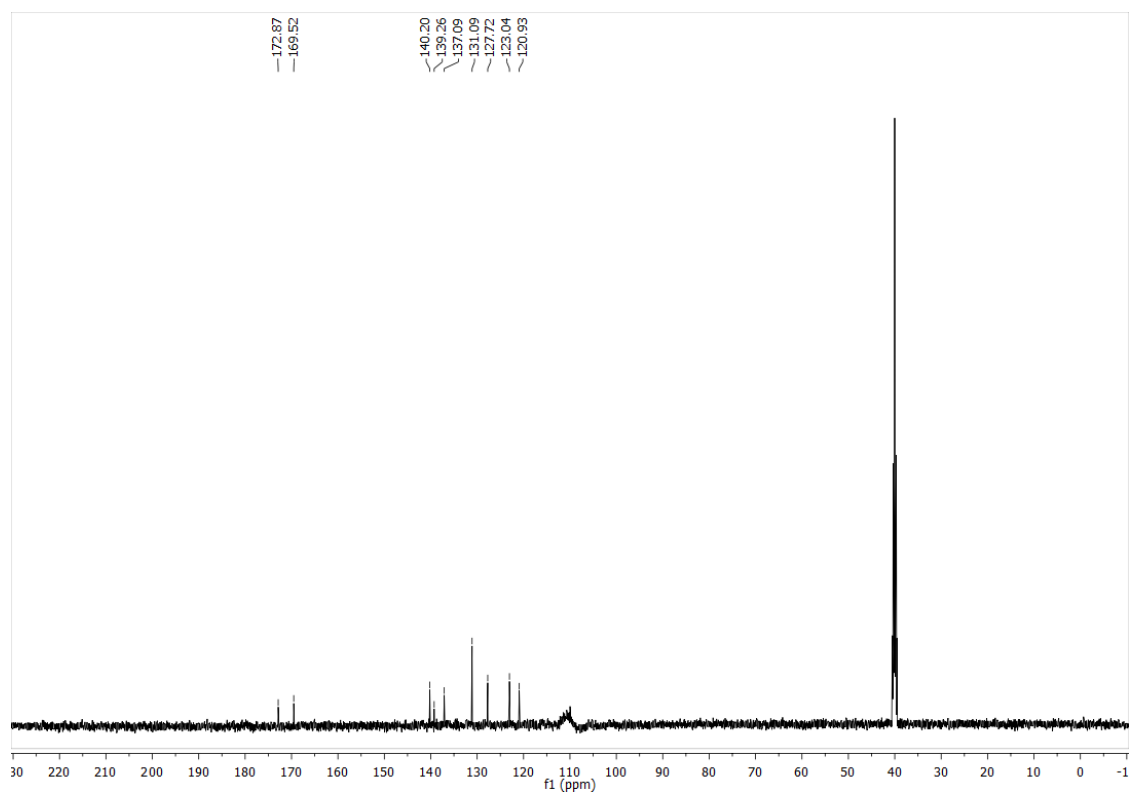
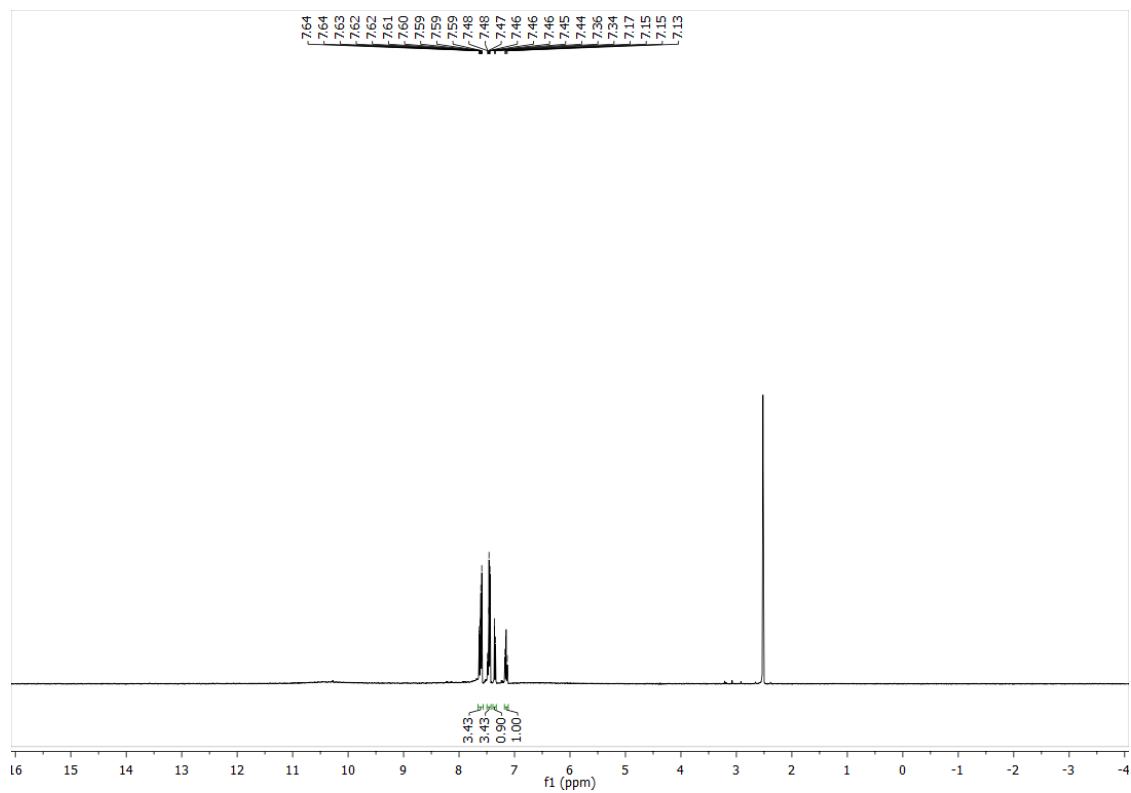
EF-4-OH

Am-NO₂-OMe

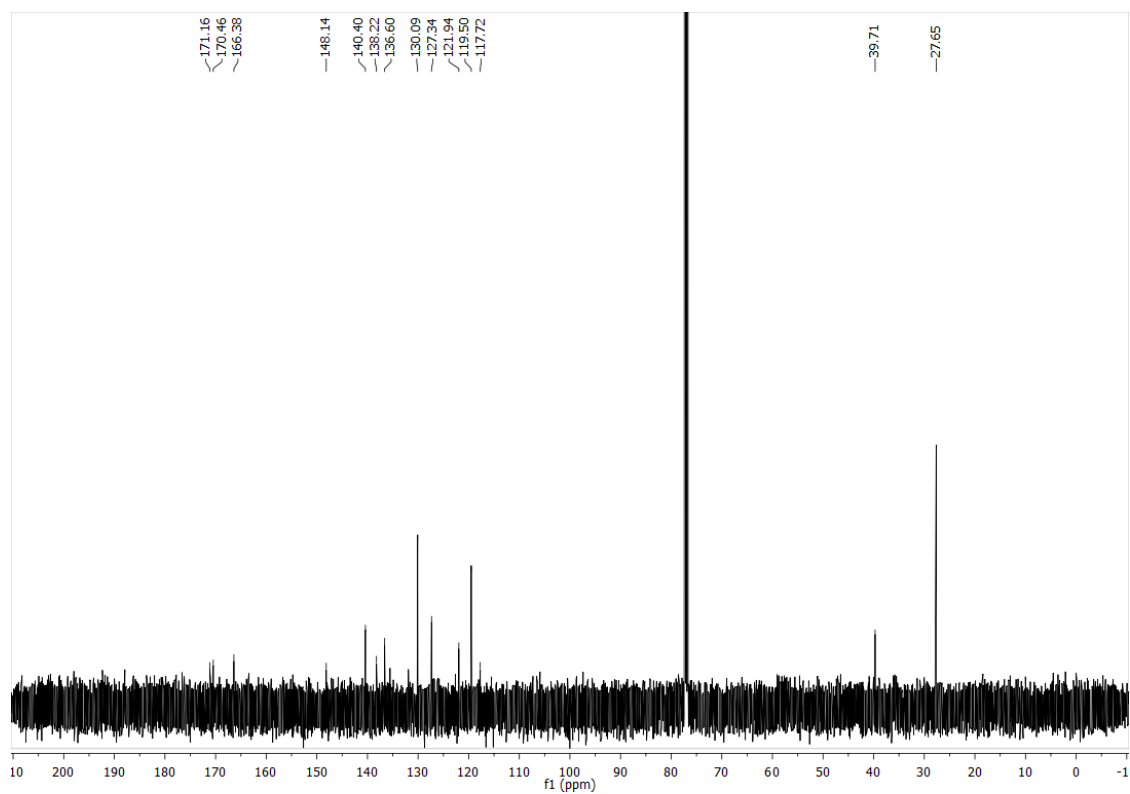
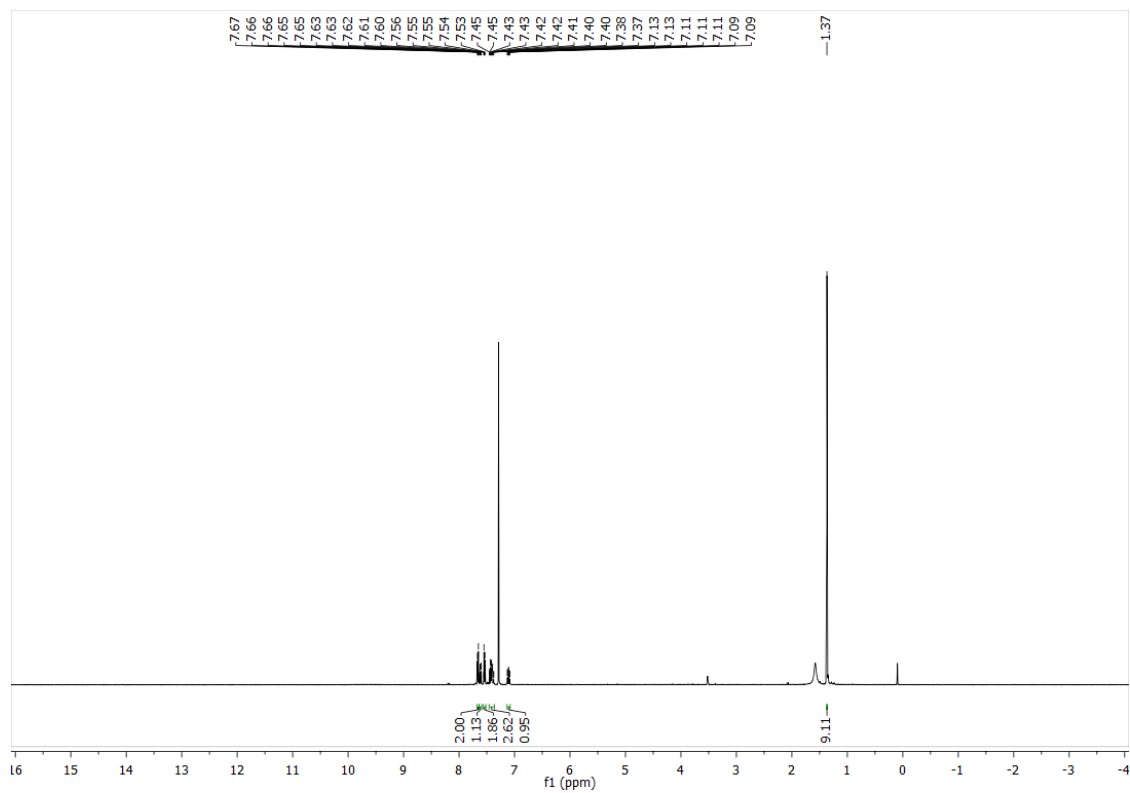
Am-NO₂-OH

Am-NHBoc-OMe

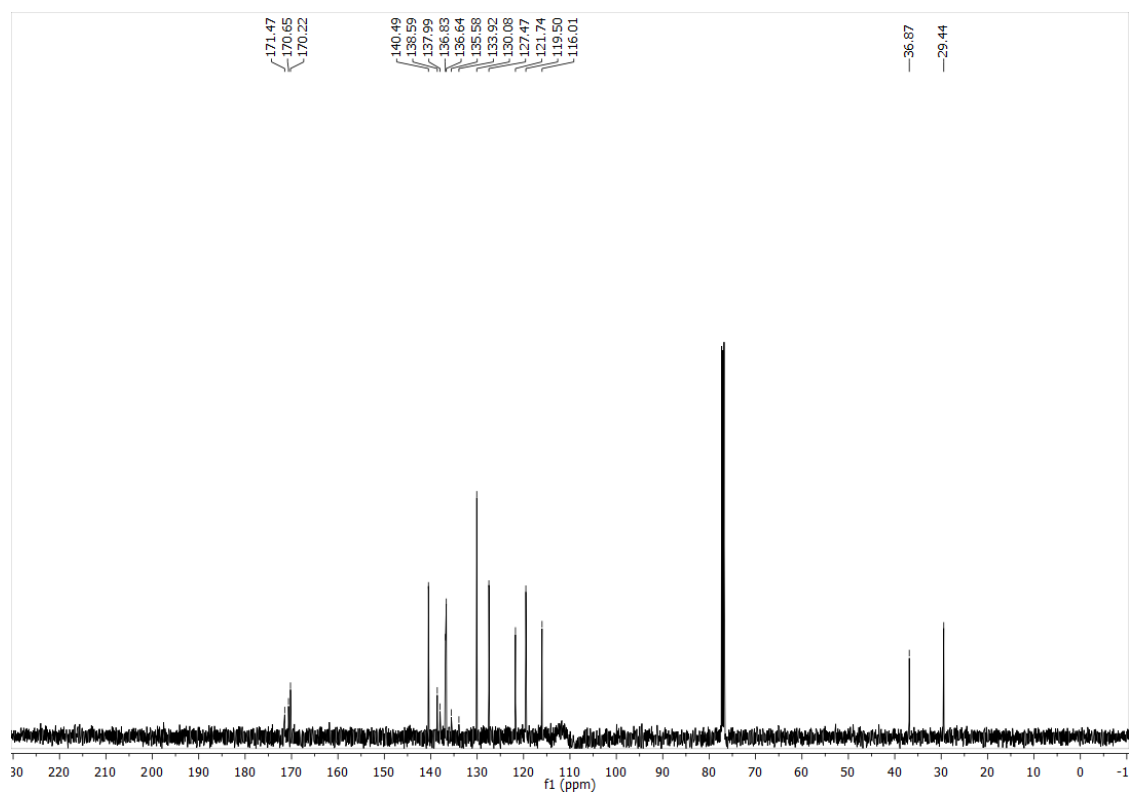
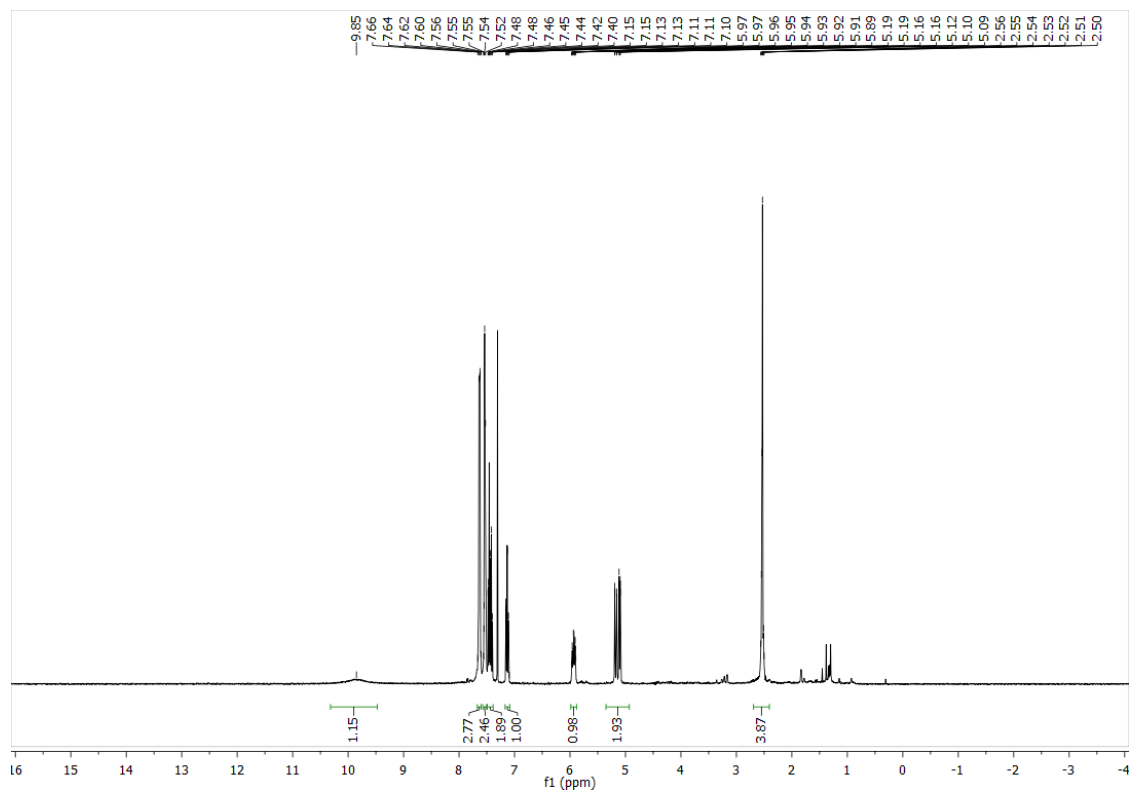


Am-NH₂-OH

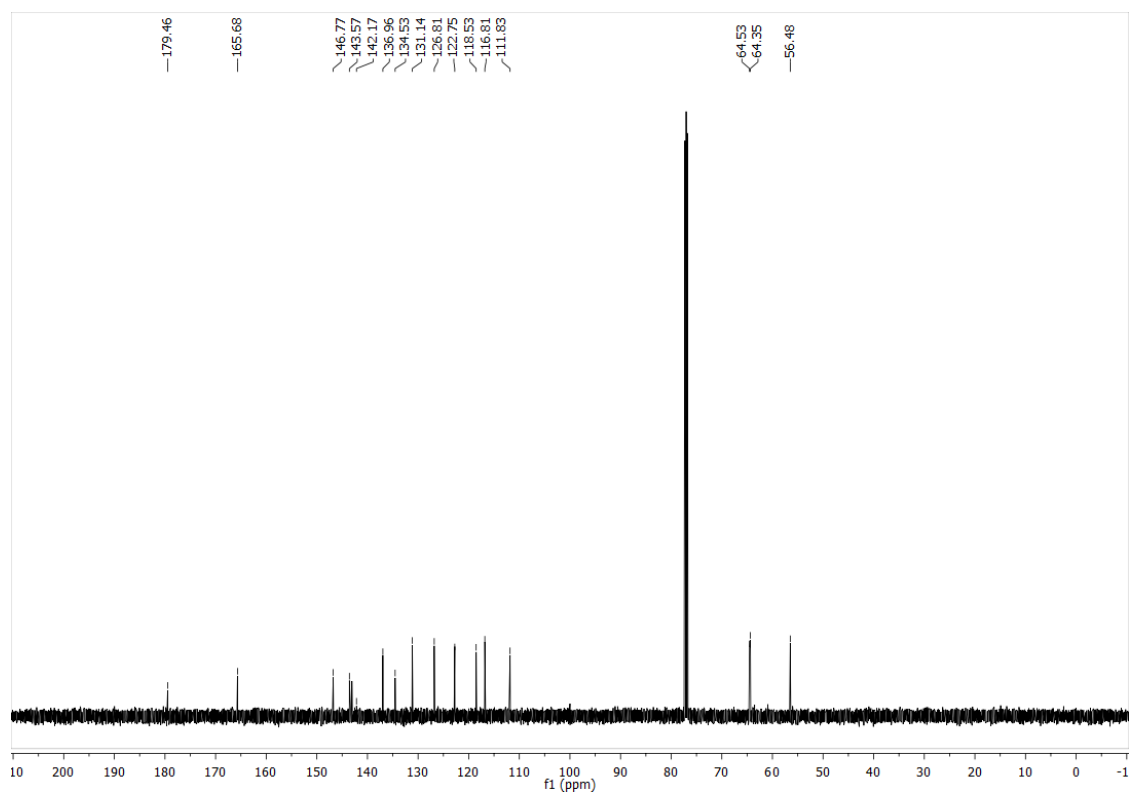
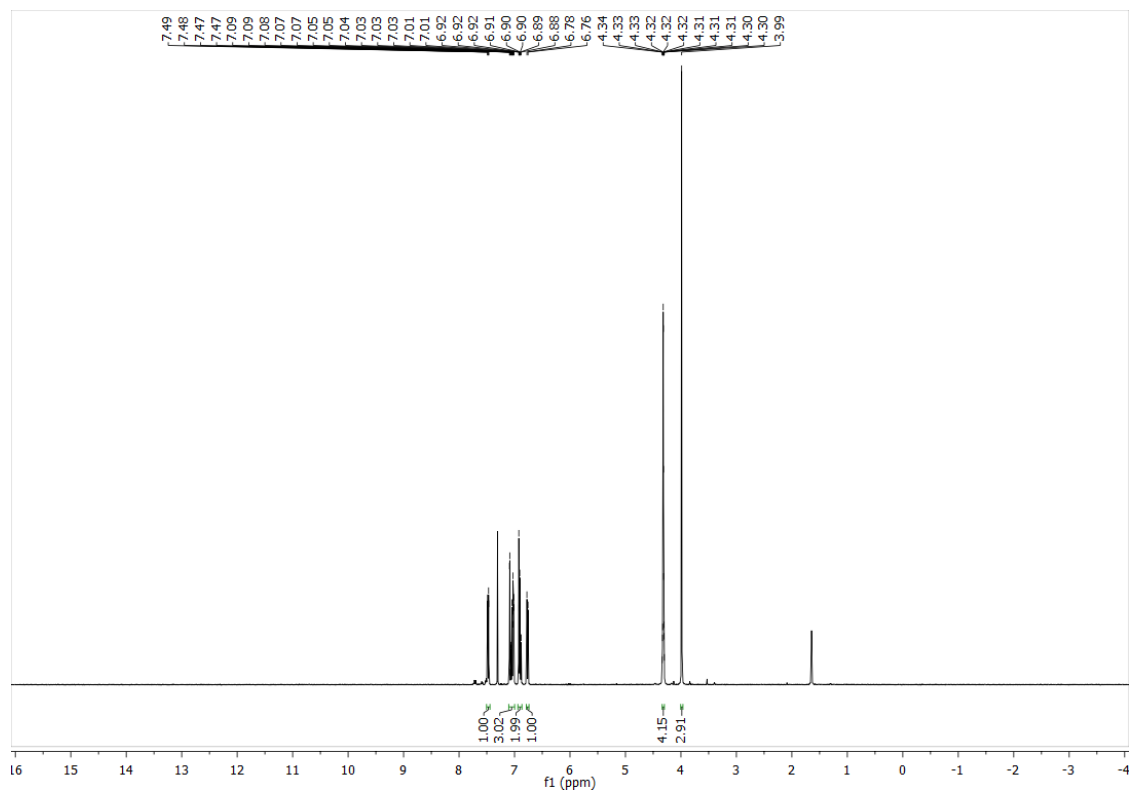
Am-Piv-OH

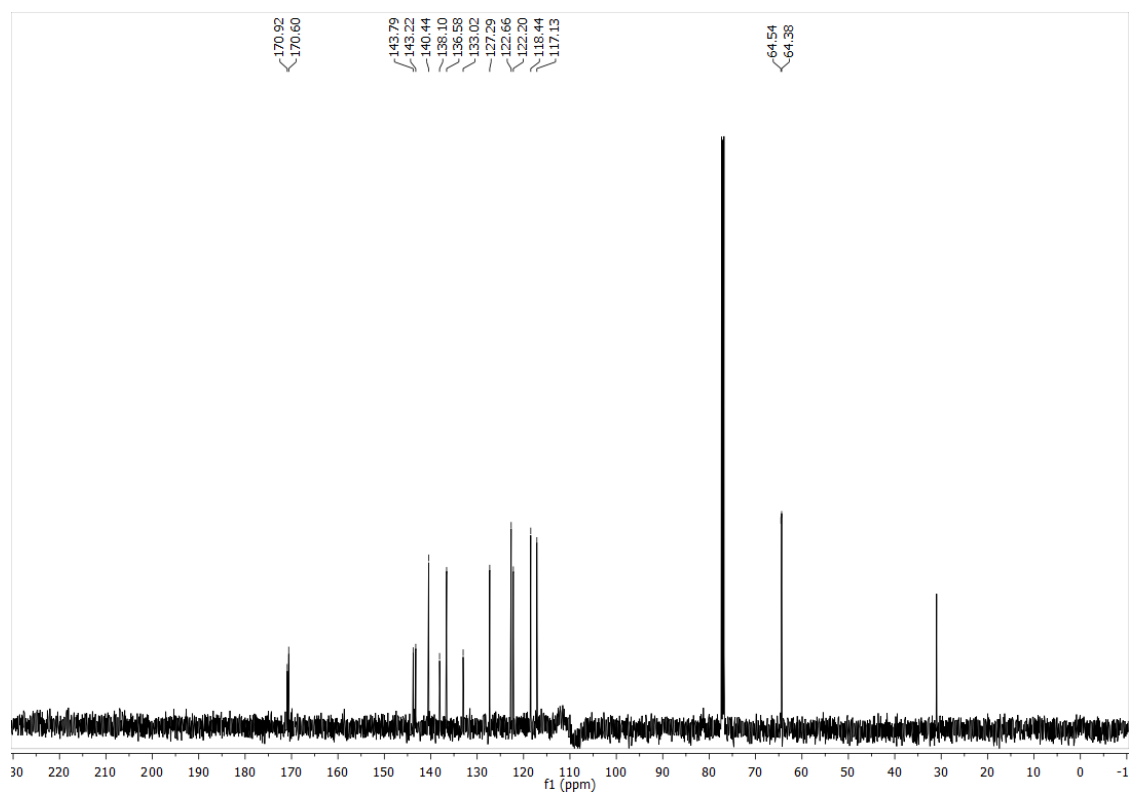


Am-P5-OH

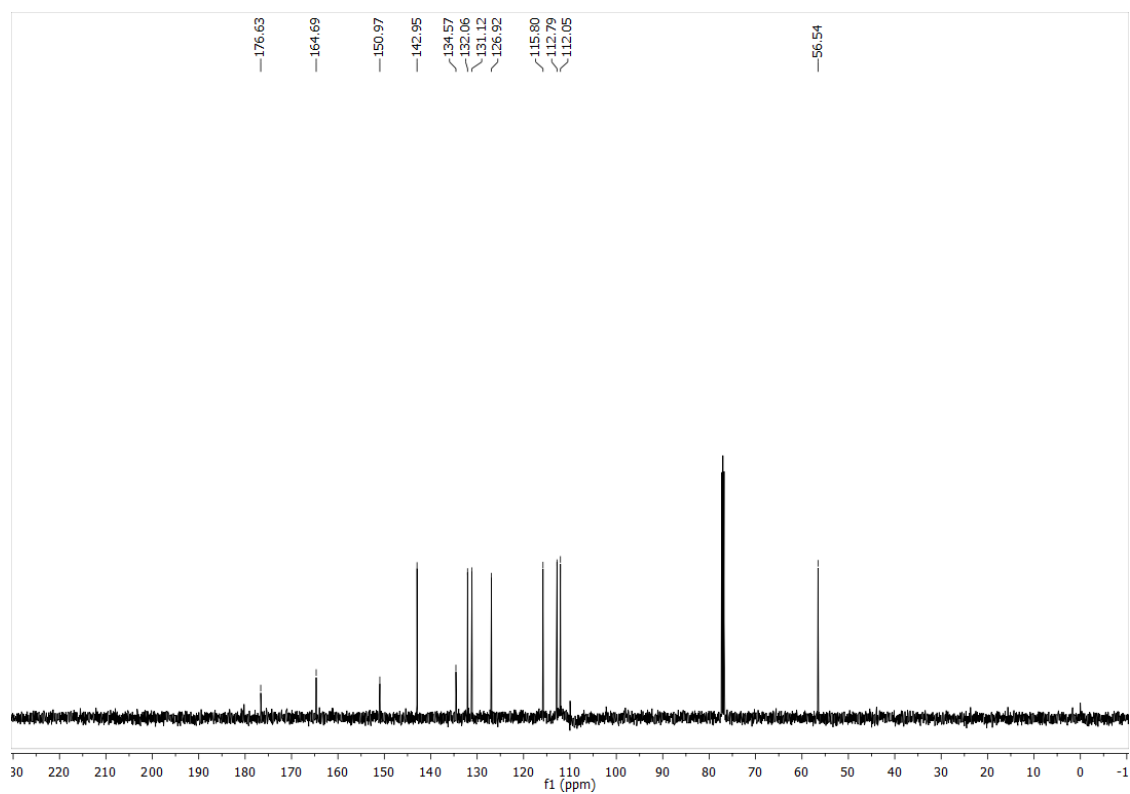
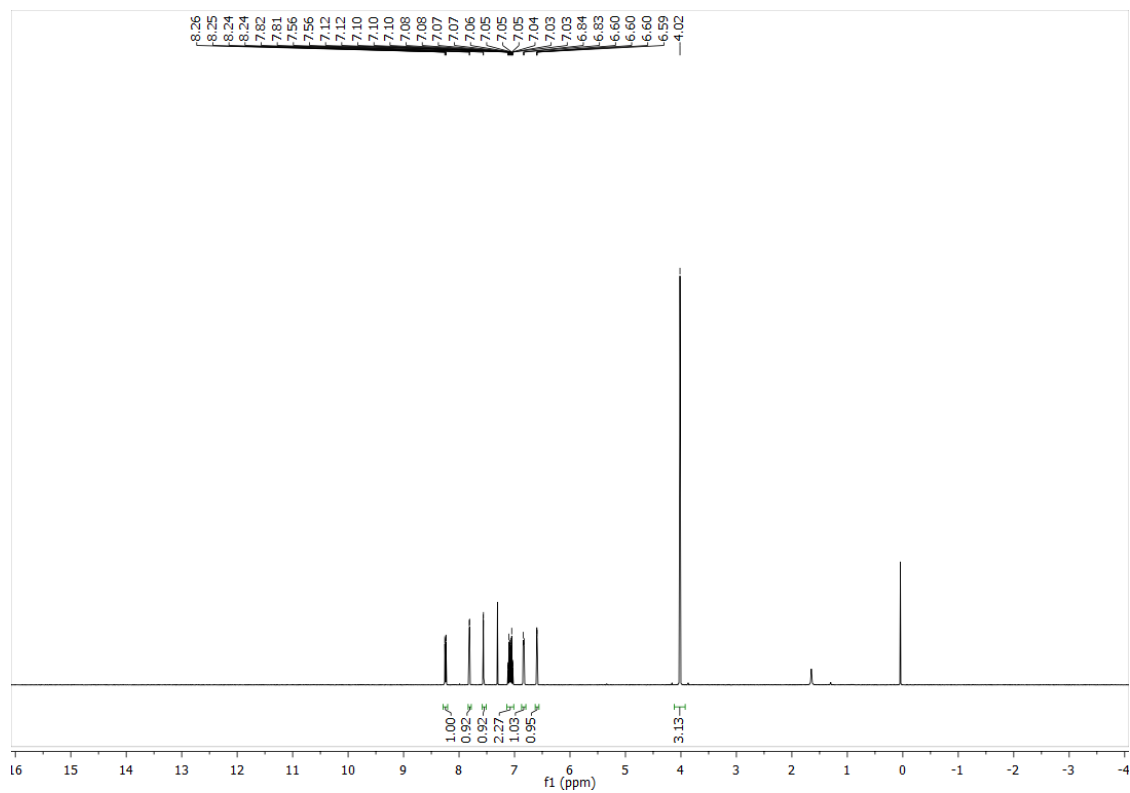


HC-1-OMe

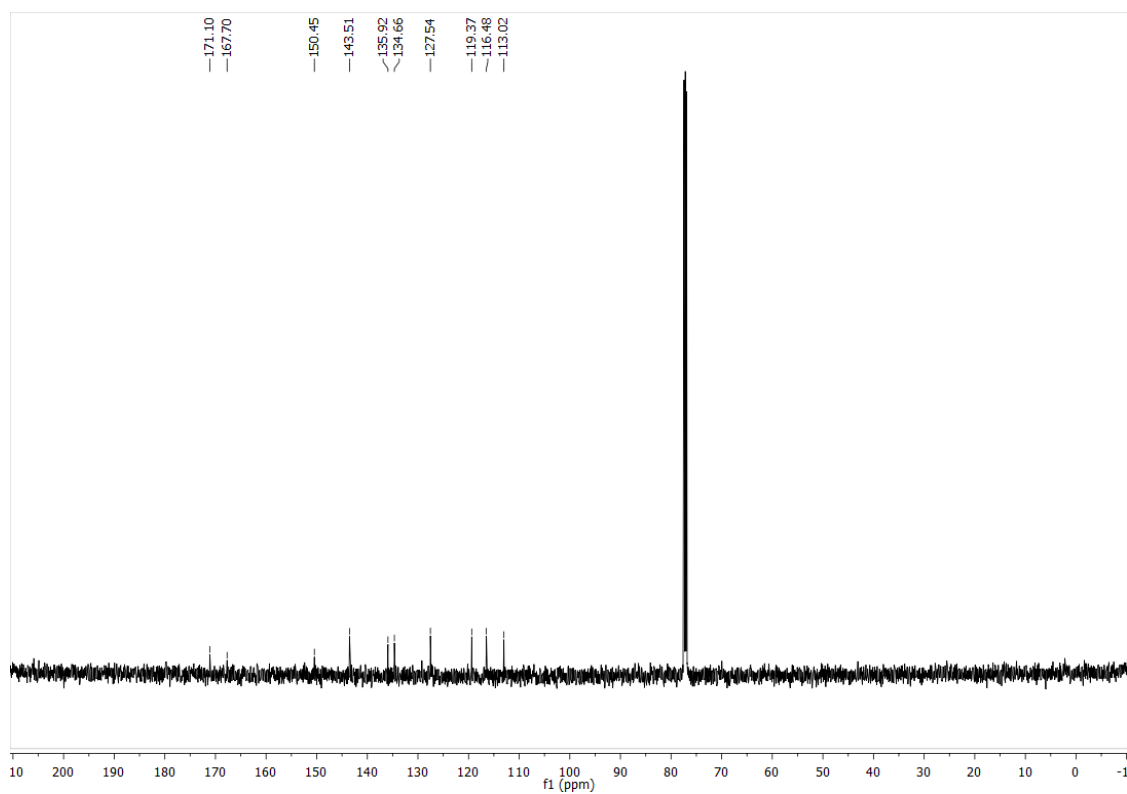
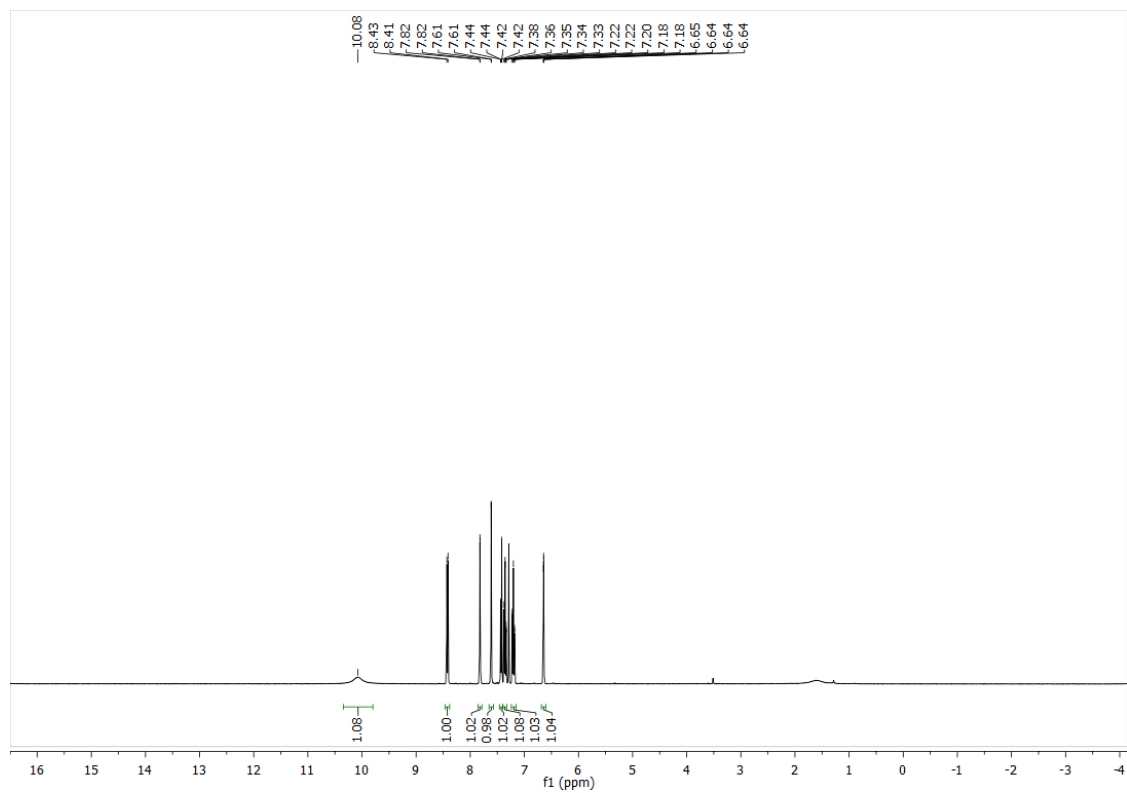




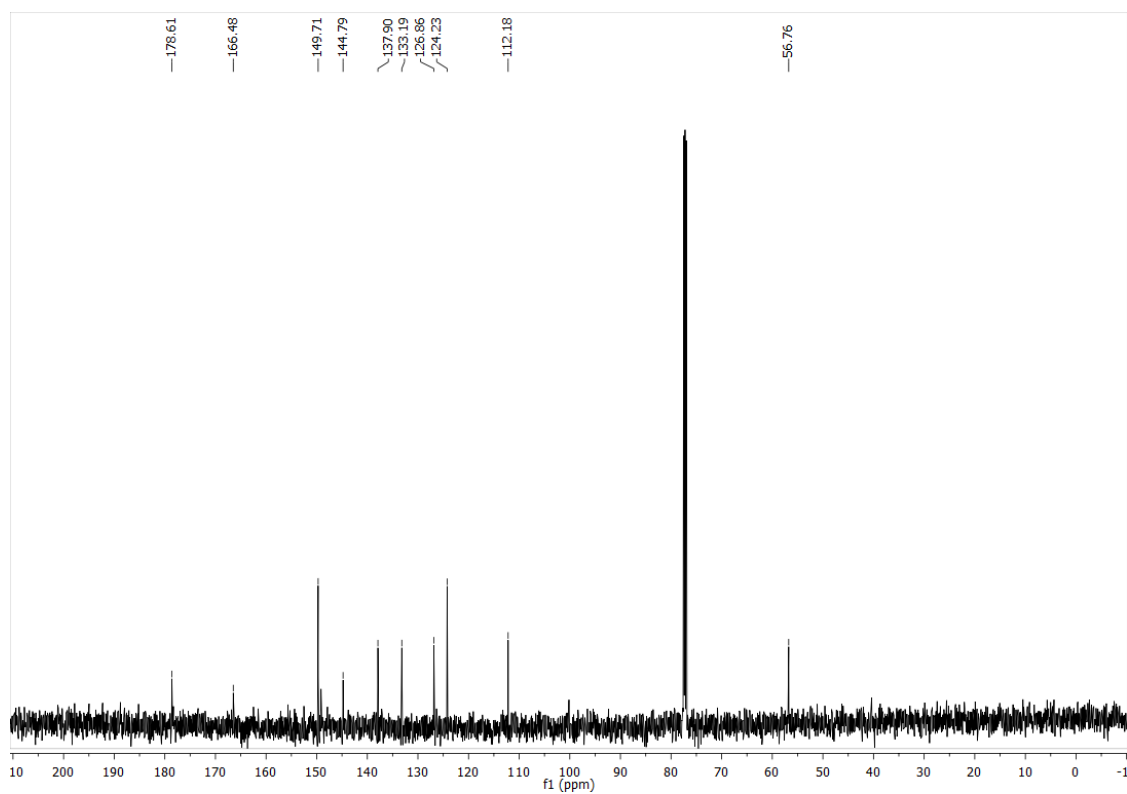
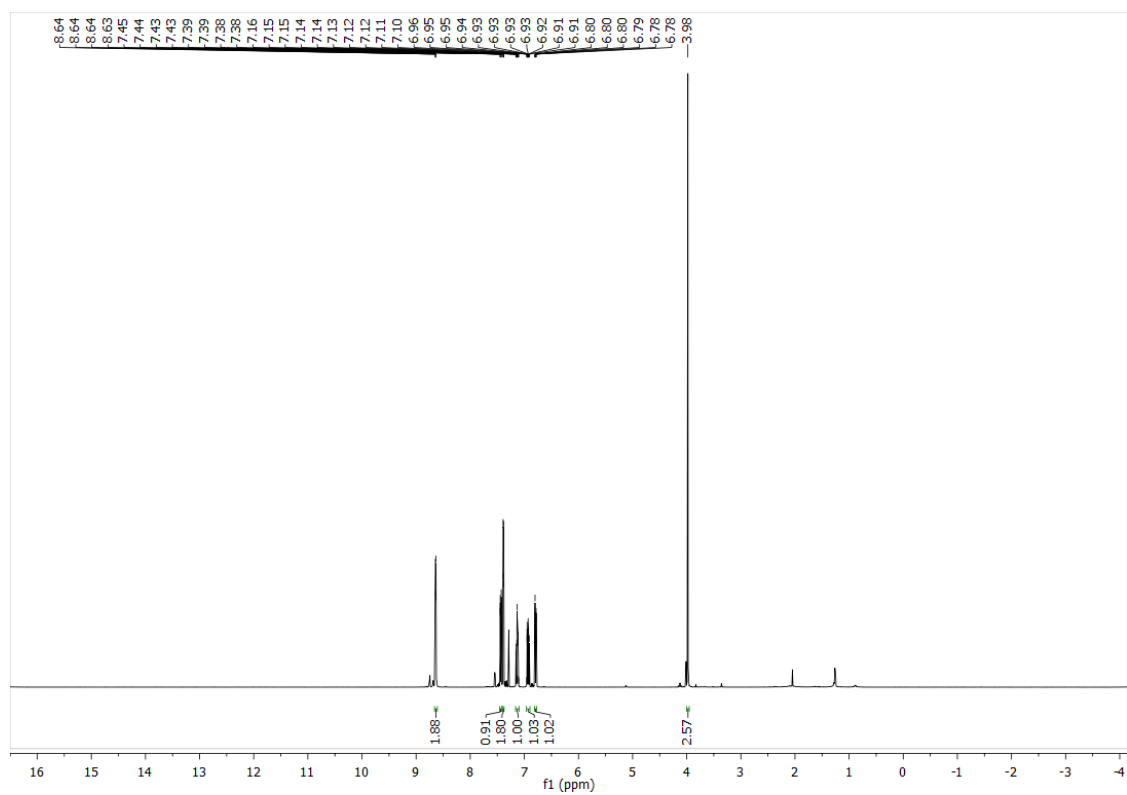
HC-2-OMe



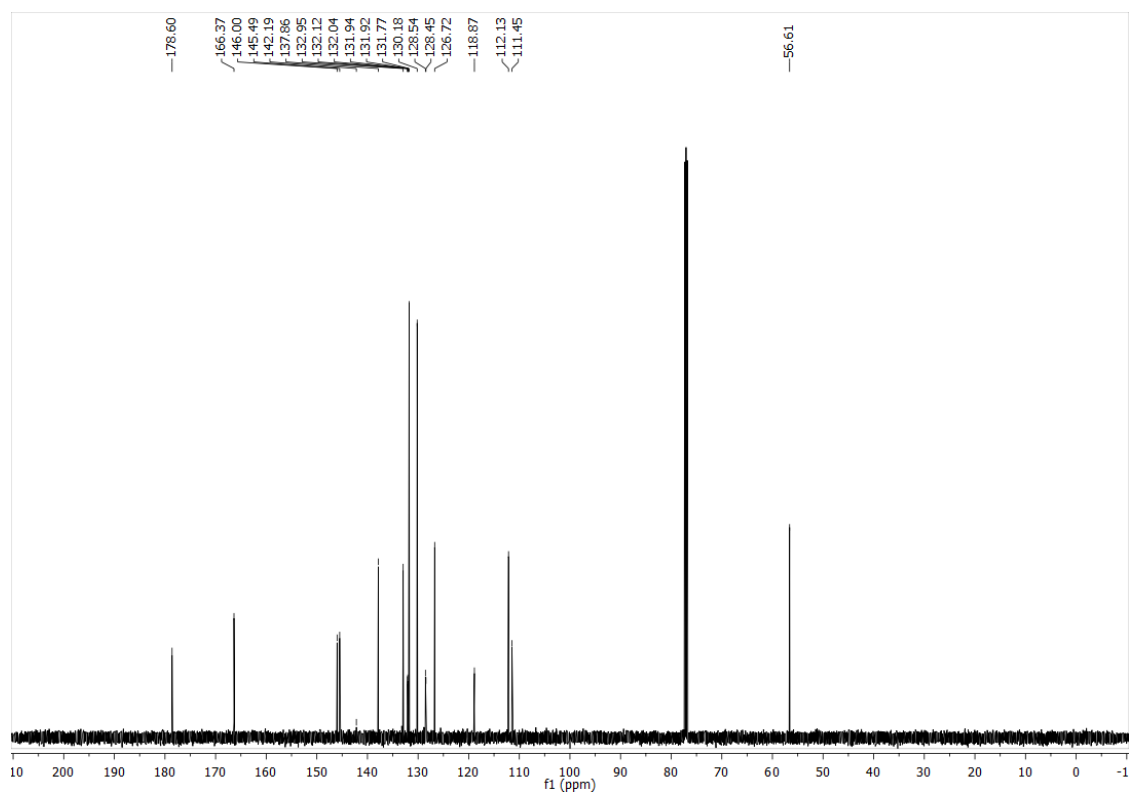
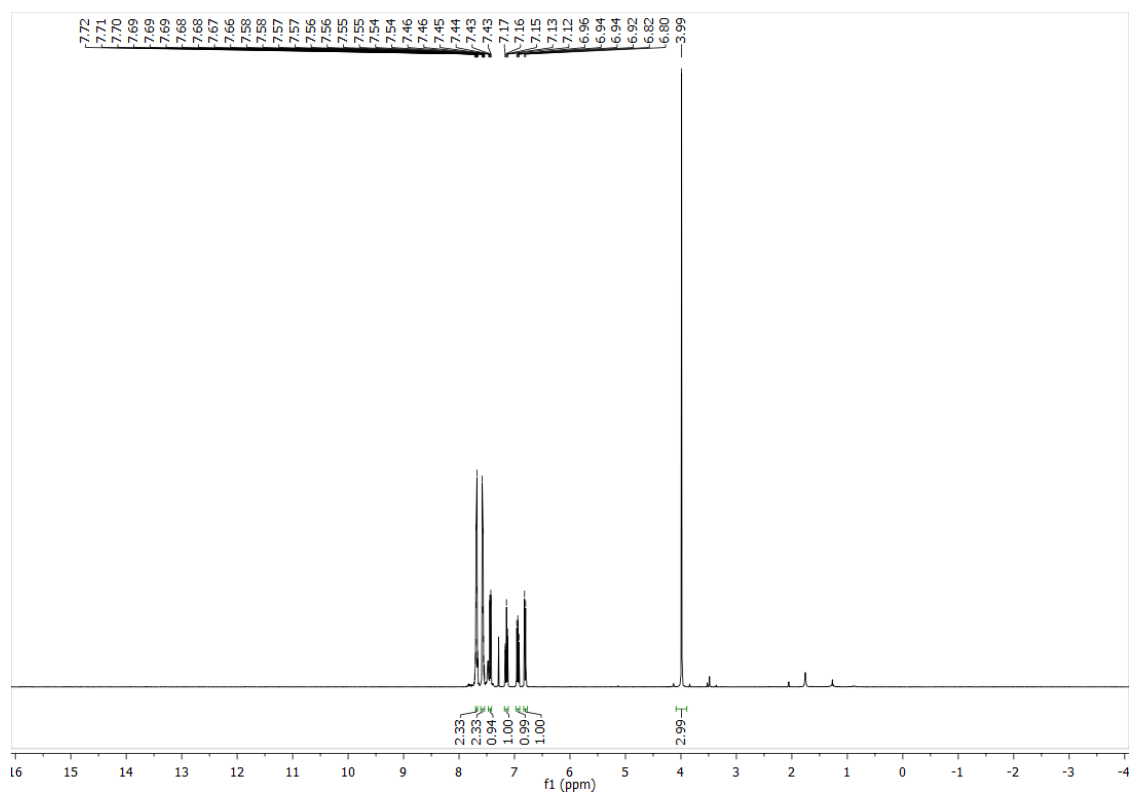
HC-2-OH



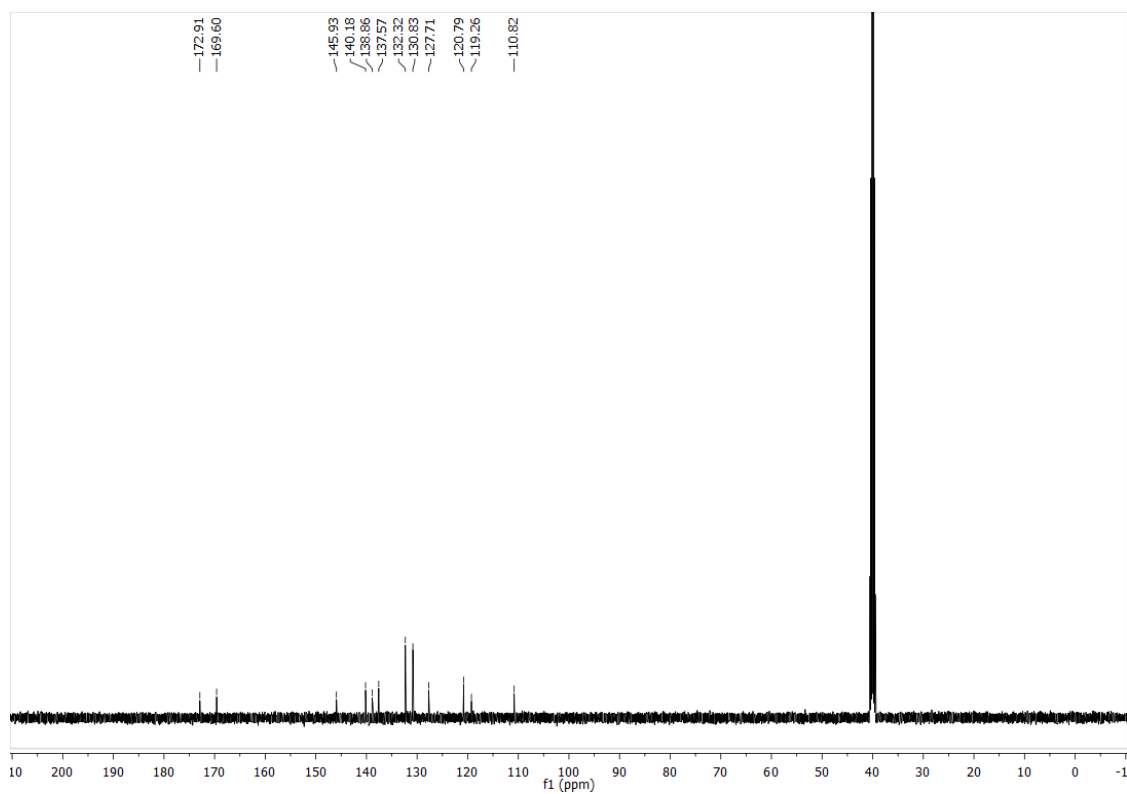
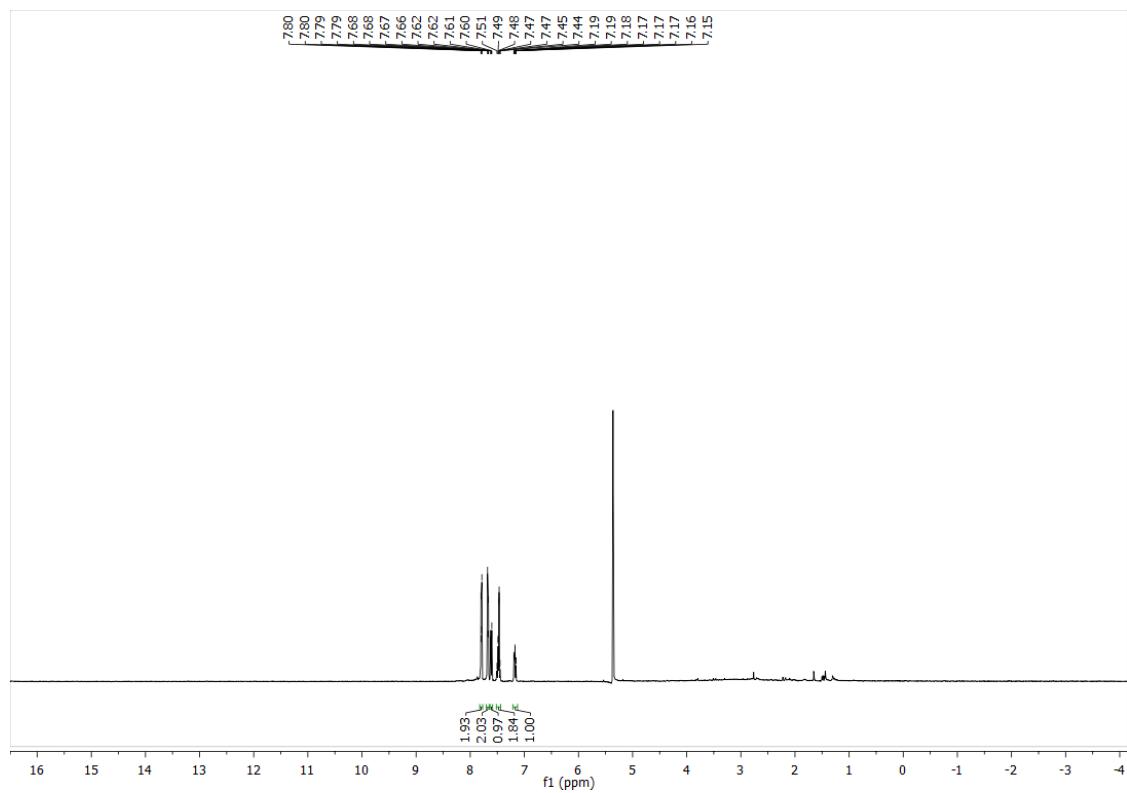
HC-3-OMe



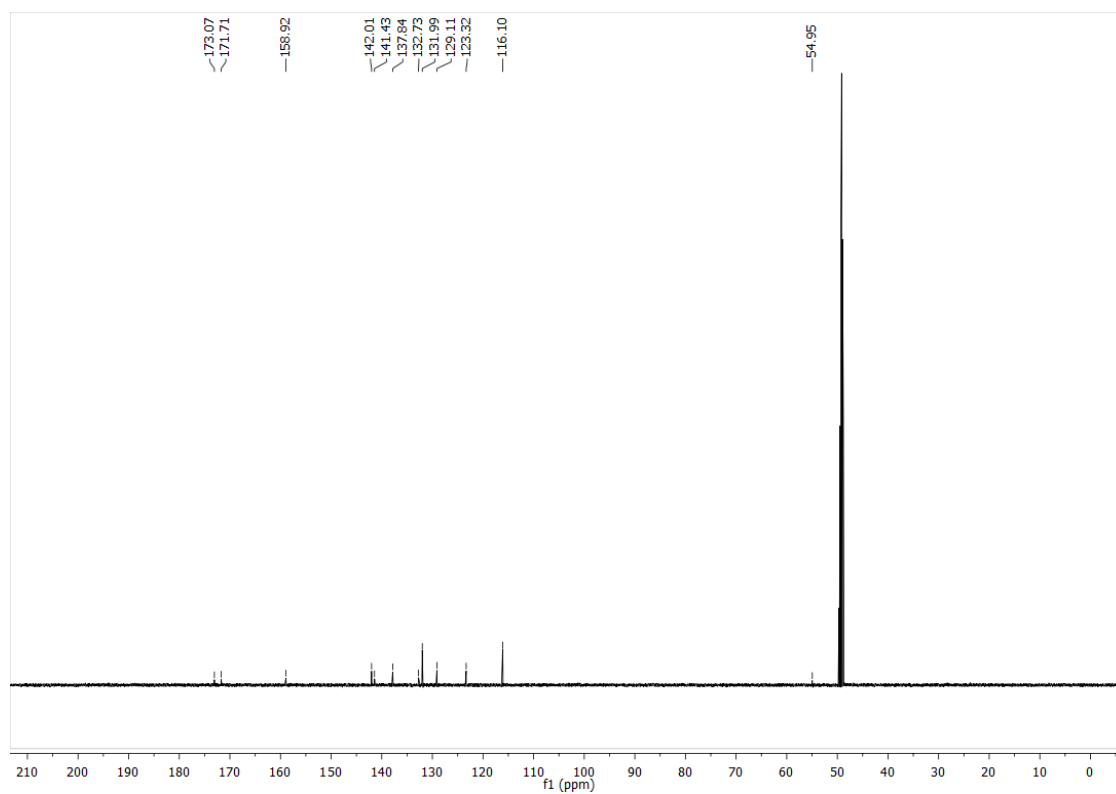
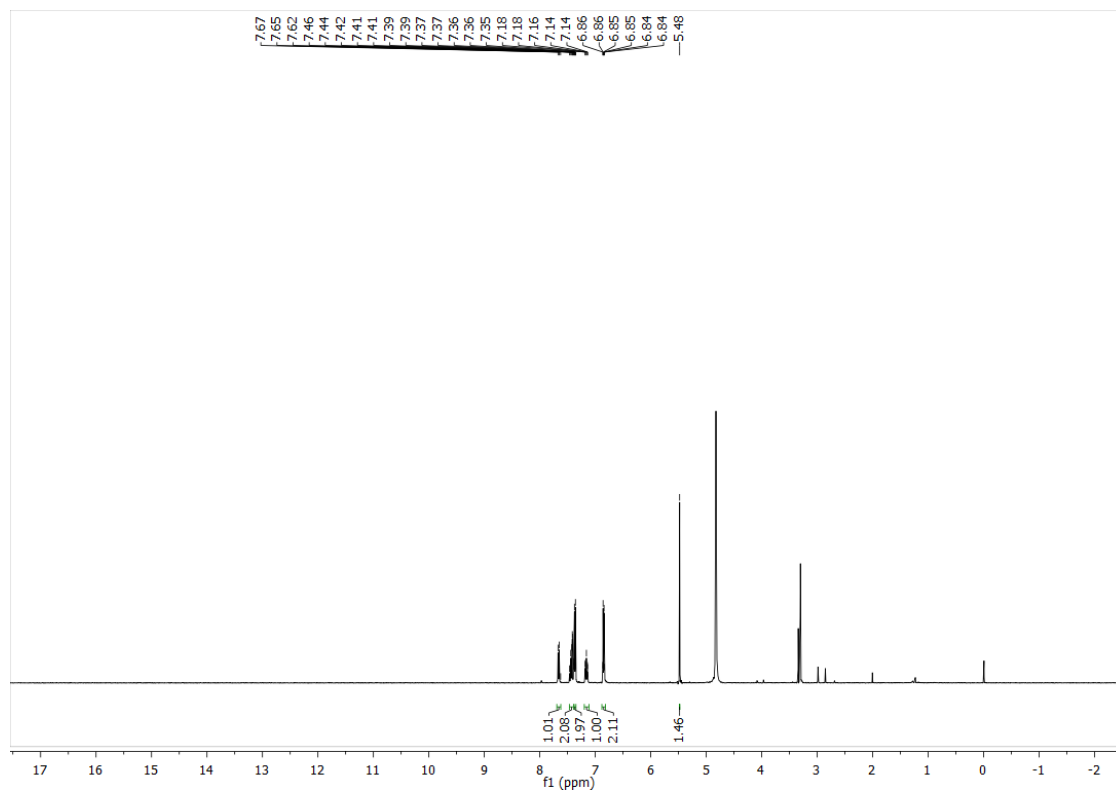
BA-pCN-OMe



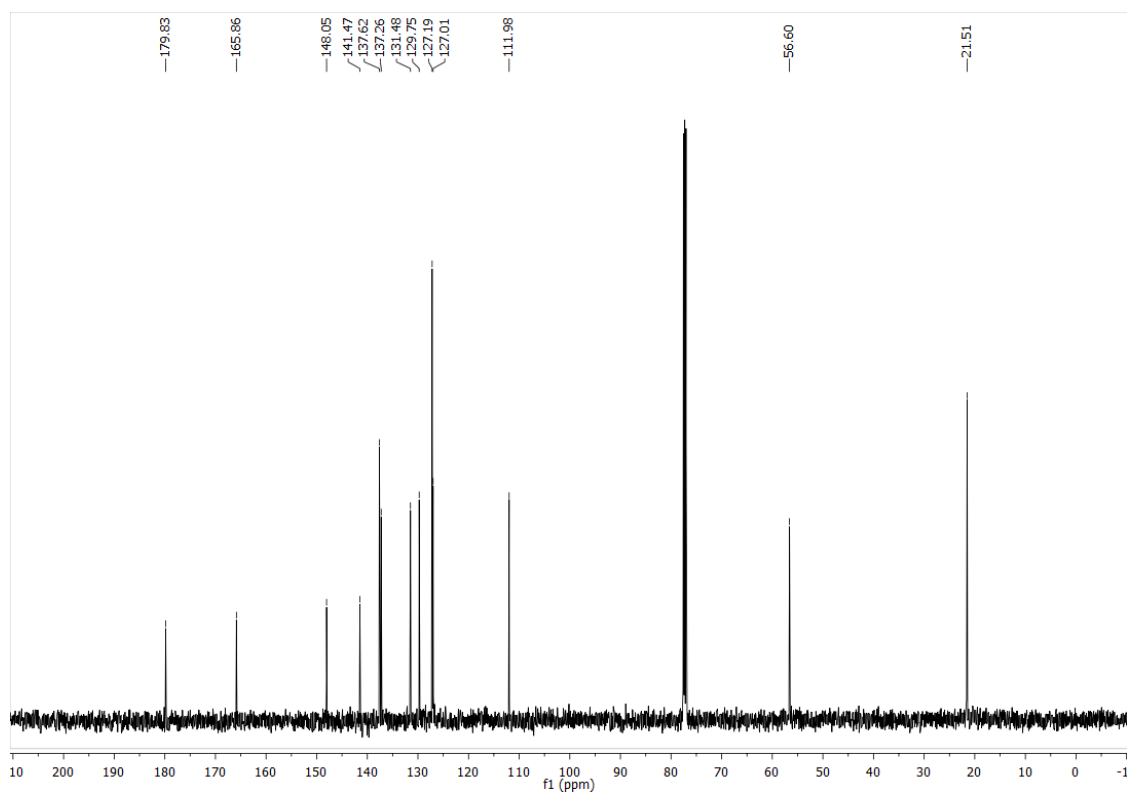
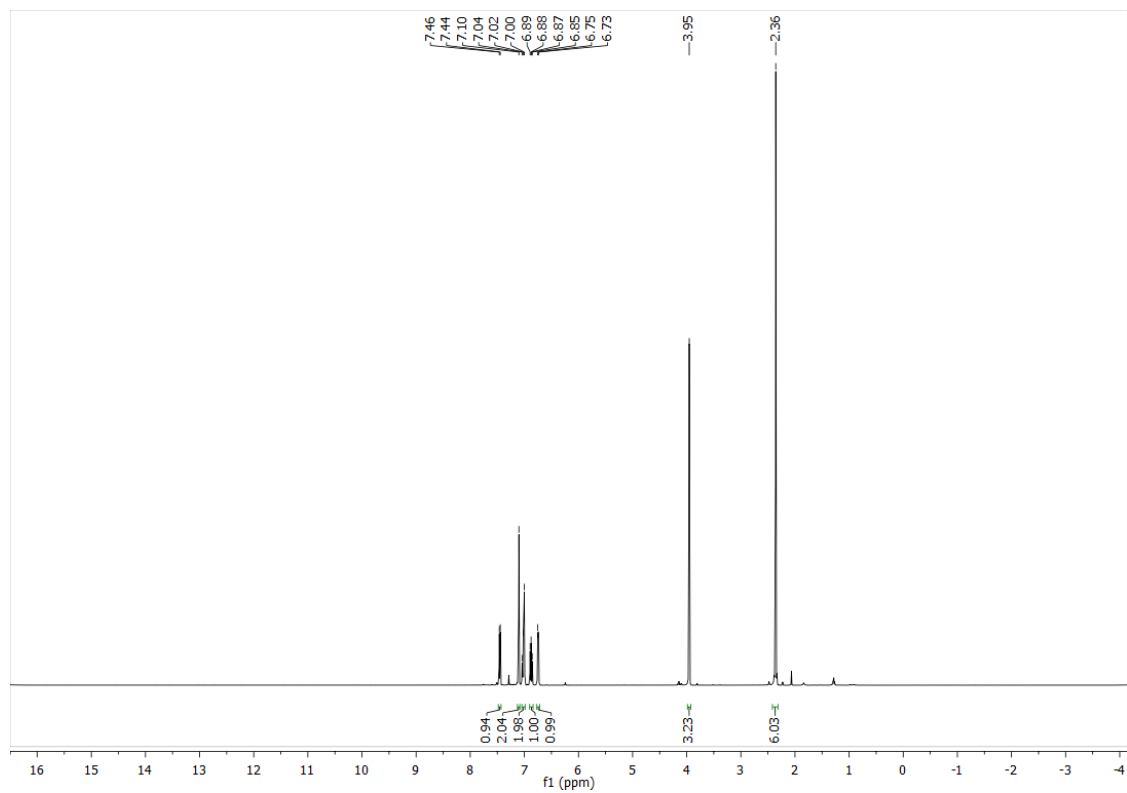
BA-pCN-OH



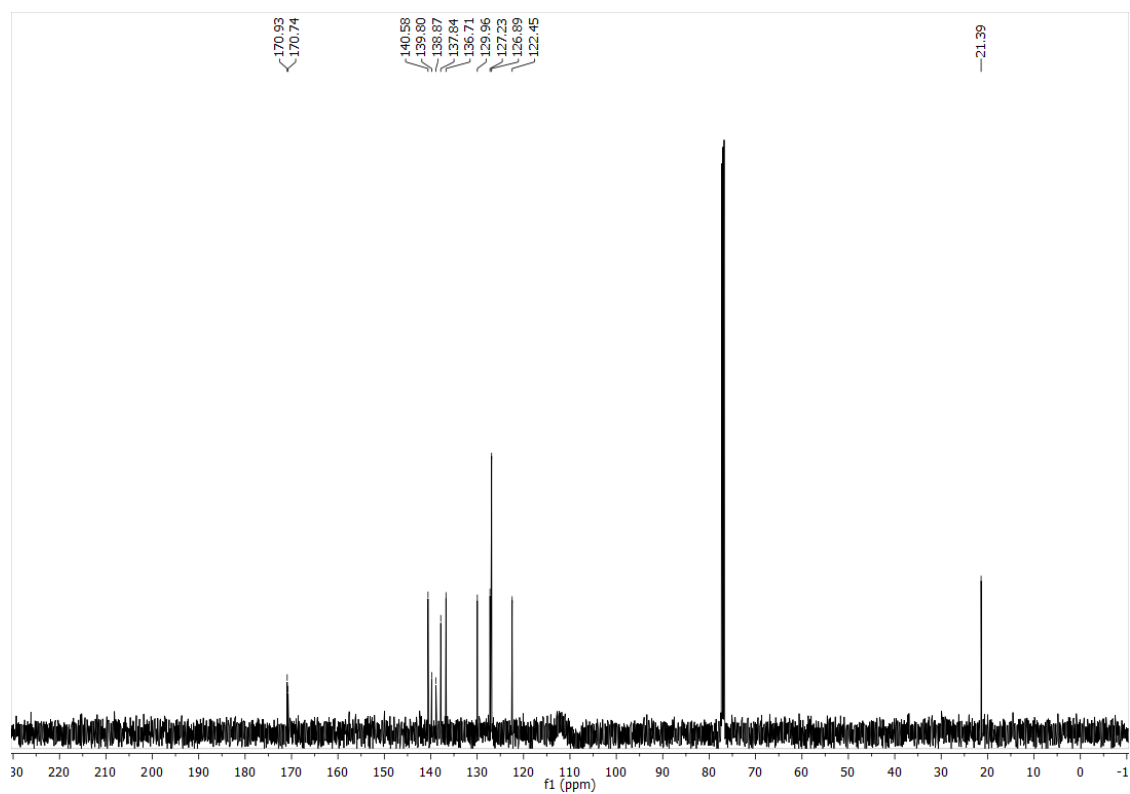
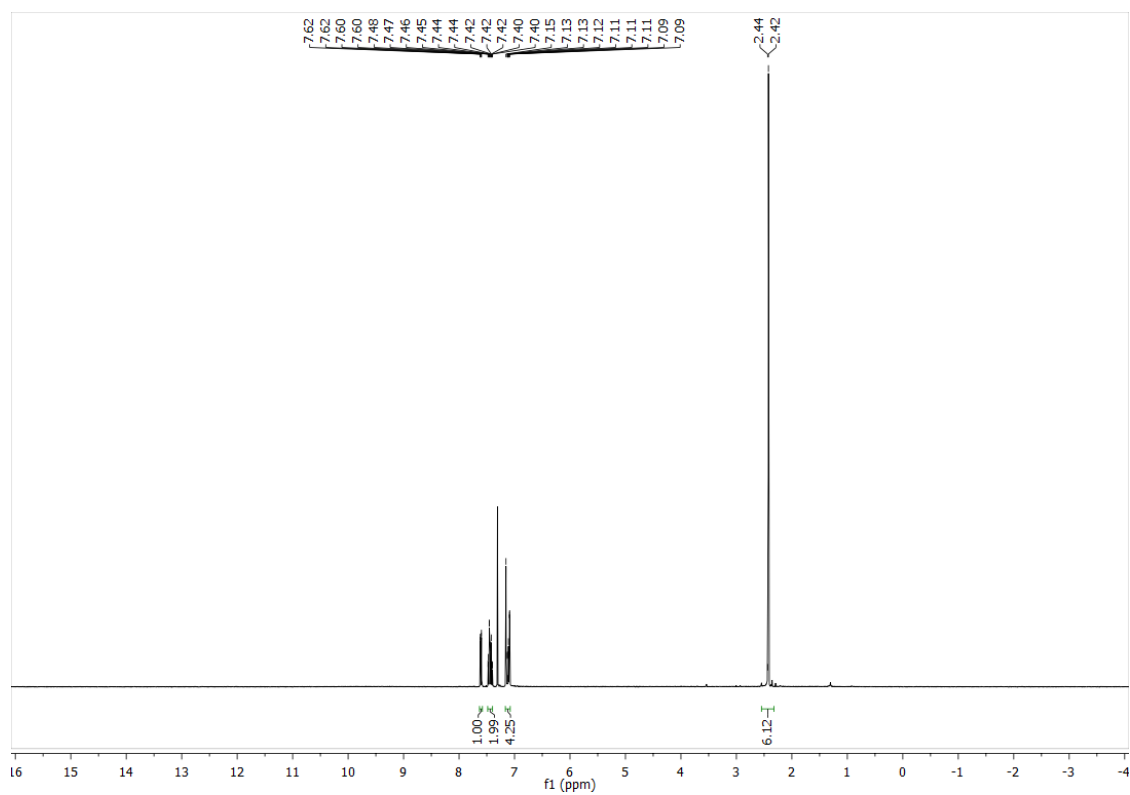
BA-pOH-OH



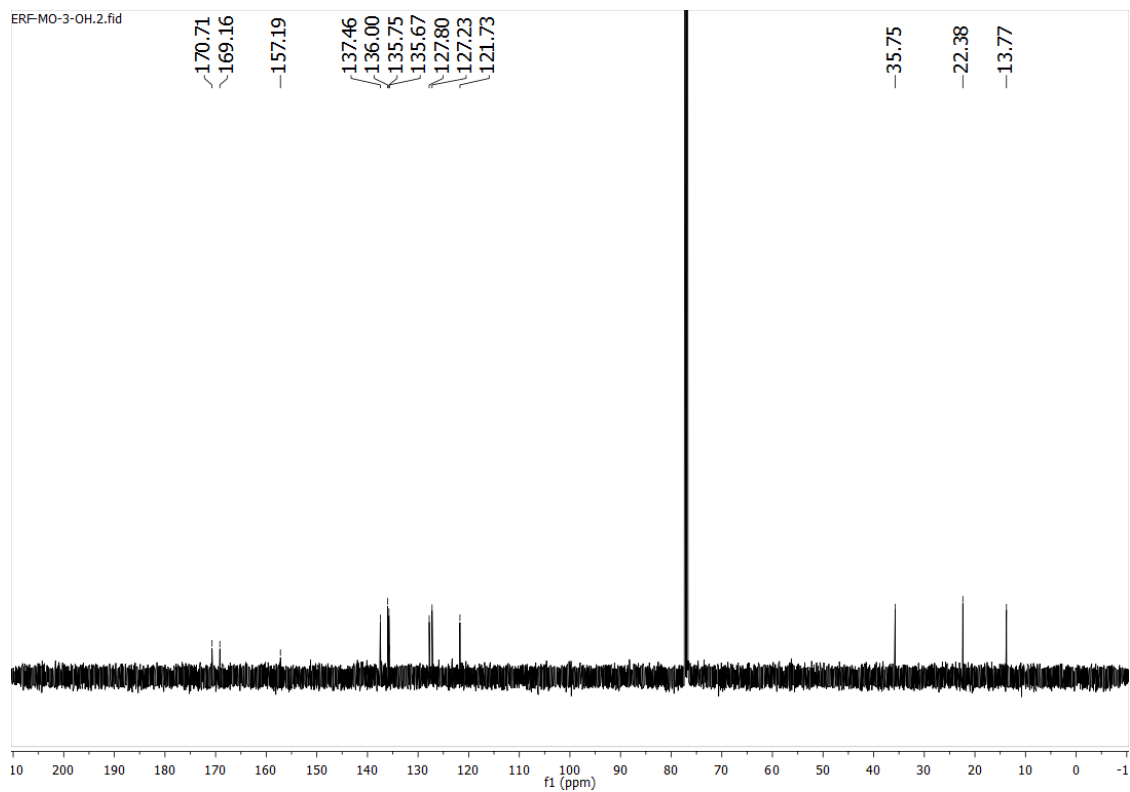
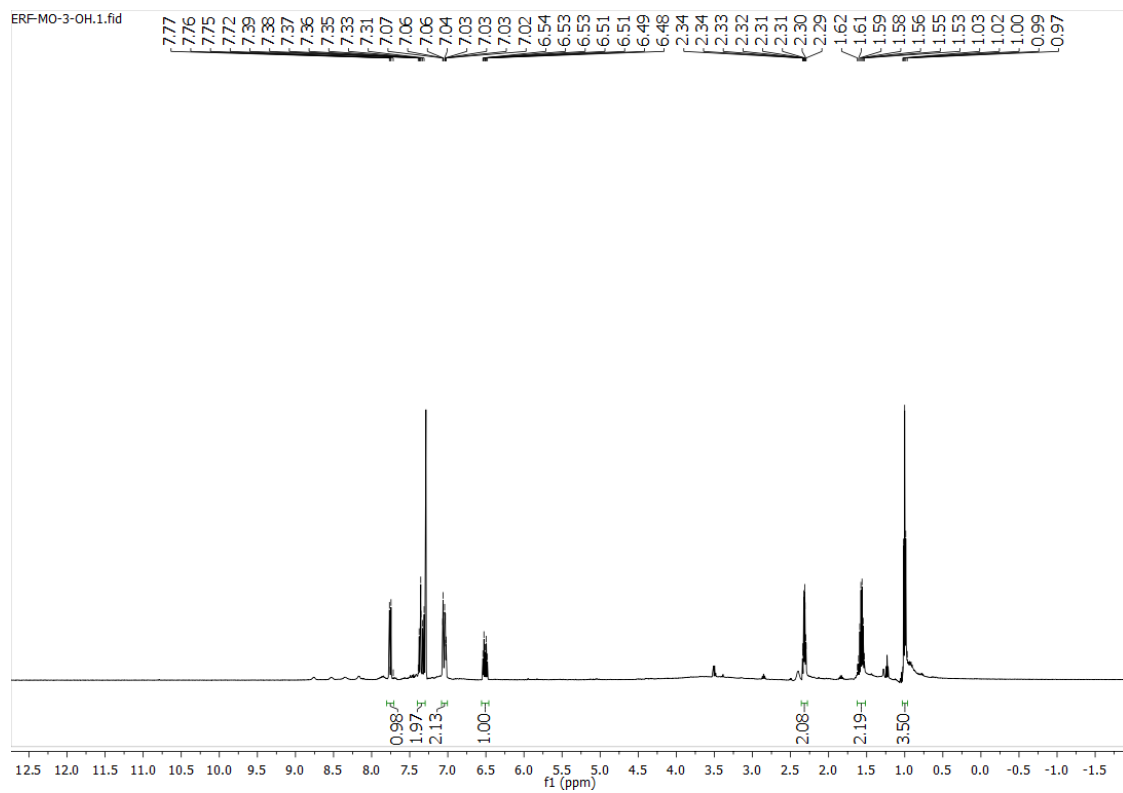
MO-DMe-OMe



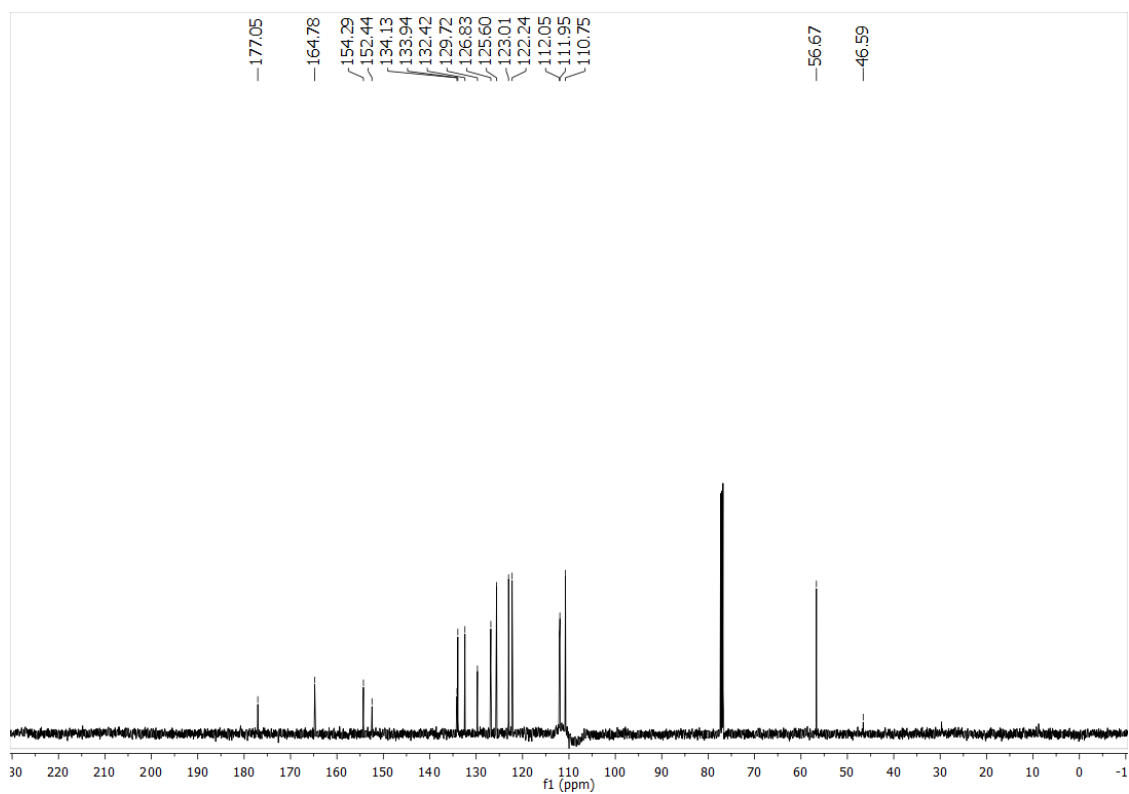
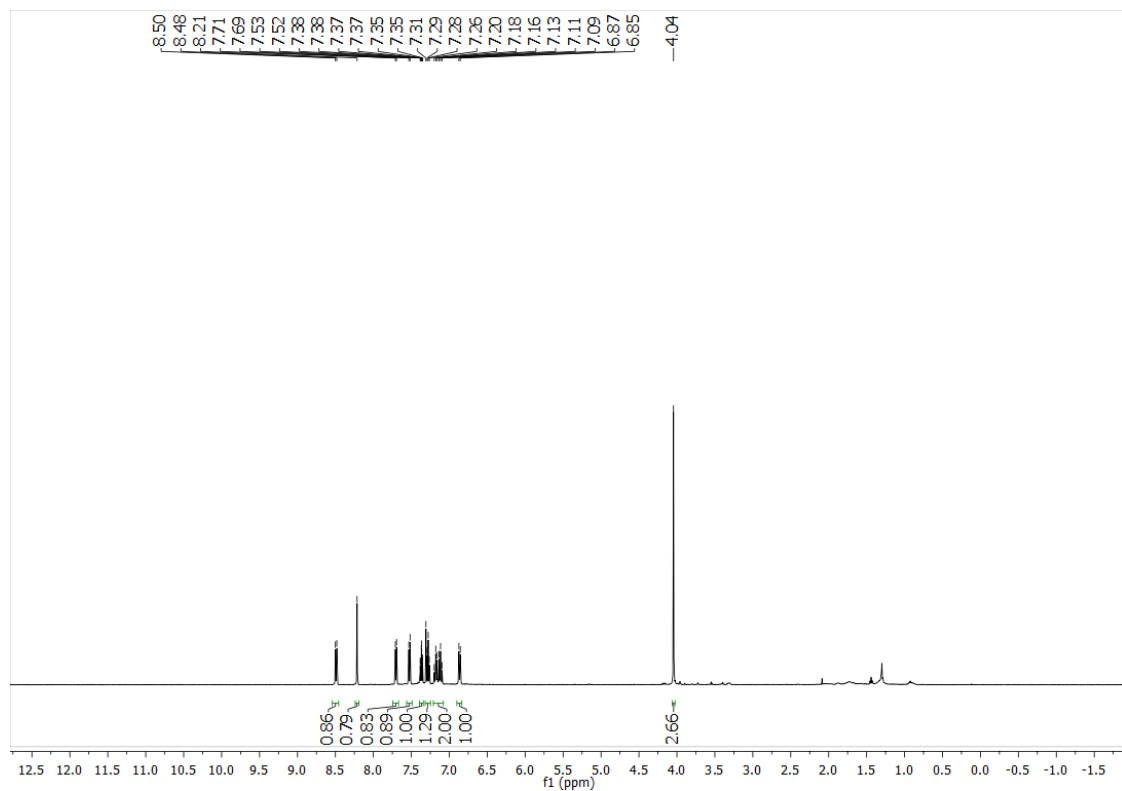
MO-DMe-OH



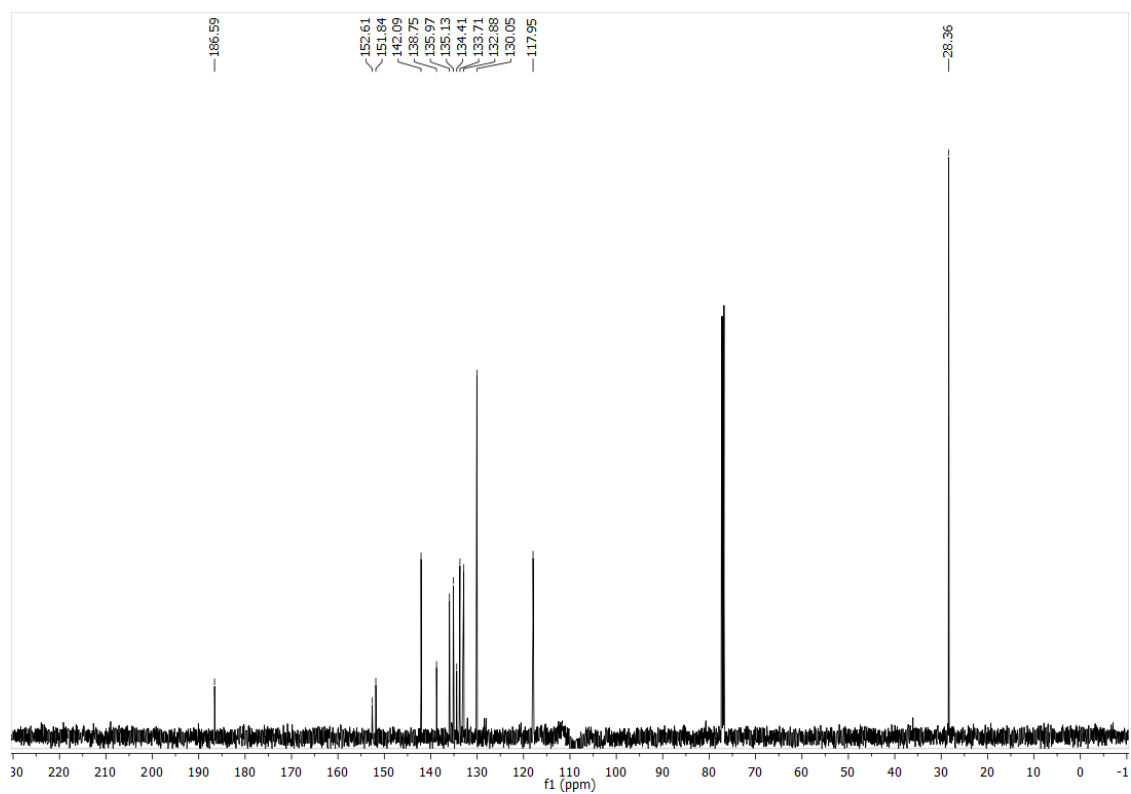
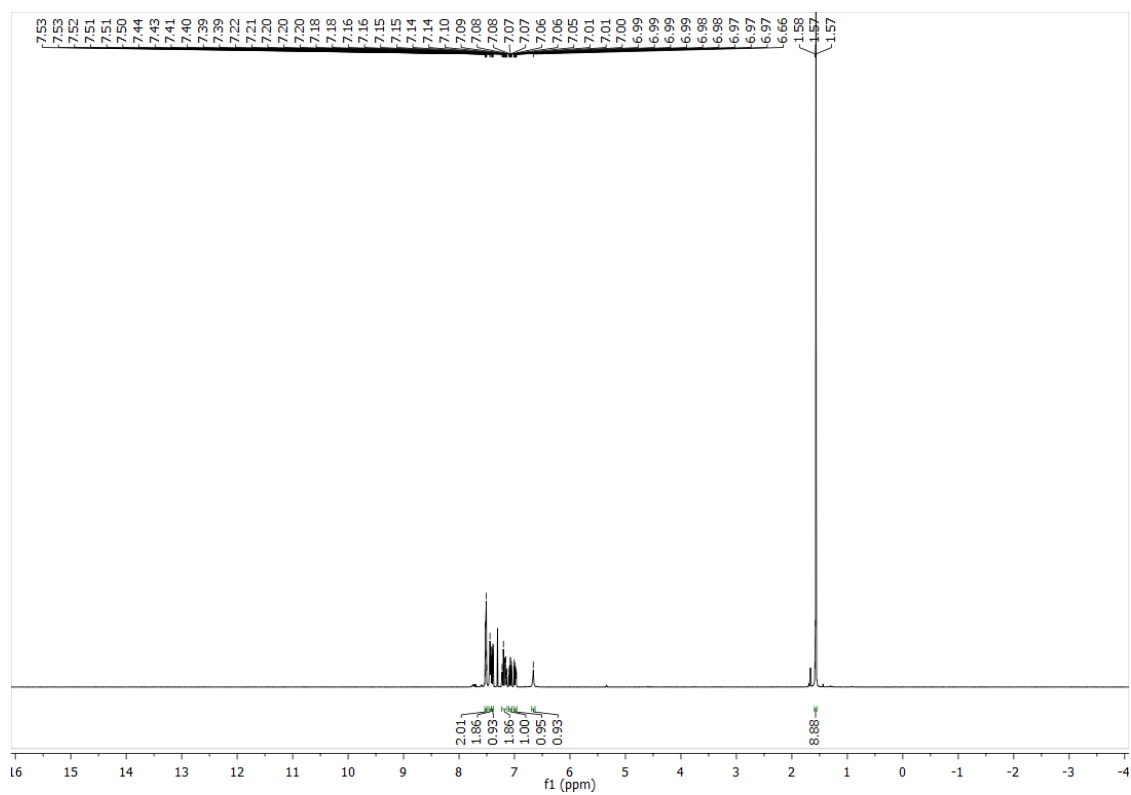
MO-3-OH

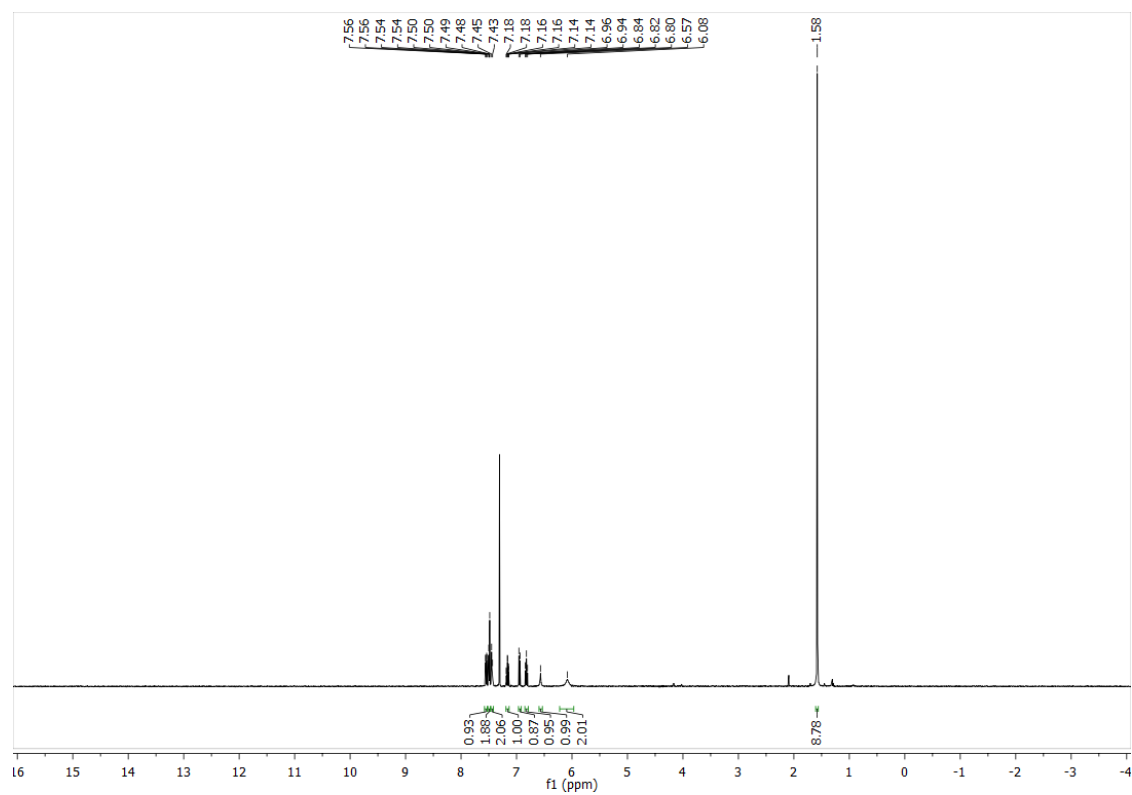


HC-4-OMe

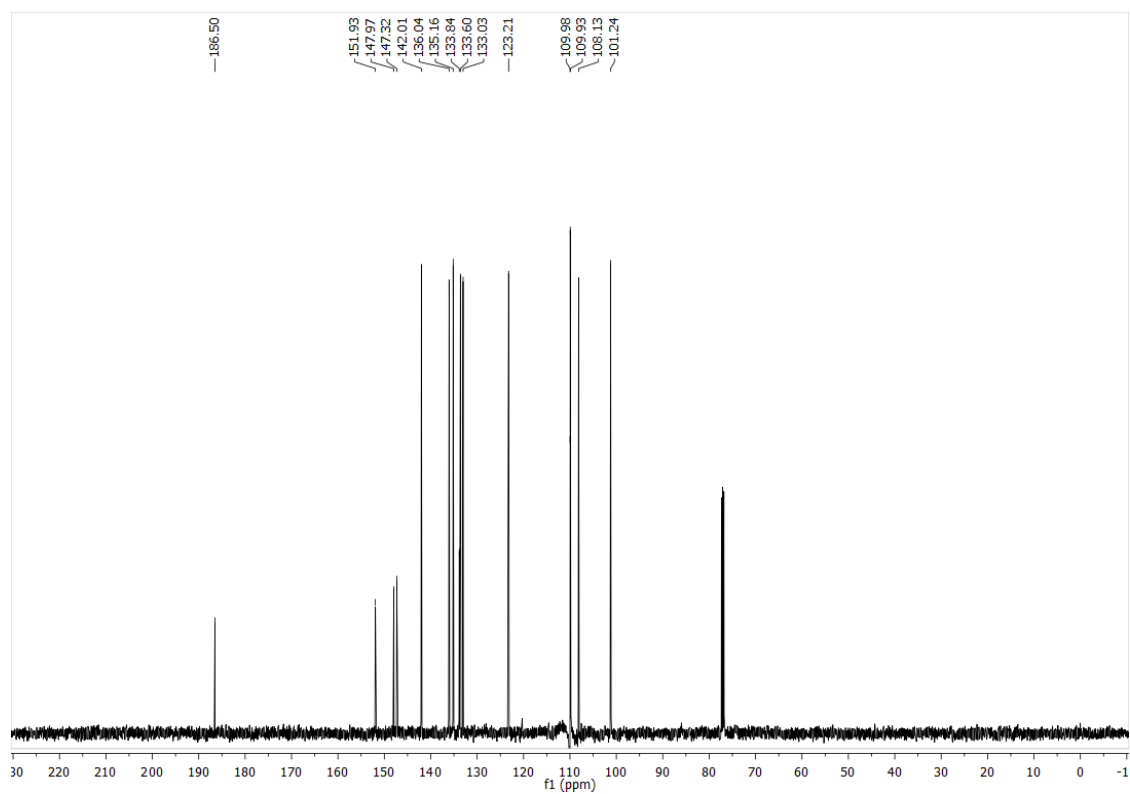
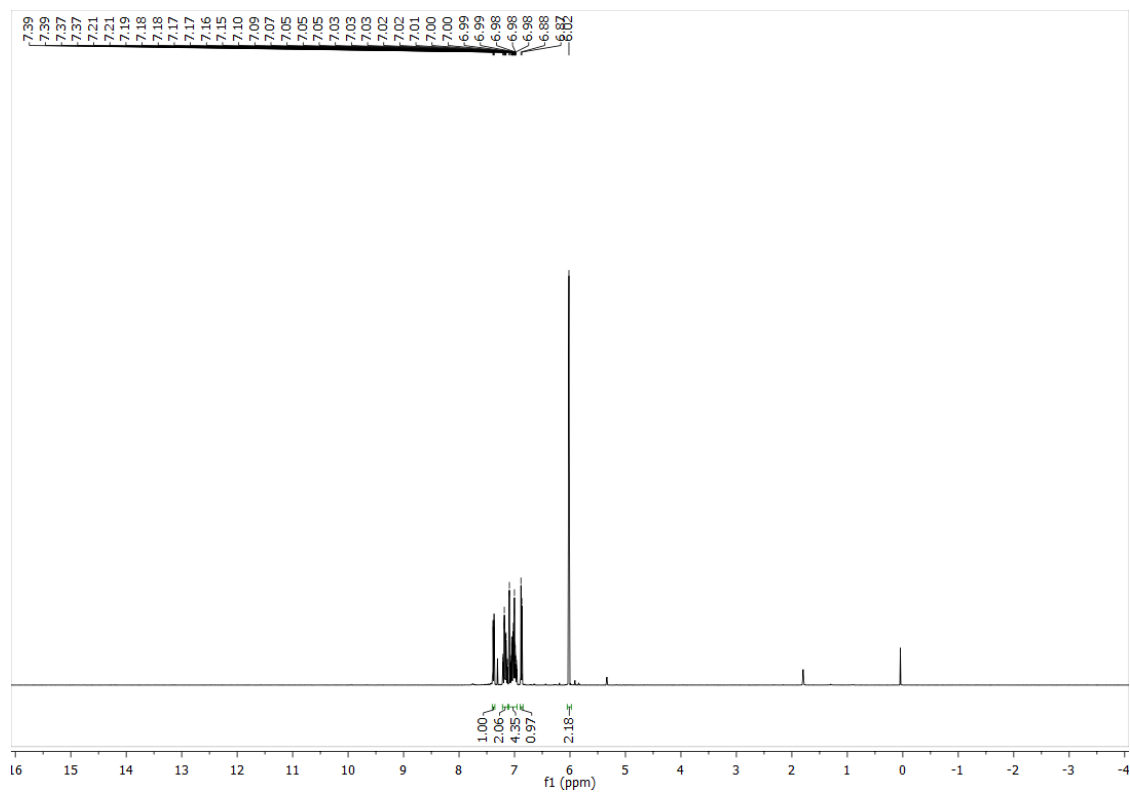


Am-Boc-H

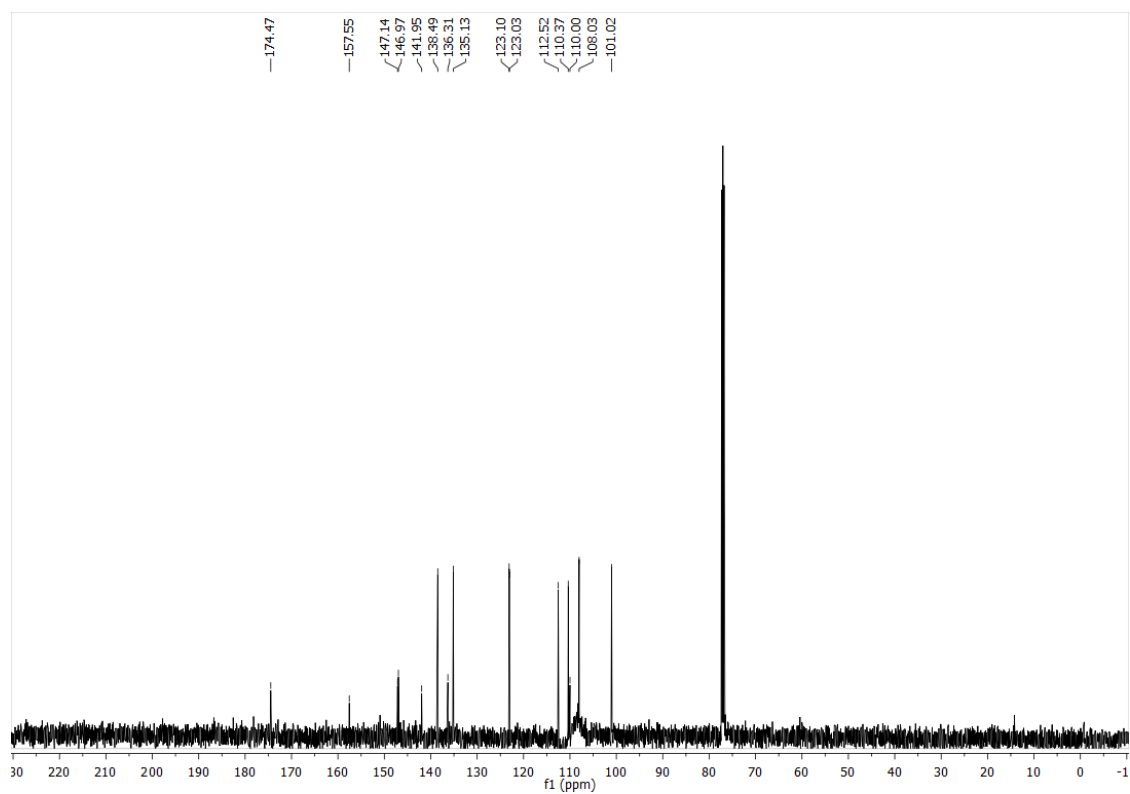
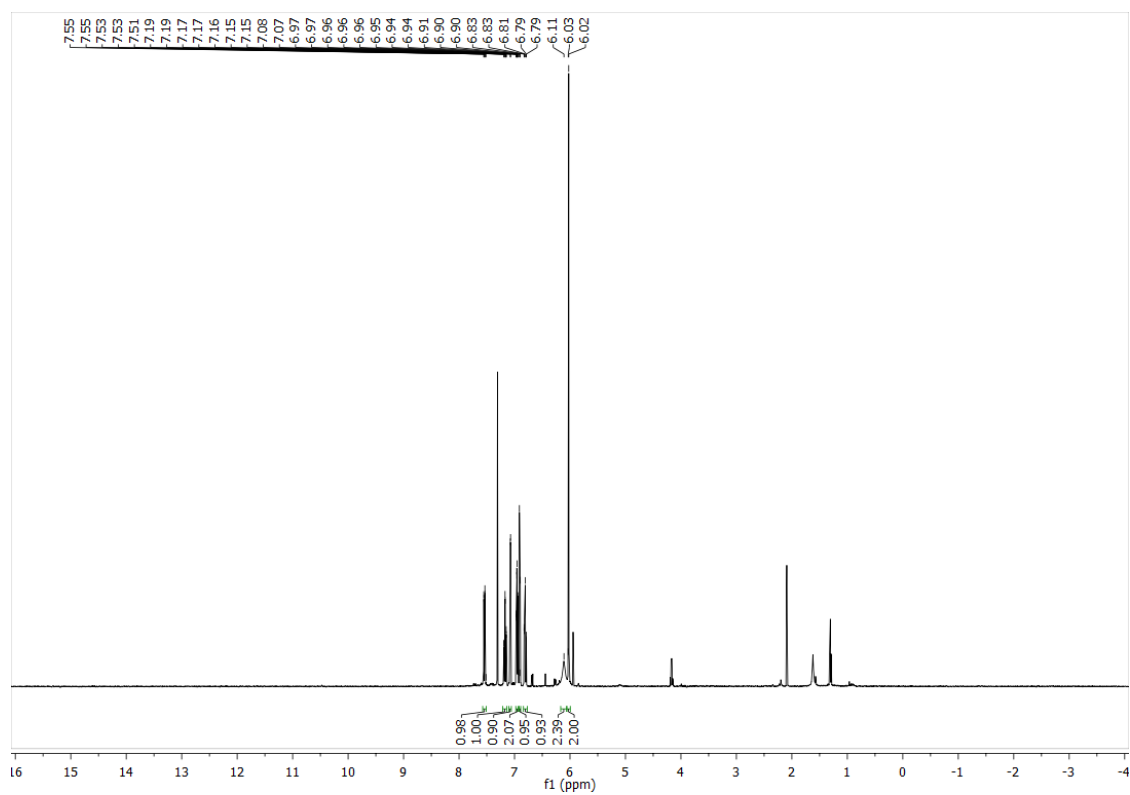


Am-Boc-NH2

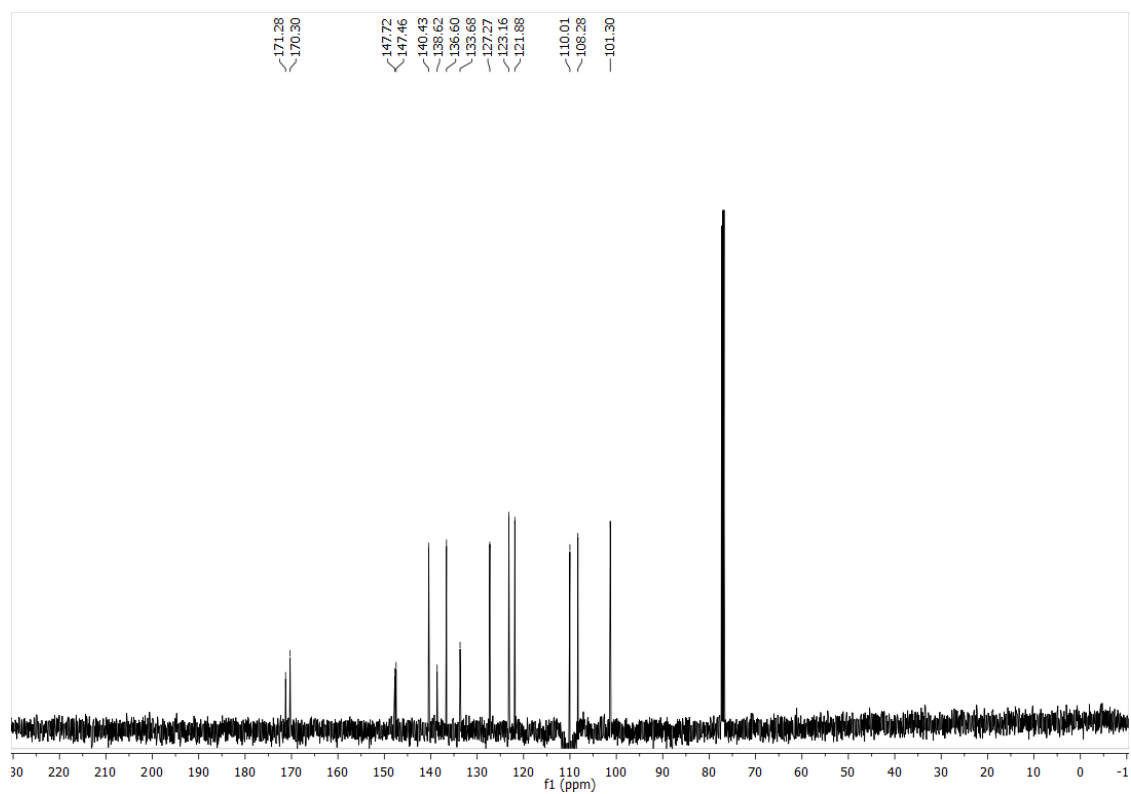
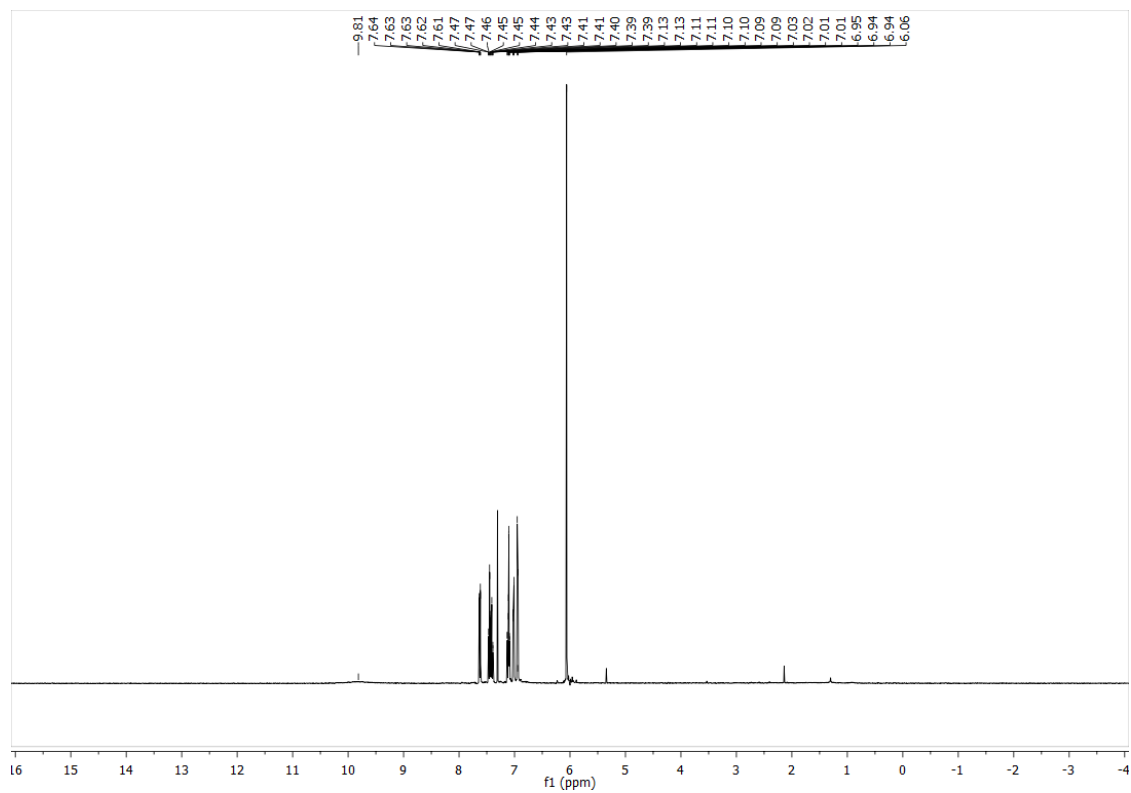
HC-5-H



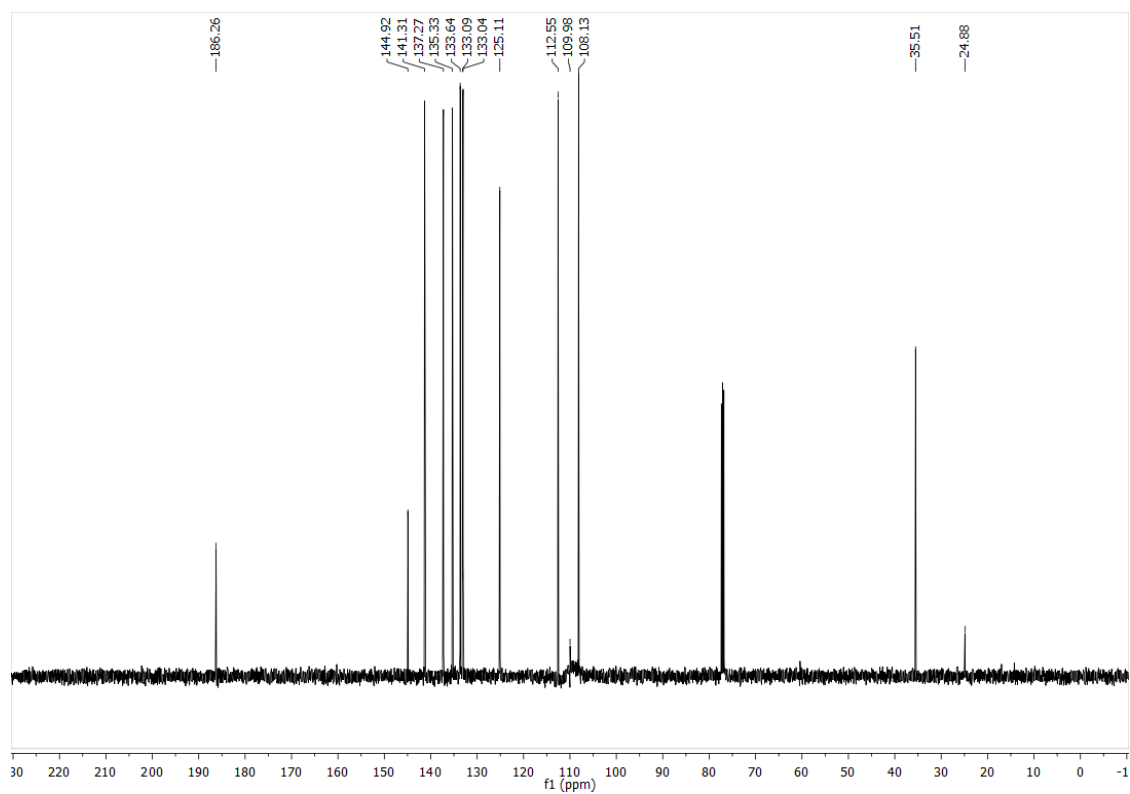
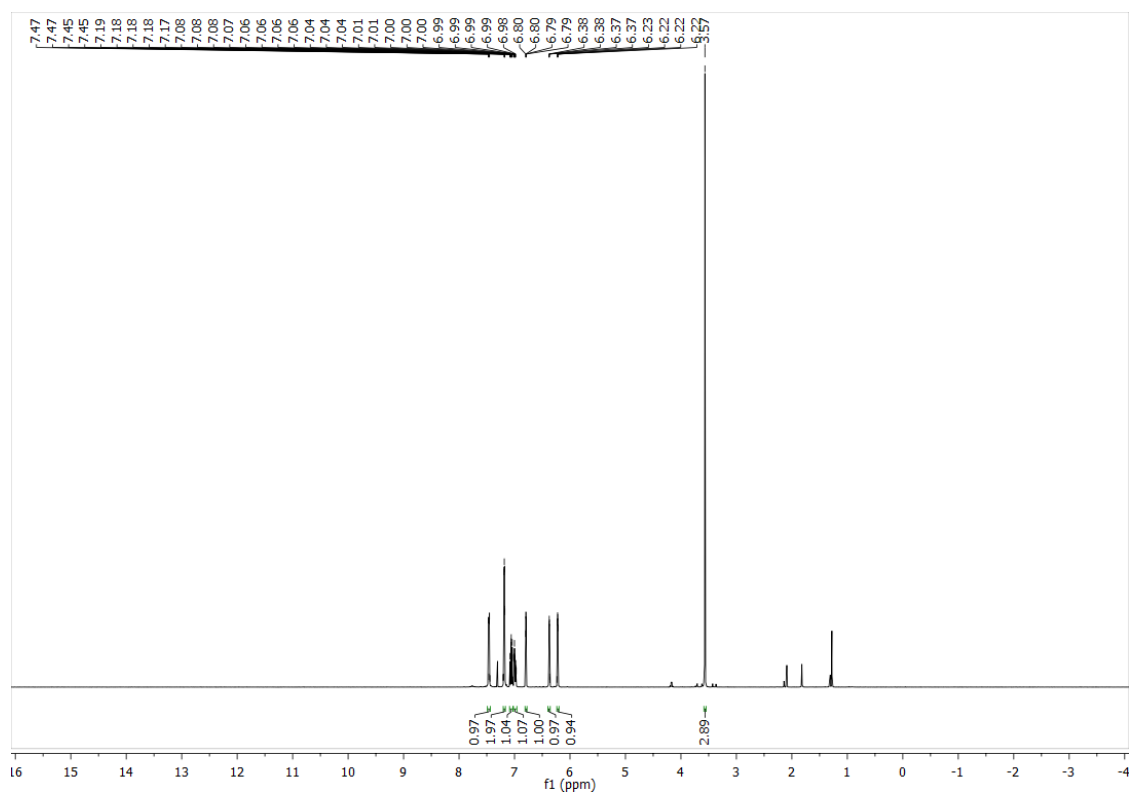
HC-5-NH2

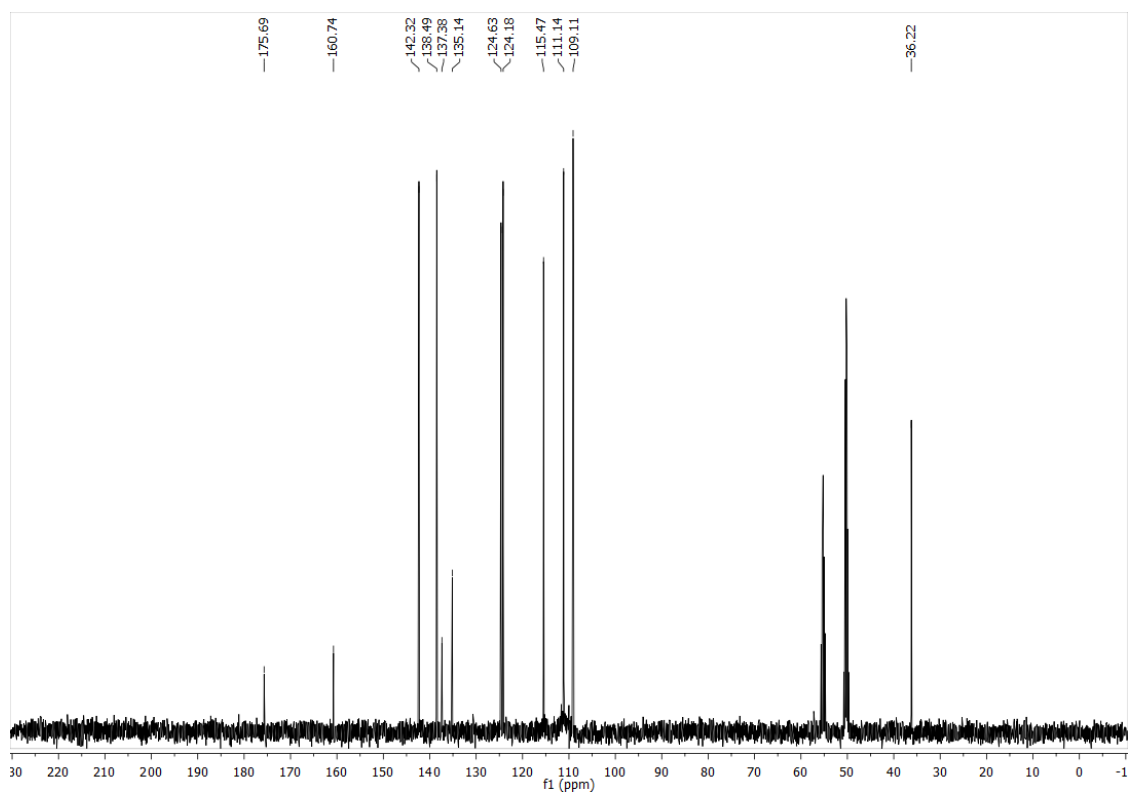
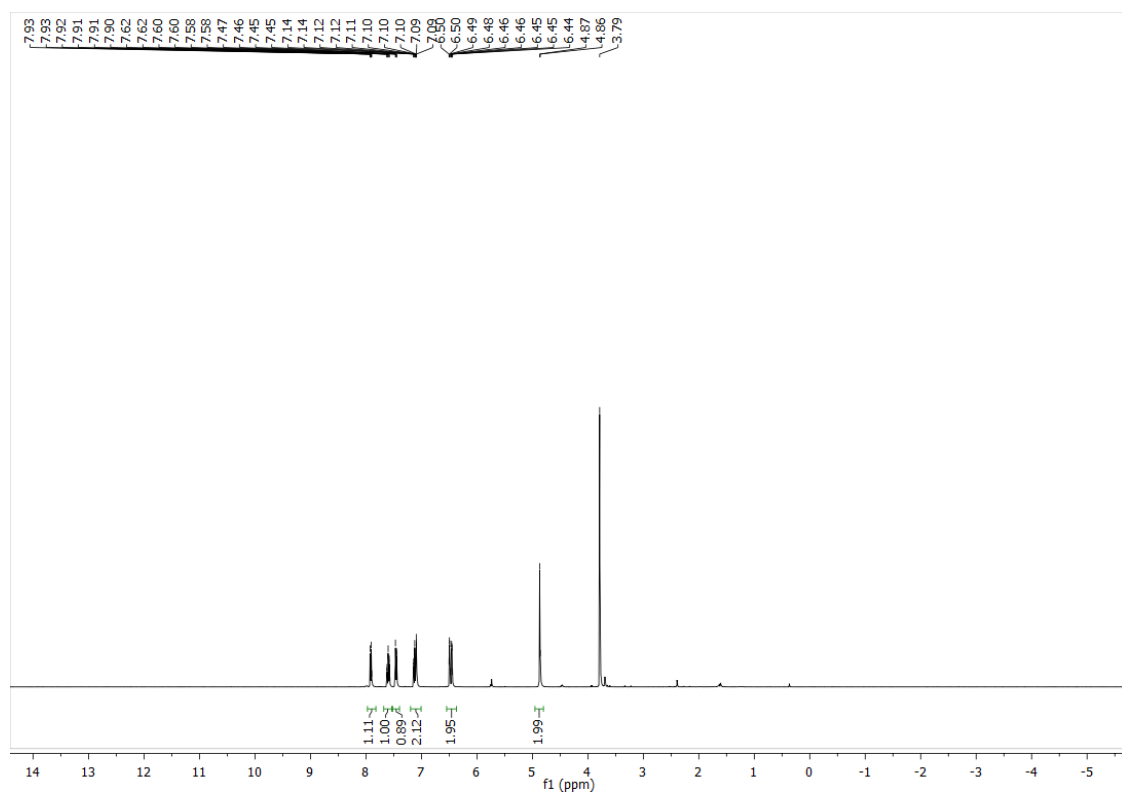


HC-5-OH

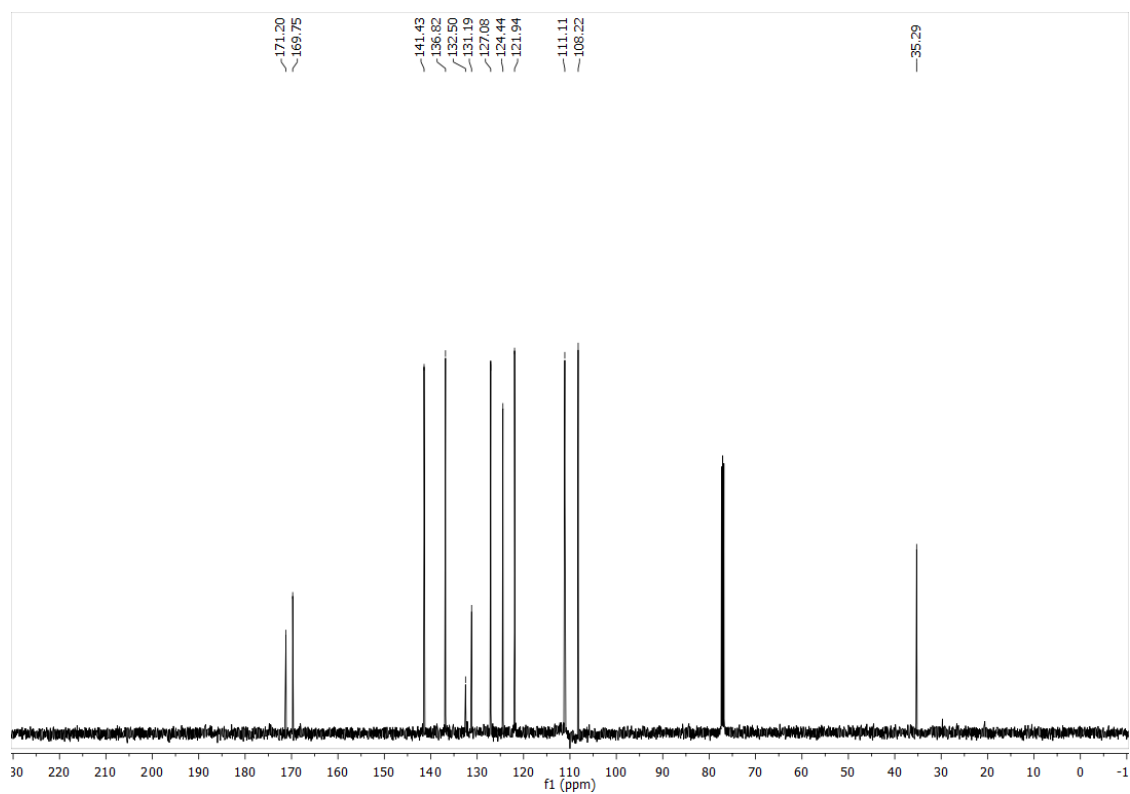
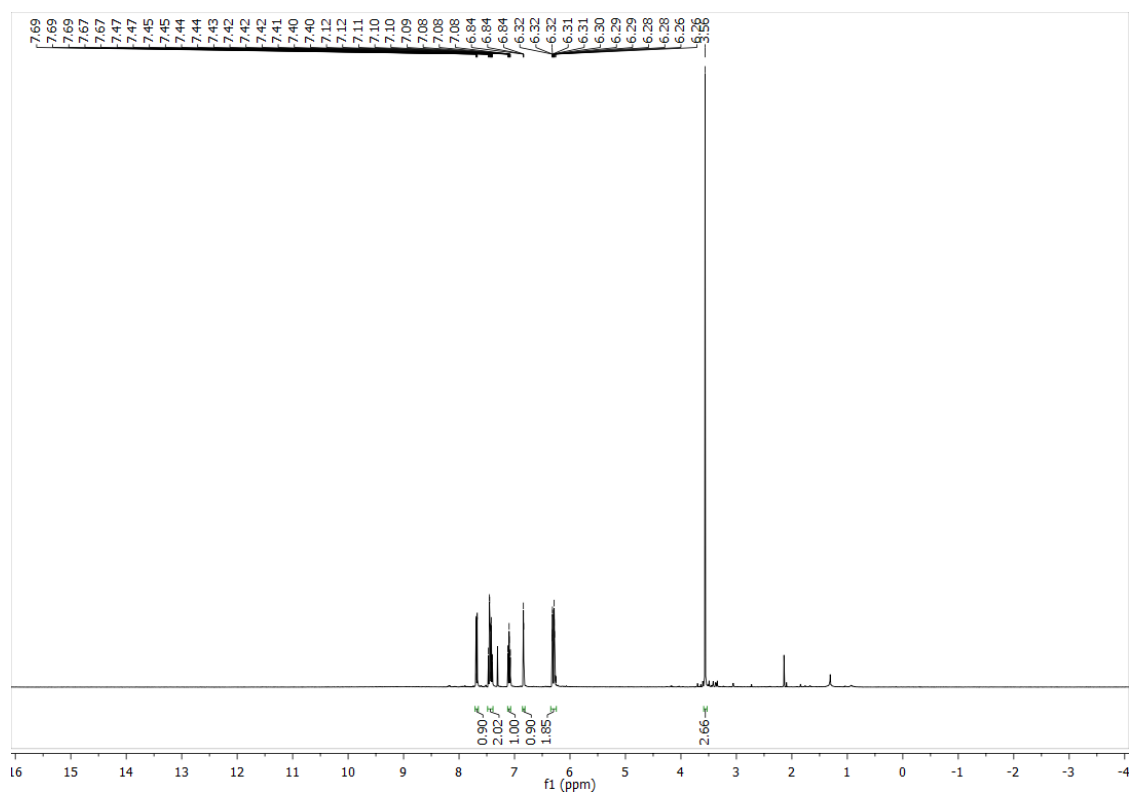


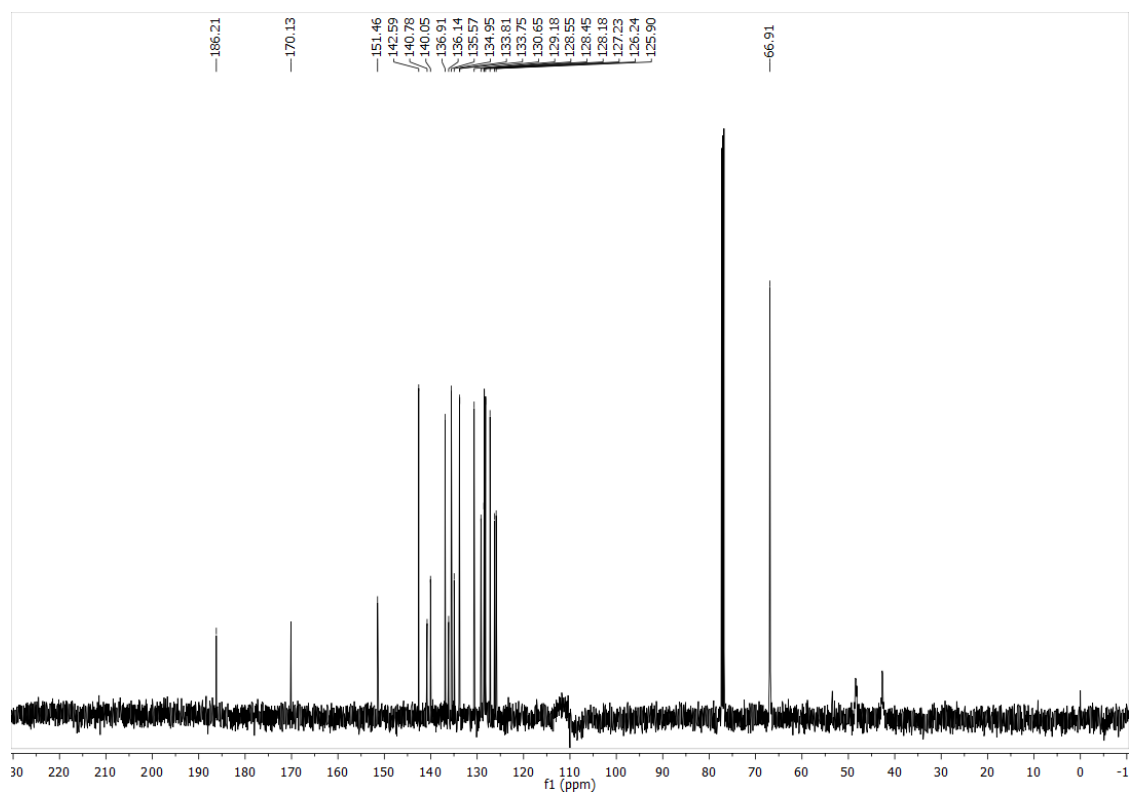
HC-6-H



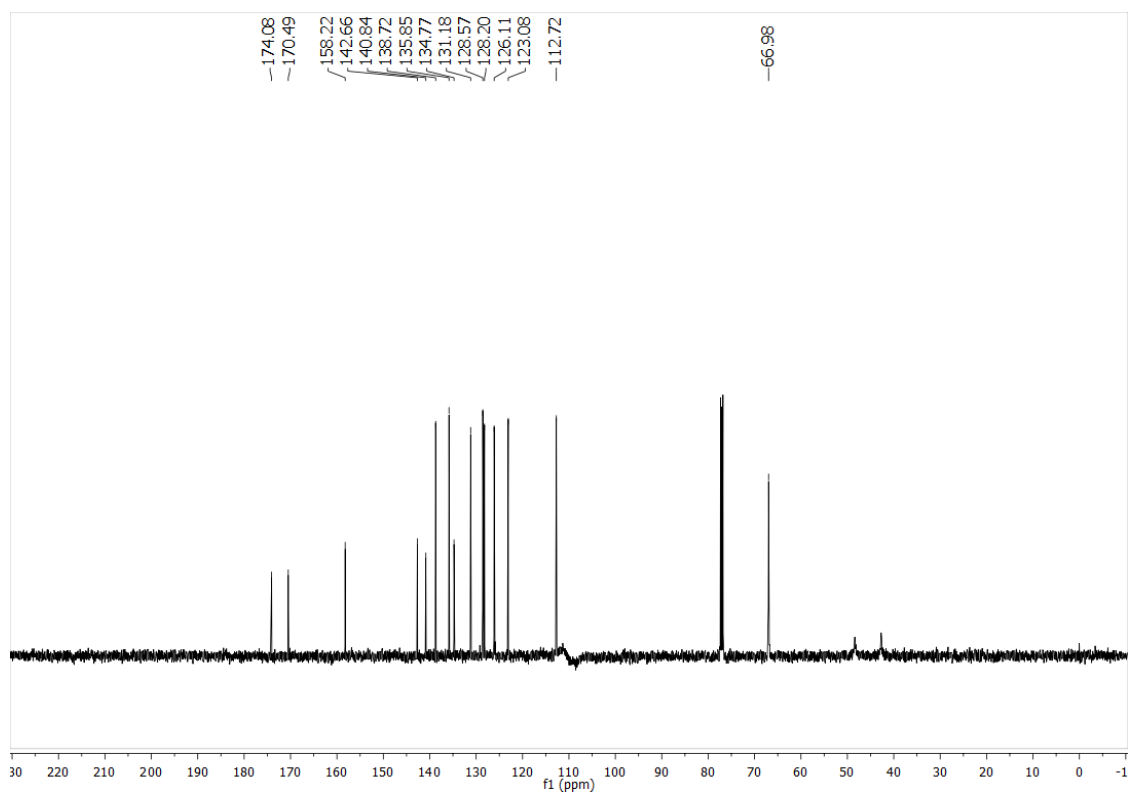
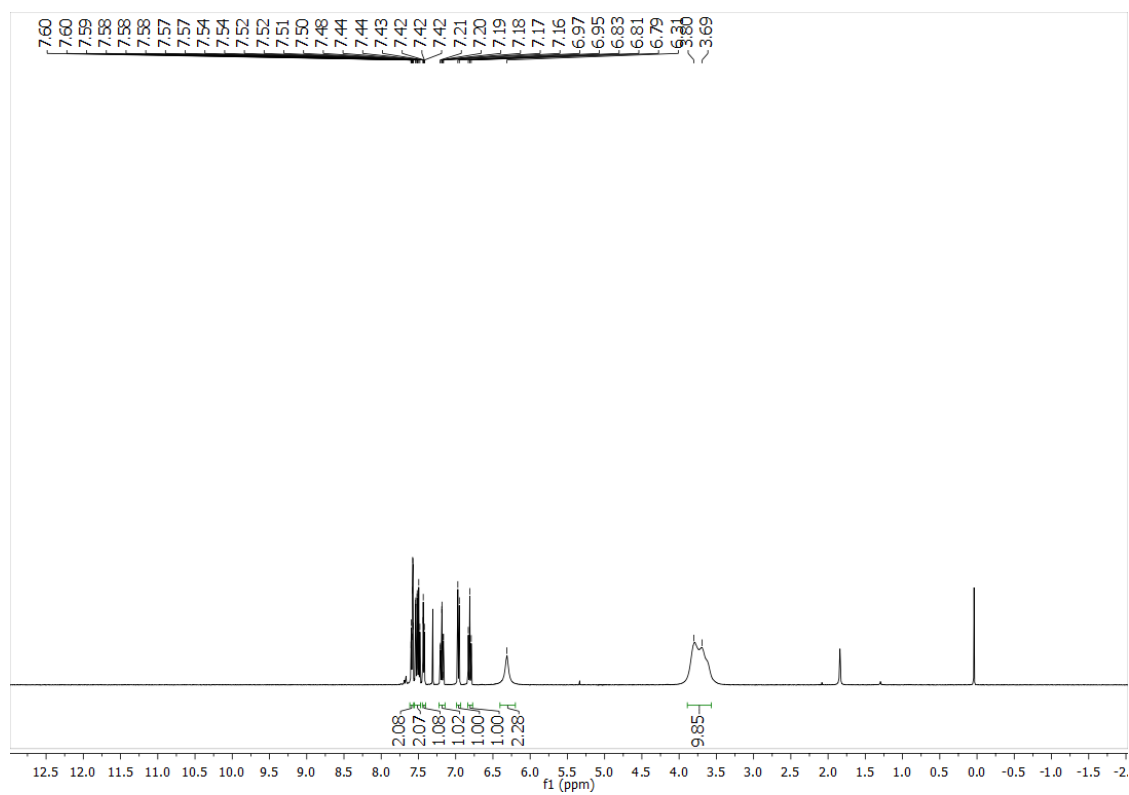
HC-6-NH₂

HC-6-OH

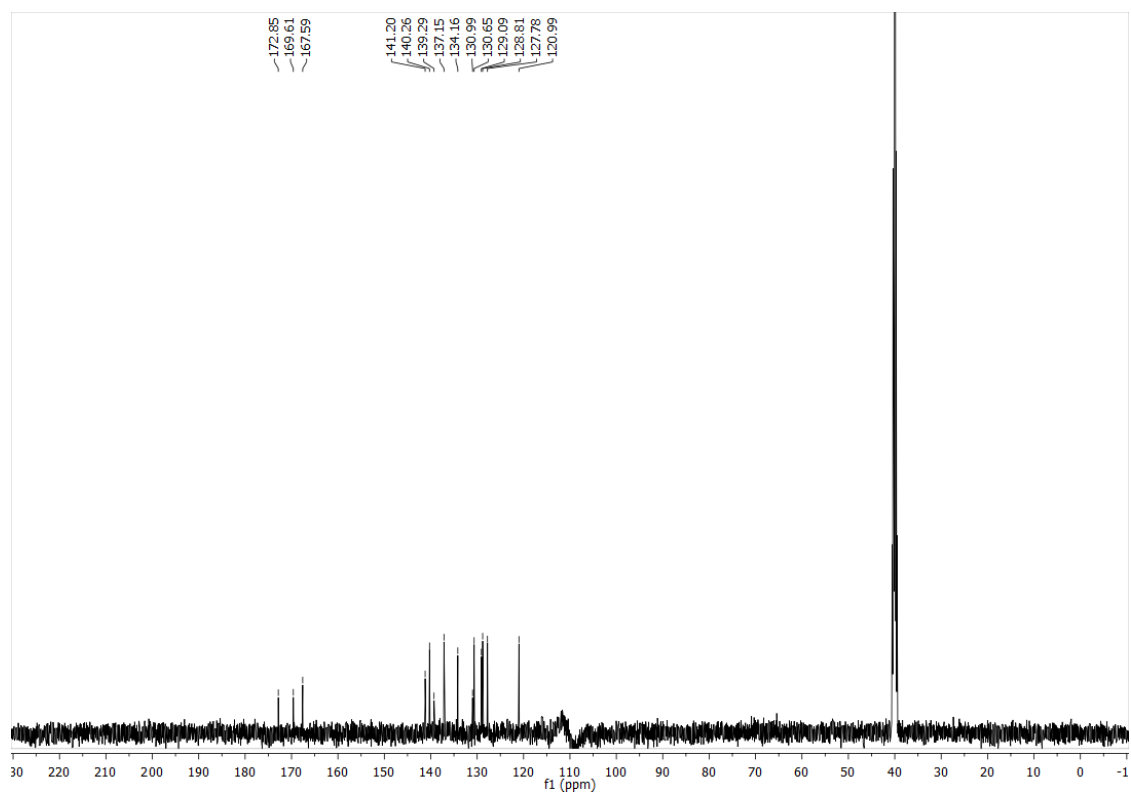
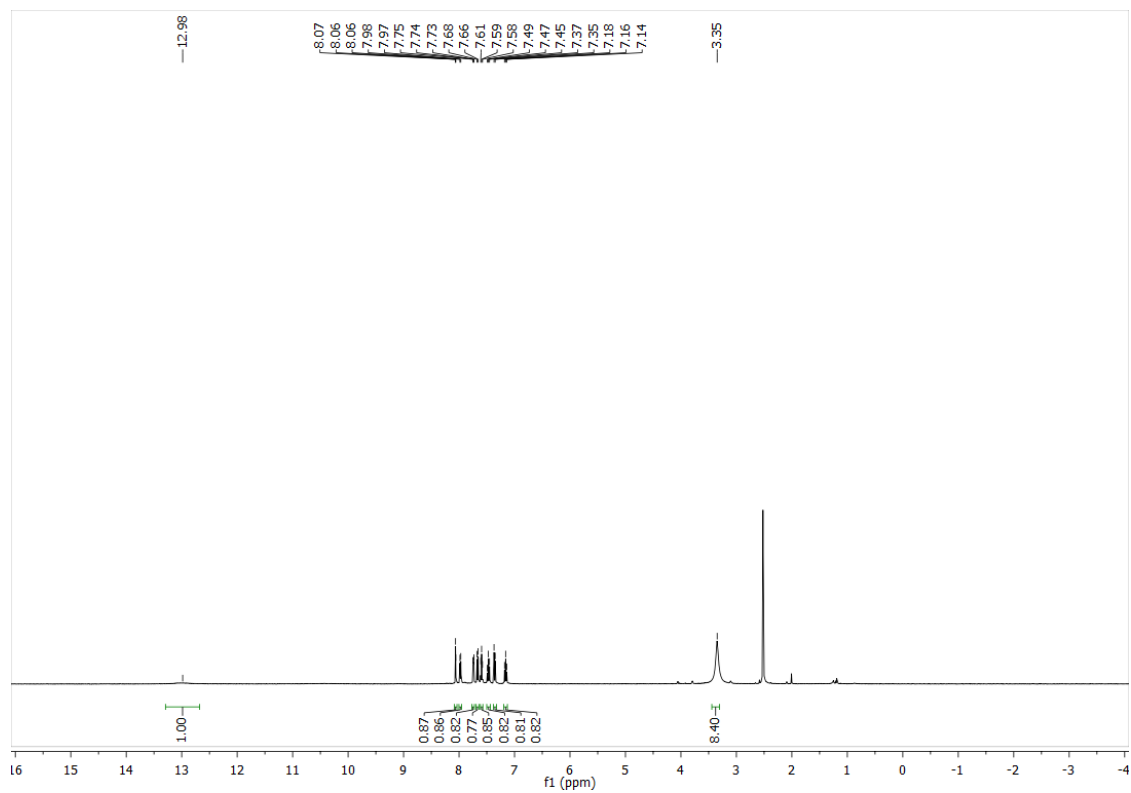


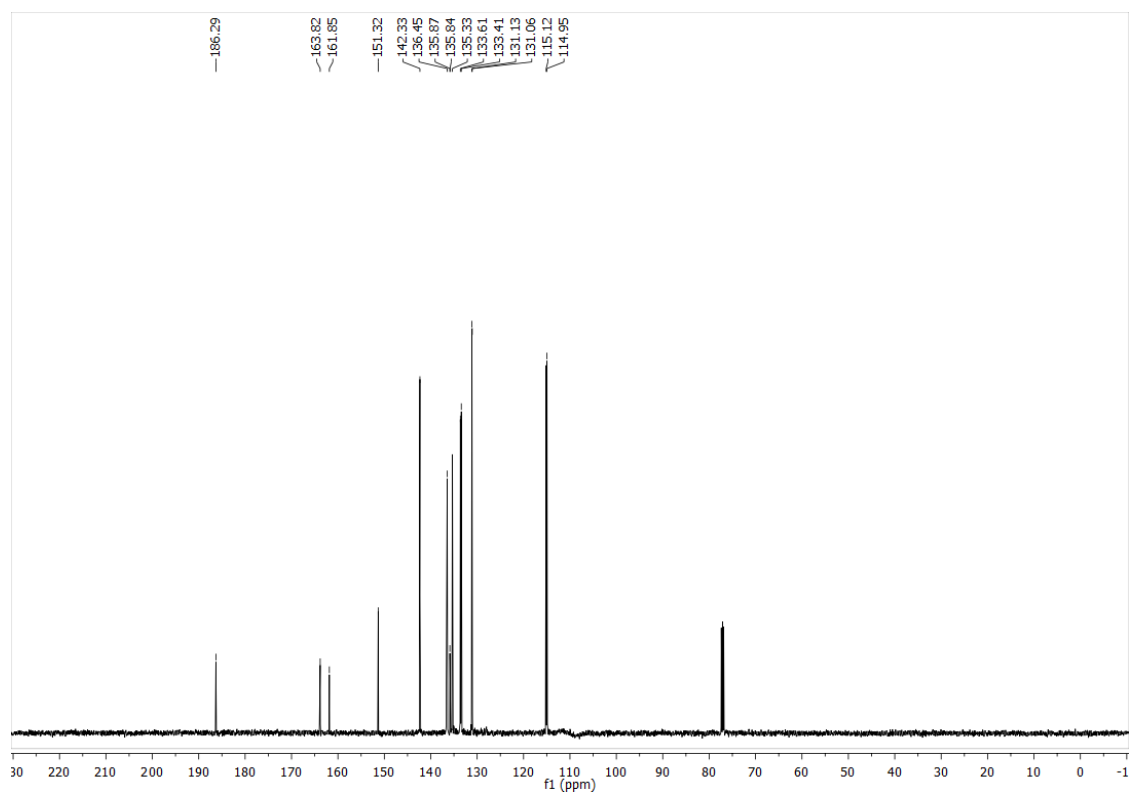
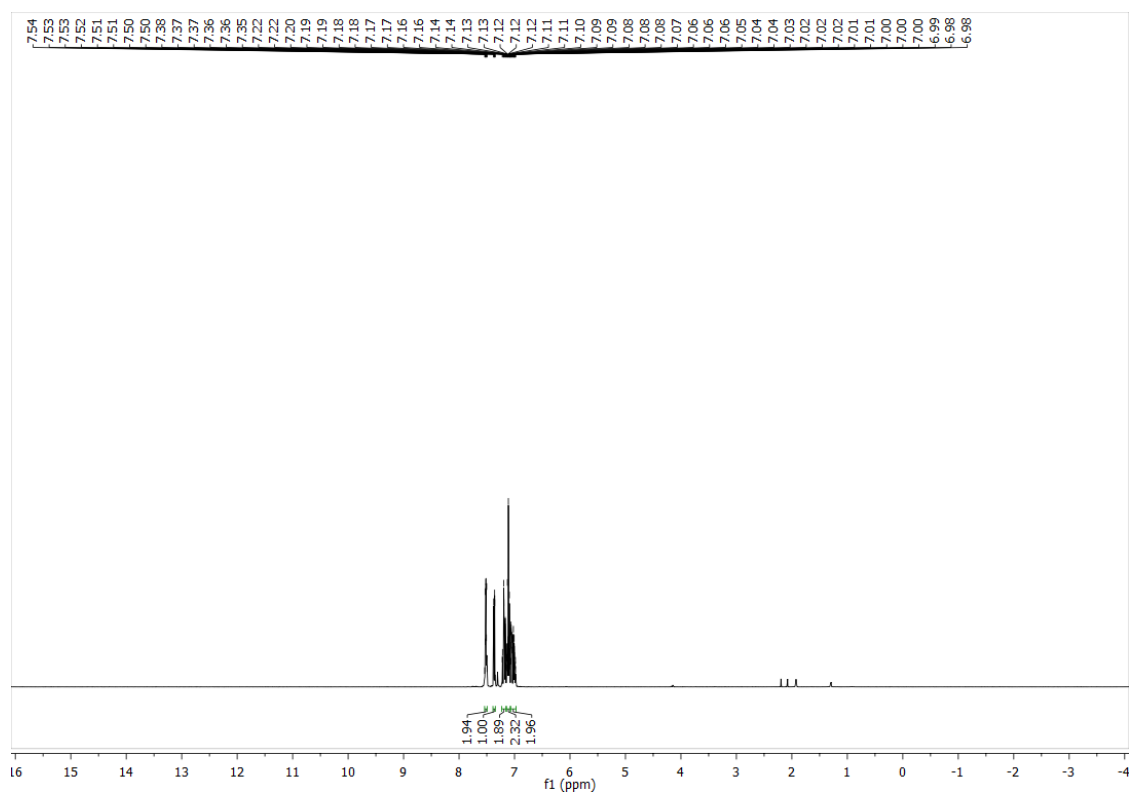


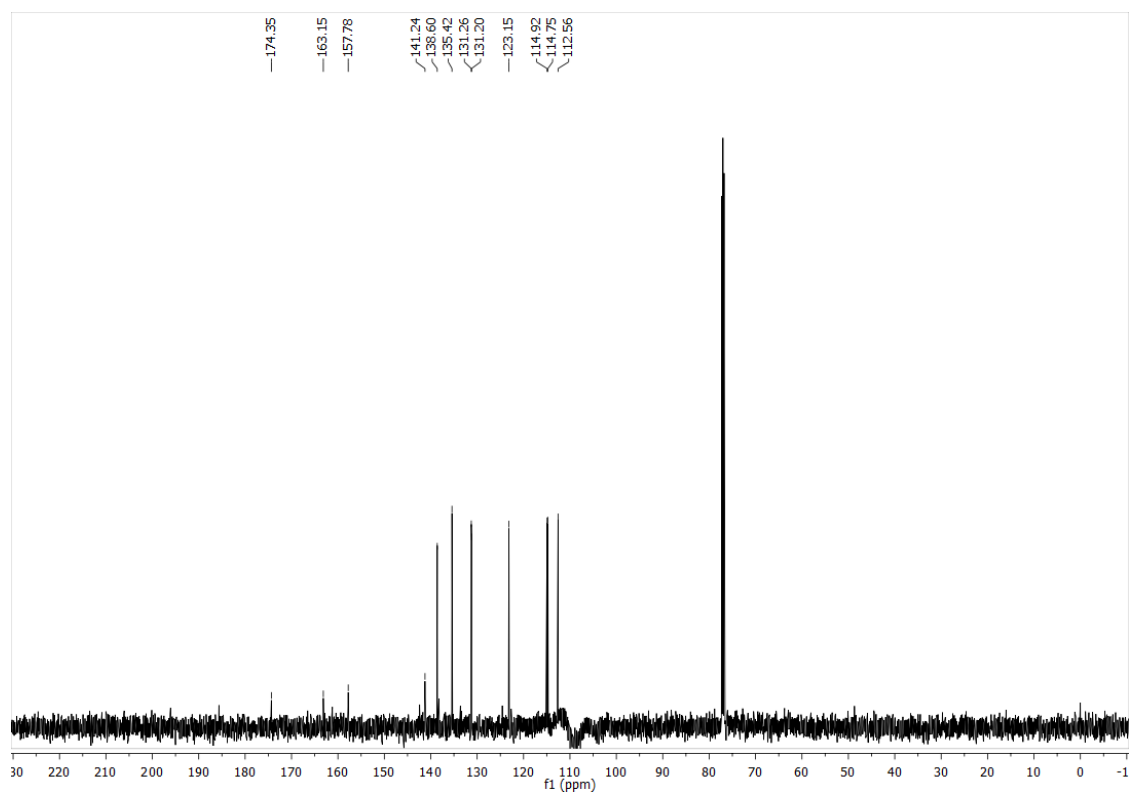
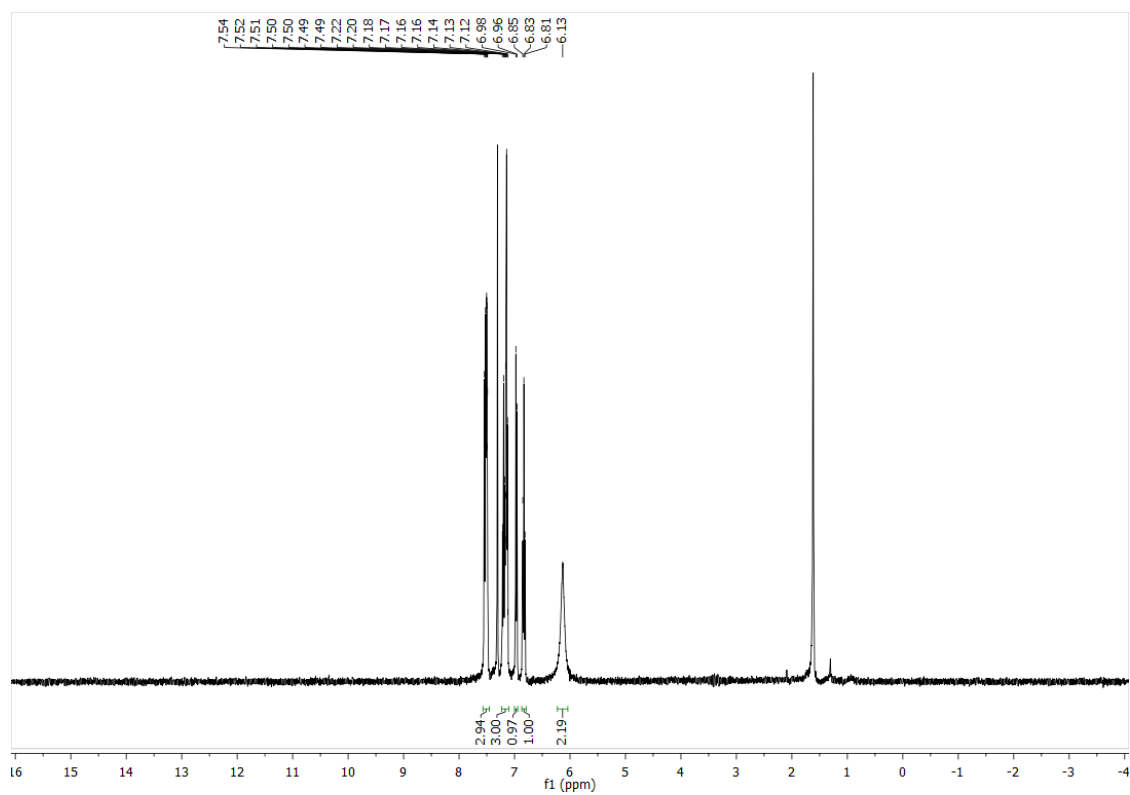
HC-7-NH2

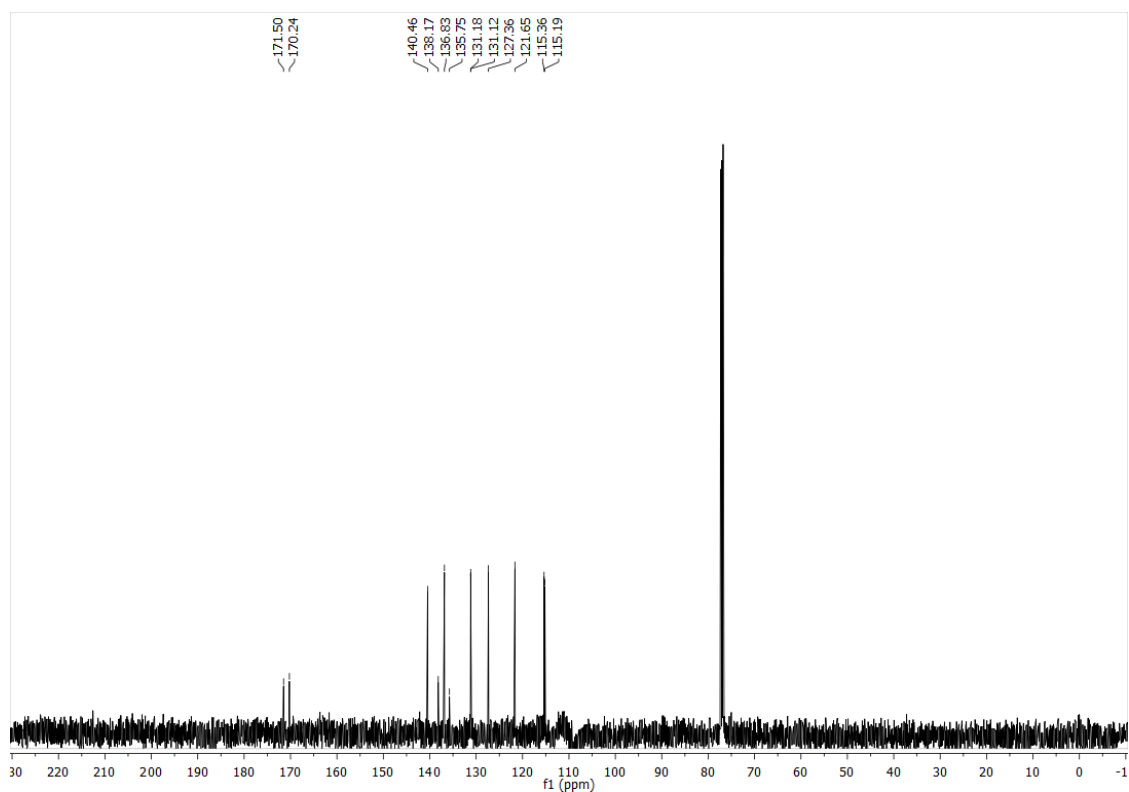
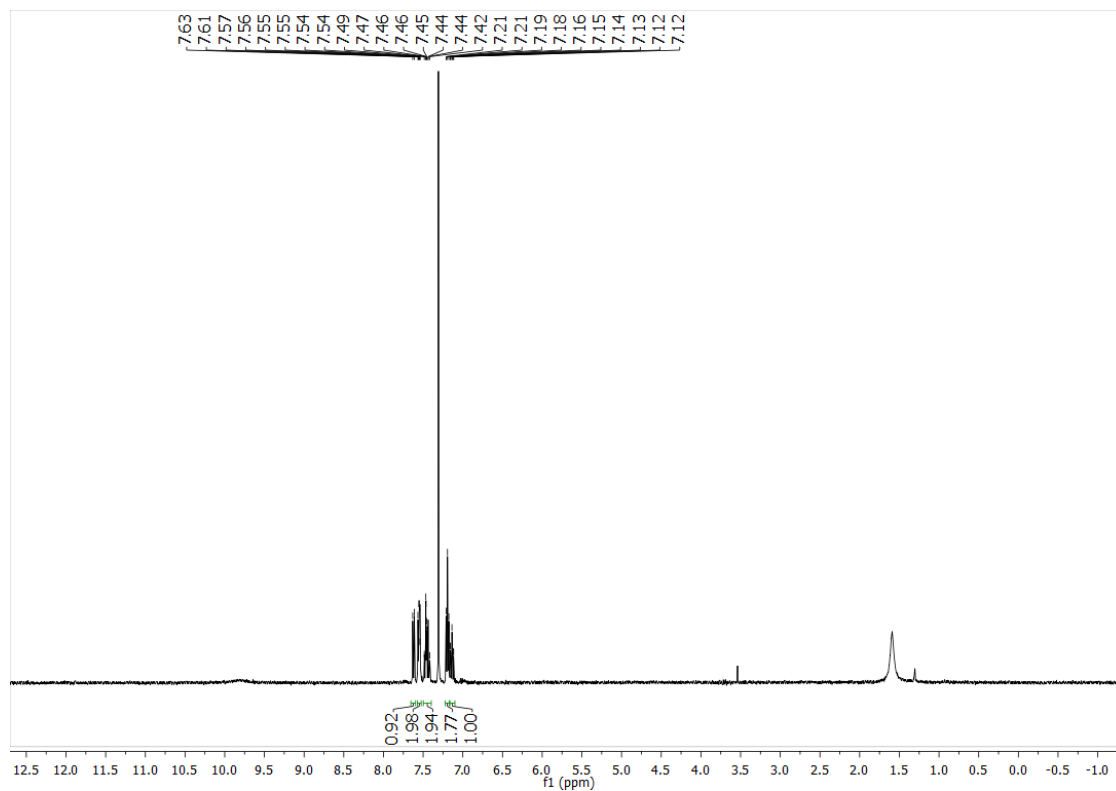


HC-7-OH

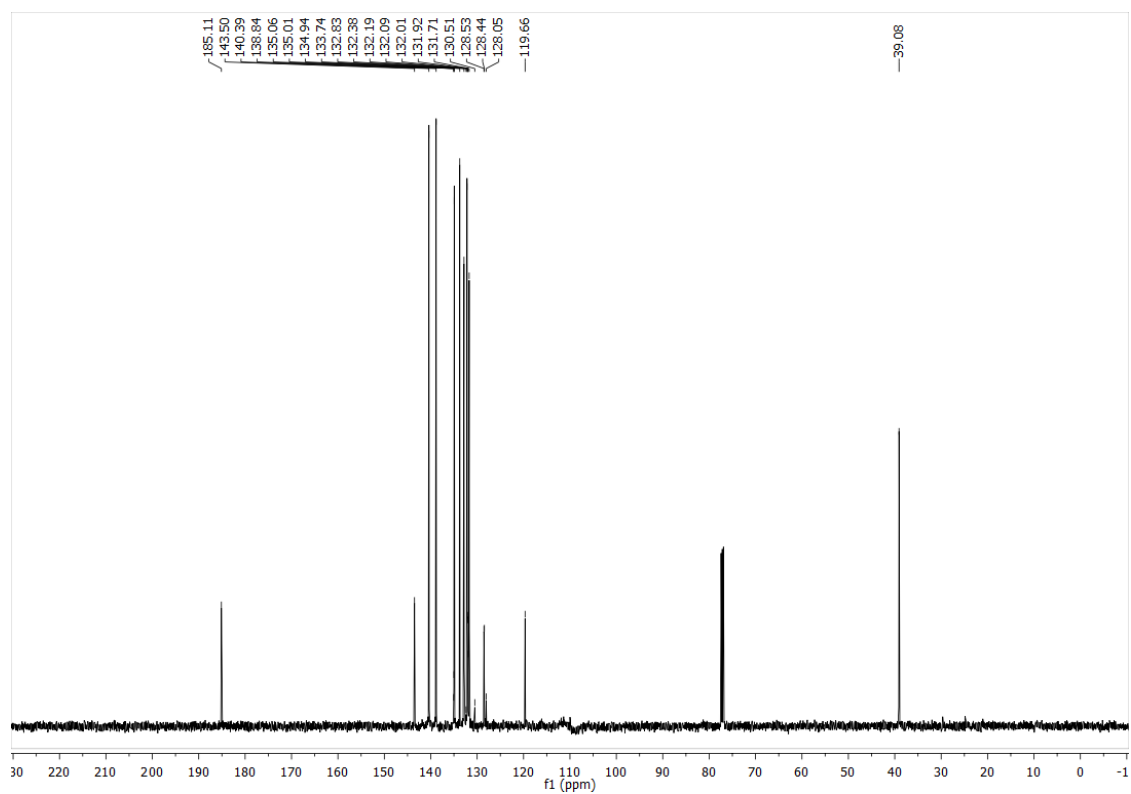
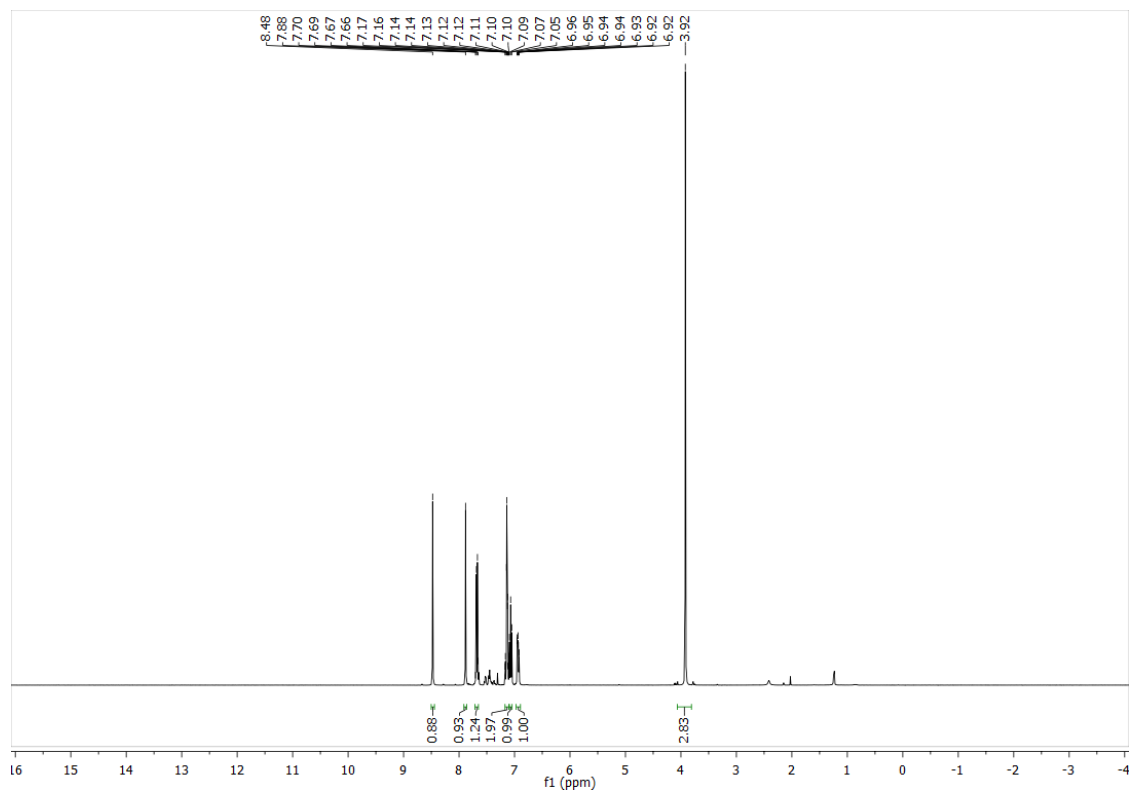


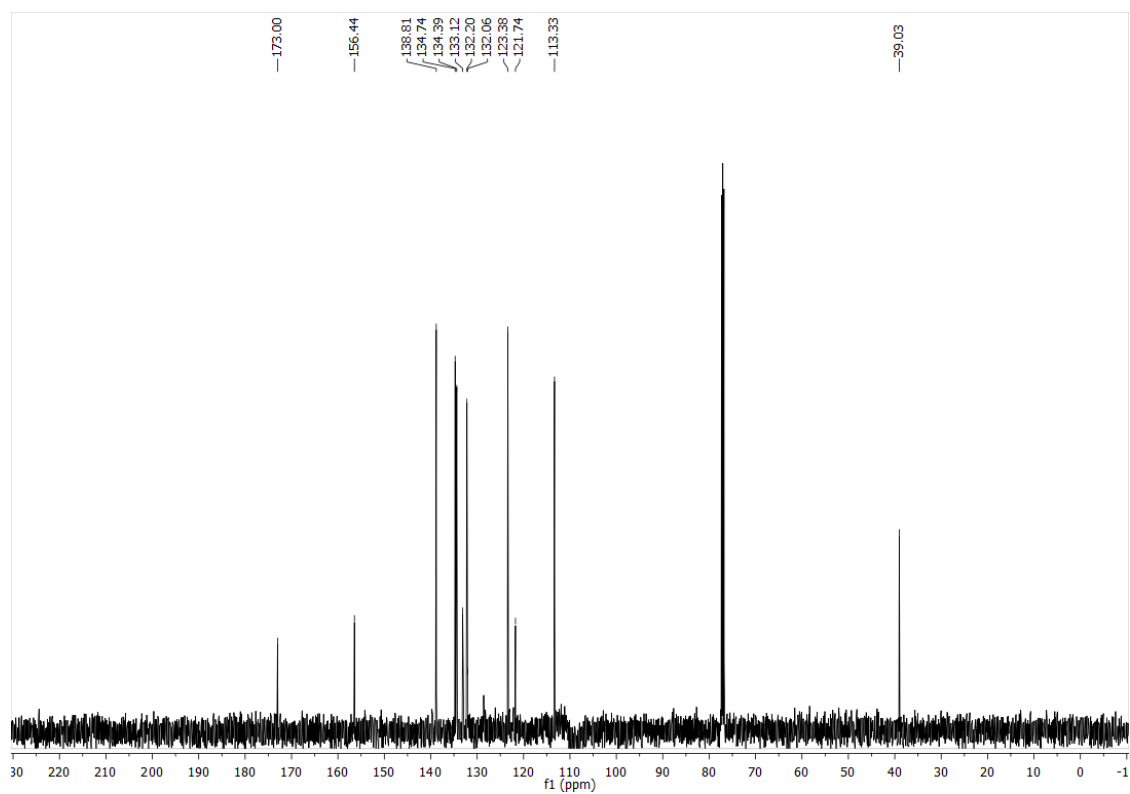
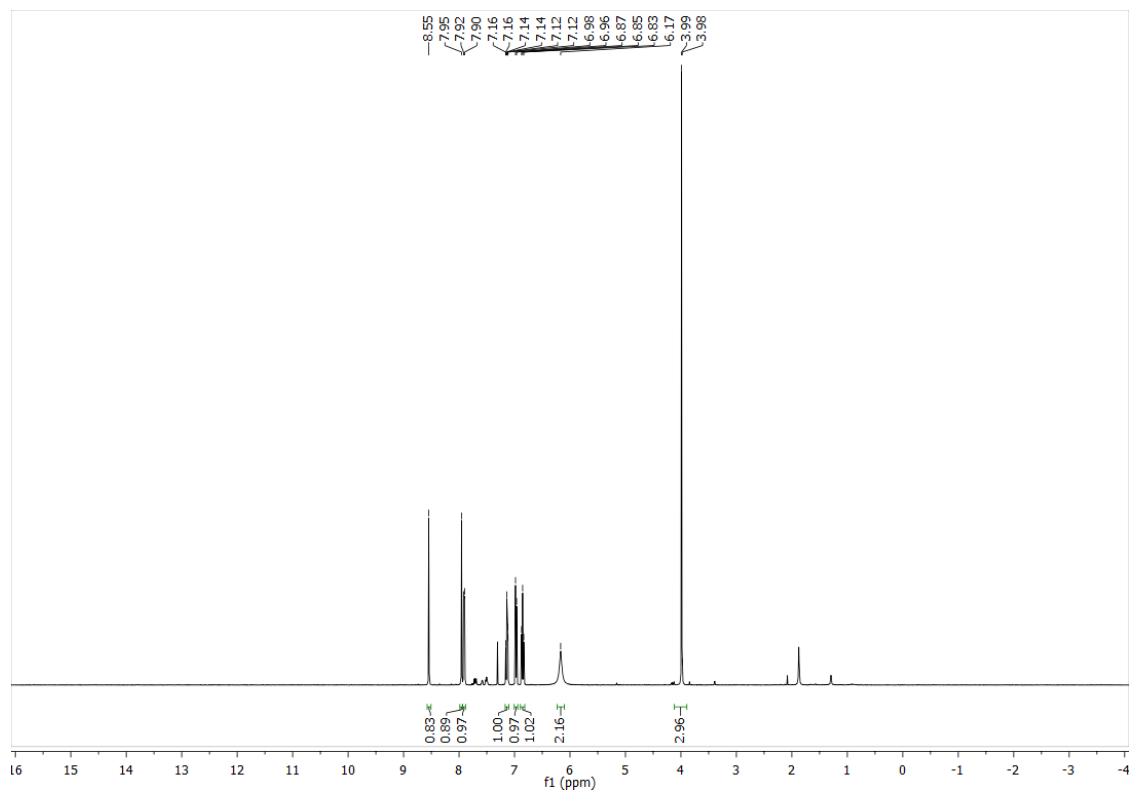
MO-pF-H

MO-pF-NH₂

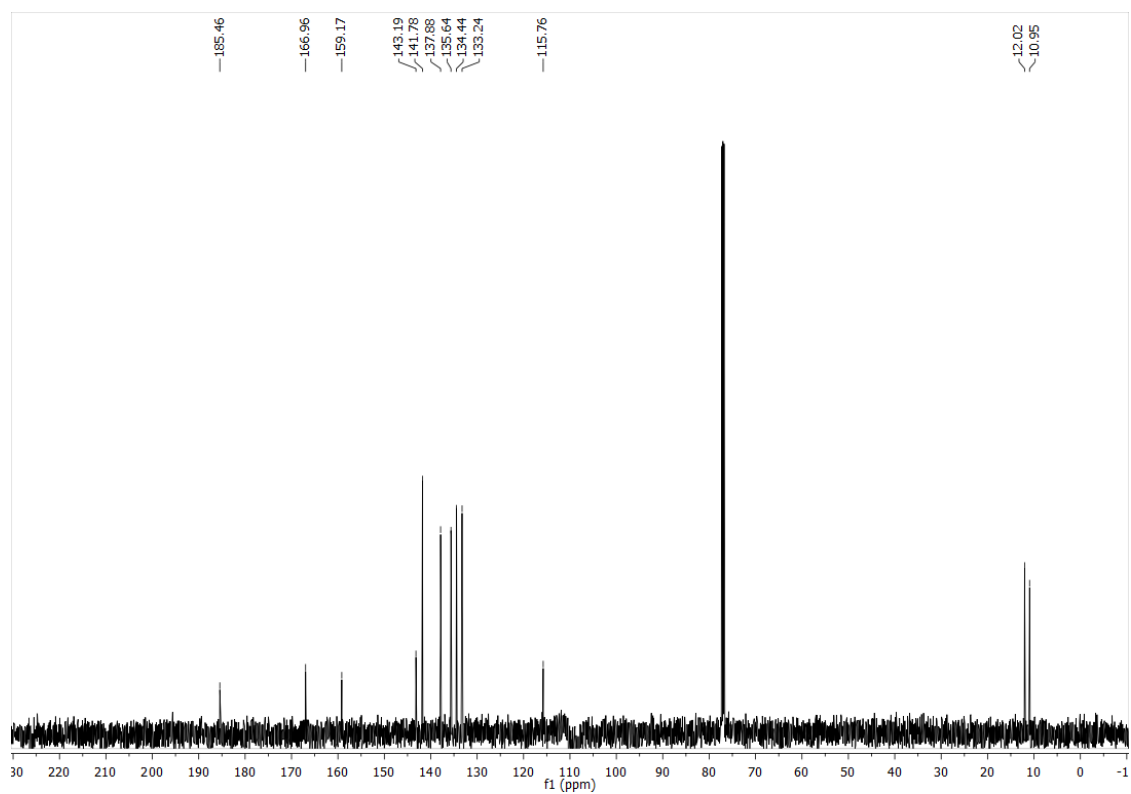
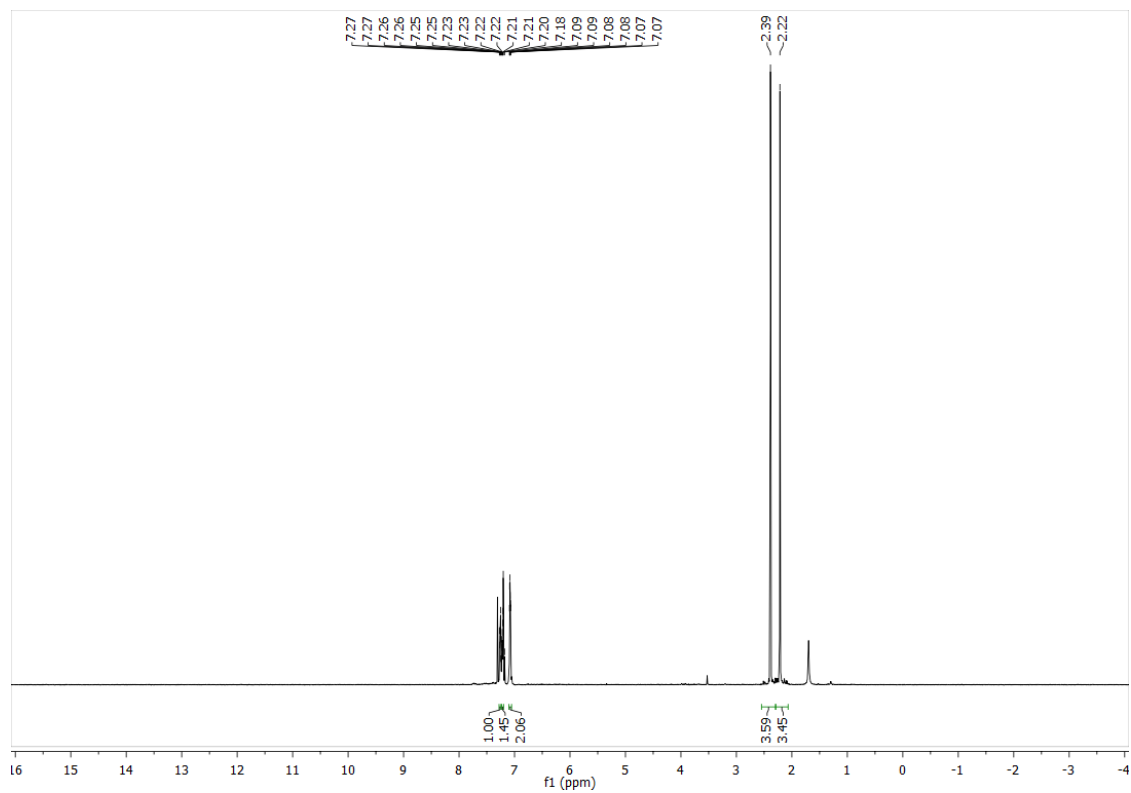
MO-pF-OH

HC-8-H

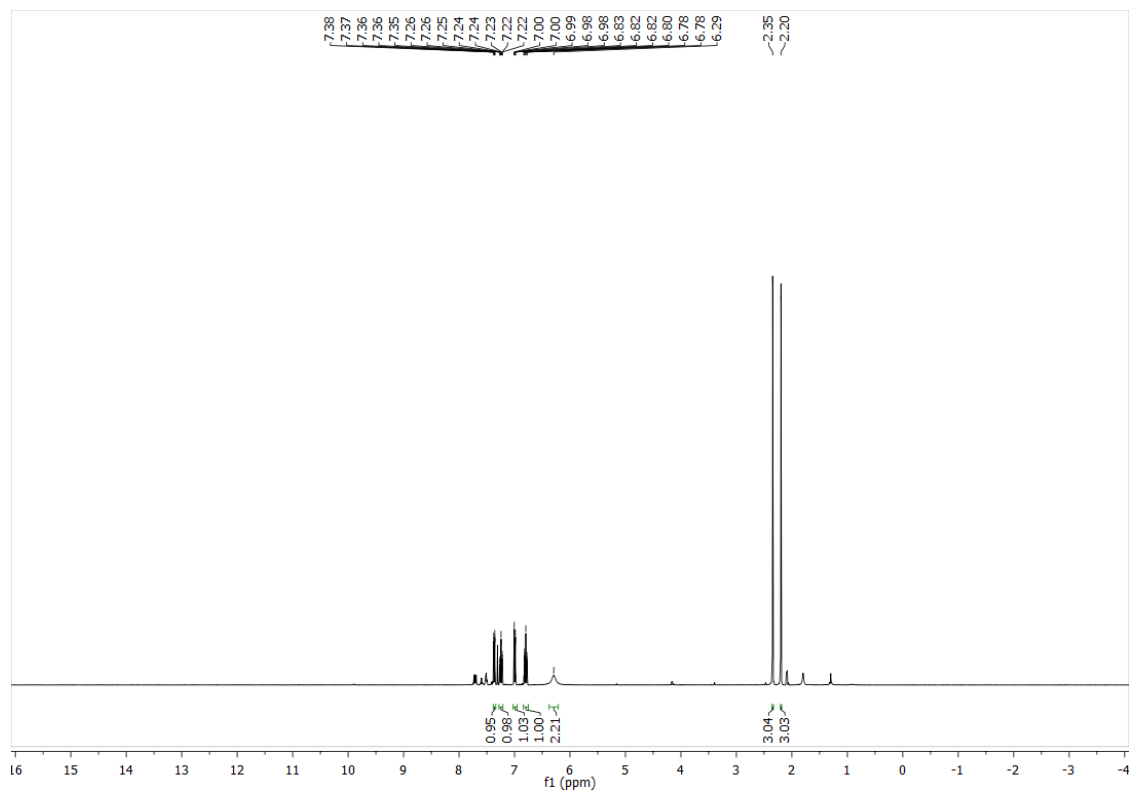


HC-8-NH2

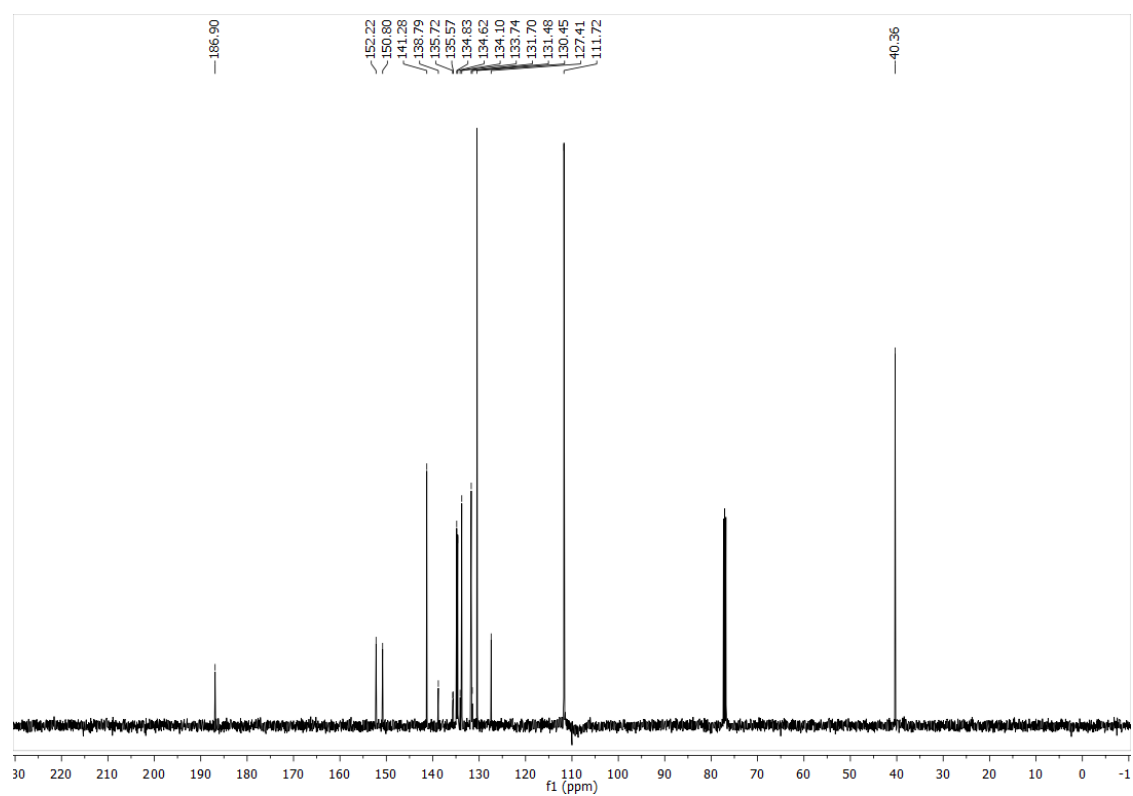
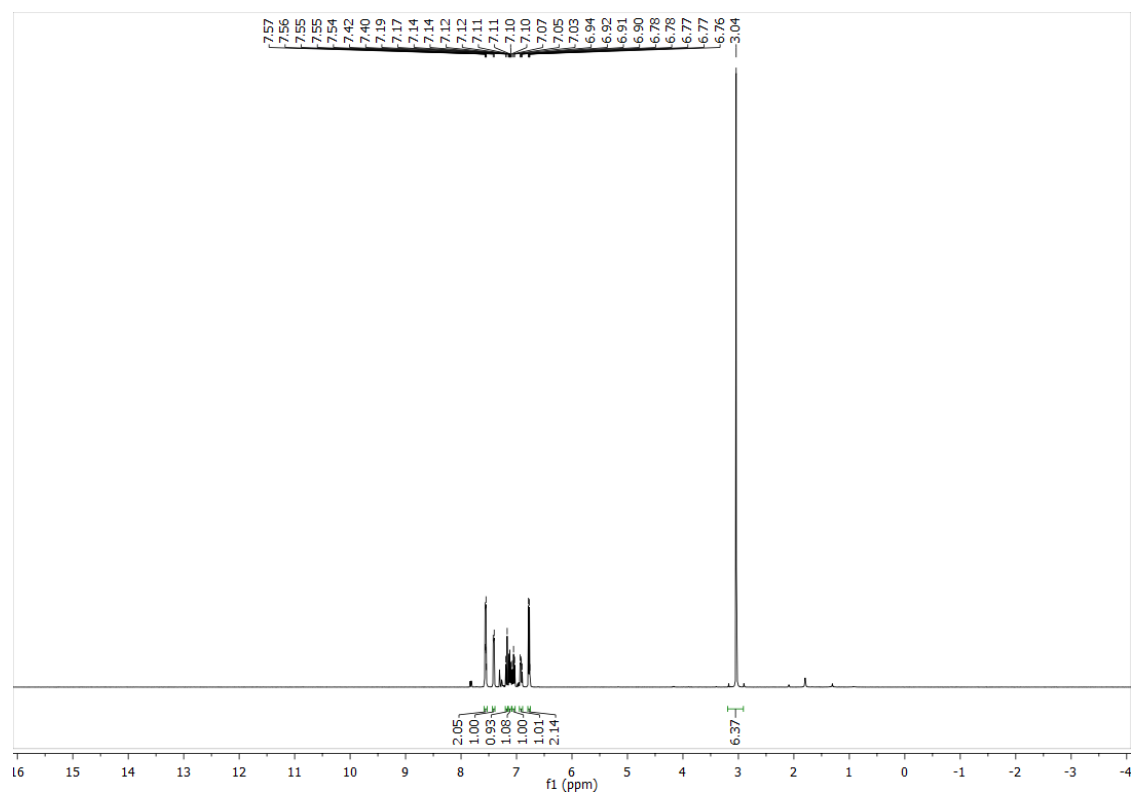
HC-9-H



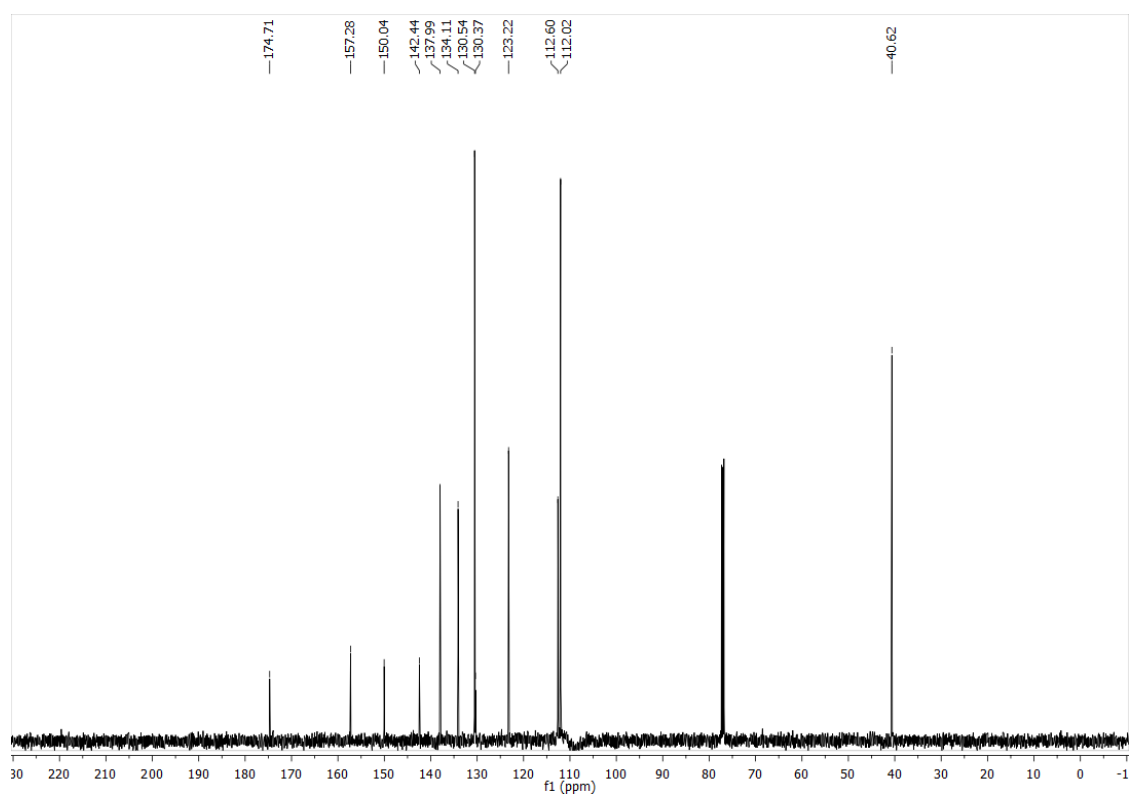
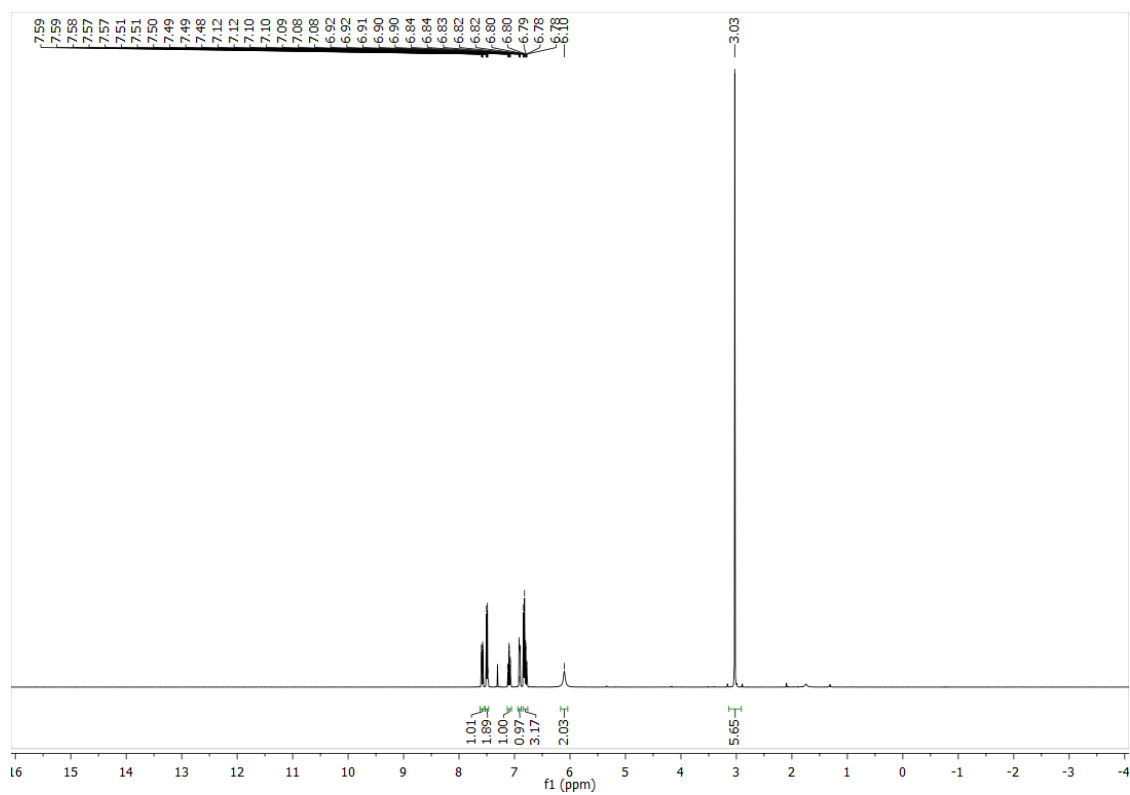
HC-9-NH2



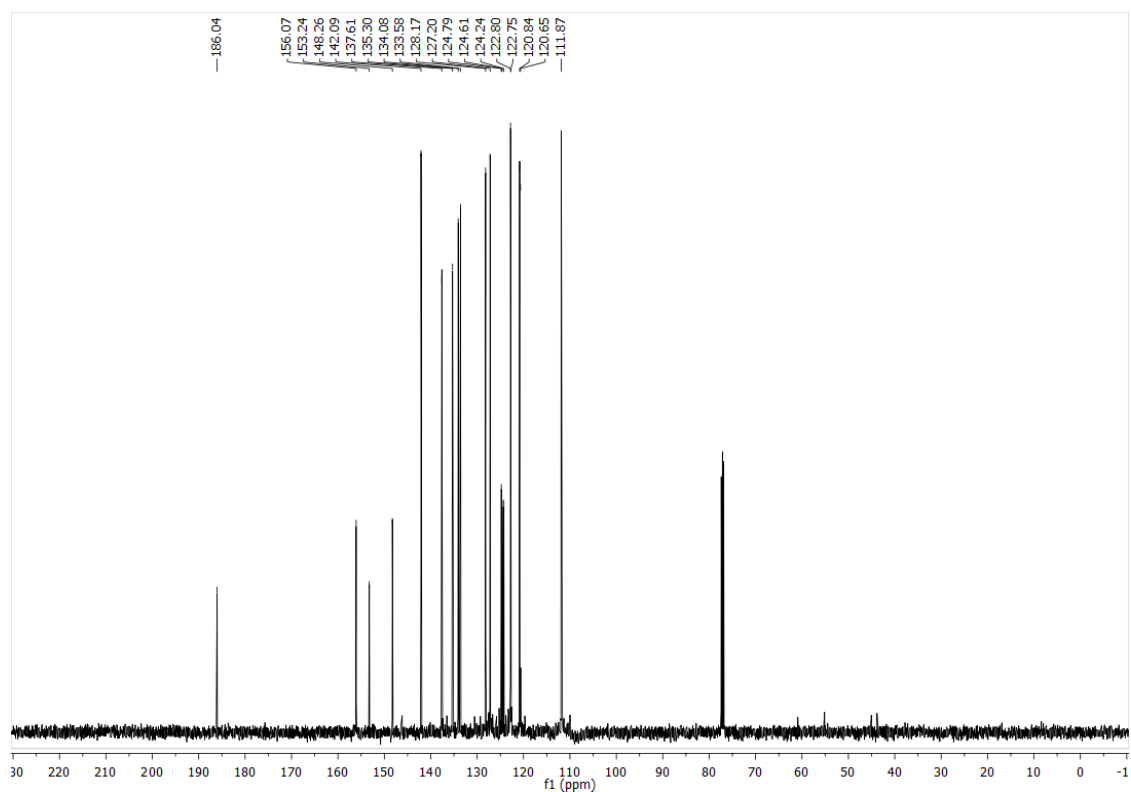
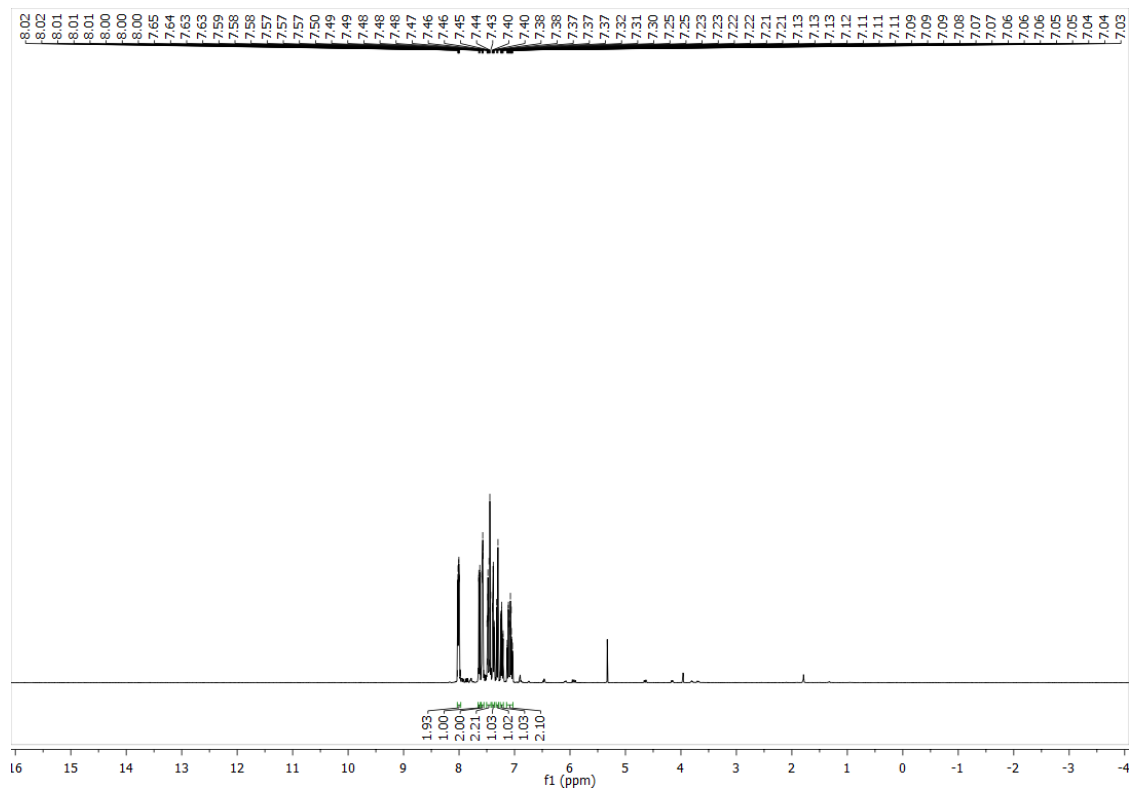
Am-DMe-H



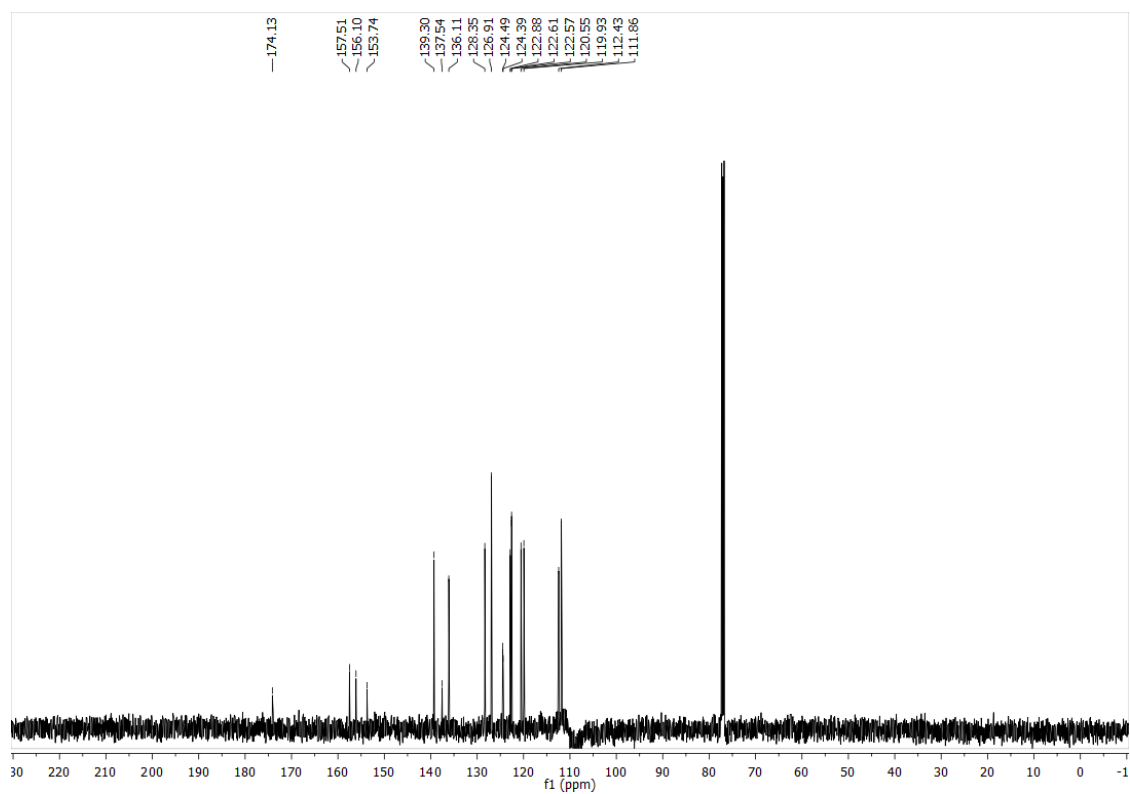
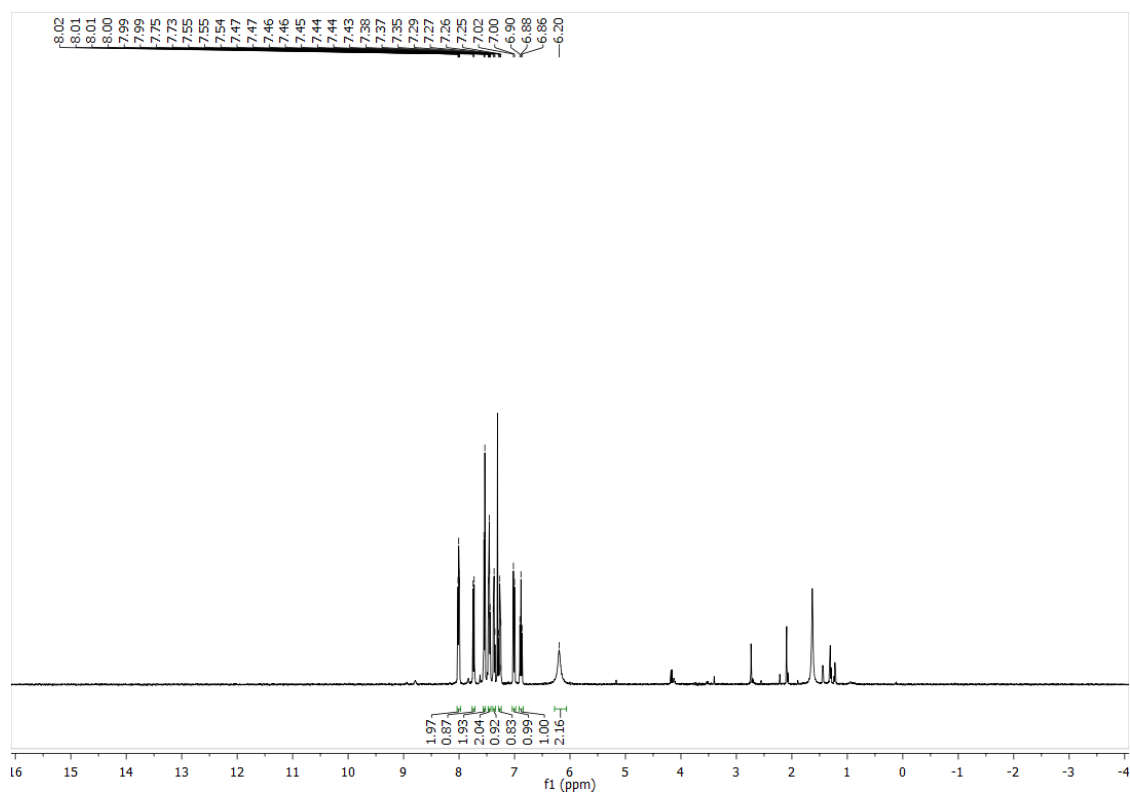
Am-DMe-NH2



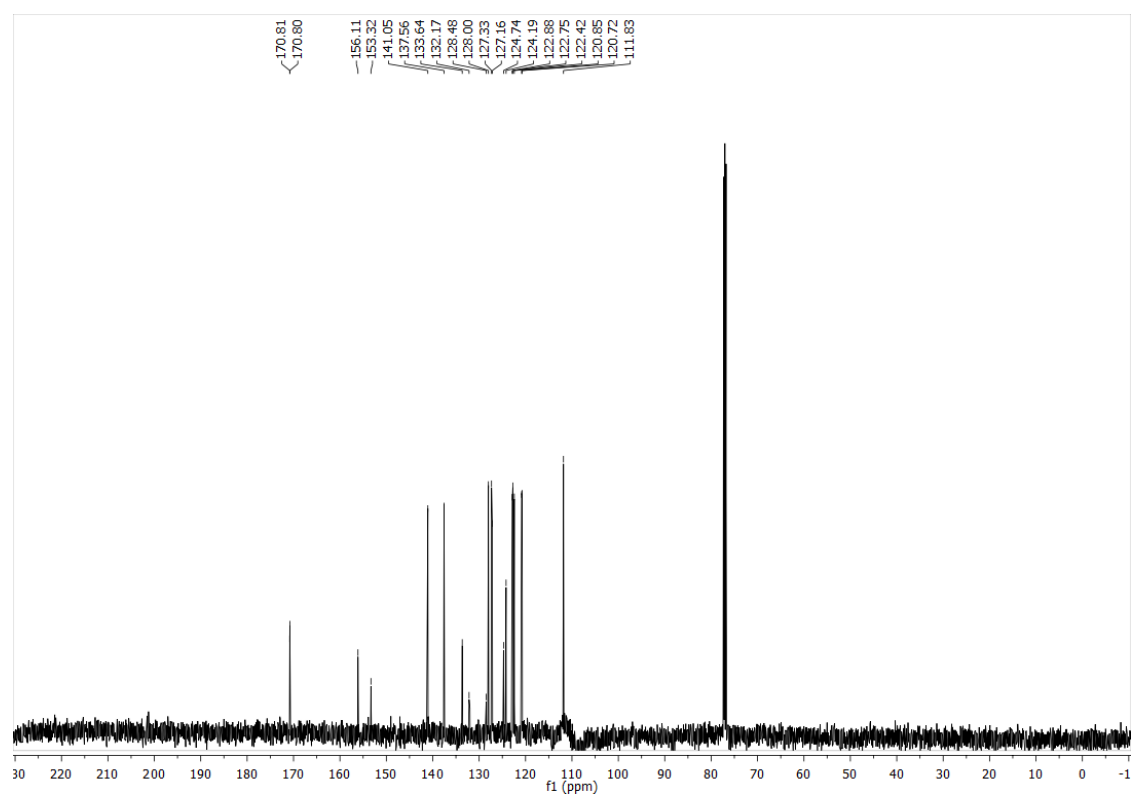
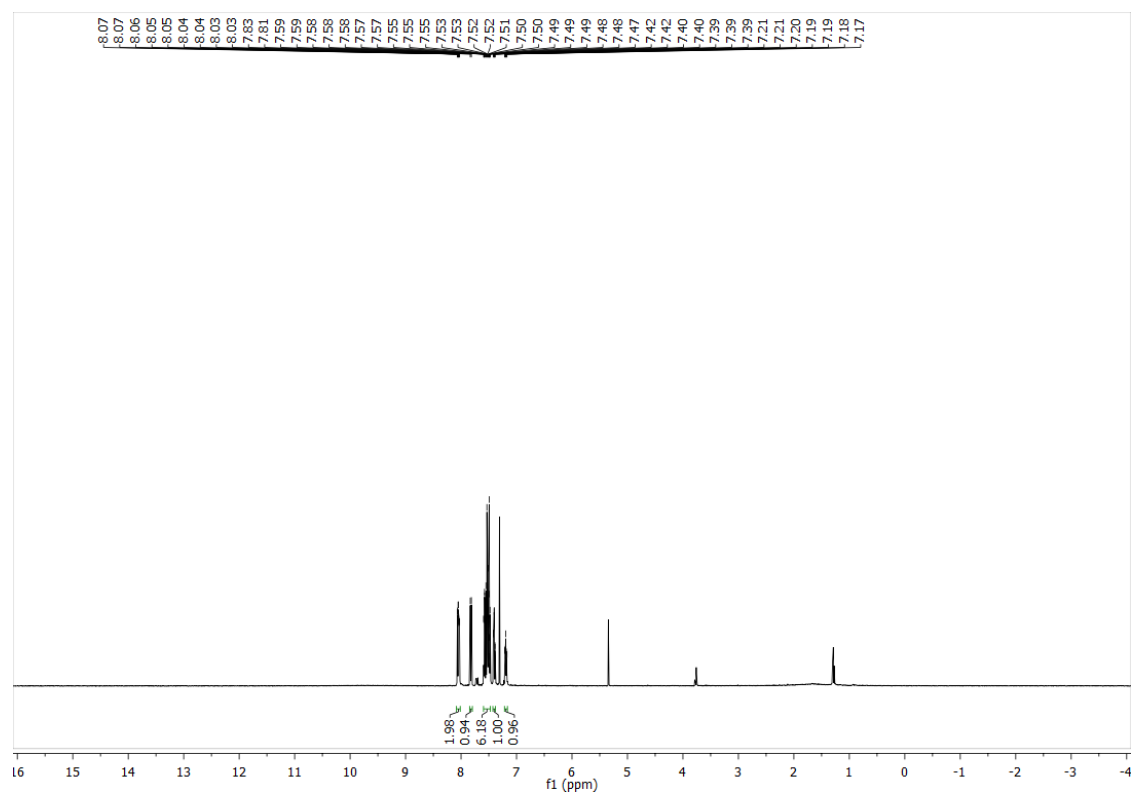
HC-10-H



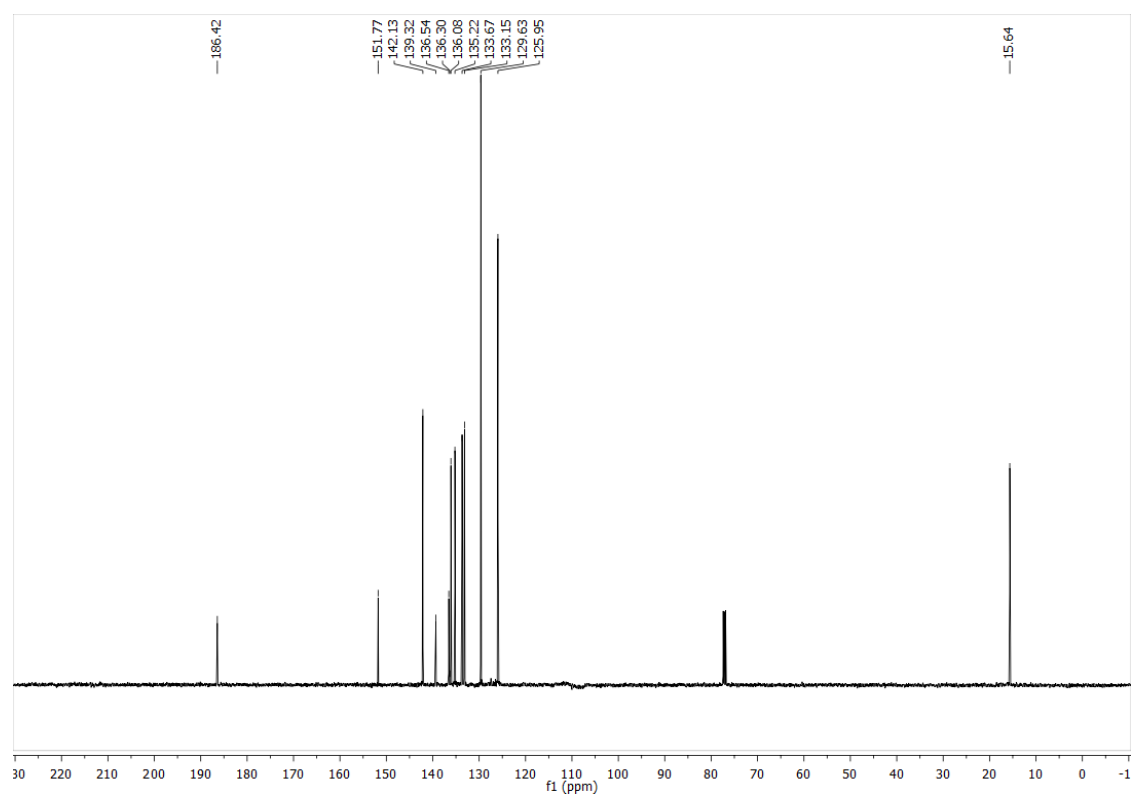
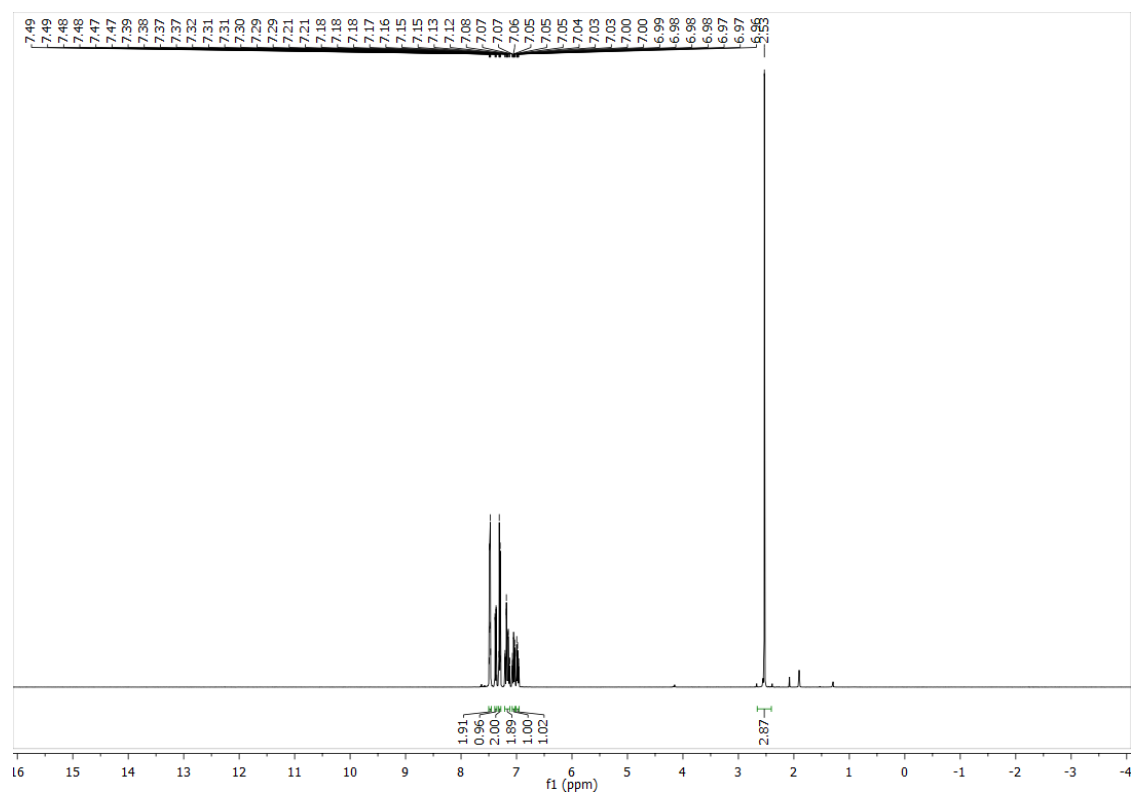
HC-10-NH2

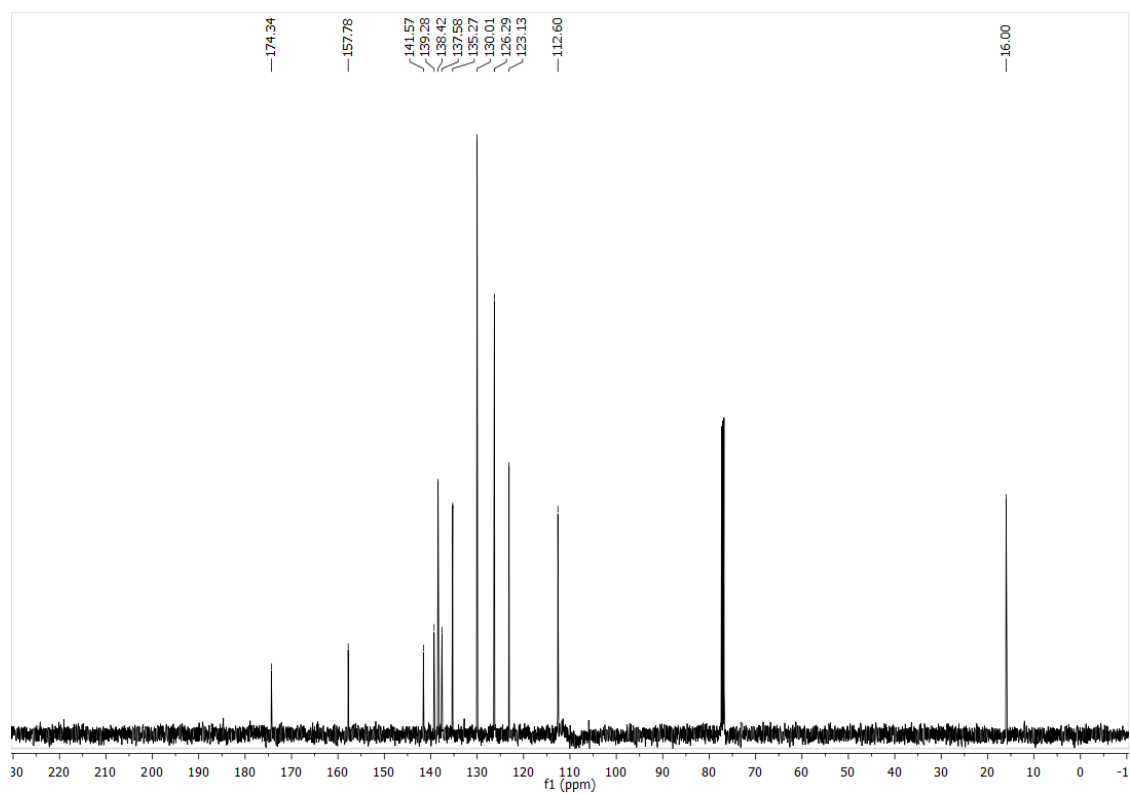
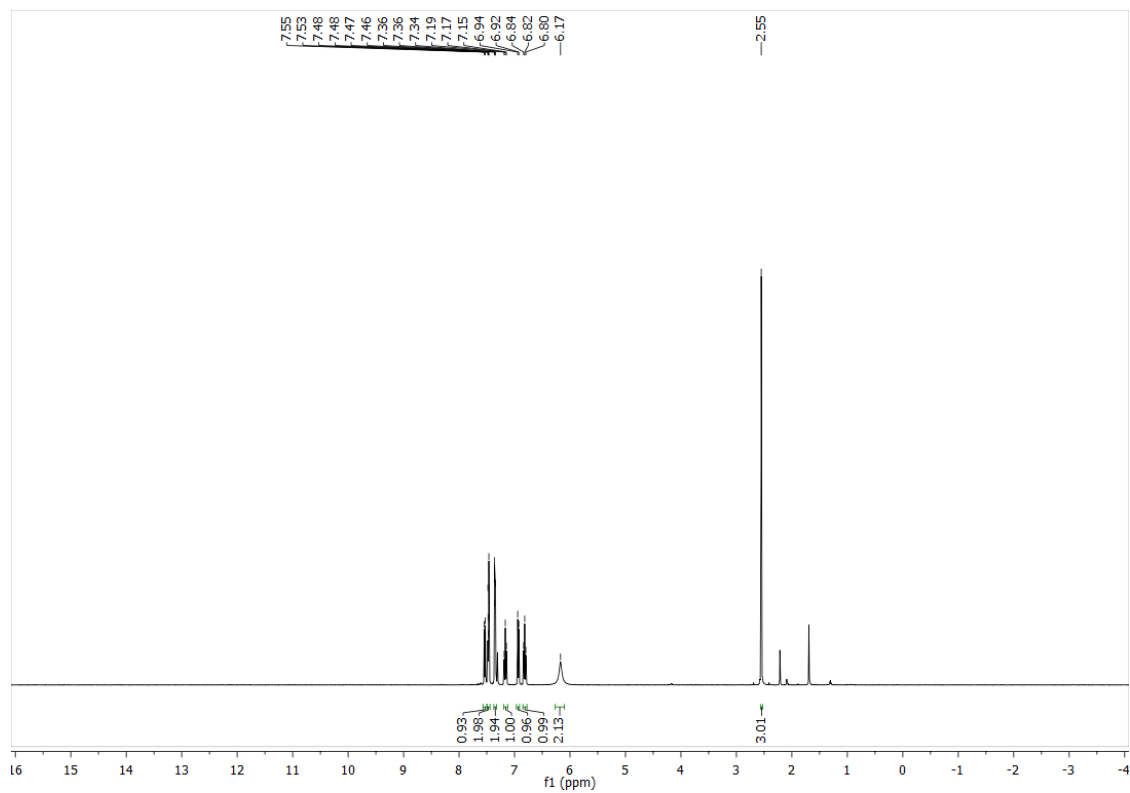


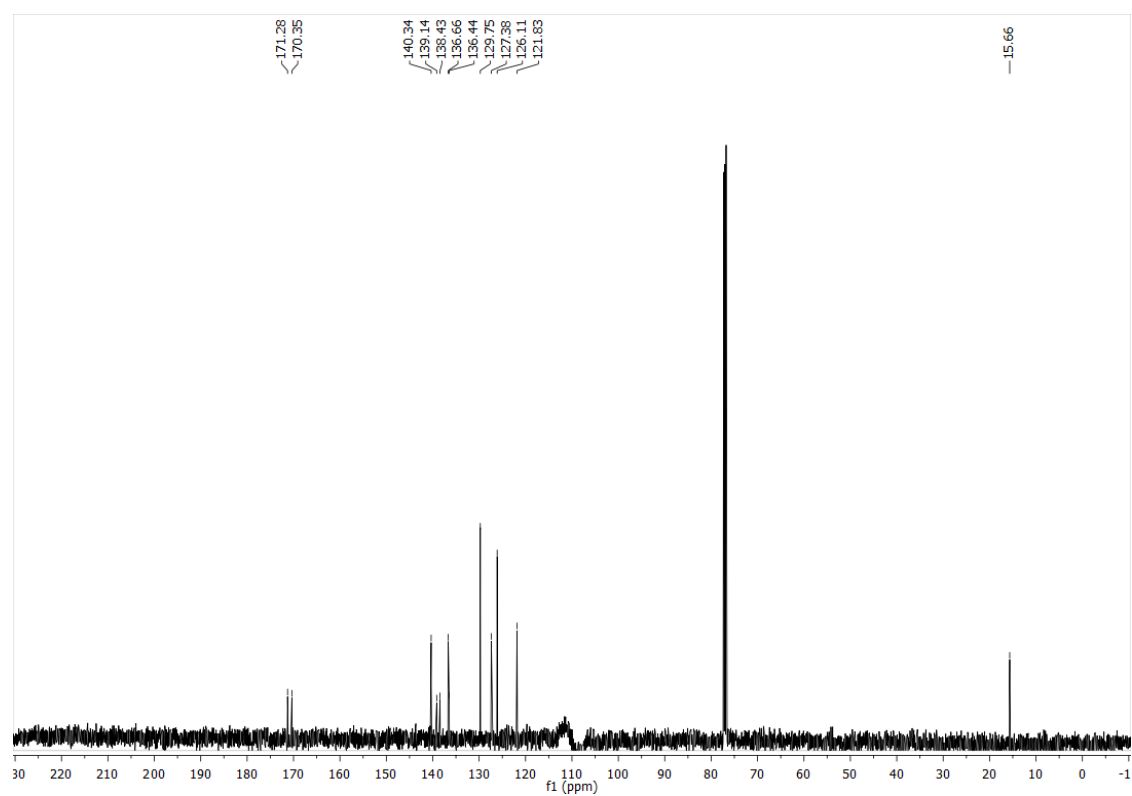
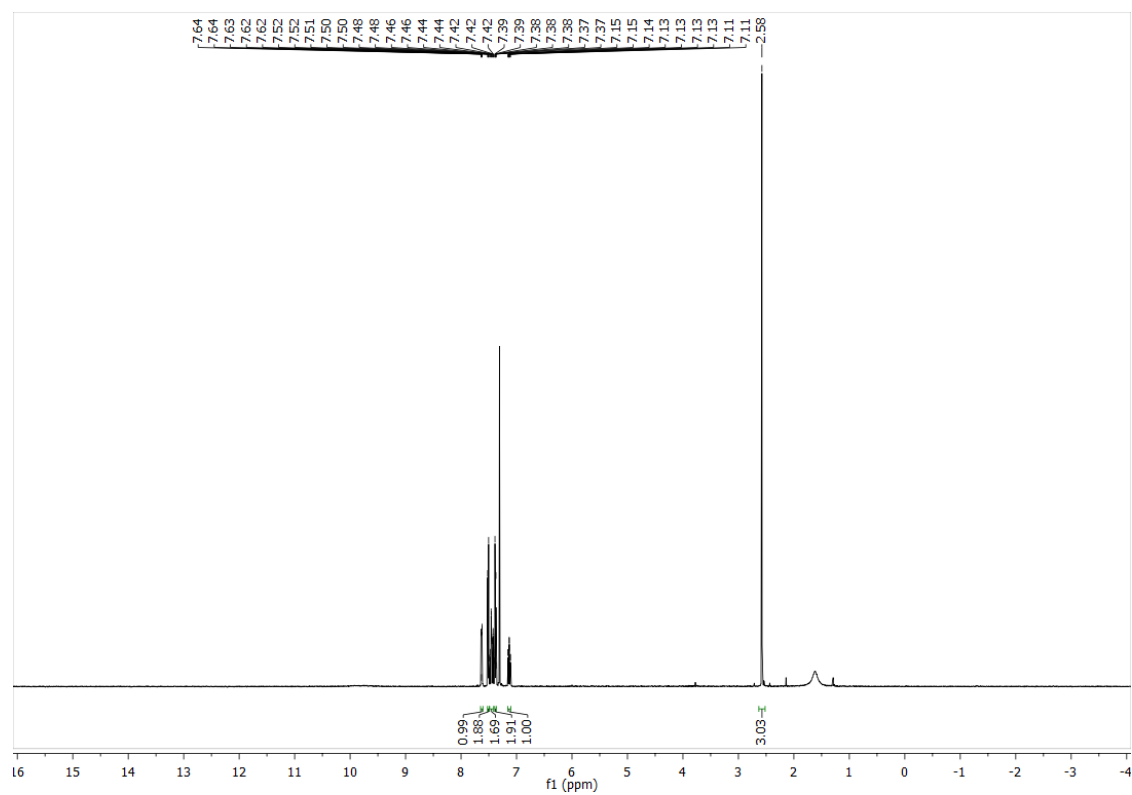
HC-10-OH



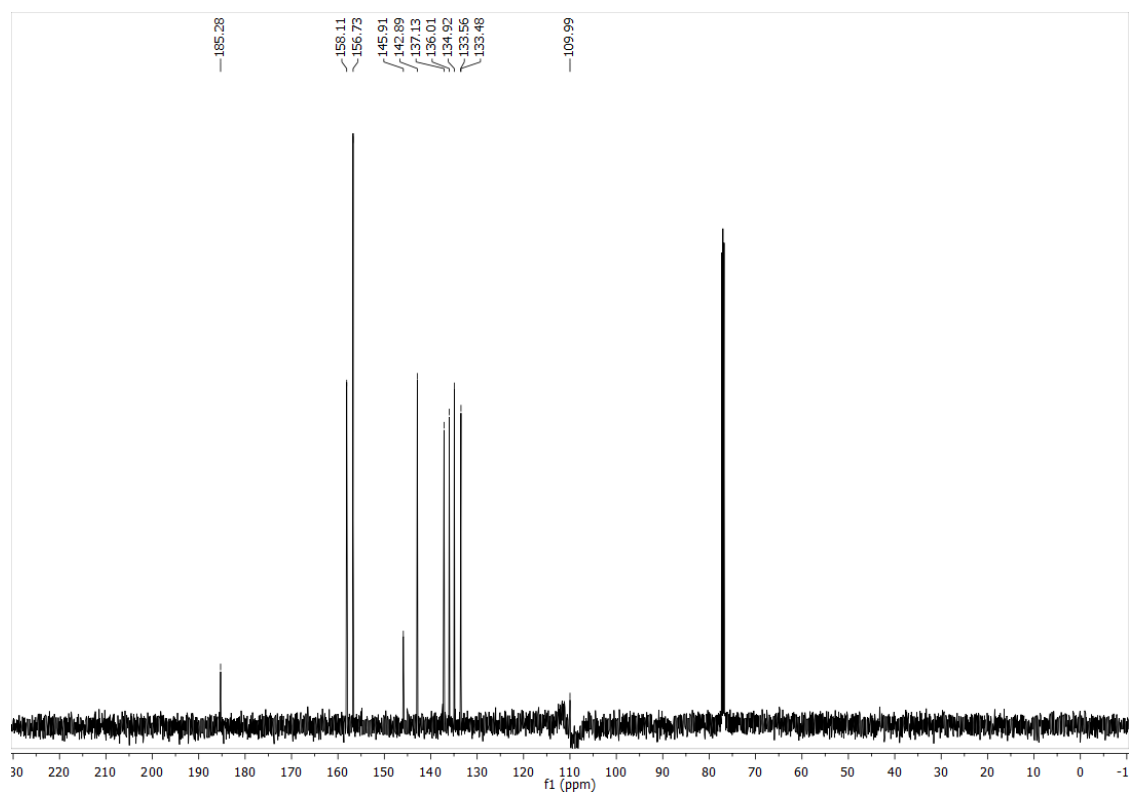
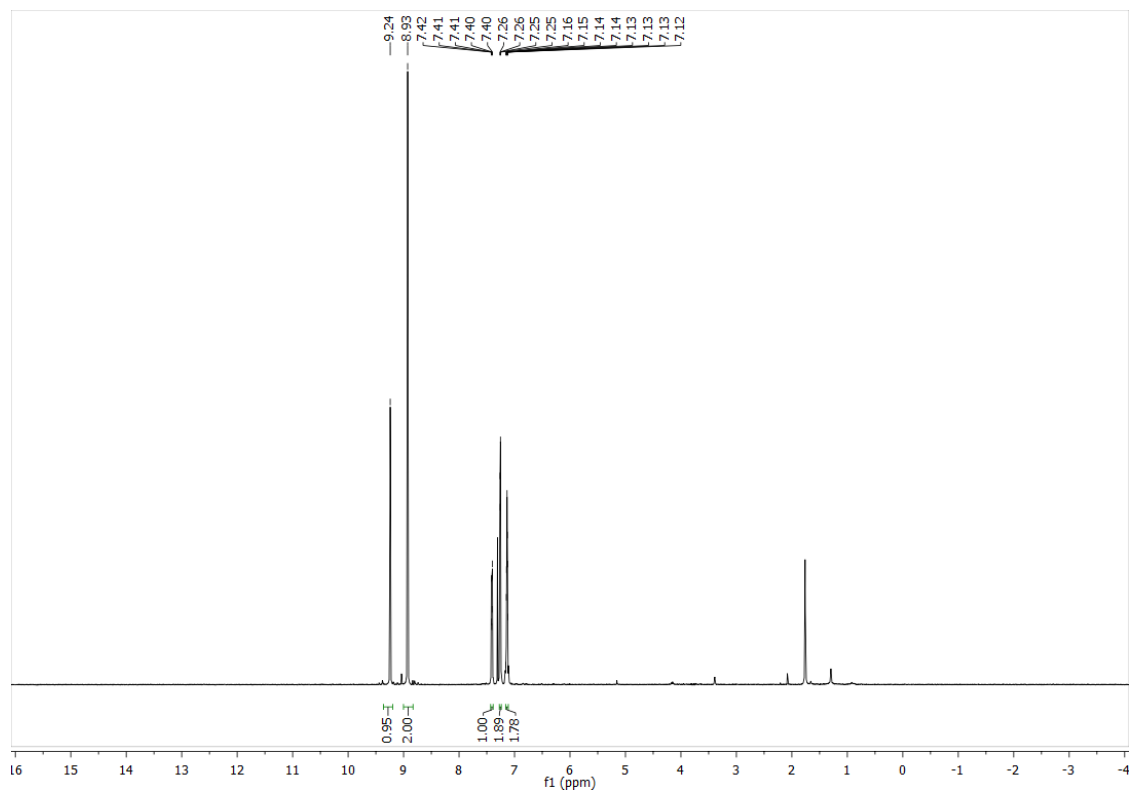
MO-pSMe-H



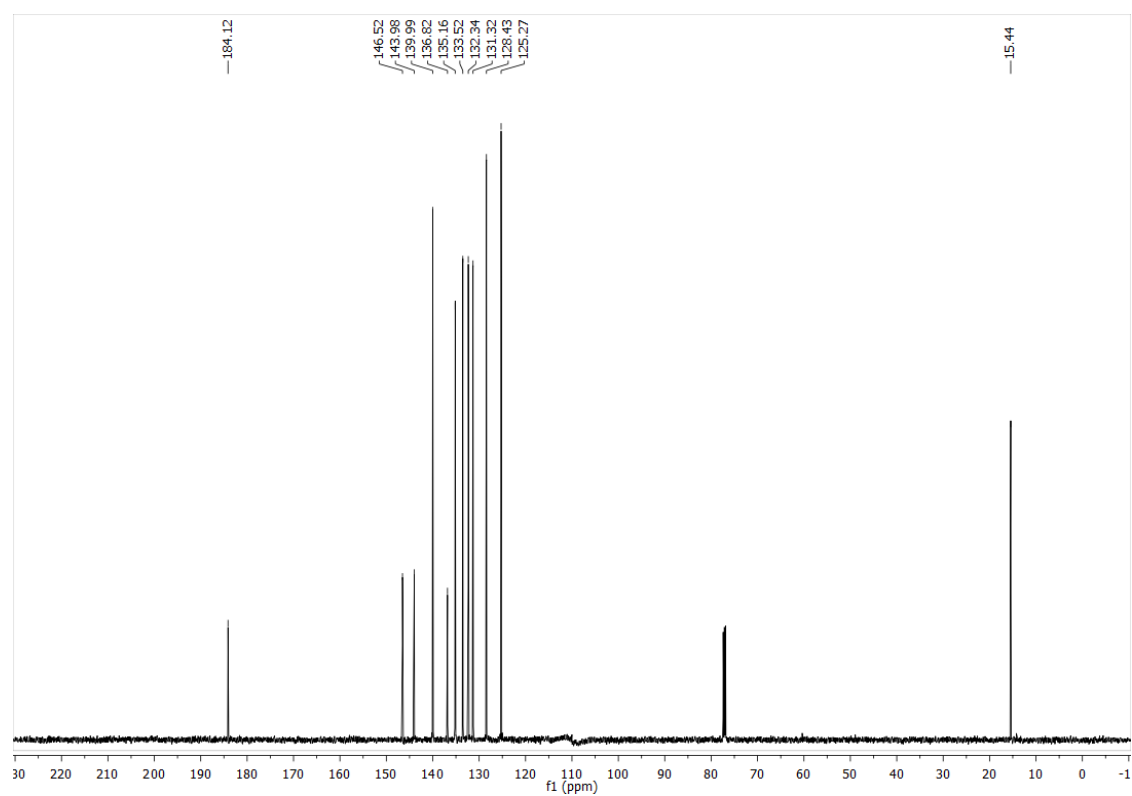
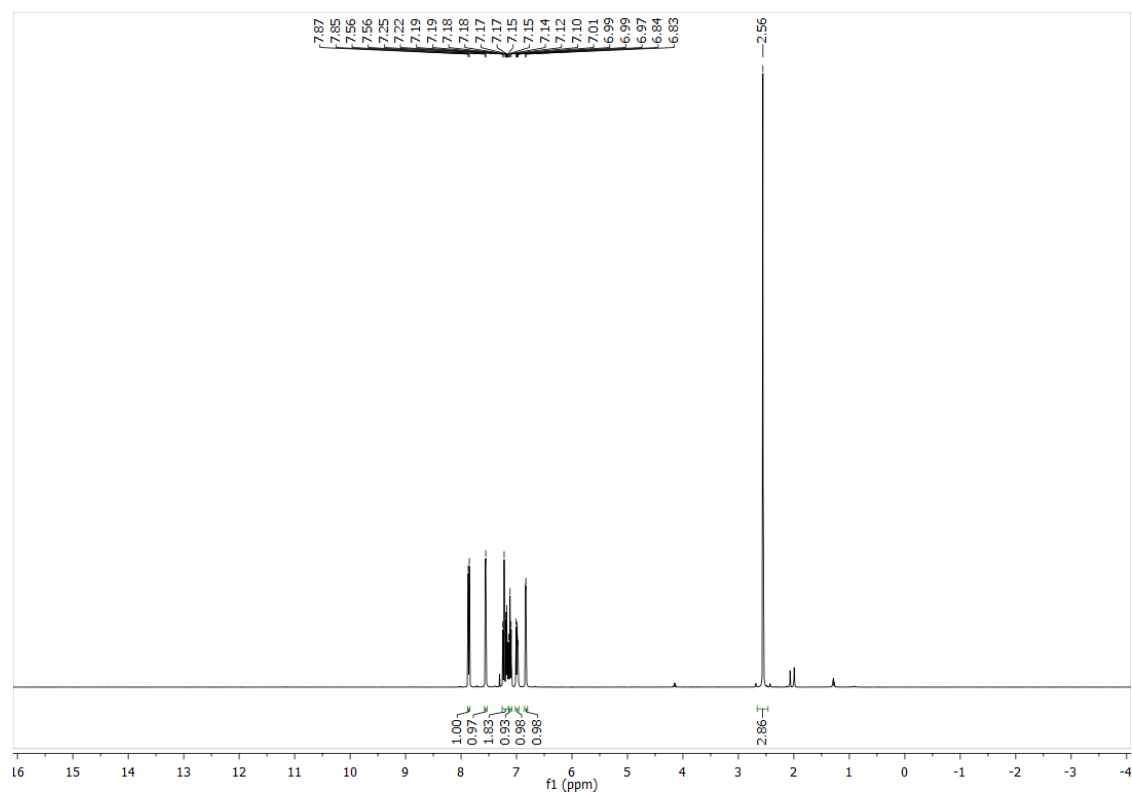
MO-pSMe-NH₂

MO-pSMe-OH

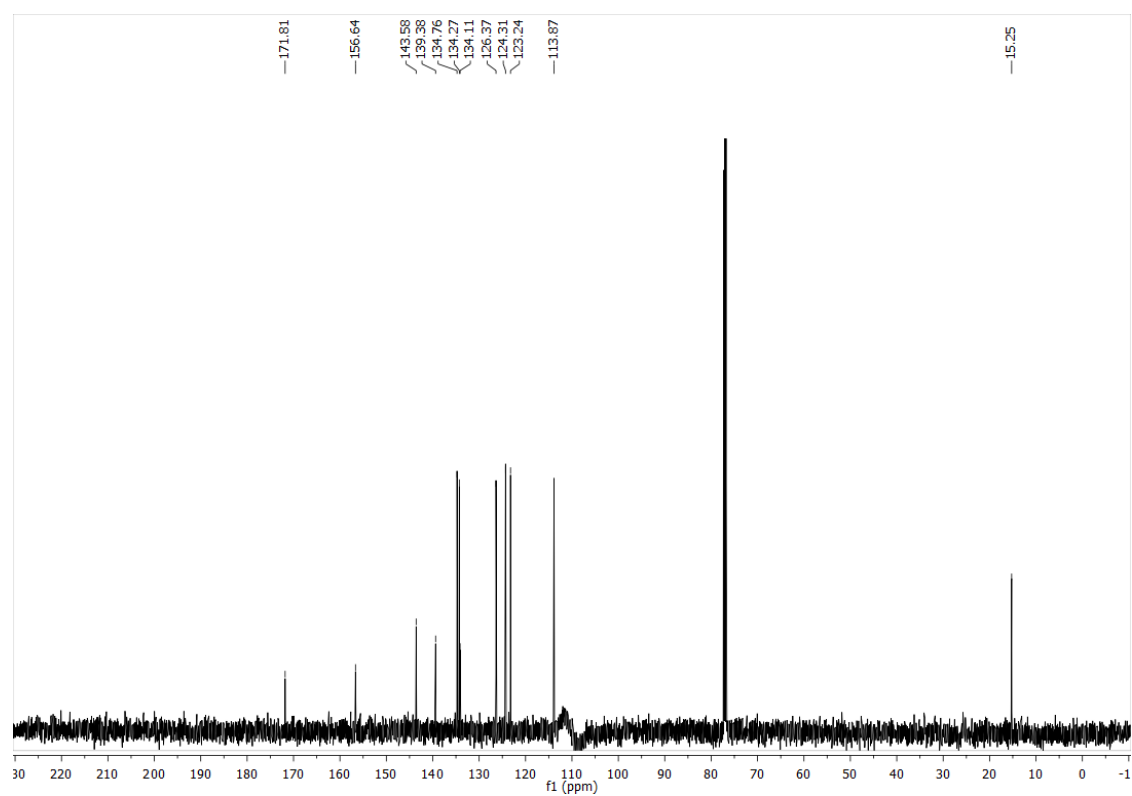
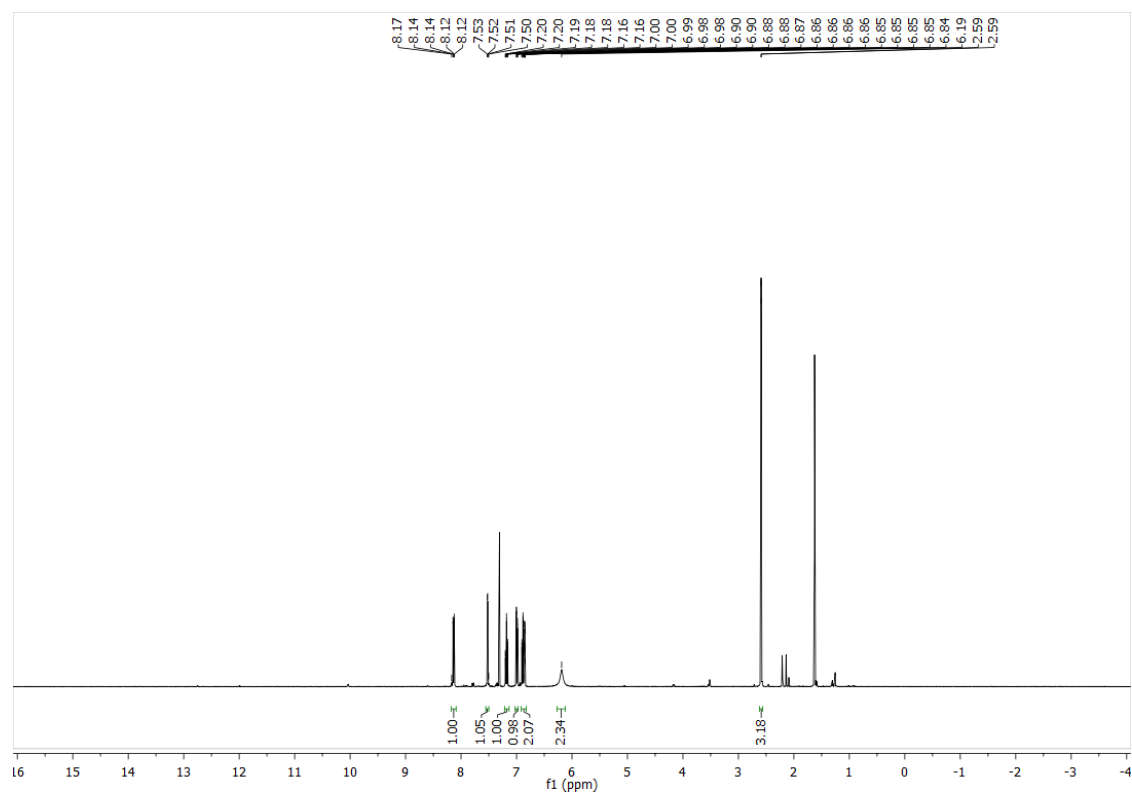
HC-11-H



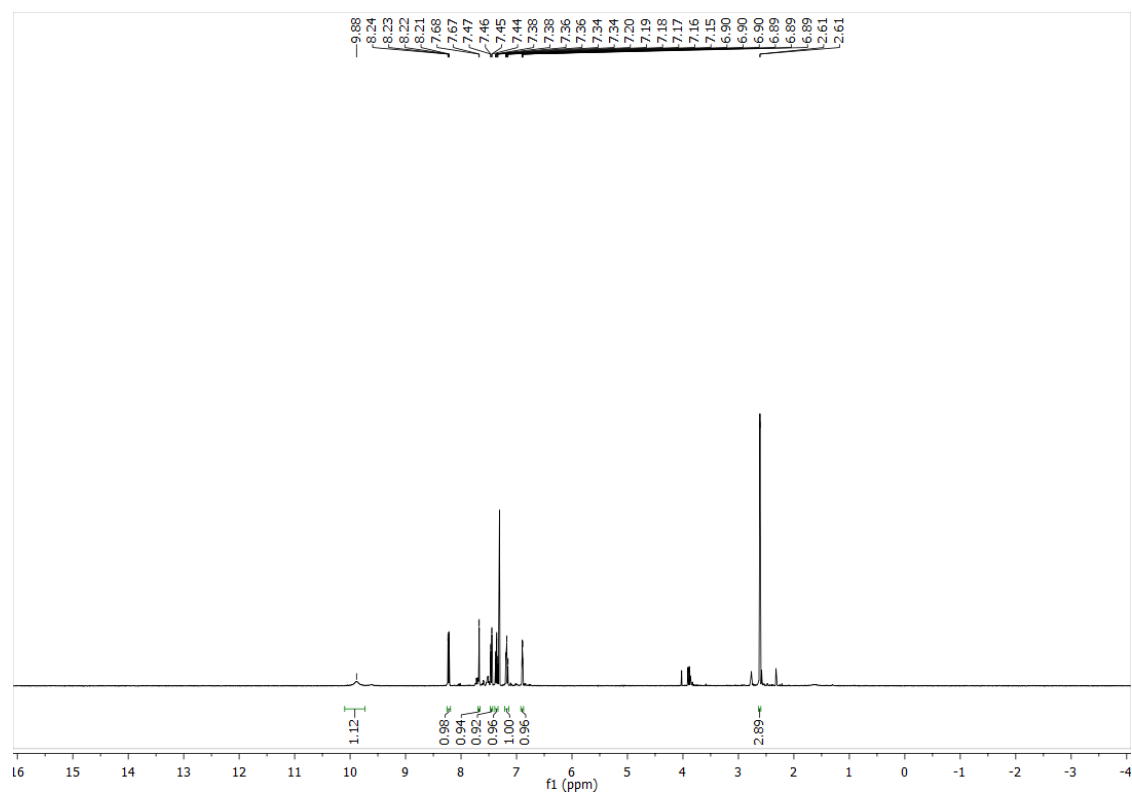
HC-12-H



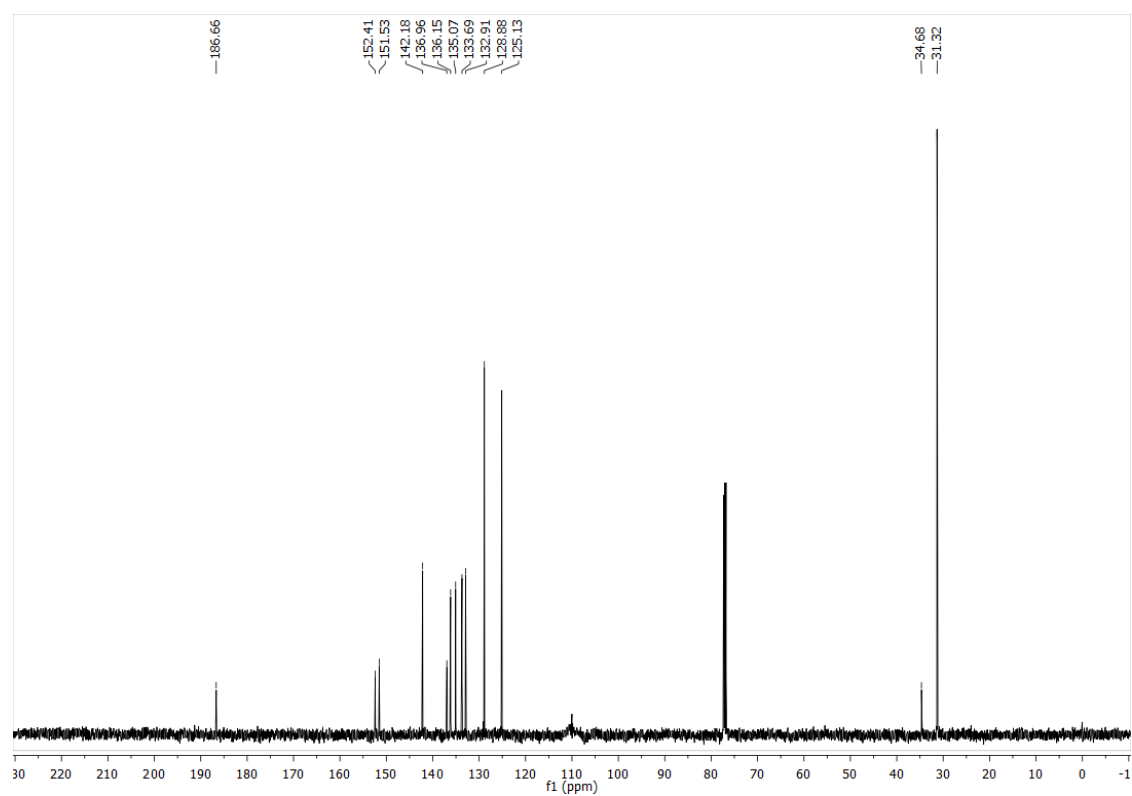
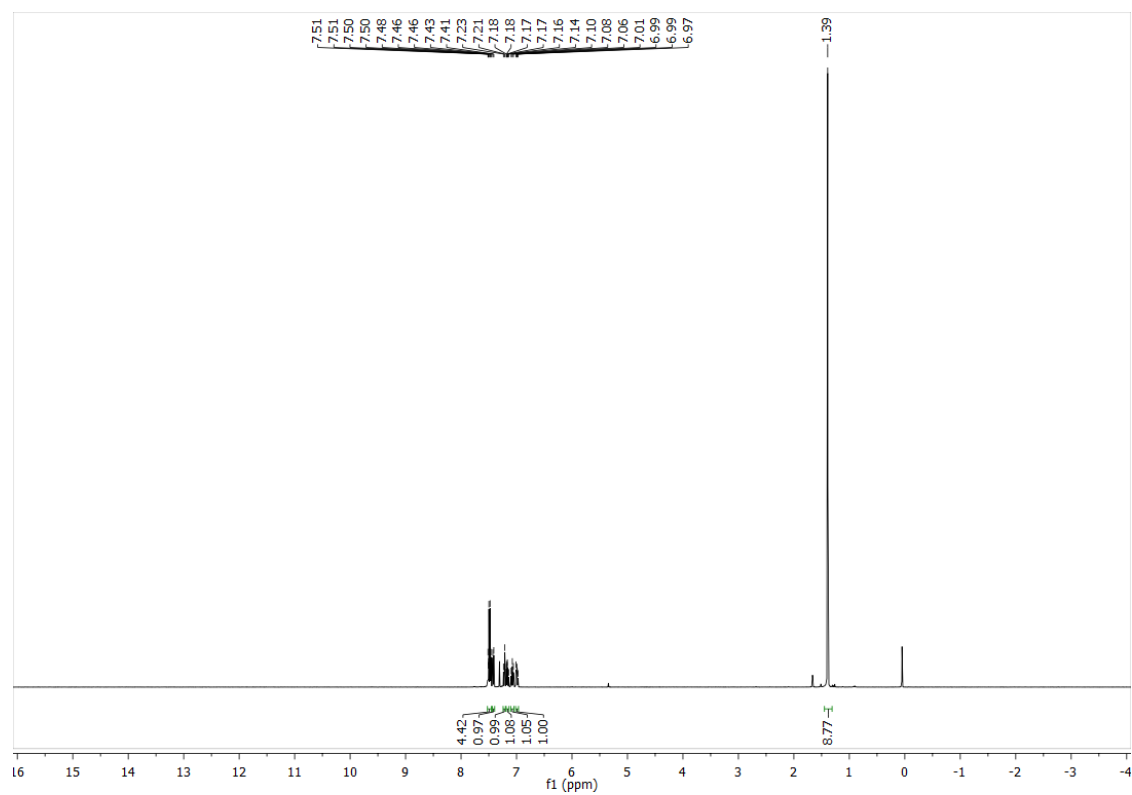
HC-12-NH2



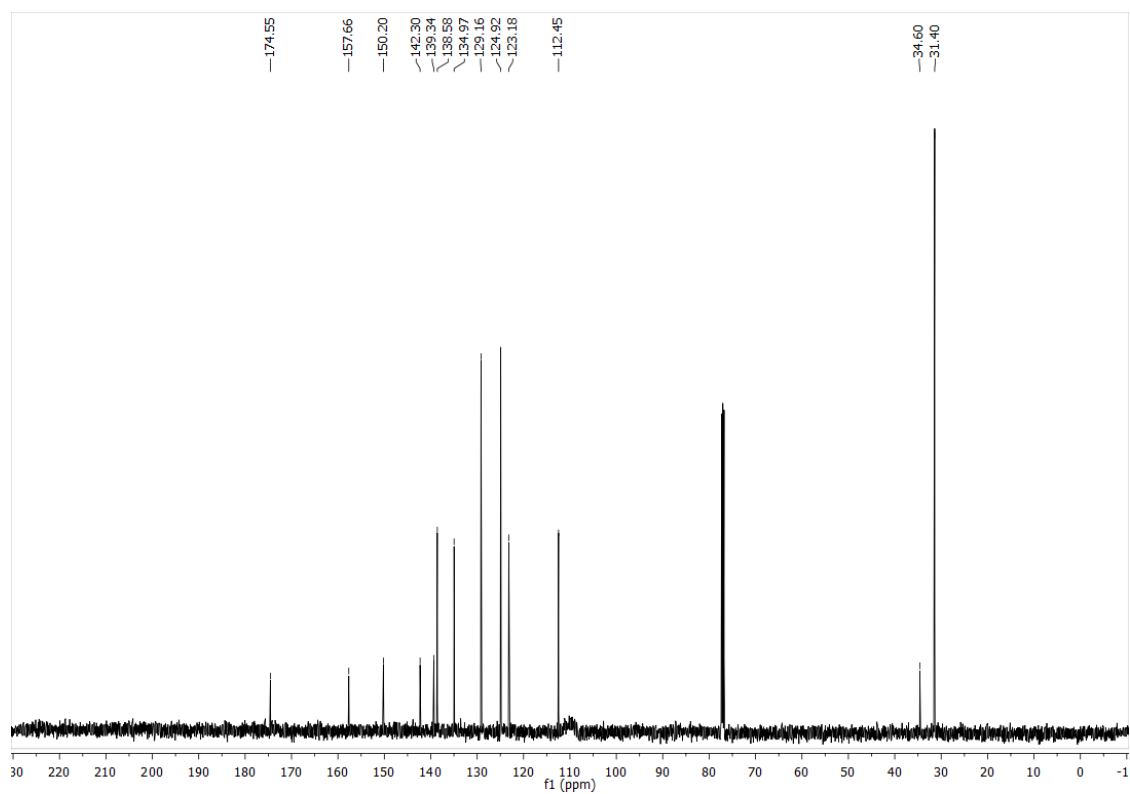
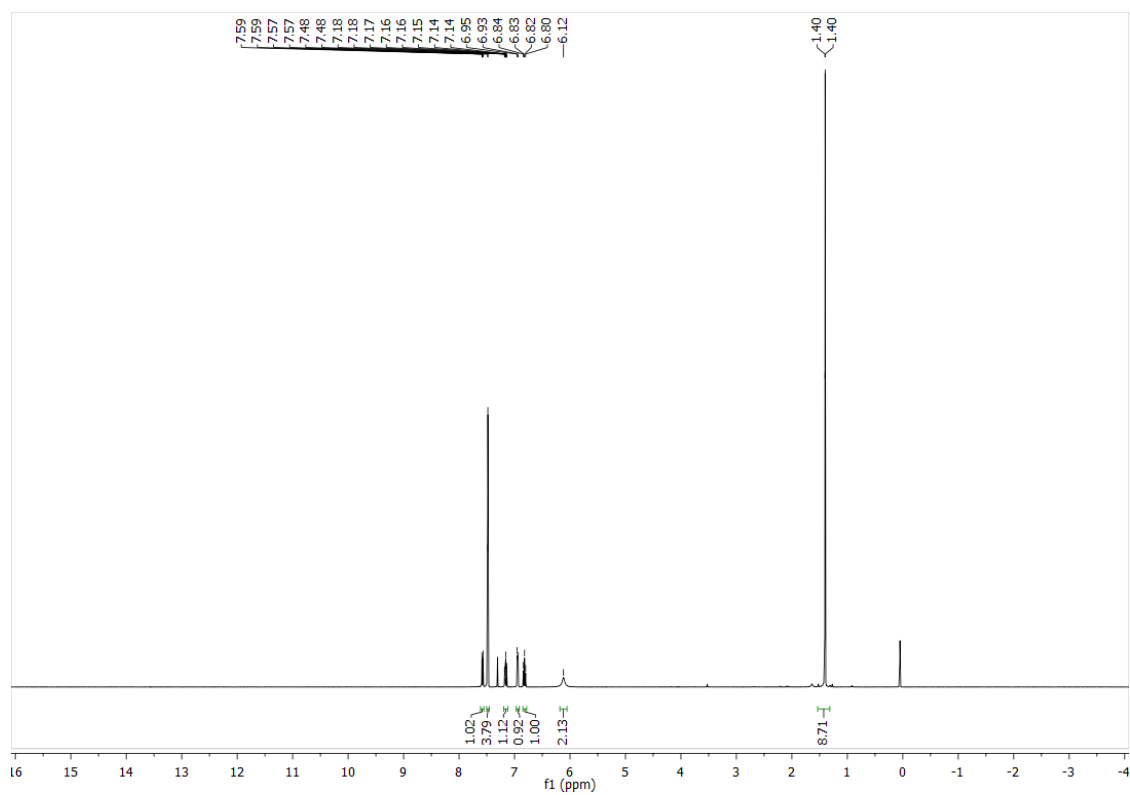
HC-12-OH



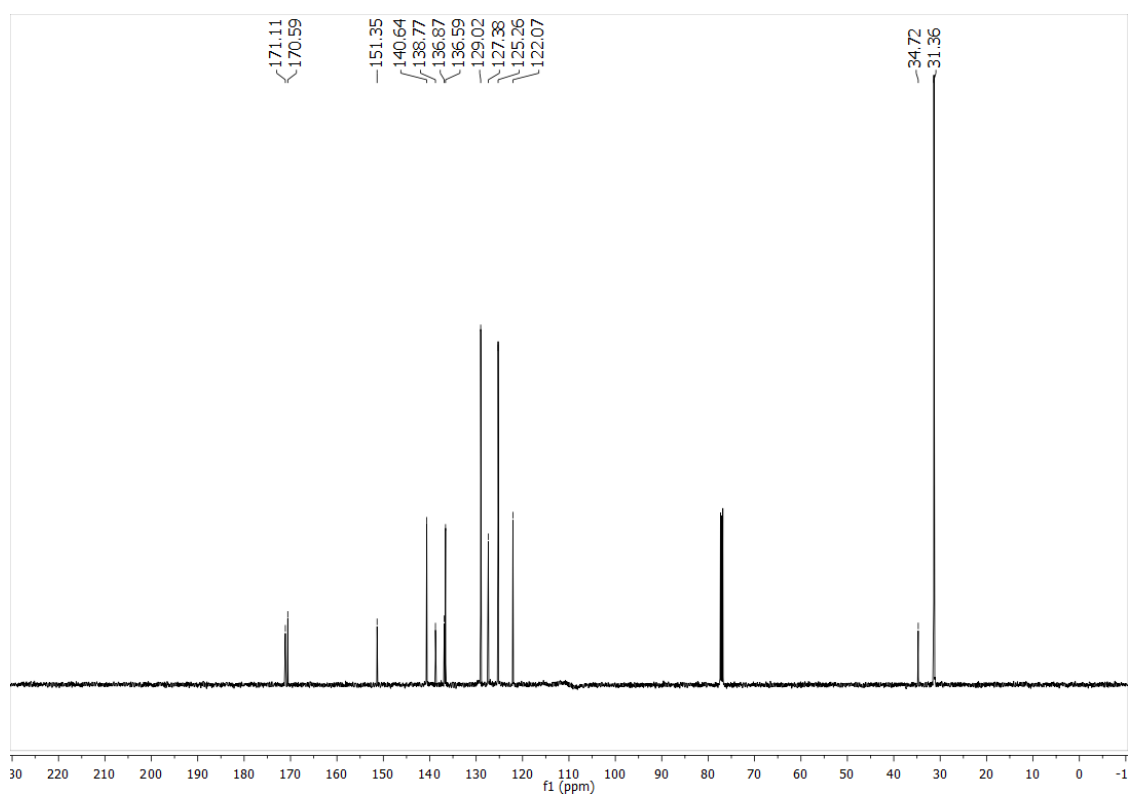
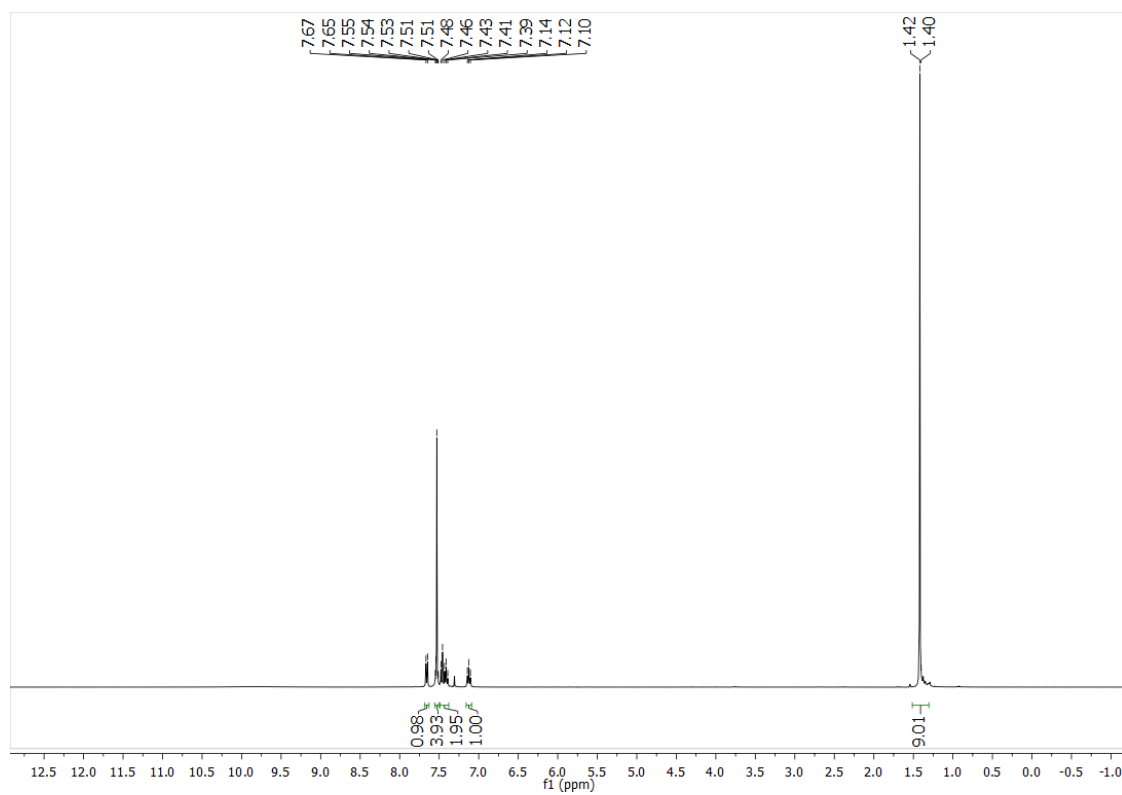
MO-11-H



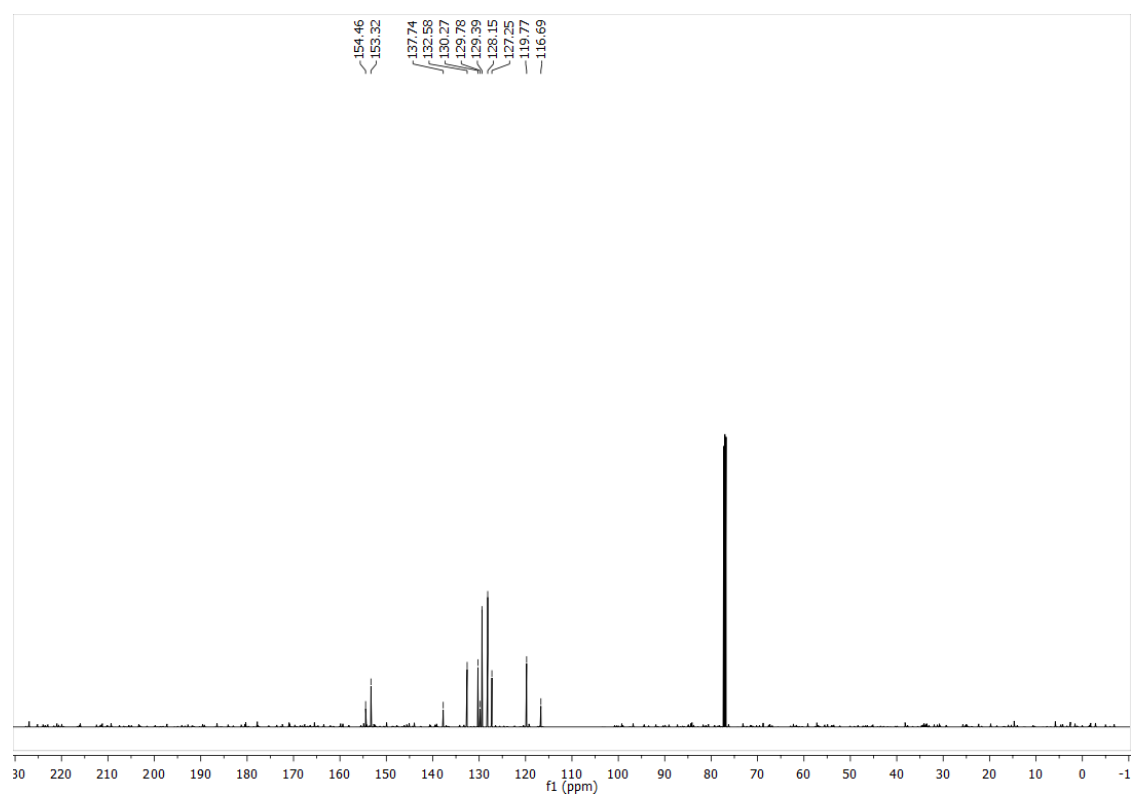
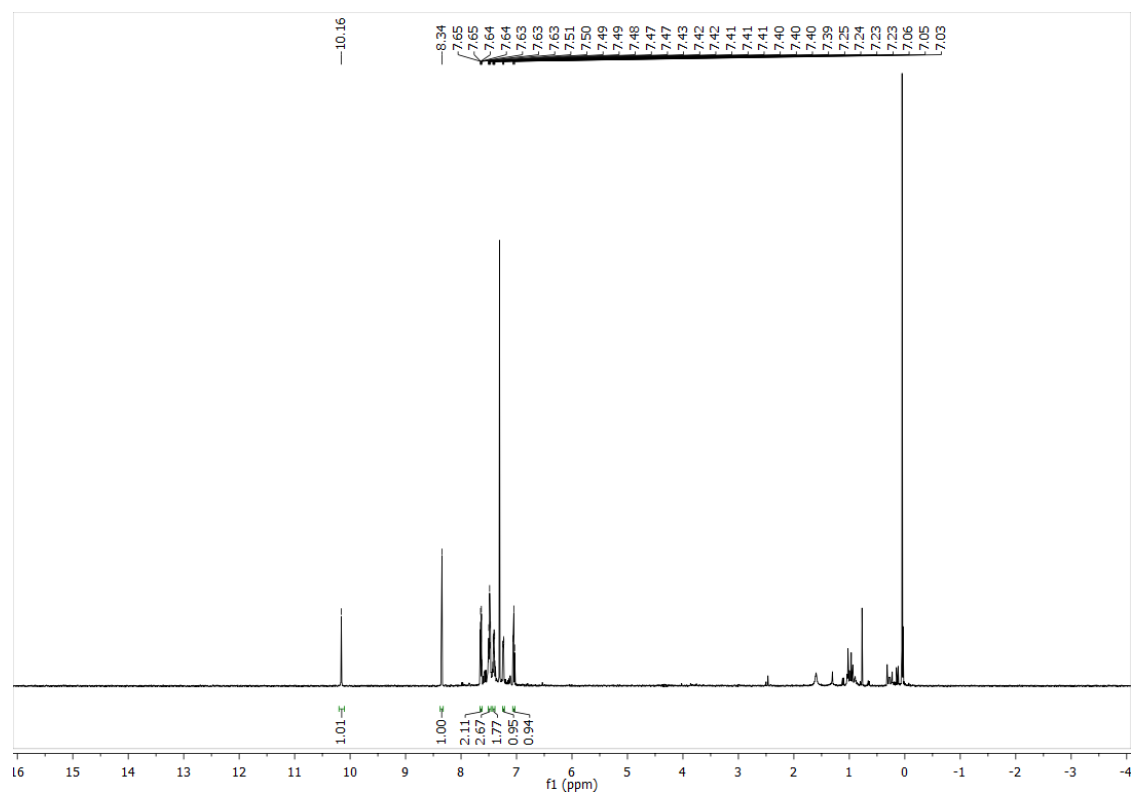
MO-11-NH2



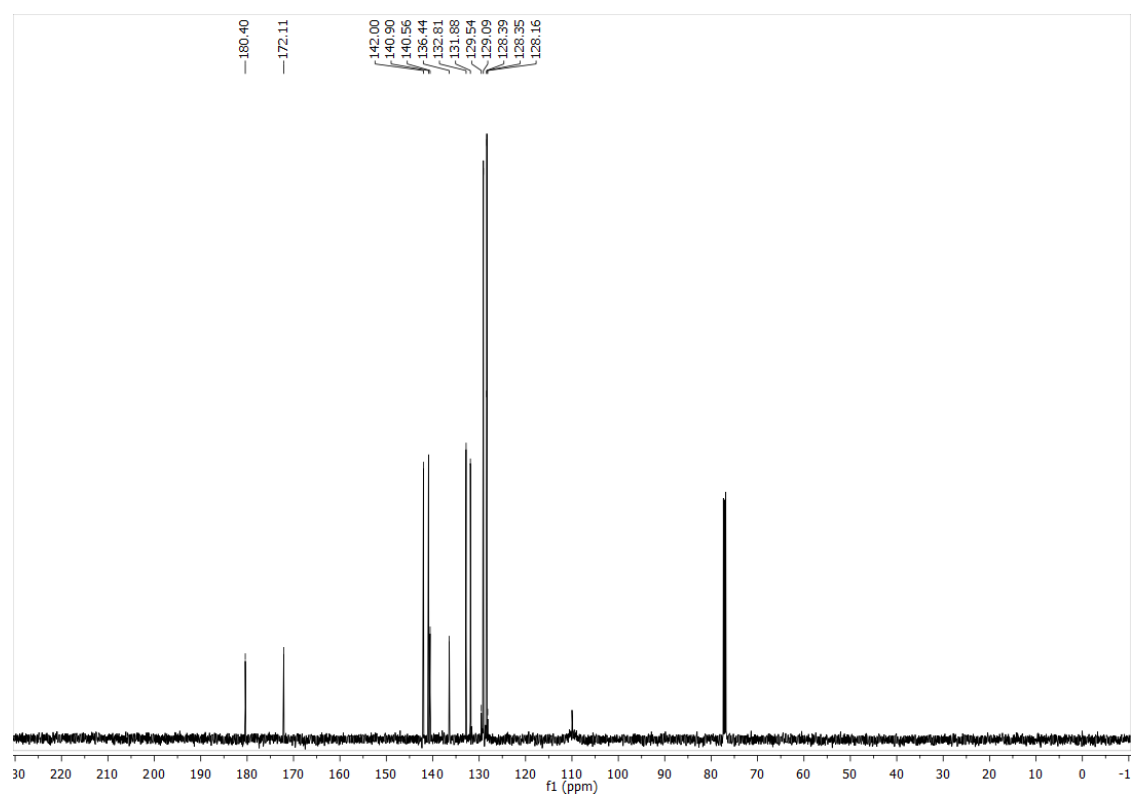
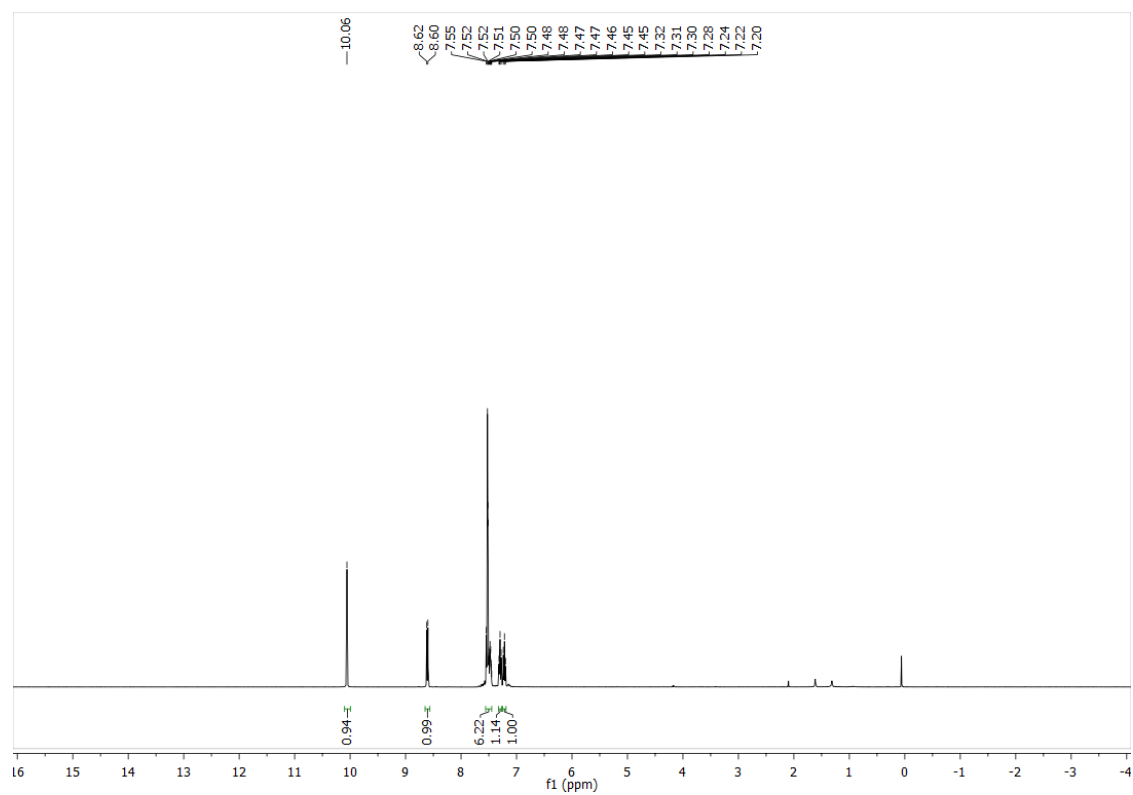
MO-11-OH



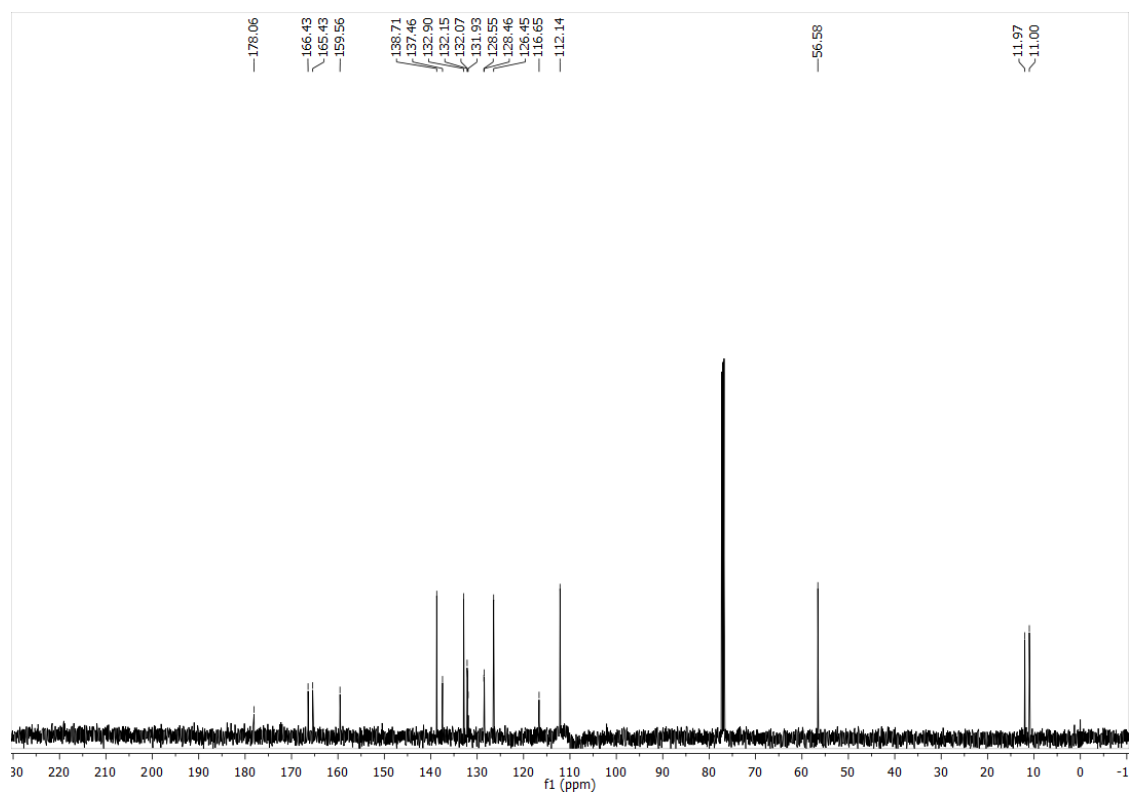
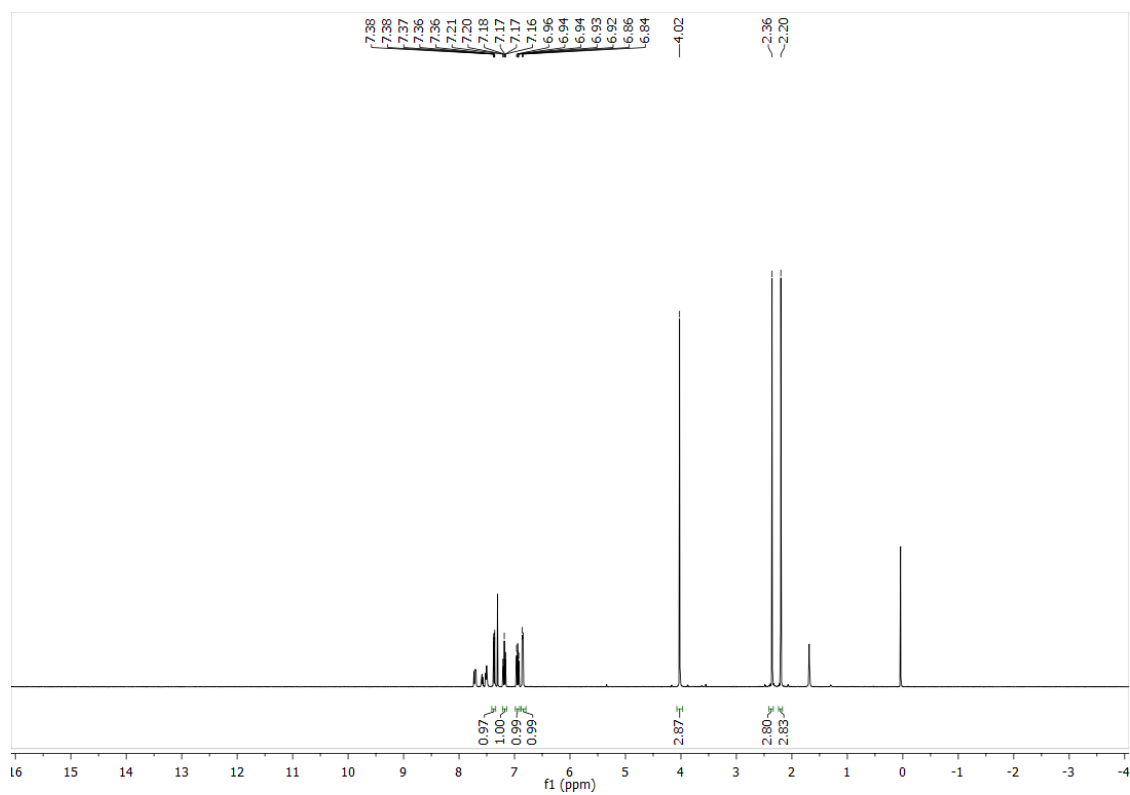
MO-NHOH-PH



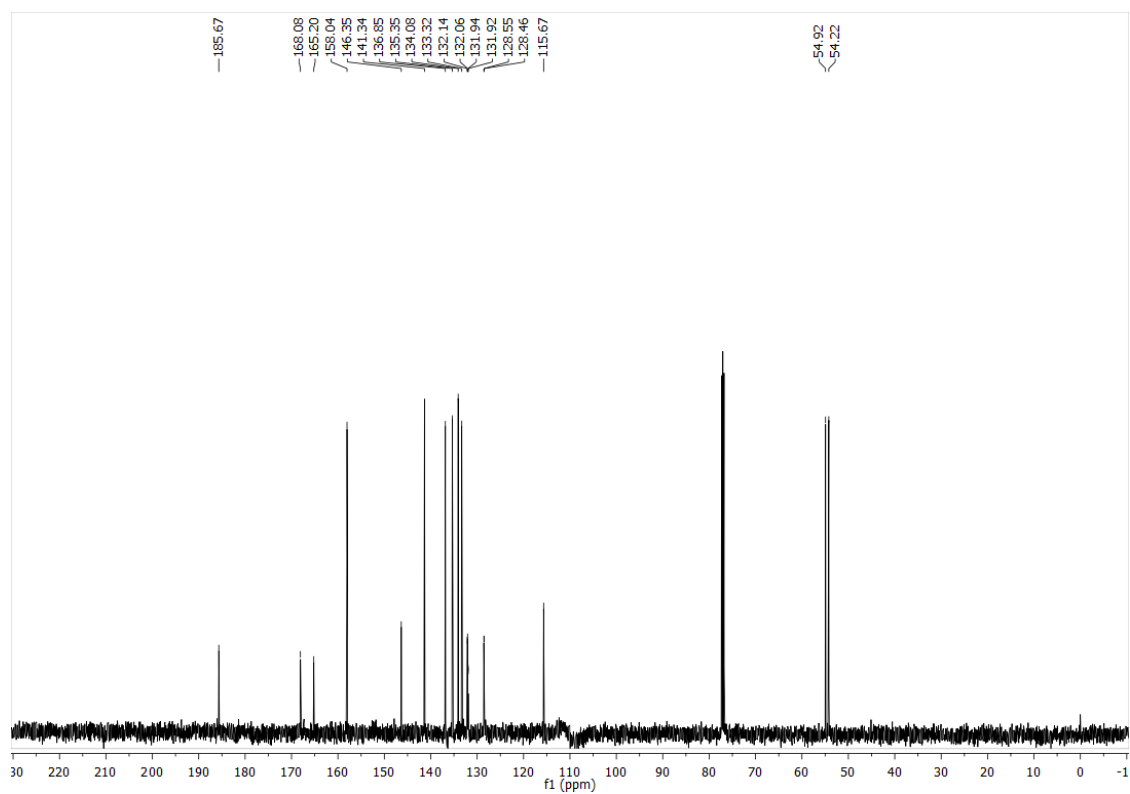
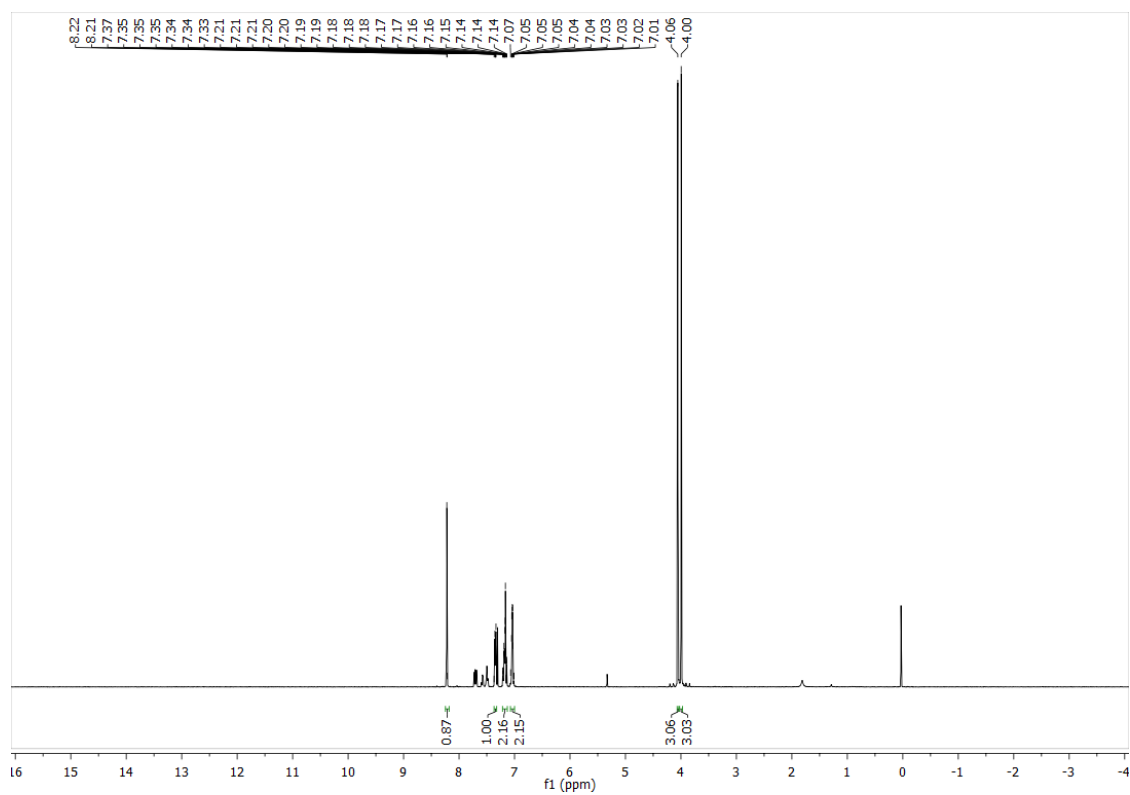
MO-SH-PH



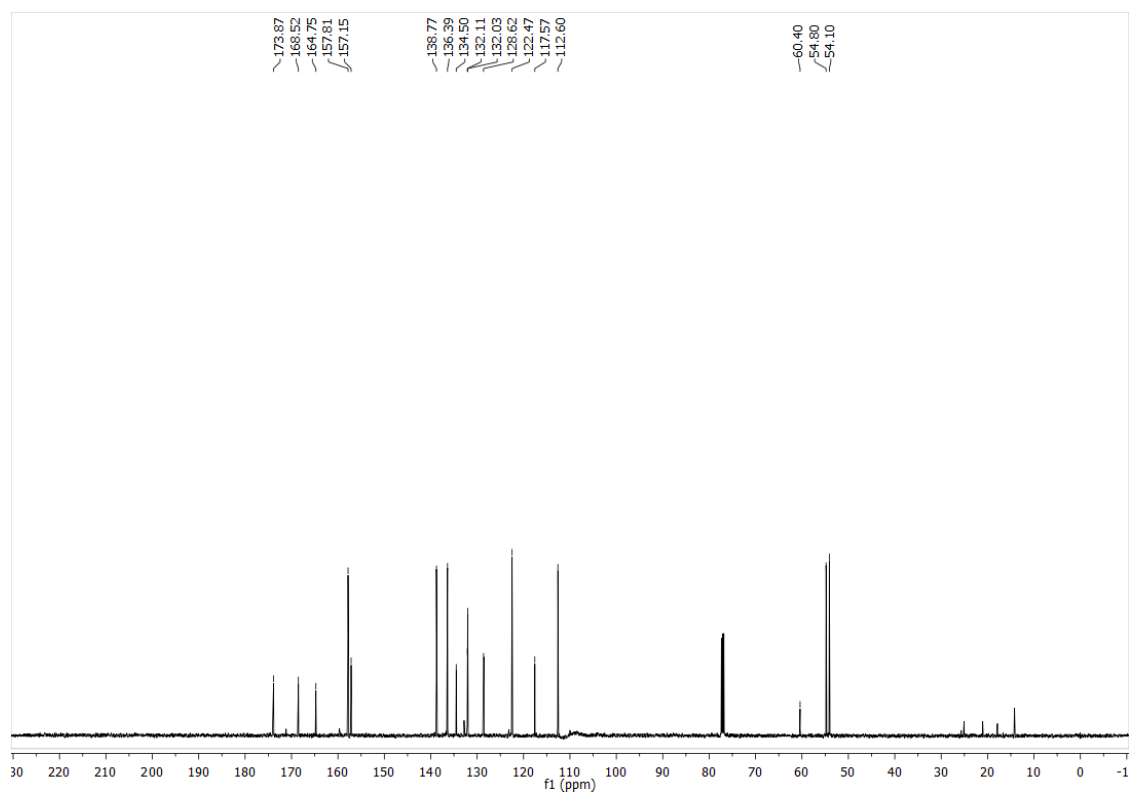
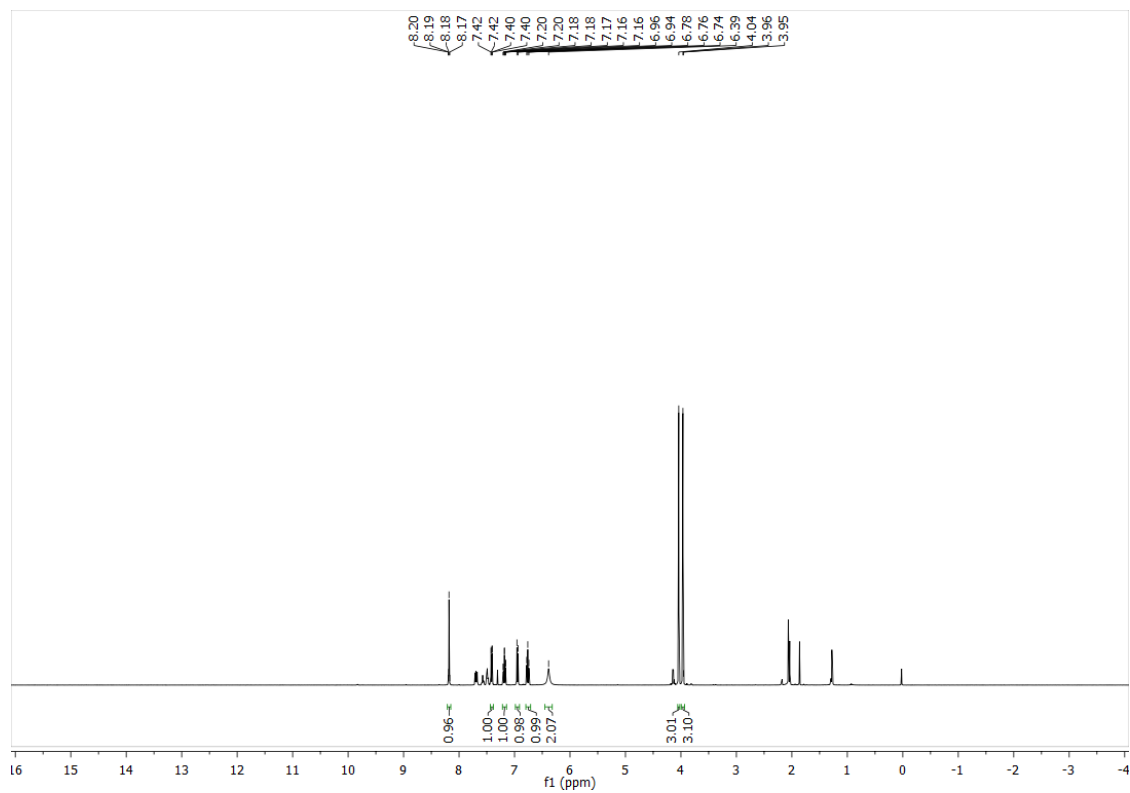
HC-9-OMe



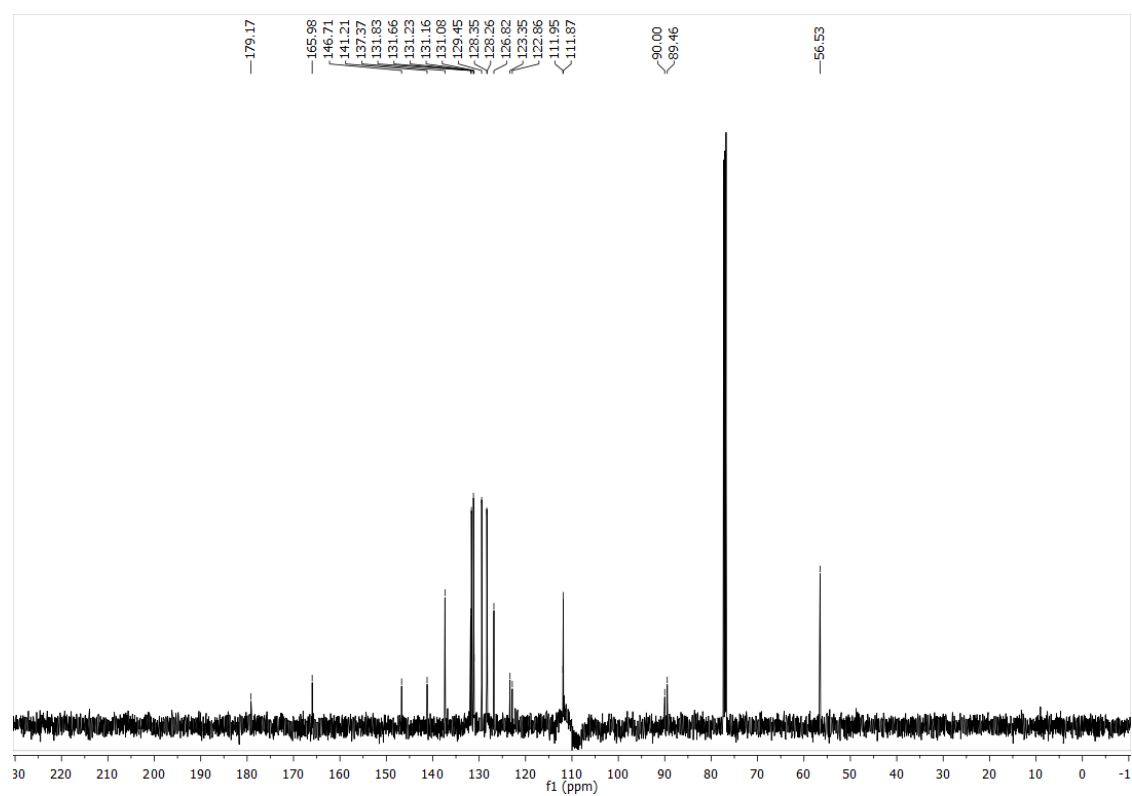
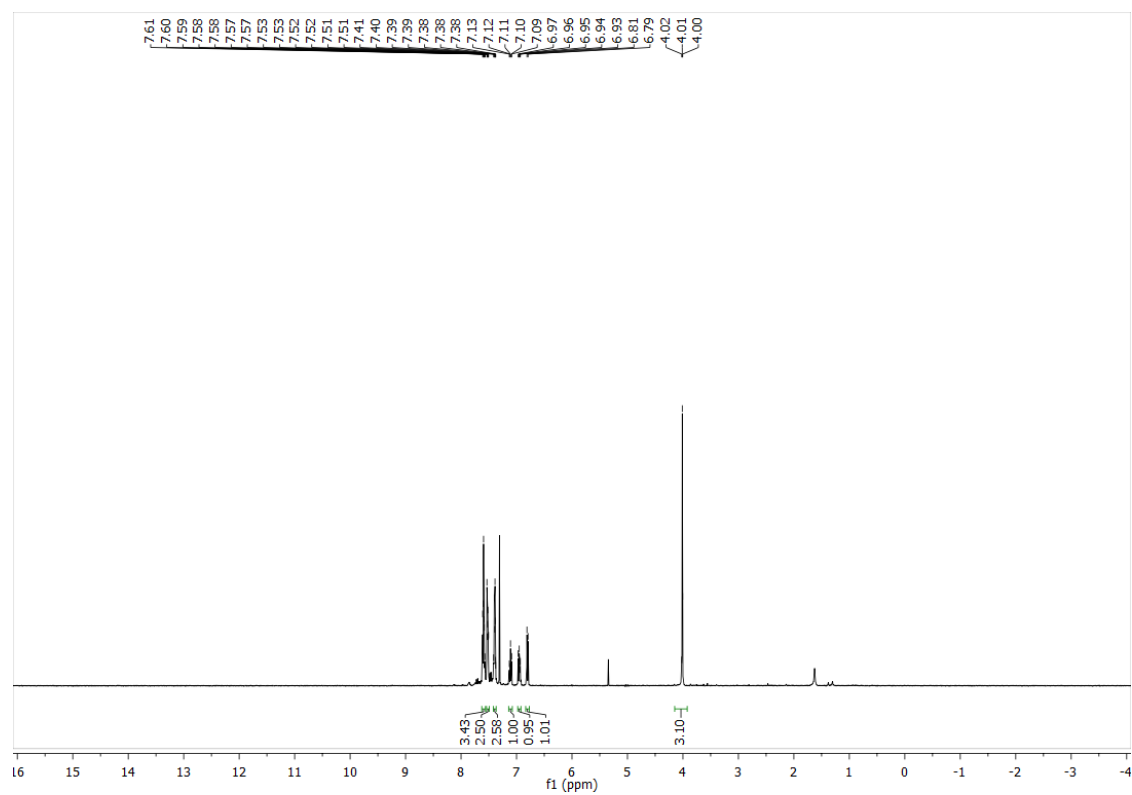
HC-13-H



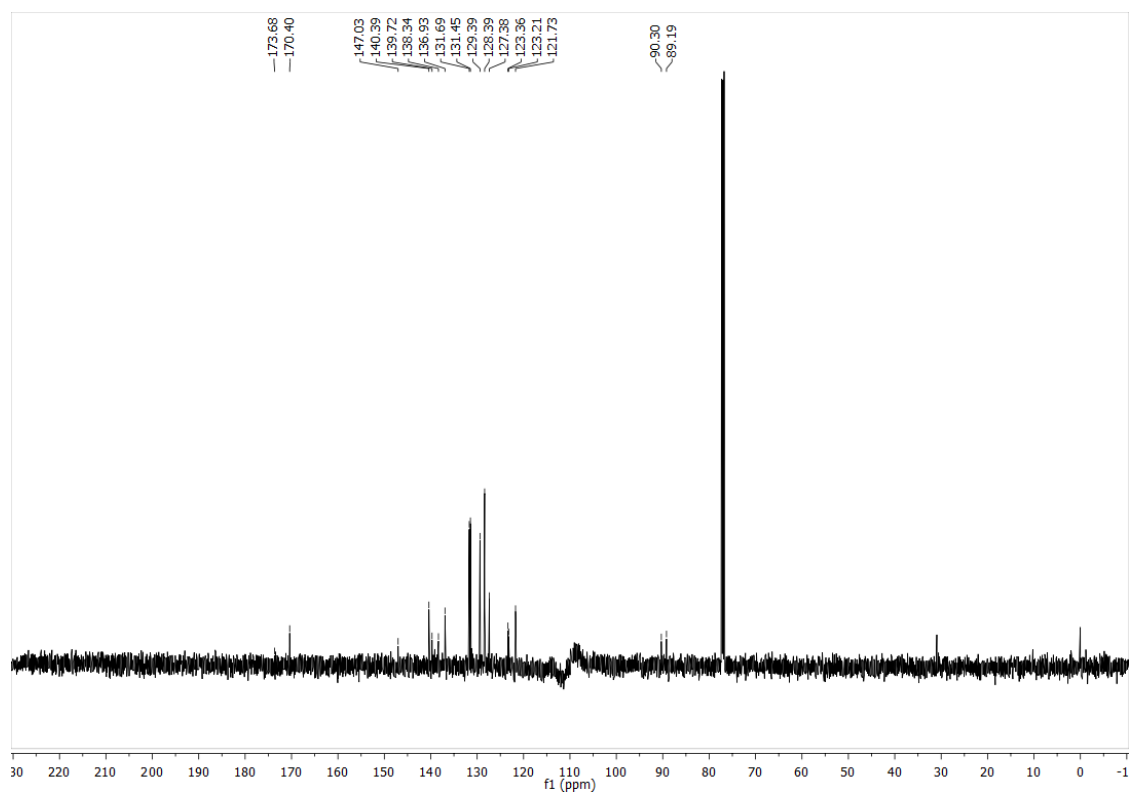
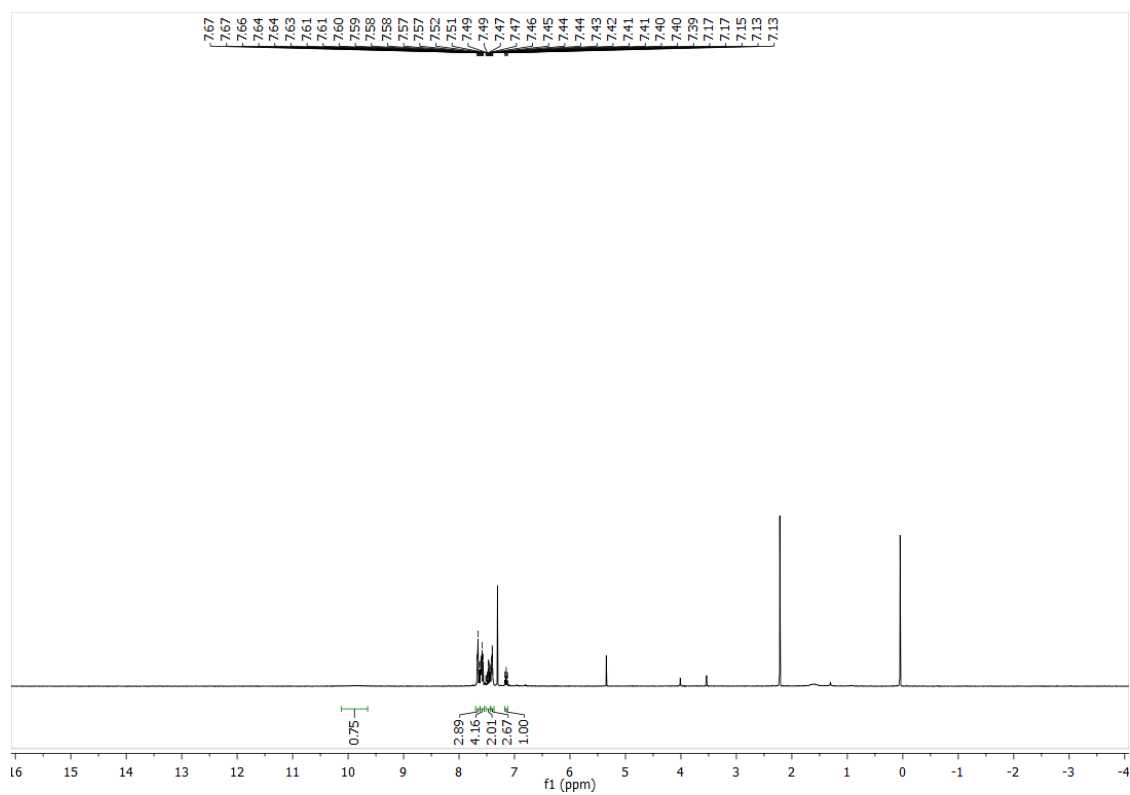
HC-13-NH2

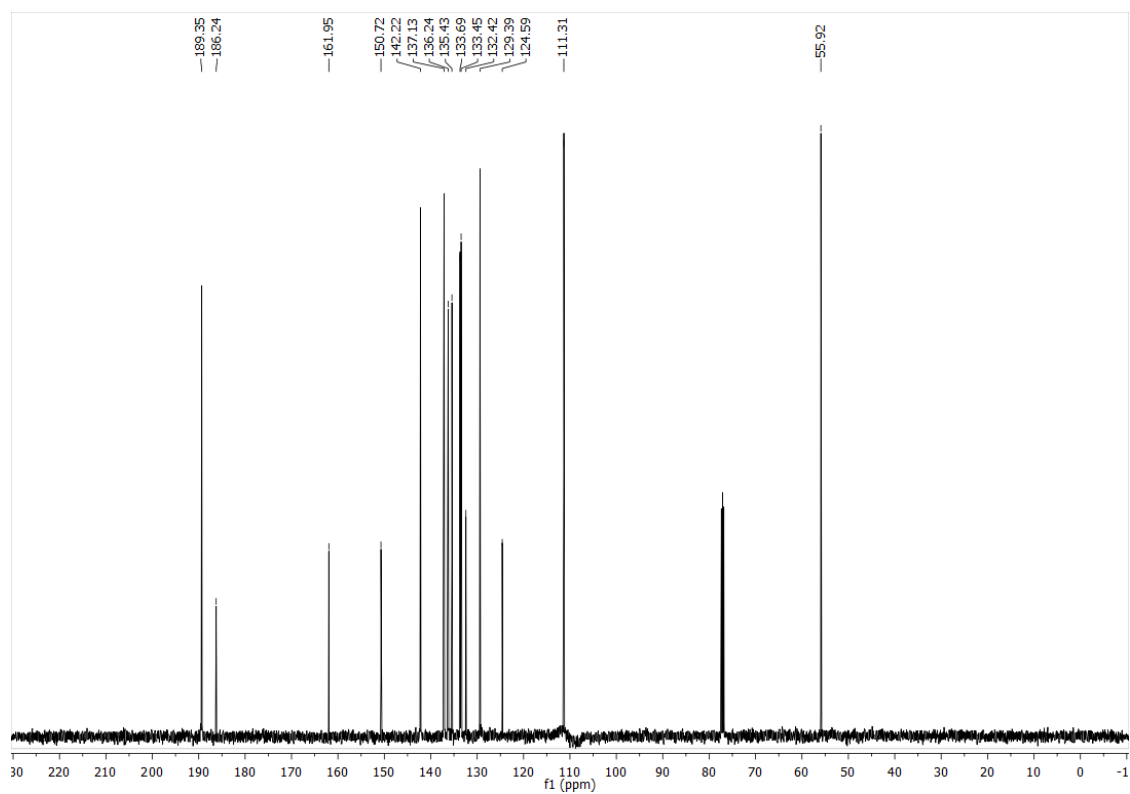
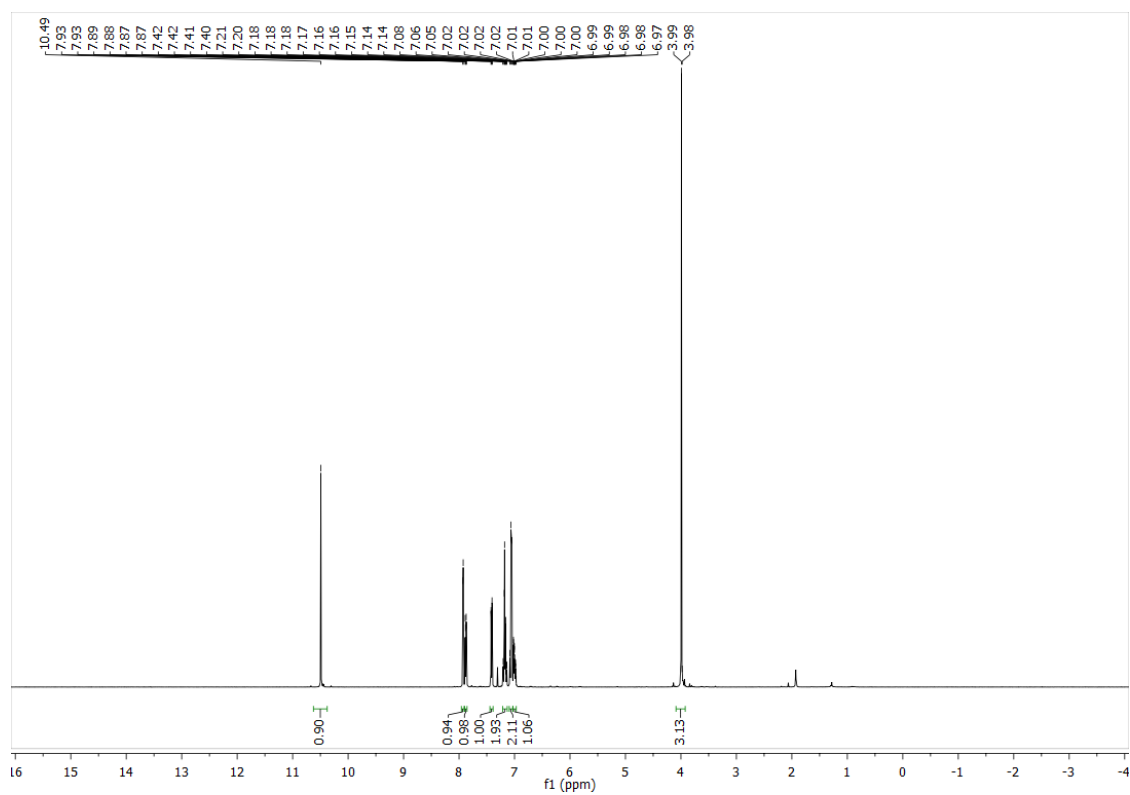


SG-PH-OMe

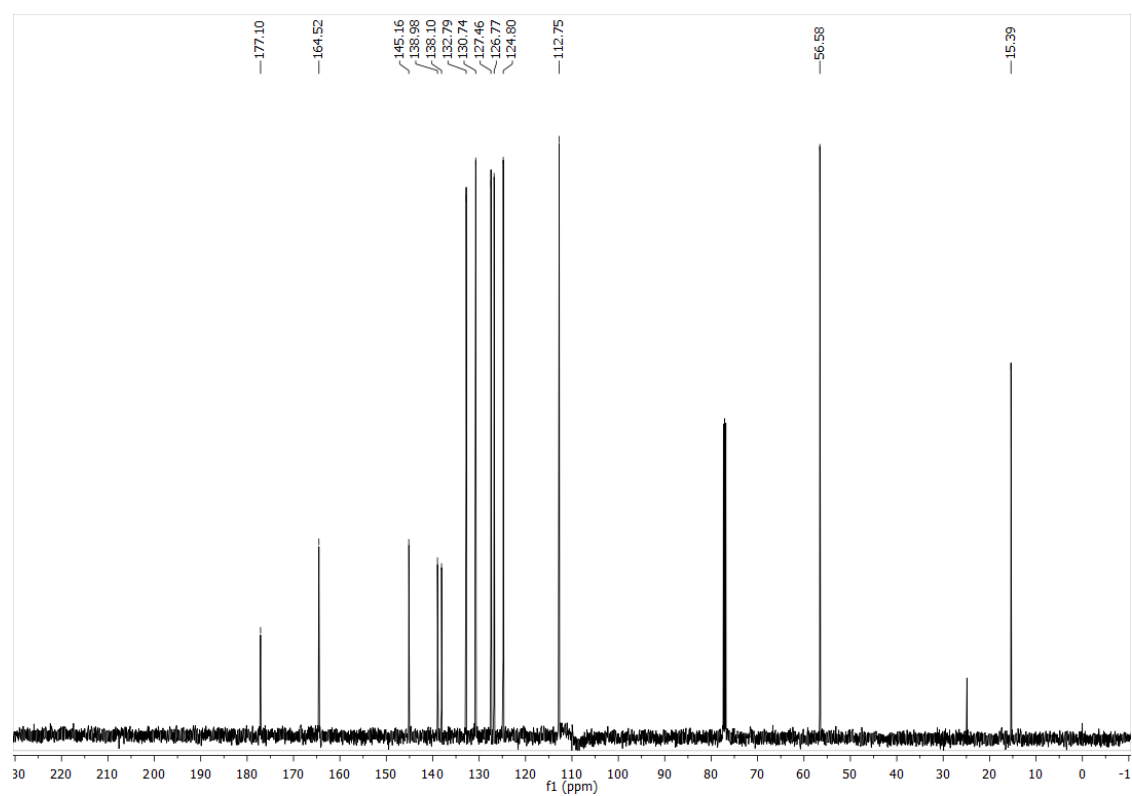
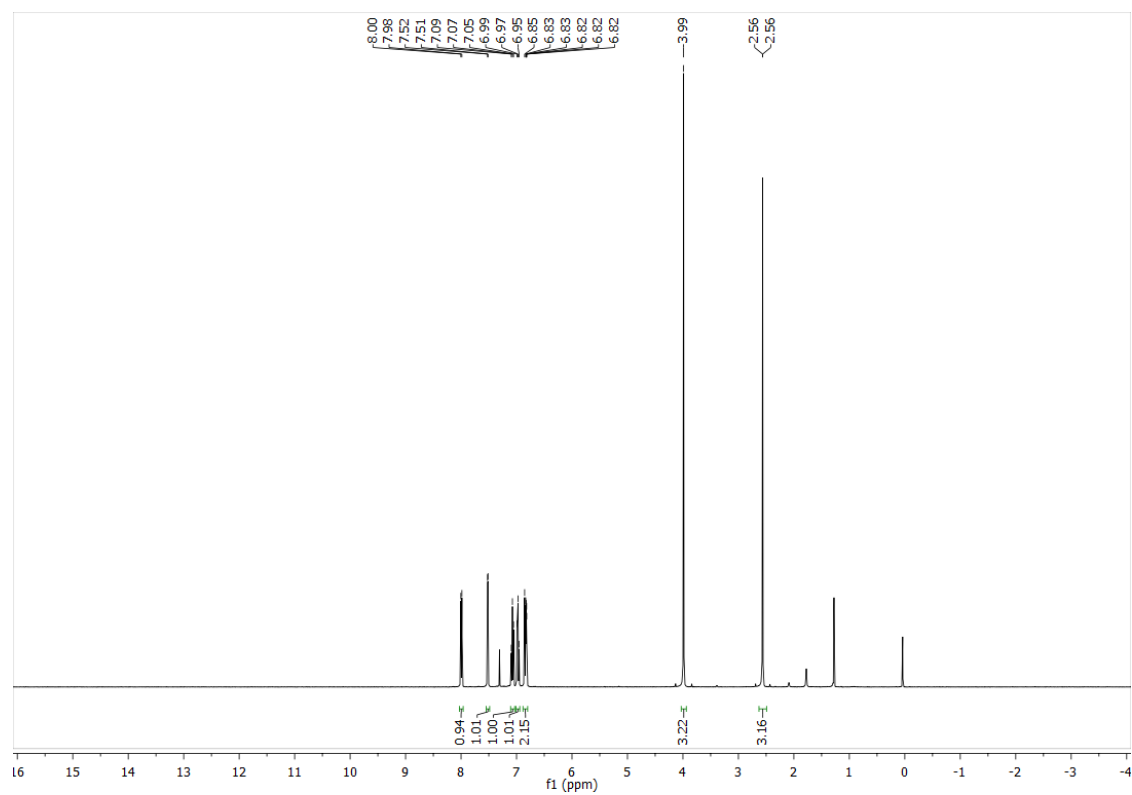


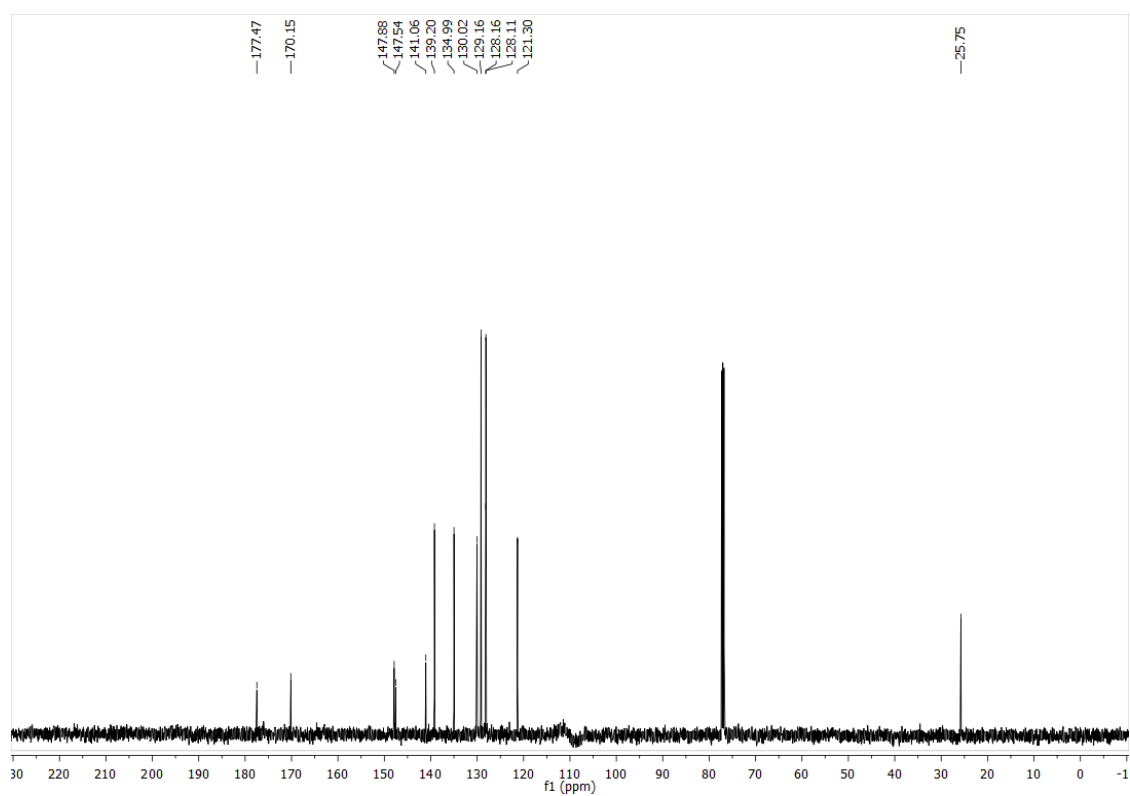
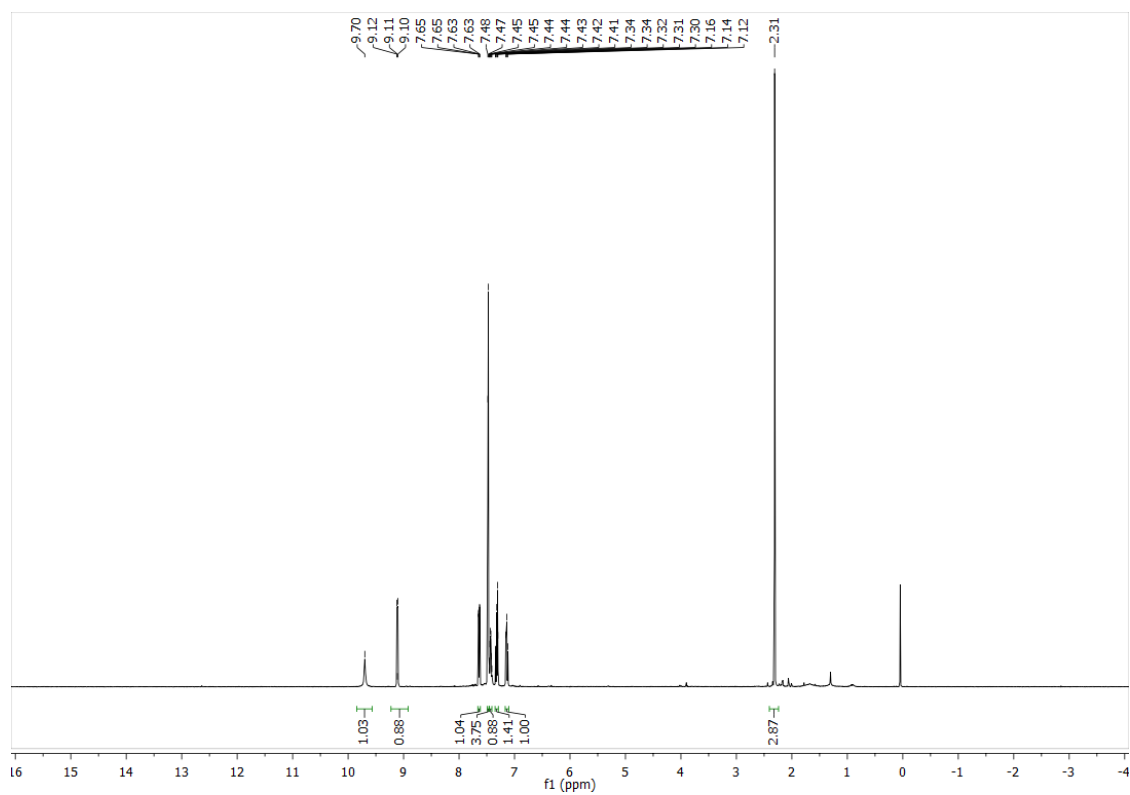
SG-PH-OH



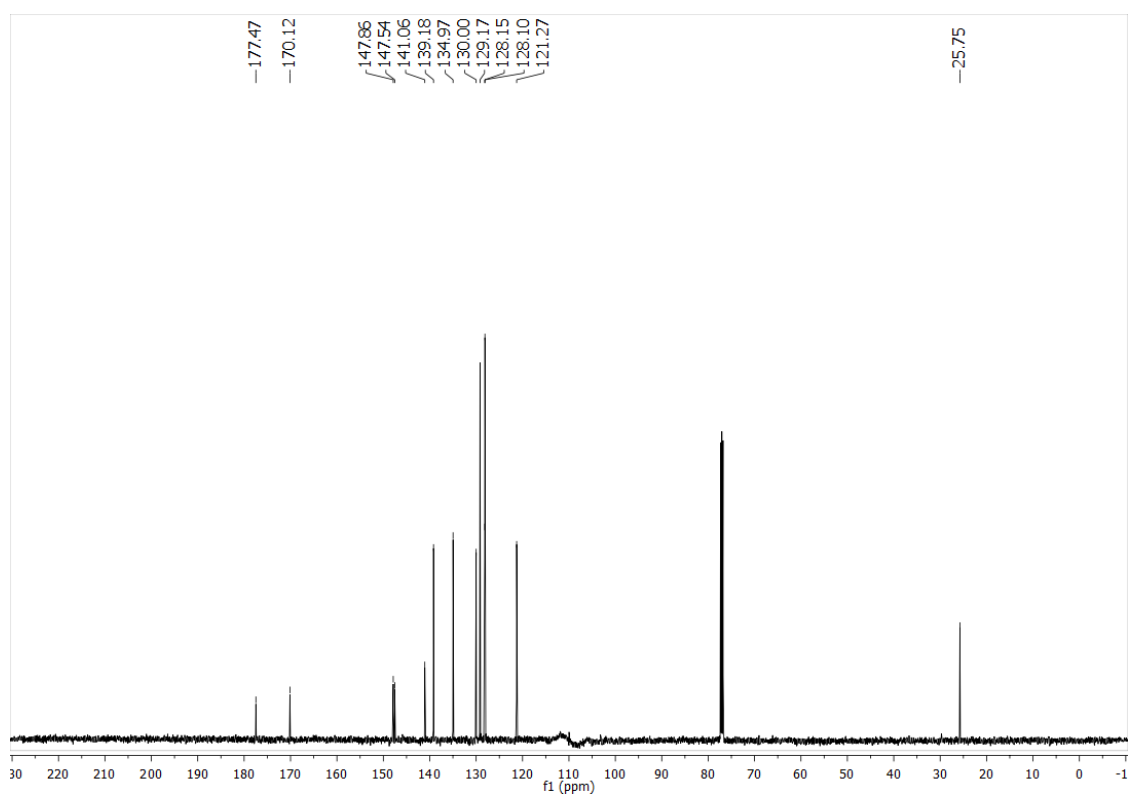
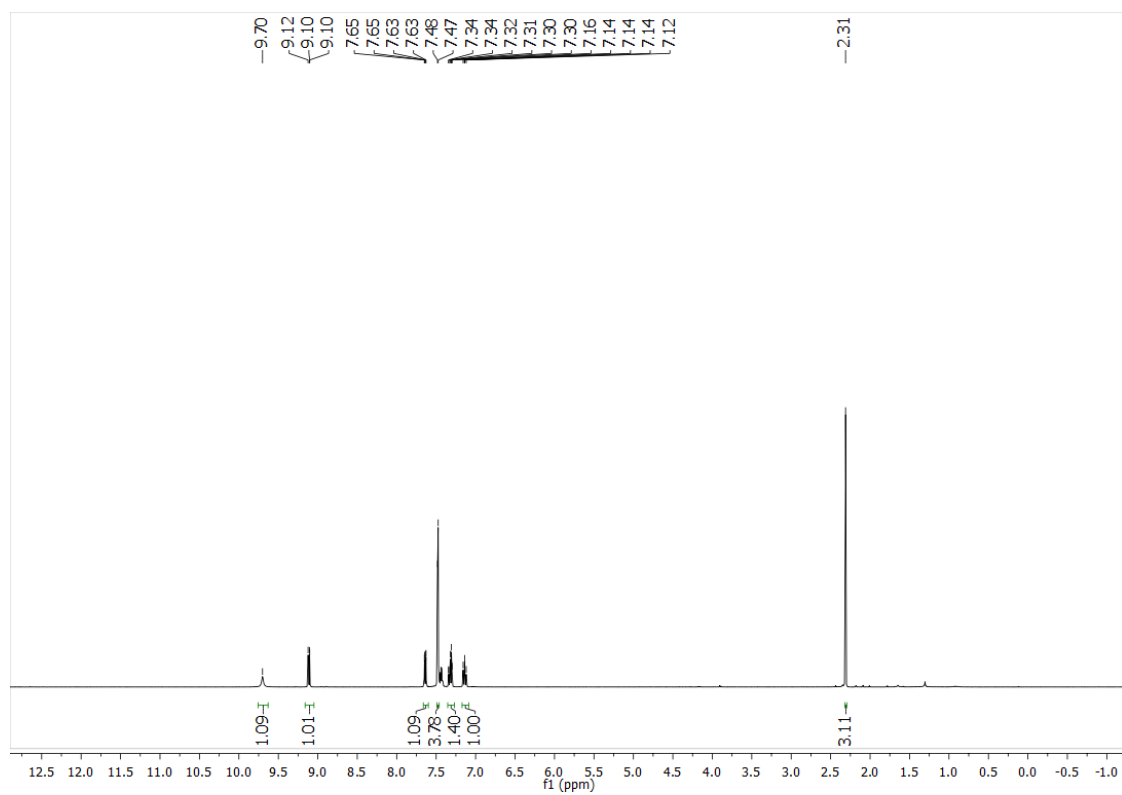
EF-5-H

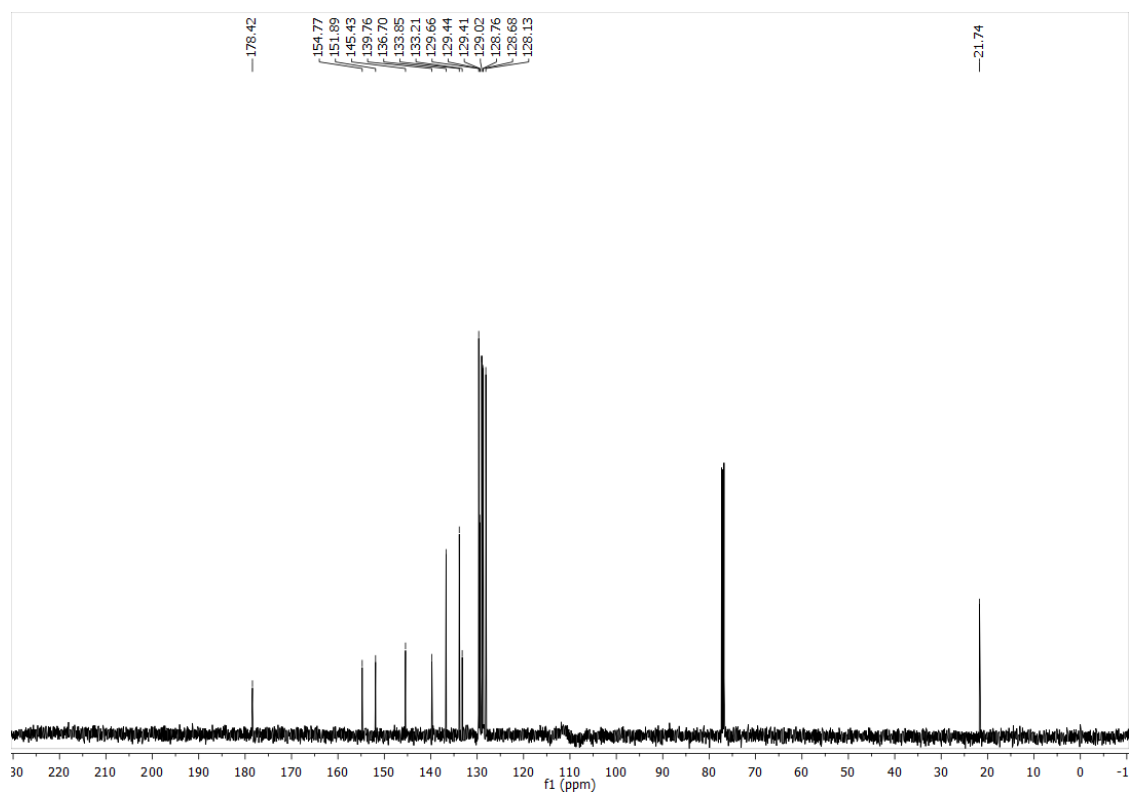
HC-12-OMe



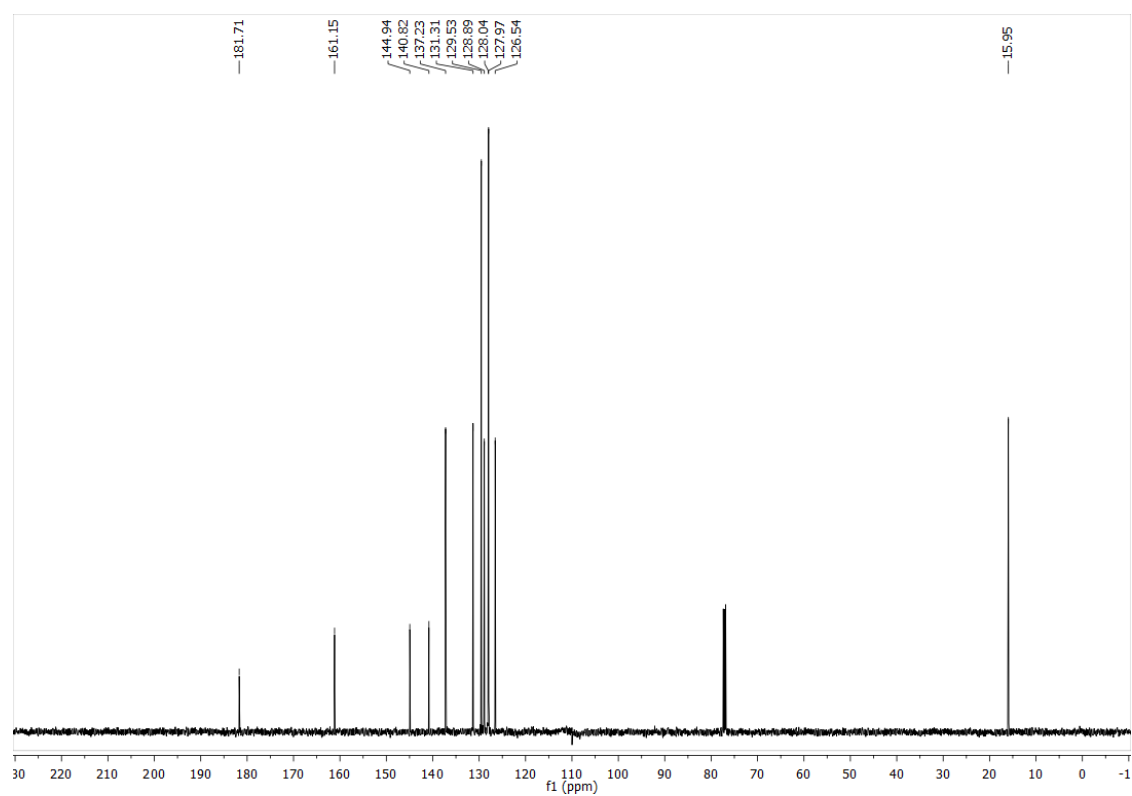
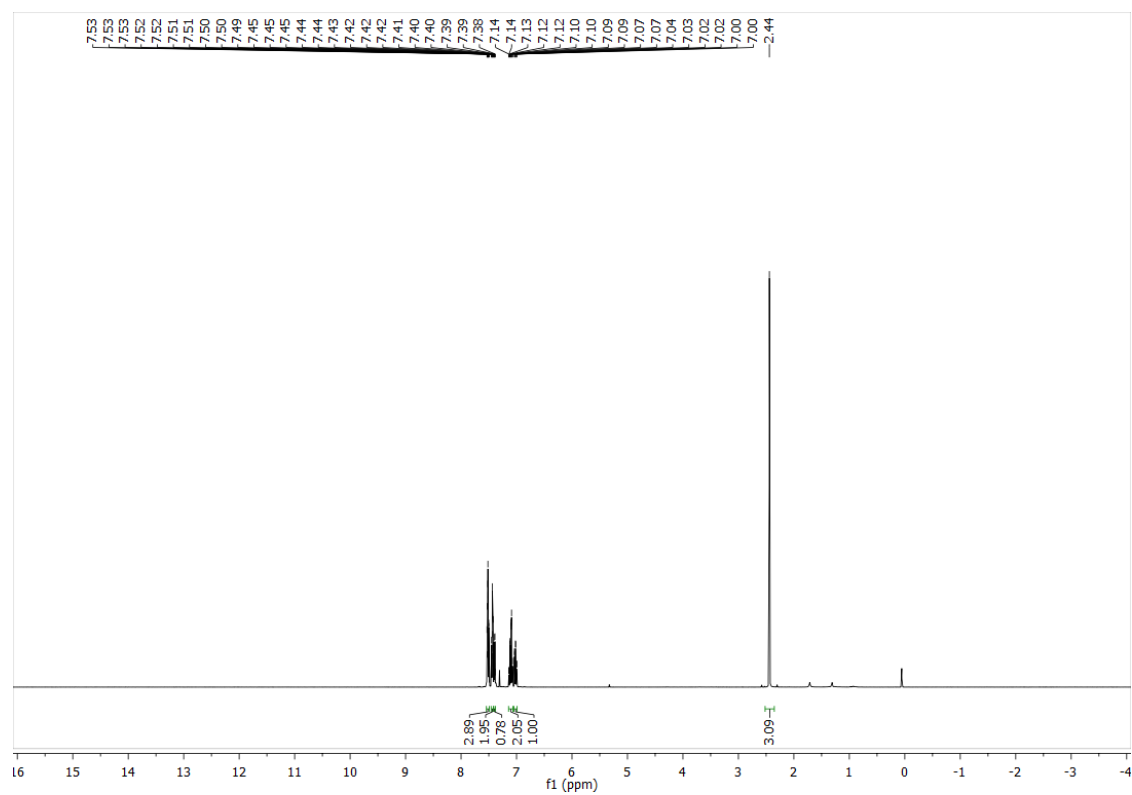
Am-Ac-OH

MO-Am-PH

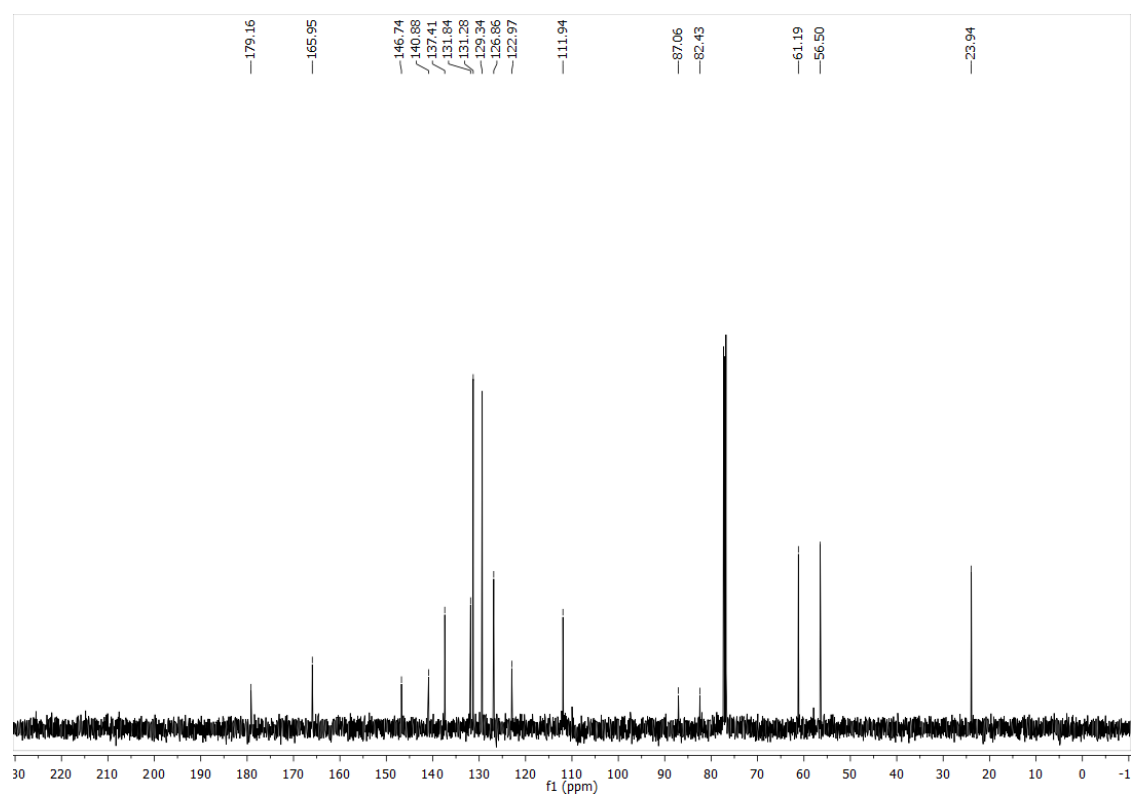
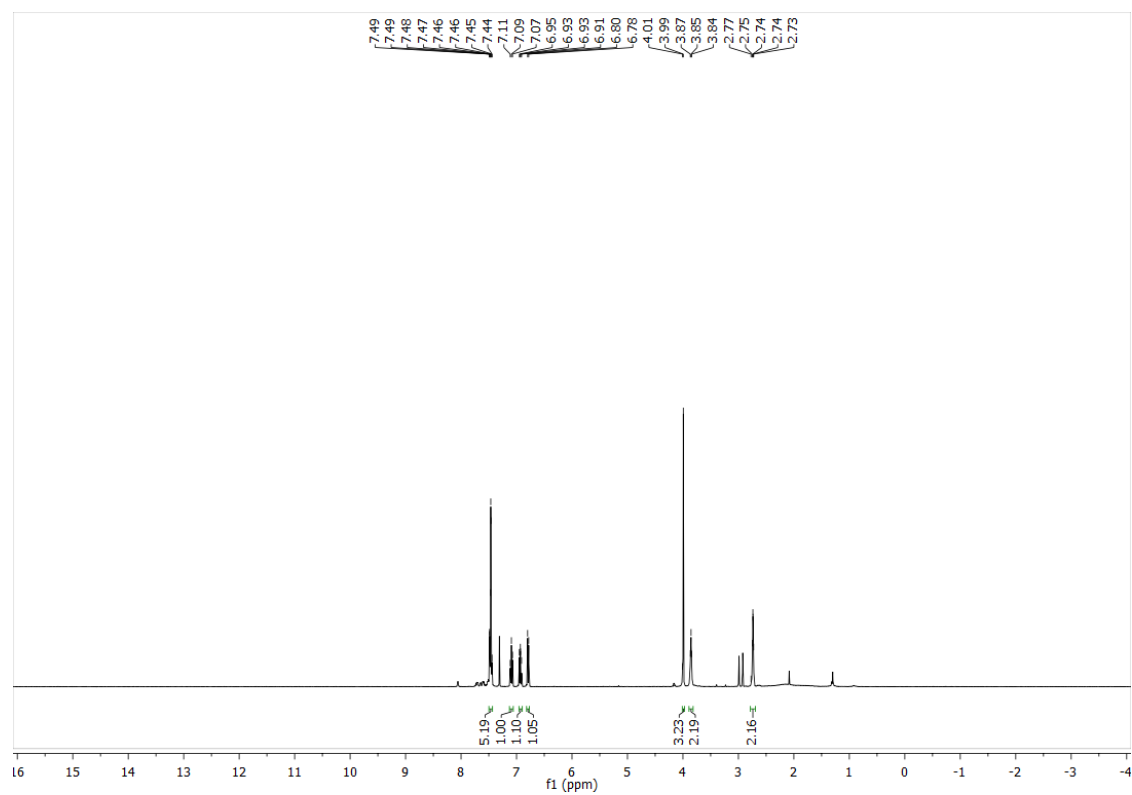




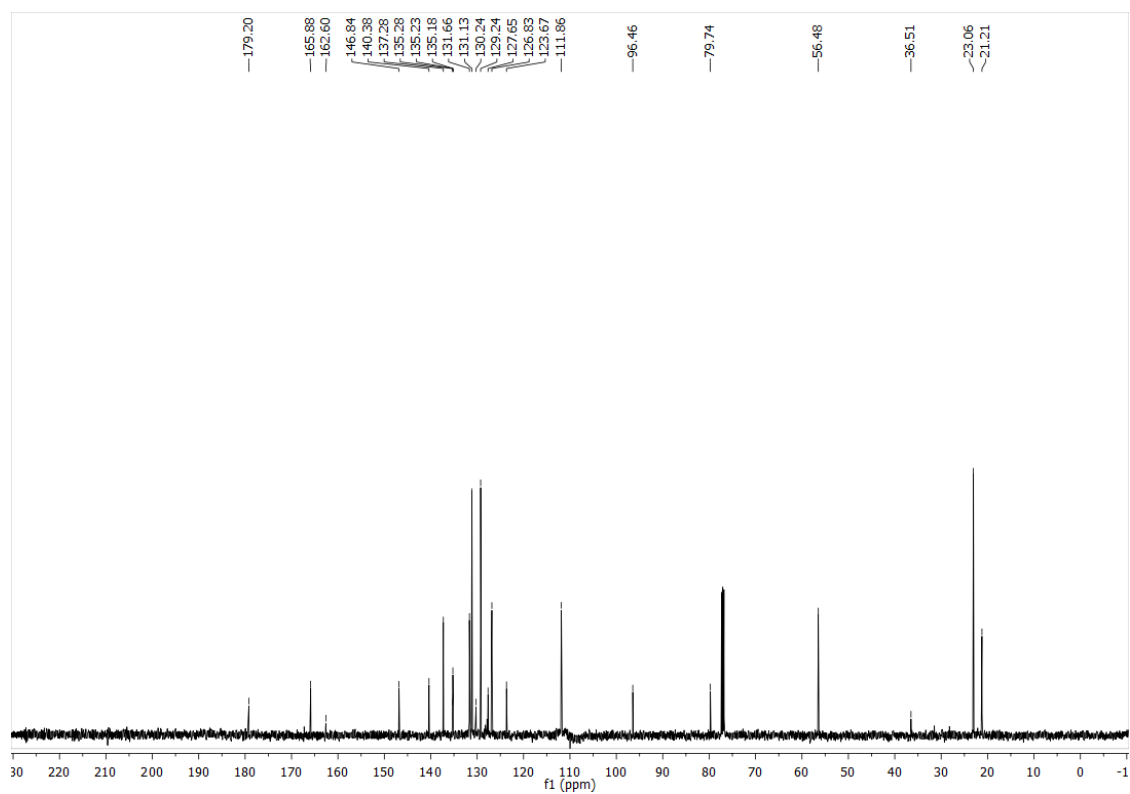
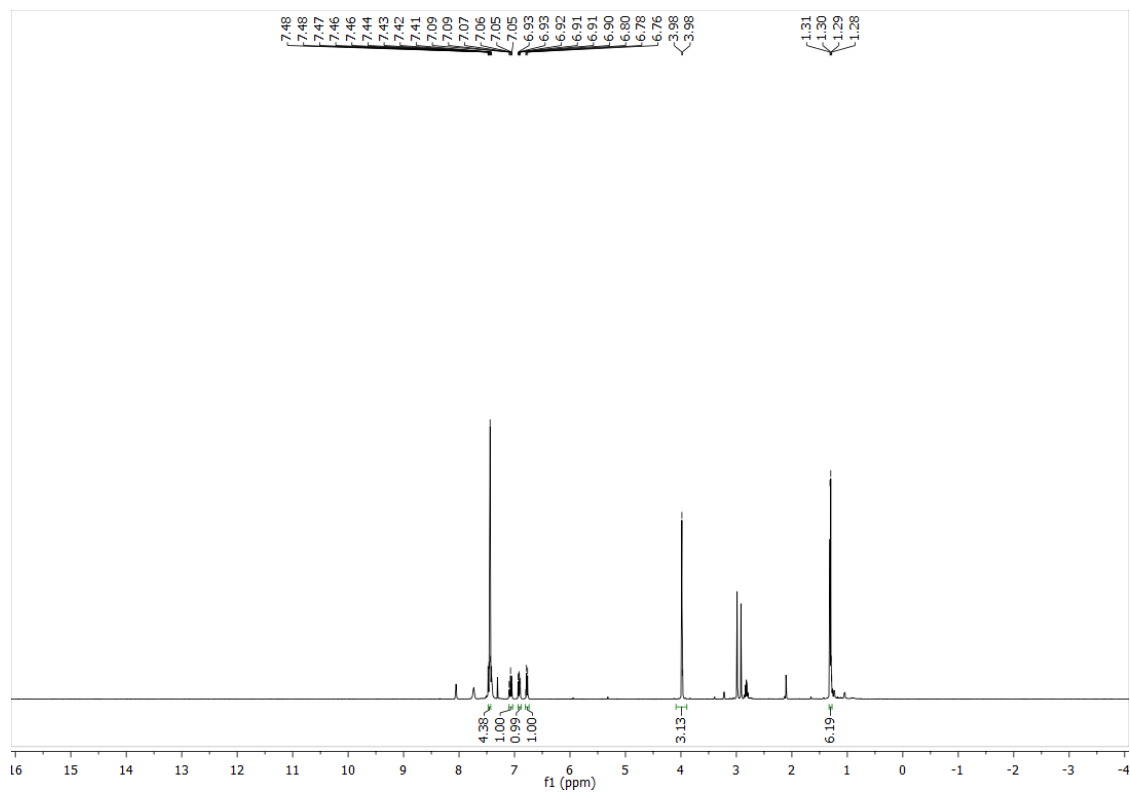
MO-SMe-PH



SG-EtOH-OMe



SG-iPr-OMe

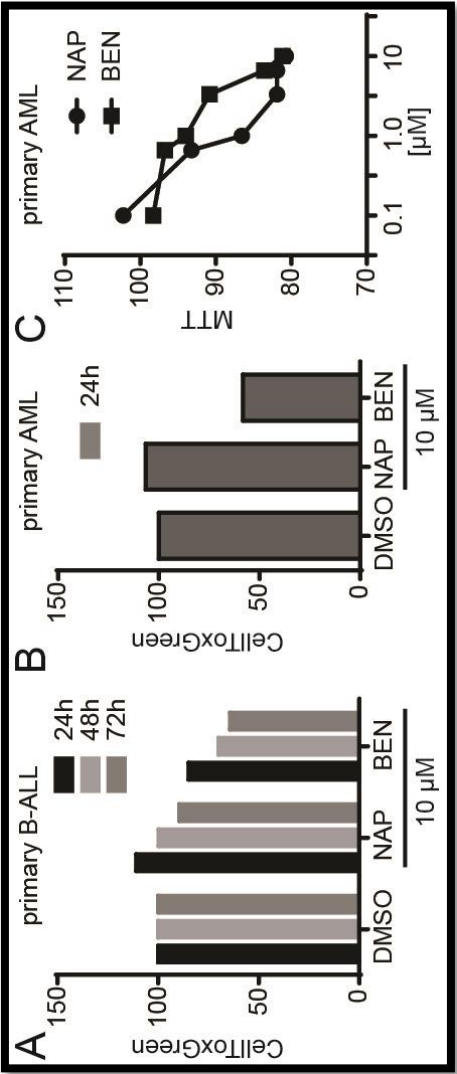


Appendix B: Biological Data

Sirt 1 Inhibition Assay		
Compound	% Inhibition	Standard Deviation
Tenovin-6	21.18	0.32
Salermide	16.84	0.28
MO-1-OH	13.89	0.49
MO-10-OH	33.53	0.17
MO-OH-Nap	30.53	0.31
BA-pBr-OH	34.18	0.38
HC-1-OH	25.92	0.52
MO-OH-DM	38.81	7.56
MO-OH-PH	29.71	0.57
MO-7-OH	36.14	0.83
BA-SM-OH	43.74	0.55
BA-TM-OH	20.77	0.37
EF-3-OH	33.87	0.54
BA-PH-OH	26.60	4.06
MO-2-OH	10.40	0.41
Am-NO ₂ -OH	18.93	1.26
EF-2-OH	22.86	0.81
MO-9-OH	-1.94	1.68
BA-P7-OH	-0.82	2.30
EF-1-OH	3.61	0.27
Am-NH ₂ -OH	32.02	0.39
HKT	21.07	1.93
TDA	61.86	0.47
HC-2-OH	13.71	0.97
BA-pOH-OH	23.23	0.37
BA-pCN-OH	2.67	1.05
Am-Piv-OH	15.38	1.35
BA-HC ₂ -OH	24.35	0.70
SG-TMS-OH	6.03	4.02
Trans-resveratrol	-30.23	1.23

Sirt 2 Inhibition Assay		
Compound	% Inhibition	Standard Deviation
Tenovin-6	65.99	0.85
MO-1-OH	-0.05	3.52
MO-10-OH	13.00	1.72
MO-OH-Nap	16.71	0.49
BA-pBr-OH	16.78	0.78
BA-Nap-OH	13.18	3.71
HC-1-OH	12.59	2.97
MO-OH-DM	5.69	2.55
MO-OH-PH	11.98	0.30
MO-7-OH	13.52	3.45
BA-SM-OH	57.48	0.79
BA-TM-OH	25.71	2.12
EF-3-OH	9.16	1.30
BA-PH-OH	18.37	2.56
MO-2-OH	15.25	2.88
Vorinostat	0.09	2.12
EF-2-OH	16.46	0.75
MO-9-OH	5.38	3.13
BA-P7-OH	10.94	5.33
EF-1-OH	4.64	1.15
Am-NH ₂ -OH	22.08	0.60
HKT	5.37	2.80
TDA	92.09	0.54
HC-2-OH	15.55	1.60
BA-pOH-OH	86.36	0.71
BA-pCN-OH	12.96	4.19
Am-Piv-OH	49.12	1.71
BA-HC2-OH	34.46	0.65
SG-TMS-OH	17.12	0.64
Trans-Resveratrol	48.11	1.12

Murine Malignant Hematologic Cell GI50 (μ M)			
Compound	Ba/F3 GC insertion	Ba/F3 88i point mutation	CH12
MO-OH-Nap	0.75	0.73	N/A
MO-OH-SM	1.01	0.93	N/A
MO-OH-DM	2.22	1.95	N/A
MO-OH-TM	3.51	3.32	N/A
MO-OH-PH	3.12	3.03	N/A
MO-1-OH	0.68	0.69	N/A
MO-2-OH	1.98	1.93	N/A
MO-7-OH	1.55	1.96	N/A
MO-10-OH	1.31	1.79	N/A
MO-9-OH	2.18	2.44	N/A
BA-P7-OH	0.29	0.46	1.84
BA-P8-OH	0.31	0.42	4.77
BA-pBr-OH	0.61	0.92	0.95
BA-Phe-OH	0.88	1.39	1.21
BA-Nap-OH	0.59	0.75	1.21
BA-SM-OH	0.8	1.13	1.27
BA-DM-OH	1.2	1.51	1.26
BA-TM-OH	1.12	1.54	1.27
EF-1-OH	0.31	0.60	2.09
EF-2-OH	0.41	0.60	1.83
EF-3-OH	0.68	0.54	2.11
HC-1-OH	0.12	0.23	>10
Am-pNH3-OH	0.32	0.31	2.35
Am-pNO2-OH	0.45	0.56	1.78
SAHA	0.16	0.35	0.68



Cancer Causing Genes Associated with Molt-4 Cells

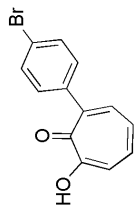
Gene	mutation type	Nap	HC-1	fold
DICER1	missense	10.44427	10.44036	10.44232
PAX8	missense	10.44427	10.44036	10.44232
EGFR		5.754676	12.84959	9.302133
HDAC9	missense	6.85147	6.856138	6.853804
TERT	missense	6.85147	6.856138	6.853804
CD79A	silent	5.208295	7.012781	6.110538
CAMTA1	missense	6.82705	4.17405	5.50055
TSC1	missense	4.101206	6.417841	5.259524
EGFR		2.573569	7.426981	5.000275
NRG1	missense	4.834759	4.832946	4.833853
BCL11B	missense	5.347897	4.206537	4.777217
EGFR	deletion/frameshift	3.214596	6.057353	4.635975
PRDM16	deletion/frameshift	2.284347	5.718419	4.001383
DNMT3A	deletion/frameshift	2.515569	5.301685	3.908627
BCAR3	missense	4.316066	2.998645	3.657356
PRDM16		2.221528	5.087109	3.654318
AZU1	silent	3.746343	3.548604	3.647474
NCOA2	missense	3.710341	3.429571	3.569956
ACVR1B	missense	4.755257	1.859933	3.307595
ATP2B3	unknown	2.14665	4.198014	3.172332
FARP2	silent	3.548126	2.575947	3.062037
HDAC7	missense	3.624204	2.23759	2.930897
KDM5A	missense	3.32002	2.47566	2.89784
PAX8		2.618842	2.850439	2.734641
PTPRB	silent	3.859757	1.581139	2.720448
TRAF7	missense	2.702256	2.704097	2.703177
LRIG3	silent	2.638993	2.670182	2.654587
ABL1	silent	2.971888	2.276293	2.624091
MUC1	insertion/frameshift	2.52445	2.718775	2.621612
TERT		2.616448	2.618231	2.61734
SF3B1	missense	2.711639	2.307232	2.509435
CREBBP	missense	1.964166	2.754203	2.359185
WHSC1	silent	2.578107	2.066212	2.322159
ATM	missense	2.585416	1.94967	2.267543
BRCA2	silent	2.232649	2.296938	2.264794
RARA		2.194239	2.28886	2.24155
HRAS	missense	2.908662	1.570436	2.239549
PMS2	unknown	2.391718	2.020761	2.20624
HNF1A	missense	2.059261	2.291288	2.175275

RARA	missense	2.265969	2.069964	2.167966
TELO2	silent	1.807135	2.46387	2.135503
ARHGEF12	missense	1.626647	2.520454	2.07355
FLT3	missense	2.221848	1.911432	2.06664
PIK3R1		2.114824	1.977994	2.046409
PPFIBP1		2.478702	1.569657	2.02418
NRG1		1.821143	2.190962	2.006053
MLL3	silent	1.511369	2.427236	1.969303
PPFIBP1	missense	1.542991	2.345792	1.944392
PHOX2B	missense	1.597356	2.287348	1.942352
FBXO11	missense	2.153459	1.663024	1.908242
PIK3R1	deletion/frameshift	1.557145	1.811219	1.684182
MEN1	missense	1.589059	1.748744	1.668901
BCL6	missense	1.657084	1.554004	1.605544

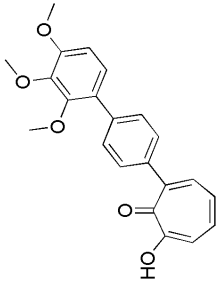
red = upregulation

green = downregulation

Non-Hematologic	
Malignant Cell GI50 (μ M)	
Compound	HepG2
MO-OH-Nap	>500
MO-OH-SM	>500
MO-OH-DM	>500
MO-OH-TM	>500
MO-OH-PH	>500
MO-1-OH	>500
Compound	MCF-7
MO-1-OH	>10
MO-2-OH	5.00
MO-7-OH	3.43
MO-9-OH	6.21
MO-10-OH	5.64
EF-C-1-OH	8.57
EF-C-2-OH	4.58
EF-C-3-OH	5.97
BA-pBr-OH	8.67
BA-Phe-OH	7.43
BA-SM-OH	4.40
BA-DM-OH	7.82
BA-TM-OH	N/A
BA-Nap-OH	6.62
BA-P7-OH	N/A
BA-P8-OH	1.00
HC-1-OH	>10
Am-NH ₂ -OH	6.84
Am-NO ₂ -OH	4.82

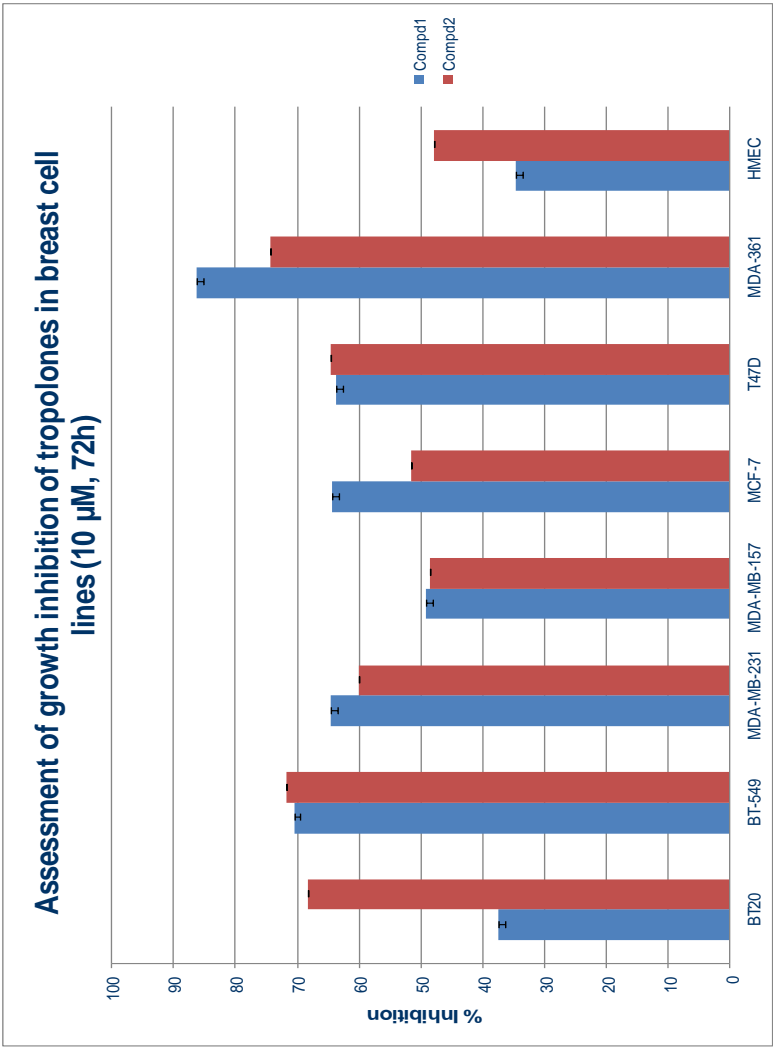


Compound 1: BA-pBr-OH



Compound 2: BA-TM-OH

Cell line Key	
<u>TNBC</u>	
•BT-20	
•BT-549	
•MDA-MB-231	
•MDA-MB-157	
<u>ER+</u>	
•MCF-7	
•T47D	
•MDA-MB-361	
<u>Non-tumorigenic</u>	
•HMEC	



MICs ($\mu\text{g/mL}$) of Tropolones against *E. coli* and *K. pneumoniae*

		MIC	MIC	MIC	MIC
	MW	<i>E. coli</i> 25922	<i>K. p</i> 10031	UCHC <i>K.p</i> 1	UCHC <i>K.p</i> 3
Tropolones					
Unsubstituted					
Tropolone	122.12	>40 $\mu\text{g/mL}$	>50 $\mu\text{g/mL}$	N/A	N/A
Negative control					
HKT-OMe	178.23	>50	>500	N/A	N/A
a-Substitution (1st gen)					
MO-OH-PH	198.22	20	25	40	20
MO-OH-SM	228.24	N/A	40	N/A	N/A
MO-OH-DM	258.27	>40	100	N/A	N/A
MO-OH-TM	288.29	>40	100	N/A	N/A
MO-OH-Nap	248.28	40	100	N/A	N/A
b-Substitution (1st gen)					
HKT	164.2	25	31.25	20	20
b-sec	178.23	N/A	N/A	N/A	N/A
b-tert	178.23	>50	125	N/A	N/A
b-cyclopentyl	190.24	50	62.5	N/A	N/A
b-Phe	198.22	25	31.25	N/A	N/A
b-SM	228.24	>50	62.5	N/A	N/A
Alkyl linker					
MO-1-OH	232.32	>40	25	>40	>40
MO-7-OH	240.3	40	25	40	20
Alkyl tail					
MO-2-OH	192.25	20/10	10	40	20
MO-3-OH	190.24	40	40	N/A	N/A
MO-9-OH	254.32	40	50	N/A	N/A
MO-10-OH	226.27	20	10	>40	40
MO-11-OH	254.32	>40	40	N/A	N/A
MO-pSMe-OH	244.31	20	20	20	20
BA-P5-OH	266.33	>40	N/A	N/A	N/A
BA-P7-OH	296.4	N/A	>40	N/A	N/A
Aniline derivatives					
Am-NO ₂ -OH	243.21	~40	20/10	40	40
Am-NH ₂ -OH	213.23	40	50	N/A	N/A
Am-Piv-OH	297.35	>40	40	N/A	N/A
Am-P5-OH	295.33	40	20	>40	>40

			MIC		MIC		MIC		MIC
Tropolones	MW		E. coli 25922		K. p 10031		UCHC K.p1		UCHC K.p3
Biaryl									
BA-pBr-OH	277.11		20		12.5		20		20
MO-pF-OH	216.21		40		40		N/A		N/A
BA-pOH-OH	214.22		>40		40		N/A		N/A
BA-pCN-OH	223.27		>40		>40		N/A		N/A
BA-Ph-OH	274.31		20		12.5		>40		>40
BA-SM-OH	304.34		N/A		>40		N/A		N/A
BA-DM-OH	334.36		40		20		>40		>40
BA-TM-OH	364.39		N/A		40		N/A		N/A
BA-NAP-OH	324.37		N/A		>40		N/A		N/A
BA-HC2-OH	264.28		20		20		40		40
Heterocycles									
HC-1-OH	256.25		40		20		>40		40
HC-2-OH	188.18		20		10		20		20
HC-3-OH	199.21		>40		>40		N/A		N/A
HC-5-OH	242.23		>40		N/A		N/A		N/A
HC-6-OH	201.22		40 > 20		40		N/A		N/A
HC-7-OH	311.33		>40		N/A		N/A		N/A
HC-10-OH	288.3		>40		N/A		N/A		N/A
HC-12-OH	218.27		40		40		N/A		N/A
Acetylene									
SG-TMS-OH	294.42		N/A		>40		N/A		N/A
Carbonyls									
EF-1-OH (p-aldehyde)	226.26		40		40		N/A		N/A
EF-2-OH (acetyl)	240.25		40		10		>40		40
EF-3-OH (methylester)	256.25		40/20		20		>40		>40
EF-4-OH (o-aldehyde)	226.26		N/A		40		N/A		N/A
Other									
TDA	212.25		20		20		20		20
Zn-ditrop-PH	459.81		20		N/A		N/A		N/A
Piv-trop	206.24		N/A		>40		N/A		N/A
ENOblock	631.18		N/A		20		N/A		N/A
Alternative chelators									
MO-SMe-PH	228.31		N/A		>40		N/A		N/A
MO-NH2-PH	197.23		N/A		>40		N/A		N/A
MO-PivAm-PH	281.35		N/A		>40		N/A		N/A

			MIC		MIC		MIC		MIC
Tropolones	MW		E. coli 25922		K. p 10031		UCHC K.p1		UCHC K.p3
Gamma substitution									
gamma amine	137.14		N/A		>40		N/A		N/A
gamma Piv	221.25		>40		>40		N/A		N/A
Amine intermediate									
MO-NH ₂ -Ph	197.23		>40		N/A		N/A		N/A
MO-NH ₂ -SM	227.26		>40		N/A		N/A		N/A
MO-NH ₂ -DM	257.28		>40		N/A		N/A		N/A
MO-NH ₂ -TM	287.31		>40		N/A		N/A		N/A
MO-NH ₂ -Nap	247.29		>40		>400		N/A		N/A

MICs in <i>E. coli</i> and <i>E. coli</i> knockout models							
Tropolones	MW		25922	BW25113	JW0451	NR698	EFFECT
a-Substitution (1st gen)							
MO-OH-PH	198.22		20	20	20	20	NONE
MO-OH-SM	228.24		N/A	>20	40	40/20	NONE
MO-OH-DMe	226.27		N/A	40	40	40	NONE
Natural Product							
HKT	164.2		25	20	20	20	NONE
tropodithietic acid	212.25		20	40	40	40/20	?
Alkyl linker							
MO-1-OH	232.32		>40	>40	>40	>40	NONE
MO-7-OH	240.3		40	20	20	20	NONE
Alkyl tail							
MO-2-OH	192.25		20/10	40	40	40	?
MO-9-OH	254.32		40	40	40	20	LPS
MO-10-OH	226.27		20	40	40/20	40/20	?
MO-11-OH	254.32		>40	40	40/20	5	LPS
MO-pSMe-OH	244.31		20	20	20	10	LPS
BA-P5-OH	266.33		>40	>20	>40	20/10	LPS
BA-P8-OH	308.41		N/A	>20	>40	>40	NONE
Biaryl							
BA-pBr-OH	277.11		20	20	20	10	LPS
MO-pF-OH	216.21		40	40	40	40	NONE
BA-pOH-OH	214.22		>40	>20	>40	40	LPS
BA-pCN-OH	223.27		>40	>40	>40	>40	NONE
BA-Ph-OH	274.31		20	>40	>40	>40	?
BA-SM-OH	304.34		N/A	>40	>40	20/10	LPS
BA-DM-OH	334.36		40	>40	20	10	EFFLUX AND LPS
BA-TM-OH	364.39		N/A	>40	40	20	LPS
BA-NAP-OH	324.37		N/A	>40	>40	40	LPS
BA-HC2-OH	264.28		20	20	20	20	NONE
Aniline derivatives							
Am-NO2-OH	243.21		40	20	20	20	NONE
Am-NH2-OH	213.23		40	>20	40/20	40/20	NONE
Am-Ac-OH	255.27		N/A	>40	>40	>40	NONE
Am-Piv-OH	297.35		>40	>20	40	40	NONE
Am-P5-OH	295.33		40	40	40	40	NONE

MICs in <i>E. coli</i> and <i>E. coli</i> knockout models							
Tropolones	MW		25922	BW25113	JW0451	NR698	EFFECT
Heterocycles							
HC-1-OH	256.25		40	40	40	40	NONE
HC-2-OH	188.18		20	20	20	20	NONE
HC-3-OH	199.21		>40	>20	>40	>40	NONE
HC-5-OH	242.23		>40	>40	>40	>40	NONE
HC-6-OH	201.22		40/20	40	20	20	?
HC-7-OH	311.33		>40	>20	>40	~40	NONE
HC-10-OH	288.3		>40	>40	40/20	10/5	LPS
HC-12-OH	218.27		40	40/20	40	40	NONE
Acetylene							
SG-TMS-OH	294.42		N/A	>20	>40	5	LPS
SG-PH-OH	298.33		N/A	>40	>40	20	LPS
Carbonyls							
EF-1-OH (p-aldehyde)	226.26		40	40	40	40	NONE
EF-2-OH (acetyl)	240.25		40	20	20	20	NONE
EF-3-OH (methylester)	256.25		40	40	40	40	NONE
EF-4-OH (o-aldehyde)	226.26		N/A	40	40	40	NONE
Other							
Chlorotrop	140.57		N/A	>40	>40	>40	NONE
Piv-trop	206.24		40/20	40	>40	40	NONE
ENOblock	631.18		40/20	40	40	10	LPS
Alternative chelators							
MO-SH-PH	214.28		N/A	>40	>40	>200	NONE
MO-NH ₂ -PH	197.23		>40	>40	>40	>200	NONE
MO-AM-PH	239.27		N/A	>40	>40	>40	NONE
MO-OMe-PH	212.24		N/A	>40	>40	>40	NONE
MO-NHOH-PH	213.23		N/A	>40	>40	>40	NONE
MO-SMe-PH	228.31		N/A	>40	>40	>40	NONE
MO-H-PH	182.22		N/A	>40	>40	>40	NONE
MO-PivAm-PH	281.35		N/A	>40	>40	20/10	LPS

Evaluation of HKT and γ -Tropolone Inhibitory Activity on E.coli Enolase (at 20 μ M concentration).

Compound	Structure	% Activity	% Inhibition
HKT	<chem>CC(C)C1=C(O)C(=O)C=CC=C1</chem>	45%	55%
γ -NH ₂	<chem>NC1=C(O)C(=O)C=CC=C1</chem>	81%	19%
γ -Piv	<chem>CC(C)(C)C(=O)NC1=C(O)C(=O)C=CC=C1</chem>	47%	53%
γ -P5	<chem>CCCC=CC(=O)NC1=C(O)C(=O)C=CC=C1</chem>	85%	15%

Salt Version of Tropolones and Its Effect on Enolase Activity.

Compound	Concentration	% Activity	% Inhibition
HKT	10 μ M	57%	43%
Na-HKT	10 μ M	63%	37%
HKT-Arginate	10 μ M	52%	48%

Compound	Concentration	% Activity	% Inhibition
HC-1-OH	10 μ M	71%	29%
HC-1-Arginate	10 μ M	63%	37%

Compound	Concentration	% Activity	% Inhibition
MO-OH-PH	20 μ M	67%	33%
Zn-ditrop-PH	20 μ M	56%	44%

Effect of Chloride and Pivalate Group on the Inhibitory Activity of the Tropone.

Compound	Concentration	% Activity	% Inhibition
Tropolone	10 μ M	61%	39%
Chlorotropone	10 μ M	45%	55%
Piv-tropone	10 μ M	27%	73%

Compound	Concentration	% Activity	% Inhibition
Tropolone	20 μ M	38%	62%
Chlorotropone	20 μ M	34%	66%
Piv-tropone	20 μ M	17%	83%

Dose-dependent Responses of α and β Substituted Tropolones.

BA-pBr-OH

Concentration	% Activity	% Inhibition
1 μ M	86%	14%
5 μ M	61%	39%
10 μ M	49%	51%
20 μ M	29%	71%

MO-2-OH

Concentration	% Activity	% Inhibition
1 μ M	80%	20%
5 μ M	65%	35%
10 μ M	52%	48%
20 μ M	22%	78%

HC-7-OH

Concentration	% Activity	% Inhibition
5 μ M	78%	22%
10 μ M	63%	37%
20 μ M	46%	54%

Tropolone

Concentration	% Activity	% Inhibition
1 μ M	94%	6%
5 μ M	74%	26%
10 μ M	63%	37%
15 μ M	54%	46%
20 μ M	39%	61%

Chlorotropone

Concentration	% Activity	% Inhibition
5 μ M	80%	20%
10 μ M	45%	55%
20 μ M	34%	66%

Piv-trop

Concentration	% Activity	% Inhibition
1 μM	94%	6%
5 μM	67%	33%
10 μM	32%	68%
15 μM	16%	84%
20 μM	11%	89%

HKT

Concentration	% Activity	% Inhibition
1 μM	89%	11%
5 μM	78%	22%
10 μM	53%	47%
20 μM	45%	55%